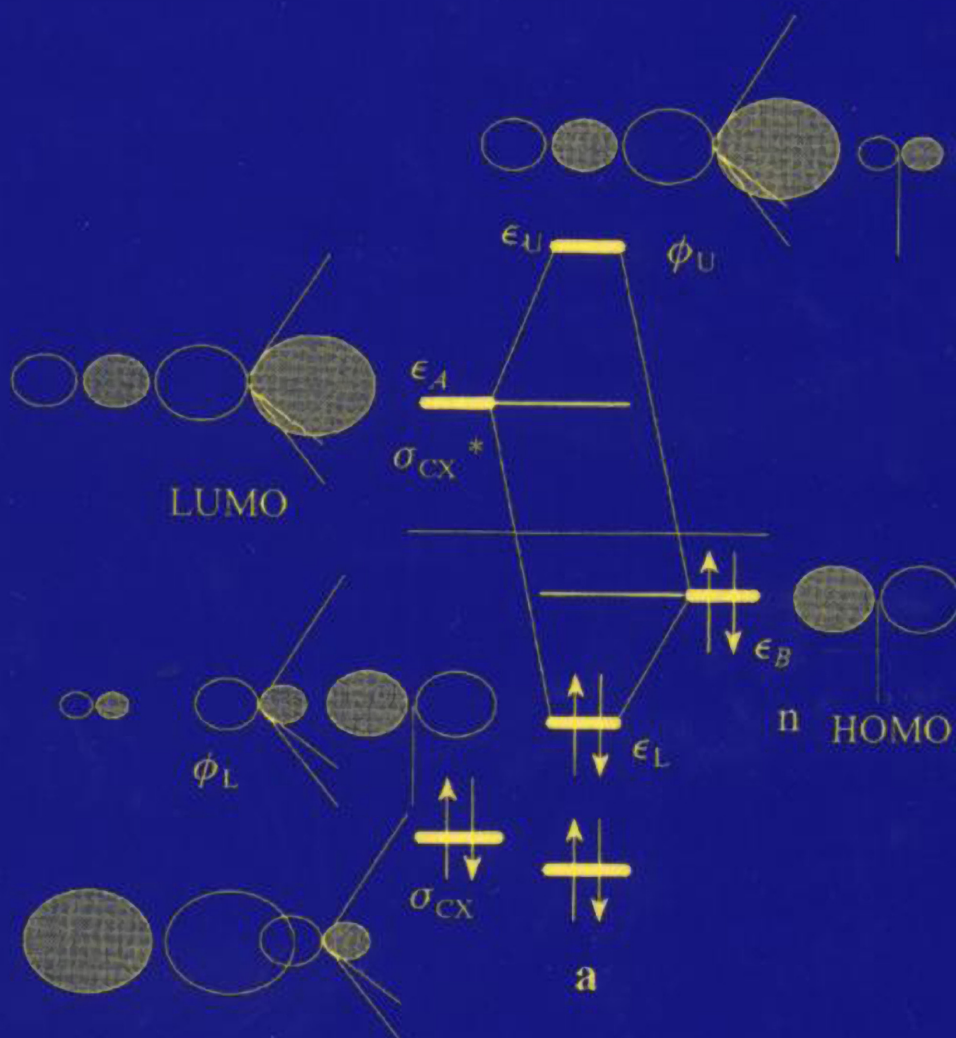


# Orbital Interaction Theory of Organic Chemistry

SECOND EDITION



ARVI RAUK

*Orbital Interaction Theory of Organic Chemistry, Second Edition.* Arvi Rauk  
Copyright © 2001 John Wiley & Sons, Inc.  
ISBNs: 0-471-35833-9 (Hardback); 0-471-22041-8 (Electronic)

# ORBITAL INTERACTION THEORY OF ORGANIC CHEMISTRY

Second Edition

---

# ORBITAL INTERACTION THEORY OF ORGANIC CHEMISTRY

---

Second Edition

**ARVI RAUK**

Professor Emeritus

University of Calgary, Canada



A John Wiley & Sons, Inc., Publication

New York • Chichester • Weinheim • Brisbane • Singapore • Toronto

Designations used by companies to distinguish their products are often claimed as trademarks. In all instances where John Wiley & Sons, Inc., is aware of a claim, the product names appear in initial capital or ALL CAPITAL LETTERS. Readers, however, should contact the appropriate companies for more complete information regarding trademarks and registration.

Copyright © 2001 by John Wiley & Sons, Inc. All rights reserved.

No part of this publication may be reproduced, stored in a retrieval system or transmitted in any form or by any means, electronic or mechanical, including uploading, downloading, printing, decompiling, recording or otherwise, except as permitted under Sections 107 or 108 of the 1976 United States Copyright Act, without the prior written permission of the Publisher. Requests to the Publisher for permission should be addressed to the Permissions Department, John Wiley & Sons, Inc., 605 Third Avenue, New York, NY 10158-0012, (212) 850-6011, fax (212) 850-6008, E-Mail: PERMREQ @ WILEY.COM.

This publication is designed to provide accurate and authoritative information in regard to the subject matter covered. It is sold with the understanding that the publisher is not engaged in rendering professional services. If professional advice or other expert assistance is required, the services of a competent professional person should be sought.

ISBN 0-471-22041-8

This title is also available in print as ISBN 0-471-35833-9.

For more information about Wiley products, visit our web site at [www.Wiley.com](http://www.Wiley.com).

# CONTENTS

---

<b>PREFACE</b>	<b>xiii</b>
<b>1 SYMMETRY AND STEREOCHEMISTRY</b>	<b>1</b>
Purpose / 1	
Definition of a Group / 2	
Molecular Point Groups / 2	
Schoenflies Notation / 2	
Interrelations of Symmetry Elements / 3	
Type Classification / 3	
Isomerism and Measurements / 6	
Stereoisomerism of Molecules / 8	
Stereotopic Relationships of Groups in Molecules / 9	
Asymmetric Synthesis and Stereochemistry / 10	
NMR and Stereochemistry / 12	
Symmetry and Structural Parameters / 14	
Note on Hybridization / 15	
Symmetry and Orbitals / 16	
Atomic Orbitals / 16	
Molecular and Group Orbitals / 17	
In What Combination? / 19	
<b>2 MOLECULAR ORBITAL THEORY</b>	<b>20</b>
Introduction / 20	
Electronic Schrödinger Equation (A.1) / 21	

Fock Equations (A.42) /	23
The Basis Set (STO-3G, 6-31G*, and All That) /	24
Orbital Energies and Orbitals /	25
Representation of MOs /	27
Total Energies and the Hartree–Fock Limit /	29
Successes and Failures of Hartree–Fock Theory /	29
Beyond Hartree–Fock /	30
Density Functional Theory /	31
Geometry Optimization /	31
Normal Coordinates and Harmonic Frequency Analysis /	32
Zero Point Vibrational Energies /	33

### 3 ORBITAL INTERACTION THEORY

34

Relationship to Hartree–Fock Equations /	34
Hückel Approximation /	34
Orbital Energies and Total Electronic Energy /	34
Case Study of a Two-Orbital Interaction /	35
Case 1: $\varepsilon_A = \varepsilon_B$ , $S_{AB} = 0$ /	38
Case 2: $\varepsilon_A = \varepsilon_B$ , $S_{AB} > 0$ , $S_{AB} \ll 1$ /	39
Case 3: $\varepsilon_A > \varepsilon_B$ , $S_{AB} = 0$ /	40
Case 4: $\varepsilon_A > \varepsilon_B$ , $S_{AB} > 0$ /	42
Effect of Overlap /	44
Energetic Effect of Overlap /	44
Orbital Effect of Overlap /	44
First Look at Bonding /	45
Relationship to Perturbation Theory /	45
Generalizations for Intermolecular Interactions /	46
Energy and Charge Distribution Changes from Orbital Interaction /	47
Four-Electron, Two-Orbital Interaction /	47
Three-Electron, Two-Orbital Interaction /	48
Two-Electron, Two-Orbital Interaction /	49
One-Electron, Two-Orbital Interaction /	51
Zero-Electron, Two-Orbital Interaction /	51
Interactions between Molecules: Many Electrons, Many Orbitals /	52
General Principles Governing the Magnitude of $h_{AB}$ and $S_{AB}$ /	52
Interactions of MOs /	52
Electrostatic Effects /	55
Group Orbitals /	56
Zero-Coordinated Atoms /	56
Monocoordinated Atoms /	57
Dicoordinated Atoms /	58
Tricoordinated Atoms /	59
Tetracoordinated Atoms /	59

Assumptions for Application of Qualitative MO Theory /	61
Example: Carbonyl Group /	62
Construction of Interaction Diagram /	62
Interpretation of Interaction Diagram /	65
Chemical Reactivity /	66
Why Does It Work and When Might it Not? /	69

#### 4 SIGMA BONDS AND ORBITAL INTERACTION THEORY 72

C—X $\sigma$ Bonds: X = C, N, O, F and X = F, Cl, Br, I /	72
$\sigma$ Bonds: Homolytic versus Heterolytic Cleavage /	74
Heterolytic Cleavage of $\sigma$ Bonds Involving C or H /	74
Homolytic Cleavage of $\sigma$ Bonds Involving C or H /	75
Homonuclear $\sigma$ Bonds C—C, N—N, O—O, F—F, Cl—Cl, Br—Br, and I—I /	76
Interactions of $\sigma$ Bonds /	77
$\sigma$ Bonds as Electron Donors or Acceptors /	81
$\sigma$ Bonds as Electron Acceptors /	81
As a $\sigma$ Acceptor /	81
As a $\pi$ Acceptor /	82
$\sigma$ Bonds as Electron Donors /	83
As a $\sigma$ Donor /	83
As a $\pi$ Donor /	84
Bonding in Cyclopropane /	84

#### 5 SIMPLE HÜCKEL MOLECULAR ORBITAL THEORY 86

Simple Hückel Assumptions /	86
Charge and Bond Order in SHMO Theory: ( $S_{AB} = 0$ , One Orbital per Atom) /	91
Electron Population and Net Charge of Center A /	91
Bond Order between Centers A and B /	92
Factors Governing Energies of MOs: SHMO Theory /	92
Reference Energy and Energy Scale /	92
Heteroatoms in SHMO Theory /	93
Effect of Coordination Number on $\alpha$ and $\beta$ /	93
Hybridization at C in Terms of $\alpha$ and $\beta$ /	96
Gross Classification of Molecules on the Basis of MO Energies /	96

#### 6 REACTIONS AND PROPERTIES OF $\pi$ BONDS 98

Reactions of Olefins (Alkenes) /	98
Effect of X: Substituents /	99
Effect of Z Substituents /	101
Effect of "C" Substituents /	101
Effect of Distortion of Molecular Skeleton /	102

Alkynes / 103

 $\pi$  Bonds to and between Higher Row Elements / 103 $\pi$  Bonds to Silicon, Phosphorus, and Sulfur / 103**7 REACTIVE INTERMEDIATES****105**Reactive Intermediates  $[\text{CH}_3]^+$ ,  $[\text{CH}_3]^-$ ,  $[\text{CH}_3]^\cdot$ , and  $[:\text{CH}_2]$  / 105

Carbocations / 105

Intermolecular Reactions of Carbocations / 106

Intramolecular Reactions of Carbocations / 107

Silyl Cations / 108

Carbanions / 108

Carbon Free Radicals / 110

Carbenes / 114

Nitrenes and Nitrenium Ions / 116

Nitrenes / 116

Nitrenium Ions / 118

**8 CARBONYL COMPOUNDS****121**

Reactions of Carbonyl Compounds / 121

Electrophilic Attack on a Carbonyl Group / 121

Basicity and Nucleophilicity of the Oxygen Atom / 122

Nucleophilic Attack on a Carbonyl Group / 124

Amide Group / 126

Thermodynamic Stability of Substituted Carbonyl Groups / 127

**9 NUCLEOPHILIC SUBSTITUTION REACTIONS****129**

Nucleophilic Substitution at Saturated Carbon / 129

Unimolecular Nucleophilic Substitution  $\text{S}_{\text{N}}1$  / 129Bimolecular Nucleophilic Substitution  $\text{S}_{\text{N}}2$  / 130Another Description of the  $\text{S}_{\text{N}}2$  Reaction: VBCM Model / 134**10 BONDS TO HYDROGEN****137**

Hydrogen Bonds and Proton Abstraction Reactions / 137

Hydrogen Bonds / 137

Symmetrical and Bifurcated Hydrogen Bonds / 139

Proton Abstraction Reactions / 141

E2 Elimination Reaction / 143

E1cB Mechanism Reaction / 144

E1 Elimination Reaction / 144

Reaction with Electrophiles: Hydride Abstraction and Hydride Bridging / 145

Activation by  $\pi$  Donors (X: and "C" Substituents) / 145



Hydride Abstraction / 145	
Hydride Bridges / 147	
Reaction with Free Radicals: Hydrogen Atom Abstraction and One- or Three-Electron Bonding / 147	
Hydrogen-Bridged Radicals / 147	
Hydrogen Atom Transfer / 148	
<b>11 AROMATIC COMPOUNDS</b>	<b>150</b>
Reactions of Aromatic Compounds / 150	
Cyclic $\pi$ Systems by Simple Hückel MO Theory / 150	
Aromaticity in $\sigma$ -Bonded Arrays? / 151	
Reactions of Substituted Benzenes / 152	
Electrophilic Substitutions / 152	
Effect of Substituents on Substrate Reactivity / 153	
Electrophilic Attack on X-Substituted Benzenes / 153	
Electrophilic Attack on Z-Substituted Benzenes / 154	
Electrophilic Attack on "C"-Substituted Benzenes / 155	
Electrophilic Attack on N Aromatics: Pyrrole and Pyridine / 155	
Nucleophilic Substitutions / 157	
Effect of Substituents on Substrate Reactivity / 158	
Nucleophilic Attack on Z-Substituted Benzenes / 158	
Nucleophilic Attack on N Aromatics: Pyrrole and Pyridine / 158	
Nucleophilic Substitution by Proton Abstraction / 159	
<b>12 PERICYCLIC REACTIONS</b>	<b>161</b>
General Considerations / 161	
Cycloadditions and Cycloreversions / 162	
Stereochemical Considerations / 162	
Electrocyclic Reactions / 165	
Stereochemical Considerations / 165	
Cheletropic Reactions / 165	
Stereochemical Considerations / 165	
Sigmatropic Rearrangements / 166	
Stereochemical Considerations / 166	
Component Analysis (Allowed or Forbidden?) / 167	
Rule for Component Analysis / 168	
Diels–Alder Reaction / 169	
Cope Rearrangement / 170	
1,3-Dipolar Cycloaddition Reactions / 171	
<b>13 ORGANOMETALLIC COMPOUNDS</b>	<b>175</b>
Transition Metals / 175	

Ligands in Transition Metal Complexes / 176  
Orbitals in Transition Metal Bonding / 176  
Orbital Energies / 178  
Valence Orbitals of Reactive Metal Complexes / 179  
Six Valence Orbitals of Tricoordinated Metal / 182  
Five Valence Orbitals of Tetracoordinated Metal / 182  
Four Valence Orbitals of Pentacoordinated Structure / 185  
Transition Metals and C—H or H—H Sigma Bonds / 186  
More About C Ligands in Transition Metal Complexes / 186  
Chelating Ligands / 187  
Organic  $\pi$ -Bonded Molecules as Ligands / 187  
Transition Metal Bonding to Alkenes: Zeise's Salt / 187  
Agostic Interaction / 191  
Ziegler–Natta Polymerization / 192  
Oxidative Addition to H—H and C—H Bonds / 194

**14 ORBITAL AND STATE CORRELATION DIAGRAMS** **196**

General Principles / 196  
Woodward–Hoffman Orbital Correlation Diagrams / 197  
    Cycloaddition Reactions / 197  
    Electrocyclic Reactions / 198  
    Cheletropic Reactions / 201  
    Photochemistry from Orbital Correlation Diagrams / 201  
Limitations of Orbital Correlation Diagrams / 203  
State Correlation Diagrams / 203  
    Electronic States from MOs / 205  
    Rules for Correlation of Electronic States / 206  
    Example: Carbene Addition to an Olefin / 206

**15 PHOTOCHEMISTRY** **209**

Photoexcitation / 209  
Jablonski Diagram / 210  
Fate of Excited Molecule in Solution / 211  
Dauben–Salem–Turro Analysis / 212  
Norrish Type II Reaction of Carbonyl Compounds / 213  
Norrish Type I Cleavage Reaction of Carbonyl Compounds / 215

**APPENDIX A: DERIVATION OF HARTREE–FOCK THEORY** **218**

Electronic Hamiltonian Operator / 218  
Electronic Schrödinger Equation / 220  
Expectation Values / 221  
Many-Electron Wave Function / 221

Electronic Hartree–Fock Energy /	222
Variation of $E_{\text{HF}}$ /	226
LCAO Solution of Fock Equations /	229
Integrals /	231
The Basis Set (STO-3G, 6-31G*, and All That) /	232
Interpretation of Solutions of HF Equations /	233
Orbital Energies and Total Electronic Energy /	233
Restricted Hartree–Fock Theory /	234
Mulliken Population Analysis /	236
Dipole Moments /	236
Total Energies /	237
Configuration Energies /	237
Post-Hartree–Fock Methods /	239
Configuration Interaction Theory /	239
Excited States from CI Calculations /	241
Many-Body Perturbation Theory /	241
Rayleigh–Schrödinger Perturbation Theory /	241
Møller–Plesset Perturbation Theory /	244
Density Functional Theory /	245

**APPENDIX B: EXERCISES****247**

Chapter 1 /	247
Chapter 2 and Appendix A /	249
Chapter 3 /	252
Chapter 4 /	262
Chapter 5 /	264
Chapter 6 /	272
Chapter 7 /	273
Chapter 8 /	278
Chapter 9 /	281
Chapter 10 /	281
Chapter 11 /	284
Chapter 12 /	288
Chapter 13 /	292
Chapter 14 /	296
Chapter 15 /	298
Miscellaneous /	301

**REFERENCES AND NOTES****313****INDEX****325**

# PREFACE

---

The premise on which this text is based is that the vast majority of chemical phenomena may be qualitatively understood by the judicious use of simple orbital interaction diagrams. The material borrows heavily from the pioneering work of Fukui [1, 2], Woodward and Hoffmann [3], Klopman [4], Salem [5], Hoffmann [6], and many others whose work will be acknowledged throughout including Fleming: *Frontier Orbitals and Organic Chemical Reactions* [7], from which a number of illustrative examples are extracted. If there is uniqueness to the present approach, it lies in the introduction of the  $\alpha$  and  $\beta$  of simple Hückel molecular orbital theory as reference energy and energy scale on which to draw the interaction diagrams, mixing  $\sigma$  and  $\sigma^*$  orbitals and nonbonded orbitals with the usual  $\pi$  orbitals of SHMO theory on the same energy scale. This approach is difficult to justify theoretically, but it provides a platform on which the reader can construct his or her interaction diagrams and is very useful in practice. Numerous illustrations from the recent literature are provided.

The book is intended for students of organic chemistry at the senior undergraduate and postgraduate levels and for chemists in general seeking qualitative understanding of the (often) quantitative data produced by modern computational chemists [8]. All reactions of organic compounds are treated within the framework of generalized Lewis acid–Lewis base theory, their reactivity being governed by the characteristics of the frontier orbitals of the two reactants. All compounds have occupied molecular orbitals and so can donate electrons, that is, act as bases in the Lewis sense. All compounds have empty molecular orbitals and so can accept electrons, that is, act as acids in the Lewis sense. The “basicity” of a compound depends on its ability to donate the electron pair. This depends on the energy of the electrons, the distribution of the electrons (shape of the molecular orbital), and also on the ability of the substrate to receive the electrons (on the shape and energy of its empty orbital). The basicity of a compound toward different substrates will be different, hence a distinction between Lowry–Bronsted basicity and nucleophilicity. A parallel definition applies for the “acidity” of the compound. The

structures of compounds are determined by the energetics of the occupied orbitals. Fine distinctions, such as conformational preferences, can be made on the basis of maximization of attractive interactions and/or minimization of repulsive interactions between the frontier localized group orbitals of a compound. All aspects are examined from the point of view of orbital interaction diagrams from which gross features of reactivity and structure flow naturally. The approach is qualitatively different from and simpler than, a number of alternative approaches, such as the VBCM (valence bond configuration mixing) model [9] and OCAMS (orbital correlation analysis using maximum symmetry) approach [10, 11].

The organization of the text follows a logical pedagogical sequence. The first chapter is not primarily about “orbitals” at all but introduces (or recalls) to the reader elements of symmetry and stereochemical relationships among molecules and among groups within a molecule. Many of the reactions of organic chemistry follow stereochemically well-defined paths, dictated, it will be argued, by the interactions of the frontier orbitals. The conceptual leap to orbitals as objects anchored to the molecular framework which have well-defined spatial relationships to each other is easier to make as a consequence. Whether or not orbitals interact can often be decided on grounds of symmetry. The chapter concludes with the examination of the symmetry properties of a few orbitals which are familiar to the student.

The second chapter introduces the student to “orbitals” proper and offers a simplified rationalization for why orbital interaction theory may be expected to work. It does so by means of a qualitative discussion of Hartree–Fock theory. A detailed derivation of Hartree–Fock theory making only the simplifying concession that all wave functions are real is provided in Appendix A. Some connection is made to the results of *ab initio* quantum chemical calculations. Postgraduate students can benefit from carrying out a project based on such calculations on a system related to their own research interests. A few exercises are provided to direct the student. For the purpose of undergraduate instruction, this chapter and Appendix A may be skipped, and the essential arguments and conclusions are provided to the students in a single lecture as the introduction to Chapter 3.

Orbital interaction theory proper is introduced in Chapter 3. The independent electron (Hückel) approximation is invoked and the effective one-electron Schrödinger equation is solved for the two-orbital case. The solutions provide the basis for the orbital interaction diagram. The effect of overlap and energy separation on the energies and polarizations of the resulting molecular orbitals are explicitly demonstrated. The consequences of zero to four electrons are examined and applications are hinted at. Group orbitals are provided as building blocks from which the student may begin to assemble more complex orbital systems.

Chapter 4 provides a brief interlude in the theoretical derivations by examining specific applications of the two-orbital interaction diagrams to the description of  $\sigma$  bonds and their reactions.

In Chapter 5, conventional simple Hückel molecular orbital (SHMO) theory is introduced. The Hückel  $\alpha$  is suggested as a reference energy, and use of  $|\beta|$  as a unit of energy is advocated. Parameters for heteroatoms and hybridized orbitals are given. An interactive computer program, SHMO, which uses the conventions introduced in this chapter, is available on the Web [12].

Chapters 6–11 describe applications of orbital interaction theory to various chemical systems in order to show how familiar concepts such as acid and base strengths, nucleo-

philicity and electrophilicity, stabilization and destabilization, and thermodynamic stability and chemical reactivity may be understood.

Pericyclic reactions are described in Chapter 12 as a special case of frontier orbital interactions, that is, following Fukui [1]. However, the stereochemical nomenclature *suprafacial* and *antarafacial* and the very useful general component analysis of Woodward and Hoffmann [3] are also introduced here.

The bonding in organometallic compounds between the metal and C and H atoms is briefly described in Chapter 13.

Chapter 14 deals with orbital correlation diagrams following Woodward and Hoffmann [3]. State wave functions and properties of electronic states are deduced from the orbital picture, and rules for state correlation diagrams are reviewed, as a prelude to an introduction to the field of organic photochemistry in Chapter 15.

In Chapter 15, the state correlation diagram approach of the previous chapter is applied to a brief discussion of photochemistry in the manner of Dauben, Salem, and Turro [13]. A more comprehensive approach to this subject may be found in the text by Michl and Bonacic-Koutecky [14], Turro [15], or Gilbert and Baggott [16].

Sample problems and quizzes, grouped approximately by chapter, are presented in Appendix B. Many are based on examples from the recent literature and references are provided. Detailed answers are worked out for many of the problems. These serve as further examples to the reader of the application of the principles of orbital interaction theory.

Arvi Rauk  
Calgary, Canada

## CHAPTER 1

---

# SYMMETRY AND STEREOCHEMISTRY

---

### PURPOSE

Symmetry is a concept that we all make use of in an unconscious fashion. We notice it every time we look in our bathroom mirror. We ourselves are (approximately) bilaterally symmetric. A reflected right hand looks like a left hand, a reflected right ear like a left ear, but the mirror image of the face as a whole or of the toothbrush does not look different from the original. The hand, a *chiral* object, is distinguishable from its mirror image; the toothbrush is not. The toothbrush is *achiral* and possesses a mirror plane of symmetry which bisects it. It would not surprise us if we were to inspect the two sides of the toothbrush and find them identical in many respects. It *may* surprise us to note that the two sides are distinguishable when held in the hand, that is, in a chiral environment (the fingers hold one side and the thumb the other). However, the achiral toothbrush fits equally comfortably into either the right or the left hand. Chiral objects do not. They interact differently with other chiral objects and often the different interactions are known by separate words. When you hold someone's right hand in your right hand, you are *shaking* hands; when it is the other person's left hand in your right, you are *holding* hands. Similar properties and interactions exist in the case of molecules as well.

In this chapter we will familiarize ourselves with basic concepts in *molecular* symmetry [17]. The presence or absence of symmetry has consequences on the appearance of spectra, the relative reactivity of groups, and many other aspects of chemistry, including the way we will make use of orbitals and their interactions. We will see that the orbitals that make up the primary description of the electronic structure of molecules or groups within a molecule have a definite relationship to the three-dimensional structure of the molecule as defined by the positions of the nuclei. The orientations of the nuclear framework will determine the orientations of the orbitals. The relationships between structural units (groups) of a molecule to each other can often be classified in terms of the symmetry that the molecule as a whole possesses. We will begin by introducing the basic termi-

nology of molecular symmetry. Finally we will apply simple symmetry classification: to local group orbitals to decide whether or not interaction is allowed in the construction of molecular orbitals; to molecular orbitals to determine the stereochemical course of electrocyclic reactions and to help determine the principal interactions in bimolecular reactions; and to electronic states to construct state correlation diagrams.

We begin by introducing molecular point groups according to the Schoenflies notation and assigning molecular and group symmetry following Jaffe and Orchin [18] where greater detail may be found.

### DEFINITION OF A GROUP

A *group*  $G = \{\dots, g_i, \dots\}$  is a set of elements related by an operation which we will call *group multiply* for convenience and which has the following properties:

1. The product of any two elements is in the set; that is, the set is *closed* under group multiplication.
2. The associative law holds: for example,  $g_i(g_j g_k) = (g_i g_j)g_k$ .
3. There is a *unit* element,  $e$ , such that  $eg_i = g_i e = g_i$ .
4. There is an *inverse*,  $g_i^{-1}$ , to each element, such that  $(g_i^{-1})g_i = g_i(g_i^{-1}) = e$ . An element may be its own inverse.

### MOLECULAR POINT GROUPS

A molecular point group is a set of symmetry elements. Each symmetry element describes an operation which when carried out on the molecular skeleton leaves the molecular skeleton unchanged. Elements of point groups may represent any of the following operations:

1. Rotations about axes through the origin:

$$C_n = \text{rotation through } 2\pi/n \text{ radians (in solids, } n = 1, 2, 3, 4, 6)$$

2. Reflections in planes containing the origin (center of mass):

$$\sigma = \text{reflection in a plane}$$

3. Improper rotations—a rotation about an axis through the origin followed by a reflection in a plane containing the origin and perpendicular to the axis of rotation:

$$S_n = \text{rotation through } 2\pi/n \text{ radians followed by } \sigma_h \text{ (see below)}$$

### SCHOENFLIES NOTATION

The symbols used to designate the elements of molecular point groups in the Schoenflies notation and their descriptions are as follows:



$E$  = identity

$C_n$  = rotation about an axis through  $2\pi/n$  radians. The *principal* axis is the axis of highest  $n$

$\sigma_h$  = reflection in a horizontal plane, that is, the plane through the origin perpendicular to the axis of highest  $n$

$\sigma_v$  = reflection in a vertical plane, that is, the plane containing the axis of highest  $n$

$\sigma_d$  = reflection in a diagonal plane, that is, the plane containing the axis of highest  $n$  and bisecting the angle between the twofold axes perpendicular to the principal axis. This is just a special case of  $\sigma_v$

$S_n$  = improper rotation through  $2\pi/n$ , that is,  $C_n$  followed by  $\sigma_h$

$i$  = inversion through the center of mass, that is,  $\mathbf{r} \rightarrow -\mathbf{r}$ ,  $=S_2$

## INTERRELATIONS OF SYMMETRY ELEMENTS

A number of relationships exist between the elements of symmetry of a point group which are a consequence of the closure property of groups. They may be used to identify difficult-to-locate symmetry elements.

1. a. The intersection of two reflection planes must be a symmetry axis. If the angle  $\phi$  between the planes is  $\pi/n$ , the axis is  $n$ -fold.
  - b. If a reflection plane contains an  $n$ -fold axis, there must be  $n - 1$  other reflection planes at angles of  $\pi/n$ .
2. a. Two twofold axes separated by an angle  $\pi/n$  require a perpendicular  $n$ -fold axis.
  - b. A twofold axis and an  $n$ -fold axis perpendicular to it require  $n - 1$  additional twofold axes separated by angles of  $\pi/n$ .
3. An even-fold axis, a reflection plane perpendicular to it, and an inversion center are interdependent. Any two of these implies the existence of the third.

## TYPE CLASSIFICATION

The following classification by types is due to Jaffe and Orchin [18]. Representative examples are given below for a number of types. The reader is challenged to find the rest.

**Type 1.** No rotation axis; point groups  $C_1$ ,  $C_s$ ,  $C_i$ .

- (a)  $C_1 = \{E\}$ . This group has no symmetry elements. It is the point group of *asymmetric* compounds.
- (b)  $C_s = \{E, \sigma\}$ . This group has only a single plane of symmetry. Methanol ( $\text{CH}_3\text{OH}$ ) is an example.
- (c)  $C_i = \{E, i\}$ . This group has only a center of inversion. Two examples are shown in Figure 1.1.

**Type 2.** Only one axis of rotation; point groups  $C_n$ ,  $S_n$ ,  $C_{nv}$ ,  $C_{nh}$ .

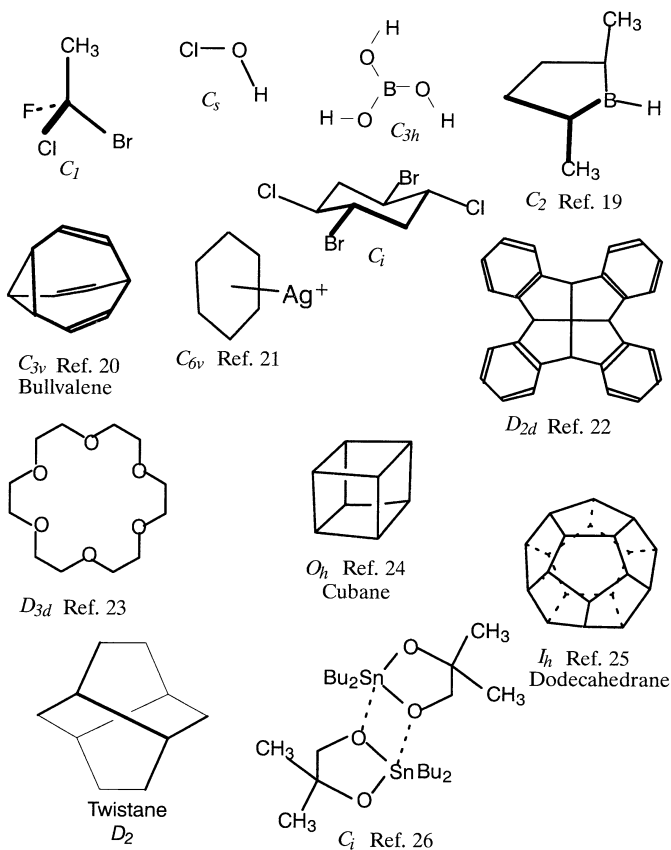


**Figure 1.1.** Examples of molecules belonging to various point groups.

- (a)  $C_n$ . This group has only a single rotational axis of order greater than 1. These molecules are *dissymmetric* (chiral) and can be made optically active unless the enantiomeric forms are readily interconvertible.

$C_2 = \{E, C_2\}$ . Hydrogen peroxide (HOOH) and *gauche*-1,2-dichloroethane are examples.

$C_3 = \{E, C_3, C_3^2\}$

$C_4 = \{E, 2C_4, C_2(=C_4^2)\}$

- (b)  $S_n$

$S_4 = \{E, C_2, S_4, S_4^3\}$ . The  $D_{2d}$  structure in Figure 1.1 actually belongs to  $S_4$  since the five-membered rings are not planar.

$S_6 = \{E, C_3, C_3^2, i, S_6, S_6^5\}$

(c)  $C_{nv}$ . This group has symmetry elements  $C_n$  and  $n \sigma_v$ :

$C_{2v} = \{E, C_2, \sigma_v, \sigma_{v'}\}$ . Water, formaldehyde, and methylene chloride ( $\text{CH}_2\text{Cl}_2$ ) are common examples.

$C_{3v} = \{E, 2C_3, 3\sigma_v\}$ . Chloroform ( $\text{CHCl}_3$ ) and ammonia are typical examples. See also bullvalene in Figure 1.1.

$C_{4v} = \{E, 2C_4, C_2, 2\sigma_v, 2\sigma_d\}$

$C_{5v} = \{E, 2C_5, C_5^2, 5\sigma_v\}$

$C_{6v} = \{E, 2C_6, 2C_3, C_2, 3\sigma_v, 3\sigma_d\}$

$C_{\infty v}$ . HCl and CO and other linear polyatomic molecules without a center of inversion.

(d)  $C_{nh}$ . This group has the symmetry element  $C_n$  and a horizontal mirror plane  $\sigma_h$ . When  $n$  is even, a  $\sigma_h$  implies an  $i$ :

$C_{2h} = \{E, C_2, i, \sigma_h\}$ , e.g., (*E*)-1,2-dichloroethene

$C_{3h} = \{E, 2C_3, \sigma_h, 2S_3\}$ , e.g., boric acid  $[\text{B}(\text{OH})_3]$ , see Figure 1.1

$C_{4h} = \{E, 2C_4, C_2, i, \sigma_h, 2S_4\}$

**Type 3.** One  $n$ -fold axis and  $n$  twofold axes; point groups  $D_n, D_{nh}, D_{nd}$ .

(a)  $D_n$ . This group has only a single rotational axis of order  $n > 1$  and  $n$  twofold axes perpendicular to the principal axis. These molecules are dissymmetric and can be made optically active unless enantiomeric conformations are readily interconvertible:

$D_2 = \{E, 3C_2\}$ , e.g., twisted ethylene, twistane (Figure 1.1)

$D_3 = \{E, 2C_3, 3C_2\}$ , e.g., trisethylenediamine complexes of transition metals

(b)  $D_{nh}$ . This group has only a single rotational axis of order  $n > 1$ ,  $n$  twofold axes perpendicular to the principal axis, and a  $\sigma_h$  (which also results in  $n \sigma_v$ ):

$D_{2h} = \{E, 3C_2, 3\sigma_v, i\}$ , e.g., ethylene, diborane, and naphthalene

$D_{3h} = \{E, 2C_3, 3C_2, 3\sigma_v, \sigma_h, 2S_3\}$ , e.g., cyclopropane

$D_{4h} = \{E, 2C_4, C_2, 2C_2', 2C_2'', i, 2S_4, \sigma_h, 2\sigma_v, 2\sigma_d\}$ , e.g., the point group of the square or planar cyclobutane. What about cyclobutadiene?

$D_{5h} = \{E, 2C_5, 2C_5^2, 5C_2, 2S_5, 2S_5^2, \sigma_h, 5\sigma_v\}$ , e.g., cyclopentadienyl anion

$D_{6h} = \{E, 2C_6, 2C_3, C_2, 3C_2', 3C_2'', i, 2S_6, 2S_3, \sigma_h, 3\sigma_v, 3\sigma_d\}$ , e.g., benzene

$D_{\infty h}$ . The other point group of linear molecules, e.g., carbon dioxide and acetylene.

- (c)  $D_{nd}$ . This group has only a single rotational axis of order  $n > 1$ ,  $n$  twofold axes perpendicular to the principal axis, and  $n$  diagonal planes  $\sigma_d$  which bisect the angles made by successive twofold axes. In general,  $D_{nd}$  contains an  $S_{2n}$ , and if  $n$  is odd, it contains  $i$ :

$D_{2d} = \{E, 3C_2, 2\sigma_d, 2S_4\}$ . Allene has this symmetry, as do puckered cyclobutane and cyclooctatetraene.

$D_{3d} = \{E, 2C_3, 3C_2, i, 3\sigma_d, 2S_6\}$ , e.g., cyclohexane and ethane. See also Figure 1.1.

$D_{4d} = \{E, 2C_4, C_2, 2C_2', 2C_2'', 2S_8, 2S_8^3, 4\sigma_d\}$

$D_{5d} = \{E, 2C_5, 2C_5^2, 5C_2, i, 2S_{10}, 2S_{10}^3, 5\sigma_d\}$

**Type 4.** More than one axis higher than twofold; point groups  $T_d, O_h, I_h, K_h$  (also  $T_h, T, O, I$ ). Methane ( $T_d$ ), cubane ( $O_h$ , Figure 1.1), dodecahedrane ( $I_h$ , Figure 1.1), and buckminsterfullerene,  $C_{60}$  ( $I_h$ , Chapter 11). The symbol  $K_h$  denotes the point group of the sphere.

*Exercise 1.1.* As an exercise, let us locate all of the symmetry elements of the  $D_{3d}$  point group as they pertain to cyclohexane. The effect of these on the cyclohexane skeleton are shown in Figure 1.2.

*Exercise 1.2.* A number of molecules representative of some of the point groups discussed are shown in Figure 1.1. Locate all of the elements of symmetry for each.

## ISOMERISM AND MEASUREMENTS

The molecular point group describes the symmetry characteristics of a particular static arrangement of the nuclei. In fact, the nuclei are not static but in constant motion, oscillating about their equilibrium positions even at 0 K! In the classical sense, we determine the symmetry on the basis of a time-averaged structure or, equivalently, a spatially averaged structure. This works because our human time scale (about 0.1 s) and the time scale of most of our measurement techniques are long compared to the time scales of molecular vibrations. The implicit conclusion is that the symmetry of a molecule may depend on the method of measurement [17]. We may therefore define *isomers* as molecules having the same molecular formula but differing in structure and separated by energy barriers. If isomers convert at immeasurably fast rates, they are *not* considered isomers. Therefore, the method of measurement used to distinguish isomers must be faster than the rate of interconversion.

Table 1.1 lists minimum lifetimes for observation of separate species and the appropriate spectroscopic methods. The time scale of nuclear magnetic resonance (NMR) experiments is particularly long, and many conformational isomers and some constitutional isomers (see below) interconvert rapidly within the time of observation and appear to be more symmetric than simple bonding considerations would imply. We will expand on these ideas after the next two sections.

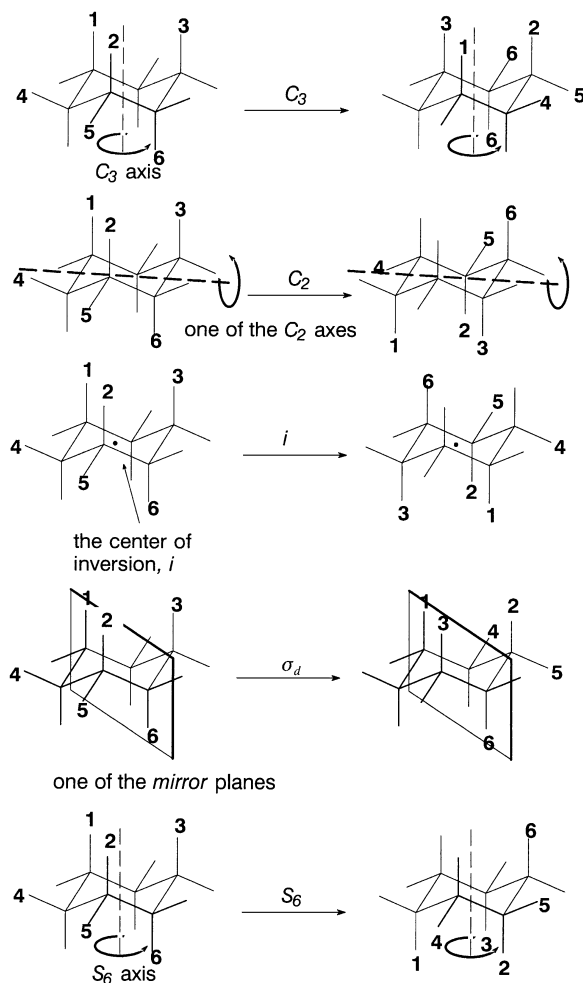


Figure 1.2. Symmetry elements of  $D_{3d}$  in cyclohexane.

TABLE 1.1. Minimum Lifetimes for Observation of Separate Species

Type of Observation	Lifetime (s)
Electron diffraction	$10^{-20}$
Neutron, X-ray diffraction	$10^{-18}$
Ultraviolet (UV) visible	$10^{-15}$
Infrared (IR) Raman	$10^{-13}$
Microwave	$10^{-4} - 10^{-10}$
Electron spin resonance (ESR)	$10^{-4} - 10^{-8}$
NMR	$10^{-1} - 10^{-9}$
Mössbauer (iron)	$10^{-7}$
Molecular beam	$10^{-6}$
Physical isolation and separation	$>10^2$

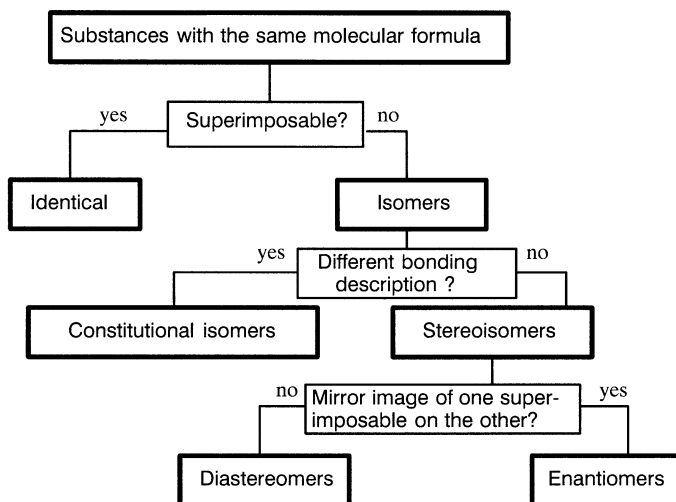


Figure 1.3. Flow chart for deciding stereomeric relationships between pairs of substances.

## STEREOISOMERISM OF MOLECULES

The stereomeric relationship between pairs of substances may be derived through the sequence of questions and answers represented by the flow diagram [17] in Figure 1.3. In terms of properties, three broad categorizations arise:

1. **Identical Molecules** Not distinguishable under any conditions, *chiral or achiral*.
2. **Enantiomers** The same in all scalar properties and distinguishable only under chiral conditions. Only molecules of which the point groups are  $C_n$  ( $n \geq 1$ ),  $D_n$  ( $n > 1$ ),  $T$ ,  $O$ , or  $I$  are chiral and can exist in enantiomeric forms.
3. **Constitutional Isomers and Diastereomers** Differ in all scalar properties and are distinguishable in principle under any conditions, chiral or achiral. Geometric isomers, which are related by the orientation of groups around a double bond, are a special case of diastereomers.

Molecules are *chiral* if their molecular point groups do *not* include any  $S_n$  ( $n \geq 1$ ) symmetry elements. Otherwise they are *achiral*. An achiral molecule is not distinguishable from its own mirror image. This is often phrased as “an achiral molecule is superimposable on its own mirror image.” A chiral molecule is *not* superimposable on its mirror image. A molecule which is identical to the mirror image of another molecule is the enantiomer of that molecule. According to the definitions above, an object is either chiral or it is not, it belongs to a particular point group or it does not. However, efforts have been made to define *degrees* of chirality [27] and continuous measures of symmetry [28].

The concepts of *chirality* and *isomerism* may readily be extended to pairs or larger assemblages of molecules, hence the reference to chiral and achiral *environments* above.

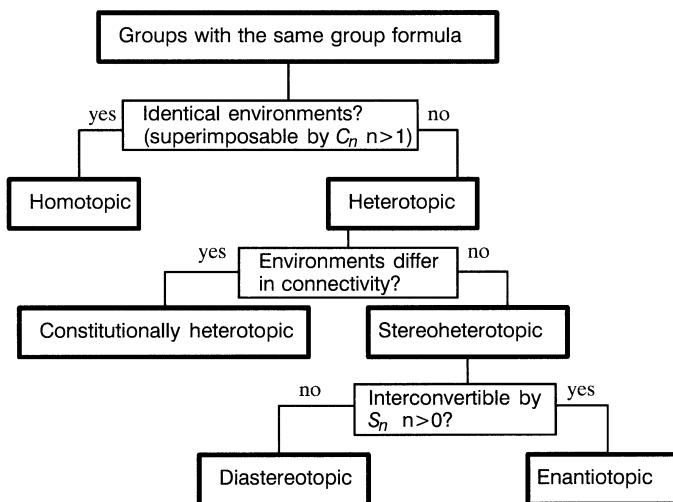


Figure 1.4. Flow chart for deciding stereotopic relationships between pairs of groups.

## STEREOTOPIC RELATIONSHIPS OF GROUPS IN MOLECULES

Many of the ideas espoused in this and the next section are due to the work of Mislow [29]. For an alternative discussion of the concepts introduced in this section, see reference 30. The reader is also directed to excellent texts by Juaristi [31] and by Eliel and Wilen [32].

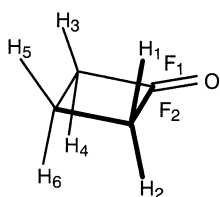
The concepts used to describe relationships between pairs of molecules may readily be extended also to pairs of groups within a molecule [17]. This is particularly useful in determining the appearance of an NMR spectrum or the possibility of selective reaction at similar functional groups. Regions (such as faces of planar portions) around molecules may be similarly classified. The same relationships could also be applied to (groups of) atomic orbitals within the molecule. These are collectively referred to as “groups” for the purpose of the flow chart in Figure 1.4. From the analysis of Figure 1.3, three broad groupings of properties emerge:

1. **Homotopic Groups** Not distinguishable under any conditions, *chiral or achiral*. To have homotopic groups, a molecule must have a finite axis of rotation. Thus the only molecules which *cannot* have homotopic groups are those whose point groups are  $C_1$ ,  $C_s$ ,  $C_i$ , and  $C_{\infty v}$ .
2. **Enantiotopic Groups** The same in all scalar properties, distinguishable only under chiral conditions.
3. **Constitutionally Heterotopic and Diastereotopic Groups** Differ in all scalar properties and are distinguishable under any conditions, chiral or achiral. Asymmetric molecules cannot contain homotopic or enantiotopic groups, only diastereotopic or constitutionally heterotopic groups.

Groups may be compared by *internal comparison* (groups in the same molecule) or by *external comparison* (groups in different molecules).

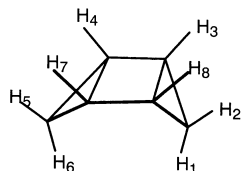
One can also compare *faces* of a molecule in the same way as groups, since the comparison actually applies to environments. Thus, the two faces of the carbonyl groups of aldehydes, unsymmetrical ketones, esters, and other acid derivatives are enantiotopic. Reaction at the two faces by a chiral nucleophile will take place at different rates, resulting in asymmetric induction.

**Exercise 1.3.** Verify the following group designations:



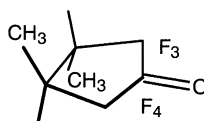
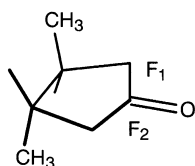
Homotopic groups—(H<sub>1</sub>, H<sub>4</sub>), (H<sub>2</sub>, H<sub>3</sub>), (H<sub>5</sub>, H<sub>6</sub>)  
 Enantiotopic groups—(H<sub>1</sub>, H<sub>2</sub>), (H<sub>3</sub>, H<sub>4</sub>), (H<sub>1</sub>, H<sub>3</sub>), (H<sub>2</sub>, H<sub>4</sub>)  
 Constitutionally heterotopic groups—any of H<sub>1</sub>, . . . , H<sub>4</sub> with H<sub>5</sub> or H<sub>6</sub>  
 F<sub>1</sub> and F<sub>2</sub> are homotopic faces.  
 There are no diastereotopic groups in this molecule.

**Exercise 1.4.** Verify the classification of the pairs of groups in tricyclo[3.1.0.0<sup>2,4</sup>]hexane.



Homotopic—(H<sub>1</sub>, H<sub>6</sub>), (H<sub>2</sub>, H<sub>5</sub>), (H<sub>3</sub>, H<sub>7</sub>), (H<sub>4</sub>, H<sub>8</sub>)  
 Enantiotopic—(H<sub>3</sub>, H<sub>4</sub>), (H<sub>3</sub>, H<sub>8</sub>), (H<sub>4</sub>, H<sub>7</sub>), (H<sub>7</sub>, H<sub>8</sub>)  
 Diastereotopic—(H<sub>1</sub>, H<sub>2</sub>), (H<sub>1</sub>, H<sub>5</sub>), (H<sub>2</sub>, H<sub>6</sub>), (H<sub>5</sub>, H<sub>6</sub>)  
 Constitutionally heterotopic—(H<sub>1</sub>, H<sub>3</sub>), (H<sub>1</sub>, H<sub>4</sub>), (H<sub>2</sub>, H<sub>8</sub>), . . .

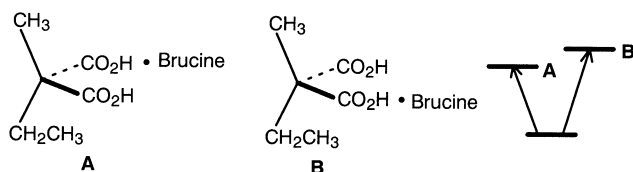
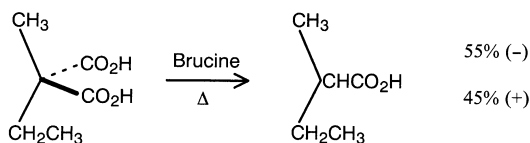
**Exercise 1.5.** Compare all of the groups and faces of the *trans*-3,4-dimethylcyclopentanones below, by both internal comparison and external comparison.



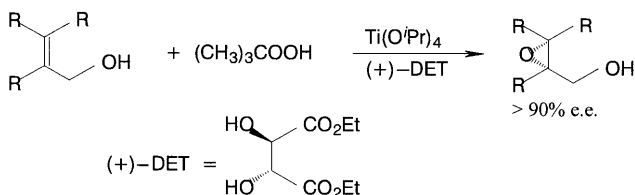
## ASYMMETRIC SYNTHESIS AND STEREOCHEMISTRY

Asymmetric synthesis is any synthesis that produces enantiomerically or diastereomerically enriched products. This is the expected result if enantiomerically enriched chiral substrates are employed. Of interest here are asymmetric syntheses where the reactants are either achiral or chiral but racemic. Many examples of this type are collected in volumes edited by Morrison [33]. The first example of an asymmetric synthesis involved use of the *chiral, optically pure* base brucine in a stereoselective decarboxylation of a diacid with enantiotopic carboxyl groups [34]:



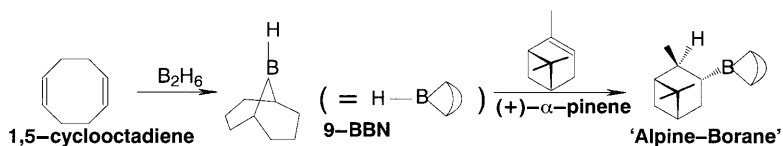


The monobrucine salts **A** and **B** are diastereomeric and therefore different in all properties, including activation energy for decarboxylation. A carbon atom which contains two enantiotopic groups is prochiral. Efficient stereoselection or asymmetric induction requires tight binding of the chiral reagent to the achiral substrate. In addition, there should be a large steric or stereoelectronic distinction between the groups in both substrate and the chiral reagent. For this purpose, the distinction between methyl and ethyl groups in Markwald's experiment shown above is less than ideal. The tight binding requirement can be satisfied by the use of transition metals to which chiral auxiliaries are attached as ligands. One example, the Katsuki–Sharpless epoxidation of allylic alcohols [35], serves to illustrate the principles:

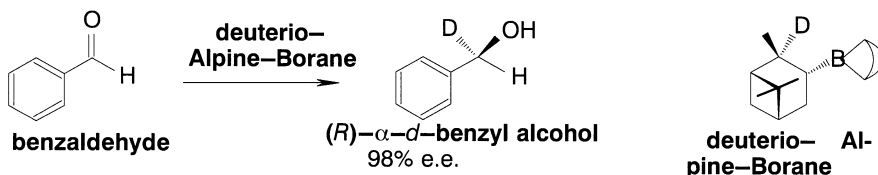


Both the allylic alcohol and *tert*-butyl hydroperoxide are achiral, but the product epoxide is formed in high optical purity. This is possible because the catalyst, titanium tetraisopropoxide, forms a chiral (possibly dimeric [36]) complex with resolved diethyl tartrate [(+)-DET] which binds the two achiral reagents together in the reactive complex. The two enantiotopic faces of the allylic double bond become diastereotopic in the chiral complex and react at different rates with the *tert*-butyl hydroperoxide. Many other examples may be found in recent reviews [31, 37–39].

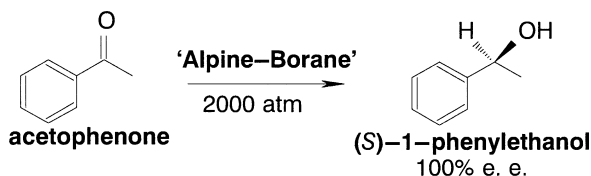
The field of organoboron chemistry pioneered by Brown [40] also provides a wealth of excellent transformations. Consider the asymmetric reduction of carbonyl compounds by Alpine-Borane [41]. Alpine-Borane is prepared by the following sequence:



In the second step, achiral 9-borabicyclo[3.3.1]nonane (9-BBN) adds to the less hindered diastereotopic face of  $\alpha$ -pinene to yield the chiral reducing agent Alpine-Borane. Aldehydes are rapidly reduced to alcohols. The reaction with deuterio-Alpine-Borane, which yields (*R*)- $\alpha$ -*d*-benzyl alcohol in 98% enantiomeric excess (ee) reveals a very high degree of selectivity of the enantiotopic faces of the aldehyde group in a crowded transition state:

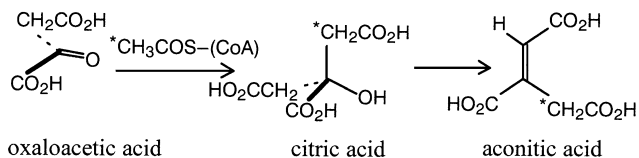


As a consequence of steric congestion in the transition state, ketones generally require high pressures to increase the reaction rate but yield optically active secondary alcohols in high ee. Thus, acetophenone yields 100% ee. of (*S*)-1-phenylethanol at 2000 atm:



Many instances of stereospecific selection of enantiotopic groups or faces may be found in nature. One such is extracted from the tricarboxylic acid cycle and is shown in Exercise 1.6. At each step, achiral reactants are transformed to achiral products with high stereospecificity!

*Exercise 1.6.* Analyze the following sequence from the tricarboxylic acid cycle (\*C denotes isotopically labeled carbon):



## NMR AND STEREOCHEMISTRY

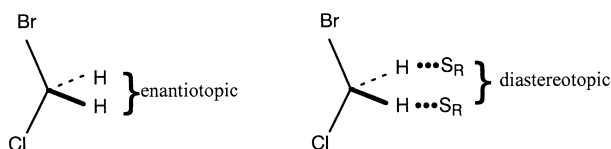
Nuclear magnetic resonance chemical shift differences can serve as an indicator of molecular symmetry. If two groups have the same chemical shift, they are *isochronous*. Isochrony is a property of homotopic groups and of enantiotopic groups under achiral conditions. Diastereotopic or constitutionally heterotopic groups will have different chemical shifts (be *anisochronous*), except by accidental equivalence and/or lack of sufficient resolution.

To be anisochronous, (1) groups may not be related by symmetry, taking into consideration internal motions which are rapid on the NMR time scale, and (2) there must be sufficient field gradient so that the difference is observable.

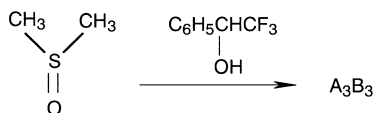
For homotopic groups, chemical shifts are indistinguishable in chiral or achiral solvents, that is, the groups are isochronous.

Enantiotopic groups are isochronous in achiral solvents and distinguishable (anisochronous) in chiral solvents.

In principle, the enantiotopic protons of bromochloromethane will be anisochronous in a chiral solvent. However, it requires a fair degree of association to make the chemical shift difference visible. This requirement may be satisfied in hydrogen-bonding solvents:



Thus the enantiotopic methyl groups of dimethylsulfoxide form an  $A_3B_3$  spin system in 1-phenyl-2,2,2-trifluoroethanol; Figure 1.5 [42]:



The hydrogen-bonding association of amino acid esters with 1-phenyl-2,2,2-trifluoroethanol is sufficient to permit NMR to be used as a method for determining the optical purities of  $\alpha$ -amino acids [43].

The same principle is involved in the use of chiral lanthanide chemical shift reagents for the determination of enantiotopic purity [44].

Figure 1.6 illustrates the expected observations when a chiral solute is dissolved in a chiral solvent and optical purities of both vary from zero (racemic) to 100%. When the optical purity of the solvent is increased, the separation of the enantiomer (actually diastereomer in the chiral solvent) signals increases. When the signal separation is sufficient, the optical purity of the solute may be determined by integration of the paired signals. When the solute optical purity is 100%, only a single signal is observed at all solvent optical purities. Recognition of the solute optical purity in the absence of the second

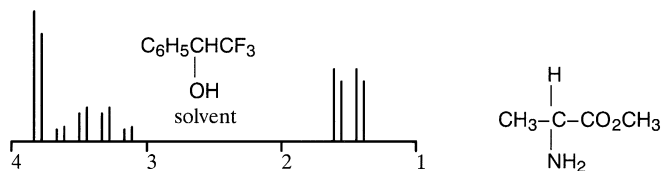
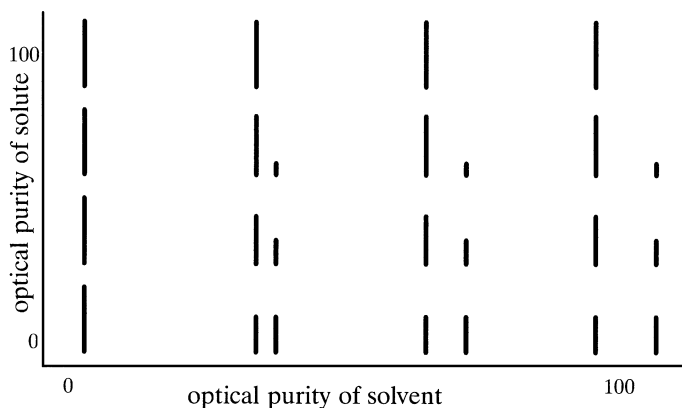


Figure 1.5. Simulated NMR spectrum of methyl alanine in a chiral solvent.



**Figure 1.6.** Effect of solvent and solute optical purity on the appearance of NMR signals of enantiomers or enantiotopic groups (bottom row).

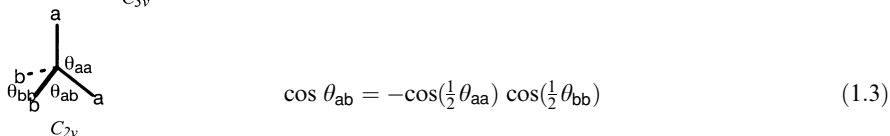
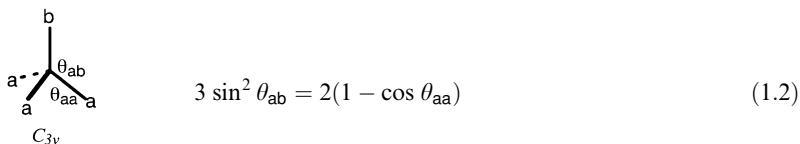
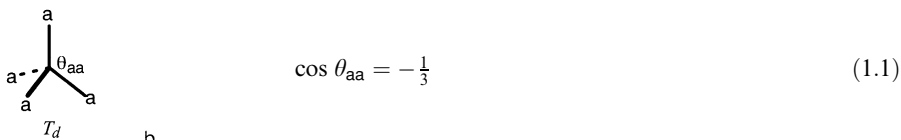
signal requires prior knowledge of the expected pure enantiomer chemical shift under the conditions of the experiment.

Enantiomeric purity is often determined by derivatization with an optically pure chiral agent. For alcohols and amines,  $\alpha$ -methoxy- $\alpha$ -trifluoromethylphenylacetic acid (MTPA) and  $\alpha$ -cyano- $\alpha$ -fluorophenylacetic acid (CFPA) [45] work well.

## SYMMETRY AND STRUCTURAL PARAMETERS

Structural parameters (bond lengths, bond angles, dihedral angles) *must* be the same in a molecule when they are interconvertible by a symmetry operation, that is, congruent. Conversely, structural parameters *cannot* be the same in a molecule when they are not congruent. If the structural parameters are not congruent, it is not possible to use symmetry arguments to predict the magnitude of the difference.

Some relationships between the bond lengths and angles of nominally tetrahedral molecules are shown below. The notation **a** and **b** denote groups which are different in some way. The point groups shown denote the *molecular* point group. For the relationships to hold *exactly*, the structures of **a** and **b** must be such as to preserve the overall symmetry. The relationships may be *approximately* obeyed if the denoted point groups are a fair representation of the *local* symmetry. For example, the first structure will have exactly  $T_d$  symmetry if **a** is H, Cl, or Me but not if **a** is Et, since the ethyl group does not have a threefold axis of symmetry. Equation (1.1) defines the tetrahedral angle. Equation (1.2) may be handy for relating the internal bond angle of a threefold symmetric species, such as ammonia, to the out-of-plane angle of the bonds. Equation (1.3) applies to molecules like methylene chloride ( $\text{CH}_2\text{Cl}_2$ ) or cyclopropane.



*Exercise 1.7.* What point groups are available for different orientations of the ethyl groups in the ‘ $T_d$ ’ structure with  $a = \text{Et}$ ?

## NOTE ON HYBRIDIZATION

The concept of hybridization was introduced to provide a mechanism for achieving directionality in bonding, recognizing implicitly that linear combinations of the  $2s$  and some of the three  $2p$  orbitals point in well-defined directions relative to other such combinations. Thus if one takes a 1 : 1 linear combination of the  $2s$  orbitals and *one* of the  $2p$  orbitals (leaving the other two  $2p$  orbitals alone), one obtains two  $sp$  hybrid orbitals which are directed at an angle of  $180^\circ$  to each other. As we shall see later, orbitals mix (or hybridize) so as to provide the best overlap for bonding. Mixing the  $2s$  orbital with *two* of the three  $2p$  orbitals yields three equivalent  $sp^2$  hybrid orbitals which are exactly arranged at  $120^\circ$  relative to each other, yielding the familiar trigonal planar pattern of bonds when each  $sp^2$  hybrid orbital forms a sigma bond to a different but identical atom or group. Likewise, four equivalent  $sp^3$  hybrid orbitals directed toward the corners of a tetrahedron with equal interorbital angles of  $109.47^\circ$  are obtained when the  $2s$  and all *three*  $2p$  orbitals are mixed. The *one*, *two* and *three* refer to the “weights” of the  $2p$  orbitals relative to the  $2s$  orbital in the  $sp$ ,  $sp^2$ , and  $sp^3$  hybrid orbitals, respectively. The angles between two equivalent hybrid orbitals are determined by the weights of the  $2p$ : $2s$  mixture. Conversely, observation of interbond angles of  $180^\circ$ ,  $120^\circ$ , and  $109.47^\circ$  between two equivalent (by symmetry) geminal C—X bonds implies that the carbon atom is using  $sp$ ,  $sp^2$ , and  $sp^3$  hybrid orbitals, respectively, to form those bonds. Hybridization can be inferred from the observed angles. Since the observed interbond angles are rarely the idealized values  $180^\circ$ ,  $120^\circ$ , and  $109.47^\circ$ , it follows that the orbitals are not the idealized hybrids but rather hybrids where the weight of the  $2p$  orbital relative to the  $2s$  orbital is a positive real number, say  $\lambda^2$ . In this case, a general hybrid orbital,  $h_i$ , will have the composition  $s + \lambda_i p$ , which is equivalent to  $sp^{\lambda_i^2}$  hybridization. The weight  $\lambda_i^2$  may range from zero to infinity (pure  $s$  to pure  $p$ ). Normalization of the hybrid orbitals requires that the following relationships hold:

$$\sum \frac{1}{1 + \lambda_i^2} = 1 \quad \frac{1}{1 + \lambda_i^2} = s \text{ character of hybrid orbital } h_i \quad (1.4)$$

$$\sum_i \frac{\lambda_i^2}{1 + \lambda_i^2} = 1, 2, 3 \quad \frac{\lambda_i^2}{1 + \lambda_i^2} = p \text{ character of hybrid orbital } h_i \quad (1.5)$$

In equations (1.4) and (1.5), the sums run over the number of *hybridized* orbitals. For any pair of hybrid orbitals,  $h_i$  and  $h_j$ , the following relationship exists:

$$1 + \lambda_i \lambda_j \cos \theta_{ij} = 0 \quad (1.6)$$

where  $\theta_{ij}$  is the angle between two *hybridized* orbitals.

**Exercise 1.8.** What is the hybridization of the carbon orbitals which form the C—H and C—C bonds of cyclopropane ( $\text{HCH} = 114^\circ$ )? Verify that if the carbon hybrids which are used for the C—H bonds are exactly  $sp^2$ , then the two equivalent hybrids for the C—C bonds must be  $sp^5$  and the interorbital angle is  $101.5^\circ$ !

Empirically,  $\text{C}^{13}$ —H spin-spin coupling constants are proportional to the “*s* character” of the hybrid orbital used in the  $\sigma$  bond to H:

$$J_{\text{CH}} \text{ (cps)} \approx \frac{500}{1 + \lambda_i^2} \quad (1.7)$$

## SYMMETRY AND ORBITALS

Symmetry properties of atomic and molecular orbitals will prove useful in a variety of contexts. We will familiarize ourselves with the characteristics of the basic types of orbitals which will be used throughout the remainder of this book. It is not proper to assign a point group label to orbitals because of the phase characteristics, but rather to the charge distribution which would result upon squaring the orbital. The orbital may then be characterized by designating the label of the *irreducible representation* according to which it transforms within the context of the local or global molecular point group. These attributes are specifically described for atomic  $s$ ,  $p$ , and  $sp^n$  (hybrid) atomic orbitals and for molecular orbitals below.

### Atomic Orbitals

The symmetry characteristics of  $s$ ,  $p$ , and  $sp^n$  (hybrid) atomic orbitals are illustrated in Figure 1.7. Thus the charge distribution due to an electron in an atomic  $s$  orbital is spherically symmetric (point group  $K_h$ ) and the  $s$  orbital itself will transform as the totally symmetric irreducible representation. Alternatively, one may assign a label,  $S$  or  $A$ , which describes the behavior of the orbital under any relevant symmetry operations. For instance, the  $s$  orbital does not change sign (phase) upon reflection in any plane containing its center or upon rotation through any angle about any axis of symmetry. It is *symmetric* with respect to any symmetry operation, and this characteristic is conveniently assigned the label  $S$  for whichever symmetry operation is considered. On the other hand, the charge distribution due to an electron in an atomic  $p$  orbital is dumbbell

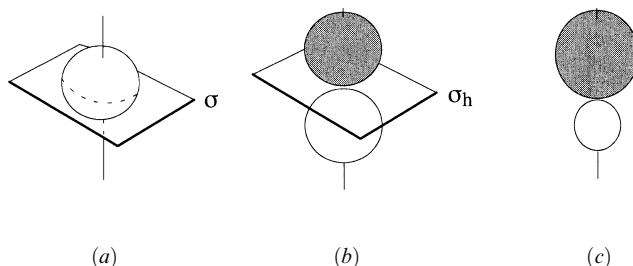
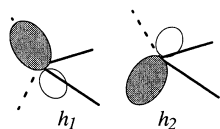


**Figure 1.7.** The symmetry characteristics of (a)  $s$ , (b)  $p$ , and (c)  $sp^n$  (hybrid) atomic orbitals. The shapes of the electron distributions are similar if one ignores the phases.

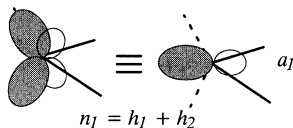
shaped (axially symmetric with a horizontal mirror plane, point group  $D_{\infty h}$ ). The  $p$  orbital itself will transform as the irreducible representation  $\Sigma_u^+$ ; that is, the  $p$  orbital does not change sign (phase) upon reflection in any plane containing its principal axis or upon rotation through any angle about the principal axis but *does* change sign (phase) upon reflection across the horizontal mirror plane (its own nodal plane) and rotation about any axis of symmetry (necessarily twofold) contained in that plane. It is symmetric ( $S$ ) with respect to any of the first set of symmetry operations, and is *antisymmetric* with respect to any of the second set of symmetry operations, and is assigned the label  $A$  for these. Hybrid atomic orbitals  $sp^n$  retain only the axial symmetry of the pure  $s$  and  $p$  orbitals. The node (boundary separating the two phases of the orbital) is now a curved surface and no longer a symmetry element. The charge distribution belongs to the point group  $C_{\infty v}$ , and the hybrid orbital transforms as the  $a_1$  irreducible representation of  $C_{\infty v}$ .

## Molecular and Group Orbitals

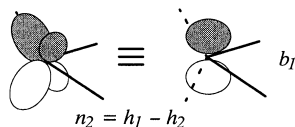
Let us accept that molecular orbitals (MOs) and group orbitals are both described as linear combinations of atomic orbitals. Exactly how and why this is the case will be seen in Chapter 2 and Appendix A. For the purpose of the present section, *proper* MOs are those linear combinations which transform as irreducible representations of the *molecular* point group, that is, are *symmetry adapted*. *Group* orbitals are linear combinations which are symmetric or antisymmetric with respect to any *local* symmetry operations of that part of the molecule which constitutes the group (e.g., a methyl group). At an intermediate level of description, MOs may be thought of as linear combinations of group orbitals. We shall frequently use the term *localized orbital*. This term has a formal definition in the literature of electronic structure theory, but we shall use it in a loose sense to describe a characteristic piece of a true MO or a group MO such as a sigma bond between a particular pair of atoms or an atomic orbital describing a nonbonded pair of electrons. A localized MO may indeed be a proper MO or a group MO which happens to be concentrated in one region of the molecule. More likely, however, a proper MO or a group MO would be described as a linear combination of localized MOs. Some examples of proper MOs and group MOs are shown in Figure 1.8. Notice that the “proper” MOs of water which describe the “lone pairs” of electrons are in- and out-of-phase combinations of the “rabbit ears” often pictured in elementary texts. The out-of-phase combination has no  $s$  character at all. It is a pure  $p$  orbital on the oxygen atom. The same is true of the proper MOs which describe the O—H bonds.



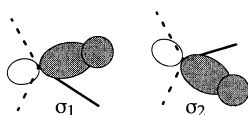
The two *localized* nonbonding orbitals,  $h_1$  and  $h_2$ , of  $\text{H}_2\text{O}$ . These are  $sp^n$  hybrids ( $n \approx 3$ ).



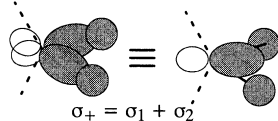
$n_1$  – A proper MO – a linear combination of the two localized orbitals which is *S* with respect to all symmetry operations of the  $C_{2v}$  point group of  $\text{H}_2\text{O}$ .



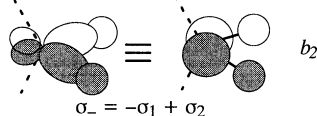
$n_2$  – A proper MO – a linear combination of the two localized orbitals which is *A* with respect to reflection in the plane of the molecule, *A* w.r.t rotation about the  $C_2$  axis and *S* w.r.t. reflection in the bisecting mirror plane of symmetry.



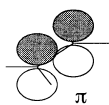
The two *localized* sigma bonding orbitals,  $\sigma_1$  and  $\sigma_2$ , of  $\text{H}_2\text{O}$ . These are linear combinations of a  $sp^n$  hybrid ( $n \approx 3$ ) of O and an *s* orbital of H.



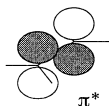
$\sigma_+$  – A proper MO – a linear combination of the two localized bond orbitals which is *S* with respect to all symmetry operations of the  $C_{2v}$  point group of  $\text{H}_2\text{O}$ .



$\sigma_-$  – A proper MO – a linear combination of the two localized bond orbitals which is *S* with respect to reflection in the plane of the molecule, *A* w.r.t rotation about the  $C_2$  axis, and *A* w.r.t. reflection in the bisecting mirror plane of symmetry.



The  $\pi$  bond of ethylene (and other olefins) is a proper MO, highly localized to the two carbon atoms. It is the linear combination of the two  $2p$  orbitals which is *S* with respect to reflection in the bisecting plane and *A* w.r.t. a  $180^\circ$  rotation about the  $C_2$  axis which contains that plane. All ' $\pi^*$ '-type orbitals are *A* w.r.t. reflection in the nodal plane of the  $p$  orbitals themselves.



The  $\pi^*$  antibonding orbital of ethylene (and other olefins) is also a proper MO, highly localized to the two carbon atoms. It is the linear combination of the two  $2p$  orbitals which is *A* with respect to reflection in the bisecting plane and *S* w.r.t. a  $180^\circ$  rotation about the  $C_2$  axis which contains that plane.

**Figure 1.8.** Examples of symmetry-adapted (proper) MOs and their constituent atomic or localized orbitals.



## IN WHAT COMBINATION?

While it is easy to make sketches of hybrid, group, and molecular orbitals such as used for illustrative purposes in Figure 1.8, the criteria for choosing the *degree* of hybridization or the specific *amount* of mixing of orbitals from different atoms to make MOs are not obvious. As we have seen, if the molecule has nontrivial symmetry (i.e., is not asymmetric, point group  $C_1$ ), then the charge distribution must have the same symmetry as the molecular framework and proper MOs should also reflect the symmetry. Elements of symmetry can serve as a guide for the amount of mixing. The  $\pi$  bonding MO of ethylene (Figure 1.8) is partly determined by the symmetry. The  $2p$  orbitals of each C must mix with equal weights. But why is the in-phase combination occupied and not the out-of-phase combination? The answer lies in the quantum mechanical theory of electronic structure (MO theory).

In Chapter 2, the physical and mathematical basis of the most familiar version of MO theory is presented in a qualitative way using a two-electron “molecule” as an example (a more rigorous treatment is given in Appendix A). It is argued that the chemical and physical properties of molecules arise in large part from the distribution of the electrons in the molecule. This has been taken as an article of faith for many years and ultimately proved in the case of the energy [46]. It will be seen that the simplest form of function which correctly describes the simultaneous distribution of all the electrons in a molecule is a product of functions (MOs) which individually describe the distribution of one electron at a time. Actually one must take a linear combination of such products to allow for the fact that any electron may have any of the one-electron distributions and to recognize the *fermion* character of electrons. In other words, a many-electron wave function is expressed as an antisymmetrized sum of products of one-electron wave functions or MOs. An optimum set of MOs is derived by *minimizing the energy* of the assemblage of electrons and atoms with respect to variations in the MOs. Since the MOs are expanded in terms of atomic orbitals (strictly speaking, atomic orbital-like functions), the process involves variation of the amount of mixing of the atomic orbitals until a mixing combination is found which yields the lowest possible energy. Indeed, a prescription for finding this optimum combination falls out of the theory. The treatment in Chapter 2 is within the grasp of any senior undergraduate student and is worth pursuing. The theory is presented in a mathematically rigorous fashion in Appendix A and concludes with a brief description of ways to improve the theory as well as a practical guide to one of the current computer programs, the GAUSSIAN package of programs, which implements the theory for solving chemical problems.

The level of treatment in Appendix A is most suitable for graduate students. Undergraduates with inadequate mathematical preparation may skip to Chapter 3 and pick up the story at the stage where the orbital interaction diagram is derived.

## CHAPTER 2

---

# MOLECULAR ORBITAL THEORY

---

### INTRODUCTION

Orbital interaction theory has its roots in molecular orbital (MO) theory. Molecular orbital theory in one form or another plays a central role in the understanding of all aspects of chemical phenomena, whether it be in the form of a discussion of *hybridization* in connection with the geometry of tetrahedral carbon, *aromaticity* and the  $4n + 2$  rule, or *orbital symmetry allowedness* of the Diels–Alder reaction. Many of the concepts are introduced in introductory general chemistry or organic chemistry courses. Indeed, for three-quarters of a century, quantum mechanics in the form of the Schrödinger equation has provided the underpinning for all but the most esoteric of chemical phenomena, and it is quite appropriate (and even essential) that students of chemistry be introduced to some aspects of it, even at a stage in their education when they do not have the mathematical background to follow the derivation of the necessary equations.

A complete derivation of the simplest correct theory for many-electron systems, Hartree–Fock theory, is given in Appendix A. The material in this appendix must appear daunting to an organic chemist not used to the formalism of quantum mechanics! However, the mathematics is not beyond the capabilities of a typical graduate student nor even a good third- or fourth-year undergraduate student. For undergraduate instruction, Appendix A may well be skipped unless it is the intention to introduce the student to the “ab initio MO” computer programs which are increasingly at the forefront of chemical research and instruction.

Presented in this chapter is a verbal and pictorial description of Hartree–Fock MO theory. No equations will be given but reference will be made to appropriate parts of Appendix A where more details may be found.

## ELECTRONIC SCHRÖDINGER EQUATION (A.1)

The properties of molecules and of intermolecular interactions may be understood by analysis of the solutions of the electronic Schrödinger equation (SE) which yield two important pieces of information: a set of complicated functions, each of which describes a different distribution of all of the electrons (the many-electron wave function), and the discrete energy of the electrons with that distribution. The lowest energy and its associated wave function correspond to the ground state of the molecule. Higher energies are those of electronically excited states. The spacing of the available energies for most molecules is such that normal thermal energy is insufficient to create a significant population of molecules in higher (excited) states than the lowest (the ground state). A molecule which finds itself in a higher energy state than the most stable will quickly lose energy by radiative emission or collisional transfer and revert to its ground state. The wave function is a rather esoteric mathematical construct with no associated physically observable object (unlike the energy). At any point in space it may be positive or negative, real or complex. However, its value *squared* is directly related to the probability of finding electrons and nuclei at that point and so from the wave function can be derived the distributions of the electrons (the electron density). We are usually interested in the wave function (or equivalently, the electron distribution) associated with the ground state of the molecule because that is the state in which most molecules exist, and this is sufficient to understand the structure of each molecule, most of the interactions between them, and most chemical reactions. However, to understand spectroscopy, photochemistry, or the homolytic fragmentation of molecules, higher electronic states must also be addressed.

The electronic SE focuses on the *energy* levels of the molecule. By obtaining the lowest energy, one assumes that the associated wave function will yield the electron distribution of the electronic ground state. An alternative theory has come into recent prominence, in which the SE is bypassed and attention focused on the electron *density* from which many desired properties including energy can be derived directly [density functional theory (DFT)].

The molecule is treated as a collection of charged particles (Figure 2.1), the positively charged nuclei and the negatively charged electrons. For any collection of particles, a classical energy expression, the Hamiltonian, can be written. The potential energy of the nuclei and electrons is obtained by application of Coulomb's law, and the kinetic energy is expressed in terms of momenta. The "zero" on the energy scale represents the case where none of the particles are moving (kinetic energy is zero) and all interparticle distances are infinite (potential energy is zero). The energy is often expressed in atomic units

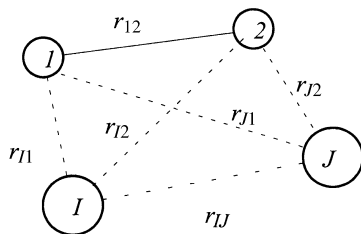


**Figure 2.1.** Hypothetical molecule with nuclei  $I$ ,  $J$  and two electrons,  $1$ ,  $2$ , and interparticle separations as shown.

called hartrees:  $1 \text{ hartree} = 27.21 \text{ eV} = 627.51 \text{ kcal/mol} = 2625.5 \text{ kJ/mol}$ . The Hamiltonian is converted to the quantum mechanical operator equivalent, the *Hamiltonian operator*, which is actually the only known part of the SE. The electronic SE is solved by use of a succession of simplifications and mathematical approximations which permit a minimization of the electronic energy. Many of these approximations can subsequently be removed to obtain more accurate solutions. It is assumed that the electron mass is a constant (the nonrelativistic approximation). This is very nearly true for the lighter elements, up to the end of the third row of the periodic table (K–Ar, including the first-row transition metals). It is also assumed that the nuclear positions are fixed [the Born–Oppenheimer (BO) approximation] at a position chosen beforehand. The BO approximation is also excellent in that electrons are much lighter than nuclei and so can respond almost instantaneously to nuclear motions. With the nuclei fixed in space, the nuclear–nuclear repulsion potential is a constant and the nuclear kinetic energy is, of course, zero. The total energy of the molecule is the sum of the constant nuclear–nuclear repulsion energy and the electronic energy determined by solution of the electronic SE. If the chosen nuclear positions (i.e., the molecular structure) do not correspond to the lowest possible energy, a new structure may be chosen and the process repeated until the lowest energy point is reached. This procedure of geometry optimization is carried out automatically by modern quantum chemistry programs. The zero-point vibrational energy of the nuclei can be reintroduced by techniques described in Appendix A.

The electrons cannot be represented as point charges, as can be done with the nuclei. Instead, a mathematical function in three dimensions is assigned to each electron. This is its *wave function*. The wave function of a single electron is called an *orbital*. Whether it is an *atomic orbital* (AO) or a *molecular orbital* (MO) depends on whether one or more nuclei are present. The square of the value of the orbital at any point in space yields the probability distribution of the electron in the space of the fixed nuclei and any other electrons which may be present. The probability integrated over a small unit of volume surrounding a point in space is the *density* due to that electron at that point. The simple sum of the density contributions of all of the electrons is the total electron density at a given point. Because the SE of the hydrogen atom can be solved exactly, the forms of AOs of not just hydrogen atoms but all of the other light atoms are accurately known. The form of the MO is more complicated. Clearly, the electrons can wander anywhere within the potential field of the nuclei but will tend to be concentrated near the nuclei. One can argue that when an electron is close to one nucleus and far from the others, its MO in the region near that nucleus should resemble an AO of that nucleus. It is reasonable that the MO can therefore be expressed as a simple linear combination of the AOs of the atoms that are present in the molecule. The precise contribution of each AO in the MO for any given collection of atoms depends on the identities and distributions and so is treated as a variable to be optimized in the solution of the SE.

The *Hamiltonian operator* consists of a set of instructions involving arithmetical operations (addition, subtraction, multiplication, and division) as well as differentiations, which must be carried out on the wave function. An expression for it is derived in Appendix A as equation (A.5). The solution of the SE consists of finding a function of the coordinates of all of the electrons, such that after carrying out the operations specified by the Hamiltonian operator, the result is just a constant multiple of the function itself. The constant multiple is the electronic energy,  $E^e$ . Very briefly, the procedure for solving the SE consists of constructing a trial wave function for the electrons of the molecule with adjustable parameters and then adjusting these parameters so as to yield the lowest possible energy. The properties of the SE guarantee that there is a lower limit

beyond which the energy cannot go and that this corresponds to an exact solution of the SE for the molecular ground state. Because the electrons are fermions, they must obey the Pauli exclusion principle, which states that no two electrons can have the same four quantum numbers. One of the quantum numbers is *spin*, which is just an add-on property in nonrelativistic quantum theory. Electron spin can only have one of two values, which we represent diagrammatically as *up* or *down* arrows. The other three “quantum numbers” describe the three-dimensional spatial distribution of the electron, that is, its MO. This means that at most two electrons can have (or occupy) the same MO and they must have different spins. A possible many-electron molecular wave function could be constructed as a simple product of all of the MOs taking into account also each electron’s spin function. This is called a *Hartree product*. To correctly reflect the physical properties of the molecular many-electron wave function, namely that it must be antisymmetric with respect to the interchange of any two electrons, and the electrons are indistinguishable from each other, the wave function is taken as an *antisymmetrized* sum over Hartree products in which the electrons are reshuffled in all possible ways between the MOs and spins. Such a wave function can be expressed as a determinant and is called a single determinantal wave function [equation (A.12)]. If, as mentioned earlier, each MO is expanded as a linear combination of AOs and the expansion coefficients are taken as variable parameters, then these parameters can be adjusted to obtain the set of MOs which, when assembled into determinantal form, yield the lowest possible energy and therefore the best possible molecular wave function (of this form). The mathematical procedure for accomplishing this is called the *variational method* and yields a set of equations, the *Fock equations*, that specify the conditions that must be met by the MOs. The full details of the derivation of the Fock equations are given in Appendix A.

## FOCK EQUATIONS (A.42)

The Fock equations are like mini-SEs for a single electron. The solutions are the MO energies and the MOs themselves, expressed as linear combinations of AO-like basis functions, the *basis set* [equation (A.43)]. The procedure for the solution of the Fock equations and a discussion of the “AO-like” basis functions is given in Appendix A. The MO energies are also discrete or quantized, as in the SE. One needs enough MOs to accommodate all of the electrons of the molecule, counting in pairs, since two electrons can occupy the same MO if they have opposite spins. An explicit expression for the total electronic energy in terms of the MO energies is given in equation (A.66). We note here only that the total electronic energy is *not* simply the sum of MO energies *but becomes so* if the electron–electron repulsive part of the potential energy is neglected. Indeed, the simplest (and first) MO theory is based on this approximation by Hückel and forms the basis of orbital interaction theory.

The most general version of Hartree–Fock (HF) theory, in which each electron is permitted to have its own spin and spatial wave function, is called *unrestricted* HF (UHF). Remarkably, when a UHF calculation is performed on most molecules which have an equal number of alpha and beta electrons, the spatial parts of the alpha and beta electrons are identical in pairs. Thus the picture that two electrons occupy the same MO with opposite spins comes naturally from this theory. A significant simplification in the solution of the Fock equations ensues if one imposes this natural outcome as a restriction. The form of HF theory where electrons are forced to occupied MOs in pairs is called *restricted* HF (RHF), and the resulting wave function is of the RHF type. A cal-

ulation on any system which does *not* have equal numbers of alpha and beta electrons should be of the UHF type.

### THE BASIS SET (STO-3G, 6-31G\*, AND ALL THAT)

Molecular orbitals will be very irregular three-dimensional functions with maxima near the nuclei since the electrons are most likely to be found there and falling off toward zero as the distance from the nuclei increases. There will also be many zeros defining nodal surfaces that separate phase changes. These requirements are satisfied by a linear combination of atom-centered basis functions. The basis functions we choose should describe as closely as possible the correct distribution of electrons in the vicinity of nuclei since, when the electron is close to one atom and far from the others, its distribution will resemble an AO of that atom. And yet they should be simple enough that mathematical operations required in the solution of the Fock equations can actually be carried out efficiently. The first requirement is easily satisfied by choosing hydrogenic AOs as a basis set. Unfortunately, the exponential radial dependence of the hydrogenic functions [see equation (A.62) and Figure 2.2a] makes the evaluation of the necessary integrals exceedingly difficult and time consuming for general computation, and so another set of functions with approximately the same behavior is now universally adopted. These are *Cartesian Gaussian functions*, centered on nuclei. The correct radial behavior of the hydrogenlike AO is as a simple exponential. Orbitals based on this radial dependence are called Slater-type orbitals (STOs). Gaussian functions are rounded at the nucleus and decrease faster than desirable (Figure 2.2b). Therefore, the actual basis functions are constructed by taking fixed linear combinations of the primitive Gaussian functions in such a way as to mimic exponential behavior, that is, resemble AOs. This is illustrated in Figure 2.2c for a linear combination of three Gaussians, which is denoted by the acronym STO-3G. The STO-nG basis sets are made up this way.

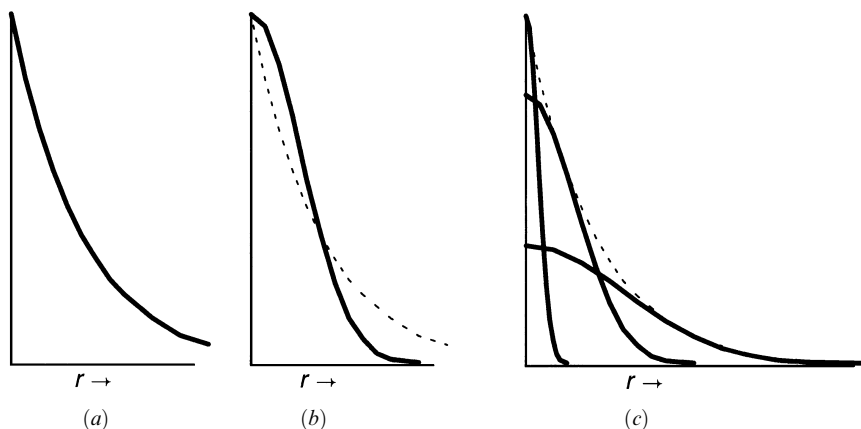


**Figure 2.2.** Radial dependence of basis functions: (a) correct exponential decay (STO); (b) primitive Gaussian-type function (solid line) vs. an STO (dotted line); (c) least-squares expansion of the STO in terms of three Gaussian-type orbitals (STO-3G).

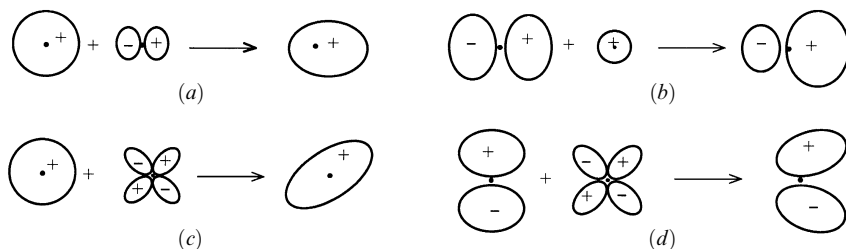


**Figure 2.3.** Action of polarization functions: (a)  $s$  polarized by  $p$ ; (b)  $p$  polarized by  $s$ ; (c)  $s$  polarized by  $d$ ; (d)  $p$  polarized by  $d$ .

A similar philosophy of *contraction* is applied to the “split-valence” basis sets, for example, 4-31G: the core  $1s$  AO is expanded as four Gaussian functions; the valence  $2s$  and  $2p$  orbitals are described by two basis functions, one of which is made up of three Gaussian functions (the inner part of the valence shell) and the other is a single more diffuse Gaussian used to provide flexibility. Commonly used split-valence basis sets are designated 3-21G, 4-31G, and 6-31G. These differ mainly in the quality of the description of the core electrons. Hydrogen atoms are not considered to have a core so only the split-valence part of the designation applies to H; that is, the split-valence basis of H consists of two  $1s$  functions only, while the corresponding basis set for C (for example) would consist of a single contracted  $1s$  orbital and two each of  $2s$ ,  $2p_x$ ,  $2p_y$ , and  $2p_z$  functions, for a total of *nine*.

The next level of improvement of the basis set involves the addition of *polarization* functions to the split-valence basis set, usually the 6-31G basis. These are designated 6-31G(d) and 6-31G(d,p), or simply 6-31G\* and 6-31G\*\*. The “d” or (first) asterisk denotes the addition to the basis sets of atoms other than hydrogen, a set of six Cartesian  $d$ -type functions to act as polarization for the  $s$  and  $p$  valence functions. The 6-31G(d) basis sets of Be, B, C, N, O, and F consist of *fifteen* functions. The “p” after the comma or second asterisk (if there is one) indicates the addition of a set of  $2p$ -like Gaussian functions to the H basis set, raising the number of H basis functions to *five*. Mixing functions of differing angular momentum quantum number (i.e.,  $s$ ,  $p$ ,  $d$ , etc.) allows the formation of functions of lower symmetry and therefore a better description of the electron distribution in the molecular environment. The process is analogous to hybridization. Some examples of polarization of the  $s$ ,  $p$  basis functions are illustrated in Figure 2.3.

## ORBITAL ENERGIES AND ORBITALS

Figure 2.4 shows the MO energies for the first row hydrides. The MOs are occupied from the lowest up until one runs out of electrons. The meaning of the empty orbitals (only one is shown in Figure 2.4) is that they would be the available energies and distributions of the next electron if another were to be added, to make the anion radical, for example. The orbitals fall into three groups, a very stable (low-energy) group called the “core,” a higher occupied “valence” group, and the group of unoccupied (or virtual) MOs. Notice the break and the difference in the energy scale between the core and valence groups. Two orbitals will have special significance for orbital interaction theory;

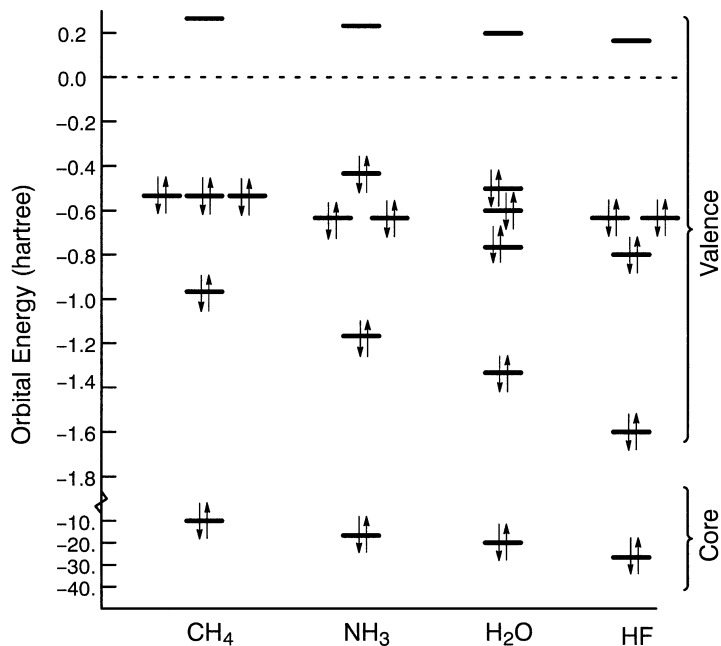


Figure 2.4. 6-31G\*\* orbital energies of the 10-electron series.

the highest occupied molecular orbital (HOMO) because it represents the distribution and energy of the least tightly held electrons in the molecule and the lowest unoccupied molecular orbital (LUMO) because it describes the easiest route to the addition of more electrons to the system. In fact, the energy of the HOMO is a good approximation to the lowest ionization potential of the molecule [see equation (A.76)] but the energy of the LUMO generally is a poor approximation to the molecule's electron affinity. A molecule whose HOMO is not doubly occupied or that does not have a large HOMO–LUMO energy gap is chemically reactive for reasons described in the next chapter. Other points to notice from Figure 2.4 are as follows:

1. The core–valence separation is very large,  $\sim 10$  hartrees for C.
2. The valence shell breaks into two groups: a single orbital which is rapidly stabilized along the series C–F and a cluster of three orbitals which remain about the same energy.
3. The question of “equivalence” of bonds or “lone pairs” is relevant here. Methane has *two* valence shell ionization potentials. Clearly, having four equivalent bonds does not imply four equal-energy bond orbitals, that is, a single ionization potential. In the same vein, ammonia has *three*, water has *four*, and HF has *three* valence shell ionization potentials.
4. Ammonia has the highest HOMO, methane and water have HOMOs of similar energy, and HF has the lowest HOMO of the group.
5. The LUMO energies decrease along the series CH<sub>4</sub>–HF.



The orbital degeneracies noted in point 3 above and seen in Figure 2.4 reflect the symmetry of the molecule's nuclear framework. Notice that the conventional picture of two equal lone pairs in water, sometimes displayed as "rabbit ears," is not supported by the energies of the two highest occupied MOs of water. In fact, the lone pairs resemble the "proper group MOs" shown in Figure 1.8.

## REPRESENTATION OF MOs

Simple balloon-type representations of orbitals were presented in the previous chapter without comment. A further example is given in Figure 2.5*b* or 2.5*c*. The boundary where

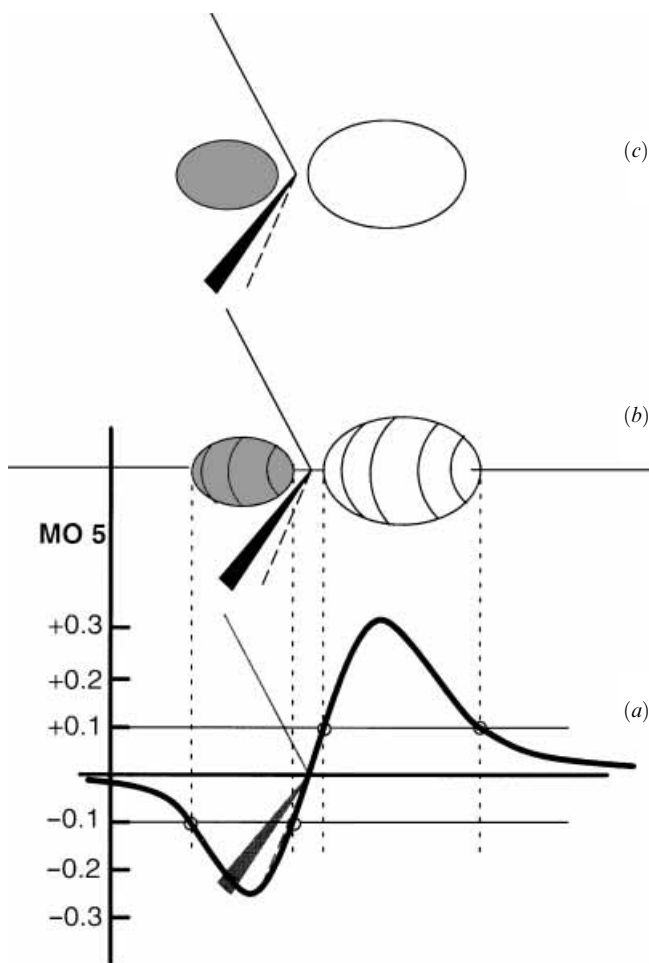


**Figure 2.5.** Three different representations of MO 5 of  $\text{NH}_3$ . (a) one-dimensional plot of orbital value along the symmetry axis. Points at which the value is  $\pm 0.1$  are marked. (b) Three-dimensional surface connecting all points at which the orbital value is  $+0.1$  (unshaded) or  $-0.1$  (shaded). (c) Two-dimensional cross section of (b) in a plane containing the symmetry axis.

an orbital stops or starts is not as well defined as these representations would suggest. The electron is free to roam over all of space but the probability of finding it (i.e., the square of its orbital) becomes very small far from any nucleus. Far from the nuclei, the MO decreases exponentially. This is illustrated in Figure 2.5a, where the value of the fifth occupied MO of ammonia at all points along the  $C_3$  axis is plotted. In this representation, the orbital actually looks like a wave which is negative inside the pyramid and positive at the top. Remember the sign is arbitrary. Just as valid is an orbital in which all of the signs are reversed. The balloon-type representation (Figure 2.5b) arises from choosing a small absolute value for the orbital and contouring in three-dimensional space to define a surface connecting all points where the MO has that absolute value. The value is chosen such that the surfaces enclose most of the electron in a qualitative sense. The surfaces are colored or shaded according to the sign, positive or negative, of the MO in that region of space. The sign represents the *phase* of the electron wave. A change of sign of an MO from one region of space to another represents a phase change and is highly significant because between the two different phases is a nodal surface where the probability of finding the electron is exactly zero and it is low anywhere near the surface. Sometimes it is convenient to use a cross section of the MO with shading to represent the phase change (Figure 2.5c). In Figure 2.5a, the four points at which this orbital has an absolute value of 0.1 are shown with white dots. Figures 2.5b and 2.5c show the three- and two-dimensional contours which arise with this value. It is important to realize that the orbital can be treated as a three-dimensional object firmly anchored to the molecular skeleton. If, for instance, one were to rotate the ammonia molecule about one of the N—H bonds, the orbital would rotate along with the nuclei. The MOs of ammonia from a HF calculation are plotted in Figure 2.6. All except MO 5 are

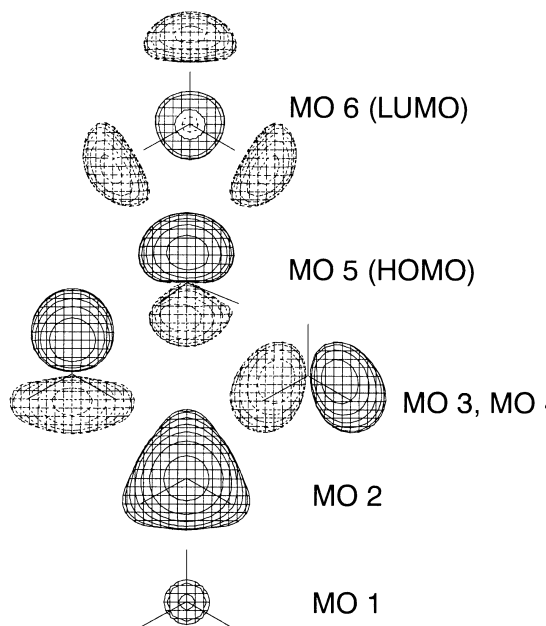


**Figure 2.6.** The 6-31G\* MOs of  $\text{NH}_3$ : MOs 1–5 are drawn at contour level  $|0.1|$  while MO 6 is drawn at  $|0.075|$ .

**TABLE 2.1. SCF Total Energies (hartrees) of CH<sub>4</sub>, NH<sub>3</sub>, H<sub>2</sub>O, and HF as a Function of Basis Set<sup>a</sup>**

Basis Set	CH <sub>4</sub>	NH <sub>3</sub>	H <sub>2</sub> O	HF
STO-3G	-39.727	-55.454	-74.963	-98.571
4-31G	-40.140	-56.102	-75.907	-99.887
6-31G*	-40.195	-56.184	-76.011	-100.003
6-31G**	-40.202	-56.195	-76.023	-100.011
HF limit <sup>b</sup>	-40.225	-56.225	-76.065	-100.071

<sup>a</sup>Table 3.13 of Ref. 47.<sup>b</sup>Ref. 48.

plotted as seen down the  $C_3$  axis. Molecular orbital 5 has the  $C_3$  axis in the plane of the paper. Notice that MOs 1 and 2 resemble atomic  $1s$  and  $2s$  orbitals, respectively, and that the other occupied MOs [3, 4, and 5 (HOMO)] resemble  $2p$  orbitals. The degenerate pair together describes the threefold symmetry of the molecule. The nodal surfaces are at right angles in the two MOs (3 and 4). The orientation of the node itself is arbitrary. As it happens, the nodal plane of MO 4 as displayed in Figure 2.6 (fortuitously) coincides with the plane containing one of the NH bonds. The HOMO would be described as the lone pair on N, but it is a true MO. The LUMO resembles a  $3s$  orbital and is made up of the out-of-phase combination of the  $2s$  of N and the  $1s$  orbitals of the H atoms.

## TOTAL ENERGIES AND THE HARTREE–FOCK LIMIT

The total energy of a substance, whether obtained from computation or “experimental,” is a very large and largely meaningless number. It is with the *difference* in total energies, for example, between conformers, or the heat of a reaction, that we make a connection to experiment. Experimental accuracy is considered to correspond to a difference of 0.001 hartree (2.6 kJ/mol). The dependence of the HF total energy on basis set size for the first-row hydrides is shown in Table 2.1. The energy decreases systematically with increasing complexity of the basis set down to a limit estimated for an infinitely large (or complete) basis set, the Hartree–Fock limit. It is evident that deviations from one level of basis set to the next are many times “experimental accuracy.” In fact, the error associated with the primary approximation of HF theory, that the wave function can be described by a single determinantal wave function, is itself hundreds of times experimental accuracy. It is not surprising, then, that this level of accuracy when taking energy differences is hardly ever achieved. Nevertheless, with the development of balanced basis sets, errors at this level of theory are remarkably constant and cancel sufficiently to allow meaningful conclusions to be drawn from differences.

## SUCCESSSES AND FAILURES OF HARTREE–FOCK THEORY

Hartree–Fock theory is a rigorous *ab initio* theory of electronic structure and has a vast array of successes to its credit. Equilibrium structures of most molecules are calculated almost to experimental accuracy, and reasonably accurate properties (e.g., dipole moments and IR and Raman intensities) can be calculated from HF wave functions. Rela-

tive energies of conformers and barriers to conformational changes are reproduced to experimental accuracy. Relative energies of structural isomers are also very well reproduced. However, the approximation involved in the derivation of HF theory (single determinantal many-electron wave function constructed of one-electron wave functions, i.e., as antisymmetrized sum of products) has a serious consequence which has not been mentioned so far, namely the treatment of electron–electron interactions as occurring between charge clouds. This means that the motion of one electron is not correlated with that of any other electrons except in an average way. The electrons can get too close to each other, and so the HF energy is higher than it should be. The *correlation error* is most severe in the region near the minimum of the potential energy hypersurface where the lowest energy solution is of the RHF type and the major part of the error involves each pair of electrons in the same orbital (pair correlation). The magnitude of the error, though large, is very constant and tends to cancel almost quantitatively if the number and nature of occupied MOs is the same in two structures being compared. Hartree–Fock theory will be expected to fail in cases where the number and nature of bonded electron pairs change. Thus, HF theory is unsatisfactory for any single-electron process, such as reduction or oxidation (including ionization) or electronic excitation (photochemistry). It also fails to describe homolytic bond dissociation, a major component of most chemical reactions in the gas phase. A secondary consequence of the averaged treatment of electron correlation error is that bond dissociation in RHF theory is always heterolytic (to ions). As a result, the local curvature of the potential energy hypersurface near minima is too steep and force constants (and harmonic frequencies) are too large. In the next section, a very brief introduction to methods of improving HF theory is presented.

## BEYOND HARTREE–FOCK

For quantitative applications, or where HF is not appropriate, it is desirable to “go beyond Hartree–Fock.” A number of methodologies for doing this are described in Appendix A. By redistributing the electron(s) out of the lowest energy MOs into some or all of the virtual MOs, one can generate more determinantal wave functions, or configurations. Addition of these to the description of the ground-state wave function has the effect of permitting electron motions to be correlated to each other. Energy minimization of such a multiconfigurational wave function, by the method of configuration interaction (CI), yields highly accurate energies which are missing only the relativistic effects. Because computational effort scales by  $n^6$  or higher (doubling the basis set size takes more than 64 times as long), it is not possible to incorporate all configurations for any but the smallest molecules. Procedures exist which differ by the selection of configurations and the manner of solution of the resulting equations, the most common known by the acronyms QCISD(T) and CCSD(T), both of which include all of the important singly and doubly excited configurations and some triply excited configurations. A CI procedure which yields results for excited states comparable to the HF description of the ground state is called CIS (CI with all singly excited configurations included).

Another way that additional configurations can be added to the the ground-state wave function is by the use of Möller–Plesset perturbation theory (MPPT). As it happens, a Hamiltonian operator constructed from a sum of Fock operators has as its set of solutions the HF single determinantal wave function and all other determinantal wave

functions that can be derived from it by single, double, and so on excitations. The corresponding energies are simple sums and differences of the MO energies. An efficient expansion of the correct wave function can be derived from these configurations by Rayleigh–Schrödinger perturbation theory where the perturbation is taken to be the difference between the true Hamiltonian and the approximate Fock-operator-derived one. The method for accomplishing this is explained in Appendix A.

If carried out with a good basis set [6-31G(d) or better], the benefits of MPPT, carried out to second order (MP2), include moderate improvements in structures and relative energies and often significant improvement in the values of secondary properties such as dipole moments, vibrational frequencies, infrared and Raman absorption intensities, and NMR chemical shifts. Modern quantum chemistry codes such as the GAUSSIAN package incorporate analytical calculation of MP2 forces and force constants. Although it adds substantially to the time required to carry out the calculations, the results of MPPT usually make the extra effort worthwhile.

## DENSITY FUNCTIONAL THEORY

A method with very different origins but with a functional form very similar to HF theory is density functional theory (DFT). Walter Kohn, who shared the 1998 Nobel Prize in Chemistry with John Pople, showed that the equations which yield the MOs which best fit the ground-state electron density are identical in form to the Fock equations except that the HF exchange term is replaced by a term which incorporates electron correlation as well. The theory does not yield the precise functional form of this “exchange-correlation” term, but numerous mathematical approximations to it have been derived in recent years, and results derived from the best of these are comparable or superior to MP2 results, often with substantially less computational effort. A variation of DFT, called B3LYP, is due to Becke who argued that some of the deficiencies of the empirical exchange-correlation functionals may be overcome by incorporating some HF exchange. Combined with the 6-31G(d) basis set, B3LYP has become the method of choice for efficient and accurate computation of most chemical properties. It has been shown to provide a significant improvement over HF and semiempirical and even MP2 methods for the study of organic reactions [49]. Also, B3LYP performs very well for molecular geometries [50], force fields [51], hydrogen-bonding energies [52], and bond dissociation energies [53].

## GEOMETRY OPTIMIZATION

A single-point calculation by any of the methods discussed above yields a point on the vibrationless BO potential energy surface. Points on the BO potential hypersurface at which the forces acting on the nuclei are all zero are called *stationary points* and correspond to, for example, local minima (stable structures), saddle points (transition structures), tops of “hills,” and so on. Derivatives of the forces constitute the *Hessian matrix*, which provides information about the curvature of the surface. The eigenvalues of the Hessian matrix serve to characterize the nature of the stationary points. A local minimum has only positive eigenvalues; a transition structure has exactly one negative eigenvalue of the Hessian. Hessians are evaluated numerically during geometry optimizations

TABLE 2.2. Bond Lengths (Å) and Bond Angles (deg) for the 10-Electron Hydrides<sup>a</sup>

Basis Set	CH <sub>4</sub> ,	NH <sub>3</sub>		H <sub>2</sub> O		HF,
	C-H	N-H	HNH	O-H	HOH	H-F
RHF/STO-3G	1.083	1.033	104.2	0.990	100.0	0.956
RHF/4-31G	1.081	0.991	115.8	0.951	111.2	0.922
RHF/6-31G(d)	1.084	1.004	107.5	0.948	105.5	0.911
RHF/6-31G(d,p)	1.084	1.004	107.6	0.943	106.0	0.901
Near HF limit	1.084	1.000	107.2	0.940	106.1	0.897
B3LYP/6-31G(d,p)	1.092	1.018	105.7	0.965	103.7	0.925
Experiment	1.085	1.012	106.7	0.957	104.5	0.917

<sup>a</sup>Data extracted from Ref. 55 except B3LYP/6-31(d,p).

by an algorithm due to Schlegel [54]. Table 2.2 presents some typical geometry optimization data as a function of basis set.

The results in Table 2.2 are reasonably representative. The HF calculations yield reasonable geometries for most molecules; errors are typically of the order of 0.02 Å for bond lengths and about 2° for bond angles. The B3LYP values are usually within 0.01 Å and 1°, respectively, of the experimental values.

## NORMAL COORDINATES AND HARMONIC FREQUENCY ANALYSIS

In mass-weighted coordinates, the hessian matrix becomes the harmonic force constant matrix, from which a normal coordinate analysis may be carried out to yield harmonic frequencies and normal modes, essentially a prediction of the fundamental IR transition

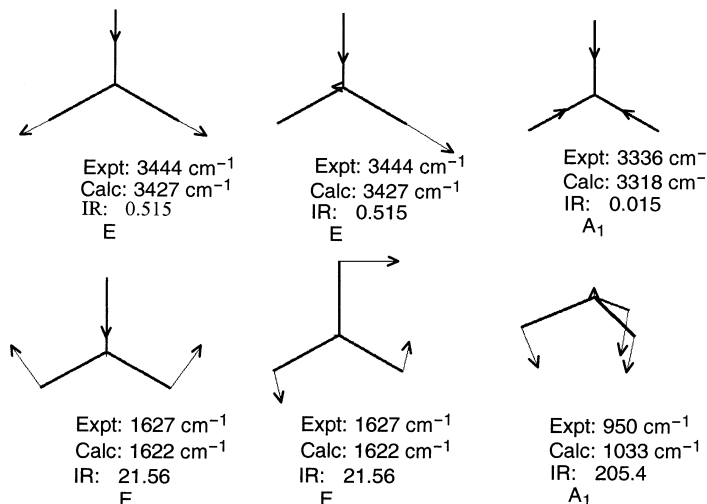


**Figure 2.7.** Experimental frequencies [56] and calculated [HF/6-31G(d,p)] normal modes, frequencies ( $\times 0.8929$ ), and IR intensities (km/mol) of ammonia.

frequencies. For frequency analysis, the Hessian matrix is derived analytically. In HF calculations, the split-valence basis sets 4-31G, 6-31G\*, and 6-31G\*\* yield very similar values for the predicted harmonic frequencies, systematically too high by about 10%. Scaling these frequencies uniformly by 0.8929 usually gives quite satisfactory results. Higher level calculations require less scaling. Recommended scale factors for MP2/6-31G(d) and B3LYP/6-31G(d) are 0.96 and 0.98, respectively. By way of example, the fundamental normal vibrational modes and calculated HF/6-31G(d,p) frequencies for ammonia are shown in Figure 2.7.

## ZERO-POINT VIBRATIONAL ENERGIES

For accurate comparison of relative energies, one must add to the BO-optimized energy the zero-point vibrational energy (ZPVE), which in the harmonic approximation is half the sum of the fundamental frequencies. This “correction” is most critical for the calculation of activation energies. The contribution of the ZPVE of the mode corresponding most closely to the reaction coordinate is lost completely. Processes that involve breaking of a bond to H are the most seriously affected; torsional changes are the least affected.

## CHAPTER 3

---

# ORBITAL INTERACTION THEORY

---

### RELATIONSHIP TO HARTREE–FOCK EQUATIONS

Orbital interaction theory forms a comprehensive model for examining the structures and kinetic and thermodynamic stabilities of molecules. It is not intended to be, nor can it be, a quantitative model. However, it can function effectively in aiding understanding of the fundamental processes in chemistry, and it can be applied in most instances without the use of a computer. The variation known as perturbative molecular orbital (PMO) theory was originally developed from the point of view of weak interactions [4, 5]. However, the interaction of orbitals is more transparently developed, and the relationship to quantitative MO theories is more easily seen by straightforward solution of the Hückel (independent electron) equations. From this point of view, the theoretical foundations lie in Hartree–Fock theory, described verbally and pictorially in Chapter 2 [57] and more rigorously in Appendix A.

### HÜCKEL APPROXIMATION

#### Orbital Energies and Total Electronic Energy

Recall that the minimum requirement for a many-electron wave function is that it be written as a suitably antisymmetrized sum of products of one-electron wave functions, that is, as a Slater determinant of MOs [see equation (A.68)] In Chapter 2 and Appendix A, we find that the condition that this be the best possible wave function of this form is that the MOs be eigenfunctions of a one-electron operator, the Fock operator [recall equation (A.42)], from which one can choose the appropriate number of the lowest energy. The Fock operator in *restricted* form,  $F(1)$  [RHF, the UHF form was given in equation (A.41)], is given by



$$F(1) = h(1) + \sum_{b=1}^M [2J_b(1) - K_b(1)] \quad (3.1)$$

The operator  $h(1)$  describes the kinetic energy of an electron and its attractive potential energy for all of the nuclei. The operators  $J_b(1)$  and  $K_b(1)$  together account for the repulsive interactions of the electron with a second electron whose distribution is given by MO  $b$ ,  $\phi_b(1)$ . The sum is only over half the number of electrons since each MO is doubly occupied,  $M = \frac{1}{2}N_e$ . The 1 in parentheses indicates that the quantities are functions of the coordinates of a single electron. The closed-shell ground-state wave function is constructed from the MOs with the lowest energies, enough for all of the electrons. Then the total RHF electronic energy [recall equation (A.69)] is given by

$$E_{\text{RHF}} = 2 \sum_{a=1}^M \varepsilon_a - \sum_{a=1}^M \sum_{b=1}^M (2J_{ab} - K_{ab}) \quad (3.2)$$

where  $\varepsilon_a$  is the energy of MO  $a$  and the term  $2J_{ab} - K_{ab}$  is an integral which yields the contribution to the electronic energy arising from the interaction of an electron described by MO  $a$ ,  $\phi_a(1)$ , with another described by MO  $b$ ,  $\phi_b(1)$ . The sums account for all electrons and all electron–electron interactions. To develop a “back-of-the-envelope” theory, we make a series of approximations. The first is the Hückel or *independent electron approximation* (IEA), in which all electron–electron interactions are ignored. Thus, the Fock operator reduces to just the *core hamiltonian*,  $h(1)$ , and the total electronic energy is just the sum of the MO energies times the appropriate occupation number, 2 (or 1 for a radical or excited state). It is too gross an approximation just to drop the electron–electron interactions and keep  $h(1)$  as is. To compensate for the loss of part of the repulsive potential,  $h(1)$  must be modified to some extent, resulting in an *effective* core hamiltonian,  $h^{\text{eff}}(1)$ . Thus,

$$F(1) \approx h^{\text{eff}}(1) \quad h^{\text{eff}}(1)\phi_a(1) = \varepsilon_a\phi_a(1) \quad E_{\text{IEA}} = 2 \sum_{a=1}^M \varepsilon_a \quad (3.3)$$

Equations (3.3) define the essence of the Hückel molecular orbital (HMO) theory. Notice that the total energy is just the sum of the energies of the individual electrons. *Simple* Hückel molecular orbital (SHMO) theory requires further approximations that we will discuss in due course.

## CASE STUDY OF A TWO-ORBITAL INTERACTION

Let us consider the simplest possible case of a system which consists of two orbitals,  $\chi_A(1)$  and  $\chi_B(1)$ , with energies  $\varepsilon_A$  and  $\varepsilon_B$  which can interact. It should be emphasized here that these may be orbitals of any kind, atomic orbitals, group orbitals, or complicated MOs. We wish to investigate the results of the interaction between them, that is, what new wave functions are created and what their energies are. Let us also be clear about what the subscripts  $A$  and  $B$  represent. The subscripts denote orbitals belonging to two *physically distinct* systems; the systems, and therefore the orbitals, are in separate positions in space. The two systems may in fact be identical, for example two water molecules or two  $sp^3$  hybrid orbitals on the same atom or on different but identical atoms (say, both C atoms). In this case,  $\varepsilon_A = \varepsilon_B$ . Or the two systems may be different in

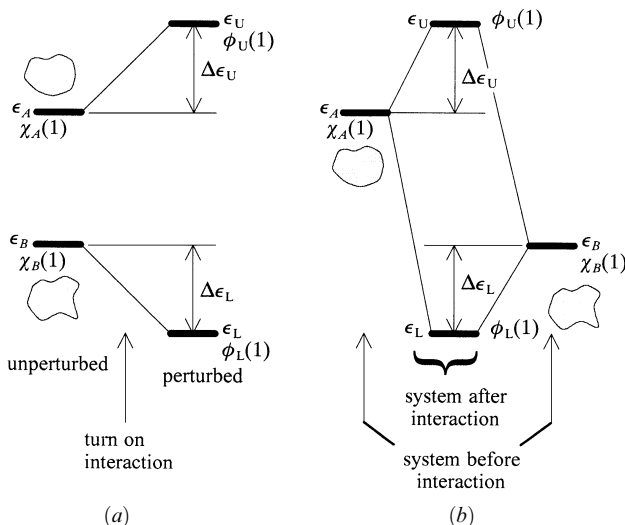


**Figure 3.1.** (a) Perturbation view of interaction of two orbitals; (b) standard interaction diagram.

all respects. Even if the systems, and the associated orbitals, are identical, they will in general differ in the way they are oriented in space relative to each other or their separation may vary. All of these factors will affect the way the orbitals of the two interact.

In the language of perturbation theory, the two orbitals will constitute the *unperturbed* system, the “perturbation” is the interaction between them, and the result of the interaction is what we wish to determine. The situation is displayed in Figure 3.1a. The diagram shown in Figure 3.1b conveys the same information in the standard representations of PMO or orbital interaction theory. The two interacting but unperturbed systems are shown on the left and the right, and the system after the interaction is turned on is displayed between them. Our task is to find out what the system looks like after the interaction. Let us start with the two unperturbed orbitals and seek the best MOs that can be constructed from them. Thus,

$$\phi(1) = c_A \chi_A(1) + c_B \chi_B(1) \quad (3.4)$$

The energy of this orbital is given by the expectation value [see equation (A.8) for the definition of expectation value]

$$\begin{aligned} \epsilon &= \frac{\int \phi(1) h^{\text{eff}}(1) \phi(1) d\tau_1}{\int |\phi(1)|^2 d\tau_1} \\ &= \frac{\int [c_A \chi_A(1) + c_B \chi_B(1)] h^{\text{eff}}(1) [c_A \chi_A(1) + c_B \chi_B(1)] d\tau_1}{\int [c_A \chi_A(1) + c_B \chi_B(1)]^2 d\tau_1} \end{aligned} \quad (3.5)$$

$$\begin{aligned} &= \frac{c_A^2 \int \chi_A(1) h^{\text{eff}}(1) \chi_A(1) d\tau_1 + c_B^2 \int \chi_B(1) h^{\text{eff}}(1) \chi_B(1) d\tau_1 + 2c_A c_B \int \chi_A(1) h^{\text{eff}}(1) \chi_B(1) d\tau_1}{c_A^2 \int |\chi_A(1)|^2 d\tau_1 + c_B^2 \int |\chi_B(1)|^2 d\tau_1 + 2c_A c_B \int \chi_A(1) \chi_B(1) d\tau_1} \\ &= \frac{c_A^2 h_{AA} + c_B^2 h_{BB} + 2c_A c_B h_{AB}}{c_A^2 + c_B^2 + 2c_A c_B S_{AB}} \end{aligned} \quad (3.6)$$

In proceeding from equation (3.5) to (3.6), we notice that the integrals

$$h_{AA} = \int \chi_A(1) h^{\text{eff}}(1) \chi_A(1) d\tau_1 \approx \varepsilon_A \quad h_{BB} = \int \chi_B(1) h^{\text{eff}}(1) \chi_B(1) d\tau_1 \approx \varepsilon_B \quad (3.7)$$

are the energies of the electron *localized* to sites  $A$  and  $B$ , respectively. These are only approximately equal to the energies of the orbitals of the isolated sites since  $h^{\text{eff}}$  includes the shielded nuclear influence of the other site. If sites  $A$  and  $B$  have identical orbitals, then  $h_{AA} = h_{BB}$ . In other words, the orbital energies are the same. The *intrinsic interaction* integral

$$h_{AB} = \int \chi_A(1) h^{\text{eff}}(1) \chi_B(1) d\tau_1 \quad (3.8)$$

provides a measure of the interference of the electron waves in energy units, in other words, how much energy may be gained if the wave functions at sites  $A$  and  $B$  overlap in a constructive manner (constructive interference or *bonding*) or how much energy must be added to the system to accommodate overlap in a destructive manner (destructive interference or *antibonding*). The wave functions at  $A$  and  $B$  are assumed to be normalized. In terms of overlap integrals,

$$\begin{aligned} S_{AA} &= \int |\chi_A(1)|^2 d\tau_1 = 1 & S_{BB} &= \int |\chi_B(1)|^2 d\tau_1 = 1 \\ S_{AB} &= \int \chi_A(1) \chi_B(1) d\tau_1 \end{aligned} \quad (3.9)$$

Notice that the overlap integral,  $S_{AB}$ , will depend on the position and orientation of the orbitals at the sites  $A$  and  $B$ , as does the intrinsic interaction integral,  $h_{AB}$ . The minimum-energy solution is found by the variational method, which we use twice in Appendix A. Equation (3.6) is differentiated with respect to  $c_A$  and with respect to  $c_B$ , resulting in two linear equations which can be solved. Thus,

$$\frac{\partial \varepsilon}{\partial c_A} = \frac{\partial}{\partial c_A} \left[ \frac{c_A^2 \varepsilon_A + c_B^2 \varepsilon_B + 2c_A c_B h_{AB}}{c_A^2 + c_B^2 + 2c_A c_B S_{AB}} \right] = 0 \quad (3.10)$$

$$\begin{aligned} 2 \frac{(\varepsilon_A - \varepsilon) c_A + (h_{AB} - S_{AB} \varepsilon) c_B}{c_A^2 + c_B^2 + 2c_A c_B S_{AB}} &= 0 \\ (\varepsilon_A - \varepsilon) c_A + (h_{AB} - S_{AB} \varepsilon) c_B &= 0 \end{aligned} \quad (3.11)$$

Similarly,

$$(h_{AB} - S_{AB} \varepsilon) c_A + (\varepsilon_B - \varepsilon) c_B = 0 \quad (3.12)$$

A solution of equations (3.11) and (3.12) may be found by setting the determinant of the coefficients of the  $c$ 's equal to zero. Thus

$$\begin{vmatrix} (\varepsilon_A - \varepsilon) & (h_{AB} - S_{AB} \varepsilon) \\ (h_{AB} - S_{AB} \varepsilon) & (\varepsilon_B - \varepsilon) \end{vmatrix} = 0 \quad (3.13)$$

Or

$$(\varepsilon_A - \varepsilon)(\varepsilon_B - \varepsilon) - (\mathbf{h}_{AB} - \mathbf{S}_{AB}\varepsilon)^2 = 0 \quad (3.14)$$

Expanding equation (3.14) yields

$$(1 - \mathbf{S}_{AB}^2)\varepsilon^2 + [2\mathbf{S}_{AB}\mathbf{h}_{AB} - (\varepsilon_A + \varepsilon_B)]\varepsilon + \varepsilon_A\varepsilon_B - \mathbf{h}_{AB}^2 = 0 \quad (3.15)$$

The two roots of equation (3.15) may be abstracted by routine application of the quadratic formula. Before we do that, let us examine the results from three simplified special cases.

**Case 1:  $\varepsilon_A = \varepsilon_B$ ,  $\mathbf{S}_{AB} = 0$**

The simplest case arises when the orbitals at the two sites are identical or accidentally have the same energy. The overlap integral will not in general be equal to zero but often is very small and may be *approximated* as zero for mathematical convenience. The solution to the entitled case is easily found from equation (3.14), which becomes

$$(\varepsilon_A - \varepsilon)^2 - \mathbf{h}_{AB}^2 = 0 \quad (3.16)$$

for which the two solutions are

$$\varepsilon = \varepsilon_A \pm \mathbf{h}_{AB} \quad (3.17)$$

To determine which of the two roots is lower in energy, one needs to know whether the wave functions of *A* and *B* suffer constructive interference (positive overlap) or destructive interference (negative overlap). Let us assume that the wave functions are in phase (positive overlap). Then  $\mathbf{h}_{AB}$  will be negative since  $h^{\text{eff}}(1)$  is negative, and the upper and lower roots,  $\varepsilon_U$  and  $\varepsilon_L$ , respectively, are

$$\varepsilon_U = \varepsilon_A - \mathbf{h}_{AB} \quad (3.18)$$

$$\varepsilon_L = \varepsilon_A + \mathbf{h}_{AB} \quad (3.19)$$

Substitution of the lower energy solution—equation (3.19) into equation (3.11)—and setting  $\mathbf{S}_{AB}$  to zero yield the relationship between the coefficients for the lower energy wave function (MO),  $\phi_L(1)$ , namely  $c_A = c_B$ . Requiring that the wave function be normalized,

$$c_A^2 + c_B^2 + 2c_Ac_B\mathbf{S}_{AB} = 1 \quad (3.20)$$

yields the result (with zero overlap)

$$\phi_L(1) = (2)^{-1/2}[\chi_A(1) + \chi_B(1)] \quad (3.21)$$

Using the upper root [equation (3.18)] in a similar manner with equations (3.12) and (3.20) yields

$$\phi_U(1) = (2)^{-1/2}[\chi_A(1) - \chi_B(1)] \quad (3.22)$$

Notice that with the case 1 assumptions the energies after the interaction are raised and lowered by equal amounts,  $h_{AB}$ , relative to the “unperturbed” energy,  $\epsilon_A (= \epsilon_B)$ , and the resulting wave functions are an *equal* admixture of the unperturbed wave functions.

**Case 2:  $\epsilon_A = \epsilon_B$ ,  $S_{AB} > 0$ ,  $S_{AB} \ll 1$**

This is a more realistic case since, if the two orbitals can interact, the overlap will not be zero. However, the overlap may be very small if the two orbitals are far apart, and in this case, a mathematical simplification ensues, as seen below.

When the overlap is not zero (assumed positive), the solutions may again conveniently be determined from equation (3.14). Thus

$$(\epsilon_A - \epsilon)^2 - (h_{AB} - S_{AB}\epsilon)^2 = 0 \quad (3.23)$$

for which the two solutions are

$$\epsilon_U = \frac{\epsilon_A - h_{AB}}{1 - S_{AB}} \approx \epsilon_A - h_{AB} + (\epsilon_A - h_{AB})S_{AB} \quad (3.24)$$

$$\epsilon_L = \frac{\epsilon_A + h_{AB}}{1 + S_{AB}} \approx \epsilon_A + h_{AB} - (\epsilon_A + h_{AB})S_{AB} \quad (3.25)$$

The second part of equations (3.24) and (3.25) arises from the expansion of  $1/(1 \pm S_{AB})$ , which converges rapidly if  $S_{AB} \ll 1$ . Thus it is apparent that inclusion of the overlap term reduces the amount of stabilization of the bonding combination of orbitals as well as the amount of destabilization of the antibonding combination. However, the reduction of the amount of destabilization,  $|(\epsilon_A - h_{AB})S_{AB}|$ , is *less* than the reduction in the amount of stabilization,  $|(\epsilon_A + h_{AB})S_{AB}|$ , leaving the antibonding combination somewhat higher in energy than the bonding combination relative to the reference unperturbed energy. The situation is illustrated in Figure 3.2. This last result, which is a consequence of overlap, is fundamental to the application of orbital interaction theory. The precise amount of destabilization for the degenerate case may be calculated by

$$\begin{aligned} \Delta\epsilon &= \epsilon_U + \epsilon_L - 2\epsilon_A \\ &= \frac{\epsilon_A - h_{AB}}{1 - S_{AB}} + \frac{\epsilon_A + h_{AB}}{1 + S_{AB}} - 2\epsilon_A \\ &= \frac{2}{1 - S_{AB}^2} [-h_{AB}S_{AB} + \epsilon_A S_{AB}^2] \end{aligned} \quad (3.26)$$

The energy change after interaction depends on two terms according to equation (3.26). The first term, involving  $-h_{AB}S_{AB}$ , is positive and contributes to the destabilization. The second term, which is proportional to the energy of the interacting orbitals, is negative since  $\epsilon_A (= h_{AA})$  is negative and leads to a stabilization. The first term is expected to dominate since  $S_{AB} < 1$ , and for valence orbitals, the intrinsic interaction energy,  $h_{AB}$ , is of the same order of magnitude (though smaller) as the orbital energy,  $\epsilon_A$ . We will return to this point in our case 4 study.

It can be easily verified by insertion of the precise value of  $\epsilon_L$  and  $\epsilon_U$ , equations (3.25) and (3.24), respectively, that the orbitals  $\phi_L(1)$  and  $\phi_U(1)$  again involve an equal

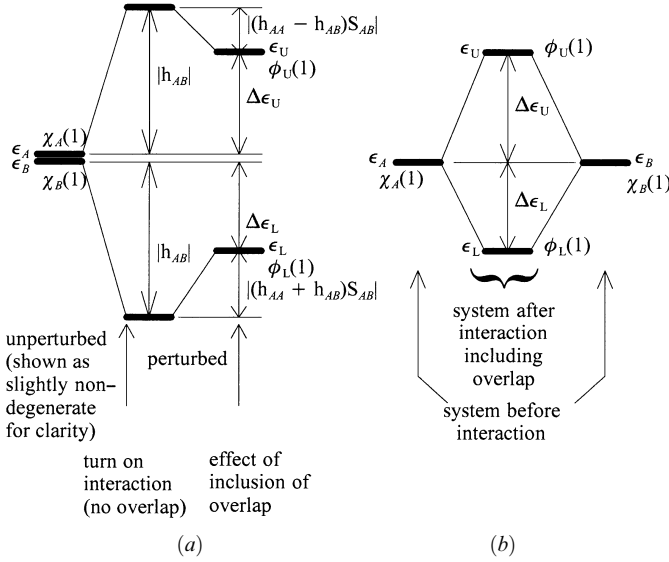


**Figure 3.2.** Case 2: (a) Perturbation view of interaction of two orbitals with inclusion of overlap; (b) standard interaction diagram showing relative destabilization of the upper orbital.

admixture of the  $\chi_A(1)$  and  $\chi_B(1)$  in phase and out of phase, respectively, as in case 1, but the coefficients are slightly different, namely

$$\phi_L(1) = [2(1 + S_{AB})]^{-1/2}[\chi_A(1) + \chi_B(1)] \quad (3.27)$$

$$\phi_U(1) = [2(1 - S_{AB})]^{-1/2}[\chi_A(1) - \chi_B(1)] \quad (3.28)$$

### Case 3: $\epsilon_A > \epsilon_B$ , $S_{AB} = 0$

For this case study, we again adopt the “zero-overlap” approximation but consider the nondegenerate case, assuming that  $\epsilon_A > \epsilon_B$ . The secular equation, from equation (3.15), becomes

$$\epsilon^2 - (\epsilon_A + \epsilon_B)\epsilon + \epsilon_A\epsilon_B - h_{AB}^2 = 0 \quad (3.29)$$

Application of the quadratic formula and some algebra leads to

$$\begin{aligned} \epsilon &= \frac{1}{2}(\epsilon_A + \epsilon_B) \pm \frac{1}{2}\sqrt{(\epsilon_A + \epsilon_B)^2 - 4\epsilon_A\epsilon_B + 4h_{AB}^2} \\ &= \frac{1}{2}(\epsilon_A + \epsilon_B) \pm \frac{1}{2}\sqrt{(\epsilon_A - \epsilon_B)^2 + 4h_{AB}^2} \\ &= \frac{1}{2}(\epsilon_A + \epsilon_B) \pm \frac{1}{2}(\epsilon_A - \epsilon_B)\sqrt{1 + \frac{4h_{AB}^2}{(\epsilon_A - \epsilon_B)^2}} \end{aligned} \quad (3.30)$$

If  $4h_{AB}^2 \ll (\epsilon_A - \epsilon_B)^2$ , that is, the interaction energy is much less than the energy differ-

ence between the interacting orbitals, one can simplify equation (3.30) by expansion of the square root:

$$\varepsilon \approx \frac{1}{2}(\varepsilon_A + \varepsilon_B) \pm \frac{1}{2}(\varepsilon_A - \varepsilon_B) \left( 1 + \frac{1}{2} \frac{4h_{AB}^2}{(\varepsilon_A - \varepsilon_B)^2} \right) \quad (3.31)$$

Notice that this situation is really only valid for separated systems. If the two orbitals are spatially close, say in the same molecule, it is unlikely that the last approximation would be appropriate. This situation is discussed further below.

In equation (3.31), the lower root is obtained by taking the minus sign. Thus

$$\varepsilon_L \approx \frac{1}{2}(\varepsilon_A + \varepsilon_B) - \frac{1}{2}(\varepsilon_A - \varepsilon_B) \left( 1 + \frac{1}{2} \frac{4h_{AB}^2}{(\varepsilon_A - \varepsilon_B)^2} \right) \quad (3.32)$$

or

$$\varepsilon_L \approx \varepsilon_B - \frac{h_{AB}^2}{\varepsilon_A - \varepsilon_B} \quad (3.33)$$

Similarly,

$$\varepsilon_U \approx \varepsilon_A + \frac{h_{AB}^2}{\varepsilon_A - \varepsilon_B} \quad (3.34)$$

Evidently, if the unperturbed orbitals are not of the same energy, and if the energy difference is large compared to the interaction energy, the effect of the interaction is to lower the lower orbital further by an amount proportional to the square of the interaction energy and inversely proportional to the energy difference. The upper orbital is raised by the same amount. One should suspect, correctly, that if overlap were to be taken into account, the amount of raising would be greater than the amount of lowering. Substitution of equations (3.33) and (3.34) separately into equations (3.11) and (3.12) yields the molecular orbitals. Specifically, insertion of equation (3.33) into equation (3.12), with  $S_{AB} = 0$ , yields

$$h_{ABCAL} + (\varepsilon_B - \varepsilon_L)c_{BL} = 0 \quad (3.35)$$

or

$$h_{ABCAL} + \left( \varepsilon_B - \varepsilon_B + \frac{h_{AB}^2}{\varepsilon_A - \varepsilon_B} \right) c_{BL} = 0 \quad (3.36)$$

Therefore,

$$c_{AL} = -\frac{h_{AB}}{\varepsilon_A - \varepsilon_B} c_{BL} \quad (3.37)$$

from which

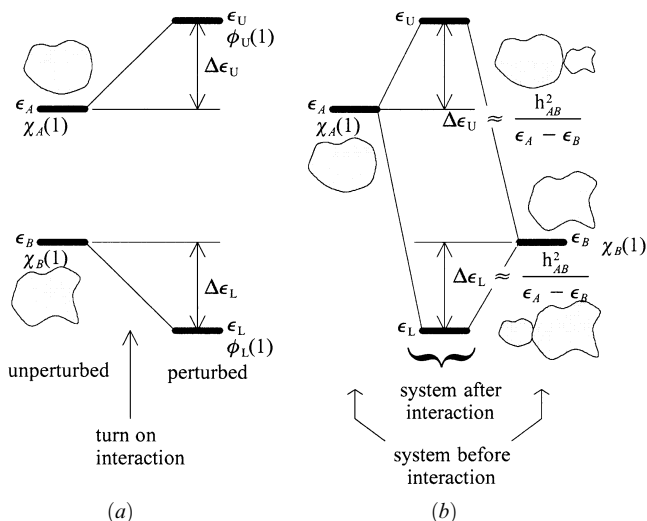


**Figure 3.3.** Case 3: (a) Perturbation view of interaction of two orbitals of unequal energy; (b) standard interaction diagram.

$$\phi_L(1) = c_{BL} \left[ -\frac{h_{AB}}{\epsilon_A - \epsilon_B} \chi_A(1) + \chi_B(1) \right] \quad (3.38)$$

Similarly, insertion of equation (3.34) into equation (3.11), with  $S_{AB} = 0$ , yields

$$\phi_U(1) = c_{AU} \left[ \chi_A(1) + \frac{h_{AB}}{\epsilon_A - \epsilon_B} \chi_B(1) \right] \quad (3.39)$$

The factors  $c_{BL}$  and  $c_{AU}$  are determined by normalization, but this is not important for our purposes. Notice that the factor  $h_{AB}/(\epsilon_A - \epsilon_B)$  is *negative* and much less than 1 in absolute magnitude. Thus the lower MO is derived from the interacting orbital which has lower energy by the admixture of a small amount of the interacting orbital of higher energy. The signs of the coefficients of the two interacting orbitals are the same, that is,  $-h_{AB}/(\epsilon_A - \epsilon_B) > 0$ . The upper MO is derived from the interacting orbital which has higher energy by the admixture of a small amount of the interacting orbital of lower energy. The signs of the coefficients of the two interacting orbitals in the antibonding MO are different. (*Note:* The assertion about the relative signs of the coefficients is contingent on the fact that the overlap of the two orbitals is positive.) The results from the case 3 study are depicted in Figure 3.3. Some of the results obtained above have been reviewed and applied by Hoffmann in an investigation of orbital interactions through space and through bonds [6] and are used extensively in the excellent book by Albright et al. [58].

#### Case 4: $\epsilon_A > \epsilon_B$ , $S_{AB} > 0$

As stated earlier, the exact algebraic solution of equation (3.15) is readily obtained but does not add to the concepts already derived. The orbital energies and wave functions



will resemble equations (3.33), (3.34) and (3.38), (3.39), respectively. The consequences of nonzero overlap will again prove to be that  $|\Delta\varepsilon_U| > |\Delta\varepsilon_L|$ . The dependence of the net destabilization,  $|\Delta\varepsilon_U| - |\Delta\varepsilon_L|$ , was discussed in the case 2 study [equation (3.26)] and found to depend on two terms, a dominant destabilizing term and a stabilizing term which is proportional to the energy of the degenerate pair. The more general expression is easily derived. The roots of equation (3.15) by the quadratic formula are

$$\varepsilon_U = \frac{-b}{2a} + \frac{1}{2a}\sqrt{b^2 - 4ac} \quad \text{and} \quad \varepsilon_L = \frac{-b}{2a} - \frac{1}{2a}\sqrt{b^2 - 4ac} \quad (3.40)$$

where

$$a = (1 - S_{AB}^2) \quad b = 2S_{AB}h_{AB} - (\varepsilon_A + \varepsilon_B) \quad c = \varepsilon_A\varepsilon_B - h_{AB}^2 \quad (3.41)$$

Thus the net destabilization is

$$\begin{aligned} |\Delta\varepsilon_U| - |\Delta\varepsilon_L| &= \varepsilon_U + \varepsilon_L - (\varepsilon_A + \varepsilon_B) \\ &= \frac{-b}{a} - (\varepsilon_A + \varepsilon_B) \\ &= \frac{S_{AB}}{1 - S_{AB}^2} [-2h_{AB} + (\varepsilon_A + \varepsilon_B)S_{AB}] \end{aligned} \quad (3.42)$$

As in the case 2 study, two terms of opposite sign are involved. The sum of orbital energies before and after interaction is the same when the quantity in square brackets [equation (3.42)] is zero, that is,

$$h_{AB} = \frac{1}{2}(\varepsilon_A + \varepsilon_B)S_{AB} \quad (3.43)$$

Equation (3.43) resembles the formula [equation (3.44)] adopted by Wolfsberg and Helmholtz [59] for the interaction matrix elements. This form, with the empirical factor  $k = 1.75$ , was adopted by Hoffmann in his derivation of extended Hückel theory [60], namely

$$h_{AB} = k \frac{h_{AA} + h_{BB}}{2} S_{AB} \quad k = 1.75 \quad (\text{recall } h_{AA} \approx \varepsilon_A \text{ and } h_{BB} \approx \varepsilon_B) \quad (3.44)$$

That  $k$  should be between 1 and 2, and consequently that the sum of orbital energies after interaction should be greater than before the interaction, was offered theoretical justification by Woolley [61]. Substitution of (3.44) into (3.42) yields the result

$$|\Delta\varepsilon_U| - |\Delta\varepsilon_L| = -\frac{|k'|}{1 - S_{AB}^2} (\varepsilon_A + \varepsilon_B) S_{AB}^2 \quad (k' \approx 0.75) \quad (3.45)$$

In summary, at least for the frontier orbitals where equation (3.45) is expected to be valid, a net destabilization depending in a complex manner on the square of the overlap integral and proportional to the sum of unperturbed orbital energies ensues from the interaction.

## EFFECT OF OVERLAP

The magnitude of the overlap of the interacting orbitals has an influence on the appearance of the interaction diagram because it affects the magnitude of the interaction integral [equation (3.44)], the difference between stabilization and destabilization [equation (3.45)], and the polarization of the resulting molecular orbitals,  $\phi_L$  and  $\phi_U$ . It is convenient to categorize the overlap dependence into two broad regimes, the regime of large overlap, which is usually the case when the interactions of interest are between adjacent regions of the same molecule (i.e., intramolecular), and the limit of small overlap, which is almost always the case when one is considering intermolecular interactions.

## ENERGETIC EFFECT OF OVERLAP

Three kinds of energetic consequences must be considered: (a) the magnitudes of  $\Delta\varepsilon_U$  and  $\Delta\varepsilon_L$ , (b) the magnitude of the difference between  $\Delta\varepsilon_U$  and  $\Delta\varepsilon_L$ ; and (c) the dependence in the difference in unperturbed orbital energies.

- (a) The magnitudes of  $\Delta\varepsilon_U$  and  $\Delta\varepsilon_L$  are directly related to the magnitude of  $h_{AB}$ ; the larger the overlap, the larger is  $h_{AB}$ , and the larger are  $\Delta\varepsilon_U$  and  $\Delta\varepsilon_L$ . Thus the energy changes which ensue from intramolecular interactions are usually much larger than those which originate intermolecularly.
- (b) The *relative* magnitudes of  $\Delta\varepsilon_U$  and  $\Delta\varepsilon_L$  are directly related to the magnitude of the overlap as seen in equation (3.45); the larger the overlap, the larger is difference between destabilization and stabilization. These considerations are important if both types (bonding and antibonding) of orbitals have to be occupied. Again, the individual energy changes which ensue from intramolecular interactions are usually much larger than those which originate intermolecularly.
- (c) Larger overlap also means that it is more difficult to meet the criterion for the results displayed in equations (3.33) and (3.34), namely that the ratio  $|h_{AB}/(\varepsilon_A - \varepsilon_B)|$  is much less than unity. In other words,  $\Delta\varepsilon_U$  and  $\Delta\varepsilon_L$  are more closely proportional to  $h_{AB}$  rather than its square and will not exhibit the inverse dependence on the difference of the initial orbital energies. For *intramolecular* considerations, the orbital energy difference becomes less important than the magnitude of  $h_{AB}$  itself whereas for *intermolecular* interactions, orbital energy differences are more important, and the inverse dependence on the energy difference is expected.

## ORBITAL EFFECT OF OVERLAP

The polarization of the resulting orbitals is also affected by the overlap, although this is more difficult to demonstrate algebraically and we do not do so here. We simply state the results: For a given energy difference (not equal to zero), the larger the overlap, the less the polarization of  $\phi_L$  and  $\phi_U$ . Less polarization means greater mixing of the initial orbitals.

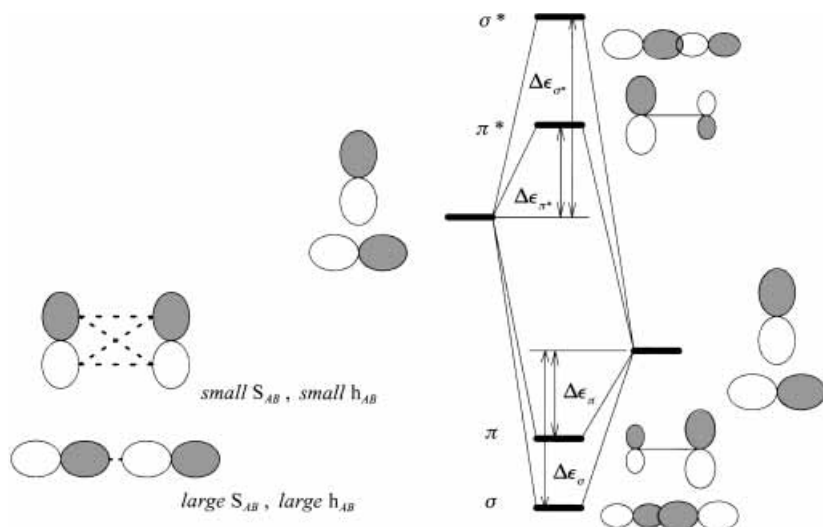


**Figure 3.4.** An  $s$ - and  $p$ -type interaction between  $p$  orbitals: The  $s$  orbitals are further apart and *less* polarized than the  $p$  orbitals. Also,  $|\Delta\epsilon_{\sigma^*} - \Delta\epsilon_{\sigma}| > |\Delta\epsilon_{\pi^*} - \Delta\epsilon_{\pi}|$ .

## FIRST LOOK AT BONDING

A distinction between  $\sigma$  and  $\pi$  orbitals may be made on the basis of the above considerations. Since the overlap of two  $p$  orbitals in a  $\pi$  fashion is smaller than in a  $\sigma$  fashion, the  $\pi$  and  $\pi^*$  orbitals are closer together than the  $\sigma$  and  $\sigma^*$  orbitals because the smaller overlap results in smaller  $\Delta\epsilon_U$  and  $\Delta\epsilon_L$ . The  $\sigma^*$  orbital is more antibonding relative to the  $\sigma$  orbital than the  $\pi^*$  orbital is relative to the  $\pi$  orbital. Because of the smaller  $\pi$ -type overlap, one expects more polarization in the  $\pi$  orbitals than in the  $\sigma$  orbitals. All three consequences are depicted in Figure 3.4.

## RELATIONSHIP TO PERTURBATION THEORY

It should be apparent that the expressions for the wave functions after interaction [equations (3.38) and (3.39)] are equivalent to the Rayleigh–Schrödinger perturbation theory (RSPT) result for the perturbed wave function correct to first order [equation (A.109)]. Similarly, the parallel between the MO energies [equations (3.33) and (3.34)] and the RSPT energy correct to second order [equation (A.110)] is obvious. The “missing” first-order correction emphasizes the correspondence of the first-order corrected wave function and the second-order corrected energy. Note that equations (3.33), (3.34), (3.38), and (3.39) are valid under the same conditions required for the application of perturbation theory, namely that the perturbation be weak compared to energy differences.

## GENERALIZATIONS FOR INTERMOLECULAR INTERACTIONS

Equations (3.33), (3.34), (3.38), and (3.39) are valid under the condition that the perturbation be weak compared to energy differences, that is,  $|h_{AB}/(\epsilon_A - \epsilon_B)| \ll 1$ . The case 1 and case 2 studies revealed the situation in the degenerate case. We now interpolate the intermediate situation, remembering that overlap will not be zero except when dictated to be so by local symmetry. However, overlap will always be small when dealing with interactions between molecules. Refer to Figures 3.1–3.4 for the defined quantities.

**Generalization 1:**  $\Delta\epsilon_L \approx \Delta\epsilon_U$ . The destabilization of the upper MO relative to the higher energy interacting orbital is approximately the same as the stabilization of the lower MO relative to the lower energy interacting orbital.

**Generalization 2:**  $|\Delta\epsilon_L| < |\Delta\epsilon_U|$ . The destabilization of the upper MO relative to the higher energy interacting orbital is always greater than the stabilization of the lower MO relative to the lower energy interacting orbital. This is a direct consequence of nonzero overlap [see equation (3.45)].

**Generalization 3:**  $(|\Delta\epsilon_U| - |\Delta\epsilon_L|) < |\Delta\epsilon_L|, |\Delta\epsilon_U|$ . The magnitude of the *difference* between destabilization and stabilization is small compared to the actual magnitudes of the stabilization and destabilization.

**Generalization 4:**  $h_{AB} \approx k(\epsilon_A + \epsilon_B)S_{AB}$  (*k a Positive Constant,  $S_{AB}$  Assumed Positive*). The interaction matrix element is not precisely proportional to the overlap integral but the behavior with respect to distance and symmetry is essentially the same. In other words,  $h_{AB}$  will be zero by symmetry when  $S_{AB}$  is zero by symmetry, but not otherwise. Also,  $h_{AB}$  decreases in magnitude as a function of increasing separation in much the same way as  $S_{AB}$ . Thus, *two orbitals will not interact if they behave differently toward local elements of symmetry*.

The proportionality to the sum of unperturbed orbital energies [see also equation (3.44)] may be misleading. Large negative values for orbital energies are associated with core orbitals for which the overlap is close to zero.

**Generalization 5:**  $\Delta\epsilon_L \approx \Delta\epsilon_U \approx h_{AB}^2/(\epsilon_A - \epsilon_B)$ . The energy raising and lowering depend directly on the square of the interaction matrix element (the square of the overlap matrix element) and inversely on the energy separation of the interacting orbitals. This relationship is precisely true only in the limit of very small interaction. The energy raising and lowering are *maximum* when the energy difference is zero, in which case they have the value approximately  $h_{AB}$ .

**Generalization 6:**  $\phi_L \approx \chi_B + d\chi_A$ ;  $\phi_U \approx \chi_A - d\chi_B$ ;  $d = -h_{AB}/(\epsilon_A - \epsilon_B)$ ;  $0 < d < 1$ . The lower MO is polarized toward the lower interacting orbital and is the in-phase (bonding) combination of the two. The upper MO is polarized toward the higher interacting orbital and is the out-of-phase (antibonding) combination of the two. In the limit of weak interaction, the amount of mixing of the minor component is approximately proportional to the interaction matrix element and inversely proportional to the energy difference between the two interacting orbitals. The orbitals mix equally ( $d = 1$ ) when the orbital energy difference is zero.

The above generalizations are summarized in Figure 3.5.

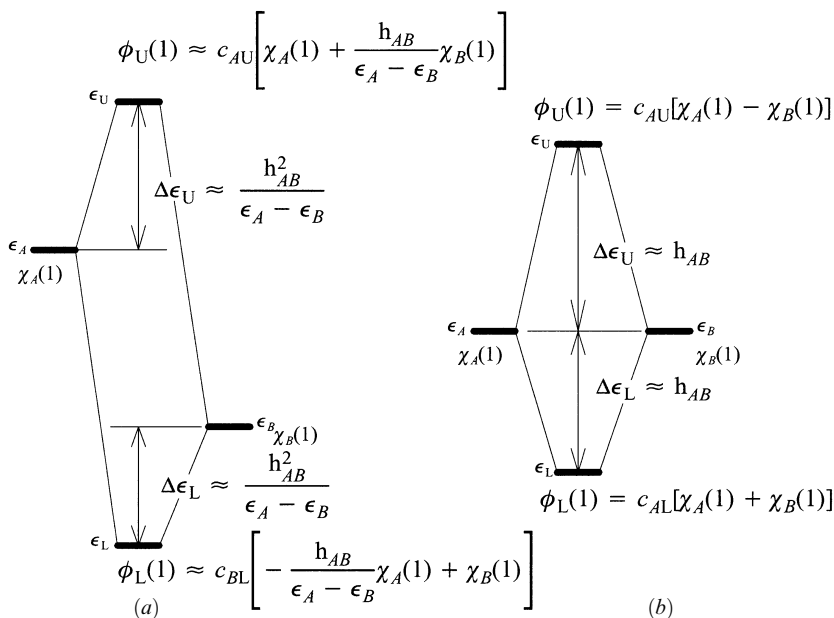


Figure 3.5. Orbital interaction diagrams: (a) nondegenerate case; (b) degenerate case.

## ENERGY AND CHARGE DISTRIBUTION CHANGES FROM ORBITAL INTERACTION

The energy change which takes place upon the mixing of two orbitals depends on the number and distribution of the electrons. If neither orbital is occupied, there is no energy change. There is no need to calculate energy changes quantitatively. Inspection of the orbital interaction diagrams will provide the qualitative assessment of the energy change, that is, large or small, stabilizing or destabilizing. We consider separately the situations which may arise as a function of the number of electrons.

### Four-Electron, Two-Orbital Interaction

With four electrons, the bonding and antibonding molecular orbitals are both filled (Figure 3.6). The interaction will be repulsive and the system will adjust in such a way as to minimize the interaction. Closed-shell molecules will tend to repel each other. The common term is *steric interaction*. The net interactions between filled orbitals of two molecules separated by more than the van der Waals contact distance will be weak; the bonding and antibonding interactions, which may individually be large, almost cancel.

Filled orbitals which cannot physically separate because they are part of the same molecule may have substantially larger overlap than the intermolecular case, and the destabilizing interaction,  $\Delta \epsilon_U$ , may be much larger than the stabilizing interaction,  $\Delta \epsilon_L$ . The net repulsion will lead to conformational changes so as to minimize the repulsive interactions. If the interaction cannot be avoided by conformational change, then as the result of the interaction, a pair of electrons is raised in energy. The system has a lower

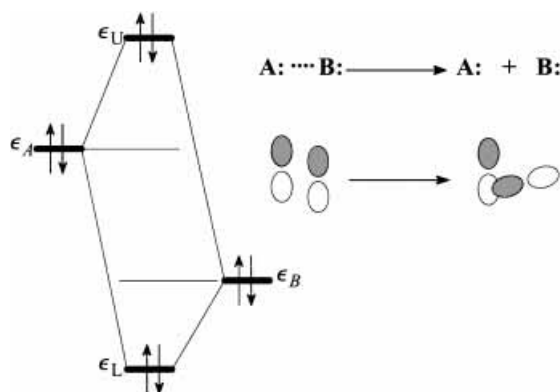


**Figure 3.6.** Repulsive four-electron, two-orbital interaction: Closed-shell species will separate, filled orbitals will tend to align in each other's nodes.

ionization potential, is more easily oxidized, and is more basic in the Lewis sense. All of these features are observed in the experimental properties of norbornadiene (Figure 3.7). The in- and out-of-phase interactions of the two occupied  $\pi$  bonding orbitals may be described by an interaction diagram such as shown in Figure 3.5*b*. Norbornadiene has two ionization potentials, 9.55 and 8.69 eV [62], which are above and below the ionization potential of (*Z*)-2-butene (9.12 eV [63]), cyclohexene (9.11 eV [64]), or norbornene (8.95 eV [64]), as expected on the basis of the orbital interaction diagram in Figure 3.7. The consequences of intramolecular interaction of  $\sigma$  bonding orbitals is further discussed in Chapter 4.

### Three-Electron, Two-Orbital Interaction

With three electrons one is dealing with a free radical. The bonding MO is doubly occupied and the antibonding molecular orbital has a single electron (Figure 3.8). In the

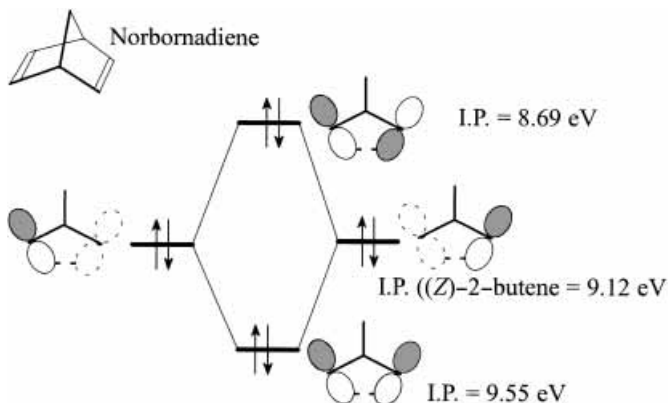


**Figure 3.7.** Four-electron, two-orbital interaction diagram for norbornadiene and its ionization potentials.

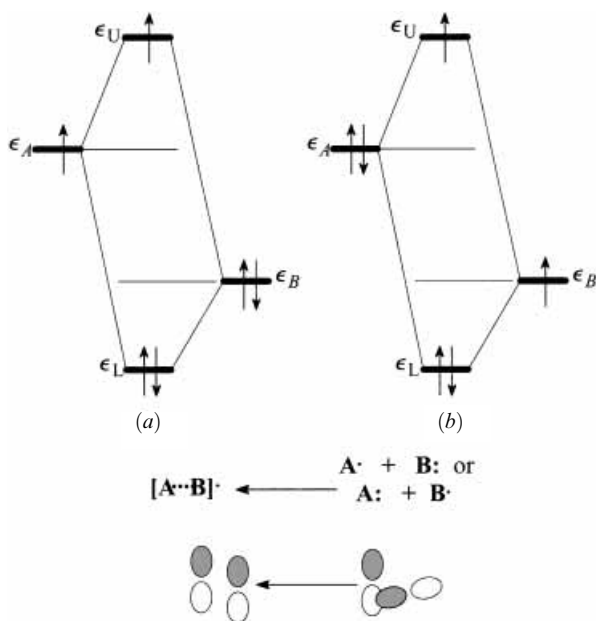


**Figure 3.8.** Three-electron, two-orbital interaction: (a) odd electron in higher orbital, moderate stabilization; (b) odd electron in the lower orbital, large stabilization and the possibility of electron transfer.

case of large overlap, the system will be only marginally stabilized because of the large difference between  $\Delta\epsilon_U$  and  $\Delta\epsilon_L$ . In fact, it has been predicted that if the overlap is greater than  $\frac{1}{3}$  (possible for  $\sigma$ -type overlap), the system is actually destabilized [65]. However, in the weak-overlap case,  $\Delta\epsilon_U$  and  $\Delta\epsilon_L$  are almost equal. The orbital interaction will be clearly attractive and the system will adjust in such a way as to maximize the interaction. The situation depicted in Figure 3.8a may arise from the interaction of a free-radical species with an inert solvent or matrix or intramolecularly when a radical site is adjacent to an electron donor substituent. The energy of the odd electron is raised and the electron is delocalized to some extent. Such a radical would be more nucleophilic. The situation depicted in Figure 3.8b arises when a species with a relatively high ionization potential is ionized. A large amount of energy is released upon complex formation, and there is a net transfer of charge from *A* to *B*. If the complex is not stable and separates, the odd electron will stay with system *A* and an electron transfer from *A* to *B* will have taken place. Free radicals are discussed in more detail in Chapter 7.

### Two-Electron, Two-Orbital Interaction

Maximum stabilization occurs in the two-electron, two-orbital interaction. A system will reorient itself to maximize such an interaction. Figure 3.9 depicts the two most common instances of this interaction. Figure 3.9a may depict the interaction of a Lewis base with a Lewis acid to form a dative bond (e.g.,  $\text{NH}_3 + \text{BF}_3 \rightarrow \text{H}_3\text{N}^+ - \text{B}^- \text{F}_3$ ), a hydrogen bond, or a tight complex, as between aryl systems and  $\text{NO}^+$  [66]. The interaction

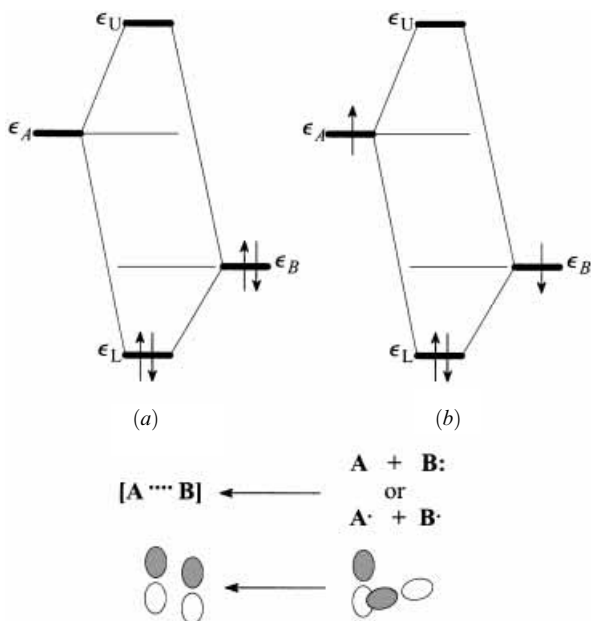


**Figure 3.9.** Two-electron, two-orbital interaction: (a) both electrons in lower orbital, dative bond formation and electron transfer from  $B$  to  $A$ ; (b) one electron in each orbital, large stabilization and covalent bond formation.

is accompanied by charge transfer from  $B$  to  $A$ . Most chemical reactions are initiated by an interaction of this type between an occupied molecular orbital of one molecule and a virtual molecular orbital of another.

Figure 3.9a may also represent the interaction of a nonbonded (“lone-pair”) orbital with an adjacent polar  $\pi$  or  $\sigma$  bond [67]. If a polar  $\pi$  bond, one can explain stabilization of a carbanionic center by an “electron-withdrawing” substituent ( $C=O$ ), or the special properties of the amide group. If a polar  $\sigma$  bond, we have the origin of the anomeric effect. The interaction is accompanied by charge transfer from  $B$  to  $A$ , an increase in the ionization potential, and a decreased Lewis basicity and acidity. These consequences of the two-electron, two-orbital interaction are discussed in greater detail in subsequent chapters.

If Figure 3.9a represents bond formation between two molecules, the reverse process would correspond to heterolytic bond cleavage. One notes, however, that in the gas phase heterolytic bond cleavage is never observed. As we shall see, the interaction depicted in Figure 3.9a is the primary interaction between any pair of molecules whether it leads to bond formation or not. It is responsible for van der Waals attraction and hydrogen bonding.

Figure 3.9b portrays homolytic bond formation by the recombination of radicals and is accompanied by charge transfer from  $A$  to  $B$ . The radicals must be singlet coupled. The interaction of triplet-coupled electron pairs is repulsive and does not lead to bond formation. The reverse process describes homolytic bond cleavage and results in singlet-coupled free radicals.



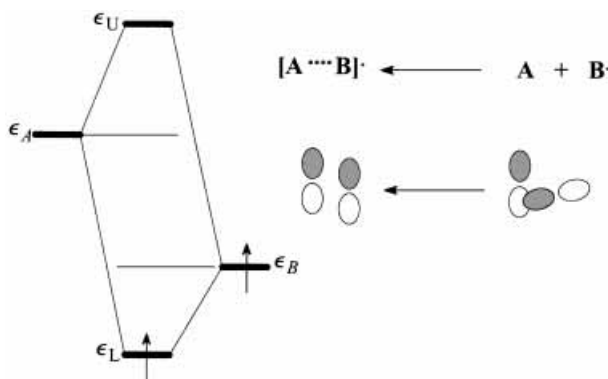


Figure 3.10. The one-electron, two-orbital interaction: half-filled orbital is stabilized.

### One-Electron, Two-Orbital Interaction

The one-electron, two-orbital interaction, portrayed in Figure 3.10, again deals with a radical. The electron in the half-filled orbital is stabilized and delocalized. If it occurs intramolecularly, Figure 3.10 illustrates the stabilization of a radical site by an electron-withdrawing substituent. Such a radical would be more electrophilic. The intermolecular process may lead to complex formation. The energies of stabilization resulting from the interaction of the singly occupied MO of methyl radical with the empty  $\sigma^*$  antibonding orbital of HCl and HBr have been estimated theoretically as 2.53 kcal/mol and 0.67, respectively [68]. An idea of the relative strengths of three-electron and one-electron interactions may be gained from a theoretical study in the gas phase of the radical cations of  $(\text{XH}_n)_2^+$ , where X is a first- or second-row element [69]. For each of the first-row systems the one-electron bonded system was more stable than the three-electron bonded system, while for  $\text{X}=\text{P}$ , the two were equivalent, and the three-electron bond was stronger than the one-electron system for S and Cl. In an absolute sense, all of the odd-electron bonds of the first-row dimers were stronger than for the second-row systems. Free radicals are discussed further in Chapter 7.

### Zero-Electron, Two-Orbital Interaction

The zero-electron, two-orbital interaction is portrayed in Figure 3.11. Since no electrons are involved and therefore there is no change in the energy, this interaction may seem trivial. This is far from the truth, however. Indeed, if the interaction of the empty orbitals occurs *intermolecularly*, Figure 3.11 illustrates the energy of the vacant MO which may determine the structure of a negatively charged complex, such as  $(\text{H}_2\text{O})_2^-$ . More importantly from the perspective of organic chemistry, an *intramolecular* interaction between a site with a low-lying empty group orbital and a neighboring site that has a high empty orbital will result in a lower empty orbital and therefore increased Lewis acidity overall. Furthermore, to the extent that  $\phi_L$  is delocalized to the A site, acidification of the A site is also indicated. Just such a diagram will describe the acidification of C—H bonds adjacent to a carbonyl group or the C—X bond of alkyl halides, as shown in some detail in Chapter 10.

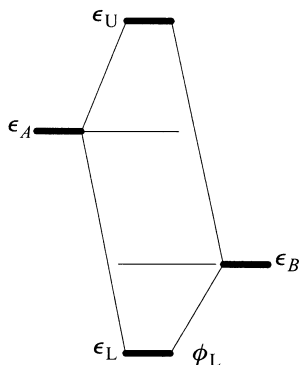


**Figure 3.11.** Zero-electron, two-orbital interaction: The system is more Lewis acidic, and some Lewis acidity is transferred to  $A$ .

## INTERACTIONS BETWEEN MOLECULES: MANY ELECTRONS, MANY ORBITALS

Most molecules consist of many electrons and many orbitals, including “virtual” orbitals. When molecules interact, all MOs and all electrons are involved in principle. Before we discuss the possible relative importance of the various interactions, some general principles need to be stressed.

### General Principles Governing the Magnitude of $h_{AB}$ and $S_{AB}$

Recall that in the case of the hydrogen atom, the *radius* of an orbital is proportional to  $n^2$ , the *energy* is proportional to  $n^{-2}$ , and the *number of nodes* is equal to  $n - 1$ , where  $n$  is the principal quantum number. A similar effect occurs in molecules. The size (spatial extension) of MOs and the number of nodes generally increase as the energy increases. The lower the energy of the orbital, the more tightly bound is the electron and the smaller is the average radius. The interaction matrix element,  $h_{AB}$ , depends approximately inversely on the average separation of the “centers of mass” of the MOs and directly on their spatial extension in the same way that the overlap integral  $S_{AB}$  does. Two orbitals will overlap more when the molecules bearing them are closer together. At a given separation, the extent of overlap depends on the size of the orbitals in a complex way. This is illustrated schematically in Figure 3.12. Very large orbitals overlap at large separations but the overlap does not reach a large absolute value, even at bonding distances, because these orbitals have a lot of nodes. At the large separations, tight orbitals do not overlap very well. At shorter separations, the overlap of a small orbital with a large one may exceed the overlap of two large orbitals, and at shorter distances still, the largest overlap and therefore the largest interaction may be between two small orbitals.

### Interactions of MOs

The interaction of two molecules is depicted in Figure 3.13. The possible orbital interactions are not shown in the form of an interaction diagram but are illustrated by labeled dashed lines in Figure 3.13a.

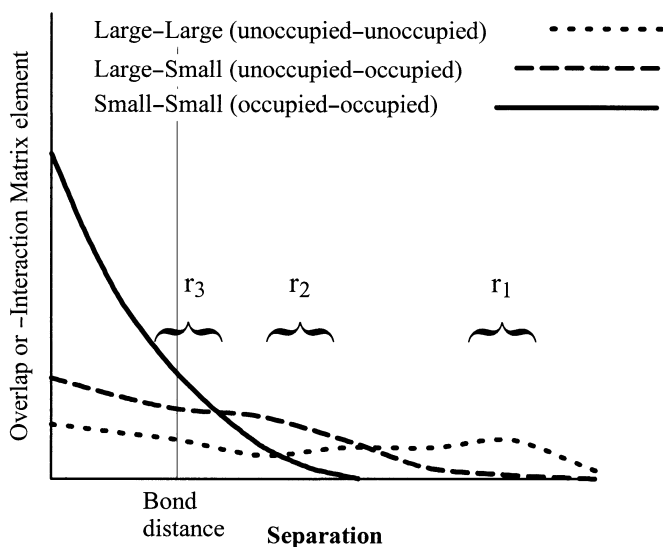


**Figure 3.12.** Schematic representation of overlap of MOs of different sizes as a function of separation.

*At large separations*  $r_1$  (Figure 3.12), interactions between filled orbitals (a, b, c) will be negligible. The largest interactions will be between the virtual orbitals (h), but since there are no electrons, there are no energetic consequences. Notice that addition of an electron to the pair (or larger assembly) of neutral molecules would lead to maximum stabilization of the electron if interaction h is maximized. The solvated electron in liquid ammonia is an example of such a system. An electron solvated by two water molecules has been detected in the gas phase. The system has been studied theoretically and found to adopt a geometry expected on the basis of maximizing LUMO–LUMO interactions ([70]; see also reference 71 for references to other studies of electrons attached to small clusters).

*At intermediate separations*  $r_2$  (Figure 3.12), interactions between occupied MOs (a, b, c) begin to become important but the four-electron, two-orbital interactions are only weakly repulsive and are outweighed by the attractive two-electron, two-orbital occupied–virtual interactions (d, e, f, g). All molecules encounter this attraction (van der Waals attraction [72]). In general, the larger the number of points of contact, the more favorable the interaction, and hence the observed relationship between “surface area” and the strength of van der Waals forces. Nodal characteristics of the interacting occupied and virtual orbitals determine the maximum magnitude of the interaction matrix element  $h_{AB}$ ; the energy contribution is proportional to the square of  $h_{AB}$ . The energy contribution is also approximately proportional to the inverse of the energy separation. Both factors tend to make the HOMO–LUMO interactions (e, f) dominant. The pair of MOs with the smaller HOMO–LUMO gap will tend to dominate the intermediate distance behavior of the molecule–molecule interaction, interaction f in Figure 3.13a. The optimum distance of approach of two neutral molecules defines the van der Waals surface of the molecules. This occurs at the point where forces due to the attractive

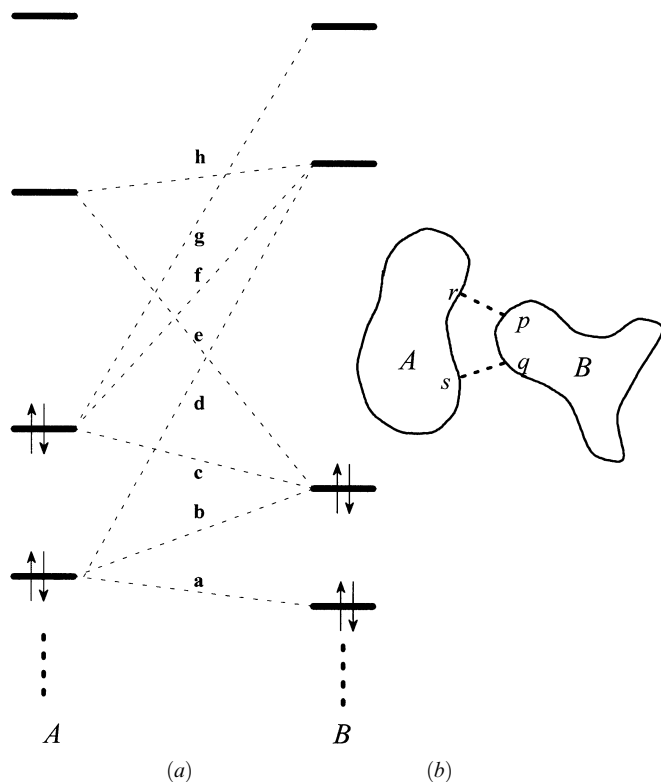


**Figure 3.13.** Interactions between two molecules: (a) orbital interactions (see text); (b) schematic showing relatively few points of contact.

two-electron, two-orbital interactions are balanced by the repulsive forces of the four-electron, two-orbital interactions, approximately  $1\text{--}1.5 \text{ \AA}$  from the outermost nuclei.

*At bonding separations*  $r_3$  (Figure 3.12), the four-electron, two-orbital interactions are strongly dominant, leading to the observed  $r^{-12}$  behavior at distances within the van der Waals separation. For two molecules in their ground states to undergo chemical reaction, there must be at least one exceptionally strong two-electron, two-orbital interaction which will permit close approach of the molecules. This interaction is necessarily accompanied by partial electron transfer.

Figure 3.13b attempts to emphasize that for large molecules, relatively few points of contact are possible, the other regions of the molecules being too far apart to interact. Two molecules which can interact favorably will tend to orient themselves to maximize the energy gain due to a two-electron, two-orbital interaction. This is the key to site-specific reactions of electrophiles and nucleophiles and the “lock and key” mechanism of enzyme–substrate binding. Let us consider the interaction of MOs,  $\phi_A$  and  $\phi_B$ , on different molecules or in different parts of the same molecule and explicitly take advantage of the approximate proportionality between  $h_{AB}$  and  $S_{AB}$ . Then, for a given energy separation, the interaction is proportional to  $h_{AB}$  (small energy separation) or  $|h_{AB}|^2$  (large

separation). Taking the former,

$$\begin{aligned} h_{AB} &\approx kS_{AB} \\ &= k \int \phi_A(1)\phi_B(1) d\tau_1 \\ &= k \sum_{a=1}^{n_A} \sum_{b=1}^{n_B} c_{aA}c_{bB} \int \chi_a(1)\chi_b(1) d\tau_1 \end{aligned} \quad (3.46)$$

$$\approx kc_{rA}c_{pB} \int \chi_r(1)\chi_p(1) d\tau_1 + kc_{sA}c_{qB} \int \chi_s(1)\chi_q(1) d\tau_1 \quad (3.47)$$

Equation (3.46) illustrates that, ultimately, the strength of the interaction between two *MOs* depends on the separation of the *AOs* of each *MO* (through the overlap integral) and on the magnitude of the product of the coefficients of those *AOs*. The last line [equation (3.47)] obtains if two atoms, *r* and *s*, of *A* can approach two atoms, *p* and *q*, respectively, of *B*, as shown by the dashed lines in Figure 3.13*b*. This is the common situation for *pericyclic* reactions discussed in Chapter 12. In the vast majority of cases, however, the contacts between two molecules are even more restrictive. Usually, only two *AOs*, one from *A* and one from *B*, are close enough to overlap; then the strength of the interaction depends just on the product of the coefficients of those orbitals and the degree of overlap that can be achieved. Conversely, two independent molecules which approach each other will orient themselves in such a way as to minimize the separation of the atomic orbitals which have the largest coefficients if the interaction is favorable or to maximize it if it is not.

## ELECTROSTATIC EFFECTS

Whenever possible, we will attempt to identify the effects of interactions between relatively few frontier orbitals, which describe the distribution of relatively few electrons of a molecule. We effectively ignore the vast numbers of the rest of the electrons in the system as well as the nuclear charges. In some cases this neglect is not justified and may lead to misleading results. When a molecule or parts of it are *charged*, coulombic interactions may dominate. The electrostatic energy of interaction of each pair of centers, *i* and *j*, with net charges, *q<sub>i</sub>* and *q<sub>j</sub>*, respectively, separated by a distance *R<sub>ij</sub>* in a medium with dielectric constant *ε<sub>m</sub>* has the form

$$E^{\text{electrostatic}} = \frac{q_i q_j}{R_{ij} \epsilon_m} \quad (3.48)$$

The energy required to separate an electron (*q<sub>e</sub>* = −1*e*) from a proton (*q<sub>p</sub>* = +1*e*) from a distance of 0.52917 Å (*R<sub>ep</sub>* = radius of H atom) to infinity in vacuum (*ε* = 1) is 13.6 or 319 kcal/mol (the ionization potential of H). This value is many times the strength of an average chemical bond. The energies involved are so large that one may generalize to say that, in any medium of low dielectric constant, charged species in solution are always paired with oppositely charged species surrounded by neutral dipolar species (if any are present) and in tight association with solvent molecules themselves.

Electrostatic effects cannot be ignored whenever a process takes place that changes the numbers of charged species. Heterolytic cleavage of *σ* bonds (see Chapter 4) would

only be expected to take place in solvents of high dielectric constant, water being the best. Electron transfer between neutral species would not be observed in the gas phase except at contact separations where salt formation is possible. Reactions of charged species with neutral but dipolar species will, at least in part, be driven by electrostatic effects.

The energies of localized orbitals will be strongly affected by the presence of formal charges. The energies of all orbitals, filled or empty, will be lowered by the presence of a formal positive charge and raised by a formal negative charge. The presence of highly polar bonds may significantly affect the energies of orbitals not directly involved in the bonding. For example, the energy of the nonbonded orbital on carbon would be expected to be lower in the  $\text{CF}_3$  free radical than in the  $\text{CH}_3$  free radical.

We will not attempt to quantify electrostatic effects but will need to be aware of possible influences as we consider our orbital interaction diagrams. Fortunately, the directions of electrostatic influences are easy to deduce from equation (3.48).

## GROUP ORBITALS

The following is a summary of the local group molecular orbitals from which one may select the primary building blocks for interaction diagrams. The orbitals are classified according to the coordination number of the central atom. The local symmetry properties and relative energies are *independent* of the atomic number of the central atom itself.

### Zero-Coordinated Atoms

The group orbitals of a zero-coordinated atom are not just the set of four valence orbitals of the atom, namely  $s$ ,  $p_x$ ,  $p_y$ , and  $p_z$ , because we will assume that for the purposes of deducing orbital interactions, it is our intention to make  $\sigma$  and possibly  $\pi$  bonds to the uncoordinated atom. Because two orbitals of the atom,  $s$  and  $p_x$ , will each interact in a  $\sigma$  fashion with a nearby atom, we mix these beforehand to form two new hybrid orbitals, one of which will interact maximally with the neighboring atom because it is pointed right at it, and another which will be polarized away from the second atom and therefore will interact minimally with it. The group orbitals of such a zero-coordinated atom are shown in Figure 3.14.

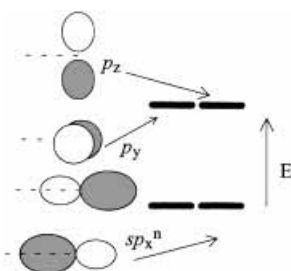


**Figure 3.14.** Group orbitals for zero-coordinated atoms hybridized for formation of a single bond.

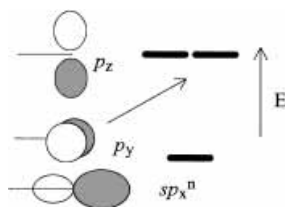


Figure 3.15. Group orbitals for monocoordinated atoms.

### Notes

- The higher energy orbitals are pure  $p$  orbitals with the same energy, that is, they are degenerate.
- One of the  $p$  orbitals will *always* be perpendicular to the plane of an adjacent group and be *antisymmetric* with respect to (w.r.t.) reflection in the plane. The other ( $p_y$ ) will lie in the plane and be *symmetric* w.r.t. reflection in the plane.
- The  $sp_x$  hybrid orbitals are shown as degenerate for convenience. One will interact maximally with an adjacent group and form a  $\sigma$  bond. The other will not interact.
- In *neutral* atoms X, the electron count for the heavy atoms is B 3, C 4, N 5, O 6, and F 7.

### Monocoordinated Atoms

Each element of coordination corresponds to the prior existence of a  $\sigma$  bond and the removal of one of the four orbitals and one of the valence electrons. In the figures that follow, the coordination is represented by an X—H  $\sigma$  bond. The group orbitals for a monocoordinated atom (excluding H) are shown in Figure 3.15. The existing bond is made from the equivalent of *one* of the hybridized valence orbitals of the atom (Figure 3.14), a hybrid orbital formed by mixing some proportion of  $s$  and  $p_x$  so as to maximize the energy associated with bond formation which is assumed to be in the  $x$  direction. This hybrid orbital is removed from the set of valence orbitals. In fact, the bond formation is accomplished using primarily the  $p_x$  orbital with minor admixture of the  $s$  orbital. The second combination of the  $s$  and  $p_x$ , mixed in inverse proportions, that is, mostly  $s$ , remains as one of the valence orbitals. It will be lower in energy than the pure  $p_y$  and  $p_z$  orbitals. The admixture (polarization) is maximum for B and C, much reduced in the case of N, and almost nonexistent for O, F, and any of the higher row elements. The remaining hybrid orbital, denoted  $sp_x^n$  in Figure 3.15, therefore is a true  $sp$  hybrid orbital for C but has a much smaller amount of  $p$  character in the case of N ( $n < 1$ ) and is almost a pure  $s$  orbital ( $n \ll 1$ ) in the case of the other first and higher row atoms. The lack of hybridization is due to the increasing energy separation between the  $2s$  and  $2p$  orbitals as one proceeds across the first row and due to the increased nodal characteristics of  $3s$ ,  $3p$ ,  $4s$ ,  $4p$ , and higher principal quantum number orbitals of the higher row elements.

### Notes

- The higher energy orbitals are pure  $p$  orbitals with the same energy; that is, they are degenerate.

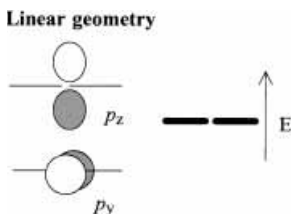


**Figure 3.16.** Group orbitals for a linear dicoordinated atom.

- (b) In a planar molecule, one  $p$  orbital ( $p_z$ ) will always be perpendicular to the plane of the molecule and be antisymmetric w.r.t. reflection in the plane. The other ( $p_y$ ) will lie in the plane and be symmetric w.r.t. reflection in the plane.
- (c) The  $sp_x$  hybrid orbital will be closest to the  $p$  orbitals for B and C and furthest for F. For O and the halogens, there will be little  $p$  character in this orbital.
- (d) In neutral hydrides  $H-X$ , the electron count for the heavy atoms is B 2, C 3, N 4, O 5, and F 6.

### Dicoordinated Atoms

Dicoordinated atoms may have either of two distinct local geometries, linear or bent. In either case, only two valence orbitals remain and the number of valence electrons for the neutral atom is reduced by 2. The valence orbitals for dicoordinated atoms in linear and bent bonding arrangements are shown in Figures 3.16 and 3.17, respectively. Which coordination geometry an atom prefers is largely a function of constraints imposed by the coordinating atoms and the number of valence electrons. For the purpose of using the group orbitals in an interaction diagram, one should have prior knowledge of which geometry is appropriate in the particular case. As in the monocoordinated case, if the dicoordinated geometry is bent, then the same factors govern the extent of hybridization of the  $sp^n$  orbital (Figure 3.17):  $n$  will be close to 2 in the case of C, less than 2 for N, and much smaller for all other atoms. In other words, the orbital will be essentially an  $s$  orbital for all atoms higher in the periodic table than C and N.

#### Notes on the Linear Geometry

- (a) The two orbitals are pure  $p$  orbitals with the same energy; that is, they are degenerate.

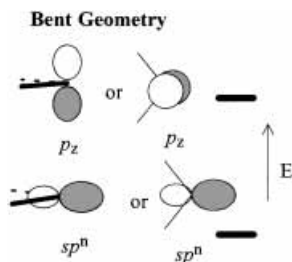


**Figure 3.17.** Group orbitals for a dicoordinated atom with a nonlinear arrangement of  $\sigma$  bonds.



- (b) In a planar molecule, one  $p$  orbital ( $p_z$ ) will always be perpendicular to the plane of the molecule and be antisymmetric w.r.t. reflection in the plane. The other ( $p_y$ ) will lie in the plane and be symmetric w.r.t. reflection in the plane.
- (c) In neutral hydrides  $H_2X$ , the electron count for the heavy atoms is B 1, C 2, N 3, and O 4.

#### Notes on the Bent Dicoordinated Geometry

- (a) The two  $\sigma$  bonds define a local plane of symmetry, assumed to be the  $xy$  plane. The  $p$  orbital ( $p_z$ ) will always be perpendicular to the local plane of the molecule and be antisymmetric w.r.t. reflection in the plane.
- (b) The  $sp$  hybrid orbital will be closest to the  $p$  orbitals for B and C and furthest for F. For O and the halogens, there will be little  $p$  character in this orbital.
- (c) The  $sp^n$  orbital lies along the bisector of the bond angle and is symmetric w.r.t. reflection in the local plane of symmetry defined by the bonds.
- (d) In neutral hydrides  $H_2X$ , the electron count for the heavy atoms is B 1, C 2, N 3, and O 4.

#### Tricoordinated Atoms

Tricoordinated atoms may also have two distinct geometric configurations, planar or pyramidal. Only one valence orbital remains, and it will be a pure  $p$  orbital in the planar case, hybridized in the pyramidal case. Both configurations for tricoordinated atoms are depicted in Figure 3.18.

#### Notes

- (a) In the planar geometry, the orbital is a pure  $p$  orbital and is antisymmetric w.r.t. reflection in the local plane of symmetry defined by the  $\sigma$  bonds.
- (b) In the pyramidal geometry, the orbital is an  $sp^n$  hybrid which lies along the local threefold axis of rotation.
- (c) In neutral hydrides  $H_3X$ , the electron count for the heavy atoms is B 0, C 1, and N 2.

#### Tetracoordinated Atoms

In many instances, the interaction of a neighboring methylene group or methyl group influences the characteristics of a functional group. The appropriate group orbitals of  $-CH_2-$  and  $-CH_3$  are shown in Figures 3.19 and 3.20, respectively.

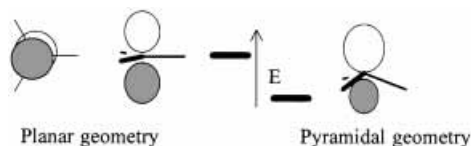


**Figure 3.18.** Group orbitals for a tricoordinated atom with planar (left) and pyramidal (right) arrangements of  $\sigma$  bonds.

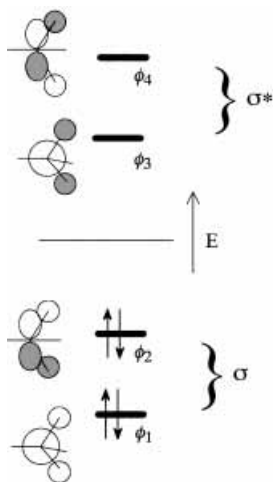


**Figure 3.19.** Group orbitals for a tetracoordinated atom as a substituent interacting through  $\sigma$  bonds. A methylene group is illustrated.

### Group Orbitals of Methylene as a Substituent ( $-\text{CH}_2-$ )

#### Notes

- (a) The bonding ( $\sigma$ ) and antibonding ( $\sigma^*$ ) MOs form two group orbitals, one of which is symmetric with respect to the local plane of symmetry ( $\phi_1$  and  $\phi_3$ ) and the other, a  $p$ -like orbital which is antisymmetric to the local plane ( $\phi_2$  and  $\phi_4$ ).

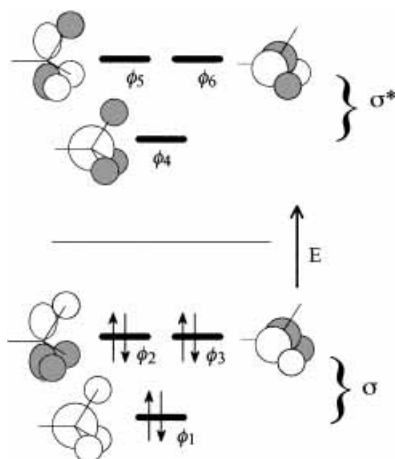


**Figure 3.20.** Group orbitals for a tetracoordinated atom as a substituent with a tetrahedral arrangement of  $\sigma$  bonds. A methyl group is illustrated.

- (b) Of each group, the higher energy orbital is formed from pure  $p$  orbitals at the central atom.
- (c) In a molecule of  $C_s$  symmetry, the  $p$ -like orbitals (e.g.,  $\phi_2$  and  $\phi_4$ ) will always be perpendicular to the plane of the molecule and be antisymmetric w.r.t. reflection in the plane. The other (e.g.,  $\phi_1$  and  $\phi_3$ ) will be symmetric w.r.t. reflection in the plane.

### ***Methyl Group as a Substituent (—CH<sub>3</sub>)***

#### **Notes**

- (a) The bonding ( $\sigma$ ) and antibonding ( $\sigma^*$ ) MOs form two group orbitals, each with a unique axially symmetric orbital ( $\phi_1$  and  $\phi_4$ ), and a pair of degenerate  $p$ -like orbitals ( $\phi_2, \phi_3$  and  $\phi_5, \phi_6$ )
- (b) Of each group, the higher energy orbitals are formed from pure  $p$  orbitals at the central atom.
- (c) In a molecule with  $C_s$  symmetry, one of the degenerate bonding and antibonding orbitals (e.g.,  $\phi_2$  and  $\phi_5$ ) will always be perpendicular to the plane of the molecule and be antisymmetric w.r.t. reflection in the plane. The other (e.g.,  $\phi_3$  and  $\phi_6$ ) will lie in the plane and be symmetric w.r.t. reflection in the plane.

## **ASSUMPTIONS FOR APPLICATION OF QUALITATIVE MO THEORY**

Gimarc has specified a set of rules for the application of qualitative MO theory [73], particularly for the determination of molecular structures and conformations, following the pioneering work of Walsh [74]. These are repeated here:

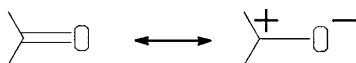
1. Electrons in molecules are completely delocalized and move in molecular orbitals which extend over the entire molecular framework.
2. For properties which can be explained by qualitative MO theory, only the valence electrons need be considered.
3. Satisfactory MOs can be formed from linear combinations of atomic orbitals (LCAO). This is the well-known LCAO–MO approximation already discussed in Chapter 2.
4. The atoms which form the molecules of a particular series or class contribute the same kinds of valence AOs from which MOs can be constructed. Therefore the MOs for each series or type of molecular framework must be qualitatively similar, and individual molecules differ primarily in the number of valence electrons occupying the common MO system.
5. The total energy of the molecule is the sum of the orbital energies of the valence electrons, or, more accurately, changes in the total energy parallel those in the orbital energy sum. Peyerimhoff and co-workers [75] have shown that this assumption results from a fortuitous cancellation of energy terms.
6. No explicit consideration of electron–electron or nuclear–nuclear repulsions are included in this simple model.
7. Molecular orbitals must be either symmetric or antisymmetric with respect to the symmetry operations of the molecule. These symmetry restrictions severely limit

the number and kinds of AOs that combine in a particular MO. This makes the job of forming the MOs even easier, since most small molecules have high symmetry. To use qualitative MO theory, the only part of group theory necessary is a knowledge of symmetry classifications (see Chapter 1).

8. From properties of AOs available on component atoms it is possible to draw pictures of what the MOs must be like and to establish the approximate order of energies without calculations.
9. Changes in molecular shape which increase the in-phase overlap between two or more AOs in a MO tend to lower the energy of that MO. Conversely, changes in shape which decrease in-phase overlap or increase out-of-phase overlap among AOs in a MO tend to raise the energy of the MO. This can be called the overlap rule.
10. No a priori assumptions about orbital hybridization are needed. As we shall see, however, simple application of the idea of hybridization will come in handy from time to time.

### EXAMPLE: CARBONYL GROUP

The carbonyl group is an important functional group in organic chemistry. It undergoes both nucleophilic and electrophilic additions and has a profound influence on the properties of neighboring groups. In this book, a separate chapter (Chapter 8) is dedicated to it. At this point we will develop the complete bonding scheme for the carbonyl group using orbital interaction diagrams:



The example will serve to illustrate application of the principles for construction of orbital interaction diagrams and also to illustrate the wealth of information which may be deduced on the basis of the diagrams. Since we are describing the existing bonding of a molecule, we imagine it to originate from the interaction of fragment orbitals. In this situation, some or all of the orbital overlaps will be large and the principles of strong interactions apply.

### CONSTRUCTION OF INTERACTION DIAGRAM

We begin the construction of the diagrams by deciding on the groups which are interacting. If we were interested in only the  $\pi$  bonds, we would note that the  $\pi$  bond is between a tricoordinated atom (the carbon atom) and a monocoordinated atom (the oxygen atom). However, we will not assume prior bonding between the carbon atom and the oxygen atom. Therefore, we will use a bent dicoordinated atom as one of our groups and a zero-coordinated atom for the other. Refer to Figure 3.21 as the development of the interaction diagram progresses. We must next decide on the placement of the groups relative to each other. Since we are attempting to understand the bonding in the carbonyl group, we will position the dicoordinated C atom and the zero-coordinated O atom in the positions and orientations that they occupy in the finished carbonyl group, using our prior knowledge of the structure of the carbonyl group. We also chose to display

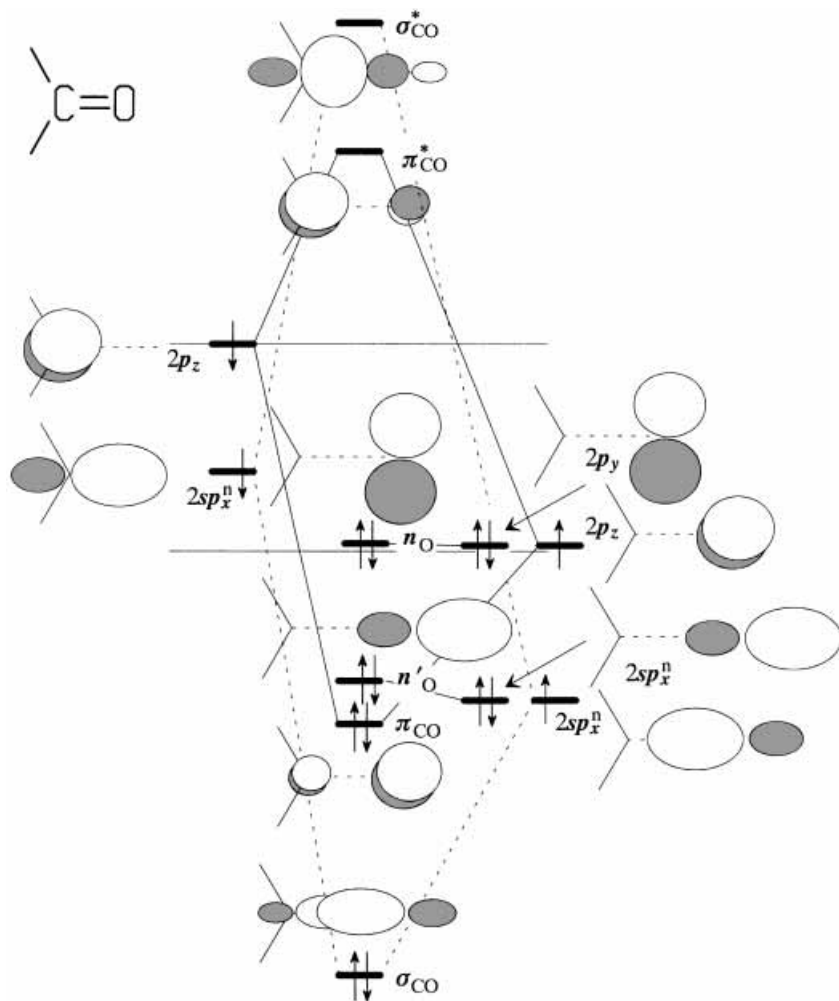


Figure 3.21. Interaction diagram for the carbonyl group.

the planar structure as lying in the plane of the paper (the  $xy$  plane), the most obvious choice. We know that the dicoordinated atom has two valence orbitals, a  $p$  orbital perpendicular to the plane of the bent  $\sigma$  bonds (a  $p_z$  orbital) and an  $sp^n$  hybrid orbital oriented along the bisector of the angle made by the  $\sigma$  bonds (the  $x$  direction) and polarized away from them (Figure 3.17). The zero-coordinated atom has four valence orbitals, two  $p$  orbitals oriented perpendicular to the direction of the incipient  $\sigma$  bond ( $p_y$  and  $p_z$ ), and two  $sp^n$  hybrids oriented along the incipient  $\sigma$  bond but polarized in opposite directions (Figure 3.14).

We must next decide on the placement of these orbitals relative to each other on the same energy scale. We have no way of doing this precisely, but we note that oxygen is substantially more electronegative than C (Table A.2 in Appendix A), and so we place the oxygen group orbitals to *lower* energy than the carbon group orbitals. The placement

on the energy scale (the vertical direction is shown by short bold horizontal lines). The positioning in space (i.e., left or right side) should be consistent with the orientation of the two groups relative to each other in space. In the present case, we have chosen oxygen to be to the right.

Our choice of orientation of the  $\sigma$  framework (as determined by the bent coordination of the dicoordinated C atom and the intended C—O  $\sigma$  bond) in the  $xy$  plane (the plane of the page) determines the orientation of the valence group orbitals. These should be drawn on the diagram beside the appropriate energy levels, each superimposed on a separate sketch of the  $\sigma$  framework, and labelled fully, as shown in Figure 3.21. All of the orbitals should be drawn about the same size, since their “weights” are equal before the interaction (their coefficients are 1).

Next we must decide which orbitals of the right and left sides interact and, approximately or relatively, how strong the interaction is. Consider first the  $sp^n$  hybrid orbital on the left-hand side. This will interact only with the  $sp^n$  hybrid orbital on the right-hand side which is pointed toward it (toward the left). The interaction is of  $\sigma$  type, and because the two orbitals overlap strongly, a large amount of stabilization ( $\Delta\varepsilon_L$ ) and destabilization ( $\Delta\varepsilon_U$ ) ensue. Make  $\Delta\varepsilon_L$  at least as large as the energy separation of the orbitals on the left- and right-hand sides of your diagram (Figure 3.21), and draw a short bold horizontal line at this position midway between the left and right energy level lines. Make  $\Delta\varepsilon_U$  even larger (by about 20%) and draw it in place the same way. Connect these four levels by thin straight lines (shown as dashed lines in Figure 3.21). The molecular orbitals,  $\phi_L$  and  $\phi_U$ , which result from the interaction must also be drawn. These should be positioned near the lines denoting their energies and positioned on the  $\sigma$  framework in a manner consistent with the uninteracted orbitals. The nature of  $\phi_L$  and  $\phi_U$  is determined by the algebra of the first part of this chapter. The lower orbital, which we may label  $\sigma_{CO}$ , consists of the two orbitals interacting in phase, with a larger contribution from the oxygen side and a smaller one from the carbon side. The actual choice of phases does not matter, only that the phases where the orbitals overlap the most are the same. The phases are best shown by shading. The *sizes* of the orbitals drawn should be proportional to the coefficients expected for them. We do not know the exact values, but we do know that the coefficients will be less than 1 as a result of the interaction, since the MO is now made up of two orbitals. Most importantly, we know that the MOs will be polarized. The lower orbital,  $\sigma_{CO}$ , is polarized toward O. The size of the contributing oxygen orbital should be drawn a little smaller than the uninteracted oxygen orbital, and the size of the in-phase carbon orbital smaller still. The upper orbital,  $\sigma_{CO}^*$ , is polarized toward C. The size of the contributing carbon orbital should be drawn a little smaller than the uninteracted carbon orbital, and the size of the out-of-phase oxygen orbital smaller still.

Consider now the  $p_z$  orbital on the left. It can overlap and therefore interact, only with one orbital on the right, the  $p_z$  orbital of oxygen. The interaction is of  $\pi$  type. Because of the smaller overlap, the  $\pi$ -type interaction is intrinsically smaller than a  $\sigma$ -type interaction between similar orbitals. This must be borne in mind in positioning the  $\pi$  and  $\pi^*$  orbitals on the diagram relative to the already placed  $\sigma$  orbitals. As a rough guide, you may take  $\Delta\varepsilon_L$  for the  $\pi$ -type interaction to be about one-half of  $\Delta\varepsilon_L$  for the  $\sigma$ -type interaction, similarly for the energies of destabilization. Having decided on the positions (Figure 3.21), draw the levels in, and label them  $\pi_{CO}$  and  $\pi_{CO}^*$ , and draw the connecting straight lines. Sketch in the MOs, bearing in mind the principles stated above in connection with the  $\sigma_{CO}$  and  $\sigma_{CO}^*$  orbitals. The only additional consideration is that the polarization of the  $\pi$  and  $\pi^*$  orbitals should be a little greater than of the  $\sigma_{CO}$  and  $\sigma_{CO}^*$  orbitals since the  $\pi$ -type overlap is smaller.

Two orbitals of the oxygen atom have not been involved in the interaction so far, the  $p_y$  orbital and the other  $sp^n$  hybrid. These are transferred to the middle of the diagram unchanged in energy or shape, although, for completeness, they should be redrawn in place; they are nonbonding orbitals of the carbonyl group,  $n'_O$  and  $n_O$ .

Lastly, one must occupy the MOs with the correct number of electrons. A neutral dicoordinated carbon atom has two valence electrons and a neutral uncoordinated oxygen atom has six, for a total of eight. Place electrons into the MOs two at a time. The HOMO is seen to be the higher nonbonding MO,  $n_O$ , and the LUMO is  $\pi_{CO}^*$ .

## INTERPRETATION OF THE INTERACTION DIAGRAM

Having carefully constructed the interaction diagram for the carbonyl group in Figure 3.21, we must now interpret it. We first make note of the frontier orbitals.

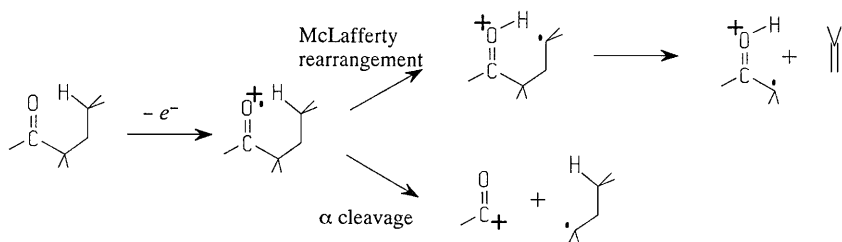
**Frontier Orbitals HOMO and LUMO.** The HOMO  $n_O$  is a nonbonding MO strongly localized to oxygen. It is predominantly a  $2p$  orbital lying in the plane of the molecule. Within the (local)  $C_{2v}$  point group, it transforms as the  $b_2$  irreducible representation. The LUMO  $\pi_{CO}^*$  is a  $\pi$  antibonding orbital strongly polarized toward the carbon atom, and relatively low in energy, at least compared to the position of the  $\pi_{CC}^*$  orbital of ethylene. We know this because the C—O  $2p-2p$   $\pi$ -type interaction matrix element  $h_{AB}$  should be similar in magnitude to the interaction between  $2p$  of carbon atoms, but the oxygen and carbon  $2p$  orbital energies are quite different, leading to a smaller  $\Delta\epsilon_U$  for  $\pi_{CO}^*$ . Within the (local)  $C_{2v}$  point group, it transforms as the  $b_1$  irreducible representation.

**Bonding.** Of the four occupied MOs, two are bonding and two are nonbonding, resulting in a net bond order of 2, that is, a double bond. Both the  $\sigma$  and  $\pi$  bonds are polarized toward oxygen, the  $\pi$  more than the  $\sigma$  because of the smaller intrinsic overlap ( $\pi$ -type overlap is smaller than  $\sigma$ -type overlap).

**Dipole Moment.** A large bond dipole moment is expected, with the negative end at oxygen and the positive end at carbon.

**Geometry.** The combination of  $\sigma$  and  $\pi$  bonds forces coplanarity of the oxygen atom, the carbon atom, and the other two atoms attached to the carbon atom.

**Ionization.** One cannot say anything about the magnitude of the ionization potential from just one interaction diagram. However, we can say with confidence that the lowest energy (strictly speaking, the ground electronic state of the) molecular ion,  $M^+$ , would correspond to a radical cation localized to the oxygen atom. With this foreknowledge, one would expect to find mass spectral fragments which arise from the McLafferty rearrangement and from rupture of the bond  $\alpha$  to the carbonyl group:



**UV Spectrum.** The lowest energy electronic transition (HOMO–LUMO) is  $n_{\text{O}}-\pi_{\text{CO}}^*$ , leading to the  $n\pi^*$  state, which has  $A_2$  symmetry in the local  $C_{2v}$  point group. The transition to this state is symmetry forbidden (it is quadrupole allowed but dipole forbidden) and will be expected to be weak.

**Photochemistry.** One might deduce that since the lowest electronic transition corresponds to transfer of an electron from an oxygen atom to a carbon atom, the  $n\pi^*$  state should have substantial diradical character and should react also by a McLafferty-type rearrangement or  $\alpha$  cleavage, as in the mass spectrometer. This is indeed the case. The photochemical  $\alpha$  cleavage is called the Norrish type I reaction, and the rearrangement is called the Norrish type II reaction. Both are discussed in Chapter 15.

## CHEMICAL REACTIVITY

To make a statement about the chemical reactivity of a substance, one must imagine *its* orbitals interacting with those of a *second* reagent. Since two reagents are involved, the initial orbital overlaps are small and the interactions will be governed by the principles of weak interactions. In the first instance, only the frontier orbitals, the HOMOs and the LUMOs, need be considered. To probe the basicity or nucleophilicity, the interaction of a proton (empty  $s$  orbital) with the HOMO is sufficient. For checking acidity in the Lewis sense, the interaction of the LUMO with the HOMO of a reference base, say the nonbonded  $sp^n$  orbital of ammonia, is appropriate. In general, the orbital interaction diagram for the interaction of two reagents is only appropriate for the initially formed van der Waals or hydrogen-bonded complex. It shows the HOMO–LUMO orbital interactions which are maximized and the HOMO–HOMO interactions which are minimized as the two reagents approach each other in the energetically most favorable way. The trajectory of approach and the orbitals involved will almost always *imply* the product, but the interaction diagram will *not* show the bonding in the product. If the orbital donating or accepting electrons is nonbonding, the newly formed bond will not greatly perturb the other bonds in the fragment. However, if a  $\sigma$  or  $\pi$  bond acts as an electron donor, that bond is weakened since it loses electrons and, in a chemical reaction, will be broken altogether. Similarly, if, as is usually the case, an empty antibonding orbital is the electron acceptor, the corresponding bond is also weakened, and if the reaction goes all the way, the bond is completely broken. The bonding of the products of a chemical reaction must be deduced with separate interaction diagrams since these are in the regime of strong interactions. In short, the weak-interaction regime and the strong-interaction regime must not be mixed in the same diagram. This can be accomplished by means of orbital *correlation* diagrams, as seen in Chapter 14.

**Basicity or Nucleophilicity.** Figure 3.22 shows the interaction diagram for the *initial* interaction between the carbonyl group and a proton (which we take to be a typical Lewis acid). This is constructed along the same principles as for the carbonyl group itself. On the left-hand side we place some or all of the orbitals derived for the carbonyl group in Figure 3.21. As stated above, only the HOMO will be required, but let us choose all of them to make the point. On the right hand side, we place the single  $1s$  orbital of the hydrogen (proton),  $s_{\text{H}}$ . Since H is slightly less electronegative than C,  $s_{\text{H}}$  should be a little above the energy level of the  $2p_{\text{C}}$  orbital of the  $\text{CH}_2$  group *prior to interaction* (see Figure 3.21). We have six carbonyl group orbitals on the left and a single



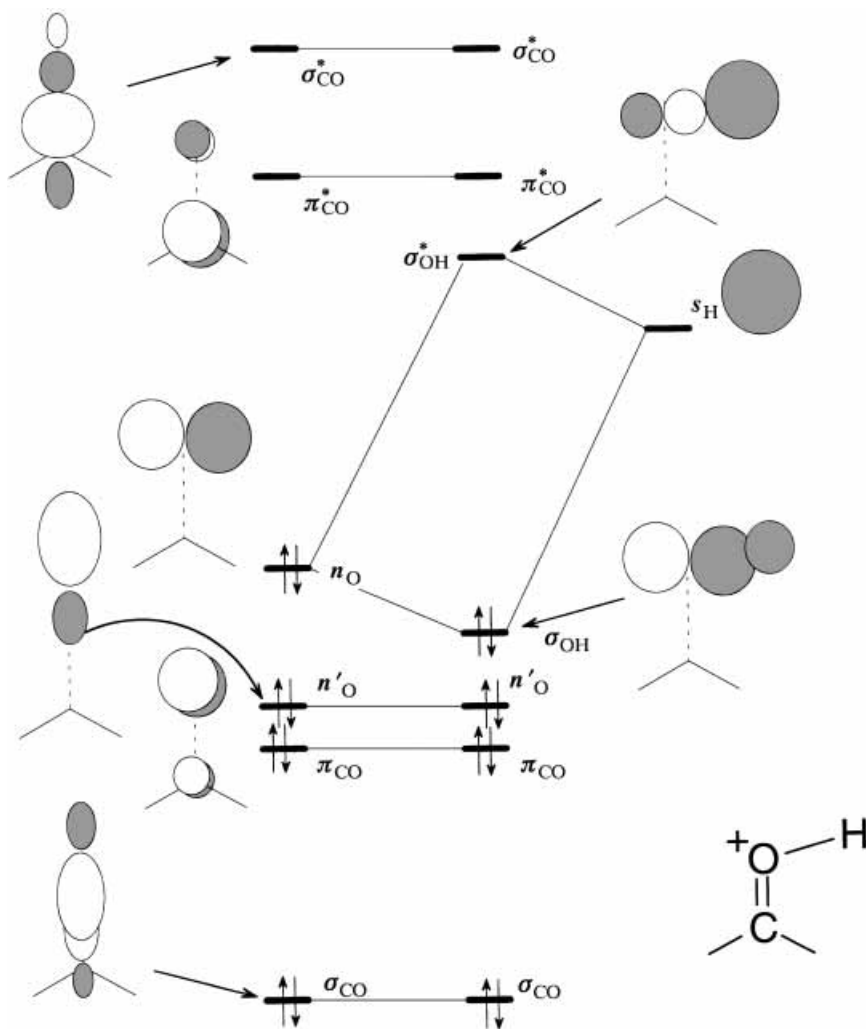


**Figure 3.22.** Interaction diagram for the carbonyl group with a proton (the electrostatic effect of the positive charge is ignored).

$s_H$  orbital on the right. What are the possible interactions between the left- and right-hand sides? Because the proton is a separate free-roaming species, the  $s_H$  orbital is not precluded by symmetry from interacting with *any* of the orbitals of the carbonyl group since it can always approach from a direction that avoids nodal surfaces. The most probable direction is the one which leads to the greatest gain in energy. Since the  $s_H$  orbital is empty, only the occupied orbitals of the carbonyl group need be considered, and it is usually safe to focus only on the HOMO since this has the smallest energy separation with an empty orbital, the LUMO  $s_H$ . Since the HOMO  $n_O$  is the  $2p_O$ , the greatest  $\sigma$ -type overlap is from a direction along the axis of the  $p$  orbital, namely in the plane of the carbonyl group, approaching the O atom from either side perpendicular to the C—O

bond. Thus, attachment of a proton or other Lewis acid would occur at the oxygen atom, in the plane of the carbonyl group, and more or less perpendicular to the C—O bond. In Figure 3.22, we show the interaction of the  $n_O$  and  $s_H$  orbitals in the most natural geometry, with the newly formed  $\sigma$  bond horizontally disposed. Notice that we have reoriented the molecular framework and all of the orbitals into the same orientation from the one in Figure 3.21. This reorientation does not affect the orbital energies. Notice that the line of approach for the HOMO–LUMO interaction brings the proton in approximately along the nodal surfaces of all of the other orbitals, so in the first instance all other possible interactions will be small and can be ignored. To make this point, Figure 3.22 is far more cluttered than it needed to be since only the orbitals connected by the interaction lines needed to be shown.

This diagram shows only the initial interaction as would be suitable for formation of a hydrogen bond. If the proton were to become attached, the  $\sigma_{OH}$  orbital would be much lower in energy and the  $\sigma_{OH}^*$  much higher. Since the donor orbital is nonbonding, addition of the Lewis acid to the oxygen is not accompanied by loss of either the  $\sigma$  or  $\pi$  bond. In this figure, we have ignored the effect of the charge. We will see in Chapters 5 and 8 that the net charge does have a dramatic effect on the remaining orbitals.

We can also crudely estimate the basicity of the carbonyl oxygen atom. Since the HOMO is strongly localized to the oxygen atom (the coefficient of  $2p_O$  is close to 1), and the oxygen atom is monocoordinated but uncharged, one should expect the Lowry–Bronsted basicity to be less than that of alkoxides, which are monocoordinated but charged.

**Acidity or Electrophilicity.** The LUMO is a  $\pi$ -type orbital polarized toward the carbon atom (the coefficient of  $2p_C$  is larger than the coefficient of  $2p_O$ ). The LUMO is also relatively low in energy. The low energy and large coefficient at carbon both suggest that the carbonyl group should be reactive as a Lewis acid or electrophile and that addition of nucleophiles (Lewis bases) would occur at the carbon atom and from a direction approximately *perpendicular* to the plane of the carbonyl group. Figure 3.23 shows another way of applying orbital interaction theory. Orbital interaction arguments are applied to deduce trajectories of attack of a nucleophile to the carbonyl group by showing the HOMO of the nucleophile (ammonia in this case) and the LUMO of the carbonyl. The best approach, which avoids both nodal surfaces of the  $\pi_{C=O}^*$  orbital (the nodal plane

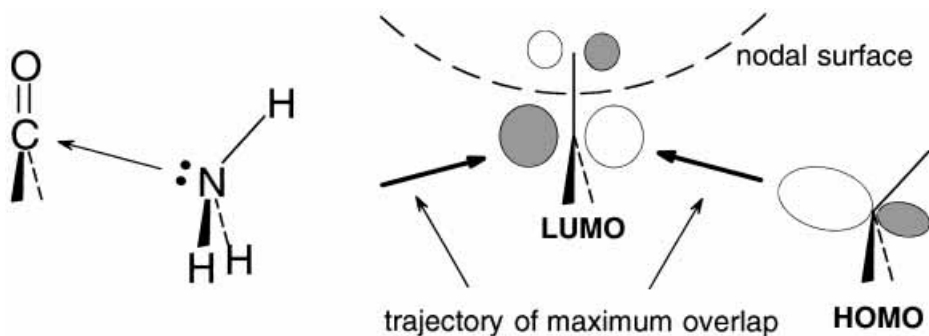


**Figure 3.23.** Trajectory of nucleophilic attack on a carbonyl group deduced from orbital interaction theory.

which defines the  $\pi$ -type orbital is not shown), is indicated by an arrow in Figure 3.23. It is along a line that makes an angle somewhat greater than  $90^\circ$  with the CO bond. Attachment of a Lewis base means addition of electrons to the  $\pi_{\text{CO}}^*$  orbital and is accompanied by loss of the  $\pi$  bond (if both bonding and antibonding orbitals are equally occupied, there is no bond).

## WHY DOES IT WORK AND WHEN MIGHT IT NOT?

The application of orbital interaction theory to understand the electronic structures of molecules, as illustrated in the case of the carbonyl group in Figure 3.21 above, is one of two conceptually distinct applications. Characteristics of the bonding and structure of the molecule were deduced from interactions of the group orbitals situated as they would be in the “finished” molecule. This application is in the regime of strong interactions and short distances, the regime in which the foundations of orbital interaction theory, one-electron theory as exemplified by Hartree–Fock theory, have a firm footing and a demonstrated record of successes. Since the electrons are confined to a small region of space, lack of specific account of electron correlation is not serious in that its inclusion would not substantially affect the one-electron description, or the error incurred may be assumed to be reasonably constant when comparing different conformations.

The second broad area of application of orbital interaction theory is in the area of intermolecular interactions, from which many aspects of chemical reactivity may be inferred. This application, as exemplified in Figures 3.22 and 3.23, is in the realm of weaker interactions and larger distances, conditions suitable to application of perturbation theories. The dominant orbital interactions in this regime are of the two-electron, two-orbital type, and usually, a single orbital interaction between the HOMO of one molecule and the LUMO of the other is sufficient for the purpose. Unfortunately, the one-electron theoretical foundation for this kind of long-range interaction involving electron transfer is much less sound. Accurate descriptions of weak interactions usually require theoretical procedures which go beyond Hartree–Fock theory for the reason that some account must be taken of the correlation of the electron motions, particularly within the same orbital. The reason for this is easy to understand and is illustrated in Figure 3.24. Prior to interaction (Figure 3.24*a*), the electrons are localized to the HOMO of the donor, B. At intermediate separations (Figure 3.24*b*), where the orbitals of A and B overlap, the space available to the electrons is greatly increased and the electrons are able to separate. After bond formation (Figure 3.24*c*), the space available to the electrons is again restricted. In the intermediate stage (Figure 3.24*b*), the lack of electron correlation inherent in one-electron theories is most strongly felt. In terms of valence bond structures, MO theory places comparable emphasis on the three structures  $R_1$ ,  $R_2$ , and  $R_3$ , whereas, in reality, resonance structure  $R_2$  alone most accurately represents the true situation. Resonance structure  $R_2$  corresponds to a configuration in which a single electron has been transferred from B to A. The reactivity of B as a donor (nucleophile) is expected to be correlated with its ionization potential [76]. Likewise, the reactivity of A as a Lewis acid should be correlated with the electron affinity of A. Post-Hartree–Fock theoretical analyses of heterolytic bond breaking [77] and the reverse, cation–anion combination reactions [78], have elucidated the role of the missing electron correlation. In the valence bond configuration mixing (VBCM) treatment of Shaik [9, 78], the valence bond configurations of reacting species are regarded as “surfaces” whose avoided crossing defines the barrier to the reaction. The Hartree–Fock model is expected to work well

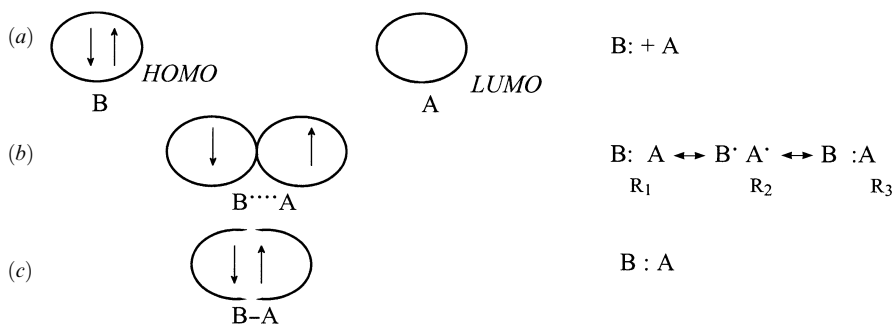


**Figure 3.24.** Stages in the interaction between two molecules, B and A, showing the effects of electron correlation and the equivalent resonance structures: (a) no interaction, the electrons are spin paired and confined to the orbital of B; (b) weak interaction (e.g., a transition structure), the electrons can separate into a larger volume of space; (c) strong interaction, a bond is formed and the electron distribution is again confined.

when the electronic description involves a single closed-shell configuration (Figures 3.24a,c) but overestimate the effect of electron–electron repulsion in the extended case (Figure 3.24b). It is not surprising, then, that Hartree–Fock calculations tend to overestimate the energy of the transition state for intermolecular reactions. This failure should not be interpreted as a general failure of the one-electron model as an interpretive device, but rather as an inappropriate energy counting for the MO description due to the fact that electron–electron repulsions are accommodated in an average way. The MO description remains as a powerful and conceptually simple means for understanding the bonding even in the region of the transition state, and such MO descriptions are derivable by the simple rules of orbital interaction theory.

Particularly for the intermolecular case illustrated by Figure 3.24, it is tempting to use experimental studies carried out in the gas phase, or the results of high quality *ab initio* calculations (carried out in *vacuo*), as a “test” of the validity of orbital interaction theoretical predictions. In the gas phase, one expects to have the “pure” orbital interactions, free of the complex contributions from the solvent. This expectation is *not* justified under some well-defined circumstances beyond those described immediately above. The effects of electrostatic interactions, discussed briefly above, are unquenched in the absence of an intervening medium. Such interactions, particularly between charged and/or strongly dipolar species, may completely overwhelm the more subtle interactions due to the frontier orbitals. Thus gas-phase experiments and theoretical calculations on ionic or polar molecules may in no way reflect on the interactions of orbitals because electrostatic interactions have a very high potential and are very long range. In a solvent of high dielectric constant, these are greatly ameliorated, permitting orbital interactions to dominate. Indeed, it has been shown by *ab initio* calculations in the presence of a medium (modeled as a continuum) that groups become less electronegative and less hard with increasing dielectric constant [79]. Thus the electronegativity of a methyl group in water is decreased by about 75% relative to its gas-phase value.

Molecular orbital calculations also do not provide an easily interpretable picture in terms of group orbital interactions for several reasons. First, the basis set does not consist of group orbitals but rather AO-like functions from which group orbitals are also constructed. Second, by definition, an MO calculation takes into account all possible

group orbital interactions, and it may be difficult to identify the dominant two-orbital interaction on which our application of orbital interaction theory depends, a matter of not seeing the forest for the trees. As a case in point, the structures of 1-methylcyclohexyl carbocation as predicted by *ab initio* MO calculations are readily interpreted in terms of a two-orbital interaction diagram such as Figure 3.9, which describes the hyperconjugative interaction between the cationic site and adjacent C—H or C—C sigma bonds. However, evidence of the bonding interaction is completely obscured among the many occupied orbitals of the molecule. One needed to seek evidence of the bonding by examining the antibonding interactions in the more highly localized LUMO [80, 81]!

## CHAPTER 4

---

# SIGMA BONDS AND ORBITAL INTERACTION THEORY

---

### C—X $\sigma$ BONDS: X = C, N, O, F AND X = F, Cl, Br, I

Consider the interaction between two  $sp^n$  hybridized orbitals of unequal energy interacting in a  $\sigma$  fashion. The interaction diagram is illustrated in Figure 4.1a. Notice that the hybridization of the  $sp^n$  group orbitals in the  $\sigma^*$  orbital appears to be turned inside out. This is in recognition that much cancellation will occur due to the node in the middle. The lowest energy configuration has two electrons with energy  $\varepsilon_L$ , as shown. Not much can be said about the absolute magnitudes of  $\Delta\varepsilon_L$  and  $\Delta\varepsilon_U$ , but we are concerned here with trends. The first series (C, N, O, F) involves atoms which are very approximately the same size but differing greatly in electronegativity. The interaction matrix element,  $h_{CX}$ , will be essentially constant across the series X = C, O, N, F. However, relatively large changes will occur in the difference in orbital energies, the quantity  $\varepsilon_C - \varepsilon_X$  increasing in the series. The consequent energies of the resulting  $\sigma$  and  $\sigma^*$  orbitals are shown in Figure 4.2. In each of the two interaction diagrams shown and the two implied in between, the energy of the  $sp^n$  orbital of the C atom is drawn at the same level. The energies of both the bonding  $\sigma$  orbital and the antibonding  $\sigma^*$  orbital decrease, being the lowest for the C—F bond. The greatest polarization also occurs in the case of the C—F bond. In particular, the low-lying  $\sigma^*$  orbital is highly polarized toward the C end of the bond.

The second series, involving bonding of C to different halogens (F, Cl, Br, I) involves atoms which are very different in size and also differing greatly in electronegativity. The halogen ends of the bonds are constructed from  $2p$ ,  $3p$ ,  $4p$ , and  $5p$  orbitals, respectively. The overlap, and therefore the interaction matrix element,  $h_{CX}$ , will decrease very rapidly across the series, X = F, Cl, Br, I. Relatively large changes will also occur in the difference in orbital energies, the quantity  $\varepsilon_C - \varepsilon_X$  decreasing in the series. The relative properties and reactivities of C—X bonds are consistent with dominance of the interaction matrix element (i.e., overlap dependence) in determining the resulting orbital

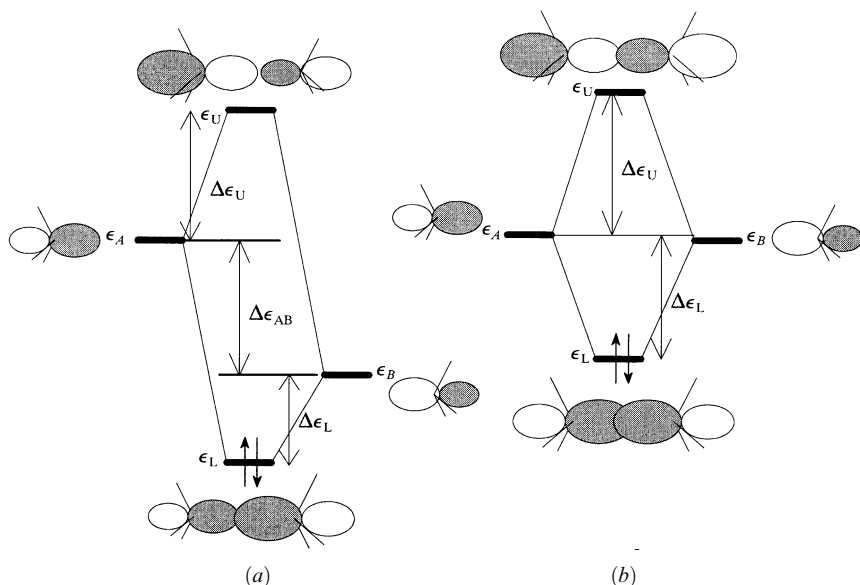


Figure 4.1. (a) A  $\sigma$  bond between atoms of different electronegativity; (b) homopolar  $\sigma$  bond.

energies. The consequent energies of the resulting  $\sigma$  and  $\sigma^*$  orbitals are shown in Figure 4.3. The  $\sigma_{CX}^*$  decreases along the series and the  $\sigma_{CX}$  bond increases. The predicted trend in  $\sigma_{CX}$  bond energies is observed in the bond ionization potentials [82]. The lowest lying  $\sigma^*$  orbital is expected to be that of the C—I bond.

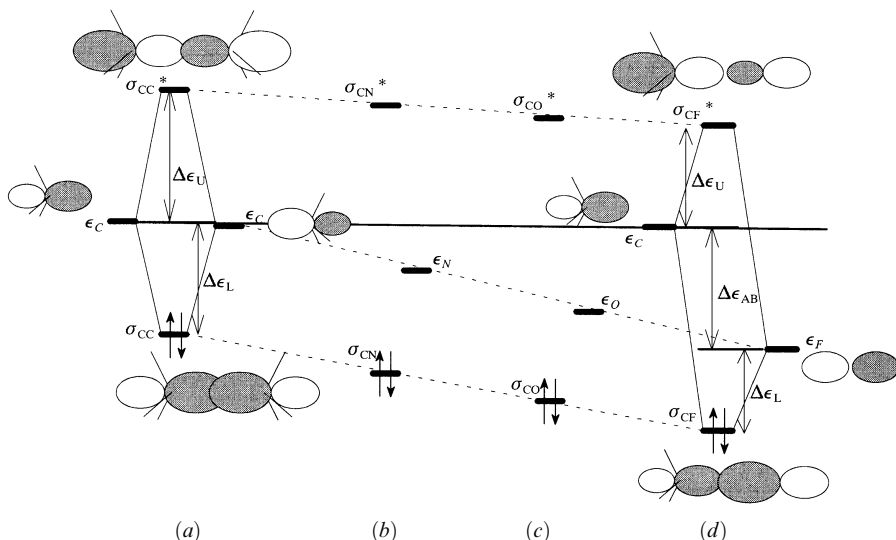
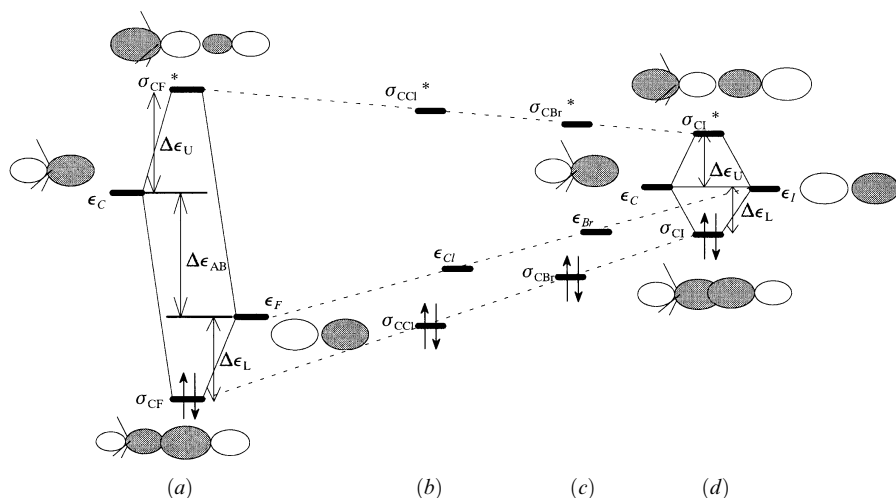


Figure 4.2. The  $\sigma_{CX}$  bond and  $\sigma_{CX}^*$  antibond between atoms of the first row: (a) X = C; (b) X = N; (c) X = O; (d) X = F.



**Figure 4.3.** The  $\sigma_{CX}$  bond and  $\sigma_{CX}^*$  antibond between different halogens: (a) X = F; (b) X = Cl; (c) X = Br; (d) X = I. No attempt has been made to show the increased size or nodal character of the  $p$  orbitals of Cl, Br, or I.

## $\sigma$ BONDS: HOMOLYTIC VERSUS HETEROLYTIC CLEAVAGE

### Heterolytic Cleavage of $\sigma$ Bonds Involving C or H

In heterolytic bond cleavage, both electrons end up on system  $B$ . The energy change associated with the bond dissociation is just the difference between electron energies before ( $2\epsilon_L$ ) and after ( $2\epsilon_B$ ), equation (4.1) and Figure 4.1:

$$\Delta E^{\text{het}} = -2(\epsilon_L - \epsilon_B) = 2\Delta\epsilon_L \approx \frac{2h_{AB}^2}{\Delta\epsilon_{AB}} \quad (4.1)$$

The last approximation in equation (4.1) is only really valid for the small-overlap regime, which this is not, but it serves to remind us of the approximately inverse energy dependence of the stabilization. One may ask how  $\Delta E^{\text{het}}$  would be expected to change in the series C—C, C—N, C—O, and C—F or the series H—C, H—N, H—O, and H—F. In the crudest approximation, one may say that the orbitals of C, N, O, and F are all approximately the same size and therefore the interaction matrix element  $h_{AB}$  will be approximately the same size for any A—B pair. The dominant factor determining the heterolysis energy therefore is the difference in orbital energies in the denominator, and one has directly the prediction (Figure 4.2) that ease of heterolytic cleavage for C—X is in the order C > N > O > F. The C—C bond is least likely to dissociate heterolytically and the C—F bond the most likely. In an absolute sense, of course, heterolytic cleavage is not a likely process for any of these bonds in the absence of other factors, as discussed below.

Similarly, one may ask how  $\Delta E^{\text{het}}$  would be expected to change in the series C—F, C—Cl, C—Br, and C—I. The situation is more complicated for this series, since both



the electronegativity and orbital size vary. Variation in orbital size is approximately proportional to  $n^2$ , where  $n$  is the principal quantum number of the valence shell. The larger the discrepancy in orbital sizes, the smaller is the effective overlap and the smaller is the interaction matrix element,  $h_{AB}$ . It should be noted that because of the smaller overlaps, the last approximation in equation (4.1) is more valid for higher elements. Thus the change in orbital energies suggests that the heterolytic cleavage should be most difficult for the C—I bond, and the change in the interaction matrix element suggests the opposite. The interaction matrix element takes on double importance since the stabilization energy varies as the square of it. Whenever orbital interaction considerations involve opposing effects, one must have recourse to experiment or higher level theory to elucidate the dominant factors. Evidently for halides, the change in  $\Delta E^{\text{het}}$  is dominated by the change in  $h_{AB}$ , and heterolytic cleavage of the C—I bond is easier than that of the C—Cl bond. The C—Br bond is intermediate. The most difficult to cleave heterolytically is the C—F bond. One must bear in mind that heterolysis occurs only in polar media where additional bond forming (to solvent) takes place. Heterolysis of the C—F bond is rarely observed. Likewise, the observed Lowry–Bronsted acidity of the H—X acids is in the order  $\text{HI} > \text{HBr} > \text{HCl} > \text{HF}$ , as is consistent with the relative energies of the  $\sigma^*$  orbitals or dominance of overlap considerations (Figure 4.3). Heterolytic cleavage of neutral molecules in the gas phase is never observed. The energy required to separate charges, of the order of the ionization potential of the H atom (13.6 eV, 1313 kJ/mol), is prohibitively high. However, it is readily compensated by solvation in polar solvents, especially water. Since solvation energies are very large, the simple theory proposed to this point could only rationalize gross trends. Heterolytic cleavage of *charged* species in mass spectrometric and negative-ion cyclotron resonance experiments is commonly observed.

### Homolytic Cleavage of $\sigma$ Bonds Involving C or H

The energy change associated with homolytic bond dissociation is given by the equation (Figure 4.1)

$$\Delta E^{\text{hom}} = -2\varepsilon_L + \varepsilon_A + \varepsilon_B = 2\Delta\varepsilon_L + \Delta\varepsilon_{AB} \approx \frac{2h_{AB}^2}{\Delta\varepsilon_{AB}} + \Delta\varepsilon_{AB} \quad (4.2)$$

Thus, the energy difference of the final singly occupied orbitals must also be considered. How would  $\Delta E^{\text{hom}}$  be expected to change in the series C—C, C—N, C—O, and C—F or the series H—C, H—N, H—O, and H—F? Recognizing, as before, that the orbitals of C, N, O, and F are all approximately the same size and therefore the interaction matrix element,  $h_{AB}$ , will be approximately the same size for any A—B pair, the dominant factor determining the homolytic bond dissociation energy therefore is the difference in orbital energies, which appears in the denominator of the first term and as the second term. The two terms have the opposite effect on the bond dissociation energy. To a first approximation, the bond energies are expected to be similar if  $\Delta\varepsilon_{AB}$  is small compared to  $|h_{AB}|$ , for example, C—C and C—N, and dominated by the second term if  $\Delta\varepsilon_{AB} > |h_{AB}|$ , for example, C—O and C—F.

Similarly, one may ask how  $\Delta E^{\text{hom}}$  would be expected to change in the series C—F, C—Cl, C—Br, and C—I or the series HF, HCl, HBr, and HI. The situation is simpler for these series, since both the electronegativity and orbital size vary but have the same effect on the bond dissociation energy. Variation in orbital size is approximately pro-

TABLE 4.1. Average Homolytic Bond Dissociation Energies (kJ/mol) of R—X

R	X = CH <sub>3</sub>	X = NH <sub>2</sub>	X = OH	X = F	X = Cl	X = Br	X = I
H	439	460	498	569	432	366	299
CH <sub>3</sub>	368	364	381	456	351	293	234

Source: *CRC Handbook*, CRC Press, Boca Raton, FL.

portional to  $n^2$ , where  $n$  is the principal quantum number of the valence shell. The larger the discrepancy in orbital sizes, the smaller is the effective overlap and the smaller is the interaction matrix element,  $h_{AB}$ . It was argued above that for halides the first term is dominated by the change in  $h_{AB}$ . Since the electronegativity, and therefore  $\Delta\epsilon_{AB}$ , also decreases, one expects homolytic bond dissociation energies of the C—X bonds to be in the order C—I < C—Br < C—Cl < C—F [83]. Likewise, the observed strengths of the bonds of the H—X acids are in the order HI < HBr < HCl < HF, as is consistent with the dominance of overlap considerations. Actual bond strengths at 298 K are shown in Table 4.1.

### Homonuclear $\sigma$ Bonds C—C, N—N, O—O, F—F, Cl—Cl, Br—Br, and I—I

Although our primary emphasis here is on  $\sigma$  bonds to C and H, we will make a brief examination of the other first-row homonuclear  $\sigma$  bonds and the interhalogen bonds. Peroxides and the halogens are important reagents in organic chemistry. Orbital interaction theory will indicate how they react and why. The  $\sigma$  bonds C—C, N—N, O—O, and F—F are compared in Figure 4.4. Following the principles expounded above, the energy changes as a consequence of the interaction,  $\Delta\epsilon_L$  and  $\Delta\epsilon_U$ , are the same for the homonuclear first-row  $\sigma$  bonds. The resulting orbitals are not shown; they are not polarized since the interacting orbitals are degenerate. The implication of constant  $\Delta\epsilon_L$  is that the homolytic bond dissociation energies (BDEs) are the same. This inference is

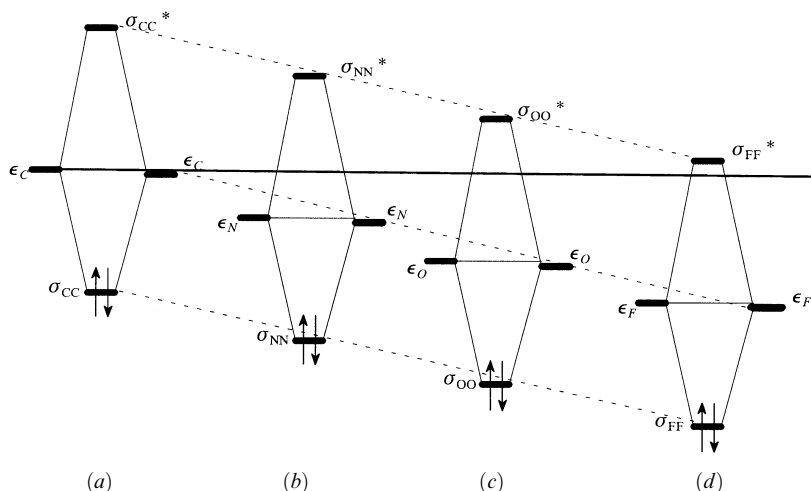
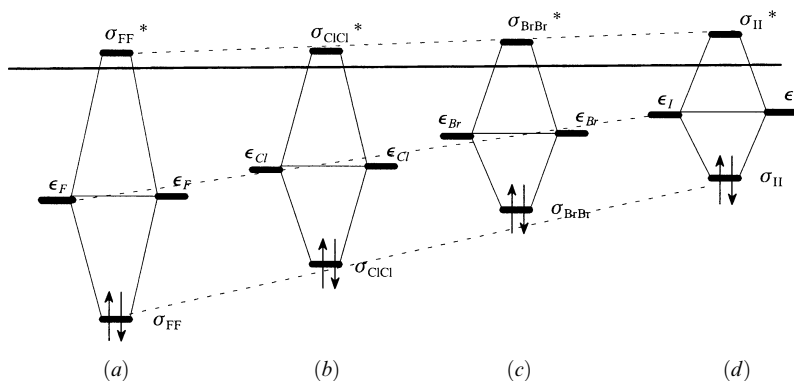


Figure 4.4. Homonuclear  $\sigma_{XX}$  bond and  $\sigma_{XX}^*$  antibond between atoms of the first row: (a) X = C; (b) X = N; (c) X = O; (d) X = F.



**Figure 4.5.** Homonuclear  $\sigma_{XX}$  bond and  $\sigma_{XX}^*$  antibond between the halogens: (a) X = F; (b) X = Cl; (c) X = Br; (d) X = I.

not quite justified since each of the heteroatoms has occupied nonbonded orbitals which interact in a repulsive four-electron, two-orbital interaction. Conformational changes occur to minimize the repulsive interactions in the case of N—N and O—O. The twisted conformations of hydrazines and peroxides arise from this avoidance. In the case of peroxides, and especially halogens, significant repulsive interactions remain and the O—O and F—F bonds are significantly weaker.

The most dramatic observation in Figure 4.4 is the reduction in the energy of the  $\sigma^*$  orbitals, the LUMO, in the series. As a consequence, the oxy and halo compounds are strong Lewis acids (subject to nucleophilic attack) and strong oxidizing agents (can readily accept electrons).

The interhalogen  $\sigma$  bonds are compared in Figure 4.5. In this case, the intrinsic interaction matrix element decreases rapidly along the series F, Cl, Br, I, as does the electronegativity. The homolytic BDE will also decrease in the series, although not as fast since there will be less repulsion due to the lone pairs; because of the very small  $\pi$ -type overlap of  $np$  orbitals ( $n > 2$ ),  $\Delta\epsilon_L \approx \Delta\epsilon_U$ . The opposite directions of  $\epsilon_X$  and  $\Delta\epsilon_L$  suggest that the  $\sigma_{XX}^*$  orbital remains low and all of the halogens are good electrophiles and strong oxidants.

## INTERACTIONS OF $\sigma$ BONDS

In our discussion of the interactions of  $\sigma$  bonds, we will focus principally on bonds to carbon or to hydrogen or both. For most organic compounds (excluding those with three-membered rings, see below), the C—C or C—H  $\sigma$  bonding orbital is too low in energy for the bond to function effectively as an electron donor toward unoccupied orbitals of other molecules or other parts of the same molecule. Likewise, the  $\sigma^*$  antibonding orbital is too high in energy to function as an electron acceptor from occupied orbitals of the main-group elements, either inter- or intramolecularly. A dramatic exception to this generalization is in their interaction with coordinatively unsaturated transition metal complexes, which may be simultaneously excellent donors and acceptors. The reactivity of  $\sigma$  bonds will be discussed in greater detail in other chapters, but general principles can be expounded here.

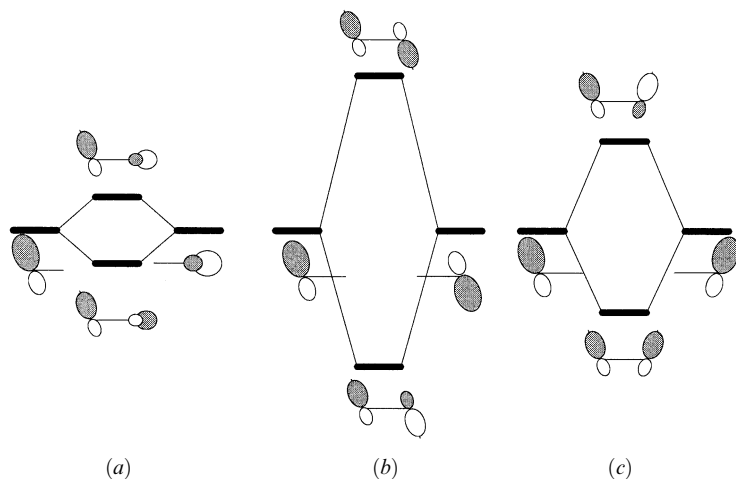


**Figure 4.6.** Diagrams for the interaction of two adjacent  $\sigma$  bonds (only the two adjacent  $sp^n$  hybrid ends are shown): (a) perpendicular geometry; (b) anti coplanar; (c) syn coplanar.

There is ample evidence that  $\sigma$  bonds do interact with other *occupied* orbitals and that  $\sigma^*$  orbitals interact with other *empty* orbitals. Evidence for the latter case is primarily in the form of chemical activation of C—H bonds by adjacent groups with low-lying empty or half-filled orbitals. The increased acidity of C—H bonds, that is, reactivity with Lewis bases, under these circumstances is discussed in Chapter 10. Several examples will serve to exemplify the interaction of  $\sigma$  bonds with adjacent filled orbitals.

In the following discussion, the  $\sigma$  bond will be represented by the  $sp^3$  hybrid orbital of the C atom. The important point to note is that this orbital is 75%  $p$  character and interacts with immediately adjacent neighbouring groups, including other  $\sigma$  bonds, in a  $\pi$  fashion. Interaction of  $\sigma$  bonds with neighboring  $\sigma$  bonds depends on the orientation of one bond relative to the other (Figure 4.6). It is clear that the interaction is minimized (but not zero) when the two bonds are perpendicular to each other (Figure 4.6a) since then the adjacent  $sp^n$  hybrid orbitals lie approximately in each other's nodal planes. It is not immediately obvious, however, whether the coplanar anti (Figure 4.6b) or the coplanar syn (Figure 4.6c) arrangement results in maximum interaction. In fact, a large body of experimental data has been interpreted to show that the coplanar anti arrangement represents the strongest interaction between adjacent  $\sigma$  bonds [6, 84]. Rates of electron transfer through chains of saturated C—C bonds confirm the anti configuration is the most effective for promoting through-bond coupling [85]. The interactions are repulsive in the four-electron case ( $\sigma$ – $\sigma$ ), attractive in the two-electron case ( $\sigma$ – $\sigma^*$ ), as expected. It has been demonstrated that the attractive  $\sigma$ – $\sigma^*$  interactions are more important than the repulsive  $\sigma$ – $\sigma$  interactions and are responsible for the rotational barrier in ethane and ethanelike molecules,  $H_3X$ — $YH_3$  (X, Y = C, Si, Ge, Sn, Pb) [86].

As well as the relative orientation of the bonds, the extent of interaction will depend on the polarizations of the bonds. Bonds from C to an element less electronegative than C will have the larger coefficient on C in the  $\sigma$  orbital and smaller in the  $\sigma^*$  orbital. Therefore, the two  $\sigma$  bonds will experience a stronger interaction than the two  $\sigma^*$  orbitals. This situation is depicted in Figure 4.7a. This is the case if the substituent is a metal.

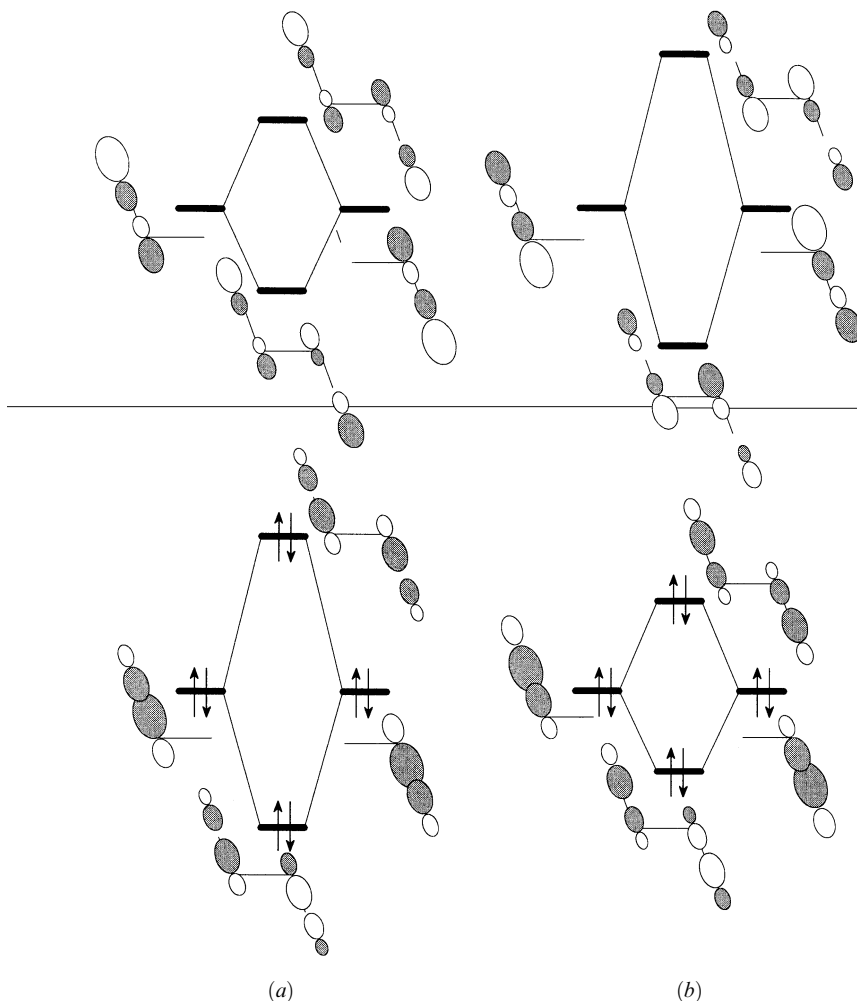
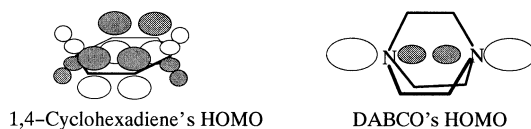


**Figure 4.7.** Diagrams for the interaction of two adjacent  $\sigma$  bonds with C bonded to (a) a less electronegative group and (b) a more electronegative group.

On the other hand, bonds from C to an element more electronegative than C (the normal situation with most substituents) will have the larger coefficient on C in the  $\sigma^*$  orbital and smaller in the  $\sigma$  orbital. Therefore, the two  $\sigma$  bonds will experience a weaker interaction than the two  $\sigma^*$  orbitals. This situation is depicted in Figure 4.7b. Carbon and hydrogen have similar electronegativities, and so C—C and C—H bonds are essentially nonpolarized. However, it does not follow that the intrinsic interaction between two  $sp^n$  hybridized orbitals (i.e., the C—C  $\sigma$  bond) is the same as the intrinsic interaction of an  $sp^n$  orbital and a  $1s$  orbital (the C—H bond). Relative C—C and C—H bond dissociation energies (see, e.g., Table 4.1) suggest that the C—C interaction is weaker and that the C—C bond will be higher in energy than a C—H bond. Conversely, the  $\sigma^*$  orbitals are reversed, that of the C—C bond being lower.

As discussed at the end of Chapter 3, one group orbital of a methyl or methylene group will always have the correct nodal characteristics to interact with an adjacent  $\pi$  orbital or with an adjacent  $sp^n$  orbital in a “ $\pi$  fashion.” The degree of interaction may be inferred from the energies of the orbitals, which may in turn be obtained by measurements of ionization potentials and application of Koopmans’ theorem. Thus, the methyl groups adjacent to the  $\pi$  bond in (*Z*)-2-butene (ionization potential IP = 9.12 eV [63]) raise the energy of the  $\pi$  orbital by 1.39 eV relative to that of ethylene (IP = 10.51 eV [87]). A similar effect is observed in cyclohexene [64].

The through-space interaction of the two  $\pi$  bonds of norbornadiene was presented in Chapter 3 as exemplifying a four-electron, two-orbital interaction. The interaction of the nonconjugated  $\pi$  bonds of 1,4-cyclohexadiene cannot be treated in the same way:



The planar molecular skeleton reduces the direct interaction between the two  $\pi$  bonds while increasing the interaction of the  $\pi$  bonds with the intervening  $\text{CH}_2$  groups. As a consequence, the *in-phase* combination of the two  $\pi$  bonds suffers a repulsive interaction with the *in-phase* combination of the higher of the  $\text{CH}_2$  group orbitals and is raised above the *out-of-phase* combination to become the HOMO of the molecule. The interaction diagram is shown in Figure 4.8. The consequences of such through-space and

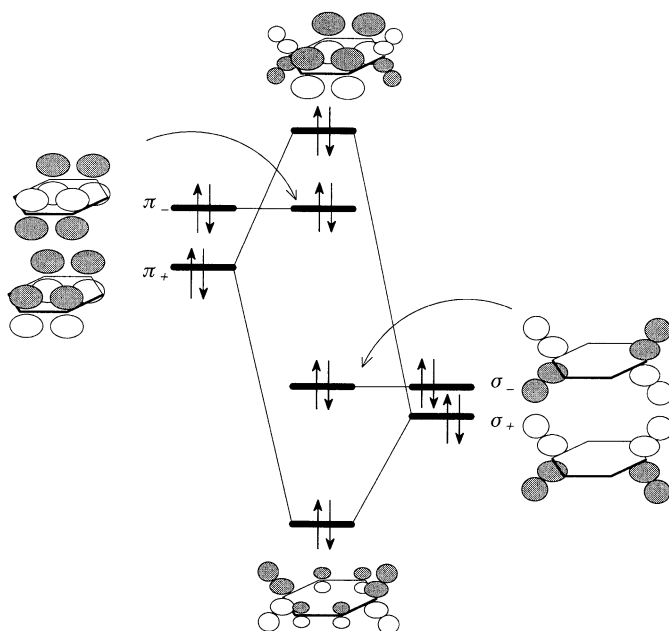


**Figure 4.8.** The  $\sigma$ - $\pi$  interactions in 1,4-cyclohexadiene.

through-bonds interactions on the ionization potentials of a number of nonconjugated dienes as a function of skeletal structure and substitution has been investigated [88].

The spectroscopic and chemical properties of 1,4-diazabicyclo[2.2.2]octane (DABCO) are consistent with a strong interaction of the in-phase combination of the nonbonded electron pairs of the nitrogen atoms with the symmetric combination of the C—C  $\sigma$  bonds, one consequence of which is that the in-phase combination is the HOMO. The two lowest IPs are 7.6 and 9.7 eV [89]. Compare these to the IPs of trimethyl amine (8.44 eV) and ammonia (10.5 eV) [90]. The relative importance of intramolecular orbital interactions through space and through bonds has been reviewed by Hoffmann [6].

## $\sigma$ BONDS AS ELECTRON DONORS OR ACCEPTORS

With respect to the ability of  $\sigma$  bonds to accept or donate electrons, several circumstances may act to change the norm (which is that they are neither donors nor acceptors). Substituents adjacent to the  $\sigma$  bond may act to raise the energy of the bonding orbital or to lower the energy of the  $\sigma^*$  antibonding orbital and thereby increase the involvement of the bond in two-electron, two-orbital interactions. Whether the bond acts as a donor in an interaction with a low-lying virtual orbital or as an acceptor in an interaction with a high-lying occupied orbital, the consequences for the bond are the same, a reduction of the bond order and a consequent weakening of the bond. The extreme consequence is a rupture of the bond, as occurs in a hydride transfer or a nucleophilic substitution ( $S_N2$ ). When the interaction does not “go all the way,” the bond weakening is often apparent in the infrared spectrum as a shift to longer wavelength of the bond-stretching frequency and a lengthening of the bond itself. The fact that both consequences are usually observed has suggested an inverse relationship between bond strength as measured by the force constant and the bond length [91]. This relationship, which is widely accepted, has no direct theoretical derivation, and exceptions, particularly in the case of N—F bonds, have been noted and attributed to “polar” effects [92].

## $\sigma$ BONDS AS ELECTRON ACCEPTORS

The acceptor ability may be improved in two ways, by lowering the energy of the  $\sigma^*$  orbital and by polarizing the orbital toward one end. The first improves the interaction between it and a potential electron donor orbital by reducing the energy difference,  $\epsilon_A - \epsilon_B$ , the second by increasing the possibility of overlap and therefore increasing the value of the intrinsic interaction matrix element,  $h_{AB}$ .

### As a $\sigma$ Acceptor

The general features (orbital distribution and energy) for a  $\sigma$  bond between C and a more electronegative element or group, X, are shown in Figures 4.1a, 4.2, and 4.3, where center *A* is carbon and center *B* is X. The energy of the  $\sigma^*$  orbital will be relatively low and the orbital is polarized toward carbon. Optimum interaction between the  $\sigma^*$  orbital and a localized nonbonding orbital of a Lewis base will occur along the axis of the orbital and from the carbon end, as shown in Figure 4.9a. The two-orbital, two-electron interaction is accompanied by charge transfer into the  $\sigma^*$  orbital and consequent reduction of

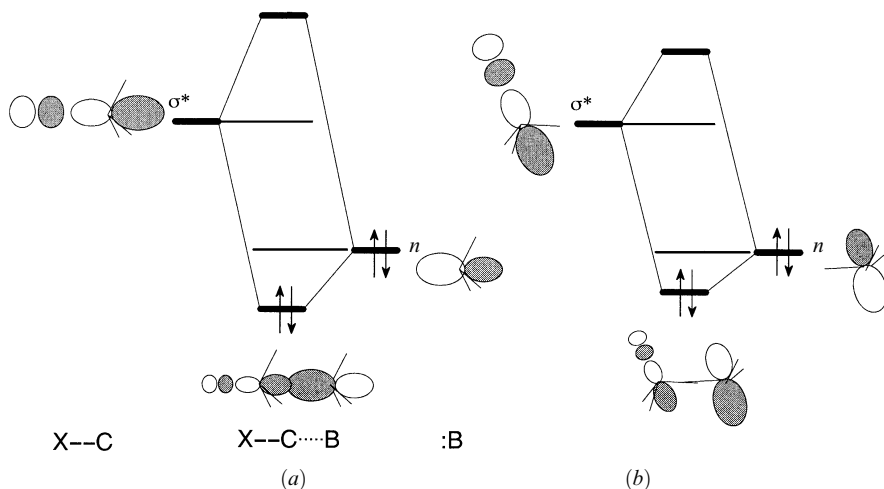


**Figure 4.9.** (a) Sigma-type acceptor interaction between the HOMO,  $n$ , of a base and the LUMO,  $\sigma^*$ , of a polarized  $\sigma$  bond. (b) Pi-type acceptor interaction between the HOMO,  $n$ , of an X-type group and the LUMO,  $\sigma^*$ , of an adjacent polar  $\sigma$  bond.

the bond order, as well as partial  $\sigma$  bond formation between C and the incoming base. Carried to the extreme, a substitution reaction with inversion of configuration at C ( $S_N2$ ) ensues, as discussed in Chapter 9. If the center  $A$  is H rather than C, the corresponding reaction is a proton abstraction, that is, a Lowry–Bronsted acid–base reaction. If the interaction falls short of proton abstraction, the attractive interaction is called a *hydrogen bond*. Both aspects are discussed further in Chapter 10.

Interhalogen bonds are accompanied by very low LUMOs ( $\sigma_{XX}^*$ ; see Figure 4.5) and thus can function as good  $\sigma$  electron acceptors. The donor–acceptor complexes between ammonia and  $F_2$ ,  $Cl_2$ , and  $ClF$  have been investigated theoretically [93] and found to have linear structures, as expected on the basis of the above discussion.

### As a $\pi$ Acceptor

The  $\sigma^*$  orbital associated with a  $\sigma$  bond between C and a more electronegative element or group, X, is polarized toward carbon. Optimum interaction between the  $\sigma^*$  orbital and an adjacent localized nonbonding orbital of an X:-type group will occur if the  $\sigma^*$  orbital and the  $p$  (or  $sp^n$ ) nonbonded orbital of the neighboring group are coplanar, as shown in Figure 4.9b. The two-orbital, two-electron interaction is accompanied by charge transfer into the  $\sigma^*$  orbital and consequent reduction of the bond order, as well as partial  $\pi$  bond formation between C and the adjacent group. Carried to the extreme, an elimination reaction ( $E1c_b$ ) ensues, as discussed in Chapter 10. The tendency of the neighboring group to assist the departure of the leaving group is called *anchimeric assistance* or the *neighboring group effect*. If the interaction falls short of elimination, the attractive interaction is called *negative hyperconjugation* [67]. The tendency to alter geometry or change conformation so as to maximize the interaction is called the *anomeric effect* [94].



## $\sigma$ BONDS AS ELECTRON DONORS

The donor ability of a  $\sigma$  bond may be improved in two ways, by raising the energy of the  $\sigma$  orbital and by polarizing the orbital toward one end. The first improves the interaction between it and a potential electron acceptor orbital by reducing the energy difference  $\varepsilon_A - \varepsilon_B$ , the second by increasing the possibility of overlap and therefore increasing the value of the intrinsic interaction matrix element,  $h_{AB}$ . Specifically, a bond between C and an element (e.g., a metal, Li, Na, Mg) or group (e.g.,  $-\text{BR}_3^-$ ,  $-\text{SiR}_3$ ) less electronegative than C will have the required features. Referring to Figure 4.1a, the role of C will be played by group B. Since H is also somewhat less electronegative than C, C—H bonds are also potential electron donors when the electron demand is high. So are bonds to H from metals or metal-centered groups (e.g., NaH,  $\text{LiAlH}_4$ ,  $\text{NaBH}_4$ ).

### As a $\sigma$ Donor

The general features (orbital distribution and energy) for a  $\sigma$  bond between C and a less electronegative element or group, M, are shown in Figure 4.1a, where center A is M and center B is C. The energy of the  $\sigma$  orbital will be relatively high and the orbital is polarized toward carbon. Optimum interaction between the  $\sigma$  orbital and a localized empty orbital of a Lewis acid will occur between the C and M, closer to the carbon end, as shown in Figure 4.10a, or from the backside if steric hindrance by M is severe. The two-orbital, two-electron interaction is accompanied by charge transfer from the  $\sigma$  orbital and consequent reduction of the  $\sigma$  bond order, as well as partial  $\sigma$  bond forma-

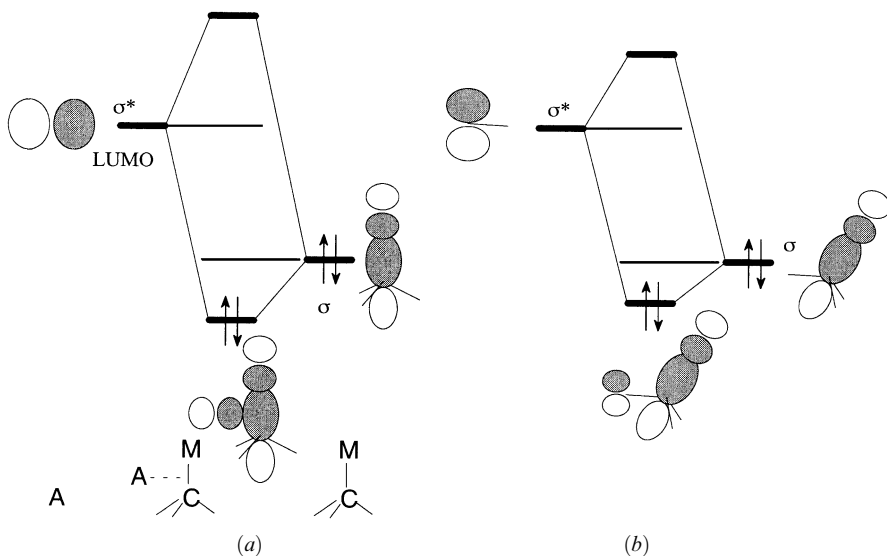


**Figure 4.10.** (a) Sigma-type donor interaction between the  $\sigma$  bond and the LUMO,  $\sigma^*$ , of a polarized  $\sigma$  bond (shown as a  $p$  orbital). (b) Pi-type donor interaction between the  $\sigma$  bond and the LUMO (shown as a  $p$  orbital), which may be the  $\pi^*$  orbital of an adjacent Z-type substituent, or  $\sigma^*$  of a polarized  $\sigma$  bond.

tion between C and the incoming acid. Carried to the extreme, a substitution reaction ensues in which the configuration at C may be *retained*. If the center *B* is H rather than C, the corresponding reaction is a hydride transfer (abstraction), as in the Cannizzaro or Meerwein–Pondorf–Verley reactions. If the interaction falls short of abstraction, a hydride bridge may be formed. Both aspects are discussed further in Chapter 10.

### As a $\pi$ Donor

A  $\sigma$  bond between C and a less electronegative element or group, M, is polarized toward carbon. Optimum interaction between the  $\sigma$  orbital and an adjacent localized empty orbital of an electron  $\pi$  acceptor group like carbonyl will occur if the  $\sigma$  orbital and the empty  $p$  orbital of the neighboring group are coplanar, as shown in Figure 4.10*b*. The two-orbital, two-electron interaction is accompanied by charge transfer from the  $\sigma$  orbital and consequent reduction of the bond order, as well as partial  $\pi$  bond formation between C and the adjacent group. The competitive  $\pi$  donation involving C—H and C—C  $\sigma$  bonds in cyclohexanones has been the subject of much discussion in the recent literature [95]. The carbonyl group distorts from planarity so as to achieve better alignment of the carbon  $2p$  component of its  $\pi^*$  orbital with the  $\sigma$  bond, a secondary consequence of which may be substantial preference for attack by nucleophiles at the face opposite to the  $\sigma$  bond involved. Where the adjacent group is a carbocationic center, distortion of the donor  $\sigma$  bond toward the acceptor site or migration of the bond (i.e., the group, M, attached to the other end) may occur. In the latter case, the reaction is a 1,2 hydride shift (M = H) or a Wagner–Meerwein rearrangement (M = alkyl). The weakening of the bond may also result in elimination of  $M^+$ . If the interaction falls short of elimination or migration, the attractive interaction is called *hyperconjugation*. The tendency to alter the geometry or change the conformation so as to maximize the attractive interaction is well documented [96]. In an extreme case, the group M may adopt a position midway between the C and the adjacent group, forming a two-electron, three-center bond as in nonclassical structures of carbocations—ethyl [97] (M = H), norbornyl [98] (M = alkyl). The bonding in (car)boranes is another example [99].

If the LUMO is the  $sp$  hybrid orbital at the C end of a polarized  $\sigma$  bond, such as to a halide, geometric distortion also occurs, particularly a lengthening of the receiving  $\sigma$  bond. Carried to the extreme, an elimination reaction occurs (E1cb, as discussed in Chapter 10). Migration of M to the adjacent group does not occur.

## BONDING IN CYCLOPROPANE

The above discussion applies to “normal”  $\sigma$  bonds in saturated compounds, as occur in molecules where the internuclear angles can reasonably approach the tetrahedral interorbital angle expected of  $sp^3$  hybridization. Many molecules exist which encompass small rings, the prototypical molecule being cyclopropane, where the internuclear angle of  $60^\circ$  is far from “ideal.” For the purpose of understanding the properties of cyclopropanes using orbital interaction diagrams, we adopt the Walsh picture [100, 101], shown in Figure 4.11. Each carbon atom is considered to be  $sp^2$  hybridized (Figure 4.11*a*). Two of the  $sp^2$  hybrid orbitals are used for the external  $\sigma$  bonds, as expected for the wider bond angle (HCH angle =  $114^\circ$  in cyclopropane). The set of three  $sp^2$  hybrid orbitals, one from each center, are directed toward the center of the ring and interact strongly to form the unique bonding combination,  $W_1$ , and the pair of antibonding MOs,

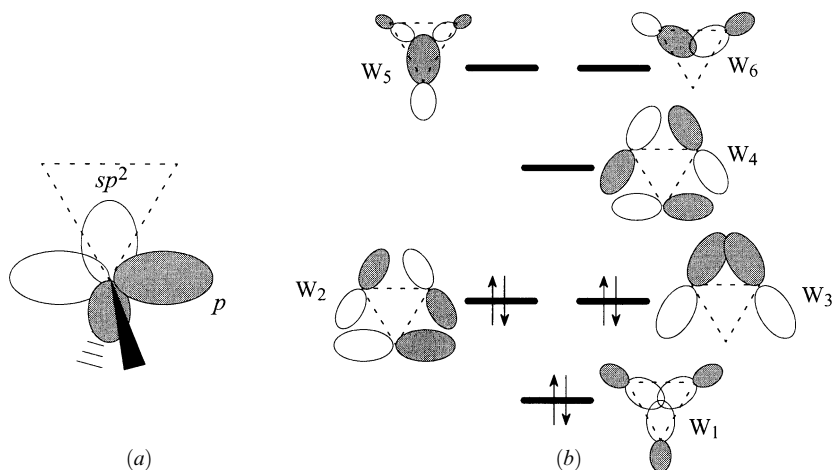


**Figure 4.11.** Bonding in cyclopropane: (a)  $2p$  and  $sp^2$  hybrid orbitals; (b) Walsh MOs. One of the degenerate HOMOs,  $W_2$ , and the LUMO,  $W_4$ , will interact in a  $\pi$  fashion with a substituent on the ring.

$W_5$  and  $W_6$ . The set of three (unhybridized)  $2p$  orbitals are oriented tangentially to the ring and interact weakly to form the degenerate pair of bonding MOs,  $W_2$  and  $W_3$ , which constitute the HOMOs, and the unique antibonding MO,  $W_4$ , which becomes the LUMO. We do not offer any explanation for why the orbital patterns originate as shown in Figure 4.11. We shall see in the next chapter that any two-dimensional cyclic array of orbitals that can overlap completely in phase (a Hückel array) will have the same orbital pattern as displayed for the  $sp^2$  set ( $W_1$ ,  $W_5$ , and  $W_6$ ), namely a unique lowest energy orbital and pairs of degenerate orbitals at higher energies. We state without proof that a cyclic array, such as the ring of  $2p$  orbitals, which cannot have all positive overlaps (a Möbius array) will have a degenerate pair of orbitals at the lowest energy and the remaining orbitals also in degenerate pairs unless there is an odd number, as in the present case. Orbitals  $W_2$ ,  $W_3$ , and  $W_4$ , are closer together simply because the  $2p$  orbitals overlap poorly in the orientation imposed by the three-membered ring geometry.

In the absence of substituents, the orientation of the nodal surfaces of the pairs of degenerate MOs is arbitrary, but the orientation will be as shown in Figure 4.11b for a substituent at the lower vertex. Notice that one of the HOMOs,  $W_2$ , and the LUMO,  $W_4$ , will interact with a substituent in this position in a  $\pi$  fashion. Because of the poor overlap of the tangentially oriented  $2p$  orbitals, the HOMO energy will be quite high, and the LUMO energy will be low. The cyclopropyl ring will therefore be expected to act both as a good  $\pi$  donor and a good  $\pi$  acceptor.

## CHAPTER 5

---

# SIMPLE HÜCKEL MOLECULAR ORBITAL THEORY

---

In this chapter, simple Hückel molecular orbital (SHMO) theory is developed. The reference energy,  $\alpha$ , and the energy scale in units of  $\beta$  are introduced.

### SIMPLE HÜCKEL ASSUMPTIONS

The SHMO theory was originally developed to describe planar hydrocarbons with conjugated  $\pi$  bonds. Each center is  $sp^2$  hybridized and has one unhybridized  $p$  orbital perpendicular to the trigonal  $sp^2$  hybrid orbitals. The  $sp^2$  hybrid orbitals form a rigid unpolarizable framework of equal C—C bonds. Hydrogen atoms are part of the framework and are not counted. The Hückel equations (3.3) described in the first part of Chapter 3 apply, namely,

$$F(1) \approx h^{\text{eff}}(1) \quad h^{\text{eff}}(1)\phi_a(1) = \varepsilon_a\phi_a(1) \quad E_{\text{IEA}} = 2 \sum_{a=1}^M \varepsilon_a \quad (5.1)$$

Each MO is expanded in terms of the unhybridized  $p$  orbitals, one per center. The overlap integral between two parallel  $p$  orbitals is small and is approximated to be exactly zero. Thus,

$$\phi(1) = \sum_{A=1}^{N_N} c_A \chi_A(1) \quad \int \chi_A(1)\chi_B(1) d\tau_1 = \delta_{AB} \quad (5.2)$$

where  $N_N$  is the number of carbon atoms which is the same as the number of orbitals. Equation (5.2) is just a generalization of equation (3.4). The subsequent steps are precisely those which were followed in Chapter 3. The energy is expressed as an expectation value of the MO [equation (5.2)] with the effective hamiltonian

$$\begin{aligned}
\varepsilon &= \frac{\int \phi(1) h^{\text{eff}}(1) \phi(1) d\tau_1}{\int |\phi(1)|^2 d\tau_1} \\
&= \frac{\sum_{A=1}^{N_N} \sum_{B=1}^{N_N} c_A c_B \int \chi_A(1) h^{\text{eff}} \chi_B(1) d\tau_1}{\sum_{A=1}^{N_N} \sum_{B=1}^{N_N} c_A c_B \int \chi_A(1) \chi_B(1) d\tau_1} \\
&= \frac{\sum_{A=1}^{N_N} c_A^2 h_{AA} + \sum_{A=1}^{N_N} \sum_{B \neq A}^{N_N} c_A c_B h_{AB}}{\sum_{A=1}^{N_N} c_A^2 + \sum_{A=1}^{N_N} \sum_{B \neq A}^{N_N} c_A c_B S_{AB}} \quad (5.3)
\end{aligned}$$

$$= \frac{\sum_{A=1}^{N_N} [c_A^2 h_{AA} + \sum_{B \neq A}^{N_N} c_A c_B h_{AB}]}{\sum_{A=1}^{N_N} c_A^2} = \frac{\mathcal{N}}{\mathcal{D}} \quad (5.4)$$

and the variational method applied. Differentiating equation (5.4) with respect to each of the coefficients,  $c_A$ ,

$$\begin{aligned}
\frac{\partial}{\partial c_A} (\mathcal{N} \mathcal{D}^{-1}) &= \frac{\partial \mathcal{N}}{\partial c_A} \mathcal{D}^{-1} - \mathcal{N} \mathcal{D}^{-2} \frac{\partial \mathcal{D}}{\partial c_A} = 0 \\
\frac{\partial \mathcal{N}}{\partial c_A} - \varepsilon \frac{\partial \mathcal{D}}{\partial c_A} &= 0 \\
(h_{AA} - \varepsilon) c_A + \sum_{B \neq A}^{N_N} h_{BA} c_B &= 0 \quad \text{for each } A = \{1, \dots, N_N\} \quad (5.5)
\end{aligned}$$

The condition that the  $N_N$  linear equations have a solution is that the determinant of coefficients (of the  $c$ 's) be equal to zero:

$$\begin{vmatrix}
h_{11} - \varepsilon & h_{12} & h_{13} & \cdots & h_{1N_N} \\
h_{21} & h_{22} - \varepsilon & h_{23} & \cdots & h_{2N_N} \\
h_{31} & h_{32} & h_{33} - \varepsilon & \cdots & h_{3N_N} \\
\vdots & \vdots & \vdots & \ddots & \vdots \\
h_{N_N 1} & h_{N_N 2} & h_{N_N 3} & \cdots & h_{N_N N_N} - \varepsilon
\end{vmatrix} = 0 \quad (5.6)$$

Within the SHMO approximations, all of the diagonal hamiltonian matrix elements,  $h_{AA}$ , are equal and are designated  $\alpha$ . The Hückel  $\alpha$  is the energy of an electron in a  $2p$  orbital of a trigonally ( $sp^2$ ) hybridized carbon atom. The off-diagonal matrix elements,  $h_{AB}$ , are all equal if the atoms involved are bonded together (since all bond distances are assumed to be equal) and these are designated  $\beta$ . The Hückel  $\beta$  is the energy of interaction of two  $2p$  orbitals of a trigonally ( $sp^2$ ) hybridized carbon atoms which are attached to each other by a  $\sigma$  bond. If the two atoms are not nearest neighbors, then  $h_{AB}$  is set equal to zero. In summary,

$$\begin{aligned}
h_{AA} &= \alpha \\
h_{AB} &= \beta \quad \text{if centers } A \text{ and } B \text{ are bonded} \\
h_{AB} &= 0 \quad \text{if centers } A \text{ and } B \text{ are not bonded}
\end{aligned}$$

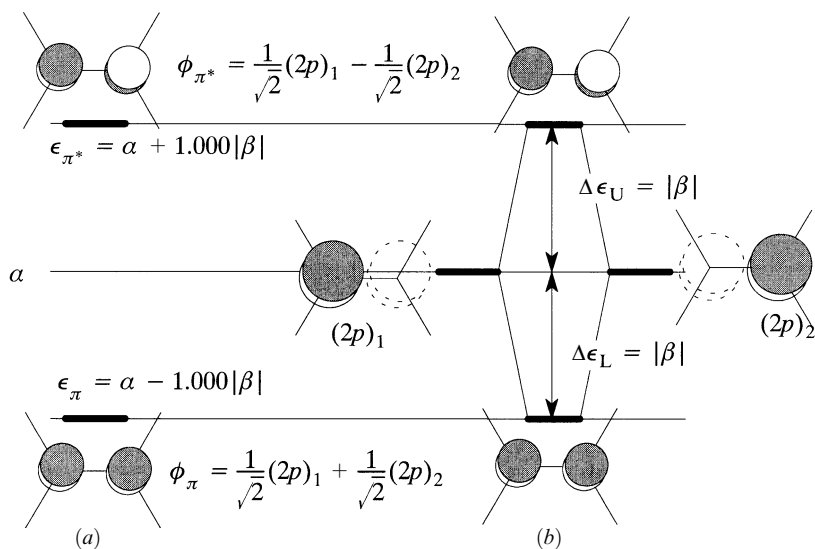


**Figure 5.1.** (a) SHMO results for ethylene. (b) The interaction diagram for ethylene: note that  $\Delta\epsilon_L = \Delta\epsilon_U$  because overlap is assumed to be zero in SHMO theory.

Thus, all of the diagonal elements are  $\alpha - \epsilon$ . The off-diagonal elements are  $\beta$  if the two atoms involved are bonded and zero if they are not. It is usual to divide each row of the determinant by  $\beta$ . This corresponds to a change of energy units and leaves either 1's or 0's in the off-diagonal positions which encode the connectivity of the molecule. The diagonal elements become  $(\alpha - \epsilon)/\beta$ , which is usually represented by  $x$ . While the determinant was expanded in Chapter 3 to yield the secular equation, it is more convenient in general to diagonalize the determinant using a computer. An interactive computer program, SHMO, has been written to accompany this book [102].

The SHMO calculation on ethylene yields the results shown in Figure 5.1a. The  $\pi$  and  $\pi^*$  orbitals are precisely one  $\beta$  unit above and below  $\alpha$ . The SHMO results are presented in Figure 5.1b in the form of an interaction diagram. In this case,  $\Delta\epsilon_L$  and  $\Delta\epsilon_U$  are assigned the same value, namely  $|\beta|$ , in the spirit of SHMO theory, but we know that the effect of proper inclusion of overlap would yield  $\Delta\epsilon_U > \Delta\epsilon_L$ .

The SHMO results for the series of “linear”  $\pi$  systems allyl, butadiene, and penta-1,3-dienyl are shown in Figure 5.2. The molecular species are portrayed with realistic angles ( $120^\circ$ ) and, in the case of the last two, in a specific conformation. Simple Hückel MO theory does not incorporate any specific geometric information since all non-nearest-neighbor interactions are set equal to zero. As a result, the SHMO results (MO energies and coefficients) are independent of whether the conformation of butadiene is s-trans, as shown in Figure 5.2, or s-cis, as may be required for the Diels–Alder reaction. Likewise the results for the penta-1,3-dienyl system shown in the “U” conformation in Figure 5.2 are identical to the results for the “W” or “sickle” conformations. The MOs are displayed as linear combinations of  $2p$  atomic orbitals seen from the top on each center, with changes of phase designated by shading. The relative contribution of each atomic  $2p$  orbital to the  $\pi$  MO is given by the magnitude of the coefficient of the eigenvector from the solution of the SHMO equations. In the display, the size of the  $2p$  orbital is proportional

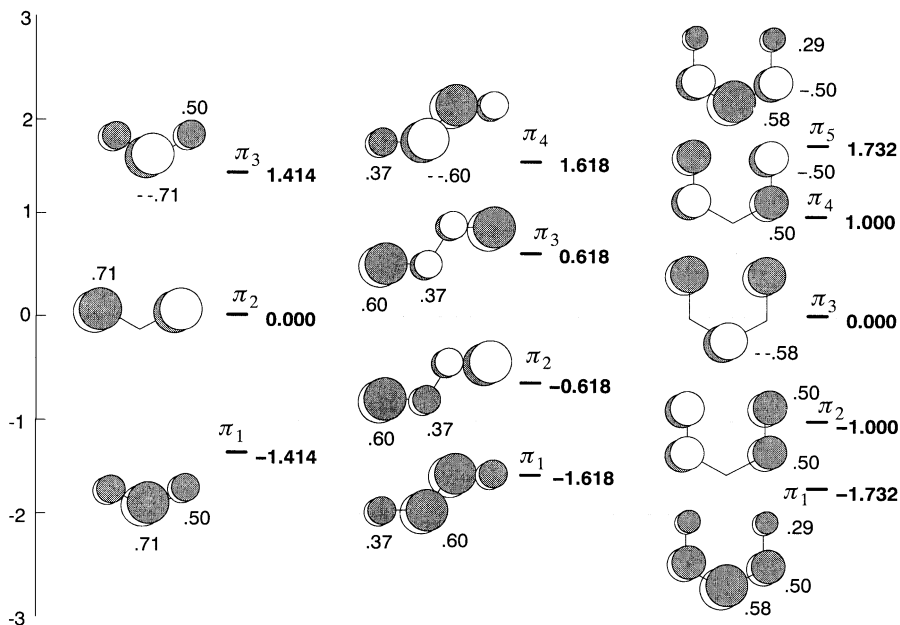


**Figure 5.2.** The SHMO orbitals of allyl, butadiene, and pentadienyl. The vertical scale is energy in units of  $|\beta|$ , relative to  $\alpha$ . Coefficients not specified may be obtained by symmetry.

to the *magnitude* of the coefficient. In some MOs, such as  $\pi_2$  of allyl, the node passes through a nucleus and a  $2p$  orbital is not shown because its coefficient is identically zero. The orbitals which are near  $\alpha$  will be of most interest in various applications. In the case of allyl, this orbital,  $\pi_2$ , is LUMO in the allyl cation, SOMO (singly occupied molecular orbital) in the allyl radical, and HOMO in the allyl carbanion. In the pentadienyl system,  $\pi_3$  plays the same role. In butadiene, the HOMO is  $\pi_2$ . Since the energy of the HOMO is higher than the energy of the HOMO of ethylene, one might conclude that butadiene is more basic than ethylene and more reactive toward electrophilic addition. Caution should be exercised in jumping to this conclusion, however, since the largest coefficient of butadiene's HOMO, 0.60, is smaller than the coefficient of the  $2p$  orbital of the HOMO of ethylene, 0.71. The smaller coefficient would imply a weaker intrinsic interaction ( $h_{AB}$ ) with Lewis acids and therefore reduced reactivity. Clearly, the energy factor and the intrinsic interaction (as judged from the coefficients) are in opposition, the first predicting higher reactivity and the second lower. As is often the case in orbital interaction theory, one must resort to experimental observations to evaluate the relative importance of opposed factors. Since, experimentally, dienes *are* more susceptible to electrophilic attack than unconjugated alkenes, we can conclude that the energy factor is more important than the relatively small difference in coefficients.

Simple Hückel MO results for the series of cyclic  $\pi$  systems cyclopropenyl, cyclobutadiene, cyclopentadienyl, and benzene are shown in Figure 5.3. Several points may be noted. The lowest MO in each case has energy identical to  $\alpha - 2|\beta|$ , a result which can be proved to be general for any regular polygon. Each ring has degenerate pairs of MOs as a consequence of the three- or higher-fold axis of symmetry. The orbitals of each

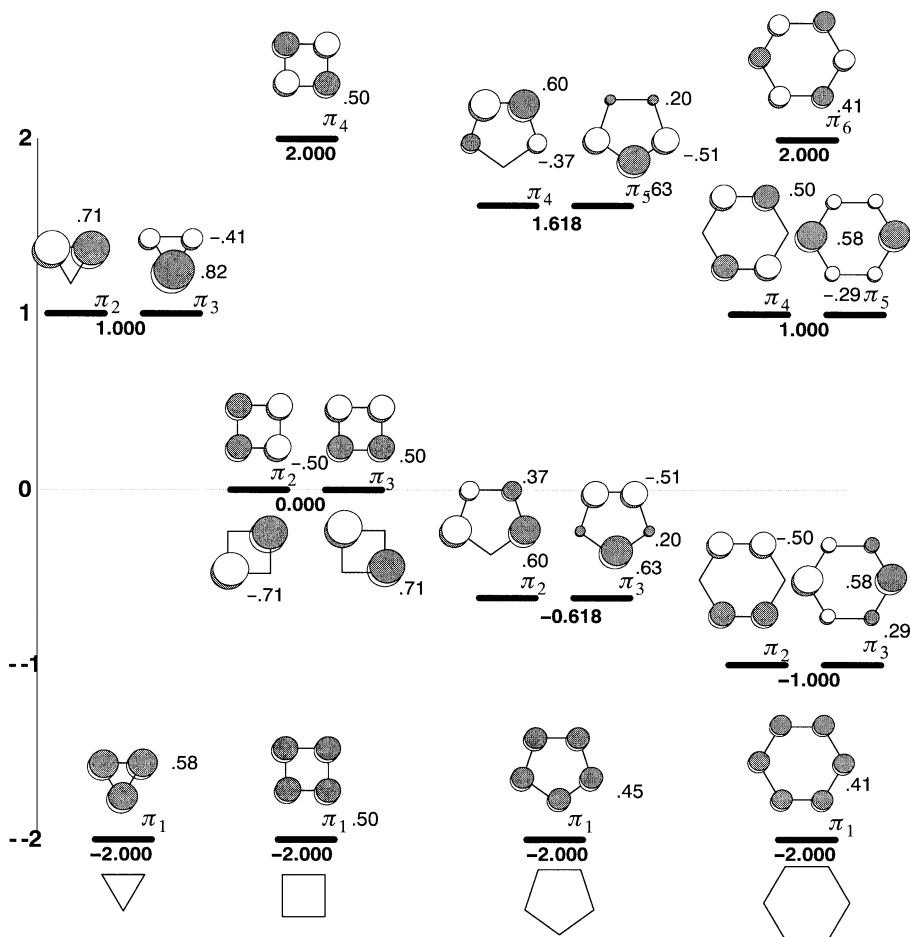


**Figure 5.3.** SHMO orbitals for cyclopropenyl, cyclobutadiene, cyclopentadienyl, and benzene. The energies are in units of  $|\beta|$  relative to  $\alpha$ . Two alternative but equivalent representations are shown for the degenerate  $\pi$  orbitals of cyclobutadiene. Sizes of the  $2p$  orbitals are shown proportional to the magnitudes of the coefficients whose numerical values are given. Coefficients not specified may be obtained by symmetry.

degenerate pair may appear very different. The orientation of the nodal surfaces of the degenerate MOs is entirely arbitrary. Two equivalent orientations are shown for cyclobutadiene. A perturbation at one of the vertices such as by a substituent will rotate the nodes of the degenerate set so that one node passes through that vertex. The orientations shown are those which should be adopted for the purposes of interaction diagrams involving a single substituent on the ring. The pairs of degenerate MOs which form the HOMO of benzene is at exactly the same energy as the HOMO of ethylene. In orbital interaction terms, we would predict that, even though the HOMOs are of the same energy, benzene would be less susceptible to electrophilic attack than ethylene for the reason that the



largest available coefficient, 0.58 in  $\pi_3$ , is smaller than 0.71, the coefficient in the HOMO of ethylene.

Conjugated  $\pi$  systems which do not contain any odd-membered rings are called *alternant*, and provided all the atoms are the same, alternant systems have a symmetrical distribution of orbital energies about the mean ( $\alpha$  for C). The coefficients also repeat in magnitude in MOs which are equidistant from the mean. These features are readily apparent in the orbitals portrayed in Figures 5.1–5.3.

Of the four cyclic conjugated  $\pi$  systems shown in Figure 5.3, only benzene, with six electrons in the  $\pi$  orbitals, is stable kinetically and thermodynamically. Neutral cyclopropenyl and cyclopentadienyl, with three and five  $\pi$  electrons, respectively, are free radicals. The cyclopropenyl cation, with two  $\pi$  electrons, and the cyclopentadienyl anion, with six, have filled shells and constitute aromatic systems in that they exhibit unusual stability, compared to other carbocations and carbanions, respectively. Cyclobutadiene is a special case. With two electrons in the degenerate HOMOs, one would expect that the electrons would separate and that the ground state would be a triplet. However, a distortion of the geometry from square to rectangular would eliminate the degeneracy and permit a singlet ground state. The ground state of cyclobutadiene has been shown experimentally to be singlet with a barrier for the rectangular-to-square deformation in the range  $7 \leq \Delta H^\ddagger \leq 42$  kJ/mol [103]. Theoretical computations suggest that the higher value may be correct [104].

### CHARGE AND BOND ORDER IN SHMO THEORY: ( $S_{AB} = 0$ , ONE ORBITAL PER ATOM)

It is of interest to enquire how the electrons are redistributed during an interaction and how a bond is affected. We use a simplified Mulliken population analysis [see Appendix A, equations (A.77)–(A.79)]. The simplification consists of dropping all terms involving the overlap of atomic orbitals and assuming that, in any given MO, there is only *one* atomic orbital on any given center). Thus, we may assume that the following relations hold:

$$\phi_a = \sum_{A=1}^n \chi_A c_{Aa} \quad S_{AB} = \delta_{AB} \quad \sum_{A=1}^n c_{Aa}^2 = 1 \quad (5.7)$$

where  $n$  is the number of atomic orbitals (which equals the number of nuclear centers, since there is one orbital per center). A measure of the *electron population* on each center is easily obtained as below.

#### Electron Population and Net Charge of Center A

The electron population of center A is defined as

$$P_A = \sum_{a=1}^n n_a c_{Aa}^2 \quad (5.8)$$

where  $n_a$  ( $= 0, 1, 2$ ) is the number of electrons in the  $a$ th MO and the sum runs over the MOs (there are as many MOs as there are AOs and atomic centers). The *net charge* of

center A,  $C_A$ , depends on the number of electrons,  $n_A$ , which are required for a neutral atomic center A. Thus

$$C_A = n_A - P_A \quad (5.9)$$

Notice that  $C_A$  is negative if the population of A,  $P_A$ , exceeds the number of electrons required to give a neutral center. It is easily verified that

$$\sum_{A=1}^n P_A = N_e \quad \sum_{A=1}^n C_A = \text{net charge on molecule} \quad (5.10)$$

*Exercise 3.1.* Verify equations (5.10).

*Exercise 3.2.* Verify that the net charge at each carbon atom of each of the *neutral* ring systems shown in Figure 5.3 is zero (to two significant figures).

### Bond Order between Centers A and B

Strictly speaking, there should be no electron population between pairs of atoms in SHMO since orbitals are assumed not to overlap. However, it is conventional to set all overlap integrals to unity for the purpose of defining a “bond order.” The *bond order*,  $B_{AB}$ , between centers A and B is defined as

$$B_{AB} = \sum_{a=1}^n n_a c_{Aa} c_{Ba} \quad (5.11)$$

where the quantities are defined as above. A positive value indicates bonding. Small negative values of  $B_{AB}$  may result. These are indications of *antibonding* or *repulsive* interaction between the centers concerned.

*Exercise 3.3.* Show that the maximum value for the bond order due to a single bond is 1 and that it occurs when  $n_a = 2$  and  $c_A = c_B = 1/\sqrt{2}$ .

*Exercise 3.4.* Show that the bond order for benzene is 0.67 from the data in Figure 5.3.

## FACTORS GOVERNING ENERGIES OF MOs: SHMO THEORY

### Reference Energy and Energy Scale

Most organic molecules are made up of the elements C, H, N, and O, with lesser amounts of S, P, and X (Cl, Br, I). Molecular orbitals are built up by the interaction of the atomic orbitals of these elements held together at bonding separations. It is convenient at this point to adopt an energy scale derived from SHMO theory, in which the “Coulomb integral”  $\alpha$  ( $=\alpha_C$ ) is the reference point on the energy scale,

$$\alpha = \alpha_C = \int [2p_C(1)] h^{\text{eff}}(1) [2p_C(1)] d\tau_1 \quad (5.12)$$

and the absolute value of the “resonance integral”  $|\beta|$  ( $=|\beta_{CC}|$ ) is the unit of energy,

$$\beta = \beta_{CC} = \int [2p_C(1)]_A h^{\text{eff}}(1) [2p_C(1)]_B d\tau_1 \quad (5.13)$$

Thus,  $\alpha$  ( $=\alpha_C$ ) is the core energy of an electron localized to the  $2p$  atomic orbital of a carbon atom, and  $\beta$  ( $=\beta_{CC}$ ) is the energy associated with the interaction of two carbon  $2p$  orbitals overlapping in a  $\pi$  (parallel) fashion at the C—C separation of benzene (or ethylene).

## HETEROATOMS IN SHMO THEORY

In SHMO, the core energies of heteroatoms, X, are specified in terms of  $\alpha$  and  $\beta$ , and the interaction matrix elements for  $p$  orbitals overlapping in a  $\pi$  fashion on any pair of atoms, X and Y, are specified in terms of  $\beta$ . Thus,

$$\alpha_X = \alpha + h_X |\beta| \quad (5.14)$$

$$\beta_{XY} = k_{XY} |\beta| \quad (5.15)$$

In SHMO theory the energy of  $\pi$  bond formation in ethylene is  $2\beta$  (since the strength of a C—C  $\pi$  bond is about 280 kJ/mol, one may consider  $|\beta|$  to be about 140 kJ/mol). The energies of electrons in  $2p$  orbitals of N and O, normally found in  $\pi$  bonding environments (i.e., as *dicoordinated* N and *monocoordinated* O) are given by  $h_{N2} = -0.51$  and  $h_{O1} = -0.98$ . These are suitable values for a pyridine N and a carbonyl O. The  $\pi$ -type interaction matrix elements of most pairs, except those involving F, are approximately given by  $k_{XY} = -1$ . The energies of electrons in  $2p$  orbitals of N and O in normal (saturated) bonding environments (i.e., as *tricoordinated* N and *dicoordinated* O) are given by  $h_{N3} = -1.37$  and  $h_{O2} = -2.05$ . Thus a tricoordinated N is more electronegative than a dicoordinated N, and similarly for dicoordinated versus monocoordinated O. The  $\pi$ -type interaction matrix elements of these kinds of orbitals with the normal C  $2p$  orbitals are approximately given by  $k_{CN} = -0.8$  and  $k_{CO} = -0.67$ , reflecting the smaller size of the orbitals. The value for the C—F interaction,  $k_{CF} = -0.5$ , is small for the same reasons. The change in effective electronegativity of the  $2p$  orbitals is a consequence of the increase in the number of atoms to which they are coordinated (see below), although in usual SHMO usage, the distinction is made in terms of the number of electrons which the atom contributes to the  $\pi$  system. A more complete list of  $h_X$  and  $k_{XY}$  parameters, derived on the basis of Pariser-Parr-Pople (PPP) calculations by Van Catledge [105], is given in Table 5.1.

### Effect of Coordination Number on $\alpha$ and $\beta$

A decrease in the coordination number at N from three to two reduces the effective electronegativity of the remaining nonbonded  $p$  orbitals at the center. The change in  $h_N$  is  $0.86|\beta|$ . A decrease in the coordination number at O from 2 to 1 similarly reduces the effective electronegativity of the remaining nonbonded  $p$  orbitals at the O center. The change in  $h_O$  is larger,  $1.12|\beta|$ . Within the same molecule, the coordination number of N or O may readily be changed by the process of protonation or deprotonation, as

TABLE 5.1. SHMO Values for Heteroatoms:  $a_X = a + h_X|\beta|$ ,  $\beta_{XY} = k_{XY}|\beta|^a$ 

X	Number of Electrons	$h_X$	$k_{XY}$ by Y Atoms														
			C <sup>b</sup>	B <sup>b</sup>	N2 <sup>c</sup>	N3 <sup>b</sup>	O1 <sup>d</sup>	O2 <sup>c</sup>	F <sup>d</sup>	Si <sup>b</sup>	P2 <sup>c</sup>	P3 <sup>b</sup>	SI <sup>d</sup>	S2 <sup>c</sup>	Cl <sup>d</sup>		
C <sup>b</sup>	1	0.00	-1.00														
B <sup>b</sup>	0	0.45	-0.73	-0.87													
N2 <sup>c</sup>	1	-0.51	-1.02	-0.66	-1.09												
N3 <sup>b</sup>	2	-1.37	-0.89	-0.53	-0.99	-0.98											
O1 <sup>d</sup>	1	-0.97	-1.06	-0.60	-1.14	-1.13	-1.26										
O2 <sup>c</sup>	2	-2.09	-0.66	-0.35	-0.80	-0.89	-1.02	-0.95									
F <sup>d</sup>	2	-2.71	-0.52	-0.26	-0.65	-0.77	-0.92	-0.94	-1.04								
Si <sup>b</sup>	1	0.00	-0.75	-0.57	-0.72	-0.43	-0.65	-0.24	-0.17	-0.64							
P2 <sup>c</sup>	1	-0.19	-0.77	-0.53	-0.78	-0.55	-0.75	-0.31	-0.21	-0.62	-0.63						
P3 <sup>b</sup>	2	-0.75	-0.76	-0.54	-0.81	-0.64	-0.82	-0.39	-0.22	-0.52	-0.58	-0.63					
SI <sup>d</sup>	1	-0.46	-0.81	-0.51	-0.83	-0.68	-0.84	-0.43	-0.28	-0.61	-0.65	-0.65	-0.68				
S2 <sup>c</sup>	2	-1.11	-0.69	-0.44	-0.78	-0.73	-0.85	-0.54	-0.32	-0.40	-0.48	-0.60	-0.58	-0.63			
Cl <sup>d</sup>	2	-1.48	-0.62	-0.41	-0.77	-0.80	-0.88	-0.70	-0.51	-0.34	-0.35	-0.55	-0.52	-0.59	-0.68		

<sup>a</sup>Ref. 105.<sup>b</sup>Ttricoordinated, planar geometry.<sup>c</sup>Dicoordinated.<sup>d</sup>Monocoordinated.

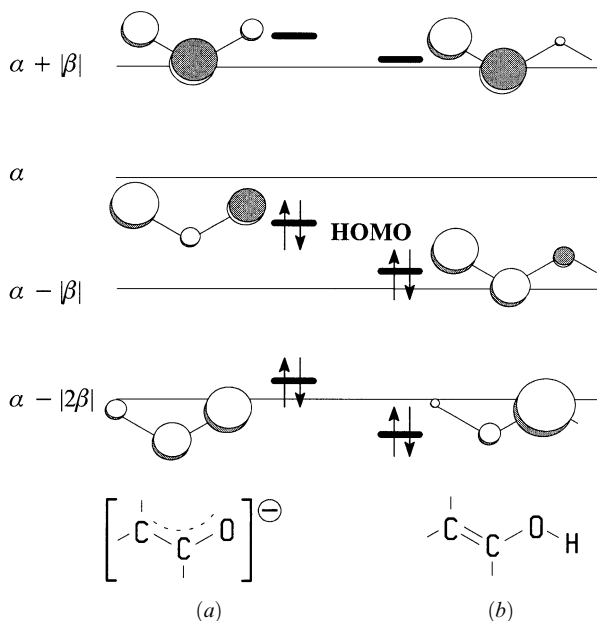


Figure 5.4. SHMO results for enolate (a, using O1 parameters) and enol (b, with O2 parameters).

a consequence of a change of pH, for instance. The results of SHMO calculations on the enolate anion and on enol are shown in Figure 5.4. In the enolate case,  $h_{O1} = -0.97$ ,  $k_{CO} = -1.06$ , while for enol, the values  $h_{O2} = -2.09$ ,  $k_{CO} = -0.66$  were used according to Table 5.1. The contributions of the individual  $2p$  orbitals of C and O are displayed with sizes proportional to the magnitudes of the coefficients. The effect of the protonation can be seen as a lowering of the energy and changed polarization of all of the MOs, including the HOMO.

Normally, no distinction is made between the kind of atom or group which is coordinated to the center of interest, but this may be a gross oversimplification in extreme cases. It is not reasonable to expect that the  $2p$  orbital of a methyl group will have approximately the same energy as the  $2p$  orbital of a trifluoromethyl group (assuming it were planar). Because of the strong inductive effect of the electronegative fluorine atoms acting in the  $\sigma$  framework, the carbon atom of trifluoromethyl would be significantly denuded of electrons. The  $2p$  orbital is in effect more electronegative and falls below  $\alpha$ .

Can one deduce reasonable values for the effective electronegativity of the  $p$  orbitals of C upon reduction of the coordination number from 3 to 2 (i.e., C2), as in alkynes, allenes, nitriles (R—CN), or carbenes, or even to 1, as in CO, isonitriles (R—NC), or acetylides? A linear extrapolation from dicoordinated O ( $\alpha_{O2} = \alpha - 2.09|\beta|$ ) and dicoordinated N ( $\alpha_{N2} = \alpha - 0.51|\beta|$ ) to dicoordinated C yields an estimate of the energy of the  $2p$  orbital as  $\alpha + 0.86|\beta|$ . This value is probably too high. It places the energy of the  $2p$  orbital of a dicoordinated carbon above that of the  $2p$  of a tricoordinated boron, but the same is not true in the case of a dicoordinated N and a tricoordinated C, and the

electronegativity differences in the series B, N, C (Table 5.1) are very similar. A reasonable compromise is to place  $\alpha_{C2}$  midway between  $\alpha_B$  and  $\alpha_C$ ,

$$\alpha_{C2} = \alpha + 0.23|\beta| \quad (5.16)$$

### Hybridization at C in Terms of $\alpha$ and $\beta$

The  $2s$  to  $2p$  promotion energy of atomic C is about 800 kJ/mol. In a molecular environment, this value is expected to be somewhat less where the presence of other nuclei may stabilize  $p$  orbitals relative to  $s$ . The coordination number of the carbon atom has a direct effect on the orbital energies, just as it had on the energies of heteroatom orbitals discussed in the previous section. Mullay has estimated the group electronegativities of  $\text{CH}_3$ ,  $\text{CHCH}_2$ , and  $\text{CCH}$  to be 2.32, 2.56, and 3.10, respectively [106]. The last value is similar to his estimate for  $\text{NH}_2$ . Boyd and Edgcombe have placed all three values near 2.6 [107]. Reed and Allen, using their bond polarity index, have assigned values of 0.000, 0.027, and 0.050, respectively (compared to H  $-0.032$  and F 0.189) [108]. Without attempting to be too quantitative, convenient values of the core energies of “hybrid” atomic orbitals, in  $|\beta|$  units, recognizing that changes in coordination number also occur, are approximately

$$\alpha_{sp} = \alpha - 0.50|\beta| \quad (\text{coordination number 1}) \quad (5.17)$$

$$\alpha_{sp^2} = \alpha - 0.33|\beta| \quad (\text{coordination number 2}) \quad (5.18)$$

$$\alpha_{sp^3} = \alpha - 0.25|\beta| \quad (\text{coordination number 3}) \quad (5.19)$$

The interaction energies of the pairs of hybridized orbitals interacting in a  $\sigma$  fashion would be strongly distance dependent. At typical single-bond distances, one may adopt  $k_\sigma = 1.5k_\pi|\beta|$  for all of them, but the value rises steeply as the separation is decreased. When the separation is that of a double bond, a value of  $k_\sigma = -2.0k_\pi|\beta|$  is more appropriate. These values are suggested only to help place  $\sigma$  bonds or  $\sigma^*$  orbitals more or less correctly relative to  $\pi$  bonds and  $\pi^*$  orbitals when both may have similar energies.

### GROSS CLASSIFICATION OF MOLECULES ON THE BASIS OF MO ENERGIES

Frontier orbital energy is not the only criterion which governs the chemical characteristics of a compound. For example, the magnitudes of the atomic orbital coefficients on any given atom may be responsible for the reduced basicity of benzene relative to ethylene, both of which have the same HOMO energy. Nevertheless, the energy criterion may be applied to deduce gross features. In Figure 5.5 are shown four extreme cases into which molecules can be categorized on the basis of their frontier orbital energies. Compounds which have a large HOMO–LUMO gap ( $>1.5|\beta|$ ) will be stable against self-reaction, for example, dimerization, polymerization, and intramolecular rearrangements. If the HOMO is low in an absolute sense ( $<\alpha - 1|\beta|$ , the HOMO of ethylene), the compound will be chemically resistant to reaction with Lewis acids. If the LUMO is high in an absolute sense ( $>\alpha + 1|\beta|$ , the LUMO of ethylene), the compound will be chemically resistant to reaction with Lewis bases:

- Compounds with a high LUMO and a low HOMO (Figure 5.5a) will be chemically inert. Saturated hydrocarbons, fluorocarbons, and to some extent ethers fall in this category.

- Compounds with a low HOMO and LUMO (Figure 5.5*b*) tend to be stable to self-reaction but are chemically reactive as Lewis acids and electrophiles. The lower the LUMO, the more reactive. Carbocations, with LUMO near  $\alpha$ , are the most powerful acids and electrophiles, followed by boranes and some metal cations. Where the LUMO is the  $\sigma^*$  of an H—X bond, the compound will be a Lowry–Bronsted acid (proton donor). A Lowry–Bronsted acid is a special case of a Lewis acid. Where the LUMO is the  $\sigma^*$  of a C—X bond, the compound will tend to be subject to nucleophilic substitution. Alkyl halides and other carbon compounds with “good leaving groups” are examples of this group. Where the LUMO is the  $\pi^*$  of a C=X bond, the compound will tend to be subject to nucleophilic addition. Carbonyls, imines, and nitriles exemplify this group.
- Compounds with a high HOMO and LUMO (Figure 5.5*c*) tend to be stable to self-reaction but are chemically reactive as Lewis bases and nucleophiles. The higher the HOMO, the more reactive. Carbanions, with HOMO near  $\alpha$ , are the most powerful bases and nucleophiles, followed by amides and alkoxides. The neutral nitrogen (amines, heteroaromatics) and oxygen bases (water, alcohols, ethers, and carbonyls) will only react with relatively strong Lewis acids. Extensive tabulations of gas-phase basicities or *proton affinities* (i.e.,  $-\Delta G^\circ$  of protonation) exist [109, 110]. These will be discussed in subsequent chapters.
- Compounds with a narrow HOMO–LUMO gap (Figure 5.5*d*) are kinetically reactive and subject to dimerization (e.g., cyclopentadiene) or reaction with Lewis acids or bases. Polyenes are the dominant *organic* examples of this group. The difficulty in isolation of cyclobutadiene lies not with any intrinsic instability of the molecule but with the self-reactivity which arises from an extremely narrow HOMO–LUMO gap. A second class of compounds also falls in this category, coordinatively unsaturated transition metal complexes. In transition metals, the atomic  $n d$  orbital set may be partially occupied and/or nearly degenerate with the partially occupied  $n + 1 sp^n$  set. Such a configuration permits exceptional reactivity, even toward C—H and C—C bonds. These systems are treated separately in Chapter 13.

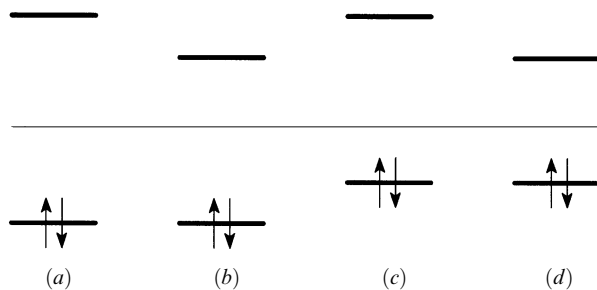


**Figure 5.5.** (a) High LUMO, low HOMO, large HOMO–LUMO gap; thermodynamically stable and chemically inert. (b) Low LUMO, low HOMO, large HOMO–LUMO gap; thermodynamically stable and chemically reactive as Lewis acid. (c) High LUMO, high HOMO, large HOMO–LUMO gap; thermodynamically stable and chemically reactive as Lewis base. (d) Low LUMO, high HOMO, small HOMO–LUMO gap; may be thermodynamically stable but chemically amphoteric and self-reactive.

## CHAPTER 6

---

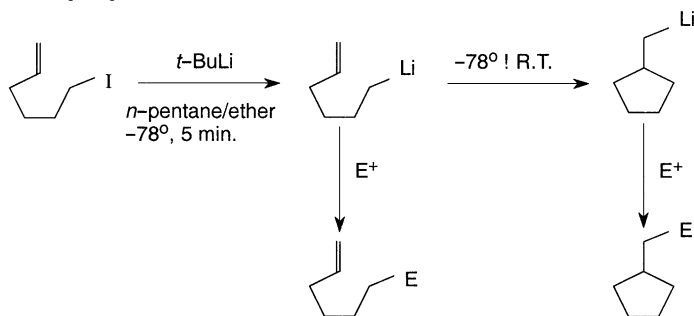
# REACTIONS AND PROPERTIES OF $\pi$ BONDS

---

### REACTIONS OF OLEFINS (ALKENES)

The orbital interaction treatment of C=C  $\pi$  bonds and other types of  $p$ - $p$   $\pi$  bonds is given here. Carbonyl compounds are treated separately in Chapter 8, and organometallic  $\pi$ -type bonding is briefly described in Chapter 13.

Ethylene is the template for olefin reactions, but ethylene itself is rather unreactive, undergoing electrophilic attack by moderately strong Lewis acids. Nucleophilic attack on the  $\pi$  bond even by the strongest Lewis bases has not been reported. The following sequence involves intramolecular addition of a carbanion to an unactivated olefin [111, 112]. The reaction is undoubtedly facilitated by active participation of the lithium cation as a Lewis acid [113].



The normal course of reaction of alkenes involves addition of Lewis acids (electrophiles) yielding an intermediate carbocation which is trapped by a weak nucleophile [114]. The most common electrophilic addition reactions are summarized in Figure 6.1. If the olefin is unsymmetrically substituted, the question of regioselectivity arises. We begin by examining the effects on the olefin  $\pi$  system of three classes of substituents as



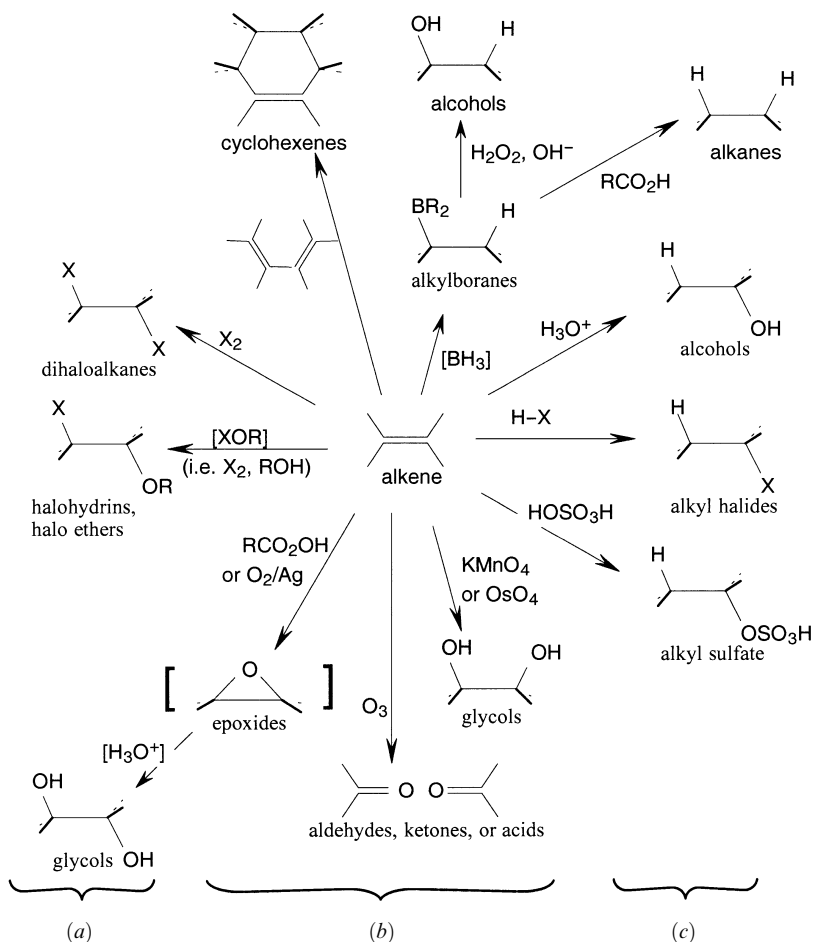


**Figure 6.1.** Summary of the most common electrophilic addition reactions of olefins. In each case, the olefin reacts as a Lewis base. All reactions are regioselective. The overall stereochemistry is (a) stereospecific anti; (b) stereospecific syn; (c) not stereospecific, in general.

defined by Fleming, namely X: ( $\pi$  electron donors), Z ( $\pi$  electron acceptors), and “C” (conjugating) [7]. An interaction diagram showing the interaction of a C—C  $\pi$  bond with each type of substituent is shown in Figure 6.2. We note the effect of the substituent on the energy and polarization of the  $\pi$  bond at its original site.

## EFFECT OF X: SUBSTITUENTS

As shown in Figure 6.2a, an X: substituent, which has a  $p$  orbital or other suitable doubly occupied orbital which will interact with the  $\pi$  bond, raises the energy of the HOMO and LUMO, thus rendering the olefin more reactive as a Lewis base. Of course, the electrons of the HOMO are also delocalized onto X. The probability of attack by an

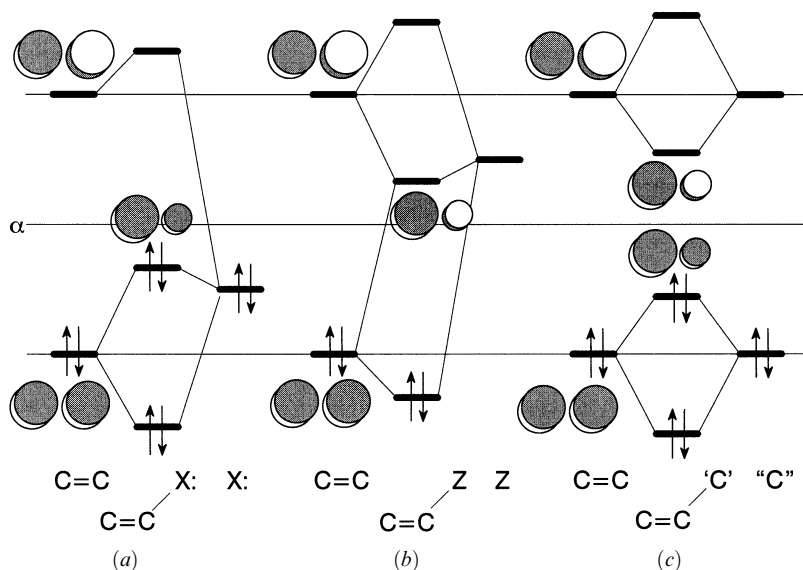
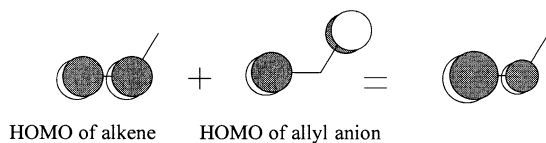
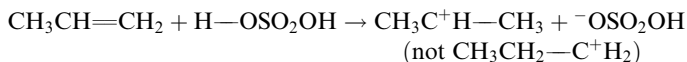


Figure 6.2. Interaction of  $\text{C}=\text{C}$  with (a) X; (b) Z; (c) C-type substituents.

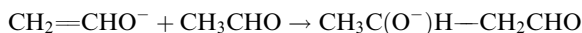
electrophile will be governed by the magnitude of the coefficient at the particular atomic position. Polarization of the HOMO away from the point of attachment of the X substituent directs electrophilic attack to that carbon. Attack may also be directed to X itself in certain cases, although this is usually reversible and may have no net consequences. The X-substituted olefin  $\pi$  system is isoelectronic to that of the allyl anion (Figure 5.2). The polarization and energy of the  $\pi$  bond can be deduced by *averaging* the HOMOs and HOMO energies of the olefin and allyl anion:



The X: substituents are  $-\text{NR}_1\text{R}_2$ ,  $-\text{OR}$ ,  $-\text{SR}$ ,  $-\text{F}$ ,  $-\text{Cl}$ ,  $-\text{Br}$ ,  $-\text{I}$ , or  $-\text{CH}_3$  (or any alkyl). The R's may be H or alkyl, or aryl, or even acyl. Thus,



As a special case, consider the aldol reaction

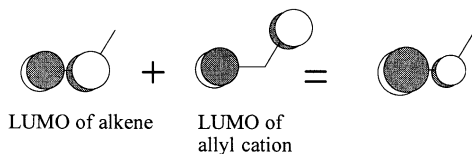


The enolate anion may be considered as an alkene with a very good powerful X-type substituent, the alkoxide oxygen. The HOMO of the  $\pi$  bond is strongly raised in energy

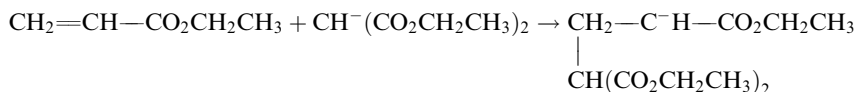
and polarized away from the alkoxy substituent. The weak electrophile, the carbonyl of acetaldehyde, adds at the distal C atom.

## EFFECT OF Z SUBSTITUENTS

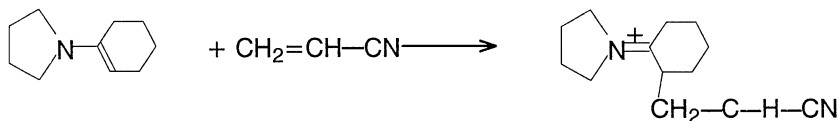
As shown in Figure 6.2*b*, a Z substituent, which has a  $p$  or  $\pi^*$  orbital or other suitable empty low-lying orbital which will interact with the  $\pi$  bond, lowers the energy of the HOMO and LUMO, thus rendering the olefin less reactive as a Lewis base but more reactive as a Lewis acid. The electrons of the HOMO are also delocalized onto Z. The probability of attack by an electrophile will be governed by the magnitude of the coefficient at the particular atomic position. Polarization of the LUMO away from the point of attachment of the Z substituent directs nucleophilic attack to that carbon. Attack may also be directed to Z itself in certain cases, and this may be irreversible, providing an alternate pathway for the reaction. The Z-substituted olefin  $\pi$  system has some characteristics of an allyl cation (Figure 5.2). The polarization and energy of the  $\pi^*$  orbital can be deduced by *averaging* the LUMOs and LUMO energies of the olefin and allyl cation:



The Z substituents are  $-\text{COR}$ ,  $-\text{CN}$ ,  $-\text{SOR}$ ,  $-\text{SO}_2\text{R}$ ,  $-\text{NO}$ , and  $-\text{NO}_2$ . The R's may be H, alkyl, aryl, or even X: substituents. Thus, the Michael addition is the best example:



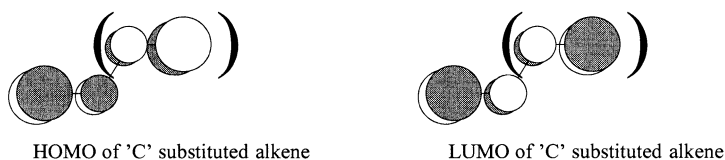
Consider also



## EFFECT OF "C" SUBSTITUENTS

As shown in Figure 6.2*c*, a "C" substituent, which has evenly spaced  $\pi$  and  $\pi^*$  orbitals, raises the energy of the HOMO and lowers the LUMO, thus rendering the olefin more reactive as both a Lewis base and a Lewis acid. The electrons of the HOMO and LUMO are also delocalized onto "C." The probability of attack by an electrophile or nucleophile will be governed by the magnitude of the coefficient at the particular atomic position. Polarization of both the HOMO and LUMO away from the point of attachment of the "C" substituent directs attack to that carbon. Attack may also be directed to "C"

itself in certain cases. The "C" substituted olefin  $\pi$  system is assumed to be butadiene-like (Figure 5.2), and hence the polarization of the  $\pi$  and  $\pi^*$  orbitals:

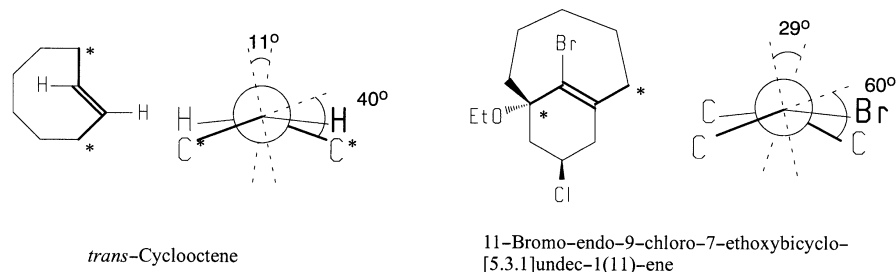


The "C" substituents are alkenyl, alkynyl, or aryl groups.

### EFFECT OF DISTORTION OF MOLECULAR SKELETON

Olefins may be synthesized in which the  $\pi$  bond must be superimposed on a  $\sigma$  framework which deviates significantly from the ideal geometry, namely coplanarity with a two  $sp^2$  hybridized carbon atoms, or in the case of alkynes, collinearity. *Twisting* of the two ends of the double bond relative to each other has the consequence of reducing the  $\pi$  overlap and hence the resonance integral is less than  $|\beta_{CC}|$ . The higher HOMO means that the twisted olefin is more susceptible to electrophilic attack, the lower LUMO implies an increased susceptibility to nucleophilic attack, and the smaller HOMO–LUMO gap suggests a bathochromic shift for the  $\pi\pi^*$  electronic transition [115]. The increased susceptibility of twisted (strained) alkenes toward electrophilic attack has been demonstrated experimentally for MCPBA (*meta*-chloroperbenzoic acid) epoxidation [116] of a variety of strained alkenes. The rate enhancement was attributed to relief of strain in the transition state, but a correlation was noted with ionization potential, and hence the energy of the HOMO. Conjugated alkenes which have high HOMO energies also were less reactive than expected on the basis of the correlation with twisted monoalkenes. In orbital interaction terms, the reduced reactivity of conjugated systems is attributed to the smaller orbital coefficients and hence lower intrinsic interaction matrix elements [see equation (3.47)].

In fact, it is difficult to effect a major perturbation to the olefin  $\pi$  system by twisting. For instance, the  $\sigma$  framework of *trans*-cyclooctene is twisted by  $40^\circ$  out of planarity, but pyramidalization at each end is such as to reduce the twist of the  $p$  orbitals to only about  $11^\circ$  [117]:



The ionization potential, 8.69 eV, is lower than in the case of *cis*-cyclooctene (8.98 eV) or cyclohexene (9.12 eV), as expected. The highly strained anti-Bredt olefin, 11-bromo-endo-9-chloro-7-ethoxybicyclo[5.3.1]undec-1(11)ene has been synthesized and its struc-

ture determined by X-ray diffraction [118]. The twist in the  $\sigma$  framework is approximately  $60^\circ$ . As in the case of *trans*-cyclooctene, both ends of the  $\pi$  bond are pyramidally distorted in such a way as to reduce the twist angle of the  $p$  orbitals to  $29^\circ$ .

## ALKYNES

At the level of simple orbital interaction theory, alkynes differ from alkenes in only two respects. First, the carbon atoms are dicoordinated, with the consequence that the  $p$  orbitals are at higher energy than  $\alpha_C$ . Second, the shorter C—C separation implies that the intrinsic interaction will be larger than  $\beta_{CC}$ . The level of the degenerate  $\pi$  MOs is expected to be about the same as in alkenes but the  $\pi^*$  MOs will be higher in energy. Additional factors such as increased coulombic repulsion of the two electrons in each  $\pi$  MO (due to the shorter separation) may further destabilize the  $\pi$  MOs. In fact, the reactivity of alkynes toward electrophilic attack is rather similar to that of alkenes when the electrophile would be expected to form an acyclic intermediate (e.g., HX) but slower when a cyclic intermediate is formed (e.g., Br<sub>2</sub>) [114]. Addition of nucleophilic free radicals to alkynes proceeds more slowly than to alkenes, an observation consistent with the expected higher  $\pi^*$  MO of the former. However, addition of nucleophiles is faster in general than to alkenes [119, pp. 670–62]. Since strong charged nucleophiles are always associated with a metallic counterion, the Lewis acidity of the cation toward the second “nonreacting”  $\pi$  MO may be responsible for the increased reactivity.

## $\pi$ BONDS TO AND BETWEEN HIGHER ROW ELEMENTS

The principles discussed in Chapter 4 for the case of  $\sigma$  bonds to higher row elements apply with a vengeance in the case of  $\pi$  bonds. Thus  $\pi$  bond orbital energies and polarizations are determined not so much by  $n$   $p$  orbital energy differences as by the smaller intrinsic interaction matrix elements,  $\beta_{CX}$  or  $\beta_{XY}$ , for  $p$  orbitals with principal quantum numbers  $n > 2$ . Smaller  $\beta_{CX}$  or  $\beta_{XY}$  values are associated with decreased HOMO–LUMO gaps, decreased LUMO energies, increased HOMO energies, and higher polarizations, all of which dictate substantially decreased thermodynamic and kinetic stabilities. Indeed, besides the  $2p$ – $2p$   $\pi$  bonds discussed above, the only other combination in which it still makes sense to consider  $p$ – $p$   $\pi$  bonds is the  $2p$ – $3p$  case, that is, bonds of the type C=Si, C=P, and C=S, the third-row analogues of alkenes, imines, and carbonyls. Note that orbital nodal characteristics and size *do* favor  $\pi$  bonds of the  $2p$ – $n$   $d$  type, especially  $2p$ – $3d$ . The case of organometallic bonding is treated in Chapter 13.

## $\pi$ BONDS TO SILICON, PHOSPHORUS, AND SULFUR

The SHMO description of  $\pi$  bonds C=C, C=Si (silaethenes), and Si=Si (disilenes) are compared in Figure 6.3 using parameters taken from Table 5.1. According to the parametrization of Van Catledge [105], C and Si have the same value of  $h_X$  (i.e., 0.0), but this may not be correct since Si is substantially less electronegative than C (Table A.2). The intrinsic interaction matrix elements decrease in the following series: C=C,  $-1.00|\beta|$ ; C=Si,  $-0.75|\beta|$ ; Si=Si,  $-0.64|\beta|$ . Thus, the  $\pi$  bond energy decreases accordingly, but significant bond polarization is not predicted. The decreased HOMO–LUMO gap,

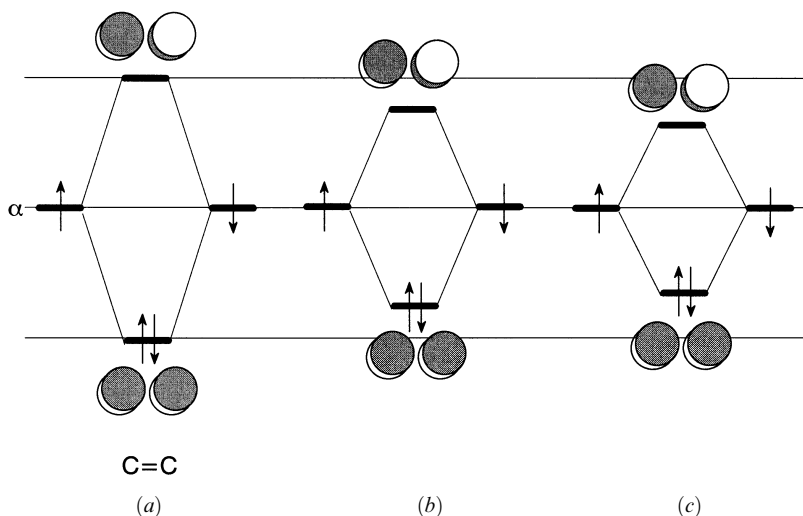


**Figure 6.3.** SHMO description of  $\pi$  bonds: (a) C=C; (b) C=Si; (c) Si=Si.

decreased LUMO energies, and increased HOMO energies of the C=Si and Si=Si species indicate substantially decreased thermodynamic and kinetic stabilities. Indeed, these species are in general not isolable but have been postulated as reactive intermediates [120, 121]. Silaethene,  $\text{CH}_2\text{SiH}_2$ , has been isolated in an argon matrix [122]. Its  $\pi$  bond energy has been determined experimentally,  $142 \pm 17$  kJ/mol [123], and theoretically, 132 kJ/mol [124], to be substantially lower than the  $\pi$  bond energy of ethylene, 269 kJ/mol [125]. The highly hindered tetramesityldisilene has been isolated [126], but not the parent,  $\text{SiH}_2\text{SiH}_2$ , whose  $\pi$  bond energy has been calculated to be only 97 kJ/mol [124]. In both silaethenes and disilenes, the silicon atom is not planar, but fairly strongly pyramidal [124].

## CHAPTER 7

---

# REACTIVE INTERMEDIATES

---

### REACTIVE INTERMEDIATES $[\text{CH}_3]^+$ , $[\text{CH}_3]^-$ , $[\text{CH}_3]^\cdot$ , AND $[\text{:CH}_2]$

The major carbon centered reaction intermediates in multistep reactions are carbocations (carbenium ions), carbanions, free radicals, and carbenes. Formation of most of these from common reactants is an endothermic process and is often rate determining. By the Hammond principle, the transition state for such a process should resemble the reactive intermediate. Thus, although it is usually difficult to assess the bonding in transition states, factors which affect the structure and stability of reactive intermediates will also be operative to a parallel extent in transition states. We examine the effect of substituents of the three kinds discussed above on the four different reactive intermediates, taking as our reference the parent systems  $[\text{CH}_3]^+$ ,  $[\text{CH}_3]^-$ ,  $[\text{CH}_3]^\cdot$ , and  $[\text{:CH}_2]$ .

#### Carbocations

Figure 7.1 shows the interaction diagrams relevant to a carbocation substituted by X:; Z, and "C" substituents:

- A carbocation is strongly stabilized by an X: substituent (Figure 7.1a) through a  $\pi$ -type interaction which also involves partial delocalization of the nonbonded electron pair of X to the formally electron-deficient center. At the same time, the LUMO is elevated, reducing the reactivity of the electron-deficient center toward attack by nucleophiles. The effects of substitution are cumulative. Thus, the more X:-type substituents there are, the more thermodynamically stable is the cation and the less reactive it is as a Lewis acid. As an extreme example, guanidinium ion, which may be written as  $[\text{C}(\text{NH}_2)_3]^+$ , is stable in water. Species of the type  $[\text{—C}(\text{OR})_2]^+$  are common intermediates in acyl hydrolysis reactions. Even cations stabilized by fluorine have been reported and recently studied theoretically [127].

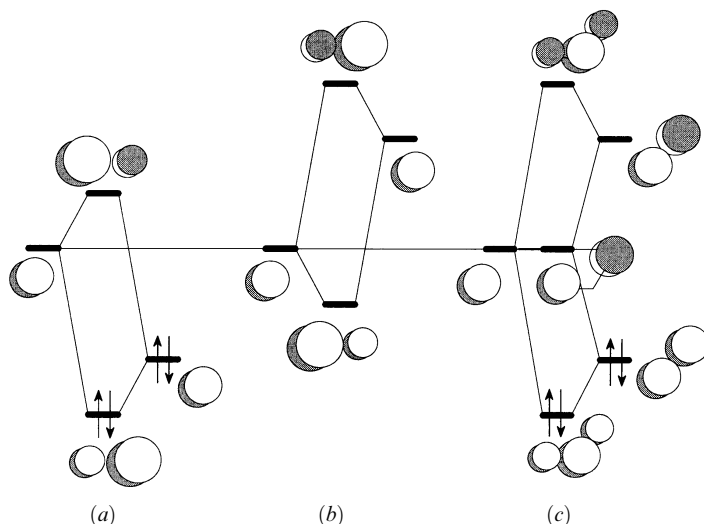


**Figure 7.1.** Carbocationic center interacting with (a) an X substituent; (b) a Z substituent; (c) a “C” substituent.

The filled bond orbitals of adjacent alkyl groups may donate electrons by  $\pi$ -type overlap (see Figures 3.19 and 3.20 in Chapter 3) to an adjacent carbocationic center. Thus, an alkyl group may be considered to be an X-type substituent. The highest combination of the C—H bonding orbitals of a methyl group has a  $\pi$  donor capability intermediate to that of the nonbonded orbitals of O and F. The donor abilities of  $\sigma$  bonds were discussed in Chapter 4.

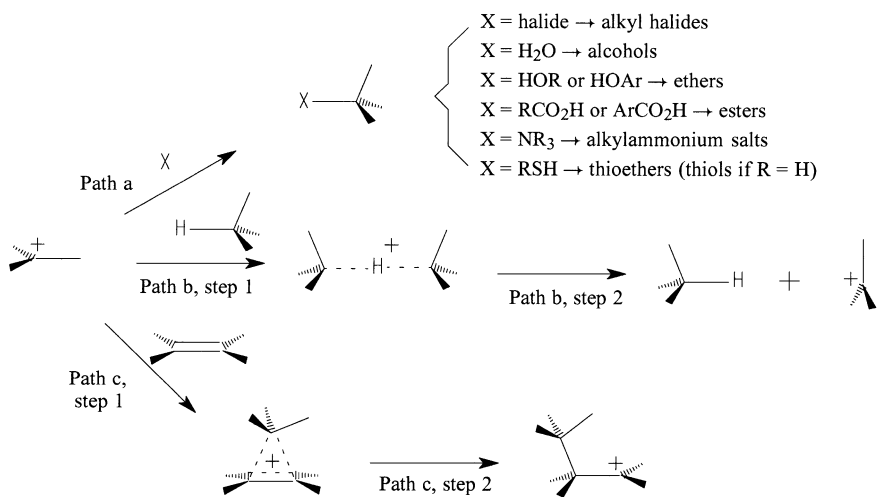
- A carbocation is only weakly stabilized by a Z substituent (Figure 7.1*b*) through a  $\pi$ -type interaction with the  $\pi$  bond of the Z group (not shown in Figure 7.1*b*). The interaction is weak because the  $\pi$  bond of a Z substituent is very low in energy and polarized away from the cationic center. The dominant interaction is with the LUMO of Z, which does not add to thermodynamic stabilization but greatly enhances the Lewis acidity of the cation, increasing the reactivity of the electron-deficient center toward attack by nucleophiles. The Z-substituted cations are being increasingly reported as intermediates in solvolysis reactions [128].
- A carbocation is strongly stabilized by a “C” substituent (Figure 7.1*c*) through  $\pi$ -type interactions which involve substantial delocalization into the substituent. The LUMO energy is relatively unchanged, but the reactivity of the electron-deficient center toward attack by nucleophiles is reduced because the orbital coefficients are smaller. Allyl and benzyl carbocations are prototypical of “C”-substituted carbocations. The effects of substitution are cumulative. Thus, the more “C”-type substituents there are, the more thermodynamically stable is the cation and the less reactive it is as a Lewis acid. A prime example is triphenyl carbocation.

### Intermolecular Reactions of Carbocations

Carbocations are strong Lewis acids which occur as intermediates in reactions following the  $S_N1$  (Chapter 9) or  $E1$  (Chapter 10) mechanistic routes. The most obvious and



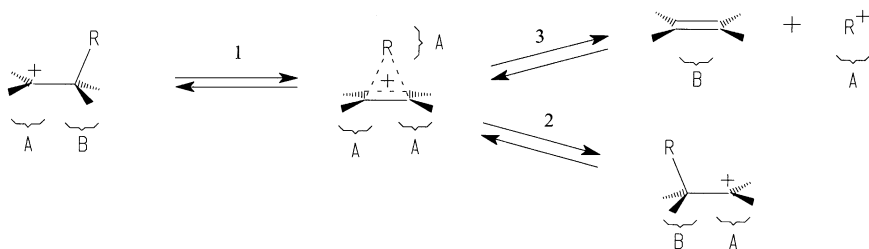
common reaction is recombination with a nucleophile (a Lewis base) to form a  $\sigma$  bond:



If the nucleophilic site (HOMO) involves a nonbonded pair of electrons (path *a*), a stable covalently bonded complex will form. If the HOMO is a  $\sigma$  bond, direct reaction is unlikely unless the bond is high in energy and sterically exposed, as in a three-membered ring, but if the bond is to H, hydride abstraction may occur (path *b*, steps 1 and 2) or a hydride bridge may form (path *b*, step 1). The last two possibilities are discussed further in Chapter 10. If the HOMO is a  $\pi$  bond, a “ $\pi$  complex” may result (path *c*, step 1), or, more commonly, donation of the  $\pi$  electrons results in the formation of a  $\sigma$  bond at the end where the  $\pi$  electron density was higher, the other end becoming Lewis acidic in the process (path *c*, steps 1 and 2). The effects of substituents on olefin reactivity were discussed in Chapter 6.

### Intramolecular Reactions of Carbocations

Intramolecular reactions of carbocations are shown in the following scheme:

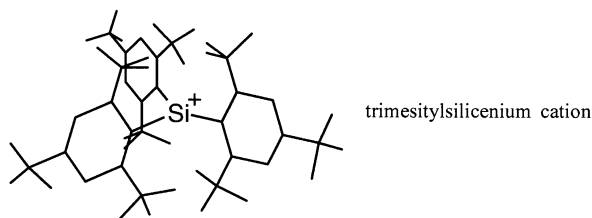


The combination of steps 1 and 2 corresponds to a 1,2 hydride shift ( $\text{R} = \text{H}$ ) or a Wagner–Meerwein rearrangement ( $\text{R} = \text{alkyl}$ ). The intermediate bridged nonclassical structure

reached after step 1 may correspond to a transition state for the rearrangement, or the stable form of the carbocation. If  $R = H$ , the bridged form is known to be stable only in the case of ethyl cation, where there are no substituents on either carbon atom (other than H). In other cases, stable bridged forms are obtained if the R group has a relatively loosely bound pair of electrons in a  $p$ - or  $\pi$ -type orbital for back donation into the  $\pi^*$ -like orbital of the C—C fragment, as in the case of  $R = \text{halide}$  (e.g., bromonium ion),  $R = \text{aryl}$  (e.g., ethylbenzenium ion [129]), or  $R = \text{vinyl}$  (cyclopropylcarbinyl cation). More or less symmetrical bridging by  $R = \text{alkyl}$  is not likely but has been shown to be the case in the 2-norbornyl cation [98, 130]. Depending on substituents in R, elimination of  $R^+$  may occur (step 3). Each of the cationic species may react intermolecularly, as shown in the previous scheme at sites labeled A. If  $R = H$ , the hydrogen end of the  $\sigma$  bond in the two “classical” structures is also liable to attack by nucleophile (the E1 mechanism, Chapter 10). Of course, step 3 would not occur in this case.

### Silyl Cations

The silicon analogs of carbocations have been reported a number of times [131], but there is only one confirmed “sighting” to date, the highly hindered trimesitylsilicenium ion as its tetrakis(pentafluorophenyl)borate salt [132]:



From the point of view of kinetic or thermodynamic stability of silyl cations, what can be deduced from orbital interaction theory? Silicon is less electronegative than carbon (Table A.2), so on the face of it, the empty  $3p$  orbital energy should be higher than the energy of the  $2p$  orbital of C. However, this is probably *not* true in the case of stabilized carbocations since strong  $2p-2p$   $\pi$ -type stabilizing interactions will raise the LUMO well above  $|\alpha|$  and result in extensive delocalization (lower the coefficient at C). On the other hand, the much weaker  $3p-2p$   $\pi$ -type interactions will have little effect in raising or delocalizing the LUMO of silyl cations, which will remain as very powerful Lewis acids, coordinating with solvent and possibly undergoing intramolecular group migrations to give the relatively much stronger  $\sigma$  bonds to Si. Thus, silyl cations are thermodynamically stable but kinetically very reactive.

### Carbanions

Except for the most highly stabilized carbanions, carbanion chemistry in solution is always complicated by the presence of the counterion, usually a metal, which is a Lewis acid and almost invariably is involved in the course of the reaction. Relative stabilities of carbanions in solution are difficult to establish for the same reason. In recent years, much information has been gathered about carbanion stabilities, structures, and reactiv-

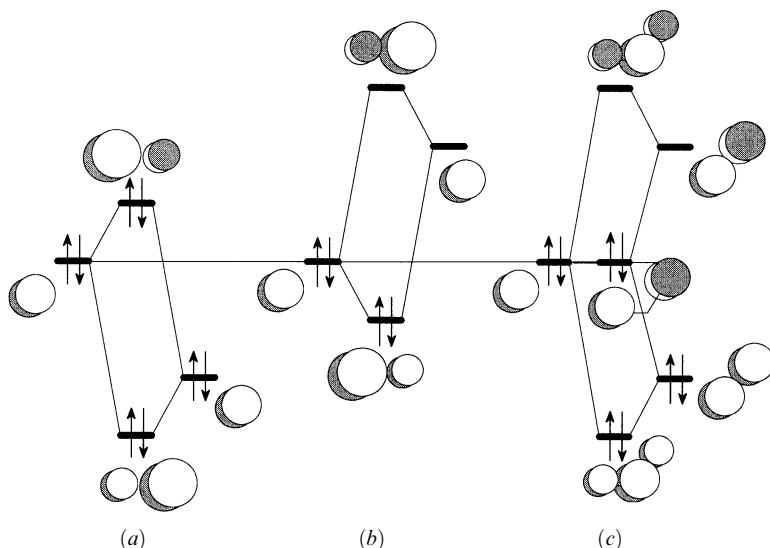
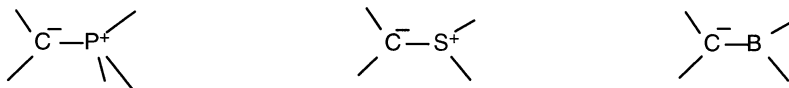


**Figure 7.2.** Carbanionic center interacting with (a) an X: substituent; (b) a Z substituent; (c) a “C” substituent.

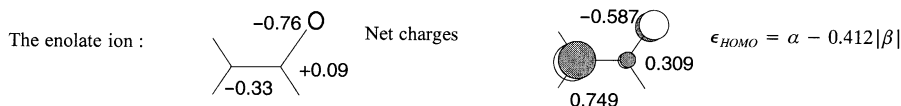
ities in the gas phase [133]. Figure 7.2 shows the interaction diagrams relevant to a carbanion substituted by X:, Z, and “C” substituents.

- A carbanion is destabilized by an X: substituent (Figure 7.2a) through a two-orbital, four-electron  $\pi$ -type interaction. The Lewis basicity and nucleophilicity are greatly increased. Because the HOMO is so high in energy, some involvement may be observed by the X: group’s LUMO, particularly in the case of alkyl-substituted carbanions where gas-phase basicities suggest that in some cases the alkyl group may act to stabilize a carbanion [133]. Carbanions are easily oxidized and may spontaneously autoionize in the gas phase. Methyl carbanion is stable in the gas phase, but ethyl, 2-propyl, and *tert*-butyl carbanions have not been observed in the gas phase [133]. Accordingly, radical intermediates should always be suspected in X:-substituted carbanionic reactions in nonpolar media. The  $\pi$  effects of X: substitution are somewhat offset by the inductive effect of the electronegative X:. There is some evidence that the inductive effect accumulates more rapidly than the resonance effect, especially if the X: substituents have  $3p$  or higher nonbonded orbitals where the intrinsic interaction matrix element is smaller and so the net repulsion is less. Carbanions next to two sulfur atoms are common. Halogen substitution also favors carbanion formation [134].
- A carbanion is strongly stabilized by a Z substituent (Figure 7.2b) through the  $\pi$ -type interaction with the LUMO of the Z group. The Z-substituted carbanions are common intermediates in solvolysis reactions and as nucleophiles in C—C bond forming reactions. The involvement of  $-\text{CF}_3$  groups as Z-type substituents has been well documented [135]. Phosphonium ( $\text{R}_3\text{P}^+-$ ) and sulfonium ( $\text{R}_2\text{S}^+-$ ) groups stabilize carbanionic centers, forming ylides. The stabilization is due in part to electrostatic effects and in part to orbital interactions via  $\sigma^*$  or  $3d$  involvement,

both of which may be lowered in energy by the formal positive charge. In the last sense, these groups are acting as Z-type substituents. The synthetic potential of trigonal boron as a Z-type substituent in stabilizing carbanionic centers has been demonstrated [136]:



The very important reactive intermediate, the enolate ion, is an example of a Z-substituted carbanion. The charge distribution and HOMO obtained by SHMO calculation are shown below:



The oxygen atom bears the majority of the negative charge, but the HOMO has the highest contribution from the carbon atom. Accordingly, charged electrophiles (hard electrophiles) should preferentially add to the oxygen atom and neutral (soft) electrophiles would be expected to add to the carbon atom. The gas-phase reactions of acyclic enolate ions have been studied by Fourier transform ion cyclotron spectroscopy [137]. The C or O selectivity was shown to depend on the HOMO energy (as measured by electron detachment threshold energies) and frontier orbital interactions as well as the charge distribution.

- A carbanion is also stabilized by a “C” substituent (Figure 7.2c) through  $\pi$ -type interactions which involve substantial delocalization into the substituent. The HOMO energy is relatively unchanged, but the reactivity of the electron-rich center toward attack by electrophiles is reduced because the orbital coefficients are smaller. The “C”-type substituents are predominantly hydrocarbons and cannot easily support a negative charge unless other factors are present.

## Carbon Free Radicals

Free radicals are molecules with an odd number of electrons. In our simple theory, all electrons are considered to be paired up in molecular orbitals, leaving one orbital with a single electron. The molecular orbital which describes the distribution of the “odd” electron is designated the SOMO (singly occupied MO). In the ground state of the radical, the SOMO is also the highest occupied MO. Often the SOMO is strongly localized. If the localization is to a tricoordinated (trigonal) carbon atom, then the radical species is described as a carbon free radical.

**Structures.** The methyl radical is planar and has  $D_{3h}$  symmetry. Probably all other carbon-centered free radicals with alkyl or heteroatom substituents are best described as shallow pyramids, driven by the necessity to stabilize the SOMO by hybridization or to align the SOMO for more efficient  $pi$ -type overlap with adjacent  $\sigma$  bonds. The planarity of the methyl radical has been attributed to steric repulsion between the H atoms [138]. The C center may be treated as planar for the purpose of constructing orbital interaction diagrams.

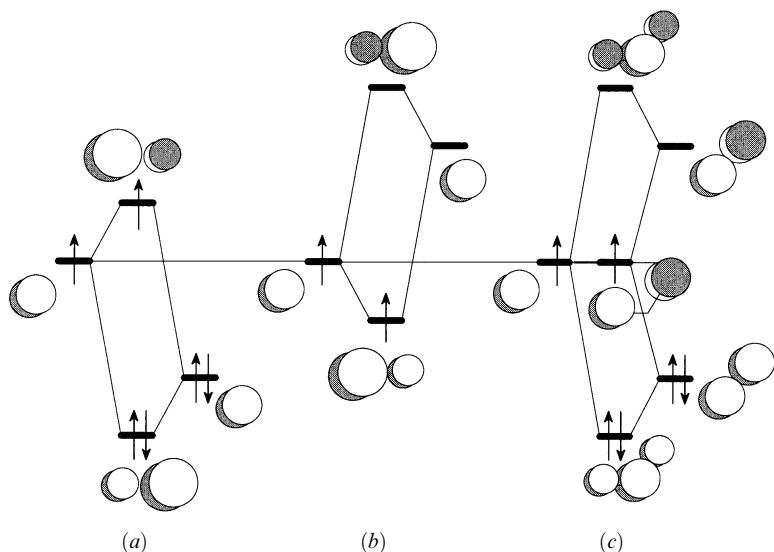


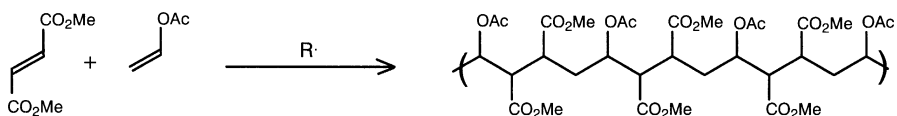
**Figure 7.3.** Carbon free radical center interacting with (a) an X: substituent; (b) a Z substituent; (c) a “C” substituent.

**Substituent Effects and Reactivity.** If the SOMO is relatively low in energy, the principal interaction with other molecules will be with the occupied MOs (three-electron, two-orbital type, Figure 3.8). In this case the radical is described as *electrophilic*. If the SOMO is relatively high in energy, the principal interaction with other molecules may be with the unoccupied MOs (one-electron, two-orbital type, Figure 3.10). In this case the radical is described as *nucleophilic*. Substituents on the radical center will affect the electrophilicity or nucleophilicity of free radicals, as shown below.

Figure 7.3 shows the interaction diagrams relevant to a carbon free radical substituted by X:, Z, and “C” substituents. The figure also applies to free radicals centered on other atoms if one takes into account the orbital energies appropriate for the heteroatom:

- A free radical is stabilized by an X: substituent (Figure 7.3a) through a two-orbital, three-electron  $\pi$ -type interaction. The nucleophilicity of the radical is greatly increased. The X:-substituted free radicals are more easily oxidized. The  $\pi$  effects of X: substitution are somewhat augmented by the inductive effect of the electro-negative X: in stabilizing the radical.
- A carbon free radical is stabilized by a Z substituent (Figure 7.3b) through the  $\pi$ -type interaction with the LUMO of the Z group. The SOMO is lowered in energy and the free radical is more electrophilic as a consequence.
- A carbon free radical is also stabilized by a “C” substituent (Figure 7.3c) through  $\pi$ -type interactions which involve substantial delocalization into the substituent. The SOMO energy is relatively unchanged, but the reactivity of the odd-electron center is reduced because the orbital coefficients are smaller.

Free-radical polymerization of a 1 : 1 mixture of dimethyl fumarate and vinyl acetate, resulting in a highly regular alternating copolymer, illustrates the importance of substitution on the properties of both the free radical and the olefinic substrate [139]:



Dimethyl fumarate is a *Z*-substituted olefin. It has a low-lying LUMO which is not polarized due to the symmetrical substitution. Because of the low-lying LUMO, dimethyl fumarate is susceptible to nucleophilic attack. On the other hand, vinyl acetate is an olefin with an X<sup>•</sup> substituent at one end. The HOMO is polarized away from the substituent acetoxy group, OAc. Since the HOMO is also raised in energy as a result of the interaction, vinyl acetate would be particularly susceptible to electrophilic attack, the preferred site being the C atom β to the substituent. Addition of a radical to dimethyl fumarate generates a *Z*-substituted carbon free radical. Addition of a radical to vinyl acetate generates an X<sup>•</sup>-substituted carbon free radical. Each of the two possible types of radicals has an equal probability of encountering either olefin. The situation is depicted in Figure 7.4 The low-lying SOMO of the electrophilic fumarate radical (left) interacts preferentially with the high HOMO of vinyl acetate, leading to selective formation of the acetoxy radical (right). The high SOMO of the acetoxy radical interacts most strongly with the low LUMO of dimethyl fumarate with selective formation of the fumarate radical. And so on.

Radical stabilities may be measured experimentally by the determination of homolytic bond dissociation energies (BDEs) in the gas phase [140] or in solution by relating them empirically to the  $pK_{\text{HA}}$  and the oxidation potentials,  $E_{\text{ox}}(\text{A}^-)$  of weak acids,

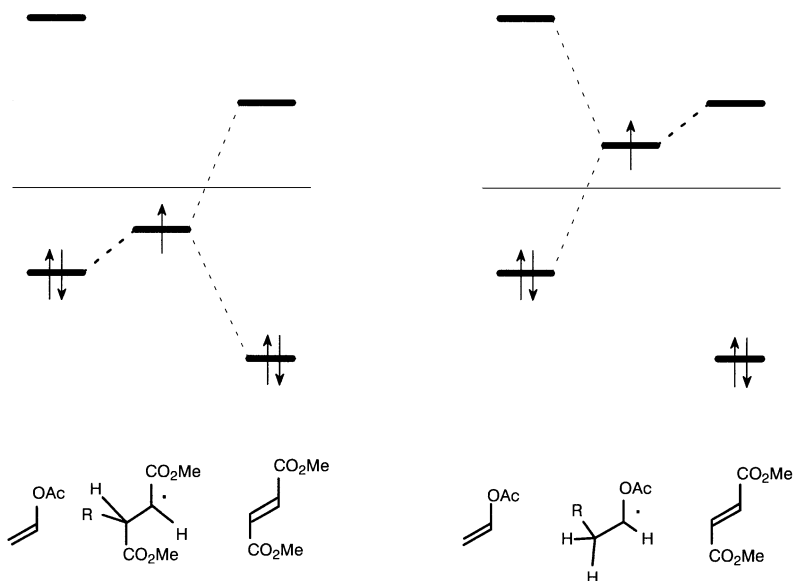


**Figure 7.4.** Interactions which determine the relative reactivities of carboxyalkyl (left) and acyloxy radicals.

H—A [141] (kJ/mol):

$$\text{BDE}_{\text{HA}} = 5.73pK_{\text{HA}} + 96.5E_{\text{ox}}(\text{A}^-) + 234.3$$

A quantity called the radical stabilization energy (RSE) may be defined to relate the stabilities of substituted carbon radicals to the methyl radical. The effects of adjacent X:, Z, and "C" substituents on the RSEs of carbon-centered radicals has been widely investigated [142, 143]. The expectations based on simple orbital interaction theory as espoused above are widely supported by the experimental findings, except that when the the  $\pi$  donor or  $\pi$  acceptor ability of the group is weak and the inductive electron-withdrawing power is large, as in  $\text{F}_3\text{C}^\bullet$  and  $(\text{Me})_3\text{N}^+\text{CH}_2^\bullet$ , the net effect is to destabilize the radical relative to the methyl radical [143]. The BDE of a C—H bond of a compound R—H is another measure of stability of the product radical, R'. It is related to the RSE by

$$\text{RSE}(\text{R}') = 439 - \text{BDE}(\text{R—H})$$

Where  $\text{BDE}(\text{CH}_4) = 439$  kJ/mol [140]. The RSE values for a number of radicals of the type  $\text{:X—CH}_2^\bullet$  are ( $\text{:X}$ , RSE in kJ/mol)  $\text{CH}_3$ , 16 [144];  $\text{NH}_2$ , 46 [145];  $\text{OH}$ , 37 [144];  $\text{F}$ , 16 [146];  $\text{SH}$ , 45 [147], 36 [146]; and  $\text{Cl}$ , 21 [146]. The trends among the  $\pi$  donor groups are generally as expected by orbital interaction considerations. The X: group with the highest  $2p$ -like HOMO ( $\text{NH}_2$ ) produces the greatest stabilization. The effect of a methyl group is similar to a fluorine substituent. Chlorine, with an electronegativity similar to oxygen but with a  $3p$  HOMO, produces a smaller RSE than OH, which has a  $2p$  HOMO and a correspondingly larger intrinsic interaction matrix element with the SOMO of the methylene group. There is a large uncertainty in the value for SH, with theoretical computations [146] favoring a lower value for RSE than the experimental value [147]. On the basis of the same electronegativity and intrinsic matrix element arguments as were applied for OH versus Cl, one would expect an RSE of the SH group to be less than that of the  $\text{NH}_2$  group.

The RSE values of some radicals of the type  $\text{Z—CH}_2^\bullet$  are (Z, RSE in kJ/mol) [146]  $\text{CHO}$ , 54;  $\text{COCH}_3$ , 54;  $\text{CN}$ , 51;  $\text{NO}_2$ , 44;  $\text{COOH}$ , 32; and  $\text{CONH}_2$ , 27. Among the carbonyl compounds, the trend is understandable in that the OH and  $\text{NH}_2$  substituents raise the energy of the LUMO ( $\pi_{\text{CO}}^*$ ), thus making the COOH and  $\text{CONH}_2$  groups poorer acceptors. The listing permits the placement of the CN and  $\text{NO}_2$  groups relative to the carbonyls.

It is instructive to compare the effects of *two* substituents, both of the same kind or one of each, on the RSE of radicals. As stated above, simple considerations imply that stabilization increases with increasing numbers of stabilizing substituents, but by how much? Table 7.1 gives the calculated RSEs of radicals of structure  $\text{G}^1\text{G}^2\text{CH}^\bullet$ . Comparison of any of the numbers with the single-substituent RSE values shown in the last column verifies that two stabilizing substituents of the same kind (diagonal numbers) or different (off-diagonal) yield more stabilization than a single substituent. The greatest stabilization ensues when both a Z-type and an X:-type substituent are present. This observation has been termed the *captodative effect* [142, 143, 148]. Thus neutral glycine, with both a donor  $\text{NH}_2$  group and an acceptor  $\text{CO}_2\text{H}$  group, is predicted to have a BDE ( $^{\circ}\text{C—H}$ ) of approximately 331 kJ/mol [149], and the BDE( $^{\circ}\text{C—H}$ ) values of all amino acid residues in proteins are predicted to be less than that of the S—H bond of cysteine or glutathione:  $\text{BDE}(\text{S—H}) = 366$  kJ/mol [150].

**TABLE 7.1. Radical Stabilization Energies (kJ/mol) of Mono- and Disubstituted Methyl Radicals,  $G^1G^2CH^a$** 

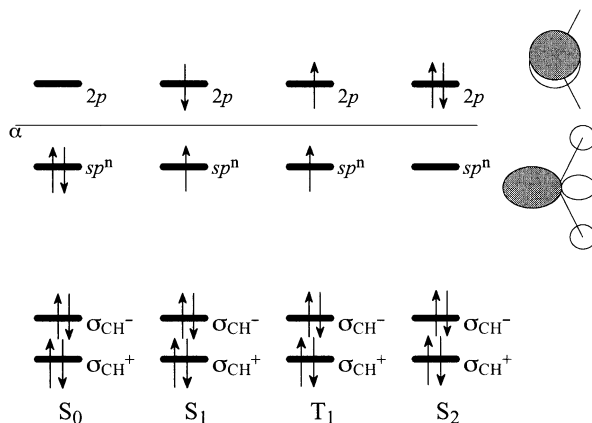
$G^1 \setminus G^2$	NH <sub>2</sub>	OH	CO <sub>2</sub> H	CN	CHO	H
NH <sub>2</sub>	69, <sup>b</sup> 42 <sup>c</sup>	73 <sup>b</sup>	105	99	119, 120 <sup>c</sup>	46, 46 <sup>c</sup>
OH	73 <sup>b</sup>	46	101	94	100	37, 32 <sup>c</sup>
CO <sub>2</sub> H	105	105	39	—	—	32, 17 <sup>c</sup>
CN	99	94	—	99	88 <sup>b</sup>	51, 28 <sup>c</sup>
CHO	119	100	—	88 <sup>b</sup>	68, <sup>b</sup> 76 <sup>c</sup>	54, 30 <sup>c</sup>

<sup>a</sup>Except as noted, data from Ref. 146.<sup>b</sup>b3lyp/6-31G\*.<sup>c</sup>RMP2/6-311+G(d)//b3lyp/6-31G\*.

## Carbenes

Carbenes are species which contain a dicoordinated carbon atom formally with two valence electrons. The possible electronic structures of the parent carbene, methylene  $:CH_2$ , are shown in Figure 7.5. The  $2p$  orbital of the dicoordinated C atom is placed above  $\alpha$  by about  $0.25|\beta|$  in order to accommodate the lower electronegativity.

One would expect on the basis of Hückel MO theory that the lowest energy configuration, i.e., the electronic ground state of  $:CH_2$ , is  $S_0$  ( $^1A_1$ ). This is incorrect. In this case we are done in by the assumption that the electron–electron coulomb repulsion can be neglected. The coulomb repulsion is most severe when two electrons are constrained to the same small MO. Although one pays a price for separation of the electrons into different MOs, this is largely compensated by the relief of electron–electron repulsion which ensues by virtue of the orthogonality of the MOs. Thus, while it is true that  $S_0$  is lower in energy than  $S_1$ , the difference is not as great as might have been expected. The *triplet* configuration,  $T_1$  ( $^3B_1$ ), is additionally stabilized by relief of “exchange repulsion,” the self-avoidance of two electrons with the same spin, that is, the principle underlying Hund’s rule. The triplet configuration  $T_1$  falls 37.7 kJ/mol *below*  $S_0$  in the case of  $:CH_2$  [151]. The geometries of singlet and triplet carbene are different: singlet, HCH = 103° [152]; triplet, HCH = 136° [153]. The chemical consequences of whether

**Figure 7.5.** Electronic configurations and state designations for  $:CH_2$ .



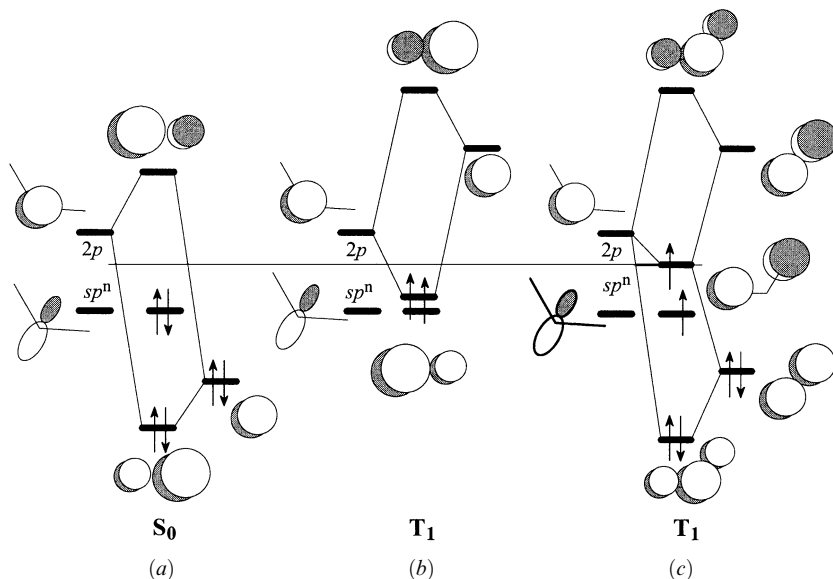


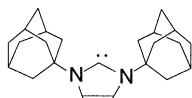
**Figure 7.6.** Carbene center interacting with (a) an X: substituent; (b) a Z substituent; (c) a “C” substituent. Only the two highest MOs of the carbene are shown.

the carbene is in its lowest singlet state ( $S_0$ ) or in its lowest triplet state ( $T_1$ ) are dramatic. With the electrons spin paired, the possibility exists for concerted reactions which preserve stereochemistry. This possibility is precluded if the carbene is in the triplet state. Chemical reactions of triplet carbenes are nonconcerted and are accompanied by undesirable side reactions, possible isomerizations, and loss of stereochemical integrity. The olefin insertion reaction which yields cyclopropanes is discussed in more detail in Chapter 14.

The small difference between the energies of  $S_0$  and  $T_1$  may easily be overturned by the effects of substituents on the carbene center. Figure 7.6 shows the interaction diagrams which are relevant to the interaction of the carbene center with each of the three types of substituent. Because of more favorable overlap, the interaction of the carbon 2p orbital with substituent p or  $\pi$  orbitals is expected to dominate. The  $sp^n$  orbital which lies in the nodal plane of the substituent p or  $\pi$  orbital will not interact except more weakly with substituent  $\sigma$  orbitals. Its energy is shown in Figure 7.6 as unperturbed by the substituent.

The 2p orbital of the carbene is raised in energy by an X: substituent (Figure 7.6a), thereby increasing the separation of the 2p and  $sp^n$  orbitals. The ground state of an X:-substituted carbene is  $S_0$ . In  $:\text{CHF}$ ,  $S_0$  is lower than  $T_1$  by 61.5 kJ/mol [154]. In  $:\text{CF}_2$ , the separation is 237 kJ/mol [155]. Many carbenes in this class are known. The most familiar is dichlorocarbene,  $:\text{CCl}_2$ , whose lower singlet electronic states have been investigated by ab initio calculations [156, 157]. The ground states of  $:\text{CBr}_2$  and  $:\text{Cl}_2$  have also been predicted to be singlet [157]. Chloromethoxy carbene,  $\text{Cl}-\text{C}-\text{OCH}_3$ , has been studied spectroscopically [158]. See also reference 159 for an experimental and theoretical study of  $:\text{C}(\text{OCH}_3)_2$  and  $\text{F}-\text{C}-\text{OCH}_3$ . Singlet carbenes have a low-lying (approximately) empty 2p orbital and so, like carbocations, can undergo 1,2 hydride or alkyl migrations

to the carbene carbon. Dimethoxy carbenes yield esters by this mechanism [160]. A stable crystalline carbene with two N substituents has been prepared and characterized [161]:



1,3-di-1-adamantylimidazol-2-ylidene

The carbene 1,3-di-1-adamantylimidazol-2-ylidene is additionally stabilized by aromaticity of the 5-membered ring and by steric protection by the neighboring adamantyl substituents. Similar carbenes with the adamantyl groups replaced by aryl groups are also stable [162]. An alkyl group may be regarded as a weak  $X\cdot$ -type substituent. The  $S_0$  state of dimethylcarbene,  $(\text{CH}_3)_2\text{C}$ , is predicted to be only 5.9 kJ/mol lower than  $T_1$  by ab initio calculations [163].

As shown in Figures 7.6*b,c*,  $Z$  and “ $C$ ” substituents either lower the  $2p$ - $sp^n$  gap or leave it about the same. In either case, the ground state for  $Z$ - or “ $C$ ”-substituted carbenes is expected to be  $T_1$ . See recent investigations of phenyl carbene,  $\text{C}_6\text{H}_5\text{CH}$ , [164]; ethynyl carbene,  $\text{HC}\equiv\text{C}-\text{CH}$  [165]; carboxylate-substituted carbenes,  $\text{R}-\text{C}-\text{CO}_2\text{R}'$  [166]; and formyl carbene,  $\text{H}-\text{C}-\text{C}(\text{O})\text{H}$  [167].

Silylenes, the silicon analogs of carbenes, are important intermediates in many thermal and photochemical reactions of organosilicon compounds [168]. Some have been isolated [169]. The chemistry is characterized both by high electrophilicity and nucleophilicity for the same reasons as discussed above in the case of silyl cations.

## NITRENES AND NITRENIUM IONS

Nitrenes ( $[\text{NH}]$ ) are the neutral nitrogen analogs of carbenes, while nitrenium ions ( $[\text{NH}_2]^+$ ) are isoelectronic to carbenes. Many of the reactions which are observed for carbenes have parallels in nitrene and nitrenium ion chemistry. Like carbenes, nitrenes and nitrenium ions can exist in both singlet and triplet states. There are some interesting divergences in chemical properties and in the effects of substituents, however, which are readily understood on the basis of orbital interaction diagrams.

### Nitrenes

Nitrenes are neutral species which contain a monocoordinated nitrogen atom formally with four valence electrons. The possible electronic structures of the parent nitrene,  $\text{NH}$ , are shown in Figure 7.7. On the basis of extrapolation from the energies of the  $2p$  orbitals of tricoordinated ( $\alpha - 1.37|\beta|$ ) and dicoordinated ( $\alpha - 0.51|\beta|$ ) nitrogen atoms, one would expect the energy of the degenerate  $2p$  orbitals of the monocoordinated N atom to be close to  $\alpha$ . The ground state is the triplet,  $T_1$ , which falls 155 kJ/mol below  $S_0$ , which has the same orbital description [170]. The singlet state,  $S_1$ , which is analogous to  $S_0$  of  $:\text{CH}_2$ , has been found spectroscopically to lie 261 kJ/mol above  $T_1$  [170]. The energy separations, which are much larger than in the corresponding carbene, represent relief of exchange and coulomb repulsion of the smaller orbitals of nitrogen. The gap between the nonbonding orbital,  $sp$ , and the degenerate  $2p$  orbitals is sufficiently large that states such as  $S_2$  (Figure 7.7) do not figure into the chemistry of nitrenes.

The singlet state,  $S_1$ , is the first state reached when a nitrene is generated by most methods, including photolysis of the corresponding azide,  $\text{R}-\text{N}_3$ . The reactions of

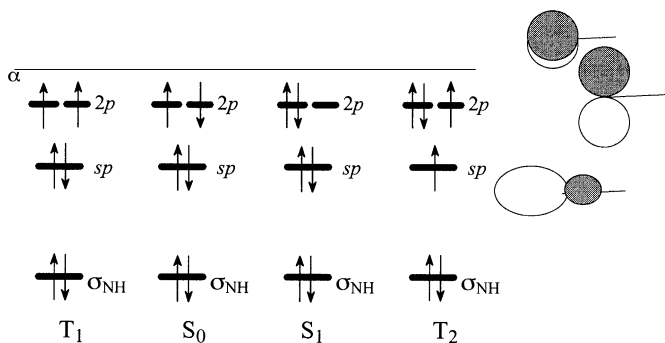


Figure 7.7. Electronic configurations and state designations for NH.

singlet nitrenes are similar to analogous reactions of singlet carbenes, with the exception that nitrenes have a much greater propensity for dimerization, yielding the azo compound,  $R-N=N-R$ .

Figure 7.8 shows the interaction diagrams which are relevant to the interaction of the nitrene nitrogen with each of the three types of substituent. The situation is somewhat more complex than in the case of carbenes because some X: substituents (i.e., halogens) are axially symmetric and do not lift the degeneracy of the  $2p$  orbitals. Alkyl substituents are also approximately three fold symmetric and probably would not lift the degeneracy enough to make the singlet state more stable. The amino group will raise the  $\pi$  system

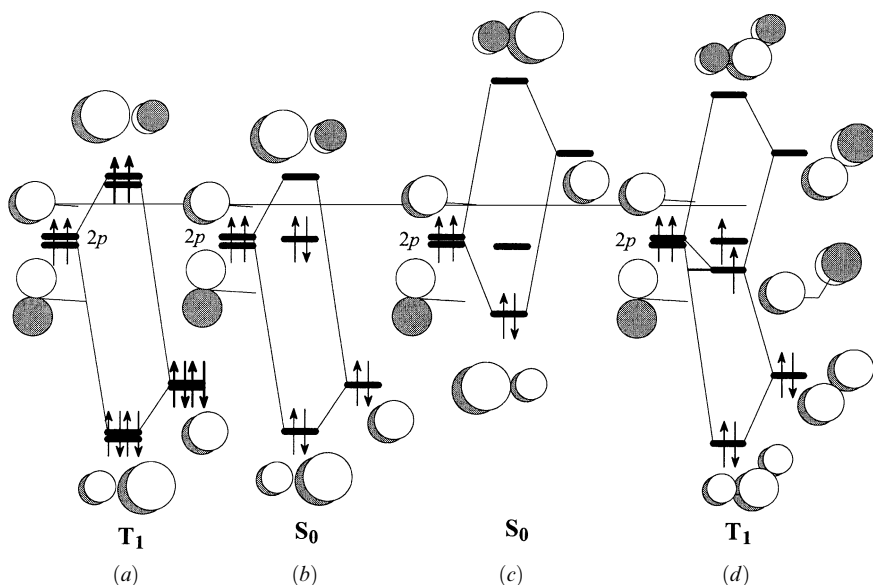
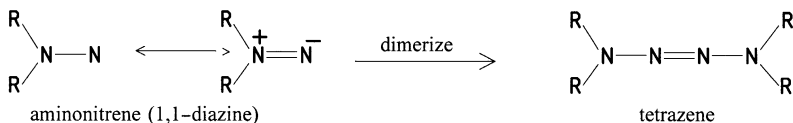


Figure 7.8. Nitrene center interacting with (a) an axially symmetric X: substituent; (b) a planar X: substituent; (c) a Z substituent; (d) a "C" substituent. Only the two highest MOs of the nitrene are shown.

sufficiently to result in a singlet closed-shell ground state. Theoretical studies on aminonitrene,  $\text{H}_2\text{N}-\text{N}$ , find the singlet state to lie 63 kJ/mol below the triplet state [171]. However, the nitrene is very strongly basic and nucleophilic. The relatively small HOMO–LUMO gap suggests that such nitrenes may be colored and have a strong tendency to dimerize. Indeed, dialkylaminonitrenes, also called 1,1-diazines, are well known and dimerize to tetrazenes [172]:



As shown in Figure 7.8c, Z substituents also may yield nitrenes with singlet ground states, in this case by lowering the energy of the  $\pi$  system. The remaining  $2p$  orbital is relatively low in energy. Thus acyl nitrenes will be strong Lewis acids at nitrogen in the  $\sigma$  plane. Such nitrenes have a strong tendency to rearrange by a 1,2 migration of the group attached to the acyl carbon to yield isocyanates. If the group is alkyl, the group migration is concurrent with nitrene formation, as in the Curtius, Hofmann, and Lossen rearrangements [173].

As with carbenes, “C” substituents will not alter the  $2p_{\pi}-2p_{\sigma}$  gap appreciably (Figure 7.8d). Thus, the ground state for “C”-substituted nitrenes is expected to be  $T_1$ . Theoretical [174, 175] and experimental [176] studies of phenylnitrene,  $\text{C}_6\text{H}_5\text{N}$ , are in agreement that the ground state is the triplet  $\pi$  radical,  ${}^3A_2$  ( $T_1$  of Figure 7.8d), which lies 75 kJ/mol below the open shell singlet,  ${}^1A_2$ . The closed-shell state,  $S_0$ , that is,  ${}^1A_1$ , is predicted to lie 162 kJ/mol above the triplet ground state [174].

## Nitrenium Ions

Nitrenium ions are isoelectronic to carbenes [177]. They contain a dicoordinated nitrogen atom formally with two valence electrons. The possible electronic structures of the parent nitrenium ion  $:\text{NH}_2^+$  are shown in Figure 7.9. On the basis of Hückel MO theory one would expect that the lowest energy configuration, that is, the electronic ground

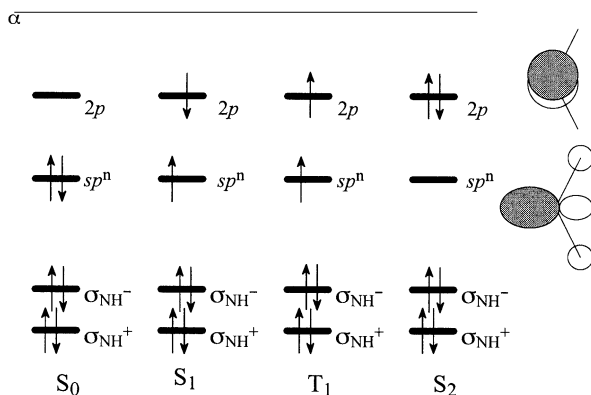
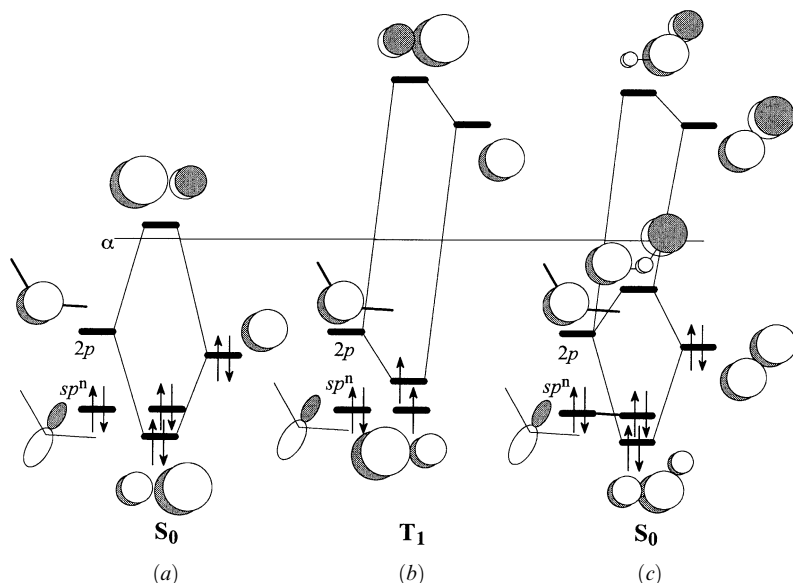


Figure 7.9. The electronic configurations and state designations for  $:\text{NH}_2^+$ .



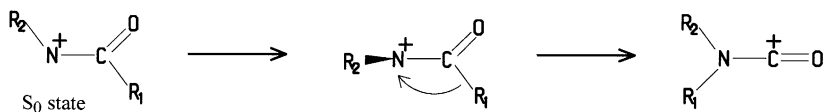
**Figure 7.10.** A nitrenium ion center interacting with: (a) an X: substituent; (b) a Z substituent; (c) a “C” substituent. Only the two highest MOs of the nitrenium ion are shown.

state of  $:\text{NH}_2^+$ , is  $S_0$  ( $^1A_1$ ). As with  $:\text{CH}_2$ , this is incorrect. The state  $T_1$  falls 126 kJ/mol below  $S_0$  in the case of  $:\text{NH}_2^+$  [178, 179].

Figure 7.10 shows the interaction diagrams which are relevant to the interaction of the nitrenium ion with each of the three types of substituent. The  $2p$  and  $sp^n$  orbitals of the nitrenium ion are lower in energy than the analogous orbitals of a carbene. Several differences in the effects of substituents ensue:

- The  $2p$  orbital of the nitrenium ion will interact strongly with the  $p$  orbital of an X: substituent (Figure 7.10a). The nitrenium ion is considerably stabilized by the two-electron, two-orbital interaction. The  $2p$ – $sp^n$  gap is widened. The ground state of an X:-substituted nitrenium ion is expected to be  $S_0$ . Apparently, according to ab initio studies, a methyl group is not a sufficiently good  $\pi$  donor. The ground state of  $\text{CH}_3\text{NH}^+$  was found computationally to be  $T_1$  [179], although the cyclic dialkyl nitrenium ion,  $\overline{\text{CH}_2(\text{CH}_2)_3\text{N}^+}$ , is predicted to have ground state  $S_0$  [179]. The LUMO remains very low in energy and the X:-substituted nitrenium ion will be a strong Lewis acid. In fact, both  $\text{CH}_3\text{NH}^+$  and  $(\text{CH}_3)_2\text{N}^+$  are predicted to rearrange without activation by a 1,2 hydride migration from methyl to N on the singlet potential energy surface [179]. The X:-substituted phosphorus and arsenic analogs of nitrenium ions (phosphenium [180] and arsenium [181], respectively) are also known.
- As shown in Figure 7.10b, Z substituents will interact relatively weakly because of the larger energy separation than is found in Z-substituted carbenes. The interaction results in some stabilization but lowers the  $2p$ – $sp^n$  gap. Thus, the ground state for Z-substituted nitrenium ions is expected to be  $T_1$ . The triplet diradical will be strongly electrophilic. The  $S_0$  state with both electrons in the  $sp^n$  orbital would gain

no stability from the interaction with the carbonyl *in the planar configuration*. In fact, on the  $S_0$  potential surface, rotation through  $90^\circ$  about the acyl—N bond occurs, placing the  $sp^n$  orbital into conjugation with the Z substituent:



Where the Z substituent is a carbonyl group, the perpendicular orientation places the other acyl substituent parallel to the vacant  $2p$  orbital, and a rearrangement ensues if the second substituent on N is not a good  $\pi$  donor [177, 182].

- As shown in Figure 7.10c, because of the lower energy of the nitrenium ion orbitals, interaction of the  $2p$  orbital with the  $\pi$  bonding orbitals of “C” substituents will be stronger than the interaction with the  $\pi^*$  orbitals. Substantial stabilization ensues. The interaction raises the separation of the  $2p$  and  $sp^n$  orbitals. Thus, the ground state for “C”-substituted nitrenium ions is expected to be  $S_0$ , unlike the situation in “C”-substituted carbenes. This expectation has been supported by ab initio calculations on phenyl nitrenium ion [183, 184]. Because the LUMO remains very low, this type of nitrenium ion will be very electrophilic.

## CHAPTER 8

---

# CARBONYL COMPOUNDS

---

### REACTIONS OF CARBONYL COMPOUNDS

The frontier orbitals of a carbonyl group may be derived from the interaction of a tri-coordinated carbon atom and a monocoordinated oxygen, assuming the  $\sigma_{CO}$  bond to be already in place. The interaction diagram is shown in Figure 8.1. The  $\pi$  and  $\pi^*$  orbitals are derived from an SHMO calculation, although this is not necessary for a qualitative analysis. The nonbonded HOMO,  $n_O$ , is raised in energy slightly relative to an oxygen  $2p$  orbital as a result of a four-electron, two-orbital interaction with the out-of-phase combination of the other two  $\sigma$  bonds to carbon (not shown). A broader analysis of the carbonyl group was presented in Chapter 3. Refer to Figure 3.21 and the discussion following it.

#### Electrophilic Attack on a Carbonyl Group

The  $\pi$  bonding orbital is polarized toward the oxygen atom. The results of an SHMO calculation yield  $\pi = 0.540(2p_C) + 0.841(2p_O)$ . Thus the smaller coefficient of the carbon  $2p$  orbital means that the carbonyl  $\pi$  bond will interact rather weakly with substituents attached to the carbon atom. The energy of the HOMO,  $\epsilon_\pi = \alpha - 1.651|\beta|$ , suggests that the  $\pi$  bond is significantly less basic than that of ethylene. Of course, the  $\pi$  bond is not the HOMO. Indeed, the HOMO,  $n_O$ , is slightly higher in energy than the  $\pi$  bond of ethylene and more polarized, suggesting significantly greater basicity [185]. The electrophile will approach the molecule from a direction which will maximize its interaction with the HOMO, namely in the plane of the carbonyl group, toward the oxygen atom, in a direction more or less perpendicular to the C=O bond, as shown in Figure 8.2a. The approach vector is relatively unhindered. Involvement of the HOMO in bonding to the electrophile does not rupture the  $\pi$  bond. However, the coordination number of the oxygen atom increases from 1 to 2, and consequently its effective electronegativity will

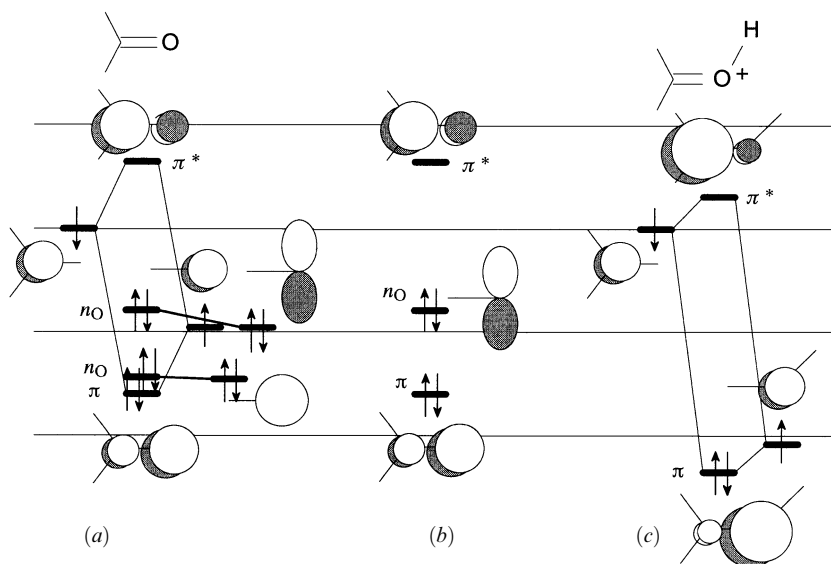


**Figure 8.1.** Carbonyl group: (a) interaction diagram; (b) the active orbitals (note the lower  $n_{\text{O}}$  has been omitted); (c) interaction diagram for a protonated carbonyl.

increase significantly as a consequence of attachment of the electrophile (e.g., a proton). Orbital interaction analysis predicts that the  $\pi^*$  (LUMO) is lowered in energy and is more highly polarized. Both factors enhance the reactivity of the carbonyl group toward nucleophilic attack, and this fact is routinely employed in the design of synthesis. The  $\pi$  system of a protonated carbonyl is shown in Figure 8.1c.

### Basicity and Nucleophilicity of the Oxygen Atom

Simple orbital interaction theory is only partially informative in distinguishing the relative basicities (nucleophilicities) of carbonyl groups in different bonding environments,

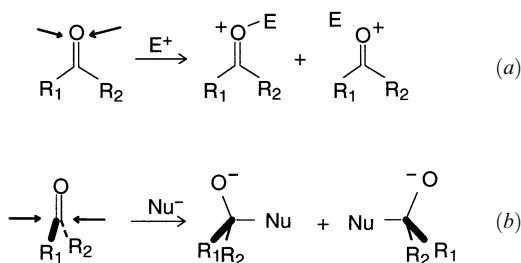


**Figure 8.2.** Reaction of a carbonyl compound with (a) an electrophile (Lewis acid) and (b) a nucleophile (Lewis base). The  $\pi$  bond is formally broken in the reaction with the nucleophile (b) but not in the reaction with the electrophile (a). Stereoisomeric forms may be generated in either case.



since the  $n_O$  energy will be perturbed only by interaction with the in-plane  $\sigma$  bonding orbitals of the attached  $sp^2$  hybridized carbon atom. Comparison of ionization potentials of formaldehyde (10.9 eV), acetaldehyde (10.2 eV), acetone (9.7 eV), and methyl acetate (10.5 eV) reveals the effect of the  $\sigma$  interaction. The HOMO ( $n_O = 2p$ ) of water, alcohols, and ethers is affected by a  $\pi$ -type interaction with neighboring  $\sigma$  bonds, as reflected in the interaction potentials (IPs) of water (12.6 eV), methanol (11.0 eV), and dimethyl ether (9.9 eV). The prediction with respect to the  $2p$  orbital energies of the oxygen atoms of the two groups, according to the heteroatom parameters of SHMO theory (Chapter 5), which suggest that the  $2p$  orbital of a monocoordinated oxygen is higher in energy than the  $2p$  orbital of a dicoordinated oxygen, is thus only partially borne out.

Basicity in the gas phase is measured by the proton affinity (PA) of the electron donor and in solution by the  $pK_b$ . A solution basicity scale for aldehydes and ketones based on hydrogen bond acceptor ability has also been established [186]. Nucleophilicity could be measured in a similar manner, in the gas phase by the affinity for a particular Lewis acid (e.g.,  $BF_3$ ) and in solution by the equilibrium constant for the complexation reaction. In Table 8.1 are collected the available data for a number of oxygen systems. It is clear from the data in Table 8.1 that the basicities of ethers and carbonyl compounds, as measured by PA and  $pK_b$ , are similar. However, the nucleophilicity, as measured by the  $BF_3$  affinity, of ethers is greater than that of carbonyl compounds, the latter values being depressed by steric interactions.

One may ask whether it is possible to coordinate *two* Lewis acids to a single carbonyl oxygen atom. This would require involvement of the second lone pair of the oxygen atom in bonding. This lone pair was placed at a significantly lower energy in Figure 8.1 on the basis of a large  $2s-2p$  separation. These considerations suggest that the attachment of a second Lewis acid to the oxygen atom is energetically unfavorable. Indeed, attempts to attach two molecules of  $TiCl_4$  to a ketone carbonyl proved unsuccessful [187].

**TABLE 8.1. Ionization Potentials (IP), Proton Affinities (PA),  $pK_b$  Values, and  $BF_3$  Affinities**

Molecule	IP <sup>a</sup> (eV)	PA <sup>b</sup> (kJ/mol)	$pK_b$ <sup>c</sup>	$BF_3$ affinity <sup>b</sup> (kJ/mol)
Water, H <sub>2</sub> O	12.6	707	15.74	46
Methanol, CH <sub>3</sub> OH	11.0	766	16	65
Dimethyl ether, CH <sub>3</sub> OCH <sub>3</sub>	9.9	798	17.5	71
Tetrahydrofuran, (CH <sub>2</sub> ) <sub>4</sub> O	9.4	825	—	85
Oxetane, (CH <sub>2</sub> ) <sub>3</sub> O	9.7	832	—	82
Formaldehyde, CH <sub>2</sub> O	10.9	704	18	26
Acetaldehyde, CH <sub>3</sub> C(O)H	10.2	770	24	50
Acetone, CH <sub>3</sub> C(O)CH <sub>3</sub>	9.7	769	21	44
Acrolein, CH <sub>2</sub> =CHC(O)H	—	814	—	58
Butenone, CH <sub>2</sub> =CHC(O)CH <sub>3</sub>	10.1	835	—	58
( <i>E</i> )-methylacrolein, CH <sub>3</sub> CH=CHC(O)H	—	835	—	60
Dimethylacrolein, (CH <sub>3</sub> ) <sub>2</sub> C=CHC(O)H	—	859	—	66
Methyl acetate, CH <sub>3</sub> C(O)OCH <sub>3</sub>	10.5	822	20.5	58
Methyl acrylate, CH <sub>2</sub> =CHC(O)OCH <sub>3</sub>	—	835	20	53

<sup>a</sup>Ref. 64.

<sup>b</sup>Computed values, MP3/6-31G\*\*//HF/6-31G\*, Ref. 188.

<sup>c</sup> $pK_b = 14 - pK_a$  (of conjugate acid), Ref. 119.

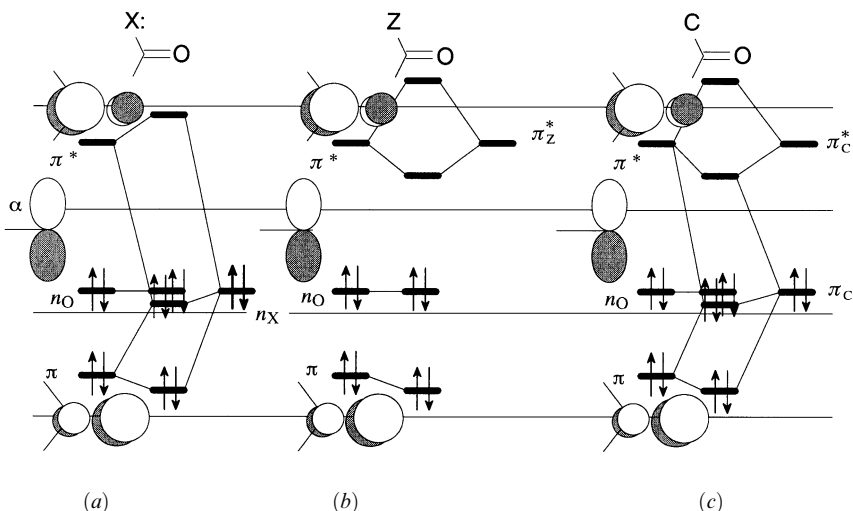
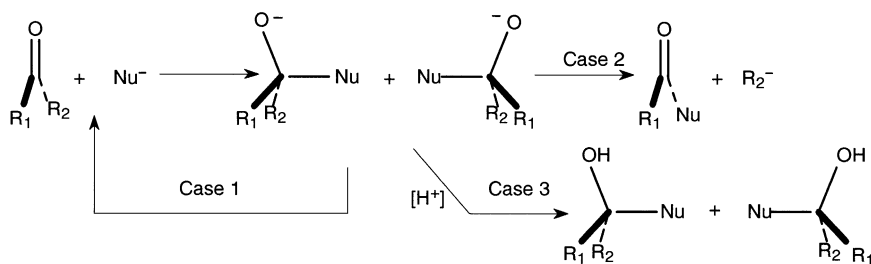


Figure 8.3. Substituted carbonyl group: (a) X substituent; (b) Z substituent; (c) "C" substituent.

### Nucleophilic Attack on a Carbonyl Group

The  $\pi^*$  antibonding orbital is polarized toward the carbon atom. The results of an SHMO calculation yield  $\pi^* = 0.841(2p_C) - 0.540(2p_O)$ . Thus the larger coefficient of the carbon  $2p$  orbital means that the carbonyl  $\pi^*$  orbital will interact strongly with substituents attached to the carbon atom. The carbonyl group as a substituent is a Z-type substituent, as discussed earlier. Since the polarized  $\pi^*$  antibonding orbital is the LUMO, with energy,  $\epsilon_{\pi^*} = \alpha - 0.681|\beta|$  (by SHMO), carbonyl compounds will be much better Lewis acids than ethylene (which, as we have seen, is not Lewis acidic at all), and the Lewis acidity will be sensitive to the presence and nature of the substituents, as shown by the interaction diagrams in Figure 8.3. Interaction with X: substituents will raise the energy of the LUMO and interaction with Z and "C" substituents will lower the LUMO energy. Approach of the nucleophile (Lewis base) will be toward the C atom of the carbonyl in a direction perpendicular to the plane of the carbonyl group. If the nucleophile is negatively charged, it will tend to be ion paired with the counterion (usually a metal ion such as  $\text{Li}^+$ ,  $\text{Na}^+$ ). The counterion will be actively involved in the reaction by coordinating to the oxygen atom [189]. The product of the reaction, the "tetrahedral intermediate," has a  $\sigma$  bond between the carbon and the base. Occupation of the  $\pi^*$  orbital results in rupture of the  $\pi$  bond, the original bonding electrons being localized to the oxygen atom. The resulting alkoxide is a strong base and a strong  $\pi$  donor. If the tetrahedral intermediate has a polarized bond, that is, a bond with a low-lying  $\sigma^*$  orbital, that bond will probably rupture, regenerating the stable carbonyl  $\pi$  bond and displacing the electronegative element at the end of the polarized bond as a Lewis base. The possible scenarios following nucleophilic attack on a carbonyl group are summarized in Scheme 8.1. Case 1, the reversal, is the normal situation if  $\text{R}_1$  and  $\text{R}_2$  are H, alkyl, or aryl and  $\text{Nu}^-$  is a halide, although if the halide is delivered by a strong Lewis acid such as  $\text{HX}$  or  $\text{SOX}_2$ , the oxygen may be eliminated (as water or sulfite) in a second step, resulting in a dihalide. If  $\text{R}_1$  is H, alkyl, or aryl and  $\text{R}_2$  is a "leaving group" such as halide,



Scheme 8.1

alkoxide, or acyl, then case 2 (nucleophilic acyl substitution) is the probable course. Hydrolyses of esters, amides, acid halides, and acid anhydrides fit this case, as do partial reductions of acids or esters to aldehydes or ketones or the addition of organometallics to esters. If  $R_1$  and  $R_2$  are H, alkyl, or aryl and  $Nu^-$  is a H, alkyl, or aryl anion (a metal hydride or organometallic), then the intermediate alkoxide will be the stable product and this is usually protonated to form the alcohol (case 3). Approach of the nucleophile to the carbon via a path perpendicular to the planar face of the carbonyl is relatively unhindered. However, steric hindrance may be sufficiently severe to prevent reaction if the carbonyl is embedded in a crowded region of the molecule or if  $R_1$  and/or  $R_2$  are sufficiently bulky that increased crowding in the transition structure (which will resemble the tetrahedral intermediate) raises the activation barrier to too high a value. The carbonyl group is particularly sensitive to attack by nucleophiles which themselves contain an X: substituent. The rate enhancement due to the presence of the X: substituent is greater than observed in the case of nucleophilic attack at saturated carbon ( $S_N2$ , see Chapter 9). Several theories have been proposed for the “extra” reactivity [190–192]. The simplest proposes a four-center interaction between the LUMO ( $\pi_{CO}^*$ ) and the HOMO of the nucleophile ( $n_{Nuc-X}$ ) which is in fact an occupied  $\pi^*$  orbital and has the correct nodal characteristics for effective overlap. The four-electron repulsive component of the interaction is easily relieved if the geometry of the transition state is as shown in Figure 8.4.

Cyclohexanones in which the chair inversion is constrained by substitution undergo diastereoselective nucleophilic addition, the nature of which (i.e., preferentially axial or preferentially equatorial) depends on the nature of the substituents. The explanation of this effect has been extensively explored [95, 189, 193–197]. The simplest explanation, shown in Figure 8.5, involves a distortion of the carbonyl group from planarity in such a way as to improve  $\pi$ -type donation from the ring C—C  $\sigma$  bond or the axial  $\sigma$  bond (often a C—H bond) in the  $\alpha$  position, whichever is the better donor. A secondary effect is the improved interaction between the distorted  $\pi^*$  orbital and the HOMO of the

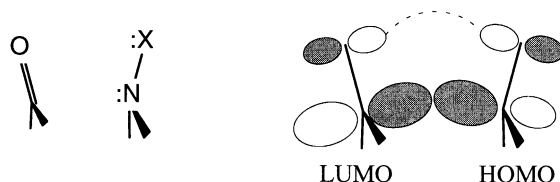
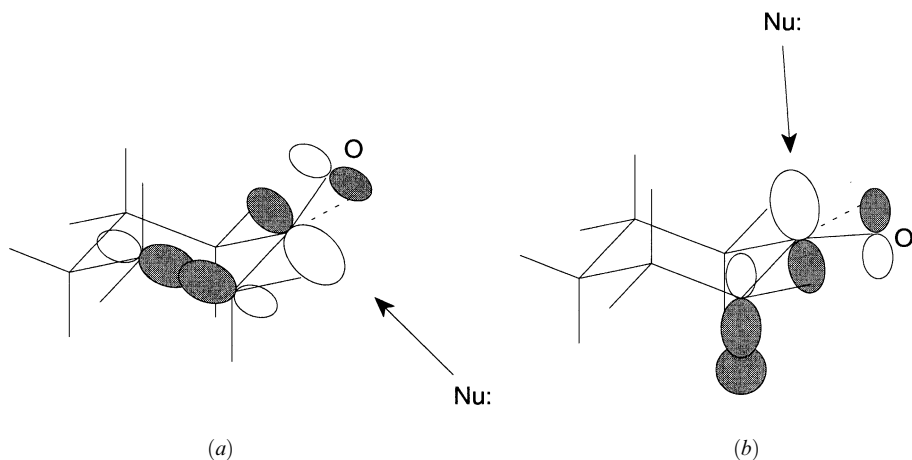


Figure 8.4. Optimal structure of the transition state for addition of an X:-substituted nucleophile to a carbonyl group according to orbital interaction considerations.



**Figure 8.5.** Pyramidalization of the  $\pi_{CO}^*$  to improve  $\pi$ -type donation of the  $\beta$   $\sigma$  bonds: (a) C—C participation favors equatorial attack by nucleophile; (b) C—H (axial) bond participation favors axial attack by nucleophiles. Figure 8.6. Amide group orbitals as an X-substituted carbonyl group.

attacking nucleophile on the side opposite to the selected  $\sigma$  bond. In unactivated carbonyl compounds, the distortion is too small realistically to account for the observed diastereoselectivity. However, the pyramidalization may be significant at carbonyls to which a Lewis acid is coordinated, as has been shown in a crystallographic structure determination [95]. The explanation of Cieplak [193] addresses stabilization of the transition state for the addition of the nucleophile (or the pathway approaching the transition state) using the interactions depicted in Figure 8.5 but substituting the incipient  $\sigma^*$  orbital of the carbonyl–nucleophile complex for the  $\pi_{CO}^*$  orbital. Substituents at the 3- or 4-position can increase or reduce the  $\pi$  donor ability of the C—C bond. The unsubstituted C—C bond is a better  $\pi$  donor than the C—H bond *in the gas phase*, but solvation effects reverse the apparent donor ability in solution [198]. However, X:-type substitution, including additional alkyl groups, can reverse this through repulsive four-electron, two-orbital  $\pi$ -type interactions with the  $\sigma$  bond. For a well-reasoned comparison of different frontier orbital related techniques for predicting diastereofacial selectivity, see the review by Dannenberg [199].

### Amide Group

The amide group is a special case of a carbonyl group substituted by a very good electron-donating X: substituent, X: = R<sub>1</sub>R<sub>2</sub>N—. It forms the backbone of every protein and of the most important commercial polymer, nylon. The bonding in an amide group is shown in Figure 8.6. The molecular  $\pi$  orbitals and their placement are as obtained by SHMO theory and are similar to those obtained by *ab initio* calculations [200], except for the relative energies of  $n_O$  and  $\pi_2$ . The *ab initio* calculations have the HOMO to be the  $\pi_2$  MO, which is slightly above the nonbonded MO,  $n_O$ . The SHMO places  $\pi_2$  at  $\alpha - 1.18|\beta|$ , slightly below the energy of the  $2p$  orbital of a monocoordinated oxygen atom (Table 5.1). The  $\pi_2$  MO (HOMO) is marginally polarized toward N. With either result, the basicity of the oxygen atom would be expected to be *greater* than the basicity

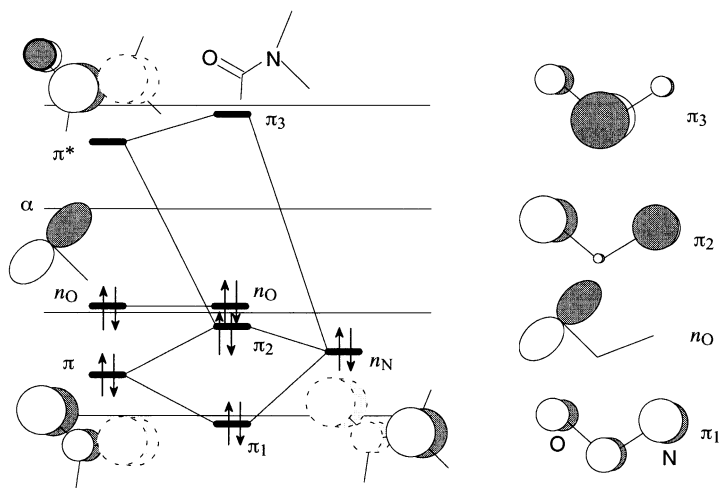


Figure 8.6. Amide group orbitals as an X-substituted carbonyl group.

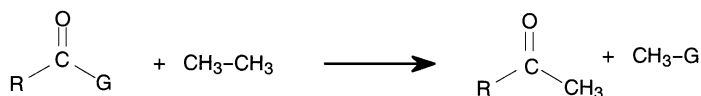
of the nitrogen atom because  $n_O$  is more localized and therefore will overlap better and interact more strongly with a typical electrophile. In other words, the coefficient of the orbital on oxygen in  $n_O$  is larger than the coefficient of the orbital on nitrogen in  $\pi_2$  [see equation (3.47) and the discussion after it]. The O-protonated form of formamide has been predicted to be 42 kJ/mol more stable than the N-protonated form by theoretical calculations [201]. The strong involvement of the nitrogen  $2p$  orbital in conjugation with the  $\pi^*$  orbital of the carbonyl group causes the nitrogen atom to adopt a nearly trigonal planar geometry and forces all of the substituents on both N and C to be approximately coplanar [202]. The barrier hindering rotation about the N—C(O) bond is 75–84 kJ/mol (75 kJ/mol in *N,N*-dimethylformamide [203]). As well as protons, metal cations also add to the carbonyl in preference to the nitrogen [204].

Because of the high-energy LUMO, nucleophilic substitution at the carbonyl is greatly slowed down compared to other X:-substituted derivatives [205]. If the geometric constraints of the molecular framework force the nitrogen to be distorted from planarity, the  $n_N$ - $\pi^*$  interaction is reduced. As a consequence, reactivity of the carbonyl toward nucleophilic attack is increased [206], as is the nucleophilicity of the nitrogen atom [207].

## THERMODYNAMIC STABILITY OF SUBSTITUTED CARBONYL GROUPS

Some aspects of the effects of substituents in the thermodynamic stability of carbonyl compounds may be deduced from the interaction diagrams of Figure 8.3. Substitution by X:-type substituents (Figure 8.3a) results in increased stabilization since there is a substantial lowering of energies of the occupied  $\pi$  orbitals, principally due to the  $n_{X:-}\pi_{CO}^*$  interaction. Stabilization will decrease in the series X: = —NH<sub>2</sub>, —OH, —F, since the  $n_{X:-}\pi_{CO}^*$  separation increases, and if the corresponding second-row elements are substituted, X: = —PH<sub>2</sub>, —SH, —Cl, because of the decreased ability to make  $\pi$  bonds between  $2p$  orbitals (part of  $\pi_{CO}^*$ ) and  $3p$  (or higher  $n p$ ) orbitals, which results in lower intrinsic interaction integrals. The phosphine group is especially weakly stabilizing

because of the high  $s$  character of  $n_p$ . Substitution by  $Z$ -type substituents (Figure 8.3*b*) is predicted to lead to modest stabilization, principally as a result of the  $\pi_{CO}-\pi_Z^*$  interaction which lowers the energy of  $\pi_{CO}$  bonding orbital. Substitution by “ $C$ ”-type substituents (Figure 8.3*c*) is predicted to lead to greater stabilization compared to  $Z$  substituents as a result of the  $\pi_{CC}-\pi_{CO}^*$  interaction which lowers the energy of  $\pi_{CC}$  bonding orbital. Additional factors such as electronegativity of the group and consequences of possible rehybridization are beyond the capabilities of simple orbital interaction theory and may affect the predictions, particularly in the case of  $Z$  and “ $C$ ” substituents. Experimentally, the effects of substituents are difficult to quantify. In a recent study, the question of stabilization was addressed in the form of a preference of a substituent to be attached to a carbonyl group rather than to a methyl group [208]. Thus, a positive  $\Delta H$  for the following reaction is taken as evidence of net stabilization of the carbonyl group by the group  $G$ :



Theoretically derived  $\Delta H$  values were compared to some which could be derived from experimental data. The calculated values agreed quite closely with the experimental values where both were available. We present here a list of the calculated  $\Delta H$  values for the above reaction as  $G$ ,  $\Delta H$  (kJ/mol), and refer the reader to the original reference for a detailed discussion [208]: H,  $-43$ ;  $\text{CH}_3$ ,  $-39$ ;  $\text{NH}_2$ ,  $+77$ ; OH,  $+93$ ; F,  $+67$ ;  $\text{SiH}_3$ ,  $-53$ ;  $\text{PH}_2$ ,  $-16$ ; SH,  $+23$ ; Cl,  $+28$ ; CN,  $-46$ ;  $\text{CH}=\text{CH}_2$ ,  $-2$ ;  $\text{C}\equiv\text{CH}$ ,  $-23$ ; and  $\text{CF}_3$ ,  $-52$ . Thus, electropositive groups ( $\text{SiH}_3$ ) and both  $Z$  (CN,  $\text{CF}_3$ ) and “ $C$ ” ( $\text{CH}=\text{CH}_2$ ,  $\text{C}\equiv\text{CH}$ ) substituents prefer attachment to methyl rather than carbonyl, possibly because more stabilization is available to them from  $\pi$ -type (hyperconjugative) interactions with the methyl group orbitals than with the carbonyl group orbitals.

## CHAPTER 9

---

# NUCLEOPHILIC SUBSTITUTION REACTIONS

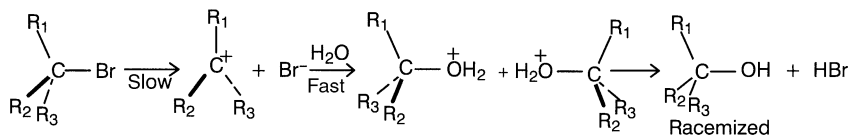
---

### NUCLEOPHILIC SUBSTITUTION AT SATURATED CARBON

The prototypical nucleophilic substitution reaction is that of an alkyl halide, although the “leaving group” may be any group which forms a polar bond to carbon and yields a weak Lewis base. The tosyl group (*p*-toluenesulfonyl) is a common leaving group displaced in a nucleophilic substitution reaction. Two mechanistic routes are distinguished,  $S_N1$  and  $S_N2$ . These are discussed separately below, although it should be recognized that the two mechanisms may compete or even merge.

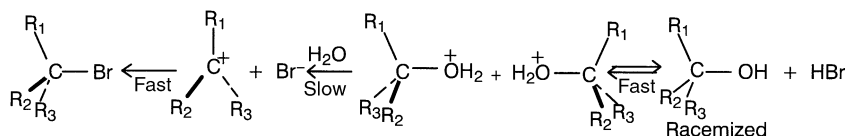
#### Unimolecular Nucleophilic Substitution $S_N1$

The  $S_N1$  mechanism involves a rate-determining heterolytic cleavage of the alkyl halide bond to yield an intermediate carbocation which undergoes rapid reaction with available electron donors, including solvent:



The typical reactions of carbocation intermediates were discussed in Chapter 7. The solvolysis of alkyl halides is an example of the involvement of carbocations in the  $S_N1$  mechanism, in other words, where the final outcome is a nucleophilic substitution. The first step is a heterolytic cleavage of the C—X bond. Properties of X which favor heterolytic cleavage, namely electronegativity difference with carbon (the larger, the better) and the degree of overlap of the X orbital with the  $sp^n$  orbital of carbon (the smaller the better), have already been elucidated (Chapter 4). The transition state has partial

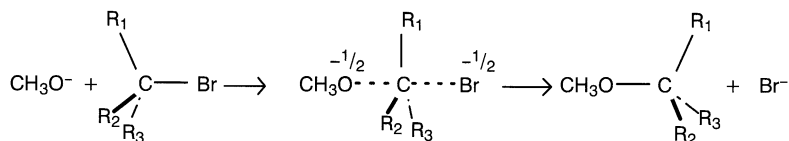
cleavage of the C—X bond and may have substantial carbocationic character. Factors which favor carbocation formation will also lower the energy of the transition state. Thus, X: or “C” substituents will accelerate the rate of the first step. The reaction is reversible. The reverse reaction provides the mechanism for the conversion of alcohols to alkyl halides. Polar solvents are necessary in order to stabilize the resulting ions. However, the direct nucleophilic involvement of solvent in the solvolysis of derivatives of tertiary C is a matter of debate [209]. We noted earlier that heterolytic rupture is easiest for the C—X bond and most difficult for C—C in the series C—C, C—N, C—O, and C—F:



In fact, in the absence of appropriate substituents at one or both ends of the bond, *none* of these bonds will undergo heterolytic rupture except under extreme conditions. However, as the above reaction sequence implies, the —OH group can be converted to a much better leaving group by the simple device of protonation. Protonation effectively increases the electronegativity of the oxygen atom. The same can be accomplished by alkylation or by the attachment to the oxygen of other Lewis acids such as metal cations  $BF_3$ ,  $AlCl_3$ ,  $FeCl_3$ , and so on. The same is true to a lesser extent for — $NR_2$  and —F for different reasons. The basicity of N makes attachment to Lewis acids an energetically favorable process, but the net difference between the effective electronegativity of N and that of C is not sufficiently large to render —N a good leaving group. On the other hand, the low basicity of —F renders attachment to most Lewis acids ineffective in competition with most solvents, especially those which are polar enough to facilitate heterolytic cleavage.

### Bimolecular Nucleophilic Substitution $S_N2$

The  $S_N2$  mechanism implies a concerted bimolecular reaction which proceeds with inversion of stereochemistry at the central carbon atom:



The transition state has a pentacoordinated carbon atom with a trigonal bipyramidal geometry, the departing and incoming groups occupying the apical positions. The  $S_N2$  mechanism is one of the most important in organic chemistry and has been the subject of numerous theoretical and experimental investigations [210]. We wish to examine this reaction using principles of orbital interaction theory to (a) explain why leaving group ability is in the order (from poorest to best), F, Cl, Br, and I, (b) discover the factors which govern *nucleophilicity*, and (c) determine which substituents may accelerate the rate of reaction. Since nucleophiles are typically Lewis bases, we expect the dominant factors which will govern the interaction of the nucleophile with the alkyl halide will be of the two-electron, two-orbital type involving the HOMO of the nucleophile and the LUMO of the alkyl halide.



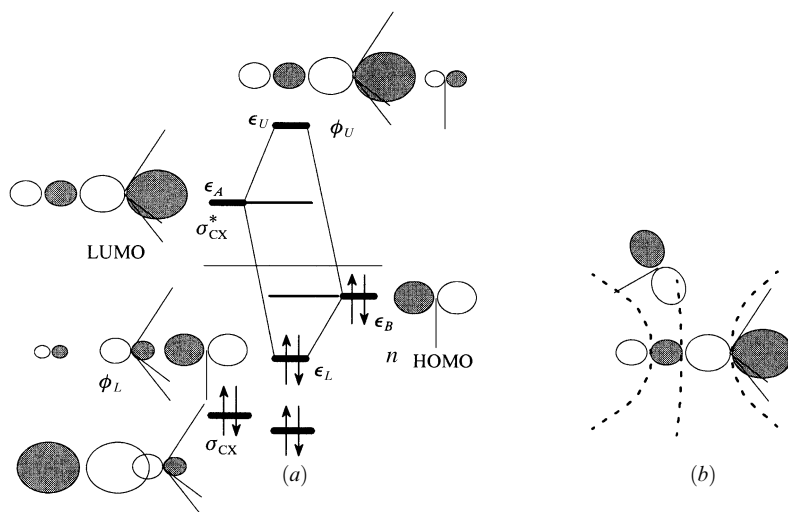


**Figure 9.1.** Two-electron, two-orbital interaction of an alkyl halide  $\sigma^*$  orbital (LUMO) and the nonbonded orbital,  $n$ , of a nucleophile: (a) most favorable approach; (b) unfavorable front-side approach on nodal surface.

**Geometry of Approach.** An interaction diagram for the approach of the nucleophile is depicted in Figure 9.1a. The  $\sigma^*$  LUMO is polarized toward C so the most favorable overlap and hence interaction occurs near the C atom. Front-side approach of the nucleophile is *not* favored since the nucleophile would have to approach amid the nodal surfaces of the  $\sigma^*$  orbital (Figure 9.1b). There is little interaction (which would be repulsive) between the nonbonded orbital and the  $\sigma_{CX}$  bond orbital since the latter is polarized toward the more electronegative X. The structures of several complexes of halide ion and methyl halides have been studied theoretically and experimentally in the gas phase where the reaction proceeds via a double-welled reaction potential with the trigonal bipyramidal structure as the transition state [211, 212]. Of course, backside approach accomplishes the observed inversion of configuration at C. Since there are three groups already on the C atom and the incoming nucleophile must squeeze between them, the incoming nucleophile must overcome destabilizing four-electron, two-orbital type interactions in order to get close enough so that overlap becomes large enough that reaction may occur. Thus, steric effects are expected to be of major concern for operation of the  $S_N2$  mechanism. In practice, the mechanism does not occur at tertiary alkyl centers. As we shall see below, steric effects in the form of the four-electron, two-orbital interactions are also responsible for the distinction between *basicity* and *nucleophilicity*.

**Nucleophilicity.** A distinction is usually made between *nucleophilicity* and Lowry–Bronsted *basicity* [213]. The latter involves specifically reaction at a proton which is complexed to a Lewis base (usually  $H_2O$ ), while the former refers to reactivity at centers other than H. Linear correlations have been shown for gas-phase basicity (proton affinity) and nucleophilicity of nitrogen bases toward  $CH_3I$  in solution [214] where the solvent is not strongly involved in charge dispersal. In each case, reaction of the base/nucleophile

is with the  $\sigma^*$  LUMO of the HX/CX acid. The  $n\text{-}\sigma^*$  attractive two-electron, two-orbital interaction is responsible for the ultimate course of the substitution reaction.

The solvent plays a major role in determining the relative nucleophilicity of closely related species. For example, among the halides in water, the observed relative nucleophilicities are:  $\text{I}^- > \text{Br}^- > \text{Cl}^- > \text{F}^-$ . However, in aprotic solvents, when the anion is not tightly associated with the cation [215], or in the gas phase [216], the order is exactly reversed and is parallel to basicity. It should be emphasized, however, that most studies in this vein have adopted a methyl halide as the reference substrate. This is the least sterically hindered substrate, in our context the most like a protic acid. The ability to overlap at longer range (vaguely expressed as polarizability) would favor larger atomic centers as opposed to small first-row atom centers as nucleophiles; additionally, reactivity is enhanced if the  $n$  orbital is higher and therefore closer in energy to the  $\sigma^*$  LUMO. Both factors predict the observed relative nucleophilicities,  $\text{I}^- > \text{Br}^- > \text{Cl}^- > \text{F}^-$ ,  $\text{—S—} > \text{—O—}$ , and  $\text{P} > \text{N}$ . The  $n$  orbital of a given kind of atom may be raised by substitution by X: substituents, a phenomenon which is known as the  $\alpha$  effect [192, 217]. Hence hydrazines ( $\text{NH}_2\text{NR}_2$ ), hydroxylamines ( $\text{NH}_2\text{OR}$ ), peroxides ( $\text{O}^-\text{OR}$ ), and similar substances exhibit enhanced nucleophilicity by virtue of their raised, and possibly more extended and polarizable, HOMOs.

**Leaving Group Ability.** As the picture of  $\phi_L$  (Figure 9.1a) implies, the HOMO–LUMO interaction involves some delocalization of charge into the alkyl halide, specifically into an orbital that is *antibonding* between the C and X. This reduces the bond order of the C—X bond and may result in rupture of the bond. Nucleophilic attack on a saturated C atom (the normal case for  $\text{S}_{\text{N}}2$  reaction) inevitably leads to rupture of the C—X bond if the incoming nucleophile can get close enough to make a bond. Clearly, the lower the LUMO, the more reactive the substrate (alkyl halide in this case). The nature of the leaving group will certainly affect the position of the LUMO. In Figure 9.2 are superimposed the expected interaction diagrams for different alkyl halide bonds. Clearly the LUMO energies are in the order consistent with the observed reactivity series. However, as the diagrams of Figure 9.2 suggest, the *polarization* of the LUMO is least for the C—I bond (C—Br shown) due to the similarity of the electronegativities of C and I. One should then question why attack of the nucleophile at the iodine end of the bond is not a competing process. Undoubtedly, such association of the nucleophile with the iodine does take place. However, for the same reason that the C—X bond is weak, there is not much energy to be gained by attempting to form a bond to I.

**The Transition State.** The MOs of the reacting complex at midpoint in the reaction are shown in Figure 9.3. The pentacoordinated structure is a true *transition structure* for the reaction at a carbon center. However, nucleophilic attack at other centers may lead to stable structures involving three-center two-electron bonds. The best known example involving H is the anion  $\text{FHF}^-$ . “Hypervalency” in second or higher row elements in compounds such as  $\text{PF}_5$ ,  $\text{SF}_4$ , or  $\text{ClF}_3$  may also be interpreted in this way. The collinear arrangement of the apical bonds may be attributed to three-center two-electron bonding without involvement of the  $3d$  orbitals.

**Substituent Effects.** The overwhelming influence of substituents on the rate of  $\text{S}_{\text{N}}2$  reactions is steric in nature; bulky groups hinder the reaction by preventing the approach of the nucleophile to the central C atom. Nevertheless, one can examine electronic effects of substituents adjacent to the site of substitution on the rate of reaction. Direct elec-

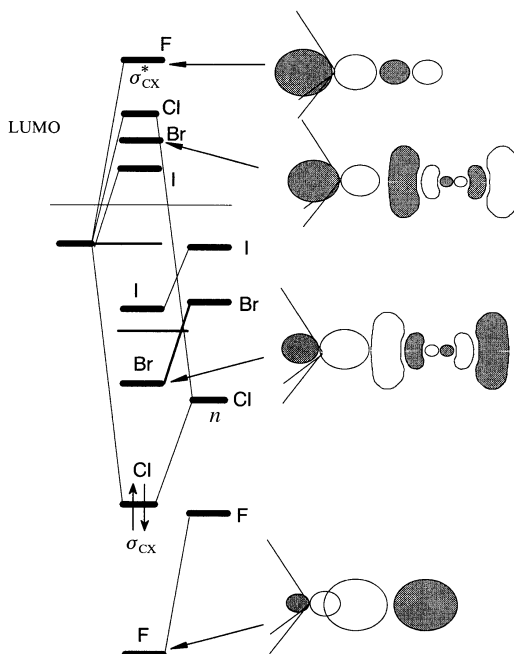


**Figure 9.2.** The  $\sigma$  and  $\sigma^*$  orbitals of alkyl halides. The fluoro and bromo systems are shown. The orbitals to bromine are less polarized.

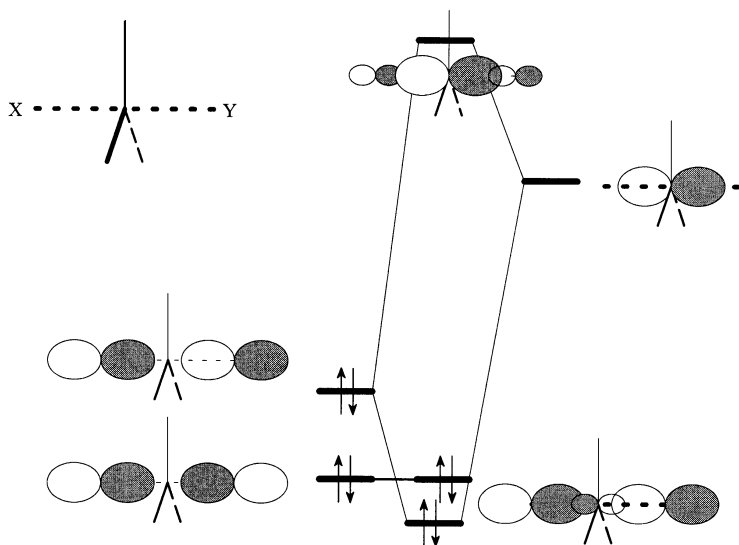


**Figure 9.3.** Interaction diagram which yields the nature of bonding in the axial bonds of a trigonal bipyramid. The HOMO is nonbonding. If enough stabilization results from the bonding combination, a stable intermediate may be formed. There are no known examples where this is the case when C is the central atom.

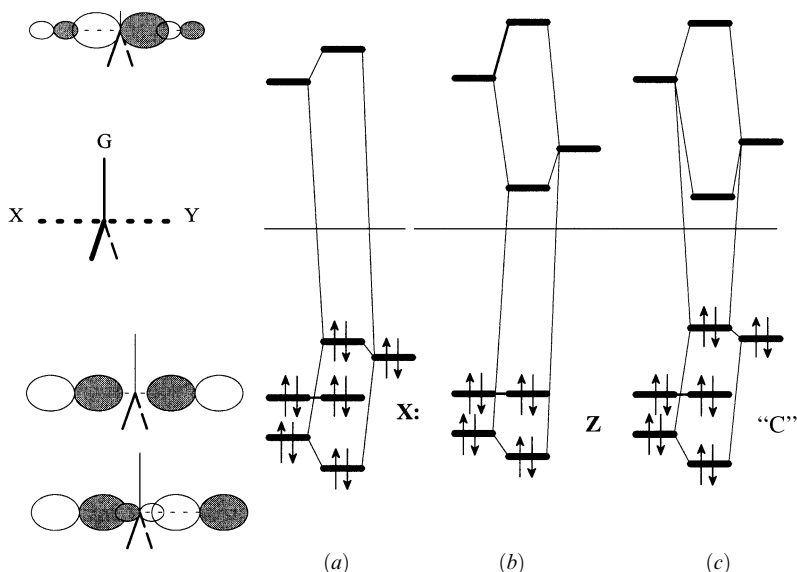


**Figure 9.4.** Interaction diagram for the MOs of the trigonal bipyramid with a substituent in the equatorial plane  $\alpha$  to the site of substitution: (a) X; (b) Z; (c) “C”. Only Z substituents are expected to have a strong stabilizing effect on the TS.

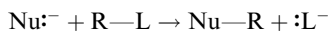
tronic interaction, which may selectively stabilize or destabilize the transition structure, will accelerate or slow down the reaction, respectively. The interaction of the transition structure orbitals with each of the three classes of substituents, X:, Z, and “C,” are shown in Figure 9.4. In the case of X: and “C” substituents, weak stabilization of the TS is predicted by the simple orbital interaction theory, while Z substituents are expected to have a stronger stabilizing effect. Experimentally, Z-substituted alkyl halides, (e.g.,  $\alpha$ -haloketones) undergo the greatest acceleration in rate of bimolecular substitution, by up to five orders of magnitude. Alkyl halides with a “C” substituent (e.g., allylic or benzylic halides) are accelerated by up to two orders of magnitude. Apparently, X substitution has a mixed effect on the rate of  $S_N2$  reaction, but the rate of  $S_N1$  reaction may be accelerated by up to eight orders of magnitude.

### Another Description of the $S_N2$ Reaction: VBCM Model

The basic features of the  $S_N2$  reaction, the site of reaction, stereochemistry (inversion), nucleophilicity, leaving group ability, and gross effects of  $\alpha$  substituents, are readily deduced from orbital interaction theory. Nevertheless, subtle distinctions having to do with nucleophilicity, the leaving group’s ability, or the effects of substituents are beyond the capability of the simple model. Recourse to quantitative electronic structure calculations is often not helpful. The Hartree–Fock procedure fails to provide a reasonable relative energy for the transition state for reasons discussed in Chapter 3, and post-Hartree–Fock calculations yield the correct relative energies, but at the expense of losing the conceptually simple orbital picture. The valence bond configuration mixing (VBCM) model developed by Shaik and co-workers [9, 218–220] preserves much of the features of

the orbital picture while providing a semiquantitative description of the  $S_N2$  reaction. The basic features are given below. The reader is directed to the book by Shaik et al. [210] for a full description.

The general  $S_N2$  reaction may be represented as



The reactants are represented by two valence bond configurations,  $R_1^R = \text{Nu}:\text{C}^- + \text{R}-\text{L}$  and  $R_2^R = \text{Nu}\cdot + \text{R}\cdots\text{L}^-$ . The second valence bond configuration,  $R_2^R$ , represents the situation where an electron has been transferred from the HOMO of the nucleophile,  $\text{Nu}:\text{C}^-$ , to the  $\sigma^*$  orbital of the bond involving the leaving group, L. Prior to interaction of the reactants, the reactant condition is described by valence bond configuration  $R_1^R$ . As the reactants approach each other, the HOMO- $\sigma^*$  interaction becomes increasingly important and the description of the reactants requires a greater contribution from  $R_2^R$ . A parallel situation applies to the products, which are described by valence bond configurations  $R_1^P = \text{Nu}-\text{R} + :\text{L}^-$  and  $R_2^P = \text{Nu}\cdots\text{R}^- + \cdot\text{L}$ . During the course of the substitution reaction, it is considered that primary reactant configuration  $R_1^R$  will have a tendency to evolve not into the primary product configuration,  $R_1^P$ , but rather into  $R_2^P$ . Similarly, the origins of  $R_1^P$  are considered to lie in  $R_2^R$ . The interplay of the valence bond configurations is displayed schematically in Figure 9.5, in which the key feature is the intended and avoided crossing of  $R_1^R$  and  $R_2^R$ . The diagram in Figure 9.5 may be interpreted semiquantitatively in as much as the energy change for the reaction may be

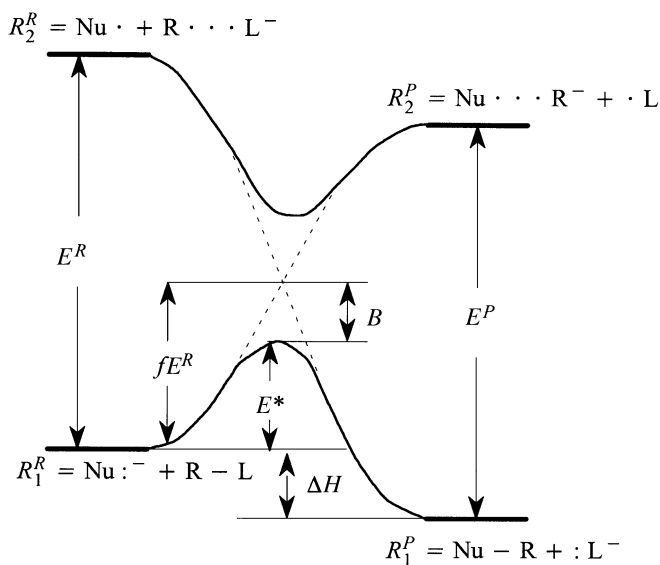


**Figure 9.5.** Schematic of the  $S_N2$  reaction coordinate according to the VBCM model. The energy gaps  $E^R$  and  $E^P$  are identified with sum of the ionization potential and electron affinities of the appropriate species. The avoided crossing occurs at a fraction of  $E^R$  determined by the reaction enthalpy,  $\Delta H$ , and the expected steepnesses of the descending curves. The activation energy for the reaction is  $E^* = fE^R - B$ , where  $B$  is the energy of the avoided crossing.

equated to the enthalpy change for the reaction,  $\Delta H$ , and the energy gaps between  $R_1^R$  and  $R_2^R$  and between  $R_1^P$  and  $R_2^P$ , may be evaluated from the vertical ionization potentials and vertical electron affinities of the donors and acceptors, respectively. The point of intended crossing is expressed as a fraction,  $f$ , of the reactant energy gap,  $E^R$ , where  $f$  depends on both  $\Delta H$  and the steepness of the descents of  $R_2^R$  and  $R_2^P$ . The latter factor is governed principally by the stability of the three-electron bonds ( $R \cdots L^-$  and  $\text{Nu} \cdots R^-$ ), which in turn may be deduced from electronic characteristics of R, Nu, and L. A strong (delocalized) three-electron bond corresponds to shallow descent and therefore large  $f$ , while a weak three-electron bond (localized) corresponds to smaller  $f$ . Various means were proposed to estimate  $B$ , the extent of the avoided crossing, or  $B$  may be assumed to be constant in a series of similar reactions. The activation energy for the reaction is given as  $E^* = fE^R - B$  and for a series of similar reactions is largely governed by the two factors which determine the magnitude of  $f$ . The VBCM approach predicts that X:-type substituents (specifically halogens, where the involvement of the substituent nonbonded electron pairs cannot be avoided) assist the delocalization of the three-electron bonds and therefore slow down the rate of reaction, the largest retardation occurring when X: and L: are the same. On the other hand, Z-type substituents reduce  $E^R$  (increase the electron affinity) without significant delocalization of the three-electron bond and therefore lead to an acceleration of the reaction, but only toward powerful nucleophiles.

## CHAPTER 10

---

# BONDS TO HYDROGEN

---

### HYDROGEN BONDS AND PROTON ABSTRACTION REACTIONS

Hydrogen atoms form the exposed outer surface of the majority of organic molecules. A reagent suffering a random collision with a substrate is most likely to encounter a bonded hydrogen atom. The interaction between a substance B and a compound in the vicinity of a hydrogen atom, *bonded to an element which is more electronegative than it is* (which includes C), is shown in Figure 10.1. The important interaction is a two-electron, two-orbital interaction between the HOMO of B and the antibonding  $\sigma$  orbital of the bond to H ( $\sigma^*$ ). If the  $\sigma^*$  orbital involves H and C, it probably will not be the LUMO, and if B is not extraordinarily basic, that is, does not have a very high energy, localized HOMO, then little consequences will ensue from the interaction other than a weak van der Waals [72] interaction which is always present. If the  $\sigma^*$  orbital is the LUMO, the interaction, which involves charge transfer may be quite strong resulting either in a complex stabilized by a hydrogen bond or rupture of the  $\sigma$  bond with concomitant transfer of the proton to B, a Lowry–Bronsted acid–base reaction. Bonds to hydrogen from O and F, and probably N, are highly polarized and there will be a substantial electrostatic component to the interaction if B is even partially negatively charged. In Figure 10.1, the HOMOs of the bases B: and A: are depicted as generic *s* orbitals. In fact, these could be nonbonded *p* or *sp<sup>n</sup>* hybrid orbitals, or also  $\pi$  orbitals as in alkenes, enolates, or enamines, or strained  $\sigma$  bonding MOs as in cyclopropanes.

### Hydrogen Bonds

Hydrogen-bonding interactions are considerably weaker than ionic interactions and covalent bonds but have a profound effect on many chemical and physical properties [221] and determine the shapes of large molecules such as proteins and nucleic acids. Protein secondary structure is determined by H bonding between the carbonyl oxygen of one amide unit and the N—H bond of another. The two strands of the double helix of

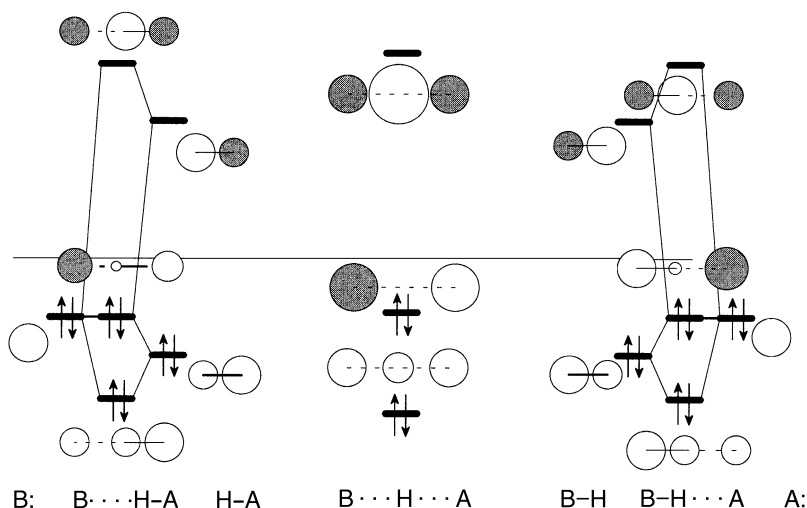
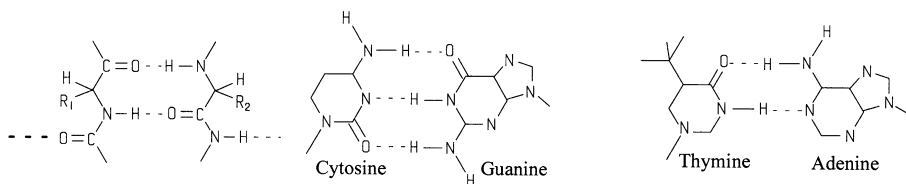


**Figure 10.1.** Orbitals for a simple acid–base reaction involving proton abstraction. Charges are ignored.

nucleic acids are held together by complementary  $N \cdots H-N$  and  $=O \cdots H-N$  bonds between thymine and adenine and between cytosine and guanine. Each H bond contributes about 20 kJ/mol to the stabilization of the complex:



This hydrogen-bond-driven large-scale structural organization has parallels in abiotic systems as well. For example, 1:1 mixtures of *trans*-1,2-diaminocyclohexane and  $C_2$  symmetric 1,2-diols self-assemble into well-defined supramolecular structures which have been characterized by X-ray diffraction analysis. The structures, some of which are stable to sublimation, are helical, the handedness of the helices being determined by the handedness of the 1,2-diamine [222].

The interaction diagram for the initial donor–acceptor complex shown on the left-hand side of Figure 10.1 is the diagram for a simple hydrogen bond. A collinear geometry for  $B \cdots H-A$  yields maximum overlap of the HOMO ( $n_B$ ) and LUMO ( $\sigma_{HA}^*$ ), but since the local symmetry of the LUMO is spherical (it is mostly  $1s_H$ ), collinearity is not a strong requirement. The extent of H transfer from A to B in the H-bonded complex  $B \cdots H-A$  and the energy associated with formation of the complex are determined by the nature of A: and B:. Numerous hydrogen-bonded complexes have been studied in the gas phase. (For a review of complexes of  $NH_3$  and a variety of proton donors, see refs. 223 and 224.) Probably the most studied hydrogen bond is that in water dimer, found to be  $-23 \pm 3$  kJ/mol experimentally [225] and  $-19.8$  kJ/mol theoretically [226]. The structure of water dimer is as expected on the basis of a dominant HOMO ( $n_O$ )–LUMO



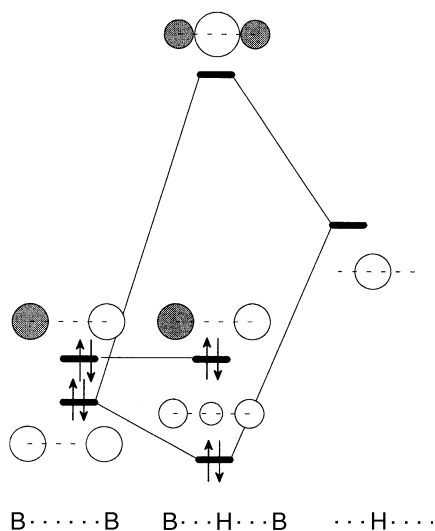


**Figure 10.2.** Orbital interaction diagrams for symmetrical two-center hydrogen bonding.

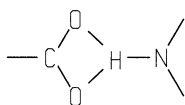
( $\sigma_{OH}^*$ ) interaction. Water trimer has been studied experimentally [227] and shown theoretically [228] to adopt a cyclic array of hydrogen bonds with an average bond strength of about 20 kJ/mol. The complex  $[H_3O^+ \cdots F^-]$ , is responsible for the anomalously low acidity of HF ( $pK_a = 3.2$ ) in aqueous solution. The HOMO is essentially nonbonding. If the HOMO is high in energy, that is, A: and B: are not very electronegative and/or interact strongly with each other, then simple orbital interaction theory would predict that it makes little difference to the thermodynamic stability whether that MO is occupied or not. Such bonding is observed in electron-deficient systems and is discussed below. If B is substantially less electronegative than A:, proton transfer will occur and the H bond will be as depicted on the right-hand side of Figure 10.1.

### Symmetrical and Bifurcated Hydrogen Bonds

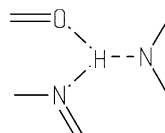
The vast majority of hydrogen-bonded systems are unsymmetrical, even when the hydrogen bond is between like atoms. The reason for this is readily understood from Figure 10.2, where the pattern of orbitals shown in the middle of Figure 10.1 is derived from the interaction of the  $1s$  orbital of a hydrogen atom (situated at the midpoint) with the in- and out-of-phase group MOs of two equal Lewis bases. It is clear that the hydrogen atom cannot interact with the HOMO of the base pair, only with the lower symmetric MO. If the hydrogen shifted away from the nodal plane, interaction with HOMO (as well as the lower MO) is possible. These considerations apply even when the two bases are not exactly equivalent. However, optimum *symmetrical* hydrogen bonding occurs when the two bases A and B are balanced in electronegativity, have maximum electronegativity, are far enough apart not to interact strongly with each other, and one is negatively charged. The strongest H-bonded complex is probably  $FHF^-$ , with a binding energy of about 210 kJ/mol. Symmetrical H bonds of the type  $[-OHO-]^-$  have

also been found between two oxygen atoms, for example in monoanions of dicarboxylic acids in nonpolar solvents [229].

It is very difficult to locate hydrogen atoms in large molecules by crystallographic methods. Nevertheless, proximity observations of heavy atoms strongly suggest the existence of *bifurcated* hydrogen bonds of the type shown below:



simple bifurcated hydrogen bond  
with a carboxylate group



symmetrical three center  
hydrogen bond

These are taken as to be expected in biological systems and are part of empirical potentials for protein and DNA structure. For example, bifurcated hydrogen bonding is assumed in the interstrand region of DNA [230], at the nucleation sites for protein  $\beta$ -sheets [231], and at other sites in proteins [232]. An examination of neutron diffraction data on 18 monosaccharide structures for hydrogen-bonding configurations revealed that “an appreciable fraction (15%) are of the bifurcated type” [233]. The symmetrical three-center case may be examined by consideration of the orbital interaction diagram in Figure 10.3*a*, where the three heavy atoms are considered to be equivalent and sym-

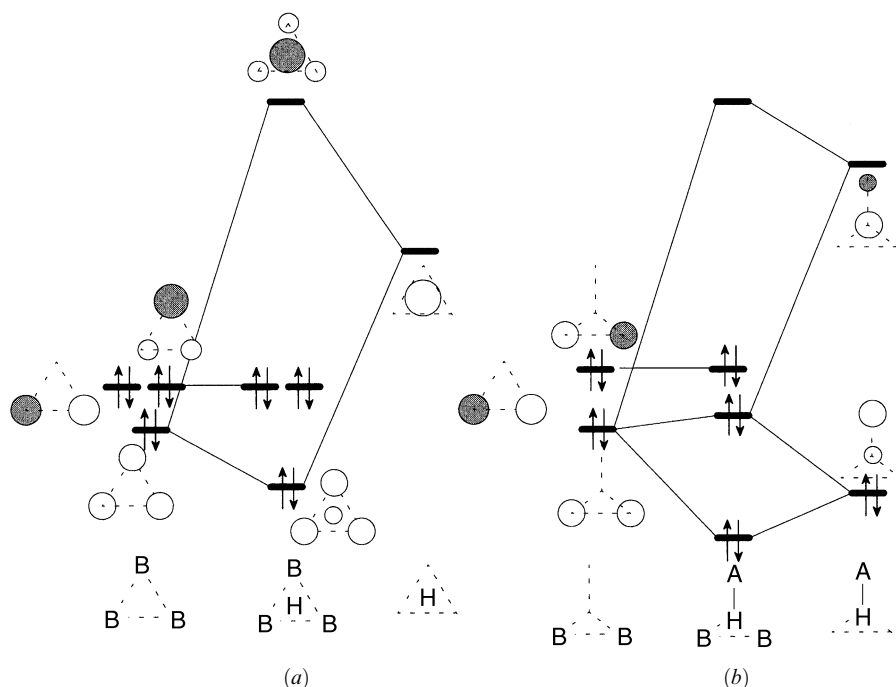


**Figure 10.3.** Orbital interaction diagrams for (a) symmetrical three-center hydrogen bonding and (b) bifurcated hydrogen bonding.

metrically disposed at the corners of an equilateral triangle, with the hydrogen atom at the center. Such an arrangement is obviously favorable energetically, but by reasoning analogous to that put forth for symmetrical two-center bonding (Figure 10.2), it is unlikely to be the *most* favorable arrangement. At the midpoint of the triangle, the hydrogen  $1s$  orbital cannot interact with *either* of the two HOMOs. On this basis, symmetrical three-center hydrogen bonding should be an extremely unlikely occurrence.

### Proton Abstraction Reactions

Many reaction steps in organic chemistry require the abstraction of a proton by a Lewis base. Interaction diagrams for the elementary stages for the reaction  $B: + H-A \rightarrow B-H + A:$  are shown in Figure 10.1. The reaction parallels the  $S_N2$  reaction; it is a nucleophilic substitution at H. We will restrict our attention to reactions which involve an abstraction of a proton from C. As stated above, the  $\sigma^*$  orbital of a C—H bond is unlikely to be the LUMO of H—A. However, if the  $\sigma^*$  orbital of a C—H bond is not too high in energy, the probability of reaction may still be relatively high due to the exposed nature of the hydrogen, the polarization toward H, and the lack of nodes. The first factor makes close approach possible; the other two factors allow large orbital overlap from a wide range of angles of approach.

The energy of the  $\sigma_{CH}^*$  may be lowered by two distinct mechanisms. A change in the hybridization of the C  $sp^n$  orbital toward smaller  $n$ , that is, more  $s$  character, is accompanied by a lowering of the energy (or increase of electronegativity) of the hybrid orbital. The orbital interaction analysis, shown in Figure 10.4, predicts two consequences, a lowering of the  $\sigma^*$  orbital and increased polarization of the  $\sigma^*$  orbital toward H. Both

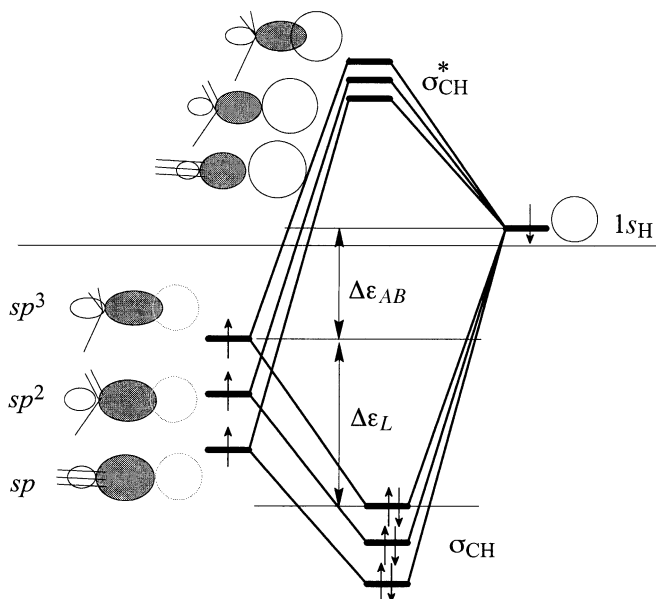


**Figure 10.4.** Trends in orbital interaction parameters in the series alkyl C—H, alkenyl C—H, and alkynyl C—H.

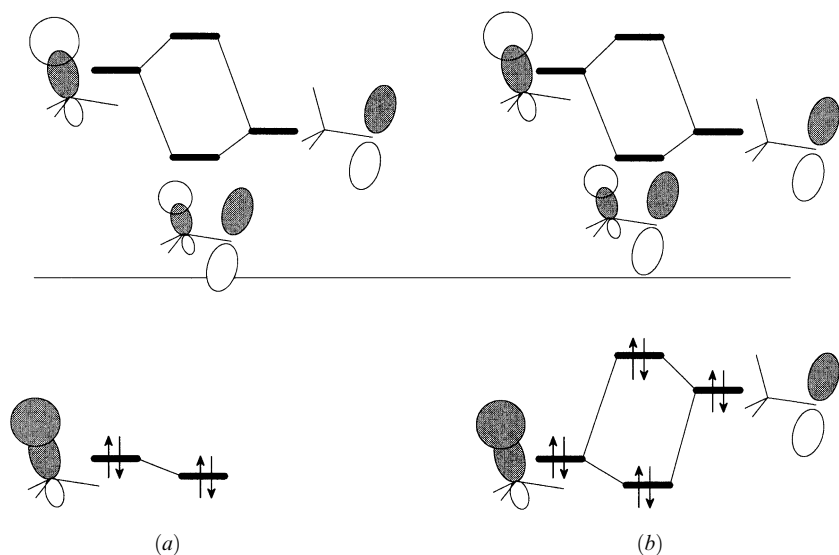


**Figure 10.5.** Activation of a C—H bond by a neighboring substituent: (a) Z substituent; (b) “C” substituent.

factors combine to increase the interaction of a base with the  $\sigma^*$  orbital and increase the reactivity toward a given base. The effect on the rate of proton abstraction is not predicted to be large since the  $\sigma^*$  orbitals are close in energy and polarization changes are small. The effects are larger on acid equilibrium values since these are governed by the stability of the conjugate bases where the orbital differences are greater; the  $\text{p}K_{\text{a}}$  values for  $\text{H—CH}_2\text{CH}_3$ ,  $\text{H—CH=CH}_2$ , and  $\text{H—C}\equiv\text{CH}$  are 48, 44, and 24, respectively, corresponding to an overall change of about 150 kJ/mol in  $\Delta G^\circ$  at 25°C.

The second mechanism for lowering the energy of the  $\sigma^*$  CH orbital is via admixture into lower energy unoccupied MOs, especially the LUMO. This occurs whenever a Z or “C” substituent is attached to the carbon atom which bears the C—H bond, as shown in Figure 10.5. The generic  $p$  orbital of the Z substituent (Figure 10.5a) or “C” substituent (Figure 10.5b) would be the orbital of a  $\pi$  system at the point of attachment of the carbon bearing the H in question. The LUMO of the Z or “C” substituent is lowered somewhat by in-phase interaction with the  $\sigma_{\text{CH}}^*$  orbital. Because the resulting LUMO has some admixture of the  $\sigma_{\text{CH}}^*$  orbital, there is an increased probability that the nucleophile will overlap with the hydrogen  $1s$  orbital, resulting in rupture of the C—H bond and yielding a  $\pi$ -delocalized carbanion. Of course, the dominant component of the new LUMO is the LUMO of the substituent, and attack of the nucleophile is most likely at that site in the absence of additional considerations such as steric effects, or strong Coulomb interactions. The  $\text{p}K_{\text{a}}$  values of several Z-substituted carbon acids are  $\text{H—CH}(\text{C}(\text{O})\text{CH}_3)_2$ , 9;  $\text{H—CH}_2\text{NO}_2$ , 10;  $\text{H—CH}_2\text{C}(\text{O})\text{CH}_3$ , 20;  $\text{H—CH}_2\text{C}(\text{O})\text{OCH}_3$ , 24;  $\text{H—CH}_2\text{SO}_2\text{CH}_3$ , 31 (DMSO); and  $\text{H—CH}_2\text{CN}$ , 31 (DMSO). Allylic and benzylic (i.e., “C” substituted) carbon acids are considerably weaker ( $\text{C}_6\text{H}_5\text{CH}_2\text{—H}$ , 41;  $\text{CH}_2=\text{CH—CH}_2\text{—H}$ , 43) unless more than one “C” substituent is present [ $(\text{C}_6\text{H}_5)_2\text{CH—H}$ , 33] or the resulting carbanion may be “aromatic” (cyclopentadiene 16).

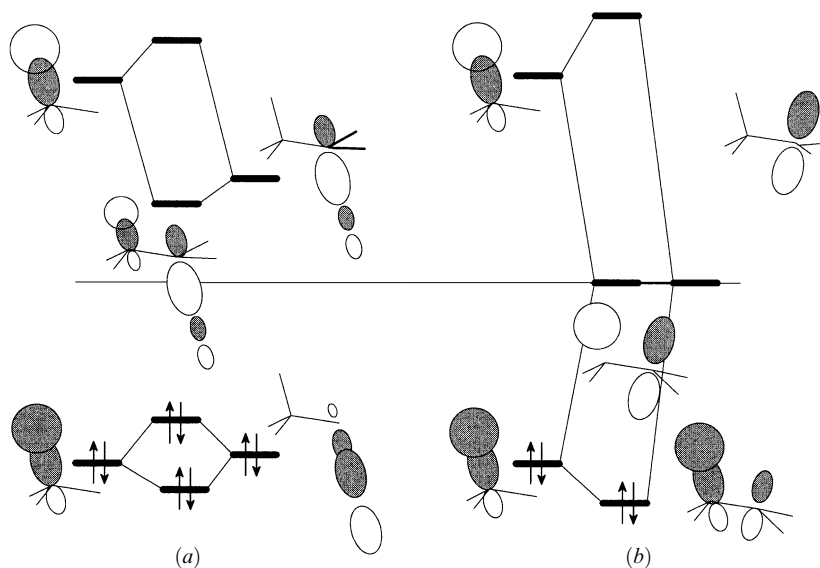


**Figure 10.6.** Activation of a C—H bond by a neighboring (a) C—X bond and (b) carbocationic center.

Two special cases need to be considered: activation by alkyl halide and by a formal cationic center. The interaction diagrams are shown in Figures 10.6a,b, respectively. These are involved in elimination reactions of alkyl halides, E2 and E1, respectively.

## E2 Elimination Reaction

The LUMO of a molecule with an alkyl halide bond flanked by a C—H bond is shown in Figure 10.6a. The LUMO is composed primarily of the  $\sigma_{CX}^*$  with some  $\sigma_{CH}^*$  mixed in *in phase*. The amount of interaction, and therefore the energy of the LUMO, depends on the orientation of the C—H and C—X bonds. Interaction is strongest when the two bonds are coplanar and slightly better if they are *anti*-coplanar. Interaction of the LUMO with the HOMO of a Lewis base (nucleophile) will direct the base to the points where the best overlap occurs, namely to the backside of the C end of the C—X bond, as already discussed, resulting in a nucleophilic substitution by the  $S_N2$  mechanism. However, there is a possibility of attack at the H end of the C—H bond, and this mode may be the most probable if the Lewis base is not a “good nucleophile” or if attack at C is sterically hindered. Attack by a Lewis base (i.e., addition of electrons) at the H end of the LUMO is accompanied by a reduction of the  $\sigma$  bond order of the C—H and C—X bonds and an increase of  $\pi$  bond order between the two carbon atoms. Thus, the overall course of the reaction is a concerted formation, by anti elimination, of a C—C  $\pi$  bond and a B—H  $\sigma$  bond and rupture of the C—H and C—X  $\sigma$  bonds. If the C—H and C—X cannot adopt a coplanar configuration, the LUMO is not lowered in energy, the C—C  $\pi$  bond cannot be formed, and there is no mechanism for breaking the C—X

bond if base attack is at the C—H bond. Operation of the E2 mechanism therefore has a very strong stereoelectronic requirement that the C—H and C—X bonds be able to achieve a (nearly) coplanar arrangement. In terms of the intrinsic stabilization, there is not much difference between the syn coplanar and anti coplanar arrangements. The observation that the E2 reaction proceeds predominantly by anti elimination is easily explained on steric grounds. The anti arrangement of two bonds at adjacent tetracoordinated centers corresponds to a minimum in the potential function for rotation about the single bond, whereas the syn (or eclipsed) arrangements corresponds to a maximum. In cyclic systems, where adjacent C—H and C—X bonds are forced into syn coplanar arrangements by ring constraints, the E2 elimination still proceeds, albeit at a reduced efficiency probably due to steric shielding of the C—H bond by the adjacent halogen.

The gas-phase E2 reaction of  $\text{CH}_3\text{CH}_2\text{Cl}$  with  $\text{F}^-$  and  $\text{PH}_2^-$  (proton affinities 1554 and 1552 kJ/mol) has been investigated by high-level ab initio computations [234]. With  $\text{F}^-$  as the nucleophile, a small difference of 4 kJ/mol was found, favoring the  $\text{S}_{\text{N}}2$  pathway over the E2 (anti) pathway. However, the E2 (anti) pathway was preferred over the E2 (syn) route by 53 kJ/mol. Fluoride was predicted to be considerably more reactive than  $\text{PH}_2^-$ , for which relative transition state energies of 0.0, 49, and 84 kJ/mol were found for the  $\text{S}_{\text{N}}2$ , E2 (anti), and E2 (syn) transition states, respectively.

### E1cB Mechanism Reaction

The E1cB mechanism has the same features as the E2 mechanism except that proton abstraction by the base proceeds essentially to completion prior to departure of the leaving group. A variant of this mechanism may intervene whenever the leaving group is a poor leaving group or an exceptionally stable carbanion may be formed (i.e., due to the presence of Z substituents in addition to the polar  $\sigma$  bond and/or a hybridization effect). The factors which lead to stabilization of carbanions have been discussed in Chapter 7.

### E1 Elimination Reaction

The rate-determining step of the E1 elimination reaction is precisely the same as previously discussed for the  $\text{S}_{\text{N}}1$  reaction. The interaction diagram for the C—H bond and an adjacent carbocationic center is shown in Figure 10.6*b*. Because the  $\sigma$  and  $\sigma^*$  C—H bond orbitals are equally spaced relative to the energy of the  $p$  orbital at the cationic site, the LUMO energy is approximately the same as the energy of the unperturbed cationic  $p$  orbital. Reactivity with Lewis bases remains very high but is reduced somewhat by delocalization of the orbital (smaller coefficient on the  $p$  orbital). Notice that the presence of the adjacent C—H bond results in stabilization of the carbocation by a lowering of the energy of the  $\sigma_{\text{CH}}$  orbital. Concomitant delocalization of the C—H bonding electrons is accompanied by weakening of the C—H bond and partial bond formation between the H and the C at the cationic site. Hydride transfer may result if this is energetically favorable. The most probable course of the reaction with a Lewis base is formation of a  $\sigma$  bond at the cationic site. However, there is a possibility of attack at the H end of the C—H bond, and this mode may be enhanced if the base is a “good” Lowry–Bronsted base (forms a strong bond to H). Both addition of the nucleophile to C and proton abstraction are reversible. The equilibrium may often be channeled toward proton abstraction by removal of the more volatile olefin by distillation.

## REACTION WITH ELECTROPHILES: HYDRIDE ABSTRACTION AND HYDRIDE BRIDGING

The C—H bond is normally not very basic and will not interact with Lewis acids as a rule. However, in the presence of very powerful Lewis acids, such as carbocations, or if substituted by powerful  $\pi$  electron donors (X: or “C” substituents), hydride abstraction from a carbon atom may be accomplished, corresponding to an *oxidation* of the C atom.

### Activation by $\pi$ Donors (X: and “C” Substituents)

Abstraction of a hydride from carbon is almost invariably an endothermic process. The rate of the reaction depends on the stability of the transition structure which closely resembles the product carbocation and is expected to be stabilized by the same factors, among them, substitution by X: and “C” substituents. Nevertheless, initial interactions set the trajectory for the hydride abstraction reaction. The interaction of a C—H bond with a “C” substituent is shown in Figure 10.7b. The feature relevant to the present discussion is that the HOMO which involves some admixture of the C—H bond has been raised in energy. Therefore, attack by electrophiles, while most likely at the  $\pi$  bond of the “C” substituent, is also possible at the C—H bond. The interaction of an X: substituent with a CH bond is shown in Figure 10.7a. In general a single X: or “C” substituent is not sufficient to activate the C—H bond toward hydride abstraction.

### Hydride Abstraction

The interaction of a C—H bond with a strong Lewis acid (low-energy LUMO) is shown in Figure 10.8a. The  $p$  orbital of a carbocation as the LUMO is shown by way of example. Examples of hydride abstraction reactions are shown in Scheme 10.1.

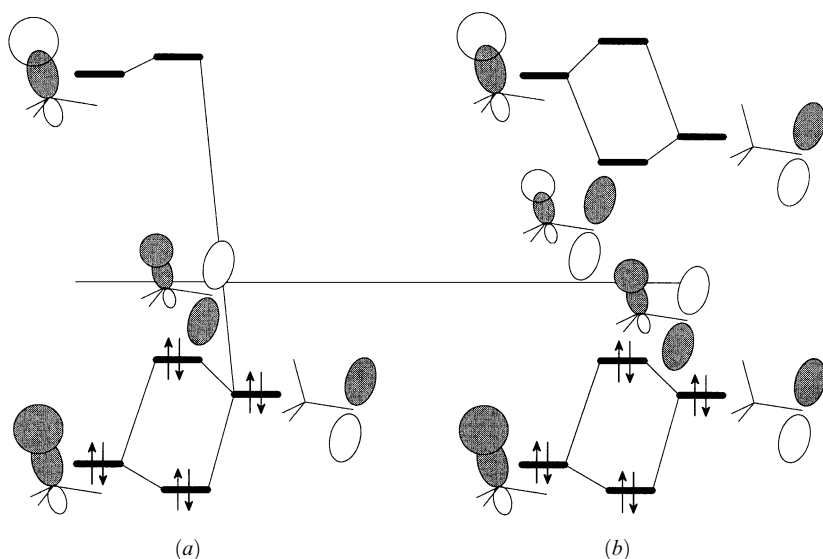


**Figure 10.7.** Activation of a C—H bond toward electrophilic attack by a neighboring substituent: (a) X: substituent; (b) “C” substituent (only the adjacent  $p$  orbital is shown).

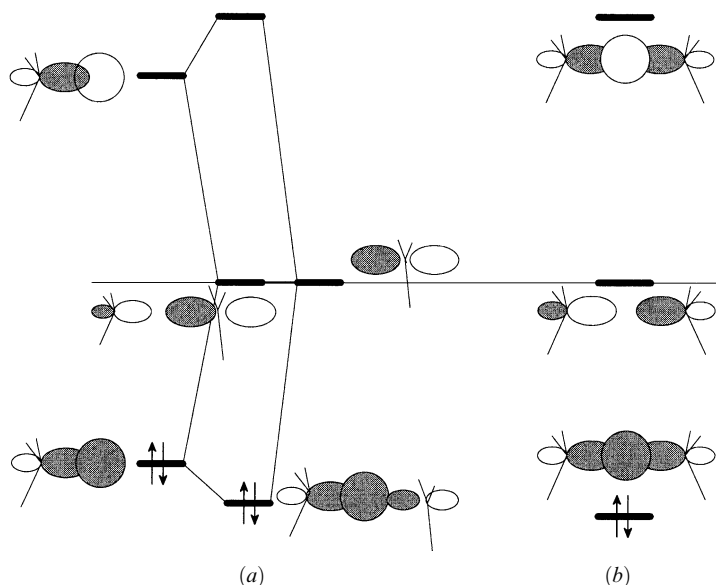
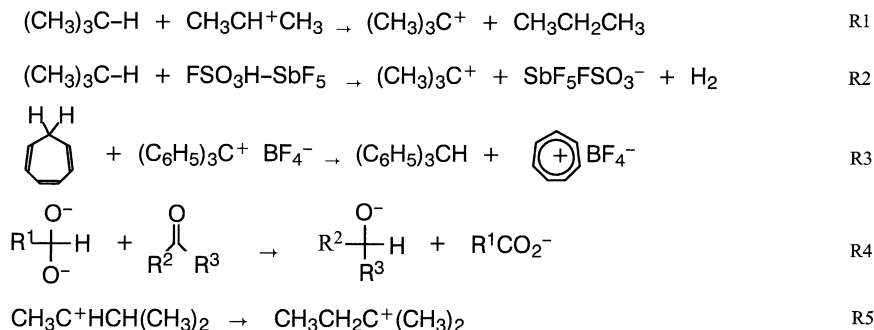


**Figure 10.8.** Interaction of a C—H bond with a strong Lewis acid: (a) initial interaction; (b) bonding MOs of a hydride bridge.

The first reaction provides a route for the reduction of alkyl halides since the carbocation (isopropyl, in R1) may be prepared from action of  $\text{AlCl}_3$  on the corresponding alkyl halide. Reactions of the type R1 are also important in the process, *catalytic cracking*, in the manufacture of gasoline. They have also been studied in mass spectroscopic experiments [235]. Reaction R2 is one route to the preparation of carbocations under stable ion conditions. Reaction R3 is employed in the laboratory synthesis of the tropylium cation. Reaction R4, the (crossed) Cannizzaro reaction, is unusual in that it takes place under strongly basic conditions. The oxy dianion is an intermediate in the reaction of concentrated hydroxide with the aldehyde,  $\text{R}^1\text{CHO}$ . None of  $\text{R}^1$ ,  $\text{R}^2$ , or  $\text{R}^3$  may have hydrogen atoms  $\alpha$  to the carbonyl groups. Formaldehyde ( $\text{R}^1 = \text{H}$ ) is readily



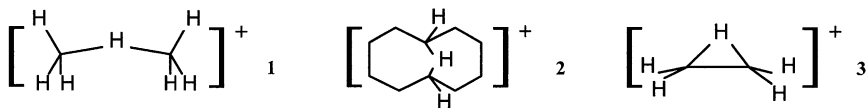
**Scheme 10.1**



oxidized and is useful in the reduction of other ketones or aldehydes. Reaction R5, a 1,2 migration of hydride, may be regarded as a special case of this class of reaction, although we will see it again in connection with the Wagner–Meerwein rearrangement as a thermally allowed [1, 2] sigmatropic rearrangement in connection with our discussion of pericyclic reactions (Chapter 12).

### Hydride Bridges

Hydride bridge bonding is common in boron compounds, the simplest example of which is  $B_2H_6$ , and in transition metal complexes. We restrict our discussion here to instances where hydride bridging occurs between carbon atoms. The MOs of a hydride bridged carbocation are shown in Figure 10.8*b*. These are entirely analogous to the MOs previously shown for two-electron three-center bonding (middle of Figure 10.7), except that the nonbonding orbital is higher in energy and unoccupied. One of the isomers of protonated ethane,  $C_2H_7^+$  **1**, has precisely the bonding shown in Figure 10.5*b*:



The C—H—C bond is not linear, the angle being about  $170^\circ$  according to high-level MO calculations. Several bridged cycloalkyl carbocations of the type **2** have been prepared [236]. Complexes between a number of alkyl cations and alkanes have been detected in mass spectrometric experiments [235]. The “nonclassical” structure of the ethyl cation, **3**, may be cited as another example of hydride bridging (for a discussion, see ref. 55).

### REACTION WITH FREE RADICALS: HYDROGEN ATOM ABSTRACTION AND ONE- OR THREE-ELECTRON BONDING

The C—H bond is normally not very polar. As a result, the  $\sigma_{CH}$  and  $\sigma_{CH}^*$  orbitals are widely separated and more or less symmetrically disposed relative to  $\alpha$ . A sluggish reaction is expected with carbon free radicals, but a rapid reaction may be anticipated with both electrophilic and nucleophilic free radicals. Examples of both kinds of reactions are ubiquitous in organic chemistry. An *ab initio* investigation of the former, involving oxygen-centered free radicals, has been carried out [237]. The reactivity spectrum may be modified by substitution on the carbon bearing the hydrogen atom. As we have seen in Chapter 7, all three kinds of substituents stabilize the carbon-centered free-radical intermediate.

### HYDROGEN-BRIDGED RADICALS

In most cases the bond to hydrogen is from an element more electronegative than it is, including carbon, and therefore the  $\sigma^*$  orbital, which may be the LUMO, is polarized toward H. Since one-electron bonding is more favorable than three-electron bonding in general, the complex formed between H—X and a free-radical center will involve a hydrogen bridge. If the interaction carries to extreme, a hydrogen atom abstraction

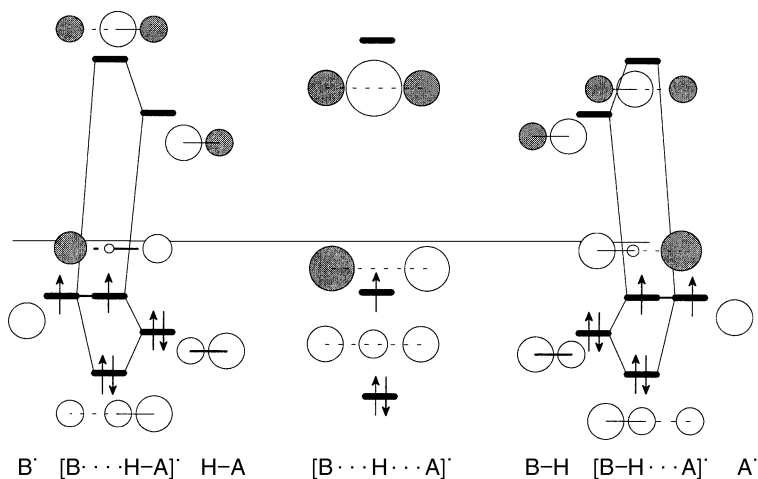


**Figure 10.9.** Orbitals for a hydrogen atom abstraction reaction. The middle is the orbital diagram for the transition state for H transfer.

occurs. The observation of negative activation energies in a number of reactions between carbon-centered free radicals and  $HX$  ( $X = Br, I$ ) [238, 239] has been interpreted as evidence of intermediate complex formation. The existence of the complex between methyl radical and  $HCl$  or  $HBr$  as a hydrogen-bridged species has been established by high-level *ab initio* calculations [68]. In the complex, the  $C-H$  bond is considerably elongated compared to the  $H-X$  bond.

## HYDROGEN ATOM TRANSFER

Figure 10.9 shows the orbital interactions for typical hydrogen atom transfer reaction. It is in fact the same diagram that described proton and hydride transfers (Figures 10.1 and 10.8, respectively). However, unlike the cationic and anionic cases, the author is not aware of any symmetrical hydrogen atom-bridged structures. The best candidate would be  $[F-H-F]^\cdot$ . The middle of Figure 10.9 would then represent the bonding of the TS to H atom transfer between equal fragments.

Sigma bonds are involved so generic  $s$  orbitals are shown for A and B in Figure 10.9. According to the principles described in Chapters 3 and 7, both the SOMO–HOMO and SOMO–LUMO interactions are attractive and a complex is expected. The SOMO–HOMO interaction becomes less important as the reagents approach each other (i.e., decreases as overlap increases) compared to the SOMO–LUMO interaction. The energy of the TS for H transfer will depend on the absolute importance of the two attractive interactions. The three-orbital interaction results in stabilization of the lowest orbital, and the middle singly occupied orbital moves slightly up or down depending on whether SOMO–HOMO or SOMO–LUMO is dominant. Because of its importance in oxidative damage by free radicals in biological systems, the activation parameters for many hydride transfer reactions have been determined experimentally or by high-level calculations, and a number of “rules” [240, 241] evolved to predict the magnitudes of the barriers,

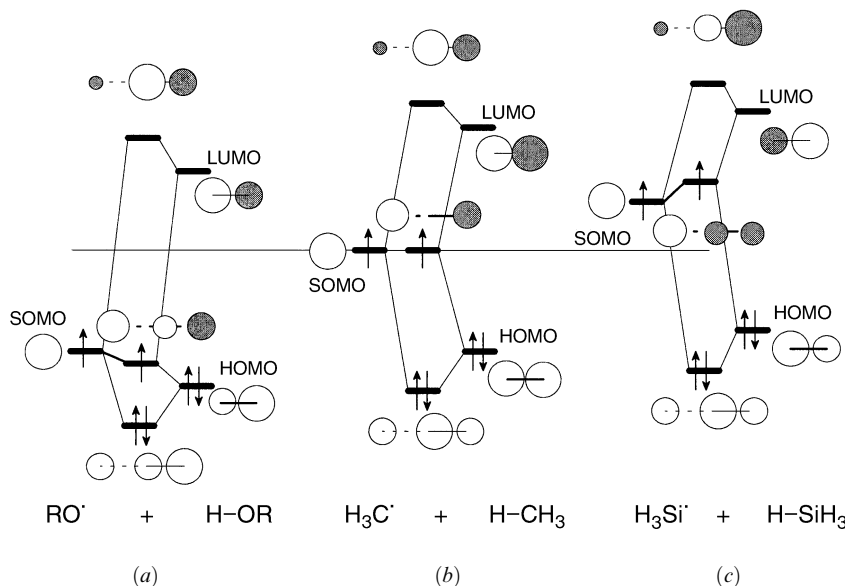


**Figure 10.10.** Orbitals for a hydrogen atom abstraction reaction by (a) alkoxy radical from H—OR; (b) methyl radical from CH<sub>4</sub> (one bond shown); (c) silyl radical from SiH<sub>4</sub> (one bond shown).

although each has notable “failures.” It seems reasonable that the barrier for H atom abstraction from H—A by B<sup>•</sup> should be dependent in some way on the strength of the H—A bond and the electronegativity difference between A<sup>•</sup> and B<sup>•</sup>, and these parameters are incorporated into the rules either directly [240] or in a more subtle fashion [241].

Polarity of the H—A bond is very important and can explain why the barriers (in kilojoules per mole) of RS<sup>•</sup> + H—SR (22 [242]) and RO<sup>•</sup> + H—OR (11 [243]) are lower than H<sub>3</sub>C<sup>•</sup> + H—CH<sub>3</sub> (57–61 [244]) and H<sup>•</sup> + H—H (40 [245]) while H<sub>3</sub>Si<sup>•</sup> + H—SiH<sub>3</sub> (58 [246]) is higher. The orbital interaction diagrams for normal polarity (H—S, H—O), nonpolar (H—C, H—H), and inverse polarity (H—Si) bonds are shown in Figure 10.10. In the normal polarity case (a), the dominant interaction is SOMO–LUMO. This has maximum stabilization and will lead to the lowest barrier. By contrast, the inverse polarization leads to a dilemma. The SOMO–HOMO favor interaction through H. Since a third-row element is involved, the smaller intrinsic interaction matrix element results in less stabilization, but also less of a repulsive component since  $|\Delta\varepsilon_U - \Delta\varepsilon_L| \approx 0$ . However, the SOMO–LUMO, which is stronger due to the smaller difference in orbital energies, favors interaction through the *other* end of the bond, that is, attack on Si. In fact, reaction of silyl radical with silane yields disilane among a host of products, but direct H abstraction seems not to be involved (see ref. 241(a) for a discussion). Thiyl radical *does* abstract a hydrogen atom from silane directly in an endothermic process with an activation energy estimated to be 34 kJ/mol from ab initio calculations [247]. Apparently the SOMO (3p orbital) of the more electronegative sulfur undergoes the expected three-electron, two-orbital interaction with the reverse polarized H—Si bond.

## CHAPTER 11

---

# AROMATIC COMPOUNDS

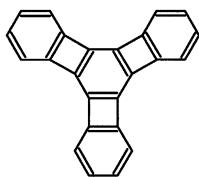
---

### REACTIONS OF AROMATIC COMPOUNDS

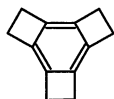
#### Cyclic $\pi$ Systems by Simple Hückel MO Theory

The MO energy level diagrams for the three- to seven-ring  $\pi$  systems are shown in Figure 11.1. The pattern may be extended. For any regular  $n$ -gon, there is a unique MO at  $\alpha - 2|\beta|$  which will describe the distribution of two electrons. The remaining orbitals are degenerate in *pairs* and able to accommodate four electrons, hence the origin of the Hückel  $4n + 2$  rule for aromaticity. All the cyclic  $\pi$  systems have exceptional stability if they have  $4n + 2$  electrons (two for the 3- and 4-membered rings and six for the others shown in Figure 11.1). Examples of each type are known experimentally. However, only benzene is stable in an absolute sense, having a relatively low pair of HOMOs, a relatively high pair of LUMOs, and a large HOMO–LUMO gap. It is electrically neutral and unstrained in the  $\sigma$  framework.

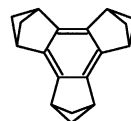
Theorists believe that the symmetry of the  $\pi$  system is imposed by the framework of  $\sigma$  bonds. Bond alternation in the  $\pi$  system can be forced by the fusion of strained bicyclic rings [248] such as in [4]phenylene [249], tricyclobutabenzene [250], or trisbicyclo[2.1.1]hexabenzene [251]:



[4]phenylene



Tricyclobutabenzene



Trisbicyclo[2.1.1]hexabenzene

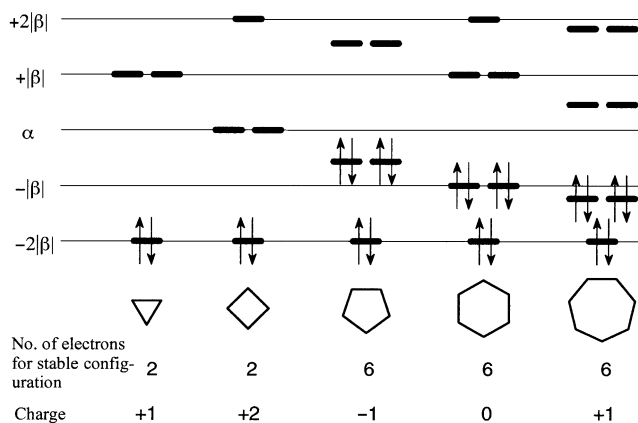
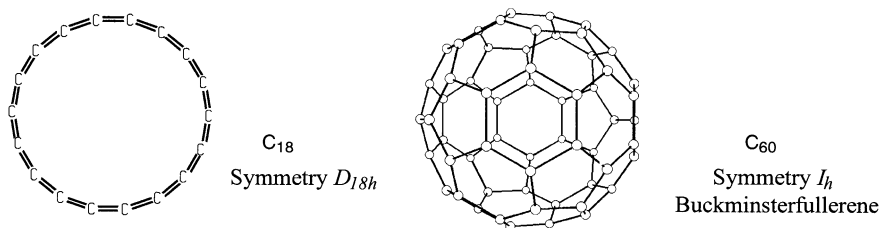


Figure 11.1. SHMO results for the smaller ring  $\pi$  systems.

### Aromaticity in $\sigma$ -Bonded Arrays?

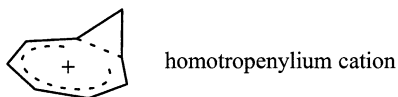
Two novel forms of carbon, with formulas  $C_{18}$  [252] and  $C_{60}$  [253] owe their stability to aromaticity with cyclic arrays of  $p$  orbitals which do not fall strictly into the class of cyclic systems discussed above:



Theoretical studies indicate that the allotrope,  $C_{18}$ , is a planar cyclic structure and therefore has one planar cyclic array of 18 electrons of the above type. It also has a *second* cyclic 18-electron array in the  $\sigma$  framework, albeit the orbitals overlap in a  $\pi$  fashion [254]. The allotrope,  $C_{60}$  [255], has a cyclic polyaromatic three-dimensional structure which has also been argued to be “aromatic” [256].

As we have already seen, the Hückel rules do not require that the orbitals be  $p$  orbitals overlapping in a  $\pi$  fashion. In fact, cyclic arrays of  $\sigma$  bonds will have substantially the same pattern of orbital energies as shown in Figure 11.1, and the  $4n + 2$  rule will apply. This observation will become especially relevant when we examine pericyclic reactions, in which more than two bonds are being made and broken at the same time. Cyclic transition structures in which  $4n + 2$  electrons are involved in the bond reorganizations will be exceptionally stabilized (i.e., aromatic), permitting relatively low activation energies for the reactions. The familiar Diels–Alder reaction is an example of this kind of reaction. Conjugation through space or through intervening cyclopropyl rings

may also exhibit aromatic character, as has been established by theoretical studies on the homotropenylium cation [257]:

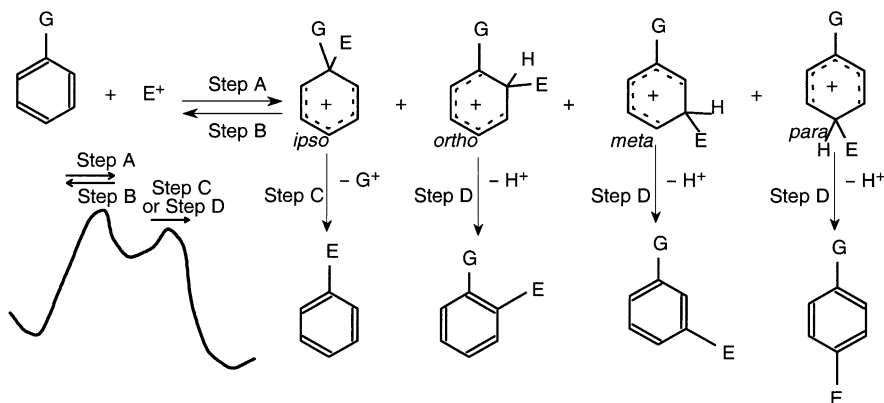


## REACTIONS OF SUBSTITUTED BENZENES

The intrinsic stability of the aromatic  $\pi$  system has two major consequences for the course of reactions involving it directly. First, the aromatic ring is less susceptible to electrophilic, nucleophilic, and free-radical attack compared to molecules containing acyclic conjugated  $\pi$  systems. Thus, reaction conditions are usually more severe than would normally be required for parallel reactions of simple olefins. Second, there is a propensity to eject a substituent from the tetrahedral center of the intermediate in such a way as to reestablish the neutral  $(4n + 2)$ -electron  $\pi$  system. Thus, the reaction is two step, an endothermic first step resulting in a four-coordinate carbon atom and an exothermic second step, mechanistically the reverse of the first, in which a group is ejected. The dominant course is therefore a *substitution* reaction rather than an addition.

## ELECTROPHILIC SUBSTITUTIONS

We will restrict our consideration to reactions of substituted benzenes and to nitrogen heteroaromatic systems in which the reaction takes place first with the  $\pi$  system. The simplest example of reaction of a monosubstituted benzene with an electrophile (Lewis acid) is shown in Scheme 11.1. The electrophile may attach itself to the  $\pi$  system (step A) in four distinct modes, ipso, ortho, meta, and para. The reactivity of the aromatic ring and the mode of attachment of the electrophile will be influenced by the specific nature of the substituent group, which may be  $X$ ;  $Z$ , or "C" type. Detachment of the electro-



Scheme 11.1

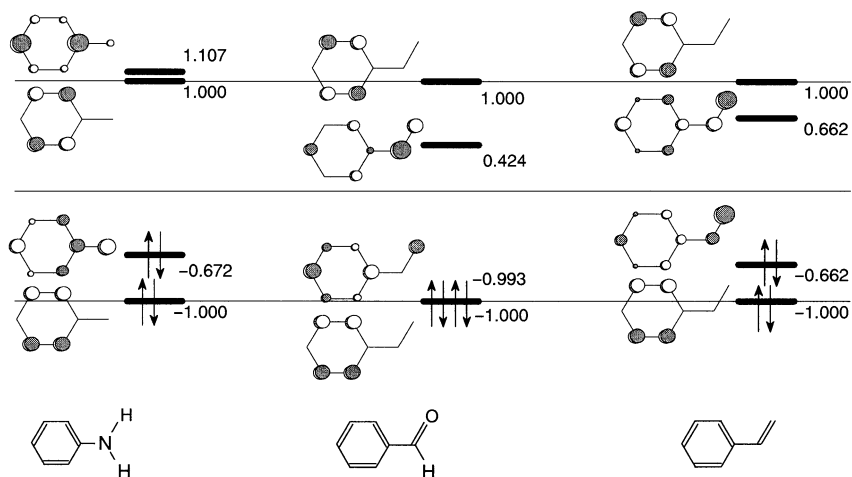


**Figure 11.2.** The SHMO frontier orbitals of aniline, benzaldehyde, and styrene as prototypes of X<sub>2</sub>-, Z-, and “C”-substituted benzenes.

phile (step B) is most probable from the ipso intermediate unless the group G itself is such that it can detach as a stable electrophile (step C). The most likely second step is abstraction of the proton by a weak base (step D) yielding a mixture of ortho, meta, and para substitution products.

### Effect of Substituents on Substrate Reactivity

The overall rate of reaction is governed by the activation energy, or more properly, the free energy of activation,  $\Delta G^\ddagger$ . Since the first step is rate determining and endothermic, or endergonic, it is expected that the effect of the substituent on the kinetics and regioselectivity of the reaction would be greatest on the transition structure which resembles the reactive intermediate. Nevertheless, as previously argued, the course of the reaction, that is to say, which of the four distinct reaction channels is favored, may well be determined by initial interactions between the electrophile and the aromatic substrate. The electronic characteristics of X<sub>2</sub>-, Z-, and “C”-substituted benzenes, using aniline, benzaldehyde, and styrene, respectively, as models, have been derived from SHMO calculations and are shown in Figure 11.2. While the relative energy levels may readily be deduced from simple orbital interaction considerations, the polarization of the HOMO and LUMO is best derived by actual SHMO calculation [12].

### Electrophilic Attack on X<sub>2</sub>-Substituted Benzenes

The X<sub>2</sub>-substituted benzene (aniline, Figure 11.2) is activated toward electrophilic attack since the HOMO is raised significantly. The electrophile would be directed to the ortho, para, and ipso positions of the ring and to the X<sub>2</sub> substituent itself. The ipso channel is usually nonproductive since the common heteroatom-based X<sub>2</sub> substituents are not easily displaced as Lewis acids. Loss of substituent is frequently observed with tertiary alkyl-substituted benzenes. Attachment of the electrophile to the X substituent is most likely if

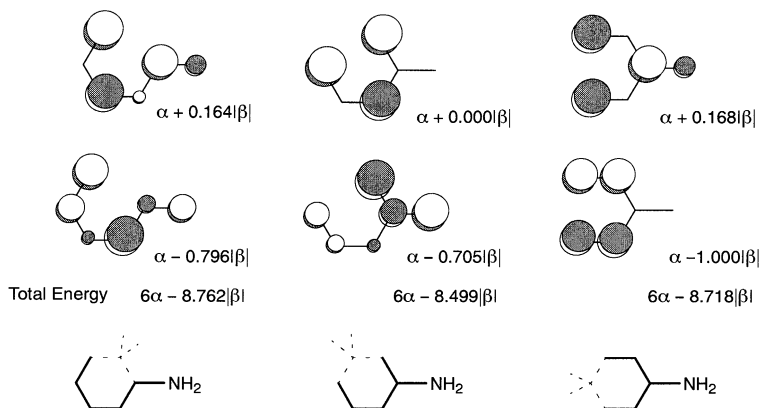


**Figure 11.3.** SHMO frontier orbitals and total energies for amino-substituted pentadienyl cations.

$X$ : is  $\text{NR}^1\text{R}^2$ . The substituent is converted to a  $Z$  substituent via the low-lying  $\sigma^*$  orbital, and the ring is deactivated toward further electrophilic attack. The ortho and para channels lead to products. The interaction diagram for an  $X$ :substituted pentadienyl cation, substituted in the 1-, 2-, and 3-positions, as models of the transition states for the ortho, meta, and para channels, are too complex to draw simple conclusions. The HOMO and LUMO of the three pentadienyl cations with an amino substituent are shown in Figure 11.3. Notice that the LUMO of each is suitable to activate the C—H bond at the saturated site toward abstraction by the base. Curiously, the meta cation has the lowest LUMO and should most readily eliminate the proton. The stabilities of the transition states should be in the order of the Hückel  $\pi$  energies. These are  $6\alpha - 8.762|\beta|$ ,  $6\alpha - 8.499|\beta|$ , and  $6\alpha - 8.718|\beta|$ , respectively. Thus the ortho and para channels are favored over the meta channel, and the ortho route is slightly preferred over the para route. Experimentally, para substitution products are often the major ones in spite of there being two ortho pathways. The predominance of para products is usually attributed to steric effects.

### Electrophilic Attack on $Z$ -Substituted Benzenes

The  $Z$ -substituted benzene (benzaldehyde, Figure 11.2) is not activated toward electrophilic attack since the HOMO of benzene is scarcely affected. No preferred site for attack of the electrophile can be deduced from inspection of the HOMOs. The interaction diagram for a  $Z$ -substituted pentadienyl cation, substituted in the 1-, 2-, and 3-positions, as models of the transition states for the ortho, meta, and para channels are too complex to draw simple conclusions. The HOMO and LUMO of the three pentadienyl cations with a formyl substituent are shown in Figure 11.4. The stabilities of the transition states should be in the order of the Hückel  $\pi$  energies. These are  $6\alpha - 9.204|\beta|$ ,  $6\alpha - 9.203|\beta|$ , and  $6\alpha - 9.129|\beta|$ , respectively. Thus, by SHMO, the ortho and meta channels are favored over the para channel, with no distinction between the ortho and meta pathways. Experimentally, meta substitution products are usually the major ones, contrary to the SHMO predictions. Either the SHMO method fails in this case or the predominance of meta products may be attributed to steric effects.



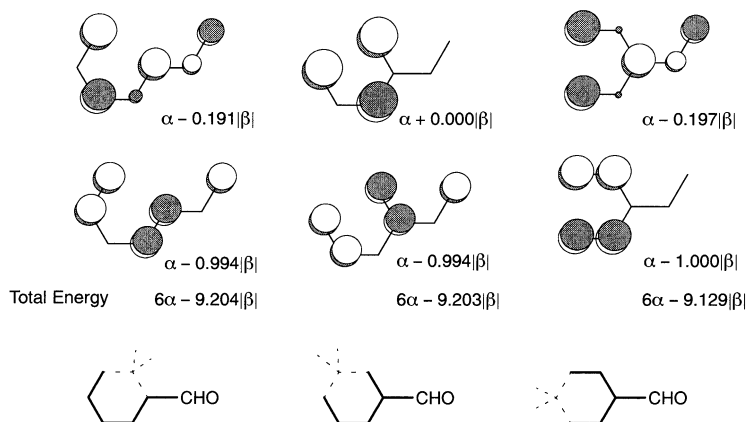


Figure 11.4. SHMO frontier orbitals and total energies for formyl-substituted pentadienyl cations.

### Electrophilic Attack on “C”-Substituted Benzenes

The “C”-substituted benzene (styrene, Figure 11.2) is activated toward electrophilic attack since the HOMO is raised significantly. The electrophile would be directed to the ortho, para, and ipso positions of the ring and to the “C” substituent itself. In fact, if the substituent is a simple olefin, electrophilic attack is almost exclusively on the external double bond. Electrophilic substitution of the ring is observed only if the “C” substituent is another aryl group. The ipso channel is nonproductive since an aryl group cannot depart as a Lewis acid. The ortho and para channels lead to products. The interaction diagram for a “C”-substituted pentadienyl cation, substituted in the 1-, 2-, and 3-positions, as models of the transition states for the ortho, meta, and para channels are too complex to draw simple conclusions. The HOMO and LUMO of the three pentadienyl cations with a vinyl substituent are shown in Figure 11.5. The stabilities of the transition states should be in the order of the Hückel  $\pi$  energies. These are  $6\alpha - 8.055|\beta|$ ,  $6\alpha - 7.878|\beta|$ , and  $6\alpha - 8.000|\beta|$ , respectively. The situation is entirely analogous to the X:-substituted case. The ortho and para channels are favored over the meta channel, and the ortho route is slightly preferred over the para route. Experimentally, the predominance of para products is usually attributed to steric effects.

### Electrophilic Attack on N Aromatics: Pyrrole and Pyridine

The SHMO orbitals of pyrrole, pyridine, and pyridinium are shown in Figure 11.6. The HOMO of pyrrole is the same as that of butadiene. Thus pyrrole is more reactive than benzene toward electrophilic attack. Attack, leading to substitution, occurs mainly at the 2- and 5-positions where the electron density of the HOMO is concentrated. In the case of pyridine (Figure 11.6*b*), the HOMO is not the  $\pi$  orbital, but the nonbonded MO,  $n_N$ , which would be situated at approximately  $\alpha - 0.5|\beta|$ . Thus, it is not pyridine but pyridinium (Figure 11.6*c*) which undergoes electrophilic attack and substitution. The reactivity is much less than that of benzene, although this could not be deduced directly from the SHMO calculation. Neither does the calculation suggest the reason that electrophilic substitution occurs mainly at the 3- and 5-positions, since the  $\pi$  HOMO is

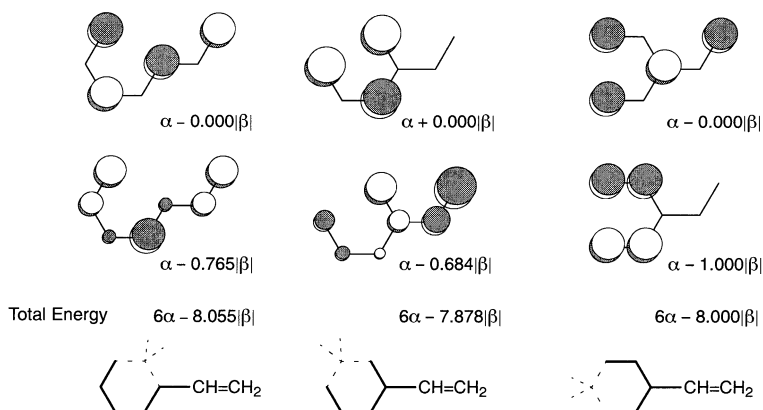


Figure 11.5. SHMO frontier orbitals and total energies for vinyl-substituted pentadienyl cations.

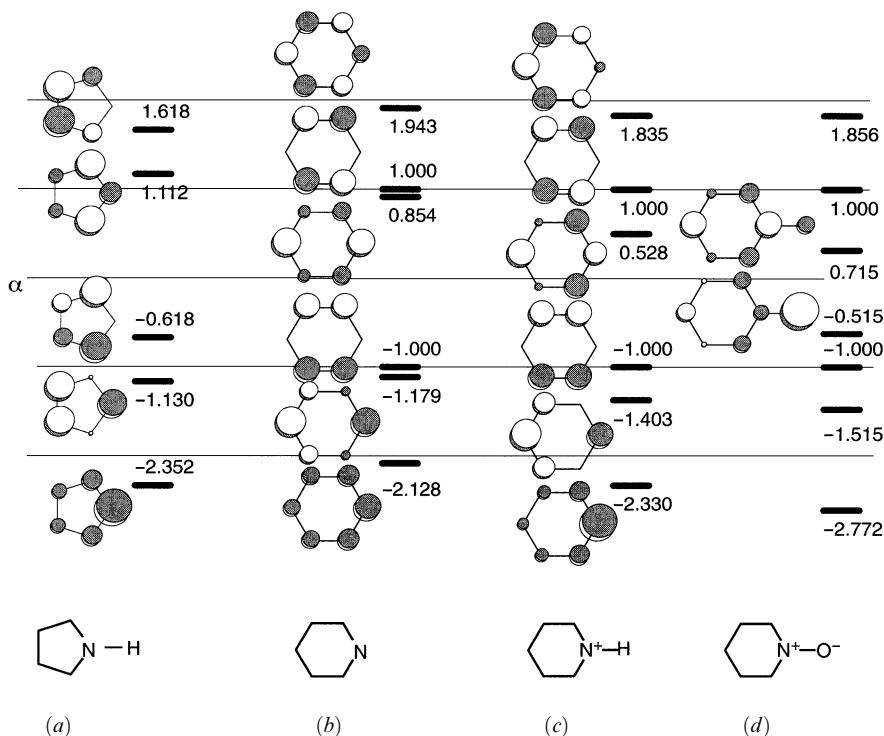
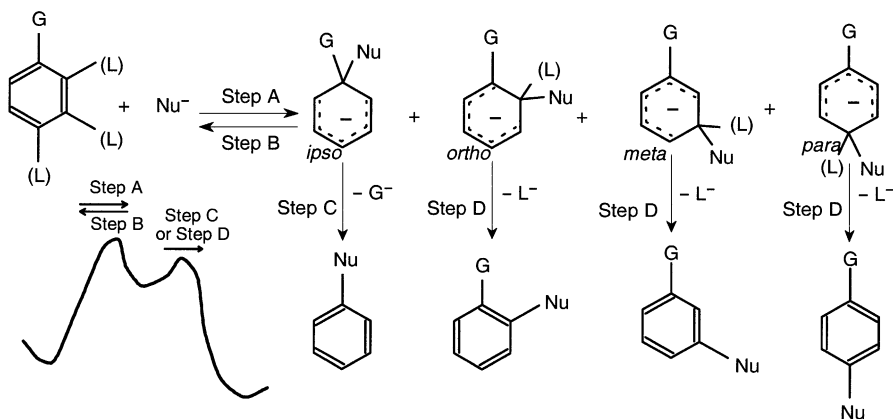


Figure 11.6. SHMO orbitals and orbital energies for (a) pyrrole; (b) pyridine; (c) pyridinium; (d) pyridine-N-oxide (HOMO and LUMO only shown).

equally distributed between the 2-, 3-, 5-, and 6-positions. It is probable that preference for the 3- and 5-positions originates from the lower activation energy, leading to the 2-azapentadienyl dication intermediate. The 2-, and 1-azapentadienyl dications serve as models for the transition states. Their SHMO  $\pi$  energies are  $4\alpha - 6.908|\beta|$  and  $4\alpha - 6.810|\beta|$ , respectively. Substitution into the 4-position of pyridine may be accomplished directly via the *N*-oxide, whose HOMO is shown in Figure 11.6*d*. On the basis of the SHMO calculation, one would expect greatly enhanced reactivity for the *N*-oxide, although polarization of the HOMO indicates that electrophilic attack would occur predominantly on the oxygen if it is not protonated under the reaction conditions.

## NUCLEOPHILIC SUBSTITUTIONS

Nucleophilic substitution in aromatic systems occurs by two very different mechanisms: initial proton abstraction and initial addition to the  $\pi$  system. The former will be discussed separately below. In the present section, we will restrict our consideration to reactions of substituted benzenes and to nitrogen heteroaromatic systems in which the reaction takes place first with the  $\pi$  system. The simplest example of reaction of a substituted benzene with a nucleophile (Lewis base) is shown in Scheme 11.2. This scheme is entirely analogous to Scheme 11.1, which described electrophilic attack, with the exception that hydrogen elimination (as hydride in step D) is not normally feasible. The nucleophile may attach itself to the  $\pi$  system (step A) in four distinct modes relative to a reference substituent, G, namely ipso, ortho, meta, and para. The reactivity of the aromatic ring and the mode of attachment of the nucleophile will be influenced by the specific nature of the substituent group, which may be X; Z, or "C" type. Detachment of the nucleophile (step B) is most probable from *all* intermediates unless the group G itself is such that it can detach as a stable nucleophile (step C) or there is such a group (L) situated at the site of attack. In the event that a leaving group, L, is present at the site of attack, the most likely second step is loss of that group (step D), yielding an ortho, meta, or para substitution product, as the case may be.



Scheme 11.2

### Effect of Substituents on Substrate Reactivity

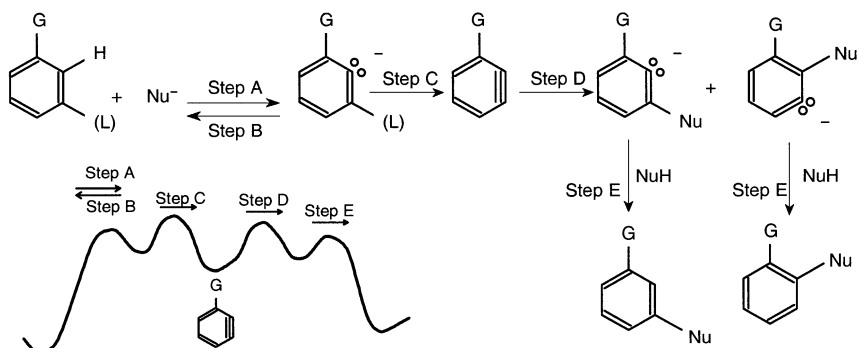
The overall rate of reaction is governed by the activation energy. Since the first step is rate determining and endothermic, it is expected that the effect of the substituent on the kinetics and regioselectivity of the reaction would be greatest on the transition structure which resembles the reactive intermediate. Nevertheless, as previously argued, the course of the reaction, that is to say, which of the four distinct reaction channels is favored, may well be determined by initial interactions between the nucleophile and the aromatic substrate. The electronic characteristics of X<sup>-</sup>, Z<sup>-</sup>, and “C”-substituted benzenes, using aniline, benzaldehyde, and styrene, respectively, as models, have been derived from SHMO calculations and are shown in Figure 11.2. The SHMO calculations on the model systems suggest that X<sup>-</sup>-substituted benzenes would not be activated toward nucleophilic attack on the  $\pi$  system, but that Z<sup>-</sup> and “C”-substituted benzenes should be reactive in this respect, Z<sup>-</sup>-substituted benzenes more so than “C”-substituted benzenes since the LUMO is lower in energy. In practice, neither X<sup>-</sup>- nor “C”-substituted benzenes undergo nucleophilic attack except by proton abstraction.

### Nucleophilic Attack on Z-Substituted Benzenes

The Z-substituted benzene (benzaldehyde, Figure 11.2) is strongly activated toward nucleophilic attack since the LUMO of benzene is substantially lowered. According to the distribution of the LUMO of benzaldehyde, nucleophilic attack is directed to the ortho and para positions in the ring and to the Z substituent also. The interaction diagram for a Z-substituted pentadienyl anion, substituted in the 1-, 2-, and 3-positions, as models of the transition states for the ortho, meta, and para channels are too complex to draw simple conclusions. The HOMOs of the three pentadienyl anions with a formyl substituent are identical to the LUMOs of the corresponding cations shown in Figure 11.4. The stabilities of the transition states should be in the order of the Hückel  $\pi$  energies. These are  $8\alpha - 9.585|\beta|$ ,  $8\alpha - 9.203|\beta|$ , and  $8\alpha - 9.513|\beta|$ , respectively. Thus, by SHMO, the ortho and para channels are favored over the meta channel, with a slight preference for the ortho pathways. Experimentally, Z substituents ortho or para to the site of substitution accelerate the reaction.

### Nucleophilic Attack on N Aromatics: Pyrrole and Pyridine

The SHMO orbitals of pyrrole, pyridine, and pyridinium are shown in Figure 11.6. The LUMO of pyrrole is higher in energy than that of benzene. As a consequence, pyrrole does not undergo nucleophilic attack in the  $\pi$  system. Just the reverse is true for pyridine, whose LUMO (Figure 11.6*b*) is somewhat lower than that of benzene. The observed reactivity of pyridine is much higher than is implied by the modest lowering of the LUMO. It is likely that the active substrate in the nucleophilic addition is not pyridine but rather metallated pyridine which will resemble pyridinium ion (Figure 11.6*c*). Complexation of the lone pair of electrons substantially lowers the energy of the LUMO which is concurrently polarized into the 2-, 4-, and 6-positions. Even hydride can be eliminated in the second step in some cases. The 1-, and 2-, and 3-azapentadienes serve as models for the metallated transition states for the pathways involving addition of the nucleophile to the 2-, 3-, and 4-positions, respectively. Their SHMO  $\pi$  energies are  $6\alpha - 7.582|\beta|$ ,  $6\alpha - 6.908|\beta|$ , and  $6\alpha - 7.408|\beta|$ , respectively, showing a clear preference for nucleophilic attack in the 2- (or 6-) and 4-positions.



Scheme 11.3

## NUCLEOPHILIC SUBSTITUTION BY PROTON ABSTRACTION

In the absence of Z substituents on the aromatic ring and aliphatic sites for nucleophilic attack, including acidic hydrogens elsewhere in the molecule, nucleophilic aromatic substitution may be accomplished by the mechanism shown in Scheme 11.3. A strong base abstracts a proton (step A) to yield an intermediate carbanion localized to the  $sp^2$  hybrid orbital of the aryl ring. The carbanion may reabstract the proton (step B) or eliminate a leaving group (step C) (or G itself if it can support a negative charge) to yield a benzyne intermediate. For this reason, this mechanism is usually referred to as the *benzyne* mechanism. The benzyne may undergo attack by the nucleophile (step D) to yield either one or both of two intermediate carbanions which are subsequently protonated (step E). Steps D and E are the microscopic reverse of steps C and A, respectively. Steps A and B may be considered to constitute a special case of the E1cB mechanism discussed briefly earlier. The carbanion which is most stabilized by adjacent low-lying  $\sigma_{CX}^*$  orbitals will most likely be formed. In step C, the better of the two leaving groups (assumed to be

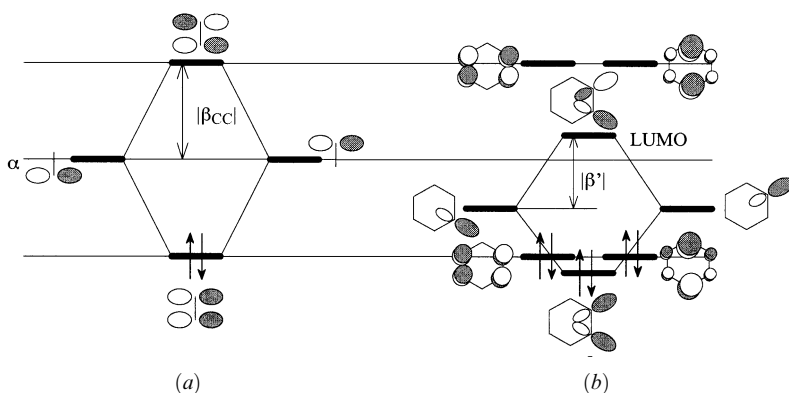


**Figure 11.7.** Interaction diagrams comparing (a) ethylene to (b) benzyne. Note that  $|\beta'| < |\beta_{CCl}|$ . The aromatic  $\pi$  system is largely unperturbed with nearly degenerate orbitals at  $\alpha - |\beta_{CCl}|$  and  $\alpha + |\beta_{CCl}|$ .

L in Scheme 11.3) departs. Nucleophilic addition to the intermediate benzyne (step D) is readily explained by perturbative MO arguments. The “extra”  $\pi$  and  $\pi^*$  orbitals of benzyne are compared to those of ethylene in Figure 11.7. *The aromatic  $\pi$  system is not involved in the special properties of benzyne.* The third benzyne  $\pi$  bond is due to the overlap in  $\pi$  fashion of the two  $sp^2$  hybrid orbitals which lie in the nodal plane of the intact  $6\pi$  electron system. Two factors contribute to a very low LUMO for benzyne. First, the  $sp^2$  hybrid orbitals are lower in energy than the  $2p$  orbitals from which the ethylene  $\pi$  orbitals are constructed. Second, the intrinsic interaction between the two  $sp^2$  orbitals is less than the normal  $\beta_{CC}$  since the orbitals have less  $p$  character and are tipped away from each other. The low LUMO of benzyne makes the molecule a strong Lewis acid, susceptible to attack by bases, and a reactive dienophile in Diels–Alder reactions, as we shall see later.

## CHAPTER 12

---

# PERICYCLIC REACTIONS

---

### GENERAL CONSIDERATIONS

In a chemical reaction, one or more bonds are broken and/or formed. Most chemical reactions in which a bond is ruptured proceed at rates which suggest that the activation energy is much less than that required to homolytically rupture the bond. Energy must be gained from the formation of one or more new bonds in order to offset that required to break bonds. The course of a typical reaction of the type  $A: + B-C \rightarrow A-B + C:$  may be followed by examination of the interaction diagrams for the reactants and products and the orbital characteristics of the TS, as shown in Figure 12.1. Repulsive four-electron, two-orbital interactions are always present but may be offset by a particularly favorable two-electron, two-orbital interaction. Often, to achieve a sufficiently large two-electron, two-orbital interaction, very stringent stereoelectronic requirements must be met. Thus, a collinear, backside approach is necessary for an  $S_N2$  reaction, and the E2 elimination reaction requires a coplanar, preferably anti arrangement of incoming base and the C—H and C—X bonds. Pericyclic reactions are reactions in which *more* than one bond is being made or broken at the same time and which have a cyclic transition state. As might be expected, even higher stereoelectronic constraints must be met in order that the reaction can proceed under moderate conditions. Stringent stereoelectronic requirements are invariably accompanied by a high degree of *diastereoselectivity*. Secondary interactions of orbitals will be applied to explain observed regioselectivity as well [258]. Pericyclic reactions are usually subclassified as *cycloadditions*, *electrocyclic reactions*, or *sigmatropic rearrangements*. These are shown in general form in Figure 12.2 and are discussed separately below. The definitions and terminology follow closely the work of Woodward and Hoffmann [3] in which more detail may be found. Treatment of the electronic effects via orbital interaction theory closely parallels the frontier orbital method of Fukui [1]. As we shall see, pericyclic reactions will fall into two categories, thermally *allowed* or thermally *forbidden* (with the implication that this

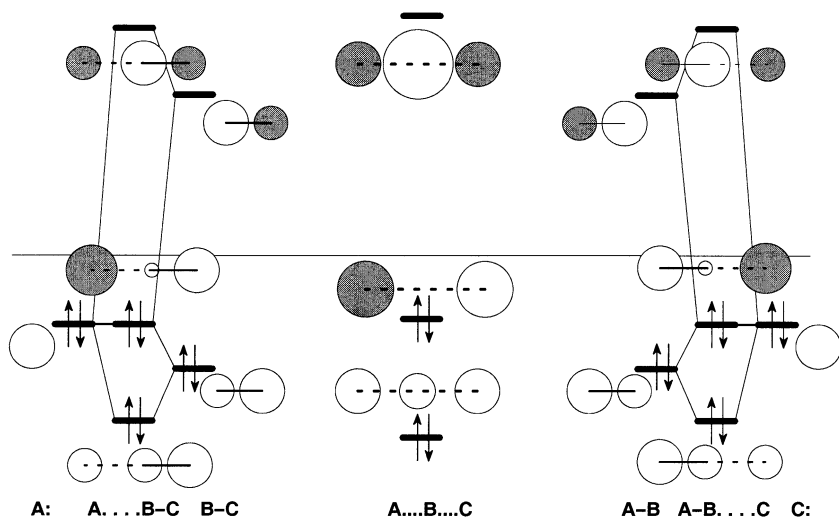


Figure 12.1. Orbitals for a simple substitution reaction:  $A + B-C \rightarrow A-B + C$ .

means photochemically allowed). The parallels to *aromatic* or *antiaromatic*, respectively, first pointed out by Dewar [259], will become evident.

## CYCLOADDITIONS AND CYCLOREVERSIONS

A general cycloaddition reaction is shown in Figure 12.2. A molecule with a conjugated system of  $m \pi$  electrons reacts with another molecule with  $n \pi$  electrons to form a cyclic molecule by the formation of two new  $\sigma$  bonds leaving conjugated systems of  $m - 2$  and  $n - 2 \pi$  electrons adjacent to the new  $\sigma$  bonds. Here  $m$  and  $n$  are even, nonzero integers. In the Diels–Alder reaction,  $m = 4$  and  $n = 2$ . Either or both  $\pi$  systems may be part of a more extended conjugated  $\pi$  system. For the purposes of the definition, the *active  $\pi$*  system of each reactant is that bridging the ends of the new  $\sigma$  bonds. In order that the formation of the two  $\sigma$  bonds may be feasible, the active  $\pi$  systems must be able to approach each other in such a way as to enable the terminal  $p$  orbitals to overlap simultaneously. In the Diels–Alder reaction, for example, the diene must be able to adopt, or be already in an *s-cis* conformation so that the  $p$  orbitals of the 1 and 4 carbon atoms can separately but simultaneously overlap the  $p$  orbitals at each end of the olefin.

### Stereochemical Considerations

In a cycloaddition reaction, the two active  $\pi$  systems may approach each other in either of two orientations, for example, head to head or head to tail. If one combination dominates, the reaction is said to be regioselective. In the course of the reaction, 4 new saturated centers are formed. With maximum labeling, a total of 16 ( $=2^4$ ) stereoisomeric forms, consisting of 8 enantiomeric pairs of diastereomers if neither polyene is chiral, may be formed. In pericyclic reactions, the stereochemistry is determined by specifying the stereochemical mode in which each component reacts. Each of the two



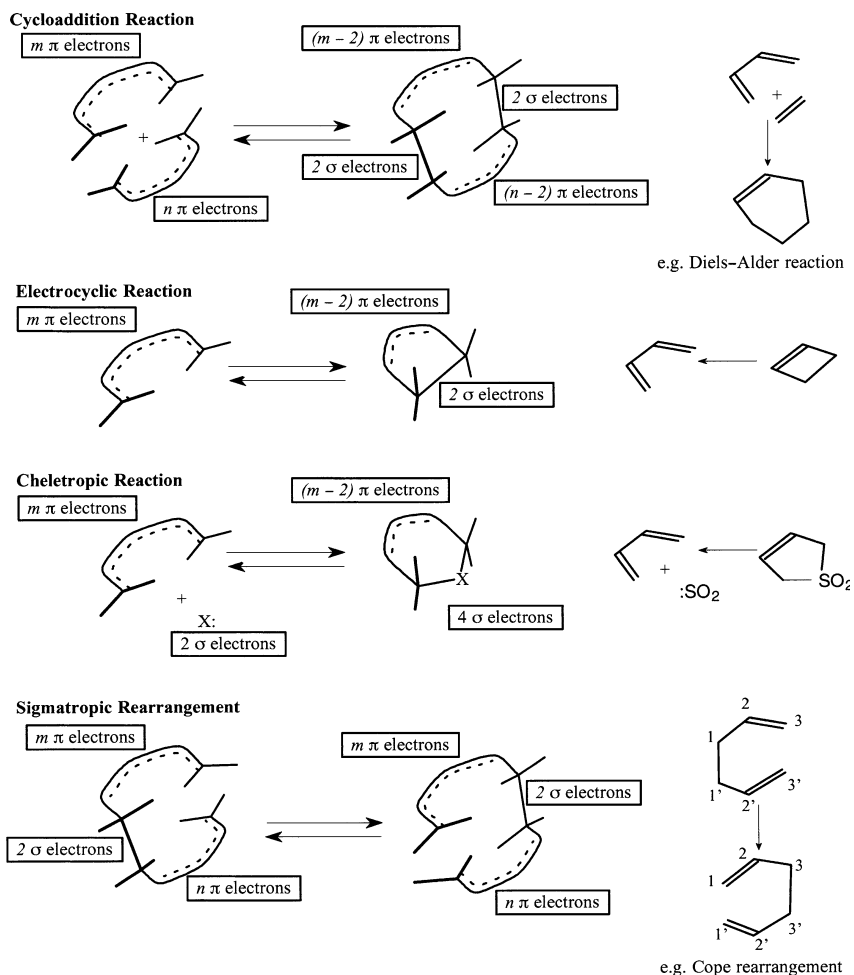


**Figure 12.2.** Three classifications of pericyclic reactions, with examples of thermally allowed reactions. *Chelotropic* is a special case of *electrocyclic*.

components of a cycloaddition reaction is a conjugated, quasiplanar  $\pi$  system for which two *faces* (top and bottom) may be distinguished. At each end of the  $\pi$  system, a new  $\sigma$  bond terminates. Each  $\sigma$  bond terminates on a line more or less perpendicular to a *face* of the  $\pi$  system. If both  $\sigma$  bonds terminate to the same face (both to the top or both to the bottom), the  $\pi$  system is said to react *suprafacially*, and the mode designation is *s*. If the two  $\sigma$  bonds are formed to opposite faces (one to the top and the other to the bottom, or vice versa), the  $\pi$  system is said to react *antarafacially*, and the mode designation is *a*. The two terminal points may be ends of two separate  $\sigma$  bonds or the opposite ends of the *same*  $\sigma$  bond (in this case, one has an *electrocyclic* reaction, which is discussed below). For example, the component designation,  $\pi 4_s$ , would indicate that a conjugated  $\pi$  system consisting of four electrons is reacting in a suprafacial manner. Examples of

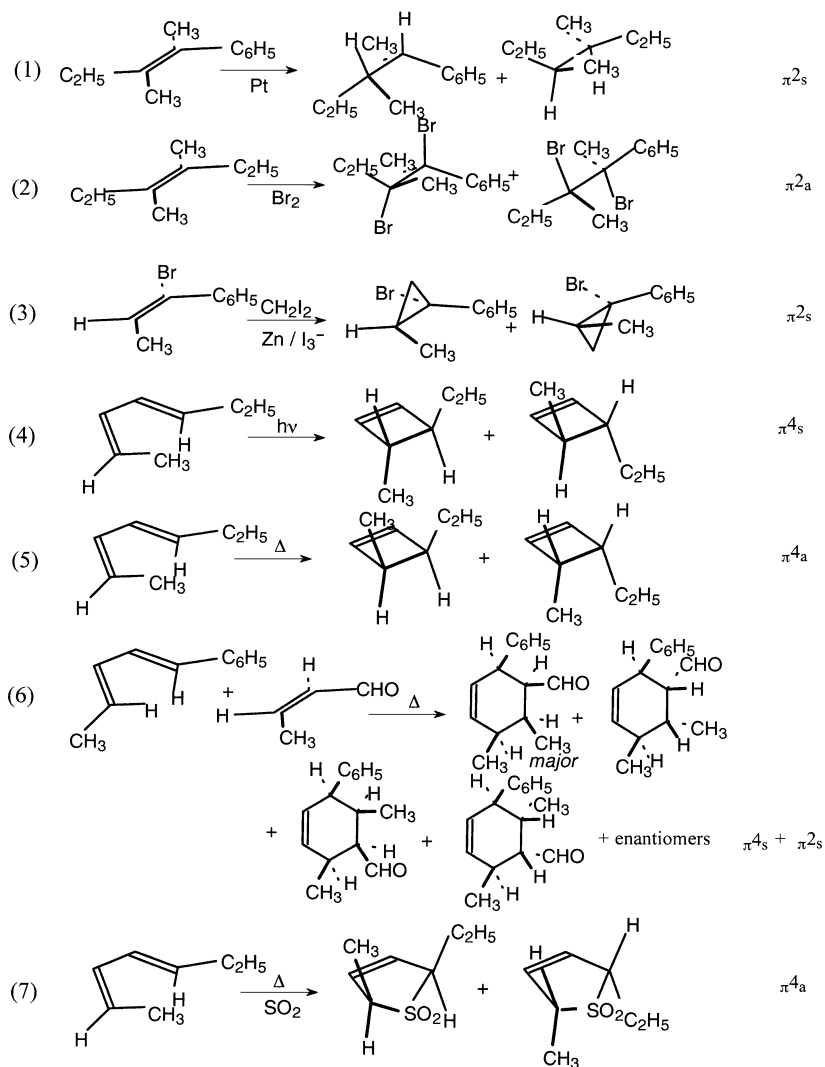


**Figure 12.3.** Examples of suprafacial and antarafacial reactions of  $\pi$  systems. Notice that the examples serve to describe the stereochemical course of the reaction only. No mechanism is implied by these examples.

suprafacial and antarafacial reactions of  $\pi$  systems are given in Figure 12.3. All of the reactions illustrated in Figure 12.3 actually give the products shown under the specified reaction conditions. Reactions (4)–(6) are pericyclic reactions.

The reverse process is also useful in synthesis. The active components of the cyclo-reversion reaction are the two  $\sigma$  bonds which will be broken and any  $\pi$  systems to which both  $\sigma$  bonds are allylic (i.e., at least one of  $m, n$  is an even number greater than 2). The stereochemistry of the reaction may also be specified in terms of the stereochemical mode of reaction of the active components of the reaction.

## ELECTROCYCLIC REACTIONS

A general electrocyclic reaction is shown in Figure 12.2. A molecule with a conjugated system of  $m$   $\pi$  electrons cyclizes to form a cyclic molecule. One new  $\sigma$  bond is formed, leaving a conjugated system of  $m - 2$   $\pi$  electrons in the ring. Here  $m$  is an even, nonzero integer. The  $\pi$  system may be part of a more extended conjugated  $\pi$  system. The *active*  $\pi$  system is that bridging the ends of the new ring-forming  $\sigma$  bond. In order that the formation of the  $\sigma$  bond may be feasible, the two ends of the active  $\pi$  system must be able to approach each other in such a way as to enable the terminal  $p$  orbitals to overlap.

### Stereochemical Considerations

In an electrocyclic reaction, a ring is formed from a nominally planar  $\pi$  system. The local plane of the carbon atom involved at each end must rotate through  $90^\circ$  in order that the  $p$  orbitals may overlap in a  $\sigma$  fashion. The active  $\pi$  system may cyclize by either of two distinct modes: conrotatory or disrotatory. *Conrotatory* ring closure occurs when the sense of rotation of the two termini is the same, that is, both clockwise or both counterclockwise. *Disrotatory* ring closure occurs when the sense of rotation of the two termini is opposite, that is, one end clockwise and the other counterclockwise, or *vice versa*. If one mode dominates, the reaction is said to be diastereoselective. In the course of the reaction, two new saturated centers are formed. With maximum labeling, a total of four ( $=2^2$ ) stereoisomeric forms, consisting of two enantiomeric pairs of diastereomers if the polyene is achiral, may be formed. Reactions (4) and (5) of Figure 12.3 illustrate the electrocyclic reaction of substituted butadiene to form a cyclobutene. Reaction (4) illustrates disrotatory closure of the ring, yielding a pair of enantiomeric 2-methyl-3-ethylcyclobutenes. Reaction (5) illustrates conrotatory closure of the ring, also yielding a pair of enantiomeric 2-methyl-3-ethylcyclobutenes which are diastereoisomers of the products of reaction (4). The active  $m$ -electron  $\pi$  system may be considered as a single component ( $m = 4$  in this case). Disrotatory ring closure corresponds to suprafacial reaction of the  $\pi$  system, the conrotatory mode being designated antarafacial. A component analysis of the reverse process involves two components, the residual  $\pi$  system and the  $\sigma$  bond which is to be lost.

## CHELETROPIC REACTIONS

A general cheletropic reaction is shown in Figure 12.2. This reaction involves the addition to, or extrusion from, a conjugated system of a group bound through a single atom. The reaction usually involves the elimination of simple stable molecules such as  $\text{SO}_2$ ,  $\text{CO}$ , or  $\text{N}_2$ . The atom to which there were two  $\sigma$  bonds carries away a pair of electrons, usually in a  $sp^n$  hybrid orbital. The addition of a carbene to a simple olefin to form a cyclopropane is also a cheletropic reaction which, as discussed in Chapter 14, is not predicted to be concerted. Cheletropic reactions incorporate features of both cycloaddition and electrocyclic reactions.

### Stereochemical Considerations

In a cheletropic reaction, a ring is formed from a nominally planar  $\pi$  system via bridging of a single atom. The local plane of the carbon atom involved at each end must rotate

through  $90^\circ$  in order that the  $p$  orbitals may overlap in a  $\sigma$  fashion. As with electrocyclic reactions, the active  $\pi$  system may cyclize by either of two distinct modes: conrotatory or disrotatory. If one mode dominates, the reaction is said to be diastereoselective. In the course of the reaction, two new saturated centers are formed. With maximum labeling, a total of four ( $=2^2$ ) stereoisomeric forms, consisting of two enantiomeric pairs of diastereomers if the polyene is achiral, may be formed. Reactions (3) and (7) of Figure 12.3 illustrate cheletropic reactions of an olefin and a carbene to form a cyclopropane and a substituted butadiene to form a 4,4-dioxo-4-thiacyclopent-1-ene. Reaction (3) illustrates suprafacial addition of  $[\text{CH}_2]$  to an olefin, yielding a pair of enantiomeric cyclopropanes. Reaction (7) illustrates conrotatory closure of the diene, yielding a pair of enantiomeric thiacyclopentenes. The forward reaction (3) or (7) has two components. Disrotatory ring closure corresponds to suprafacial reaction of the  $\pi$  system, the conrotatory mode being designated antarafacial. A component analysis of the reverse process involves three components, the residual  $\pi$  system and the two  $\sigma$  bonds which are to be lost.

## SIGMATROPIC REARRANGEMENTS

A general sigmatropic rearrangement is shown in Figure 12.2. A molecule with two conjugated systems of  $m$  and  $n$   $\pi$  electrons rearranges in such a way that the  $\sigma$  bond appears to migrate across each  $\pi$  system, forming a molecule with the same description but with the  $\pi$  bonds shifted by one carbon atom and the  $\sigma$  bond in a new position. Here  $m$  and  $n$  are even integers. One or *both* may be zero. A "zero" may indicate either that there is no active  $\pi$  system adjacent to that end of the  $\sigma$  bond or that there is an active  $\pi$  system which consists of a single empty  $p$  orbital (a trivial  $\pi$  system with no electrons). In order that a sigmatropic rearrangement takes place, there must be at least *one* active  $\pi$  system. Sigmatropic rearrangements are sometimes described by a pair of numbers  $[i, j]$ . These count the number of *atoms* over which the two ends of the  $\sigma$  bond migrate, counting the atom at each end as "1." Thus the Cope rearrangement illustrated in Figure 12.3 is a [3,3] rearrangement since each end of the migrating  $\sigma$  bond moves over three atoms. In order that the formation of the new (rearranged)  $\sigma$  bond may be feasible, the two ends of the active  $\pi$  systems must be able to approach each other in such a way as to enable the terminal  $p$  orbitals to overlap, or, in the case of a  $[1, j]$  rearrangement (i.e., only one end of the  $\sigma$  bond migrates), the nonmigrating end of the  $\sigma$  bond must be able to approach the other end of the active  $\pi$  system closely enough so that new bond formation can be initiated.

### Stereochemical Considerations

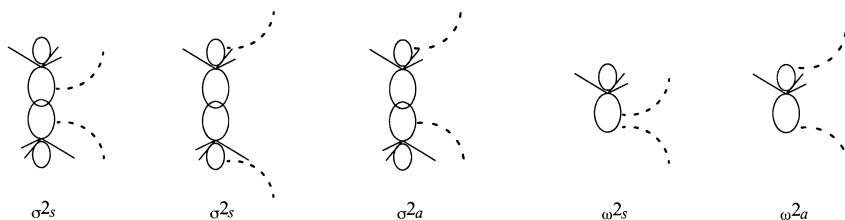
In a sigmatropic rearrangement, with maximum labeling, the number of elements of stereochemistry is preserved. There are four: chirality at each end of the  $\sigma$  bond and geometric isomerism at the far end of each active  $\pi$  system. After the rearrangement, the roles are reversed. A maximum of 16 ( $=2^4$ ) stereoisomeric products may be formed. Even if one end of the  $\sigma$  bond does not migrate but is an asymmetric center, the stereochemistry of that center may change. The stereochemical mode of reaction of a  $\sigma$  bond (as a component) may be specified as suprafacial or antarafacial in a fashion parallel to the  $\pi$  components. A sigma component of the reaction always has two electrons (a  $\pi$  component may have any even number, including zero). A  $\sigma$  bond component is

regarded as reacting suprafacially if the stereochemical fate at each end is the same, that is, the configuration is retained or inverted at each end. A  $\sigma$  component is regarded as reacting antarafacially if the stereochemical fate at the two ends is different, that is, the configuration is retained at one end and inverted at the other, or vice versa. If one end of the bond is a hydrogen atom, that end is considered to react with retention of configuration. The stereochemical mode of reaction of that bond is then determined by whether configuration at the other end is retained (*s*) or inverted (*a*).

### COMPONENT ANALYSIS (ALLOWED OR FORBIDDEN?)

A component analysis of pericyclic reactions proceeds by the following steps, which are illustrated for each of the classes of reaction in Figure 12.4:

1. Examine the reactants and products identifying the *active* components of each. The active components are those  $\sigma$  and/or  $\pi$  bonds which are broken in the reactants and formed in the products.
2. Draw the constituent orbitals for each component. These are *p* orbitals at each end of the  $\pi$  system and (usually) *sp*<sup>3</sup> hybrid orbitals at each end of  $\sigma$  components (if the  $\sigma$  bond terminates at H, the orbital there is an *s* orbital). *Disregard orbital phases.*
3. Identify which orbitals of the reactants must overlap to form the newly formed bonds of the products and connect these with a curved line. When orbitals overlap in a  $\pi$  fashion, one may *arbitrarily* choose the pair of lobes (top or bottom) when making the connection.
4. Examine the components of the reactants. Each component should have *two* curved lines entering it, one to each end. The curved lines indicate the stereochemical mode of reaction of each component. For a  $\pi$  component, if the two curved lines are connected to the same face, the mode is *s*; if to opposite faces, *a*. For a  $\sigma$  component, the mode is *s* if both curved lines are connected to the larger (inner) lobes of the *sp*<sup>3</sup> orbitals or both to the smaller (backside) lobes. Otherwise the mode is *a*, as in the illustrated sigmatropic rearrangement in Figure 12.4. If the component is a single *sp*<sup>*n*</sup> orbital, it is called  $\omega$ . If both curved lines terminate to the same lobe, that component is reacting as *s*; if to different lobes, then *a*.



5. Add up the components, counting only  $4n + 2$  components if they are *s* and  $4m$  components if they are *a*. Remember that  $4n + 2$  and  $4m$  are the numbers of electrons. Thus the allylic  $\pi$  system in Figure 12.4 is a two-electron component, i.e.,

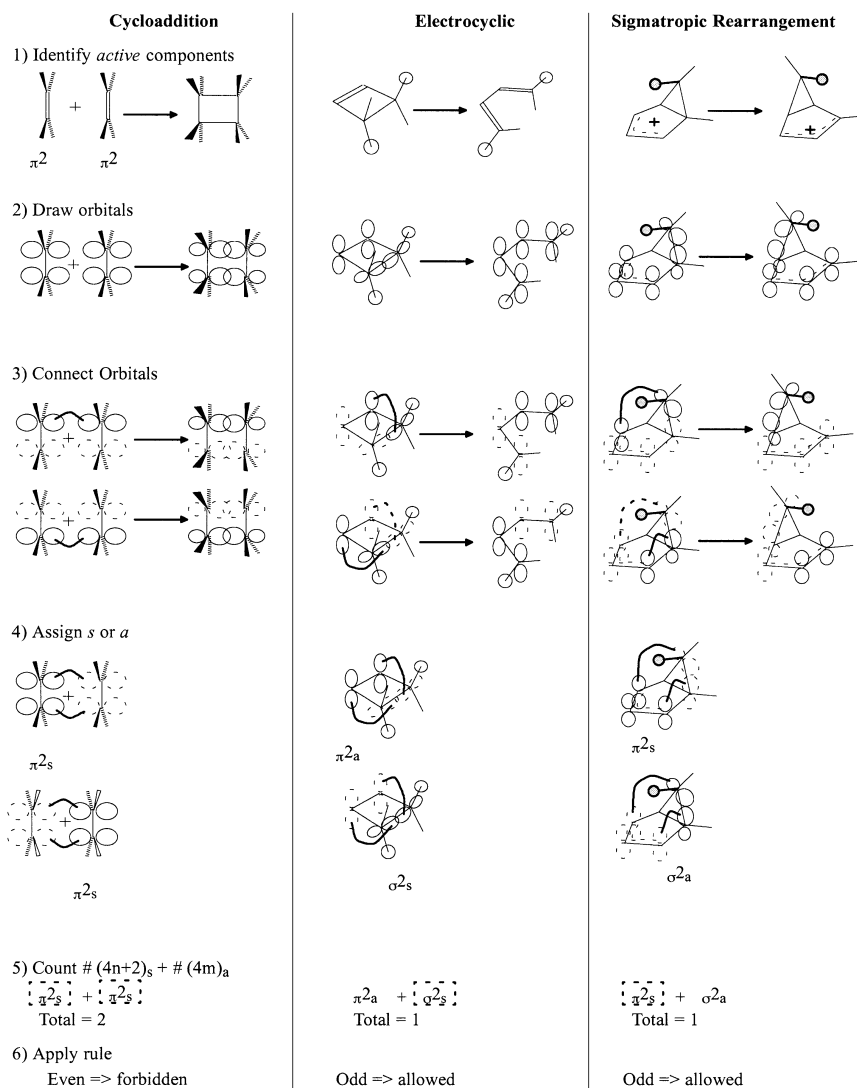


**Figure 12.4.** Procedure for general component analysis illustrated for each of the three types of pericyclic reactions.

$4n + 2$  with  $n = 0$ . A component may have no electrons, in which case it is a  $4m$  component ( $m = 0$ ).

6. Apply the rule (see below).

### Rule for Component Analysis

The general rule for all pericyclic reactions was formulated by Woodward and Hoffmann ([3], p. 169). *A ground-state pericyclic change is symmetry allowed if the total number of  $(4n + 2)_s$  and  $(4m)_a$  components is odd.*

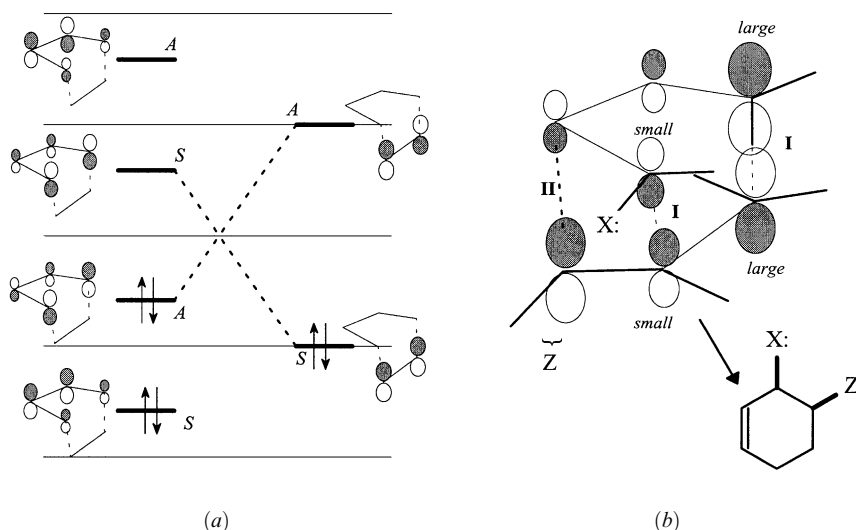


**Figure 12.5.** (a) Orbital interaction diagram for an s-cis diene and an olefin in the orientation for maximum overlap. (b) Interaction frontier MOs of an X-substituted diene and a Z-substituted dienophile showing primary (I) and secondary (II) interactions.

## Diels–Alder Reaction

The Diels–Alder reaction, shown in Figure 12.5, reaction (6), is probably the best known and synthetically the most useful of all pericyclic reactions. The diene must be in, or be able to achieve, a quasi-s-cis geometry. The Diels–Alder reaction of the parent molecules, 1,3-butadiene and ethene, is difficult, requiring high temperature and pressure (e.g., 36 h at 185°C at 1800 psi [260]) but has been shown to proceed in a concerted synchronous fashion both experimentally [260] and theoretically [260, 261]. The reaction is accelerated by substitution by electron donors (X: or “C” substituents) on the diene moiety and by the presence of electron-withdrawing substituents (Z type) on the alkene, which then becomes a “good dienophile.” Many examples of the Diels–Alder reaction with the reverse substitution pattern (reverse-demand Diels–Alder) are also known. The reaction proceeds with a high degree of stereospecificity at both diene and dienophile moieties as expected from its component analysis,  $\pi 4_s + \pi 2_s$ , and often in the case of unsymmetrically substituted components a high degree of regioselectivity (head-to-head vs. head-to-tail selectivity). Additionally, the longitudinal orientation of the Z-substituted dienophile in the reaction is consistent with a degree of preference for the more crowded endo transition state leading to endo diastereoselectivity. All aspects of the Diels–Alder reaction are readily understood in terms of the orbital interaction diagram.

**Orbital Interaction Analysis.** An orbital interaction diagram for the Diels–Alder reaction is shown in Figure 12.5a. The geometry of approach of the two reagents which ensures a maximum favorable interaction between the frontier MOs (dashed lines) preserves a plane of symmetry at all separations. The MOs are labeled according to whether they are symmetric (S) or antisymmetric (A) with respect to reflection in the plane. Simultaneous overlap of *both* HOMO–LUMO pairs is a necessary feature of all peri-

cyclic reactions, permitting charge transfer in both directions in the multiple bond-forming process. The charge transfer and back transfer are required to avoid excessive charge separation in the reaction but are not necessarily synchronous in the sense that the extent of charge transfer in each direction is the same. In the normal course of the Diels–Alder reaction, the reactivity is controlled by a dominant HOMO(diene)–LUMO(dienophile) interaction. The polarization and energies of unsymmetrically substituted frontier MOs of olefins and dienes were discussed in Chapter 6. The orbitals are shown in Figure 12.5*b* in the orientation which provides maximum overlap (the *large–large, small–small* orientation) in the primary interactions (I). The reaction is therefore regioselective, producing 3*X*,4*Z*-cyclohex-1-enes. The secondary interaction (II) [258] leads to endo diastereoselectivity and *cis* diastereomers, namely an enantiomeric pair of *cis*-3*X*,4*Z*-cyclohex-1-enes (Figure 12.5*b*). Substantial progress has been achieved in enantioselective Diels–Alder reactions where one or both components are substituted by chiral groups or complexed to chiral organometallic groups.

### Cope Rearrangement

The Cope rearrangement, illustrated in Figure 12.6, and variations of it are synthetically important reactions ([119], p. 1021). Reaction of the parent 1,5-hexadiene has an activation energy of 33.5 kcal/mol [262] and has been shown by *ab initio* computations [263, 264] to proceed in a synchronous concerted manner. The chairlike transition state is slightly preferred over the boatlike form (Figure 12.6*a*). Variations include the anionic oxy-Cope rearrangement shown in Figure 12.6*b* [265] and the rearrangement of divinyl cyclopropanes to 1,4-cycloheptadienes (Figure 12.6*c*). The 1,209,600-fold degenerate rearrangement of bullvalene (Figure 12.6*d*) is rapid at room temperature, displaying only a single peak in the NMR spectrum. The structure has been shown to have  $C_{3v}$  symmetry by neutron diffraction studies [266] and by temperature-dependent solid-state NMR [267].

**Orbital Interaction Analysis.** An orbital interaction diagram for the Cope rearrangement is shown in Figure 12.7*a*. The reaction may be initiated by electron donation from

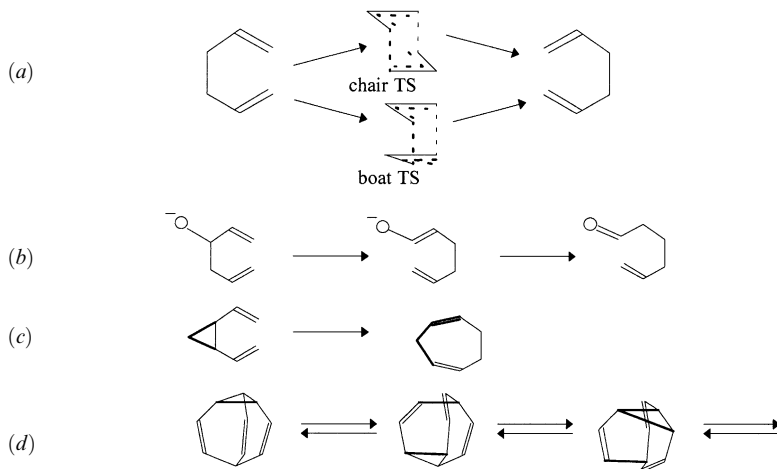


**Figure 12.6.** (a) Cope rearrangement of 1,5-hexadiene; (b) oxy-Cope rearrangement; (c) divinylcyclopropane rearrangement; (d) degenerate rearrangements of bullvalene.



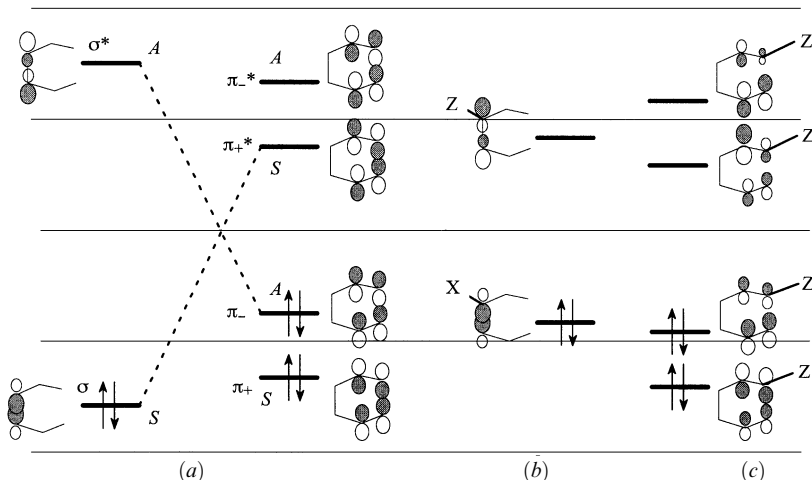


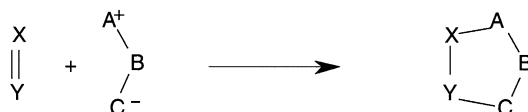
**Figure 12.7.** Orbital interactions in the Cope rearrangement: (a) symmetry-allowed interactions of the  $\sigma$  and  $\pi$  orbitals; (b) effect of X: (or "C") and Z (or "C") substituents in the 3-position; (c) effect of Z substituents at the 1-position.

the  $\sigma$  bonding orbital into  $\pi_+^*$  or from  $\pi_-$  into  $\sigma^*$  (dashed lines). The effect of a Z-type substituent at the 3-position (Figure 12.7b) is to lower the energy of the  $\sigma^*$  orbital, thereby increasing the interaction with the  $\pi_-$  orbital and facilitating the reaction. After rearrangement the Z substituent would occupy the 1-position of the resulting 1,5 diene (Figure 12.7c). While the LUMO energy is lowered by the Z substituent, the concomitant polarization of the adjacent  $\pi^*$  orbital and energy separation of the two  $\pi^*$  orbitals act to reduce the bonding interaction (positive overlap) between the two  $\pi^*$  orbitals. These factors, together with the energy lowering of one of the  $\pi$  bonding orbitals, combine to shift the equilibrium of the Cope rearrangement so as to leave the Z substituent in the 1-position. The effect of an X-type substituent in the 3-position is also shown in Figure 12.7b. The raised  $\sigma$  bonding orbital also serves to facilitate the reaction, placing the X: substituent in the 1-position. The effect of the X: substituent in this position (not shown) is the inverse of that of the Z substituent, but the result is the same; the equilibrium is shifted in this direction. The oxy-Cope rearrangement shown in Figure 12.6b is an example.

The  $\sigma$  bonding orbital may also be raised by incorporation into a 3- or 4-membered ring. The divinylcyclopropane to cyclohepta-1,4-diene (Figure 12.6c) is an example, as is the rapid degenerate rearrangement of bullvalene (Figure 12.6d) and related compounds.

## 1,3-DIPOLAR CYCLOADDITION REACTIONS

A general 1,3-dipolar cycloaddition reaction is shown:

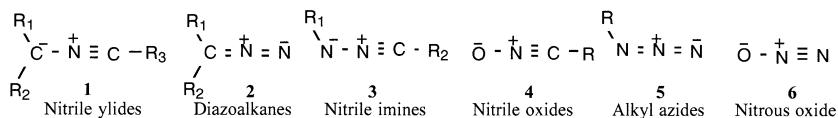


The "dipole" is a triad of atoms which has a  $\pi$  system of four electrons and for which a dipolar resonance form provides an important component of its bonding description. The requirements have also been described as "atom A must have a sextet of outer electrons and C has an octet with at least one unshared pair" ([119], p. 743). The substrate is an olefin and an alkyne or a carbonyl. The reaction therefore is of  $\pi 4 + \pi 2$  type like the related Diels–Alder reaction and has proved to be very useful synthetically for the construction of 5-membered ring heterocycles [268, 269]. Evidence suggests the reaction is concerted and regioselective. "Dipoles" fall into two general categories [119]:

1. *Sixteen-Electron*. Those for which the dipolar canonical form has a double bond on the sextet atom and the other resonance structure has a triple bond. Examples are azides ( $R-N_3$ ), diazoalkanes ( $R_2C=N=N$ ), and nitriloxides ( $R-C\equiv N-O$ ). These have also been labeled as "propargyl/allenyl anion type" [270].
2. *Eighteen-Electron*. Those in which the dipolar canonical form has a single bond on the sextet atom and the other forms a double bond. Examples are ketocarbenes [ $R-C:C(O)R$ ], azoxy compounds [ $R-N=N(O)R$ ], and nitrones [ $R_2C=N(O)R$ ]. These have also been labeled as "allyl anion type" [270].

If all three atoms of the triad belong to the first row, a total of 18 different uncharged species, 6 of the 16-electron kind and 12 of the 18-electron kind, are possible.

The reactivity and regioselectivity of 1,3-dipolar cycloadditions have been discussed in terms of the frontier orbitals [271]. Most of the features may be understood on the basis of simple Hückel MO theory. The HOMO and LUMO  $\pi$  orbitals and  $\pi$  orbital energies for all 18 combinations of the parent dipoles are shown in Figure 12.8. The frontier orbitals of many of the 1,3-dipoles have previously been derived by CNDO/2 and extended Hückel theory [272]. The first six structures, all of 16-electron type, are shown in greater detail:



The SHMO parameters for the dicoordinated C atom of **1**, **3**, and **4** and the mono-coordinated N atom of **2**, **5**, and **6** were derived by the addition of  $0.25 |\beta|$  to the normal Coulomb integrals ( $\alpha$ 's) of the tricoordinated C and dicoordinated N atoms, respectively, as discussed in Chapter 7. It is apparent that each of the first six parent or alkyl substituted dipoles has a very high LUMO and so will not function in the first instance as an electrophile. All have quite a high HOMO which decreases rapidly across the series **1**–**6**. The nucleophilicity is predicted to be relatively high for the first stable dipole, **2**, and lower for the others, **4**, **5**, and **6**. In fact,  $N_2O$  has been shown to react with "C"-substituted and X-substituted olefins but does not react with Z-substituted olefins [273]. The orbital energies of  $N_2O$  appear to be seriously overestimated in SHMO theory, perhaps because no account is taken of substitution by strongly electronegative groups. The experimental ionization potential of  $N_2O$  is quite high, 12.9 eV [274]. For the rest of these dipoles, a good dipolarophile is analogous to a good dienophile in the normal Diels–Alder reaction, in other words, a Z-substituted olefin.

The HOMO of none of the first six parent dipoles is strongly polarized. Little regioselectivity is expected due to the primary interaction, HOMO(dipole)–LUMO(dipo-

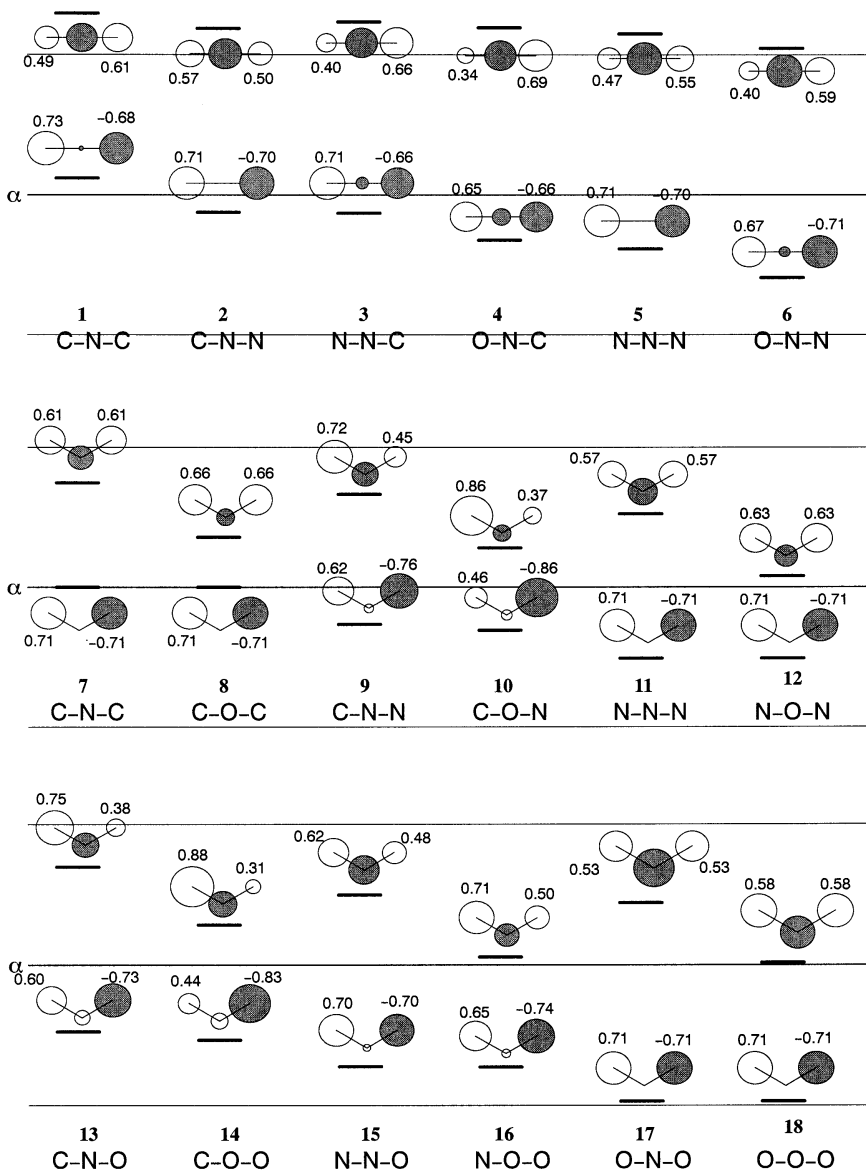
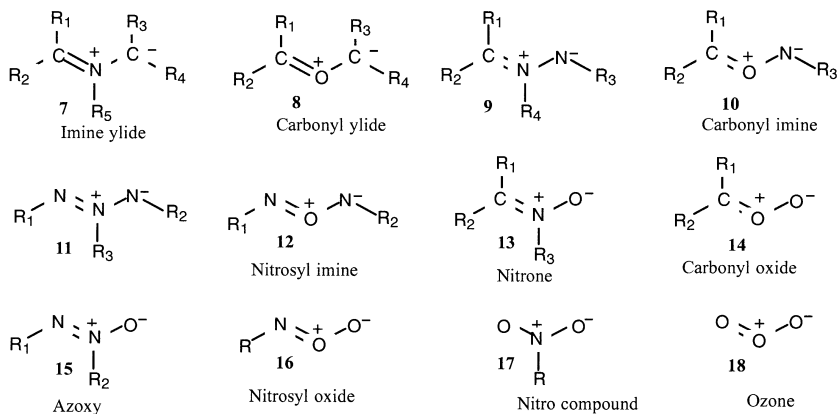


Figure 12.8. SHMO orbitals and orbital energies of the 18 first-row "1,3-dipoles."

larophile). For dipoles 4–6, the LUMO is relatively strongly polarized, but it should not be expected that significant regioselectivity be observed due to the secondary interaction, LUMO(dipole)–HOMO(dipolarophile), since the HOMOs of good dipolarophiles for these dipoles are not strongly polarized themselves. While the HOMO orbitals of the parent dipoles are not strongly polarized, this will probably not be the case for substituted dipoles. Substituents in the terminal positions will perturb the  $\pi$  system in the

same direction as already discussed in Chapter 6 in connection with olefin reactivity. Substituents of the X: and "C" type will raise the HOMO further and polarize it away from the substituent. Substituents of the Z and "C" type will lower the LUMO and also polarize it away from the substituent. Substitution at the middle position is not possible for neutral dipoles of the 16-electron type.

The remaining 12 dipoles, which are of the 18-electron type, are shown explicitly:



Imine ylides **7** and carbonyl ylides **8** are not stable but may be generated in situ by pyrolysis of suitably substituted aziridines and oxiranes. The energy of the HOMO, and therefore the nucleophilicity of the parent 18-electron dipoles, decreases from very high to very low across the series **7–18**. In the same series, the electrophilicity increases from moderate to high, being consistently higher when the central atom is oxygen.

The ozonolysis of olefins may be analyzed as a sequence of two 1,3-dipolar cycloadditions; initial electrophilic attack by ozone **18** to form the first intermediate, which decomposes into a carbonyl compound and a carbonyl oxide **14**; followed by nucleophilic 1,3-dipolar addition of the carbonyl ylide **14** to the ketone, yielding the molozonide.

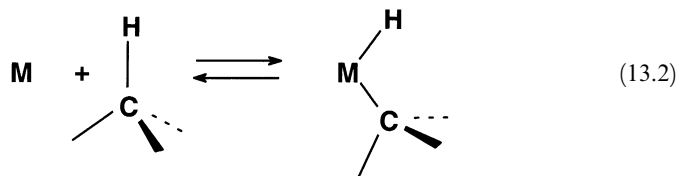
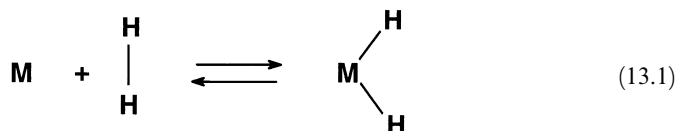
## CHAPTER 13

---

# ORGANOMETALLIC COMPOUNDS

---

The variety of bonding in organometallic compounds is enormous. We focus fairly narrowly here on the types of bonding found between transition metals and carbon and hydrogen atoms and on the interactions between metals and  $\sigma$  and  $\pi$  bonds between C atoms and C and H atoms. In particular, we seek to understand in some detail the process known as “oxidative addition,” as shown in reactions (13.1) and (13.2).



### TRANSITION METALS

The chart in Figure 13.1 provides a handy reference for the electron count in the transition metals in their M(0) configurations. Occupancy occurs in the  $n d$  and  $n + 1 s$  orbitals. The  $n + 1 p$  orbitals are also counted as part of the valence level and are used in hybridization of the metal center by mixing with the  $n d$  and  $n + 1 s$  orbitals, giving a total valence shell capacity of 18 electrons.

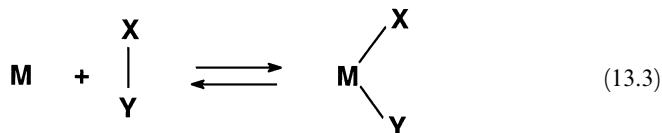
Number of Valence Electrons	3	4	5	6	7	8	9	10	11	12
Row 1	21 Sc	22 Ti	23 V	24 Cr	25 Mn	26 Fe	27 Co	28 Ni	29 Cu	30 Zn
Row 2	39 Y	40 Zr	41 Nb	42 Mo	43 Tc	44 Ru	45 Rh	46 Pd	47 Ag	48 Cd
Row 3	57 La	72 Hf	73 Ta	74 W	75 Re	76 Os	77 Ir	78 Pt	79 Au	80 Hg

Figure 13.1. Number of valence electrons in the neutral transition metals.

## LIGANDS IN TRANSITION METAL COMPLEXES

For the purpose of assigning formal oxidation numbers, the established convention is to regard all ligands on the metal as  $2e$  donors, even if this is unrealistic, as in the case of H and  $\text{CH}_3$  (or alkyl). Two-electron  $\sigma$  donors come in two flavors, negatively charged ( $\text{X}^-$ ) and neutral ( $\text{L}$ ). The distinction is important since neutral complexes of the type  $\text{ML}_n\text{X}_m$  ( $m \neq 0$ ) will have the metal in a *formal oxidation state*,  $+m$ . Much more so than in main group chemistry, the formal oxidation state of the metal is a useful measure of the energy of the remaining valence orbitals, which we shall see are normally polarized toward the metal center. The  $\text{X}^-$  ligands are  $\text{H}^-$ ,  $\text{CH}_3^-$ ,  $\text{CN}^-$ ,  $\text{Cl}^-$ ,  $\text{Br}^-$ ,  $\text{I}^-$ , and so on. The  $\text{L}$  ligands include  $\text{CO}$ ,  $\text{PPh}_3$ ,  $\text{NH}_3$ ,  $\text{H}_2\text{O}$ , and so on.

The addition reaction (13.3) of a  $\sigma$ -bonded pair of groups,  $\text{X}-\text{Y}$ , forming two  $\sigma$  bonds to the metal is, by definition, an *oxidative* addition since the bonding electrons are assigned to the ligands and the formal oxidation state of the metal increases by 2:



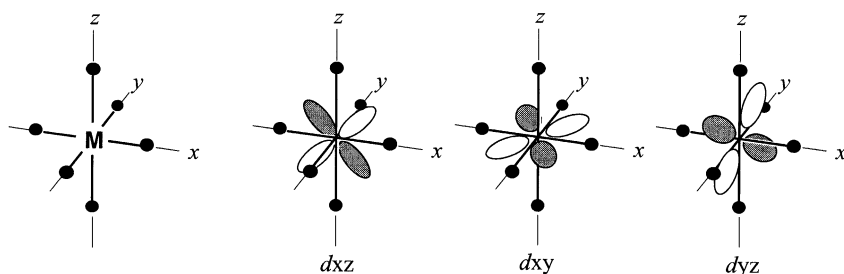
The reverse reaction is *reductive elimination*. No mechanism is implied in reaction (13.3). The addition may be stepwise, radical, electrophilic, or nucleophilic or concerted. Oxidative additions of  $\text{H}-\text{H}$  [reaction (13.1)] or  $\text{H}-\text{R}$  [reaction (13.2)] tend to be concerted.

A further distinction must be made between ligands of both types, namely the ability to receive electrons by *pi* back donation from the metal. This ability has a number of important consequences, beside the obvious one of increased thermodynamic stability of the bond. The energy of the nonbonded valence orbitals, chiefly of the  $d_{xy}$ ,  $d_{xz}$ , or  $d_{yz}$  type, is lowered by the in-phase interaction.

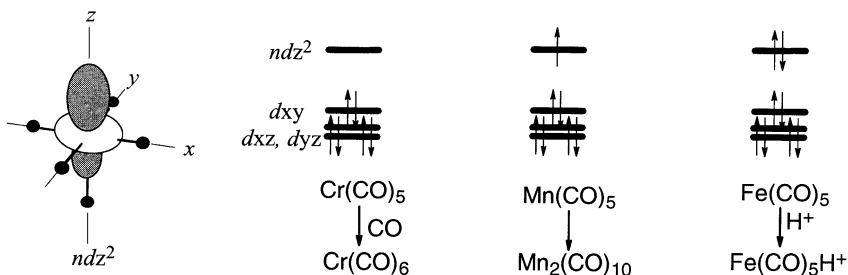
## ORBITALS IN TRANSITION METAL BONDING

The bonding in transition metal complexes has been elucidated in some detail by Albright et al. [58]. The reader is directed to that source for a thorough development

using principles similar to those of the present work. With five  $d$  orbitals as well as a set of  $s$  and  $p$  orbitals in the valence shell, a metal can accommodate up to 18 electrons in its valence shell. Multiple and complex coordination patterns are found, the most common being octahedral coordination of six ligands. It can readily be shown on the basis of symmetry [58] that this arrangement of substituents permits the formation of six  $\sigma$  bonds, accounting for 12 of the 18 electrons for which there is room in the valence shell. These six  $\sigma$  bonds and the corresponding  $\sigma^*$  orbitals are considered to be removed from the frontier orbital region in the same way as the main group  $\sigma$  and  $\sigma^*$  orbitals are (Chapter 3). Three of the  $d$  orbitals are not of the correct symmetry to participate in  $\sigma$  bonding (in an octahedral environment) and, in the absence of suitably arranged  $p$  orbitals on the ligands, remain as nonbonding orbitals accommodating the remaining six electrons. Although the metal in such a bonding situation has three pairs of nonbonded electrons and could potentially function as a Lewis base, the octahedral packing of ligands effectively hinders access by Lewis acids, and a thermodynamically and chemically stable structure ensues.



If a ligand is removed from the octahedral arrangement, say from the  $+z$  position, the orbital which remains at the metal end of the bond is essentially the  $dz^2$  orbital polarized by  $s$ ,  $p$  mixing toward the site of the missing ligand. Such a hybrid orbital is entirely analogous to the  $sp^n$  hybrid orbital that remains when a substituent is removed from a tetracoordinated carbon atom. It is essentially nonbonding and higher in energy than the preexisting nonbonding orbitals ( $dxy$ ,  $dxz$ , and  $dyz$ ). Such a coordinatively unsaturated complex may function as a powerful electron donor or acceptor in the  $\sigma$  sense, depending on the occupancy of the orbital. Thus chromium pentacarbonyl is Lewis acidic and adds a sixth two-electron  $\sigma$ -donating ligand:



Manganese pentacarbonyl is a free radical and spontaneously dimerizes to dimanganese decacarbonyl. Iron pentacarbonyl is a weak Lewis base and can be protonated by sulfuric acid, forming a metal–hydrogen bond. We will make extensive use of the isolobal

analogy expounded by Hoffmann and co-workers [275] and direct our attention directly to the specific application of transition metal-based systems as reagents for organic transformations, some of which have no direct correspondence in the “main group” chemistry we have examined so far.

## ORBITAL ENERGIES

The orbital interaction theoretical approach requires an appreciation of the effective overlap of the interacting orbitals, their relative energies, and the amount of interaction which ensues. We here attempt to place the transition metal orbitals on the same energy scale as was found useful for the first- and second-row elements.

**Neutral Metals (0 Oxidation State).** The orbital energies of the transition row atoms and the atoms of adjacent elements could be deduced in principle from experimental ionization potentials and spectroscopic information [276]. However, analysis of the experimental data is complicated by the large number of spin configurations available to most of the elements. A more convenient source of orbital energies, and one more in keeping with the development of the method, is the tabulation by Clementi and Roetti [277] of the results of Hartree–Fock (HF) calculations of the neutral atoms in various spin configurations. The HF energies of the valence orbitals of the first- and second-row transition elements and of neighboring atoms are plotted as a function of atomic number in Figure 13.2. The  $2p$  orbital energies of B, C, N, O, and F are also plotted, and these form the basis for the orbital energies in terms of the  $|\beta|$  scale shown at the right. In the case of the first-row transition elements, Sc–Zn, the  $3d$  orbital energies shown in Figure 13.2 correspond to atomic configurations  $s^2d^n$ . The  $s^1d^{n+1}$  configurations (not shown) are higher by from 0.1 hartree (Sc) to 0.25 hartree (Zn) due to the excess coulombic repulsion which ensues upon increasing the electron population of the  $d$  orbital by one electron. The Coulombic repulsion within the  $4s$  orbital is offset by increased penetration to the nucleus and the energy of the  $4s$  orbital between the  $s^2d^n$  and  $s^1d^{n+1}$  configurations changes by only about one-tenth of the  $3d$  orbital change. The average value is shown in Figure 13.2. The  $d$  orbital energies shown should be representative of the energies of the lowest nonbonding orbitals in the metal complexes shown later in Figures 13.4–13.6. It is clear that while the early transition elements, Sc and Ti, have  $3d$  orbital energies which are higher than the  $2p$  orbital energy of C, the  $3d$  orbital energies fall sharply across the row, with the later energies comparable to the  $2p$  orbital energies of O and F.

The  $4d$  orbital energies of the  $s^2d^n$  configuration of the second-row transition metals, Y–Cd, are also plotted in Figure 13.2. The valence configurations  $s^0d^{n+2}$  and  $s^1d^{n+1}$  (not shown) are higher by 0.07 hartree (Y) to 0.16 hartree (Cd). The smaller values compared to the  $3d$  orbital case may be due to the intrinsically larger  $4d$  orbitals. The  $4d$  orbital energies are a little higher and parallel to the corresponding  $3d$  energies. The  $5d$  orbital energies of the third-row transition metals were not calculated. Their position shown in Figure 13.2 is based on extrapolation. In each of the valence orbital sets shown in the preceding figures, the highest was essentially the unoccupied  $n + 1 p$  orbital, the energies of which were also not determined by the calculations. Their position, shown in Figure 13.2 near  $\alpha + 1.5|\beta|$ , is anticipated on the basis that the occupied  $p$  orbitals of Ga and In are similar and start at  $\alpha + 1|\beta|$ .



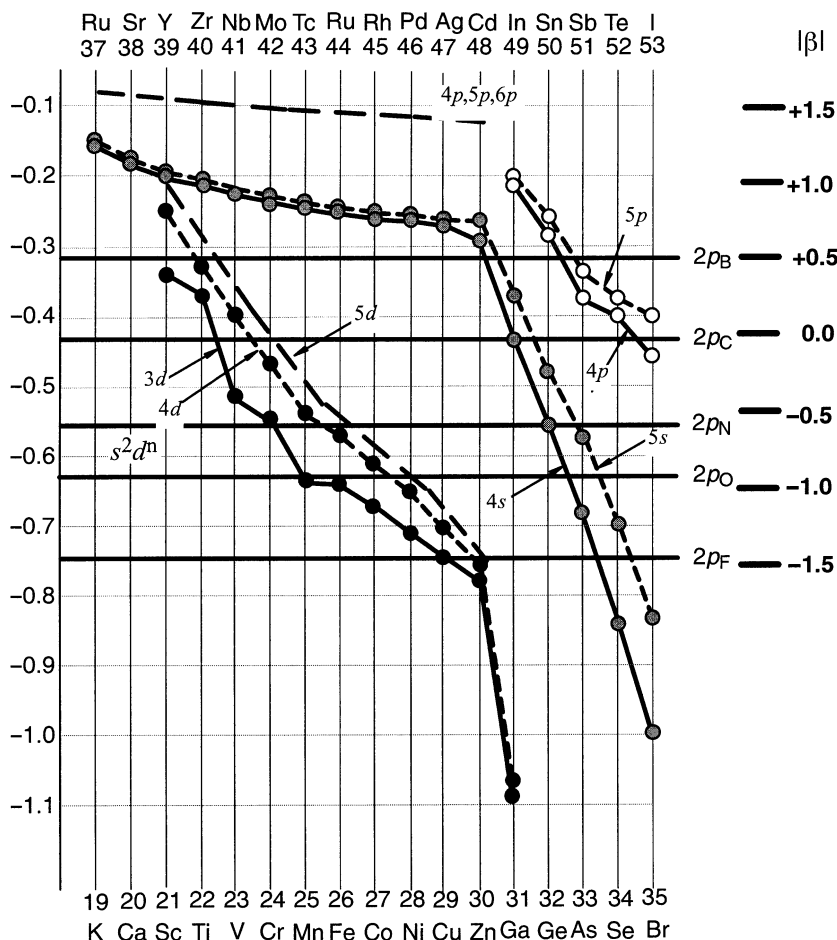


**Figure 13.2.** Occupied valence orbital energies of the first-row (-----) and second-row (----) transition metals and adjacent elements (circles): black,  $d$  orbitals; gray,  $s$  orbitals; white,  $p$  orbitals. The effect on  $d$  orbital energies of three electronic configurations of the metals is shown. The vertical scale on the left is in hartrees. The scale at right is in units of  $|\beta|$  relative to  $\alpha_C$ .

## VALENCE ORBITALS OF REACTIVE METAL COMPLEXES

As the above discussion shows, we will adopt the simple view that an octahedrally hexacoordinated metal complex,  $ML_6$ , is coordinatively saturated, just as is a tetracoordinated carbon atom. Metal complexes with fewer than six ligands will be treated on the same footing as organic reactive intermediates. The distinction we are making is that direct involvement of the metal center in a reactive process (bond making or breaking) is easy only at coordinatively unsaturated metal centers, just as it is at carbon. Of course, just as at saturated carbon, ligand substitution by association or dissociation can take place, and the presence of the center (C or M) with its array of substituents can influence

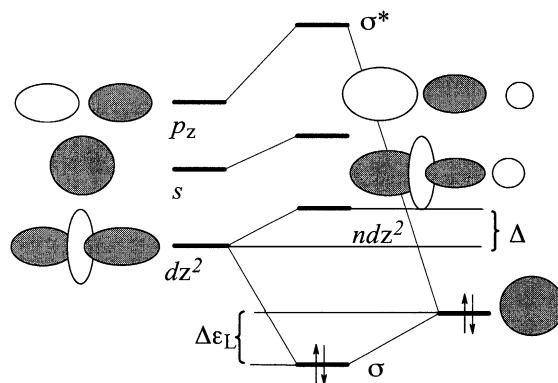


**Figure 13.3.** Four-orbital interaction forms a  $\sigma$  bond to the metal (mostly ligand) and removes one of the metal orbitals from the valence set. The remaining metal orbitals are shown.

the chemistry of the “ligands” themselves in hexacoordinated metal complexes. We begin in the same way as in the case of main group fragments, by building up the library of fragment valence orbitals, beginning with a fragment in which the metal is bound to three groups,  $ML_3$ , and working our way up to pentacoordination,  $ML_5$ . A discussion of mono- and dicoordinated complexes may be found in standard sources [58, 275, 278]. We emphasize here, as earlier, that bonding means  $\sigma$  bonding only. If, after we have accommodated all ligands by  $\sigma$  bonds, there are valence orbitals and electrons left over, multiple bonding can be considered. The bare (0-coordinated) metal has nine valence orbitals, in ascending order, five  $d$ ’s, one  $s$ , and three  $p$ ’s. Each  $\sigma$  bond formed removes one of the metal’s valence orbitals. Since a potential ligand always has the opportunity (by symmetry) to interact with one of the  $d$  orbitals, the  $s$  orbital, and one of the  $p$  orbitals, a complex mixing pattern arises from the hybridization of the three. By virtue of relative electronegativities, the usual situation (see below) is that all of the metal orbitals lie to higher energy than the ligand, even if it is a hydrogen or carbon atom. The consequences of this four-orbital interaction are shown in Figure 13.3. As in the case of two- and three-orbital interactions, the orbitals of the four-orbital interaction move apart. The lowest orbital is the  $\sigma$  bond to the ligand. If the ligand is highly electronegative, this orbital is highly polarized toward the ligand. Since the ligand also introduced an orbital to the set, this does not count. The highest, most antibonding orbital may be considered to be the  $\sigma^*$  orbital. It is metal centered and counts as the one removed from the valence set. The middle two orbitals, both  $spd$  hybrids, are left in the valence set. Both are mostly nonbonding. The upper is chiefly the  $p_z$  orbital. The lower is chiefly the  $dz^2$  orbital polarized away from the coordinated atom. The same principle, namely that the middle two orbitals are essentially metal centered nonbonding and polarized away from the  $\sigma$ -bonded substituent, applies to metal centers with multiple  $\sigma$  bonds.

**Intrinsic Interaction Matrix Element,  $h_{AB}$ , Between  $d$  Orbitals and Orbitals of C and H.** The quantities  $\Delta$ , the separation of the weakly antibonding  $d$  orbital from the nonbonded  $d$  orbitals (Figure 13.3), and  $\Delta\epsilon_L$ , the amount of lowering of the bonding orbital, will be of special interest. Here,  $\Delta$  is not directly analogous to  $\Delta\epsilon_U$  of earlier orbital interaction diagrams because of the mixing with higher energy orbitals, but its magnitude is governed by the same principles, namely the energy separation of the

ligand orbital from the metal  $d$  orbitals and the intrinsic interaction matrix element, which is approximately proportional to the overlap of the two orbitals and the average of their energies [e.g., equation (3.44)]. Judging from Figure 13.2 and parametrizations of extended Hückel theory [279], the energies of the  $d$  orbitals are similar to the  $2p$  orbital energies of C, N, and O. Hence the principal factor governing the magnitude of  $h_{AB}$ , and therefore  $\Delta_{\varepsilon_L}$  and  $\Delta$ , will be the overlap. Overlap of orbitals decreases with increasing numbers of nodes and mismatch of sizes. For both reasons, both  $\sigma$ - and  $\pi$ -type overlap between  $d$  orbitals and the orbitals of the first-row elements will be smaller than equivalent overlaps between the first-row elements themselves. As a consequence, one expects smaller  $\Delta_{\varepsilon_L}$  and  $\Delta$  and weaker bond dissociation energies.

In the octahedral environment,  $\Delta$  will be related to  $\Delta_O$ , the spectroscopically derived octahedral crystal field-splitting parameter [280]. One can gain some insight into the variation of  $h_{AB}$  as a function of ligand type and metal by noting how these factors affect  $\Delta_O$ . Ligands may be ranked according to their effect on  $\Delta_O$ . Thus  $\Delta_O$  increases in the series:  $I^- < Br^- < Cl^- < F^- < OH^- < H_2O < NH_3 < en < PPh_3 < CN^- < CO$  [280]. The halogens have the weakest effect on  $\Delta_O$  while CO has the greatest effect, probably because the “nonbonded” orbitals are lowered by in-phase interaction with the  $\pi_{CO}^*$ . Another effect of ligands, which is also attributed to overlap, namely the *trans effect*, may be a measure of  $\Delta$  (and of  $h_{AB}$ ) (Figure 13.3). In square planar complexes, the *trans effect* of a  $\sigma$ -bonding ligand,  $L_1$ , measures the rate enhancement for ligand substitution of another ligand,  $L_2$ , when  $L_1$  is in the *trans* position in the complex. Presumably,  $L_1$  raises the energy of  $n dz^2$  (Figure 13.3), thereby decreasing its bonding to  $L_2$ . Sigma-bonding ligands, in order of increasing *trans effect* in square planar complexes of Pt(II), are  $OH^- < NH_3 < Cl^- < Br^- < CN^-, CO, CH_3^- < I^- < PR_3 < H^-$  [280]. We note particularly that  $H^-$  has the largest *trans effect* and that  $CH_3^-$  (and other alkyl groups) is also high on the list. Comparing the  $\Delta_O$  series with the *trans effect* series reveals that they differ principally in the *softness* or *nucleophilicity* property which reverses the order of the halogens and of amines and phosphines.

**Effect of Formal Oxidation State.** Since the valence orbitals are largely localized to the metal, their energies will be sensitive to the net charge of the metal, of which the formal oxidation number will be a good guide provided the ligands are poor  $\sigma$  donors, like the halogens or oxygen. It is suggested here that for the purpose of assigning nonbonding  $d$  orbital energies, a metal with formal charge  $+m$  be treated as equivalent to the neutral metal with  $m$  higher atomic number; that is, the  $d$  orbital energies of Pd(II) will be those of Cd(0) in Figure 13.2. Thus the nonbonding  $d$  orbitals drop sharply with increasing oxidation. However, the antibonding hybrid  $d$  orbitals drop less since  $\Delta$  increases (see below). A good  $\sigma$  donor, like H or alkyl, will have a maximum effect in supporting the antibonding  $d$  orbitals, especially if it is in the *trans* position.

In addition to the effects of ligands,  $\Delta_O$  (and  $\Delta$ ) depends on the type of metal and its oxidation state [280]:

$\Delta_O$  increases with increasing formal oxidation state

$\Delta_O$  increases down a group

The dependence on formal oxidation state can be attributed to electrostatic lowering of the metal  $d$  orbitals thereby narrowing the gap with ligand orbitals. The effect of principal quantum number may be due to better overlap of the larger  $4d$  and  $5d$  orbitals with ligand orbitals, compared to the more compact  $3d$  orbitals. Thus  $\Delta_O$  increases in the

series  $\text{Mn}^{2+} < \text{Ni}^{2+} < \text{Co}^{2+} < \text{Fe}^{2+} < \text{V}^{2+} < \text{Fe}^{3+} < \text{Co}^{3+} < \text{Mn}^{4+} < \text{Mo}^{3+} < \text{Rh}^{3+} < \text{Ru}^{3+} < \text{Pd}^{4+} < \text{Ir}^{3+} < \text{Pt}^{2+}$  [280]. We will return to these points below as we discuss the valence orbitals of metal fragments which are 3-, 4-, and 5-coordinated.

## SIX VALENCE ORBITALS OF TRICOORDINATED METAL

Three distinct geometric configurations need to be considered for tricoordination. Only two, a trigonal planar structure and a pyramidal configuration of  $C_{3v}$  symmetry, were available to main group tricoordinated systems. The addition of  $d$  orbitals into the valence shell introduces the third possibility, a T-shaped structure with local  $C_{2v}$  symmetry. The six valence orbitals of each of the structures in their individual standard orientations are shown in Figure 13.4. In the case of the T-structure, the most convenient orientation has the fragment in the  $xy$  plane with the symmetry axis aligned with the  $x$  axis. The valence orbitals, in ascending order, are  $dxz = b_1$ ,  $dyz = a_2$ ,  $dxy = b_2$ ,  $nz^2 = a_1$ ,  $nx^2 - y^2 = a_1$ , and  $pz = b_1$ .

The standard orientation of the trigonal planar structure has the molecule in the  $xy$  plane and the  $C_3$  axis coinciding with the  $z$  axis. It is derived from the T-structure by movement of the ligands away from the  $y$  axis. The resulting valence orbitals and correspondence of the energy levels is shown in Figure 13.4. Two of the T-shaped fragment orbitals are significantly affected by the change in geometry, namely the  $dxy = b_2$  orbital, which suffers a strongly repulsive interaction and rises in energy, and the  $nx^2 - y^2 = a_1$  orbital, which obtains a relief in repulsion and moves to lower energy. The result is that the quasidegenerate set of three lowest orbitals is broken apart, leaving only two orbitals at low energy. The valence orbitals, in ascending order, are  $(dxz, dyz) = e''$ ,  $nz^2 = a'_2$ ,  $(nxy, nx^2 - y^2) = e'$ , and  $pz = a'_2$ .

Movement of all three ligands of the  $D_{3h}$  structure symmetrically out of the plane leads to the pyramidal  $C_{3v}$  structure. All valence orbitals are affected by the geometry change. The  $(dxz, dyz) = e''$  set can interact with the ligands and are raised in energy. Repulsion is reduced significantly in  $nz^2 = a'_1$  and somewhat in the  $(nxy, nx^2 - y^2) = e'$  set, and these move to lower energy in a corresponding fashion. The  $npz = a'_2$  orbital rises. In ascending order, the six valence orbitals of the trigonal pyramidal structure are  $(dxz, dyz) = e$ ,  $nz^2 = a_1$ ,  $(nxy, nx^2 - y^2) = e$ , and  $npz = a_1$ .

A tricoordinated metal is highly unsaturated. Relatively stable fragments occur as follows:  $16e$  ( $s^2d^8$ ), structure  $C_{3v}$ , e.g.,  $\text{Ni}(\text{C}_2\text{H}_4)_3$ ;  $12e$  ( $s^2d^4$ ), structure  $C_{2v}$ , e.g.,  $\text{HFe}(\text{CO})\text{CH}_3$ ; and  $10e$  ( $s^2d^2$ ), structure  $D_{3h}$ , e.g.,  $\text{Ti}(\text{NH}_3)_3$ . The  $10e$  and  $12e$  structures occur only in the case of the early transition metals, which have the highest energy valence orbitals. By the same token, late transition metals can only support higher valence occupancies if they are in high formal oxidation states since the high central positive charge lowers the energy of the higher valence orbitals.

## FIVE VALENCE ORBITALS OF TETRACOORDINATED METAL

Three distinct structural types are available for a tetraordinated fragment: a square planar structure of  $D_{4h}$  symmetry, a nonplanar square pyramid with  $C_{4v}$  symmetry, a nonplanar structure with  $C_{2v}$  symmetry (which would result from the removal of two cis ligands from an octahedral  $\text{ML}_6$ ), and the tetrahedral structure of symmetry  $T_d$ . These are shown in Figure 13.5 in the standard orientation. The orbitals of the  $D_{4h}$  structure

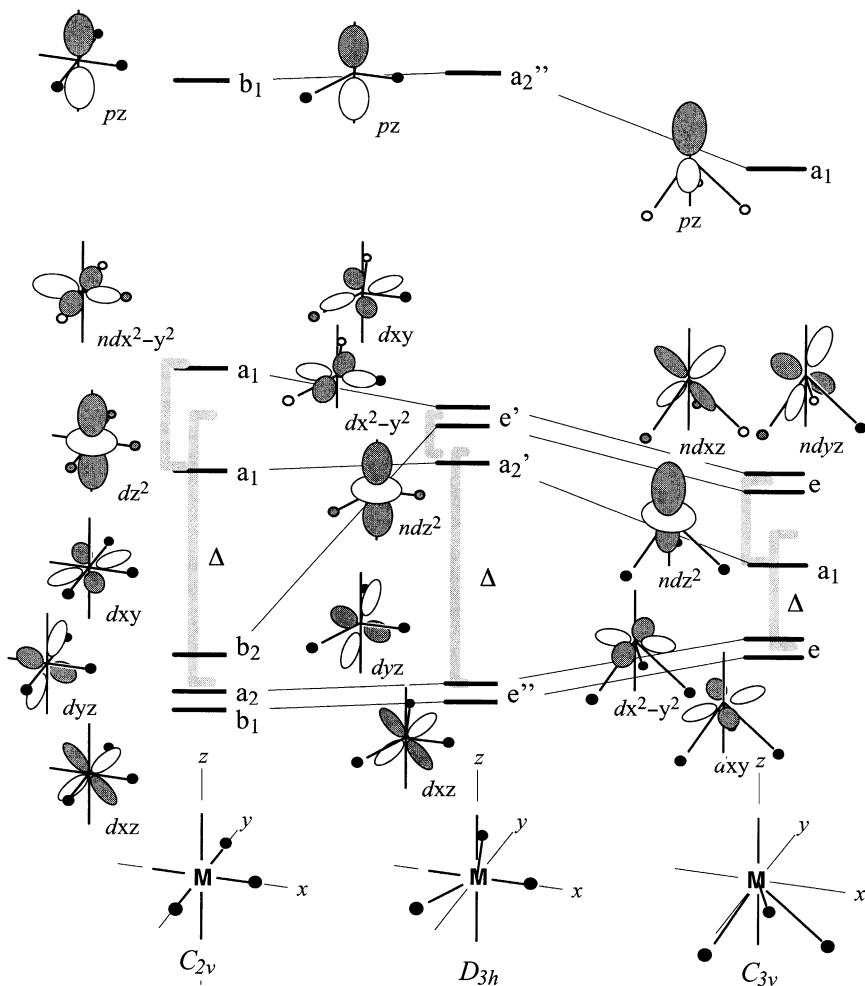


**Figure 13.4.** Valence orbitals of a tricoordinated metal;  $\Delta$  (longer gray bracket) is analogous to  $\Delta\varepsilon_U$ . The splitting of the upper levels (shorter gray bracket) is a measure of the trans effect.

are readily derived from symmetry considerations [58]. In ascending order, they are  $(dxz, dyz) = e_g$ ,  $dxy = b_{2g}$ ,  $ndz^2 = a_{1g}$ , and  $pz = b_{1g}$ .

Movement of all four ligands symmetrically to one side of the plane yields the square pyramidal  $C_{4v}$  structure. The highest two orbitals of the  $D_{4h}$  structure,  $pz = b_{1g}$  and  $ndz^2 = a_{1g}$ , are substantially stabilized, the former by in-phase mixing of the ligand orbitals and the latter by relief of repulsion with the ligand orbitals. In ascending order, the five valence orbitals of the  $C_{4v}$  structure are  $dxy = a_2$ ,  $(nxz, nyz) = e$ ;  $nz^2 = a_1$ , and  $npz = a_1$ .

Movement of the two opposite ligands of the  $D_{4h}$  structure out of the  $xy$  plane yields the tetracoordinated  $C_{2v}$  fragment. The  $b_{1g}$  and  $a_{1g}$  orbitals are again stabilized and one of the members of the  $e_g$  set is destabilized. The position of the orbitals shown is that

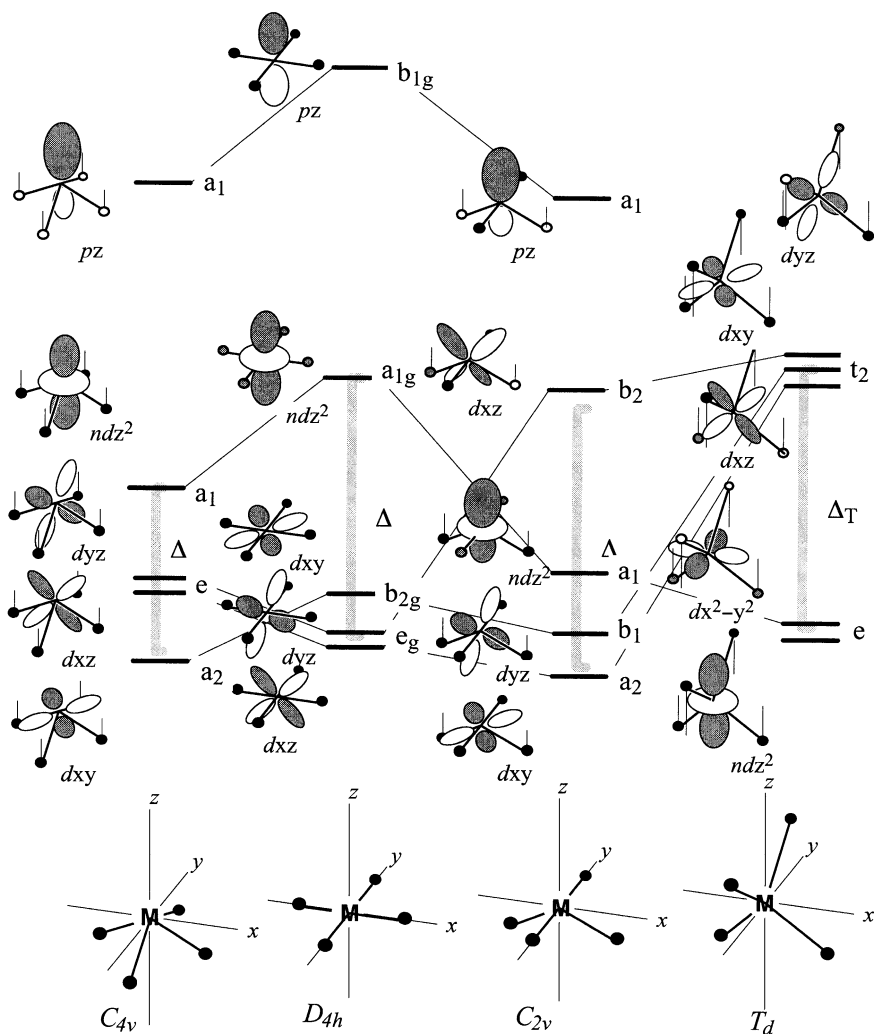


**Figure 13.5.** Valence orbitals of a tetracoordinated metal;  $\Delta$  (long gray bracket) is analogous to  $\Delta\epsilon_U$ .

expected if the out-of-plane ligand bond angle is reduced to  $90^\circ$ . The orbitals in order of increasing energy are  $d_{xy} = a_2$ ,  $d_{yz} = b_1$ ,  $nz^2 = a_1$ ,  $nxz = b_2$ , and  $npz = a_1$ .

The  $C_{2v}$  structure may be transformed into a tetrahedral structure by movement of the remaining collinear ligands out of the  $xy$  plane in the opposite direction. When the structure has  $T_d$  symmetry or close to it, the bonding pattern shown in Figure 13.5 is obtained. From lower energy to higher, the valence orbitals are  $(dz^2, dx^2 - y^2) = e$  and  $(d_{xy}, dxz, d_{yz}) = t_2$ . Thus the  $d_{yz} = b_1$  orbital of the  $C_{2v}$  structure is severely destabilized upon deformation toward  $T_d$ . A tetracoordinated transition metal is also highly unsaturated. Stable fragments occur as follows:  $18e$  ( $s^2d^6$ ), structure  $T_d$ , e.g.,  $\text{Ni}(\text{CO})_4$ ;  $16e$  ( $s^2d^6$ ), structure  $C_{4v}$  or  $C_{2v}$ , e.g.,  $\text{Fe}(\text{CO})_4$ ;  $14e$  ( $s^2d^4$ ), structure  $C_{4v}$ ,  $D_{4h}$ , or  $C_{2v}$ , e.g.,  $12e$  ( $s^2d^2$ ), structure  $T_d$ , e.g.,  $\text{FeCl}_4$ .

## FOUR VALENCE ORBITALS OF PENTACOORDINATED STRUCTURE

Two distinct structural types may be considered for the pentacoordinated metal complex: a trigonal bipyramid and a structure of  $C_{4v}$  symmetry in which four of the ligands lie in a common plane. If the metal atom also lies in the same plane, then the structure is trivially derivable from the  $ML_6$  structure by removal of a ligand, as already described above. We describe this case and the more general case where the metal and fifth ligand are out of the plane separately. All  $ML_5$  structures in their respective coordinate frames are shown in Figure 13.6. For the “octahedral”  $C_{4v}$  structure, three of the valence orbitals form a nearly degenerate set at low energy. These are  $d_{xy} = b_2$  and  $(d_{xz}, d_{yz}) = e$ . The fourth,  $nz^2 = a_1$ , is well separated from the others because it suffers repulsive interactions with all five ligands.

Movement of the metal and apical ligand out of the plane relieves the repulsive interactions of  $nz^2 = a_1$ , and it is substantially stabilized. At the same time, the degenerate

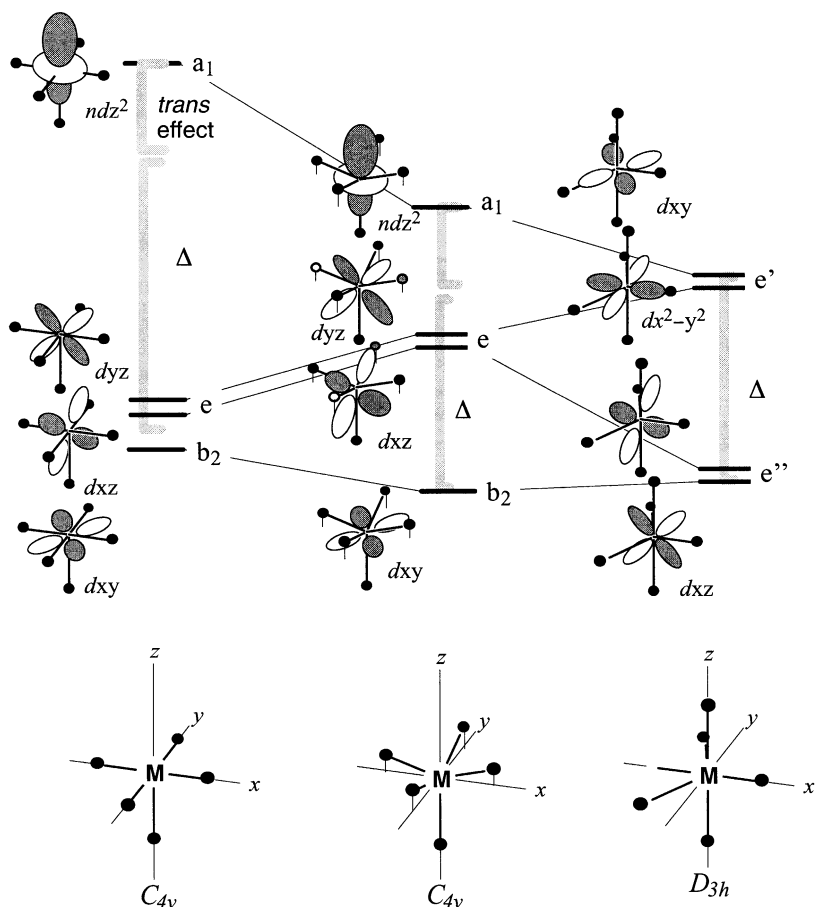


**Figure 13.6.** Valence orbitals of a pentacoordinated metal;  $\Delta$  (longer gray bracket) is analogous to  $\Delta_{\epsilon U}$ . The splitting of the upper levels (shorter gray bracket) is a measure of the trans effect.

pair,  $(dxz, dyz) = e$ , is destabilized and moves to higher energy, approaching the descending  $nz^2 = a_1$  orbital as the out-of-plane deformation increases.

The natural orientation of the  $D_{3h}$  trigonal bipyramidal system requires a reorientation of the coordinate frame relative to that used for the  $C_{4v}$  structures. The four valence orbitals resolve themselves into two degenerate groups (in ascending order)  $(dxz, dyz) = e''$  and  $(dxy, dx^2 - y^2) = e'$ . The correspondence to the orbitals of the  $C_{4v}$  structures is shown in Figure 13.6.

## TRANSITION METALS AND C—H OR H—H SIGMA BONDS

Nonpolar  $\sigma$  bonds such as C—H and H—H are chemically inert to acids and bases under normal circumstances. The primary reason is that the  $\sigma$  bonding orbital is very low in energy and not polarized. Both aspects reduce its ability as a  $\sigma$  or  $\pi$  donor of electrons. As we have seen in Chapter 4, such  $\sigma$  bonds are directly susceptible to attack by only the strongest Lewis acids, such as carbocations. By the same token, the  $\sigma^*$  orbital is very high in energy and also not polarized. Both aspects reduce its ability to act as an electron acceptor. An additional factor which we did not dwell upon in the earlier discussions is that both ends of the C—H or H—H bond are of intermediate electronegativity and so are unable to support a substantial positive or negative charge. Donation of electrons in a two-electron, two-orbital interaction in which the C—C, C—H, or H—H bond acts as a donor or as an acceptor necessarily is accompanied by charge transfer and the accumulation of charge on C or H. Only if it were possible to donate and accept at the same time could the build-up of substantial charge be avoided. This is normally not possible in main group chemistry because there are no stable molecular species which simultaneously are at least moderately strong donors and acceptors. An additional requirement is that the system must be a strong acceptor in the *sigma* sense because the  $\sigma$  bond is a nodeless donor. To be able to react with a  $\sigma$  bond, the agent must be a  $\pi$  donor (because maximum overlap with the  $\sigma^*$  acceptor orbital requires accommodation of the node across the middle of the bond). Transition metals can satisfy the last requirement because an occupied  $dxz$  or  $dyz$  orbital has the nodal characteristics to be a  $\pi$  donor if the  $\sigma$  bond approaches from the  $z$  direction in an edgewise ( $\eta^2$ ) fashion. At the same time, the metal may also satisfy the requirement of being an effective nodeless  $\sigma$  acceptor because advantageous mixing of the  $s$ ,  $pz$ , and  $dz^2$  orbitals can take place.

The last requirement to be met is that the metal  $d$  orbitals are close enough in energy to the C—H and H—H orbitals for effective interaction to take place. This requirement is readily met across most of the first and second transition row series. The energies of the  $d$  orbitals sweep a broad range as the atomic number and formal oxidation state are changed, and the size, shape, and energy may be finely tuned by the appropriate choice of ligands.

## MORE ABOUT C LIGANDS IN TRANSITION METAL COMPLEXES

A tricoordinated carbon center acting as a ligand to a transition metal is a powerful  $\sigma$  donor because of the high energy of its valence ( $sp^n$ ) orbital, and it is not a  $\pi$  acceptor.

A dicoordinated carbon atom bonded to a metal may vary greatly in its  $\pi$  acceptor ability. If the atom is formally bonded by a  $\pi$  bond to another atom, the  $\pi$  acceptor ability ranges from poor to moderate depending upon whether the other atom is C (i.e.,



vinyl), N (i.e., iminyl), or O (i.e., carbonyl). If the dicoordinated carbon atom is not involved in formal  $\pi$  bonding, then it is considered to be a carbene center and its  $\pi$  acceptor ability ranges from moderate to high, depending upon whether its two substituents are themselves good  $\pi$  donors (N or O) or not (alkyl or H).

Similar considerations apply to a monocoordinated carbon atom which functions as a ligand to a transition metal. The carbon atom may have two formal  $\pi$  bonds to its attached atom, as in acetylides, cyanide anion, or carbon monoxide. Such compounds coordinate in a linear fashion and can accept  $\pi$  electrons equally in the two orthogonal planes. The  $\pi$  acceptor ability ranges from poor to moderate. The electrically neutral carbonyl group may formally donate electrons to one metal and accept electrons from another and therefore bridge the two. If the two metals are similar, the CO molecule acting in this fashion is functionally equivalent to a ketone carbonyl group. Acetylides and cyanide cannot function in the same way because neither the carbon atom nor the nitrogen atom are electronegative enough to support the extra nonbonded electron pair and the negative charge. Substitution by an alkyl group on N or a second alkyl or hydrogen on C permits the carbon atoms of these groups to coordinate to two metals as well. The groups are vinylidene and isonitrile, respectively.

## CHELATING LIGANDS

Chelating ligands such as *en* (ethylenediamine), *acac* (acetylacetonate), and alkyl separated phoshines can be regarded as the equivalent number of L: and X: groups. Thus *en* = L<sub>2</sub> and *acac* = LX. The length of the chelating bridge may impose a geometry restriction, however, forcing an interligand bond angle to be less than 90°, for instance.

## ORGANIC $\pi$ -BONDED MOLECULES AS LIGANDS

A simple alkene is just an L:-type ligand, donating 2e in a  $\sigma$  fashion from one face of the  $\pi$  bond. It is also a modest  $\pi$  acceptor through its  $\pi^*$  orbital. Unsaturated molecules with multiple but isolated  $\pi$  bonds, like 1,5-cyclooctadiene, behave as chelating ligands. Conjugated  $\pi$  systems of four or six electrons can donate any number of pairs of electrons up to the maximum. Thus benzene may act as L, L<sub>2</sub>, or L<sub>3</sub> and cyclopentadienyl as X, LX, or L<sub>2</sub>X. If acting as multiple donors, then they necessarily impose geometry restrictions consistent with the dimensions of their  $\sigma$  framework and in this sense behave as chelating ligands. To a much greater extent than is true for simple chelating ligands, however, multiple conjugated  $\pi$  donor ligands can change their donating characteristics in response to the electronic demand of the metal. For instance, a cyclopentadienyl complex in which the cyclopentadiene is acting as a four-electron donor (hapto-3,  $\eta^3$ ) can readily use the cyclopentadienyl ring to occupy a coordination site vacated by the departure of another ligand. The cyclopentadienyl then assumes the role of a six-electron donor (hapto-5,  $\eta^5$ ). The "hapto" number describes phenomenologically the number of (more or less) equivalent short metal-to-ligand distances, but from it can be inferred the number of donated electrons.

## TRANSITION METAL BONDING TO ALKENES: ZEISE'S SALT

Zeise's salt, KPtCl<sub>3</sub>( $\eta^2$ -C<sub>2</sub>H<sub>4</sub>), exemplifies transition metal bonding to unsaturated hydrocarbons. The orbital interaction diagram for the T-shaped metal fragment PtCl<sub>3</sub><sup>-</sup> and

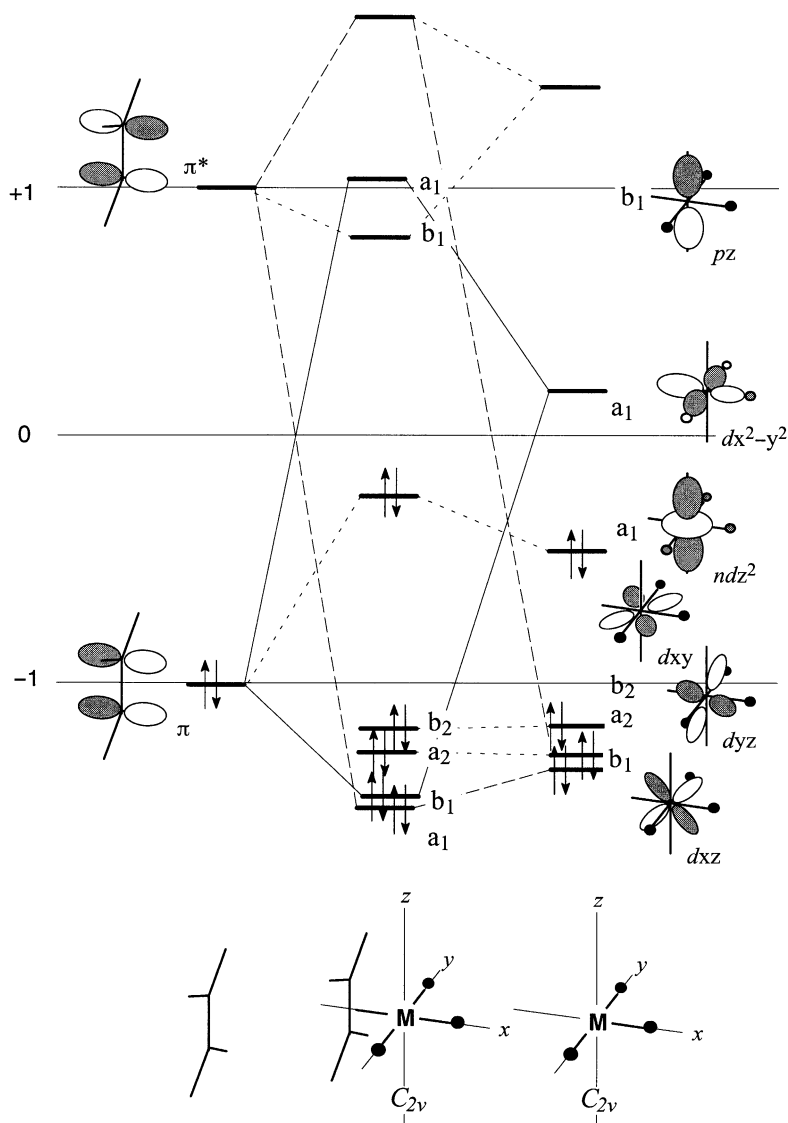


Figure 13.7. Orbital interaction diagram for Zeise's anion,  $[\text{PtCl}_3(\text{CH}_2\text{CH}_2)]^-$ .

ethylene shown in Figure 13.7 describes the bonding. Construction of the interaction diagram requires one to place the metal fragment orbitals and the alkene orbitals on the same scale. We already know that the  $\pi$  and  $\pi^*$  orbitals are placed at  $\alpha - |\beta|$  and  $\alpha + |\beta|$ , respectively. The placement of the metal fragment orbitals is accomplished with reference to Figures 13.4 and 13.2. The Cl ligands are poor  $\sigma$  donors so Pt(II) will be treated as Pd(II) = Cd(0). The energy scale is adjusted to the  $|\beta|$  scale, as recommended in Figure 13.2. The energies of the  $p$  orbitals are not very row dependent. It was recommended above that these be placed at  $\alpha + 1.5|\beta|$ . The nonbonded  $d_{xy}$ ,  $d_{xz}$ , and  $d_{yz}$  orbitals will

fall near  $\alpha - 1.5|\beta|$ . The *relative* vertical spacing of the metal valence orbitals of the T-shaped ( $C_{2v}$ ) fragment is as shown in Figure 13.4. On this basis, the upper of the two  $a_1$  orbitals,  $ndz^2$  and  $dx^2 - y^2$ , is placed near  $\alpha_C$ , the zero of the  $|\beta|$  scale. In  $\text{PtCl}_3^-$ , platinum is in the +2 formal oxidation state and contributes  $8e$ , all of which are assigned to the valence levels. Therefore, the two  $a_1$  levels,  $ndz^2$  and  $dx^2 - y^2$ , are the HOMO and LUMO, respectively. It is clear that the principal attractive interaction, shown by solid lines, is between the HOMO of ethylene and the LUMO of the metal. Optimum overlap between the  $\pi$  orbital and the  $dx^2 - y^2$  occurs if the ethylene is oriented perpendicular to the  $xy$  plane (the plane of the metal complex). This orientation also minimizes the repulsive interaction with the  $ndz^2$  orbital. It is the observed structure of Zeise's salt [281]. Back donation from the occupied  $b_1 = dxz$  orbital of the metal to the  $\pi^*$  of ethylene, shown by the dashed lines in Figure 13.7, is not very important because of the large energy separation of the two orbitals. The C—C distance of the bound ethylene, 1.37 Å [281], is similar to that in free ethylene, 1.34 Å. The structure is best described as a  $\pi$  complex (rather than a metalacyclopropane). These conclusions are essentially the same as reached from DFT calculations [282], although greater significance was attributed to the extent of  $\pi$  back bonding on the basis of B3LYP calculations [283].

We note two features of the bonding picture of Zeise's salt (and similar complexes). First, the LUMO of the complex is predominantly the  $\pi^*$  orbital of ethylene—it is lowered in energy by interaction with the  $pz$  orbital. One might expect reactivity toward nucleophiles. As we shall see in the next sections, intramolecular nucleophilic attack at the alkene carbon atom by hydride or alkyl ligands on the metal is a key step in olefin polymerization. Second, the  $ndz^2$  orbital is raised in energy by interaction with the  $\pi$  orbital of ethylene to quite a high value and is the HOMO—the square planar Pt complex should be quite reactive toward Lewis acids from the direction perpendicular to the plane. In fact, the presence of the low-lying  $pz$  orbital complicates matters since attachment of an electrophile to one face of the square-planar complex lowers the symmetry and permits mixing of the two, resulting in a very much lower empty  $pd$  hybrid and attachment of a nucleophilic sixth ligand and a formal oxidation state of Pt(IV). The pentacoordinated species has to be regarded as a reactive intermediate [284]. The observed trans addition of HCl to square planar Pt(II) complexes is consistent with this expectation [285].

The perpendicular orientation of the alkene in such complexes is favored because it maximizes the overlap of the  $\pi$  bond with the LUMO ( $dx^2 - y^2$ , Figure 13.7) and minimizes  $4e$  repulsive interactions with the HOMO ( $ndz^2$ ). The in-plane orientation is not expected to be strongly disfavored, however, because of the secondary interaction between the  $\pi^*$  orbital and the  $dxy$  orbital. The rotational barrier of ethylene in Zeise's anion was theoretically estimated to be 55 kJ/mol [282], within the range 42–63 kJ/mol measured by NMR for related complexes [286].

The binding of ethylene in Zeise's-like anions was investigated as a function of metal (Ni, Pd, Pt) and ligand ( $\text{Cl}^-$ ,  $\text{NH}_3$ ) by B3LYP calculations [283]. The binding energy of ethylene to Zeise's anion,  $\text{PtCl}_3^-$ , was found to be 142 kJ/mol and was calculated to decrease in the series,  $\text{PdCl}_3^-$  (79 kJ/mol) and  $\text{NiCl}_3^-$  (26 kJ/mol). Substitution of chloride for ammonia, a poorer  $\sigma$  donor, led to increases in binding energies but did not change the relative order of stabilities—binding energies of ethylene to  $c\text{-MCl}(\text{NH}_3)_2^-$ : Pt, 193; Pd, 142; Ni 105 [283]. We shall attempt to rationalize these trends on the basis of orbital interaction theory.

The effect of variation of metal and ligand on the energies of the orbitals of the T-shaped complex is shown in Figure 13.8 in which a number of principles are illustrated.

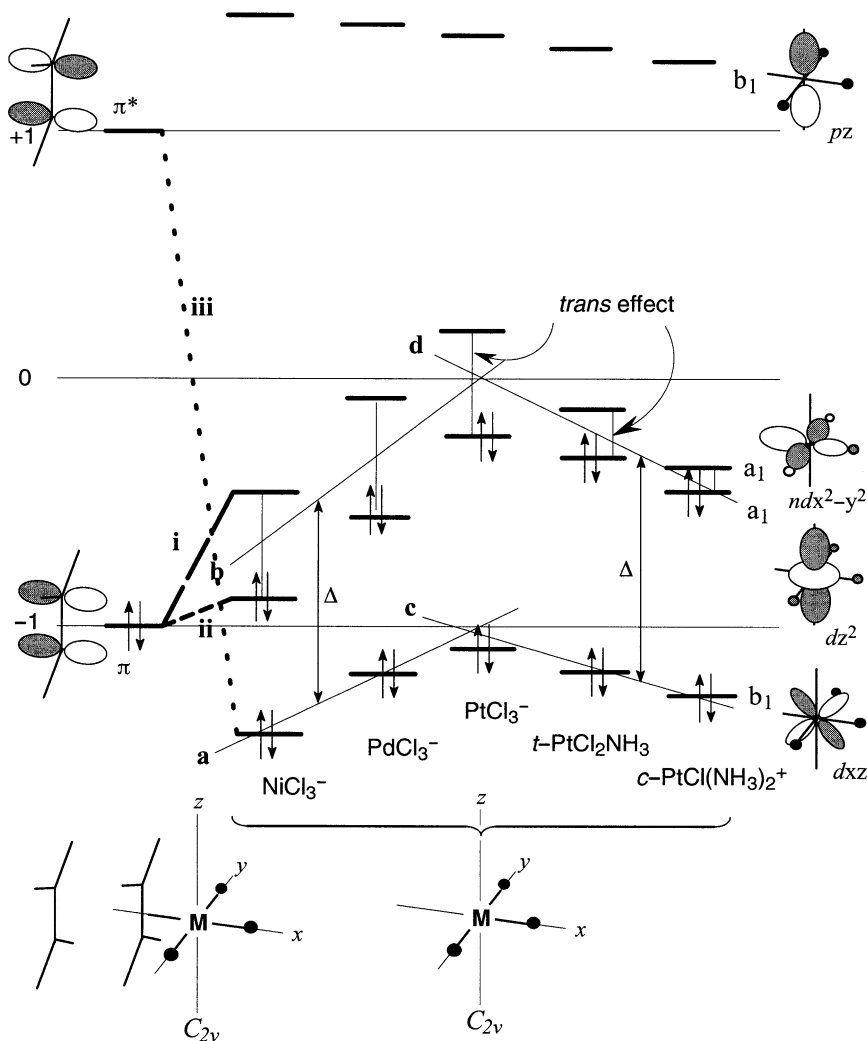


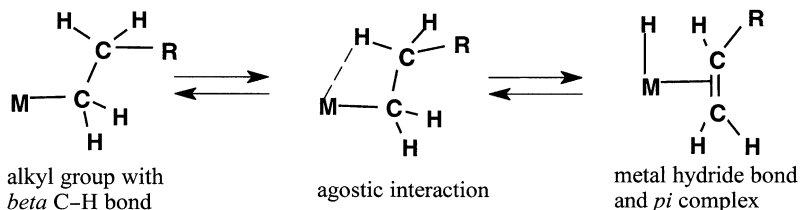
Figure 13.8. Analysis of alkene binding to different tricoordinated metal complexes.

The frontier orbitals of ethylene are shown on the left-hand side. On the right, occupying most of the figure, are five sets of orbitals of the T-shaped complex. For clarity, only the  $a_1$  and  $b_1$  orbitals are shown since these can interact with the  $\pi$  ( $a_1$ ) and  $\pi^*$  ( $b_1$ ) orbitals of ethylene. The middle set is that of the  $\text{PtCl}_3^-$  complex (see also Figure 13.7). Lines  $a$  and  $b$  show the trend in  $d$  orbital energies as a function of the change of the metal, following Figure 13.2. Line  $b$  represents an average of the LUMO–HOMO gap, which was attributed to the trans effect above. The separation between lines  $a$  and  $b$  is attributed to the *ligand field splitting parameter*,  $\Delta$  (or  $\Delta_0$ ), which decreases in the series  $\text{Pt} > \text{Pd} > \text{Ni}$ . Lines  $c$  and  $d$  depict the corresponding changes with successive replacements of  $\text{Cl}^-$  by  $\text{NH}_3$ . In this case, the downward slope of the fragment orbitals is due to increasing

charge. There should be little difference in the slopes of lines *c* and *d* since the metal center is the same. However, the HOMO–LUMO gap decreases since  $\text{NH}_3$  has a weaker trans effect than  $\text{Cl}^-$  (see above). The interactions primarily responsible for the binding of the alkene are shown by bold dashed or dotted lines labeled i, ii, and iii. The attractive interaction, i, which is responsible for the majority of the binding energy, clearly is the weakest in Zeise's complex and increases in both series due to the slopes of lines *b* and *d*. At the same time, in both series, the attractive interaction, iii, decreases due to the slopes of lines *a* and *c*. In reference 283, the computed decrease in binding energy in both series was attributed to decreased  $\pi$  back donation in the series on the basis of the length of the C—C bond. We note, however, that the length of the C—C bond would also be increased by donation from the  $\pi$  bonding orbital, the primary bonding interaction in Figure 13.8 (or 13.7). On the basis of the diagram in Figure 13.8, it would be difficult to blame the reduced binding to a further weakening of the already much weaker  $\pi$  back donation. It seems more likely that the culprit is the repulsive four-electron interaction, ii, which becomes more effective in both series. Indeed, the difference in the two series, namely that the binding energies are higher in the ligand substitution and lower in the metal substitution (relative to Zeise's complex), may be explained as due to the balance of interactions i and ii. Because of the constant HOMO–LUMO gap, interaction ii is relatively more important in the metal substitution series and has a greater effect on the binding energy. In the ligand substitution series, the *lower* trans effect of  $\text{NH}_3$  manifests itself as reducing the gap between the  $\pi$  orbital and the  $dx^2 - y^2$  LUMO, thereby increasing the primary interaction.

## AGOSTIC INTERACTION

A common motif in organometallic chemistry is the *agostic interaction*, which can act to stabilize low-coordination low-*e*-count complexes. The requirement is an alkyl group with a  $\beta$ - or a  $\gamma$ -C—H bond attached to the metal within reach of (i.e., cis to) an empty coordination site. An attractive interaction occurs with the C—H bond acting as a  $2e$  donor into the low-lying metal valence orbital that occupies that site. In the case of a  $\beta$ -C—H bond, hydride transfer may occur with little activation, resulting in an M—H sigma bond and a  $\pi$  complex with an alkene as discussed above.



The reverse reaction corresponds to intramolecular C—H bond formation. It requires that the alkene rotate from its equilibrium perpendicular orientation toward the less favored parallel orientation. The barrier hindering the rotation of the alkene may be partially or totally offset by the incipient agostic interaction. If the alkene is unsymmetrical, the question of regioselectivity of hydride transfer arises. In the case of an unsymmetrical alkene with an X: or "C" substituent, the donor  $\pi$  orbital is polarized away from the substituent (Figure 13.9) and the metal lies closer to that end. Conversely,

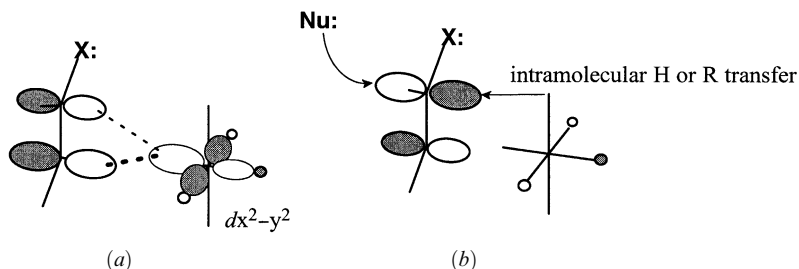


**Figure 13.9.** (a) Biased bonding in the  $\pi$  complex of a X-substituted alkene; (b) regio- and stereochemistry of intermolecular and intramolecular nucleophilic attack.

the acceptor  $\pi^*$  orbital is polarized toward the substituent. In this case, M-to-C hydride transfer occurs at the more highly substituted carbon.

It has been shown experimentally that attack by strong nucleophiles also occurs regioselectively at this C atom, stereoselectively from the face opposite to the metal [287]. Since the alkyl group  $\sigma$  bonded to the metal is very carbanion-like, it is susceptible to protonation by acids, yielding an alkane. The overall reaction provides the mechanism for homogeneous hydrogenation of alkenes. It may be extended to hydrogenation of C=N and C=O pi bonds.

## ZIEGLER-NATTA POLYMERIZATION

In the scheme above, the role of the hydride may very well be played by an alkyl group, particularly for the reverse reaction. Figure 13.10 shows the basis for the most important industrial application of organometallic chemistry, the homogeneous polymerization of alkenes, modeled on the heterogeneous system first discovered by Ziegler et al. [288]. The

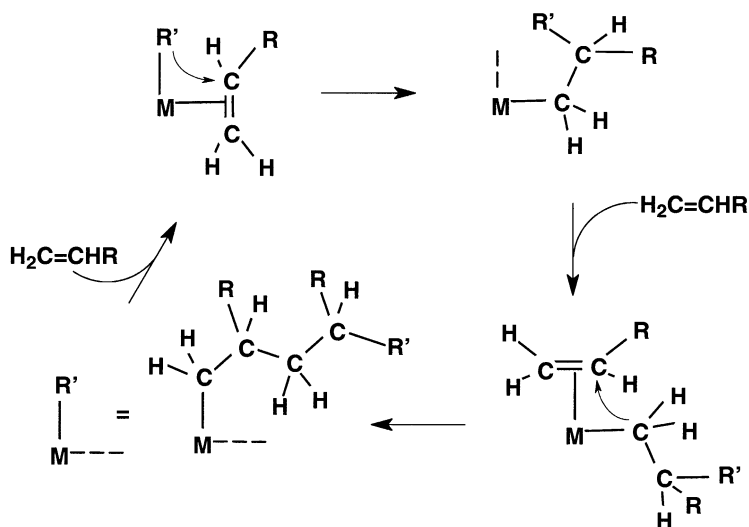
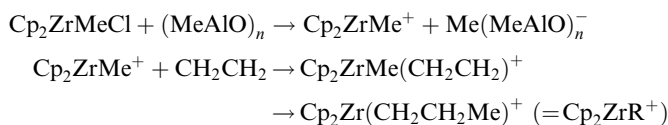


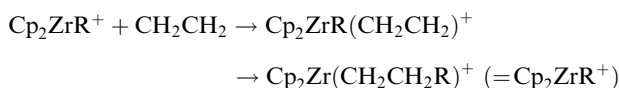
**Figure 13.10.** A typical olefin polymerization cycle, consisting of olefin binding followed by M—C rearrangement of alkyl group.

catalytic systems consist of quasi-tetrahedral chloro or methyl complexes of  $d^0$  metals with one or two cyclopentadienyl (Cp) ligands and a Lewis acidic aluminium-based cocatalyst whose function is to remove a ligand and produce the active metal catalyst, a coordinatively unsaturated complex [289]. Typically, the active metal catalysts are cationic species (e.g.,  $\text{Cp}_2\text{TiMe}^+$  or  $\text{Cp}_2\text{ZrMe}^+$ ). For example, the following sequence based on Kaminsky and co-workers [290] yields high-density polyethylene:

Initiation with an alumoxane (large excess):



Propagation:



The electronic structure of such a  $d^0$  complex (e.g.,  $\text{Cp}_2\text{TiMe}^+$ ) is shown in Figure 13.11.

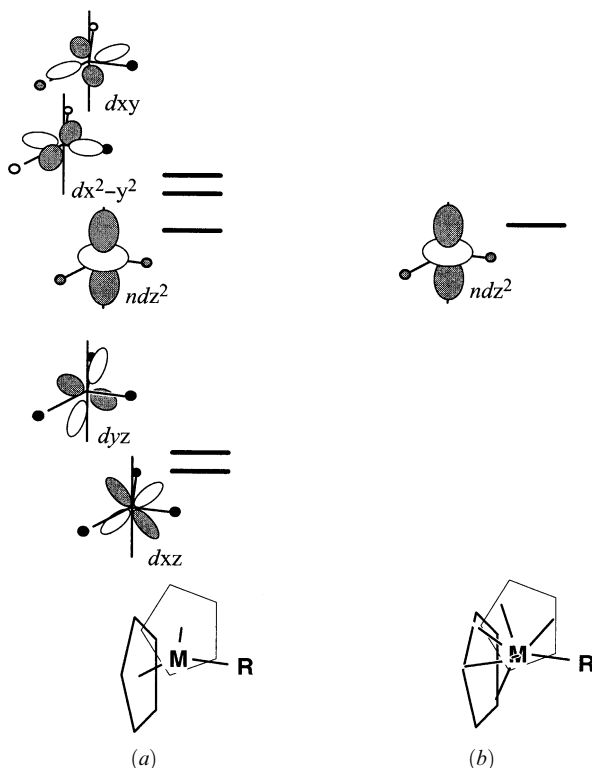


**Figure 13.11.** R = alkyl, M = a  $d^0$  metal [e.g., Ti(IV) or Zr(IV)]: (a) cyclopentadienyl anion as a 2e donor ligand; (b) cyclopentadienyl as a 6e donor ligand.

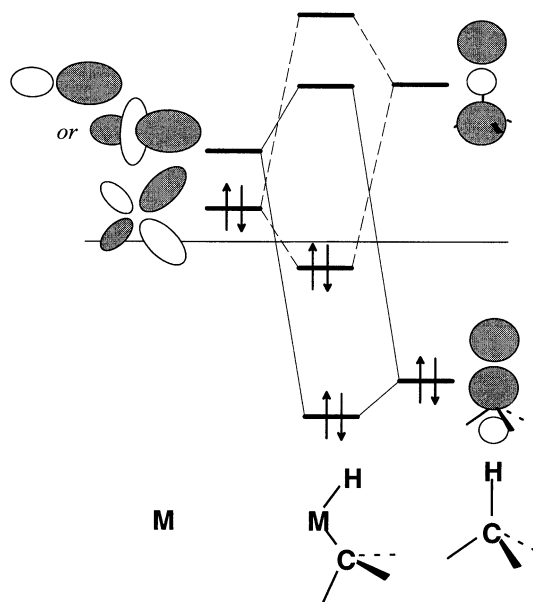


**Figure 13.12.** Transition metal orbitals required for oxidative addition, a  $\sigma$ -type acceptor and a  $\pi$ -type donor.

It may be derived from the “ $D_{3h}$ ” structure of Figure 13.4, in which both sets of degenerate orbitals are removed, leaving only an empty  $dz^2$  orbital. Such a complex is a weak Lewis acid, coordinating with the alkene through the latter’s  $\pi$  bonding orbital. There are no occupied  $d$  orbitals to partake of  $\pi$  back bonding so the  $\pi^*$  orbital remains low and is receptive to transfer of the alkyl group, as in Figure 13.10. The nature of the transition structure and energetics of the alkyl transfer step (14 kJ/mol) have been studied by DFT [291]. The “vacant” site in the coordinatively unsaturated active catalyst is weakly occupied by solvent or by an intramolecular agostic interaction. A complete computational description of the intermediates and barriers involved in catalytic cycles of the type shown in Figure 13.10 has been carried out by Margl and co-workers [292].

## OXIDATIVE ADDITION TO H—H AND C—H BONDS

Oxidative addition, reactions (13.1) and (13.2), was introduced in the opening paragraph of this chapter as one of the reactions of transition metal compounds of particular interest to organic chemists. Figure 13.12 shows a generic orbital interaction diagram for oxidative addition to  $H_2$ . One notes that the coordination number of the metal increases by 2 in this process, as does the formal oxidation state of the metal. This effectively limits the metal fragments which provide the occupied  $\pi$  donor (typically  $dxz$ -type orbital and unoccupied  $\sigma$  acceptor [usually  $(n+1)sp_z^n$  or  $ndz^2$ ] orbital to 3-coordinated (Figure 13.4) and 4-coordinated (Figure 13.5) fragments. Examination of the fragment orbitals from Figure 13.4 reveals that a  $C_{3v}$  fragment with  $s^2d^2$  (10e) configuration and  $C_{2v}$  fragments with  $s^2d^4$  (12e) or  $s^2d^6$  (14e) configurations are the most likely candidates



since each has a LUMO suitable for interaction with a  $\sigma$  bond donor and a HOMO which can act as a  $\pi$  donor. In the case of the  $s^2d^6 C_{2v}$  structure, this role would be filled by  $ndz^2$ , and the midpoint of the incoming  $\sigma$  bond will not be along the  $C_2$  axis but rather out of the plane of the metal's ligands. The  $16e$  complexes of the type  $M(\text{dmpe})_2$ ,  $\text{dmpe} = (\text{CH}_3)_2\text{PCH}_2\text{CH}_2\text{P}(\text{CH}_3)_2$ ,  $M = \text{Fe}, \text{Ru}$ , have been shown experimentally and theoretically to add  $\text{H}_2$  essentially without activation [293]. Theoretical calculations on the model system,  $M(\text{PH}_3)_4$ , indicate that an initially formed complex between the metal LUMO ( $p_z$  of the  $C_{2v}$  structure in Figure 13.5) and the H—H bond coordinated endwise ( $\eta^1\text{-H}_2$ ) collapses with little or no activation to an  $\eta^2\text{-H}_2$  adduct as the metal HOMO ( $dxz$  of the  $C_{2v}$  structure, Figure 13.5) comes into play. Reaction with methane (with  $\text{Ru}(\text{CO})_4$ ) is predicted to follow the same pattern but with higher activation energy [294]. Oxidative addition of  $\text{H}_2$  to  $\text{Fe}(\text{CO})_4$  has been shown experimentally to have an activation barrier less than 8 kJ/mol. Reductive elimination of  $\text{H}_2$  from  $\text{Fe}(\text{CO})_4\text{H}_2$  has an activation barrier of  $86 \pm 9$  kJ/mol. The average Fe—H bond dissociation energy (BDE) is  $259 \pm 8$  kJ/mol [295]. Computed M—H and M—C BDEs are available for  $\text{CpMPH}_3\text{R}^+$  complexes ( $M = \text{Co}, \text{Rh}, \text{Ir}$ ;  $\text{R} = \text{H}, \text{Me}, \text{Et}, \text{Pr}$ ) [296].

## CHAPTER 14

---

# ORBITAL AND STATE CORRELATION DIAGRAMS

---

### GENERAL PRINCIPLES

Orbital interaction theory as introduced and utilized in the previous chapters of the book has served to point us in a direction along a reaction coordinate. We have been able to find the most favorable geometry in which two molecules can approach each other by considering the interactions of the frontier orbitals, and we have seen that, *carried to the logical extreme*, the initial interactions imply making and breaking of bonds and the formation of new molecules. Indeed, the initial trajectory implied from the orbital interaction theory very often does indeed lead to the expected products when the reaction is exothermic. For endothermic reactions, information with respect to the structure and stability of the transition state is necessary to decide upon the reaction pathway, and this could be deduced from examination of the reactive intermediates (or products if the reaction is concerted). The purpose of *correlation* diagrams is to follow a system *continuously* from one description to another, assuming that material balance is maintained, for example, a chemical reaction from reactants to products or a molecule from one conformation to another. A correlation diagram, or a comparison of several correlation diagrams, would permit one to identify preferred reaction pathways or more stable conformations and offer an explanation for experimentally observed preferences.

What should be correlated? In an *orbital* correlation diagram, the shapes and energies of orbitals are examined to see if the electronic structure of the reactants could be smoothly converted into the electronic structure of the products, each defined by the structures and occupancies of their respective orbitals. The nodal characteristics of orbitals are very resistant even to rather large perturbations and will tend to be conserved in chemical reactions. If an element of symmetry, for example, a mirror plane, is maintained during the course of the reaction, the nodal characteristics separate the orbitals into two sets, the members of one set being symmetric with respect to reflection

in the symmetry plane, the others being antisymmetric with respect to reflection. Orbital symmetries are conserved in the reaction. If the number of orbitals of each symmetry type is not the same in the reactants as in the products, that reaction will not take place readily. Even if symmetry is not present, *local* symmetry usually is sufficient to distinguish the orbitals, hence the principle of *conservation of orbital symmetry* which formed the title of the classic text by Woodward and Hoffmann [3a] or the *orbital correlation analysis using maximum symmetry* (OCAMS) approach of Halevi [10].

## WOODWARD–HOFFMANN ORBITAL CORRELATION DIAGRAMS

An abbreviated description of the generation of Woodward–Hoffmann orbital correlation diagrams is presented here. A full description is available in numerous sources, most notably reference 3. To begin with, a reaction coordinate is proposed. The active components of the reactants and products are maximally symmetrized by ignoring substituents and the presence of embedded heteroatoms. Symmetry elements conserved in the course of the reaction (at least those which intersect bonds being formed or broken) are identified, and group orbitals are combined to provide symmetry-adapted MOs if necessary. In- and out-of-phase combinations of like-symmetry reactant orbitals are taken if they are close in energy. The orbitals of products are treated in like manner. Inspection of the reactant and product orbitals may suggest obvious correlations. However, orbitals of like symmetry will not cross, while orbitals of different symmetry may. The lowest energy MO of the reactants is connected to the lowest energy product MO which has the same symmetry. The next higher reactant MO is similarly correlated with a product MO of the same symmetry type, and so on until the highest energy reactant MO has been correlated. The numbers and symmetry types of reactant and product orbitals must be the same, so that all orbitals are connected. If all reactant orbitals which are occupied in the ground-state electronic configuration correlate with ground-state occupied MOs of the product(s), the reaction is thermally allowed by the postulated mechanism. If one or more reactant MOs correlate with product orbitals which are empty in the ground state, the reaction is not allowed.

Orbital correlation diagrams are useful for cycloadditions and electrocyclic reactions but not for sigmatropic rearrangements since no element of symmetry is preserved.

### Cycloaddition Reactions

The orbital correlation diagrams for the attempted face-to-face dimerization of two olefins ( $\pi 2_s + \pi 2_s$ ) to form a cyclobutane and for the Diels–Alder reaction are shown in Figures 14.1a and 14.1b, respectively. Figure 14.1a displays a typical correlation diagram for a reaction which is orbital-symmetry forbidden. The HOMO of the olefin pair (the out-of-phase combination of the two  $\pi$  bonds correlates with an unoccupied MO of cyclobutane. Therefore, an attempt to squeeze two olefins together in a face-to-face geometry (the least motion pathway to cyclobutane) would tend to yield a highly excited state of the cyclobutane. The reverse is also true. Rupturing a cyclobutane into two olefins would produce one or both olefins in a highly excited state. On the other hand, the orbital correlation diagram for the Diels–Alder reaction (Figure 14.1b) is typical of thermally allowed pericyclic reactions. Ground-state reactants would yield ground-state product(s) directly.

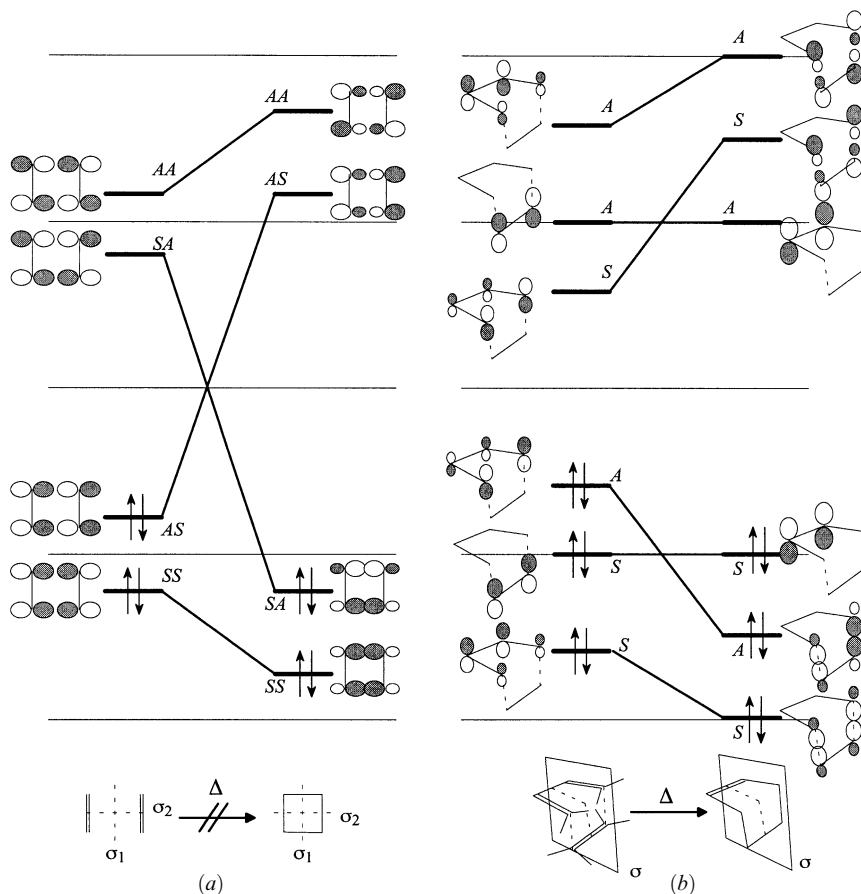


**Figure 14.1.** (a) Orbital correlation diagram for  $\pi 2_s + \pi 2_s$  dimerization of two olefins to form a cyclobutane. (b) Orbital correlation diagram for  $\pi 4_s + \pi 2_s$  cycloaddition of a diene and an olefin (the Diels–Alder reaction).

## Electrocyclic Reactions

As discussed in Chapter 12, electrocyclic reactions may proceed in a conrotatory or disrotatory fashion, that is, the  $\pi$  system cyclizes in an antarafacial or suprafacial manner, respectively. Since there is only a single component, it should be *counted* according to the general component analysis for a thermally allowed reaction, that is,  $\pi(4m)_a$  = conrotatory and  $\pi(4n+2)_s$  = disrotatory. Thus, the cyclization of butadienes to cyclobutenes (or more likely the reverse reaction) should proceed in a conrotatory fashion ( $m = 1$ ), and the reaction of 1,3,5-hexatrienes should proceed in a disrotatory manner ( $n = 1$ ). As illustrated in Figure 14.2, using butadiene as an example, a two-fold axis of symmetry is maintained throughout a conrotatory electrocyclic closure or opening, while a mirror plane of symmetry is preserved during disrotatory ring closure. The orbital correlation diagrams for electrocyclic reactions of butadiene and hexatriene are shown in Figures 14.3a and 14.3b, respectively. In each case, the solid lines connecting reactant and product MOs show the correlation for *conrotatory* ring closure, the MOs

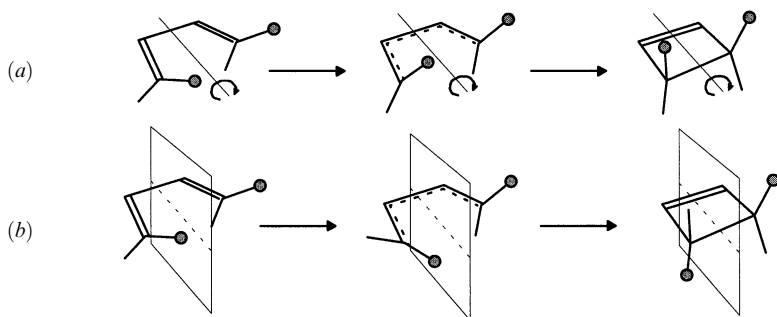


**Figure 14.2.** (a) Conrotatory electrocyclic reaction showing preservation of a  $C_2$  axis of symmetry. (b) Disrotatory ring closure showing preservation of a mirror plane of symmetry.

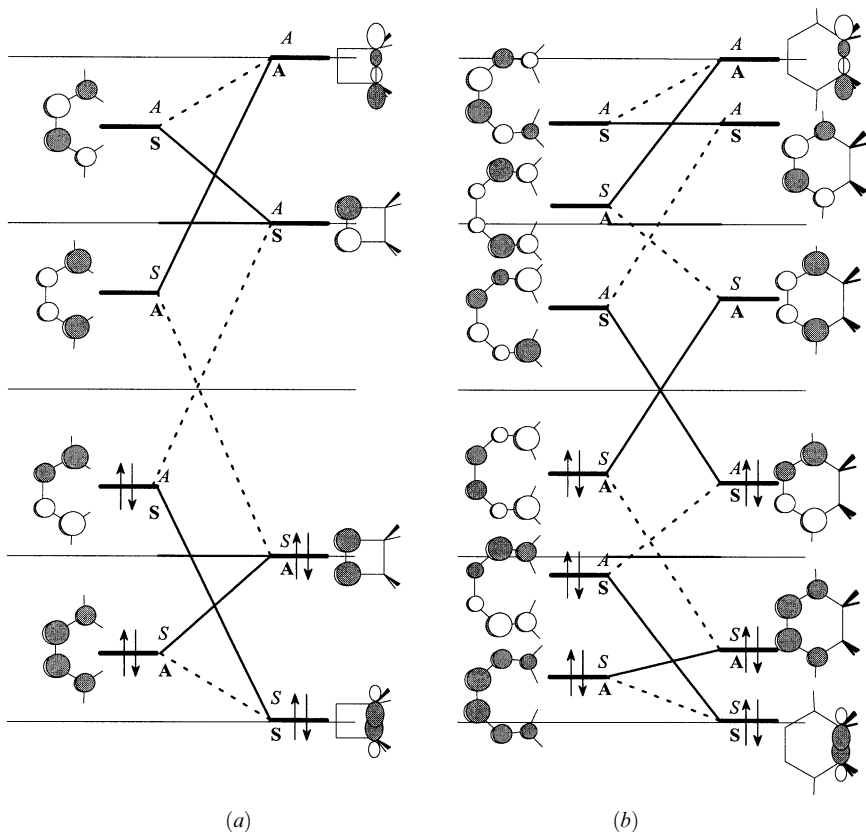


**Figure 14.3.** (a) Orbital correlation diagram for electrocyclic reaction of butadienes (b) Orbital correlation diagram for electrocyclic reaction of hexatrienes. Solid lines and S, A denote correlation for *conrotatory* motion; dashed lines and S, A denote correlation for *disrotatory* motion.

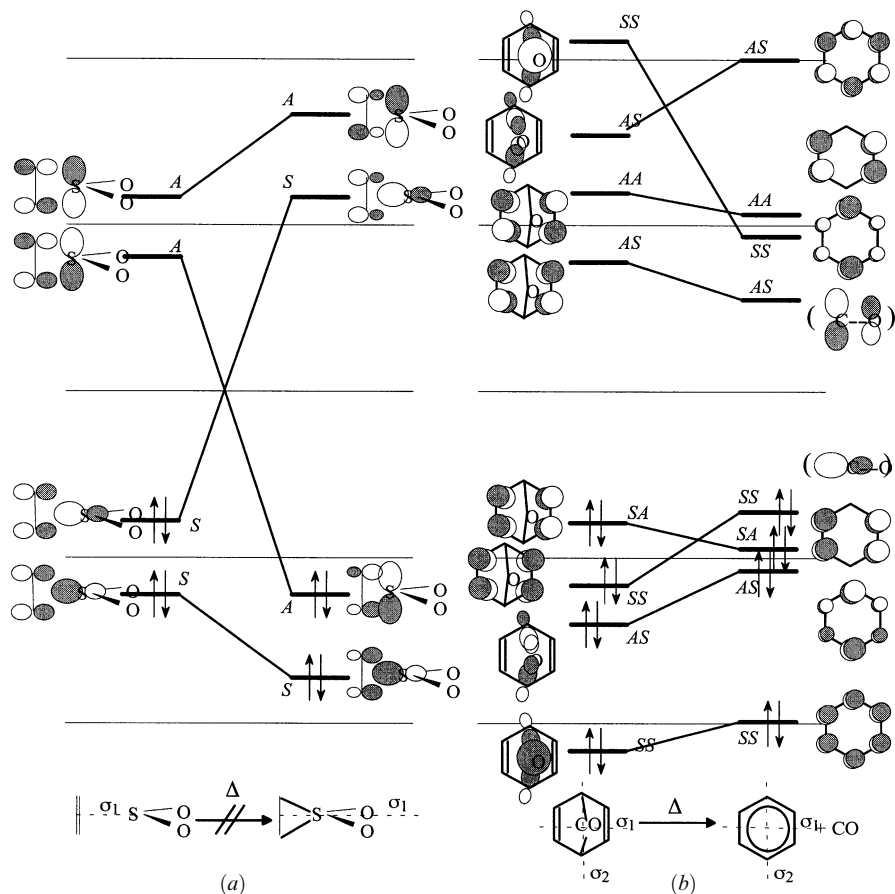


**Figure 14.4.** (a) Orbital correlation diagram for  $\pi 2_s + \omega 2_s$  cheletropic addition of  $\text{SO}_2$  to an olefin. The symmetry element preserved is a vertical mirror plane. (b) Orbital correlation diagram for elimination of  $\text{CO}$  from a norbornadienone. Two vertical planes of symmetry are preserved.

being classified according to their properties, *S* or *A*, with respect to a preserved  $C_2$  axis of symmetry. The dashed lines show the correlation for *disrotatory* ring closure, the MOs being classified *S* or *A* with respect to a preserved *mirror plane* of symmetry. The thermally allowed conrotatory opening of cyclobutenes has been confirmed experimentally. Likewise, the disrotatory mode of ring closure of (*Z*)-1,3,5-hexatriene has been demonstrated [297]. As predicted, (3*Z*,5*Z*)-1,3,5,7-octatetraenes cyclize in a conrotatory manner [298, 299].

The electrocyclic reactions of 3-membered rings, cyclopropyl cation and cyclopropyl anion, may be treated as special cases of the general reaction. Thus the cyclopropyl cation opens to the allyl cation in a disrotatory manner (i.e., allyl cation,  $n = 0$ ), and the cyclopropyl anion opens thermally to the allyl anion in a conrotatory manner (i.e., allyl anion,  $m = 1$ ). Heterocyclic systems isoelectronic to cyclopropyl anion, namely oxiranes, thiiranes, and aziridines, have also been shown experimentally and theoretically to open in a conrotatory manner [300].

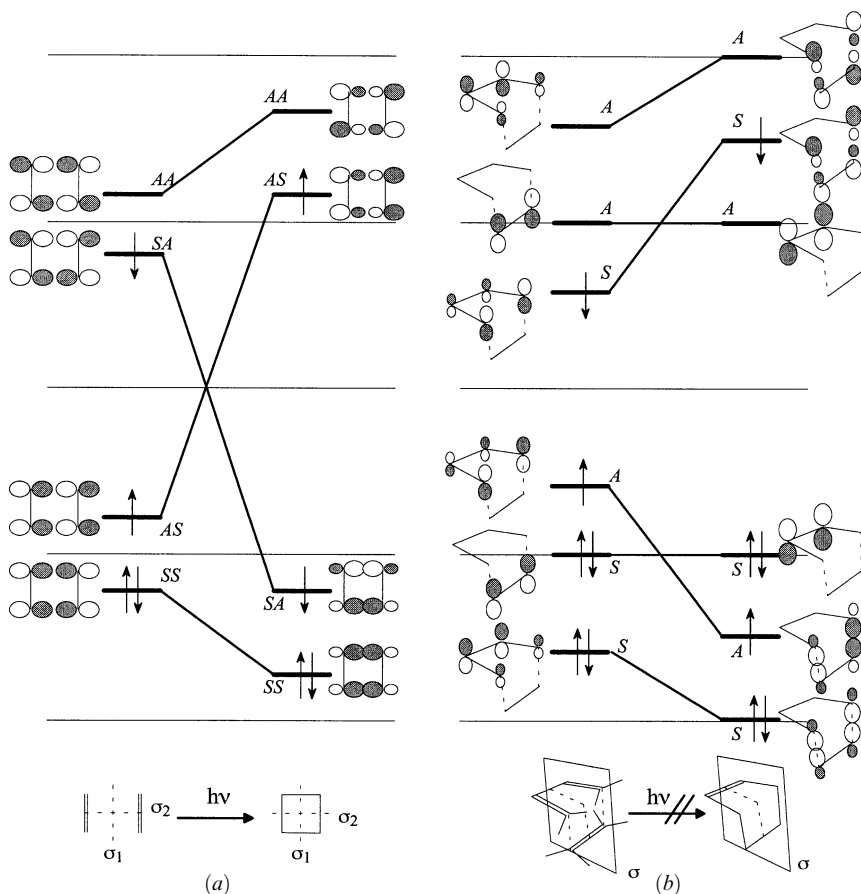


**Figure 14.5.** (a) Orbital correlation diagram for the photochemical  $\pi 2_s + \pi 2_s$  dimerization of two olefins to form a cyclobutane. (b) Orbital correlation diagram for the photochemical  $\pi 4_s + \pi 2_s$  cycloaddition of a diene and an olefin.

### Cheletropic Reactions

*Cheletropic* reactions, in which a single atom is added or extruded, comprise a special case of cycloaddition reactions. Figure 14.4 displays correlation diagrams for two typical cheletropic reactions, the loss of SO<sub>2</sub> from a thiirane dioxide (Figure 14.4a) and the loss of CO from a norbornadienone (Figure 14.4b). The addition of a carbene to an olefin is another example which is discussed below (Figure 14.9a).

### Photochemistry from Orbital Correlation Diagrams

Photochemical processes are best examined using *state* correlation diagrams, as shown below and in Chapter 15. Nevertheless, some information may be derived from orbital correlation diagrams. The orbital correlation diagrams for cycloaddition reactions shown in Figure 14.1 are repeated in Figure 14.5, showing the reactants in their lowest excited states. In simple Hückel theory, this corresponds to a single electron jump from

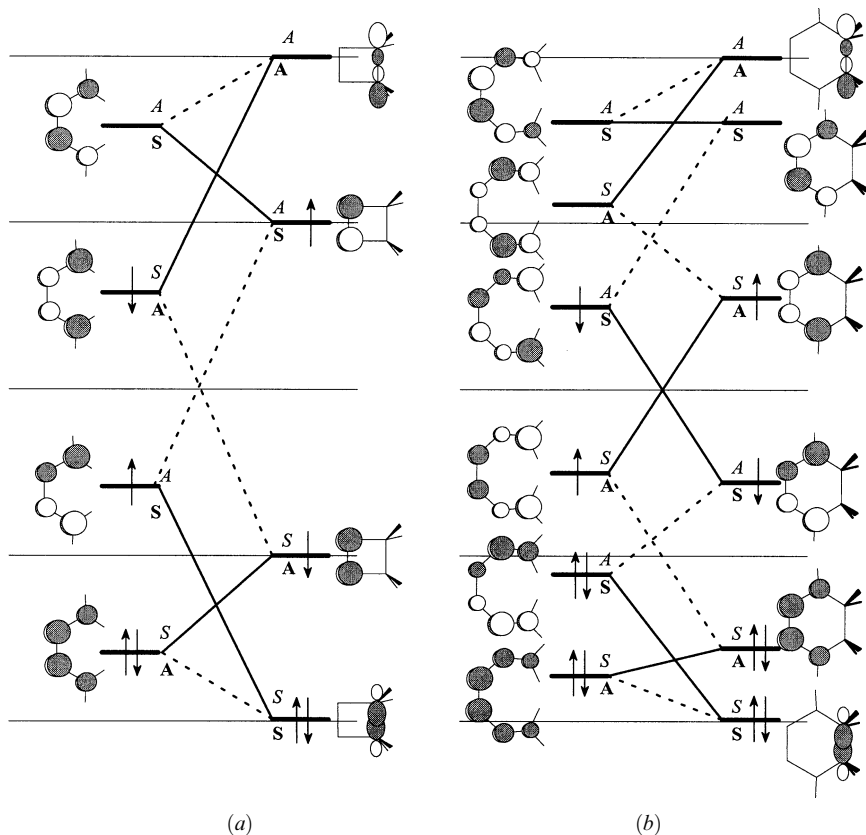
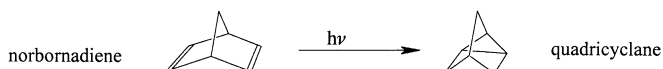


**Figure 14.6.** (a) Orbital correlation diagram for the photochemical electrocyclic reaction of butadienes. (b) Orbital correlation diagram for the photochemical electrocyclic reaction of hexatrienes. Solid lines and S, A denote correlation for conrotatory motion; dashed lines and S, A denote correlation for disrotatory motion.

the HOMO to the LUMO. The photochemical correlation shown in Figure 14.5a suggests that if the reactants are in their lowest excited state, then the product cyclobutane would also be formed in its lowest excited state. This is considered to be a photochemically *allowed* reaction. This should be contrasted with the situation depicted in Figure 14.5b, where the lowest excited state of reactants correlates with a highly excited state of the product cyclohexene. Thus the Diels–Alder reaction would not proceed with the observed stereochemistry ( $\pi 4_s + \pi 2_s$ ) under photolysis conditions. This does not imply that a diene and an olefin will not react under these conditions, but it does suggest that the mechanism will be other than the thermally allowed route. The  $\pi 2_s + \pi 2_s$  *unsensitized* photodimerization of *cis*- and *trans*-2-butene has been carried out and shown to proceed with complete stereospecificity [301]. Another well-studied case involves the  $\pi 2_s + \pi 2_s$  photochemical conversion of norbornadiene to quadricyclene [302], possibly as a system for the chemical storage of solar energy.





The orbital correlation diagrams for electrocyclic reactions shown in Figure 14.3 are repeated in Figure 14.6, with the reactants in their lowest excited states. In the case of butadienes (Figure 14.6*a*), the reactant in its first excited state would yield product in its first excited state if the disrotatory pathway (correlation by dashed lines) were followed. The situation is reversed for hexatrienes (Figure 14.6*b*). In that case, reactant in its first excited state would yield product in its first excited state if the conrotatory pathway (correlation by solid lines) were to be followed. Thus the expected stereochemistry upon photolysis is the opposite of that expected and observed for the thermal (ground-state) reactions. In fact, the photolytic ring opening of simple alkylcyclobutenes has been shown *not* to be stereospecific [303]. One of the possible reasons for the lack of observed stereoselectivity is competitive radiationless transition to the vibrationally excited ground state and subsequent thermal ring opening in the allowed conrotatory fashion. Partial orbital symmetry control is observed in the photochemical ring opening of a constrained cyclobutene [304]. An alternative mechanism for the loss of stereospecificity in the photolysis of cyclobutenes has been proposed on the basis of theoretical calculations [305] which suggested the existence of three stereochemically distinct transition points for deexcitation of the excited ring-opening cyclobutene.

By contrast with the photochemical cyclobutene-to-butadiene conversion, the photochemical conversion of 1,3-cyclohexadiene has been shown to proceed in a highly stereospecific conrotatory manner to yield the *cis*-hexatriene [306].

## LIMITATIONS OF ORBITAL CORRELATION DIAGRAMS

Although very useful in the vast majority of cases, orbital correlation diagrams are known to yield incorrect, or at least suspect, results in a few cases and may be difficult to interpret in others. The rearrangement of benzvalene to benzene provides an example. The most direct path for the rearrangement preserves a  $C_2$  axis of symmetry. The correlation diagram for the reaction, shown in Figure 14.7, suggests the reaction is thermally allowed. On the contrary, a moderately high barrier is observed for this highly exothermic reaction. In a similar vein, the direct thermal conversion of cyclooctatetraene to cubane is not observed and was considered by Woodward and Hoffmann to be forbidden on the basis of *intended* orbital correlation. Recent experimental results reveal that in the *retro* process, which is exothermic, cubane may be rearranged to cyclooctatetraene with a relatively low activation barrier,  $180 \pm 4$  kJ/mol [307]. The rearrangement is thought to involve a number of intermediates which were not observed [307].

## STATE CORRELATION DIAGRAMS

Although orbital correlation diagrams often give a reliable indication of the course of a reaction, it is not possible to follow a reaction in any quantitative fashion in this way, even if highly accurate *ab initio* MO energies are available at all points along a reaction coordinate. The ground state and electronically excited states are separated from each other within the Born–Oppenheimer approximation and by total spin angular momen-

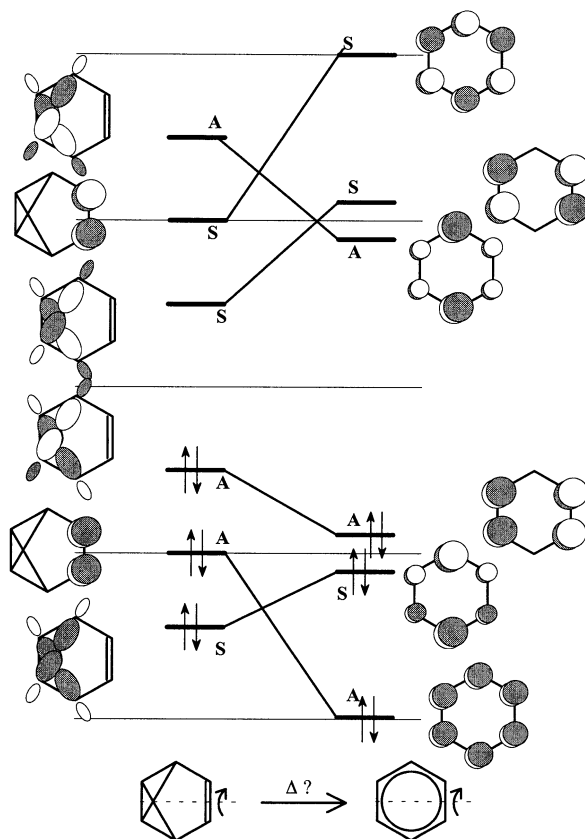


**Figure 14.7.** Orbital correlation diagram for the thermal rearrangement of benzvalene to benzene. A  $C_2$  axis of symmetry is preserved.

tum (since the usual electronic Hamiltonian does not have terms derived from electron and nuclear spins). *Ab initio* CI or other post-Hartree–Fock techniques are able in principle to produce quantitatively correct correlations of the ground and lower excited states of reactant(s) and trace these accurately along the reaction coordinate to products. However, since, often, only the few lower electronic states are of chemical interest, quite adequate *state* correlation diagrams may usually be derived from the simple orbital correlation diagrams which we have examined above. Different electronic states may be generated from the set of occupied and empty MOs by redistributing the electrons. Relative energies of the states may be estimated by simple summation of the electron (MO) energies, and state symmetries may be deduced from the symmetries of the electron distributions (the state symmetry is the direct product of the individual electron symmetries). Singlet and triplet spin configurations are simply represented by the simple artifice of showing electrons in singly occupied MOs as spins antiparallel (singlet) or parallel (triplet). Triplet states derived from the same MOs as singlet states have the same spatial symmetry but are lower in energy by a magnitude which depends on the magnitude of the exchange integral. Qualitatively, if the SOMOs are spatially close (e.g.,

$\pi$  and  $\pi^*$ ), the singlet–triplet spacing will be large, whereas for spatially remote MOs or orbitals which lie in each other's nodal planes (e.g.,  $n_O$  and  $\pi^*$  of carbonyls), the singlet–triplet splitting will be small. Once the states of reactants and products are qualitatively ordered in energy and their spin and symmetry properties assigned, the states may be correlated by a few simple rules which parallel the rules laid out above for orbital correlation diagrams.

### Electronic States from MOs

The procedure for obtaining electronic state wave functions from the MOs for a molecule is illustrated for a carbonyl group in Figure 14.8. The frontier MOs are sketched, placed on an energy scale, and, if applicable, their symmetry properties designated relative to the molecular point group or the local point group. Thus the important MOs of carbonyls are the occupied  $\pi$  and  $n_O$  (HOMO) MOs and the unoccupied  $\pi^*$  (LUMO), as were developed in Chapter 8. The local symmetry in the absence of strongly conjugating substituents is  $C_{2v}$ . In Figure 14.8a, the MOs are classified as  $S$  or  $A$  with respect to the three symmetry operations or given the appropriate labels of the irreducible representations. In Figure 14.8b, electronic configurations of the lower electronic states are obtained by redistributing the electrons among the MOs. The spatial composition of the state may be specified by the *configuration*, that is, a statement of the occupancies of the MOs. The ground state, designated  $S_0$  or  $G$ , is obtained when all of the lowest energy MOs are doubly occupied in most cases (we have seen an exception in the case

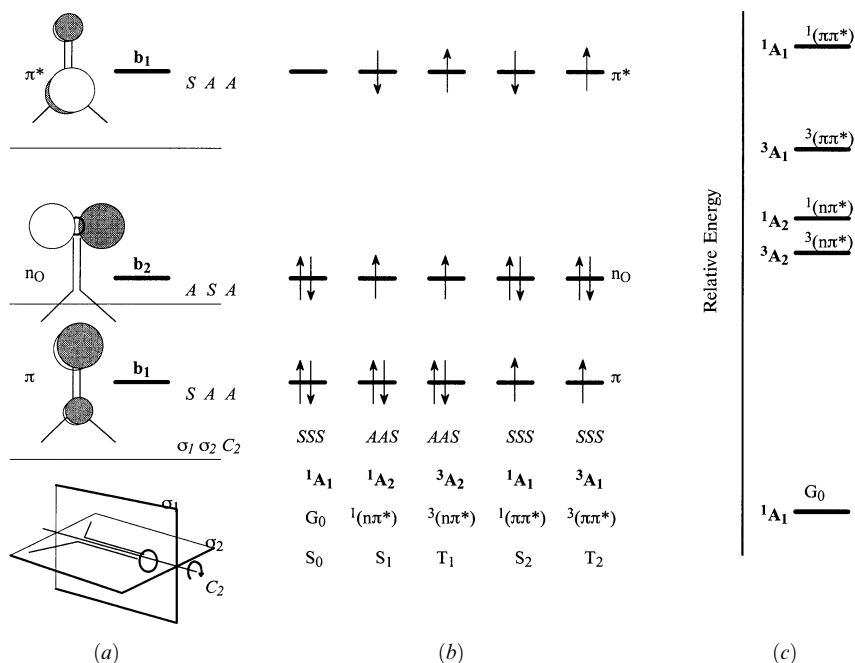


**Figure 14.8.** (a) The MOs of the carbonyl group. Symmetry classification is with respect to the local symmetry group  $C_{2v}$ . (b) The electronic states which can be constructed from the three frontier MOs. (c) The electronic states ranked approximately in relative energy.

of carbenes in Chapter 7). Thus the configuration of  $S_0$  is  $\dots(\phi_{\text{HOMO}-1})^2(\phi_{\text{HOMO}})^2$ . Excited *singlet* states are obtained by single (or multiple) electron excitations from the occupied MOs. The first (lowest energy) excited singlet state is usually that obtained from a HOMO-to-LUMO excitation and is designated  $S_1$ , with configuration  $\dots(\phi_{\text{HOMO}-1})^2(\phi_{\text{HOMO}})^1(\phi_{\text{LUMO}})^1$  or, more descriptively, by the MOs involved in the transition (if the MOs are known), for example,  $^1(n_{\text{O}}\pi^*)$ . States with doubly occupied MOs only must be singlet states. Where “open shells” are involved, additional states must be considered from reversal of electron spin(s). When two electrons have the same spin, the state is a *triplet*, designated  $T_1, T_2, \dots$ , in order of increasing energy, or by a superscript in front of the state descriptor, for example,  $^3(n_{\text{O}}\pi^*)$ . The spatial symmetry of the state is, in practice, determined by the cross product of the spatial symmetries of the SOMOs by the following rules:  $S \times S \Rightarrow S$ ,  $A \times A \Rightarrow S$ ,  $S \times A \Rightarrow A$ ,  $A \times S \Rightarrow A$ . The “closed-shell” states, like the ground state, are  $S$  with respect to every symmetry operation or transform as the totally symmetric irreducible representation of any point group. The energies of the electronic states may be derived from simple Hückel considerations (MO energy differences). Triplet states are lower than the singlets with the same MO configuration. The separation of  $^3(n_{\text{O}}\pi^*)$  and  $^1(n_{\text{O}}\pi^*)$  is relatively small, whereas the separation of  $^3(\pi\pi^*)$  and  $^1(\pi\pi^*)$  is large. Singlet states may be reached directly from the ground state by photoexcitation at the appropriate frequency. The electron rearrangement associated with the excitation process is very rapid (about  $10^{-15}$  s), and the nuclei do not have time to move to their new equilibrium positions. The dynamics of the excitation process and the fate of excited electronic states are discussed in Chapter 15.

### Rules for Correlation of Electronic States

When the electronic states of both the reactants and products have been determined and characterized, a correlation diagram may be constructed by connecting the states according to the following rules:

1. As with orbital correlation diagrams, states are correlated from the lowest to the highest.
2. Reactant states will only correlate with product states of the same spatial symmetry and spin multiplicity.
3. Correlation lines define potential energy “surfaces.” Surfaces are allowed to cross (intersect) if the states involved are different in spatial symmetry or spin multiplicity but may *not* cross if both characteristics are the same.
4. Inspection of the orbital make-up of reactant and product states may imply *intended* correlations which would lead to state crossings. If the states involved may not cross by rule 3, an *avoided* crossing occurs. The intention to cross is often depicted by dashed lines.

### Example: Carbene Addition to an Olefin

The MOs and electronic states of carbene have been discussed in Chapter 7. The orbital and state correlation diagrams for addition of  $:\text{CH}_2$  to ethylene is shown in Figure 14.9. The Walsh bonding picture for the MOs of cyclopropane requires that the  $\sigma$  and  $\sigma^*$  MOs of the ethylene also be included in the diagram. The  $\sigma_2$  and  $\sigma_3$  orbitals are degenerate but are shown separated for clarity. The postulated least-motion pathway preserves a vertical plane of symmetry (as well as the other elements of the  $C_{2v}$  point group), and the

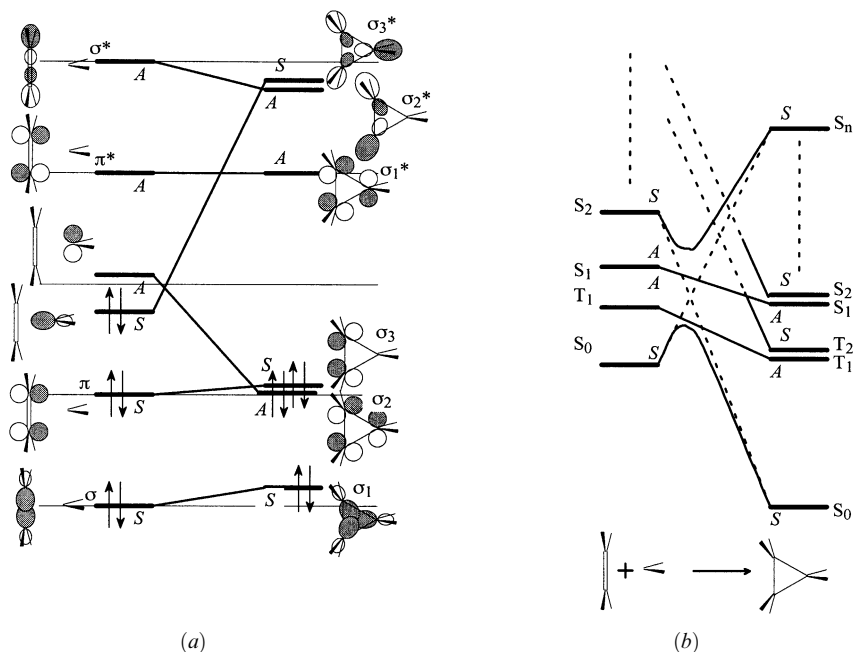


**Figure 14.9.** (a) Orbital correlation diagram for the direct insertion of carbene into an olefin to form cyclopropane. Symmetry classification is with respect to the vertical bisecting mirror plane. (b) State correlation diagram showing the intended correlations and the avoided crossing of states  $S_0$  and  $S_2$ .

orbitals of reactants and the product cyclopropane are characterized by their behavior toward reflection in this plane. The orbital correlation is shown (Figure 14.9a) with the carbene in its  $S_0$  electronic state. Direct insertion by the least-motion pathway is clearly forbidden on the basis of the diagram. Yet it is well known that singlet carbenes add smoothly and stereospecifically to olefins to yield cyclopropanes. The apparent contradiction may be resolved by inspection of the state correlation diagram. The electronic configurations of carbene were shown in Figure 7.5. The lower electronic states of the reactants are entirely derived from redistribution of the two valence electrons between the two frontier MOs of the carbene and are labeled as in Figure 7.5:  $S_0, \dots(\pi)^2(sp^n)^2$ , symmetry  $S$ ;  $T_1, \dots(\pi)^2(sp^n)^1(p)^1$ , symmetry  $A$ ;  $S_1, \dots(\pi)^2(sp^n)^1(p)^1$ , symmetry  $A$ ;  $S_2, \dots(\pi)^2(p)^2$ , symmetry  $S$ . The lower electronic states of cyclopropane by simple Hückel theory are:  $S_0, \dots(\sigma_2)^2(\sigma_3)^2$ , symmetry  $S$ ;  $T_1, S_1, \dots(\sigma_2)^2(\sigma_3)^1(\sigma_1^*)^1$ , symmetry  $A$ ;  $T_2, S_2, \dots(\sigma_2)^1(\sigma_3)^2(\sigma_1^*)^1$ , symmetry  $S$ . The pairs of states  $S_1, S_2$  and  $T_1, T_2$  are degenerate. The high-energy cyclopropane excited state  $S_n, \dots(\sigma_2)^0(\sigma_3)^2(\sigma_3^*)^2$ , is shown as the intended correlation partner of the carbene (+ethylene)  $S_0$  state. The doubly excited but relatively low energy carbene (+ethylene) state  $S_2$  would correlate directly with the ground state of cyclopropane but is prevented from doing so by the avoided crossing with the ascending  $S_0$  state. The reaction is highly exothermic, and the avoided crossing occurs early in the reaction coordinate. The resulting barrier hindering reaction is relatively low, thus explaining the apparent allowedness and concerted character of singlet carbene insertions into olefins. In fact, the barrier may be further lowered if the carbene

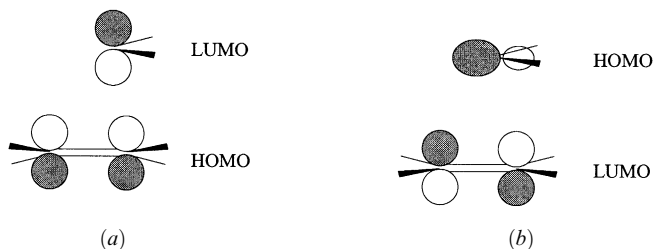


**Figure 14.10.** Non-least-motion approach of a singlet carbene to an olefin showing the most favorable HOMO–LUMO interaction: (a) primary interaction; (b) secondary interaction.

approaches the olefin in a non-least-motion pathway, as would be expected from orbital interaction considerations (Figure 14.10) and shown by computation [308, 309]. Similar non-least-motion reaction pathways have been theoretically predicted for rapid singlet carbene insertion into C–H bonds [310] and in carbene dimerization to ethylenes [311].

The orbital and state correlation diagrams for the pyrolysis of dioxetanes are shown in Figure 14.11. The formally forbidden  $\sigma 2_s + \sigma 2_s$  reaction proceeds with activation energy in the range 90–120 kJ/mol, is highly exothermic, and is accompanied by emission of light. One of the product carbonyl compounds is produced in an electronically excited state. The chemiluminescence is due to phosphorescence with high quantum efficiency [312, 313], indicating that the final product state is a triplet.

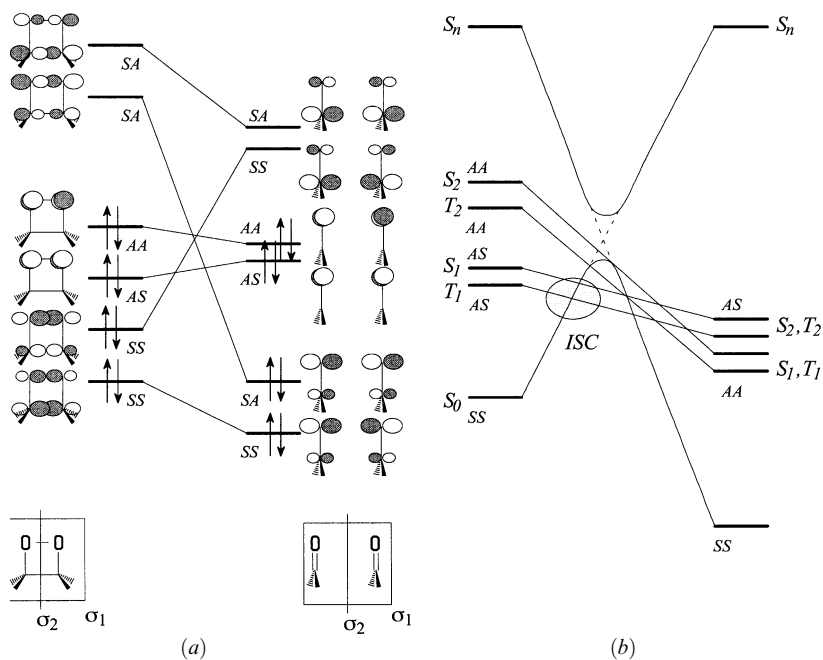


**Figure 14.11.** (a) Orbital and (b) state correlation diagrams for the decomposition of dioxetane. The observed chemiluminescence may be due to intersystem crossing (ISC) to the triplet manifold in the region denoted by the shaded circle in (b).

## CHAPTER 15

---

# PHOTOCHEMISTRY

---

The ground state of a molecule represents only one of, in principle, an infinite number of electronic states. Because the electron distribution is different for each state, the bonding, structure, and reactivity will be different from the ground state. Each electronic state is de facto a separate chemical species, with its own set of chemical and physical properties. Excited electronic states are higher in energy than the ground state so energy must be introduced in some manner to excite the molecule. In *photochemistry* the energy is introduced to the molecule by the absorption of a photon of light ( $h\nu$ ) which falls in the UV/visible spectral region.

### PHOTOEXCITATION

The geometry of a molecule in its ground state represents but one point on a  $(3N - 6)$ -dimensional potential hypersurface ( $3N - 5$  in the case of linear molecules). It is a stationary point (all forces acting on the nuclei are zero) corresponding to a local minimum (all displacements of nuclei from their equilibrium positions lead to a rise in the potential energy). Other stationary points on the ground-state potential energy hypersurface may represent different conformations of the same molecule or different molecules (including dissociation fragments). Each excited state has a similar potential hypersurface associated with it. Stationary points on excited-state surfaces will not in general coincide with those on the ground-state surface. Figure 15.1 shows a one-dimensional cross section of the ground state,  $S_0$ , and two excited-state potential surfaces, one of which is *bound* like the ground state,  $S_1$ , and the other of which is *unbound*,  $S_2$ . In fact, Figure 15.1 may depict a state correlation diagram of the kind discussed in Chapter 14. On bound surfaces, the vibrational motion is also quantized. The spacing of the vibrational energy levels ( $400\text{--}4000\text{ cm}^{-1}$  or  $4\text{--}40\text{ kJ/mol}$ ) is such that at room temperature most of the molecules are in the lowest vibrational state. In addition, *rotational* motion of the molecule about its center of mass is also quantized. The spacing of the rotational energy levels depends

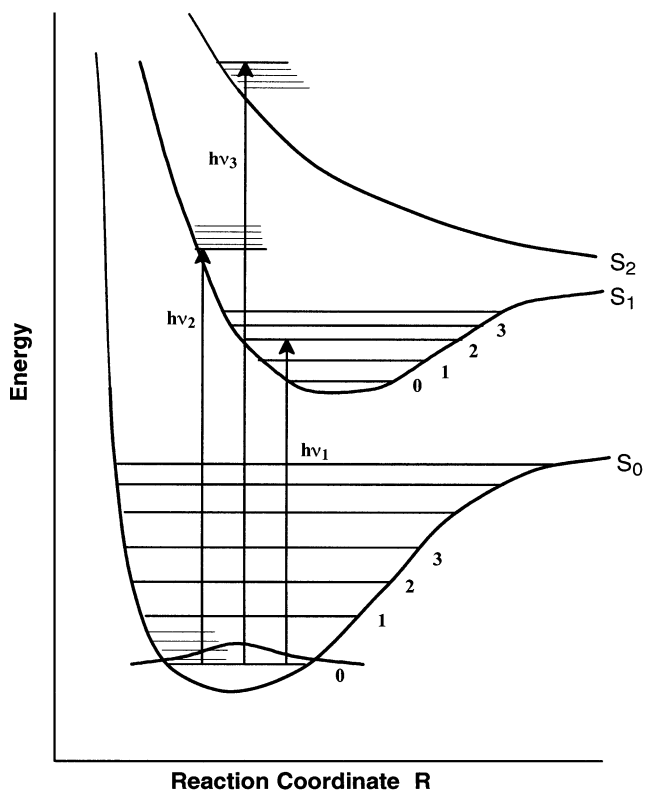


**Figure 15.1.** Potential energy surfaces for bound states,  $S_0$  and  $S_1$ , and a dissociative state,  $S_2$ .

inversely on the moment of inertia. For large molecules (more than a few first- or higher row atoms) or in solution, the rotational structure is not resolved, although at room temperature, a number of rotational levels will be populated. The range of structures in the ground vibrational state is given by the vibrational wave function shown for the lowest vibrational level of  $S_0$  in Figure 15.1. The time required to excite the electron ( $10^{-15}$  s) is very short compared to vibrational periods ( $>10^{-13}$  s). The shaded area in Figure 15.1 represents the range of structures from which *vertical* excitation may take place if the energy of the photon corresponds to the approximate energy difference between the ground-state lowest vibrational level and some vibrational level of an excited-state potential energy surface. In general, the excited state reached by vertical excitation from the ground state will be *hot* (vibrationally excited) and may dissociate if the vibrational mode of the excited state corresponds to bond stretching. A more detailed representation of the sequence of events after photoexcitation is given by a Jablonski diagram.

## JABLONSKI DIAGRAM

A generic Jablonski diagram for a molecular system is shown in Figure 15.2. Singlet states and triplet states are shown as separate stacks. Associated with each electronic state is a vibrational/rotational manifold. The vibrational/rotational manifolds of dif-



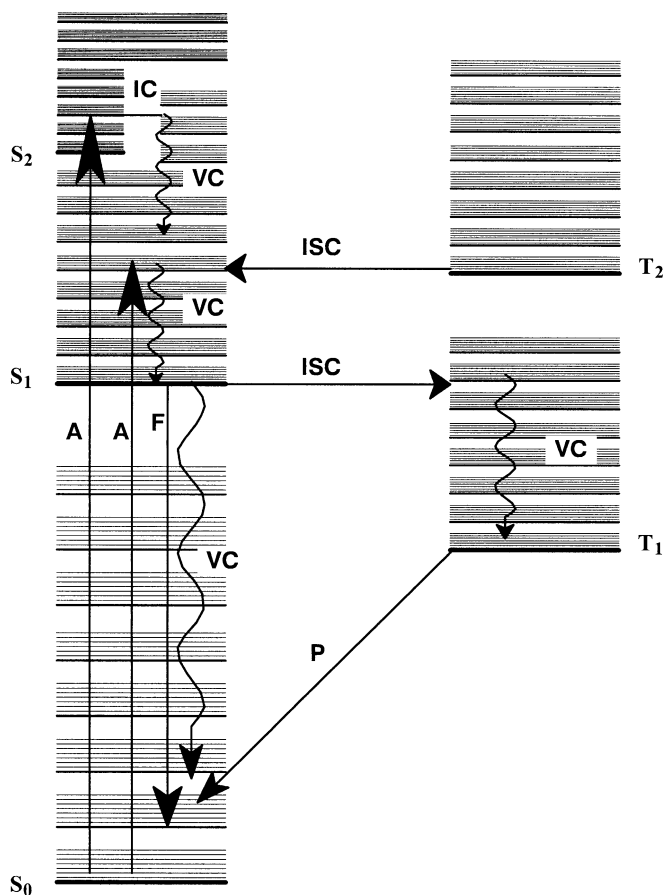


**Figure 15.2.** Modified Jablonski diagram: A = absorption; F = fluorescence; P = phosphorescence; IC = internal conversion; ISC = intersystem crossing; VC = vibrational cascade.

ferent electronic states will in general overlap each other. Straight lines represent photon absorption (A) or emission, the latter as *fluorescence* (F) or *phosphorescence* (P). Wavy lines correspond to radiationless transitions which involve vibrational relaxation via a *vibrational cascade* (VC) to the zero vibrational level of the same electronic state. Energy is carried away through collisions with solvent. If vibrational/rotational levels of two electronic states overlap, then it is possible to move from one state to the other (lower) without a change in energy. If a change in spin multiplicity is not involved ( $S \rightarrow S$  or  $T \rightarrow T$ ), the process is called *internal conversion* (IC); if a change in spin multiplicity is involved ( $S \rightarrow T$  or  $T \rightarrow S$ ), the process is called *intersystem crossing* (ISC). Both IC and ISC are immediately followed by VC.

## FATE OF EXCITED MOLECULE IN SOLUTION

The fate of an excited molecule depends on the rates (time scales) of competing processes. As already mentioned above, the time scale for photon absorption (A) is very

fast,  $10^{-15}$  s. For molecules containing elements with atomic number less than about 50, electron spin is strongly conserved. As a result, only singlet states are accessible in the primary excitation process. The time scale for the vibrational cascade and for internal conversion between higher excited states is governed by vibrational motions or collision frequencies in dense medium. Both are about  $10^{-12}$ – $10^{-13}$  s. Internal conversion between  $S_1$  and  $S_0$  may be substantially slower,  $10^{-6}$ – $10^{-12}$  s, of the same magnitude approximately as fluorescence,  $10^{-5}$ – $10^{-9}$  s. Ultimately, useful photochemistry is limited by the fluorescence lifetime,  $\tau_F$ , which for absorptions in the near UV may be estimated from the molar extinction coefficient as [314]

$$\tau_F (s) \approx \frac{10^{-4}}{\epsilon_{\max}}$$

A photochemical transformation can be accomplished only if the photoexcited molecule has a chance to do something before it fluoresces. Intersystem crossing time scales may vary considerably,  $10$ – $10^{-11}$  s. Return to the ground state by means of phosphorescence is comparatively slow,  $10^2$ – $10^{-4}$  s. The rates of chemical processes depend on the magnitudes of barriers hindering the change. Intermolecular processes depend additionally on collision frequency between reactant (the photoexcited molecule) and substrate as well as possible orientational (stereoelectronic) criteria. Effective barriers hindering reaction tend to be lower in photochemical processes, partly because bonding in the excited molecule is weaker and partly because the excited molecule may be vibrationally excited (hot). The collision frequency for intermolecular reactions may be maximized if the substrate can function as the solvent or if the reaction is intramolecular.

## DAUBEN–SALEM–TURRO ANALYSIS

The following very useful approach for the analysis of photochemical reactions is due to Dauben, Salem, and Turro [13]. A bond, a—b, made from fragment orbitals  $\phi_a$  and  $\phi_b$  of molecular fragments, a and b, is broken in the process under consideration. The relationship to the orbital interaction diagram is transparent (see Figure 15.3). The orbitals  $\phi_a$  and  $\phi_b$  are the left- and right-hand sides of the interaction diagram, while the assembly a—b is the middle. The “middle” constitutes the reactant. The noninteracting right- and left-hand sides constitute the products. Assume that the orbital  $\phi_b$  is lower in energy than  $\phi_a$ . The two electrons originally in the bonding orbital may be distributed in four distinct ways between the two fragment orbitals,  $\phi_a$  and  $\phi_b$ , yielding four states,  $Z_1 = \dots(\phi_b)^2(\phi_a)^0$ ,  $Z_2 = \dots(\phi_b)^0(\phi_a)^2$ ,  ${}^1D = \dots(\phi_b)^1(\phi_a)^1$ , and  ${}^3D = \dots(\phi_b)^1(\phi_a)^1$ . The first two states are *zwitterionic*, since the bond dissociates heterolytically. Also, since both electrons occupy the same orbital, both zwitterionic states are *singlet* states and will be totally symmetric with respect to any symmetry operation which may be preserved in the dissociation. By our assumption that  $E(\phi_b) < E(\phi_a)$ , it is expected that  $E(Z_1) < E(Z_2)$ . The remaining two states arise from homolytic dissociation of the bond and therefore are *diradical* in character. Both *singlet* and *triplet* states arise. If any residual interaction persists (i.e., if the bond broken was a  $\pi$  bond or the products are held together in a solvent cage), then the triplet diradical state is lower than the singlet diradical state. Otherwise the two have the same energy. Since the electrons end up in different orbitals, the spatial symmetry of the diradical states is determined by the symmetry properties of  $\phi_a$  and  $\phi_b$ . The diradical is symmetric (*S*) if  $\phi_a$  and  $\phi_b$  are both

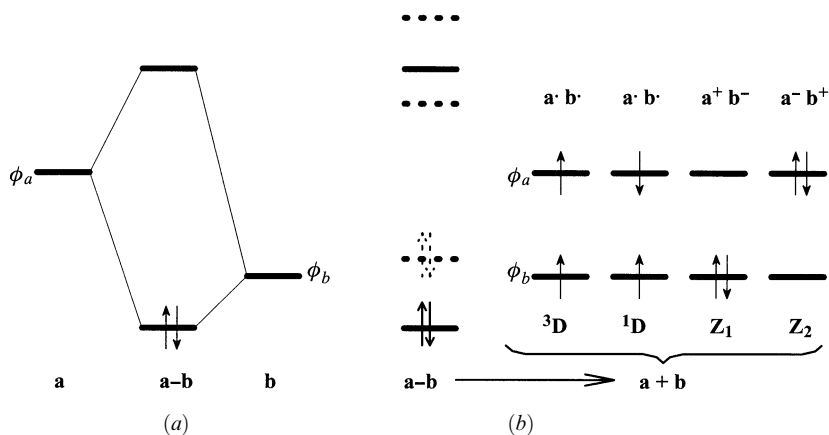


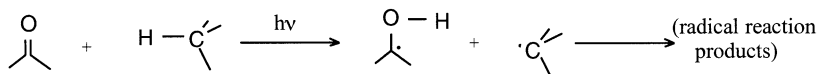
**Figure 15.3.** (a) Orbital interaction diagram for the formation of a bond between molecule fragments *a* and *b*. (b) Orbitals for Dauben–Salem–Turro analysis of the rupture of the *a*–*b* bond: left-hand side, orbitals of the bond with other occupied and unoccupied MOs of the reactant (molecule *a*–*b*); right-hand side, configurations which arise from the orbitals which made up the bond (other orbitals of fragments *a* and *b* not shown).

symmetric (*S*) or both antisymmetric (*A*) with respect to a preserved symmetry operation. If  $\phi_a$  and  $\phi_b$  have different symmetry properties, one *S* and the other *A*, then the spatial symmetry of the diradical states is *A*. Notice that the latter case could not arise if  $\phi_a$  and  $\phi_b$  are the orbitals involved in the original bond, since they could not have interacted to form the bond if they were of different symmetry. It will generally happen that one or more of the orbitals of the fragments *a* and *b* will be comparable in energy to  $\phi_a$  and  $\phi_b$  so that other diradical and zwitterionic states must be considered and the situation of different symmetries may occur among these. The same holds true for the reactant excited states.

As mentioned earlier, heterolytic cleavage of a bond to form charged species is never observed in the gas phase and is very unlikely in nonpolar solvent. Thus the expected overall order of the energies of the product states arising from the bond rupture is  $E(^3D) \leq E(^1D) < E(Z_1) < E(Z_2)$ . If the energy separation of  $\phi_a$  and  $\phi_b$  is large, or if  $\phi_a$  and/or  $\phi_b$  are diffuse, that is, the Coulomb repulsion of two electrons in the same MO (neglected in Hückel theory) is not large, the energy separation of the diradical states from  $Z_1$  may not be very large and may indeed be reversed if the dissociation is carried out in a highly polar solvent like water. Examination of several reactions of carbonyl compounds will serve to exemplify the principles of Dauben–Salem–Turro analysis.

## NORRISH TYPE II REACTION OF CARBONYL COMPOUNDS

A common photochemical reaction of carbonyl compounds is the transfer of a hydrogen atom to the carbonyl oxygen atom:



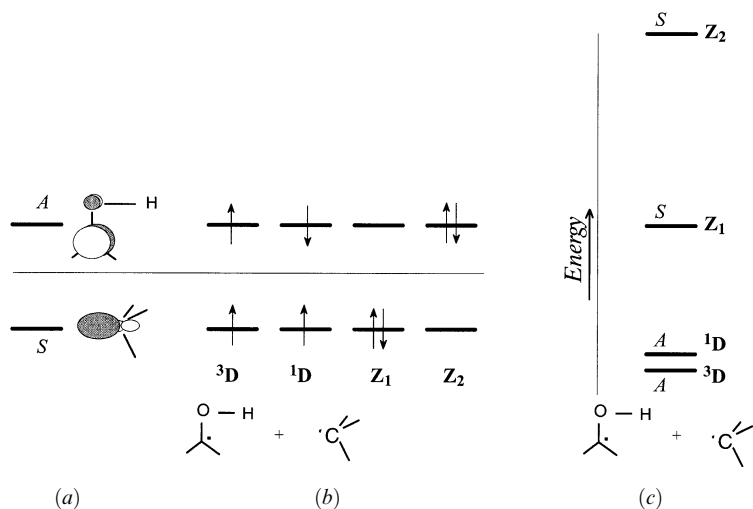


**Figure 15.4.** (a) Frontier orbitals of the fragments; (b) electronic configurations with two electrons; (c) order of the energies of the electronic states.

The lower electronic states of the reactants (left-hand side) are those of the carbonyl group shown in Figure 14.8c, since the  $\sigma_{CH}$  and  $\sigma_{CH}^*$  orbitals are too far apart to participate in the lower electronic states. In other words, the light will be absorbed by the carbonyl compound. The local group orbitals of the product fragments and the states which arise from them are shown in Figure 15.4. The reaction is considered to take place in the plane of the carbonyl group, and the orbitals are symmetry typed according to their behavior with respect to reflection in this plane.

A Dauben–Salem–Turro state correlation diagram for the photochemical step of the Norrish Type II hydrogen abstraction reaction is shown in Figure 15.5. The reactant (carbonyl) states are classified in point group  $C_s$  and also as  $S$  or  $A$ . The placement of the reactant and product states on the same energy diagram need only be approximate. The singlet and triplet  $n\pi^*$  states are located by virtue of the observed lowest electronic transition in the UV spectra of carbonyls, about 250 nm or 5 eV relative to the ground state. The  $\pi\pi^*$  states are higher, with a larger singlet–triplet gap. Assuming the ground states of reactants and products to be of similar energy, the diradical states may be placed at about the energy required to dissociate a C–C or C–H bond, about 360 kJ/mol or 4 eV.

The state correlation diagram indicates that the reaction should proceed via the  $n\pi^*$  states which correlate directly with the product states of the respective multiplicity. The  $\pi\pi^*$  states of the carbonyl group correlate with higher electronic states of the products. The carbonyl ground state correlates with the  $Z_1$  state of products. Both singlet and triplet  $n\pi^*$  states cross with the ascending ground state at the regions marked by shaded circles. At the crossing of singlet states, IC may allow a substantial fraction of the reaction to revert to the reactants. Intersystem crossing is usually much less efficient, and therefore a higher quantum yield would result if the reaction were carried out on the triplet potential energy surface.

The efficiency of photon capture to form the  $^1(n\pi^*)$  state is very low since the excitation is electric dipole forbidden in the local  $C_{2v}$  point group of the carbonyl. Direct

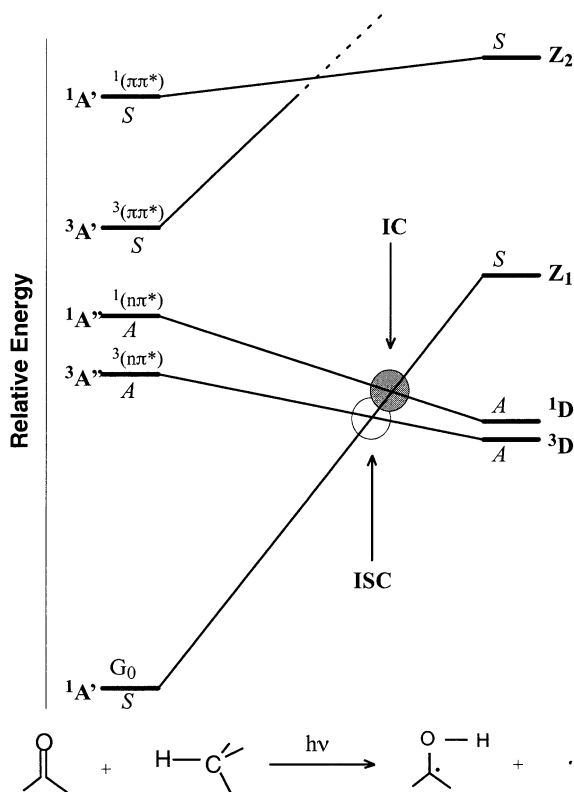
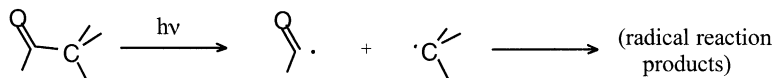


**Figure 15.5.** Dauben–Salem–Turro analysis of the photochemical step of the Norrish Type II reaction. The reaction is efficient on the  $^3(n\pi^*)$  surface to yield triplet diradical products. It is less efficient on the  $^1(n\pi^*)$  surface since IC is relatively efficient.

excitation to the  $^3(n\pi^*)$  state is both space and spin forbidden. The triplet state,  $^3(n\pi^*)$ , may be reached via *sensitization* using compounds which undergo ISC very efficiently and whose lowest triplet states are above the  $^3(n\pi^*)$  state of the carbonyl. Conversely, the presence of compounds whose triplet states are below the  $^3(n\pi^*)$  state of the carbonyl will result in *quenching* of the reaction.

## NORRISH TYPE I CLEAVAGE REACTION OF CARBONYL COMPOUNDS

A second common photochemical reaction of carbonyl compounds is the cleavage of the bond adjacent to the carbonyl group:



As with the Norrish Type II reaction, the lower electronic states of the reactants (left-hand side) are those of the carbonyl group shown in Figure 14.8c. The local group

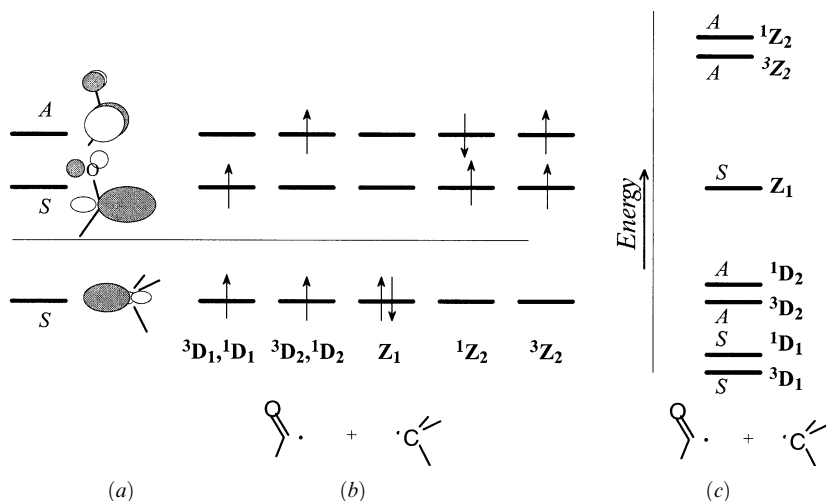


**Figure 15.6.** (a) Frontier orbitals of the fragments of a Norrish Type I cleavage; (b) electronic configurations with two electrons; (c) order of the energies of the electronic states.

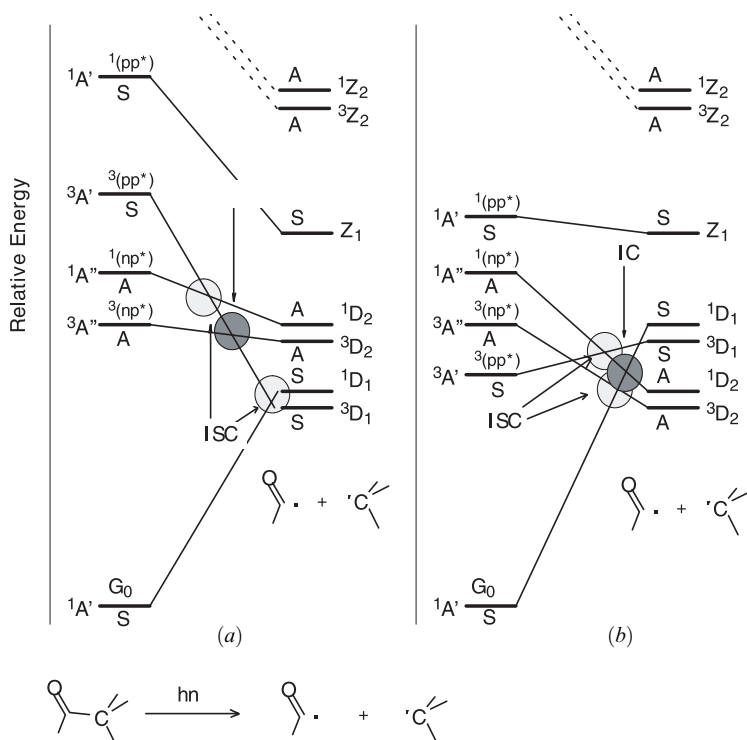


**Figure 15.7.** Dauben–Salem–Turro analysis of the photochemical step of the Norrish Type I reaction for (a) saturated carbonyls and (b) conjugated carbonyls. The reaction is most efficient on the  $^3(\pi\pi^*)$  surface to yield triplet diradical products. It is also efficient on the  $^3(n\pi^*)$  surface since IC permits formation of products in their ground state.

orbitals of the product fragments and the states which arise from them are shown in Figure 15.6. The reaction is again considered to take place in the plane of the carbonyl group and the orbitals are symmetry typed according to their behavior with respect to reflection in this plane.

A Dauben–Salem–Turro state correlation diagram for the photochemical step of the Norrish Type I  $\alpha$  cleavage reaction is shown in Figure 15.7. The reactant (carbonyl) states are classified in point group  $C_s$  and also as  $S$  or  $A$ . The state correlation diagram indicates that the reaction should proceed most efficiently via the triplet  $\pi\pi^*$  state which correlates directly with the ground state of the products. The  $^3(n\pi^*)$  state of the carbonyl group also cleaves relatively efficiently via internal conversion at the crossing of the triplet surfaces. Reaction via  $^1(n\pi^*)$  also occurs since the  $^1(n\pi^*)$  state correlates with a higher singlet electronic state of the products and can then undergo internal conversion and vibrational cascade to the lowest singlet state of products. However, in this case, recombination of the radical pair is very fast if the radicals have been held together in a solvent cage or within the same fragment, as in the case of  $\alpha$ -cleavage of cyclic ketones. The carbonyl ground state correlates with the  $^1D_1$  state of products. This reaction corresponds to thermal cleavage of the  $\alpha$  C—C bond.

## APPENDIX A

---

# DERIVATION OF HARTREE–FOCK THEORY

---

The purpose of this appendix is to give the reader a firm understanding of the requirements for the description of many-electron wave functions, the standard procedures used to obtain energies and wave functions, and the role of one-electron wave functions (orbitals) in the scheme of things. It should be read in parallel with Chapter 2. It provides in as simple a way as possible the theory behind the most straightforward applications of prevailing nonempirical quantum chemistry computer codes such as the GAUSSIAN package of quantum chemistry codes [315]. A brief description of procedures for systematic improvement of the theoretical description and an introduction to the alternative density functional methods are also provided. At the same time, the simplifications which can be made to derive the “empirical or semiempirical MO” methods are placed in proper perspective. More complete descriptions of the theoretical methods used by computational chemists may be found in references 55 and 316.

### ELECTRONIC HAMILTONIAN OPERATOR

The properties of molecules and of intermolecular interactions may be understood by analysis of the solutions of the electronic Schrödinger equation:

$$H^e\Psi = E^e\Psi \quad (\text{A.1})$$

where  $\Psi$  is the *wave function* which describes the distribution of all of the electrons in the presence of the fixed nuclei. The total energy of the electron distribution is  $E^e$ . The *Hamiltonian operator*  $H^e$  is the only known quantity (by virtue of a postulate of quantum mechanics) in equation (A.1). It consists of a set of instructions involving arithmetical operations (addition, subtraction, multiplication, and division) as well as differentiations, which must be carried out on the wave function, and we will derive an



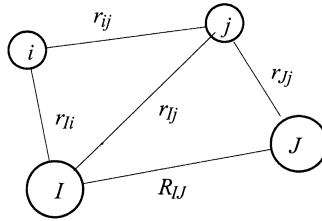


**Figure A.1.** Hypothetical molecule with nuclei  $I, J$  and electrons,  $i, j$  and interparticle separations as shown.

expression for it. The solution of equation (A.1) consists of finding a function of the coordinates of all of the electrons such that after carrying out the Hamiltonian operations, the resulting function is just a constant multiple of the function itself. The constant multiple is the electronic energy  $E^e$ . While no *exact* solution for equation (A.1) exists yet, well-defined procedures have been developed for finding solutions of arbitrary accuracy. We describe these procedures and carry out an approximate solution of the Schrödinger equation, beginning with a definition of  $H^e$ .

The starting point is the classical energy expression for a molecule. A molecule, after all, is just a collection of charged particles (Figure A.1) in motion interacting through electrostatic forces (i.e., obey Newtonian mechanics and Coulomb's law). Thus the potential energy of interaction between any two electrons is  $e^2/r_{ij}$ , where  $r_{ij}$  is the separation between the electrons  $i$  and  $j$  and  $e$  is the electron charge. For any two nuclei  $I$  and  $J$  with atomic numbers  $Z_I$  and  $Z_J$  separated by a distance  $R_{IJ}$ , the interaction potential is  $Z_I Z_J e^2 / R_{IJ}$ . With corresponding labeling, the potential energy of an electron  $i$  with a nucleus  $I$  is  $-Z_I e^2 / r_{Ii}$ . The kinetic energies of the  $i$ th electron and the  $I$ th nucleus in momentum formulation are  $p_i^2 / 2m_e$  and  $P_I^2 / 2M_I$ , respectively, where the electron mass  $m_e$  and the nuclear mass  $M_I$  are assumed constant. We will use the convention that lowercase letters refer to electrons and capital letters refer to nuclei. Thus, for an *isolated system* of  $N_N$  nuclei and  $N_e$  electrons, the classical *nonrelativistic* total energy may be written as the sum of the kinetic energies of the individual particles and the sum of all pairs of interparticle potentials:

$$E = \sum_{i=1}^{N_e} \frac{p_i^2}{2m_e} + \sum_{I=1}^{N_N} \frac{P_I^2}{2M_I} - \sum_{i=1}^{N_e} \sum_{I=1}^{N_N} \frac{Z_I e^2}{r_{Ii}} + \sum_{i=1}^{N_e-1} \sum_{j=i+1}^{N_e} \frac{e^2}{r_{ij}} + \sum_{I=1}^{N_N-1} \sum_{J=I+1}^{N_N} \frac{Z_I Z_J e^2}{R_{IJ}} \quad (\text{A.2})$$

The first two terms of equation (A.2) describe the kinetic energy of the system due to electrons and nuclei, respectively. The last three terms describe the potential energy, given by Coulomb's law, of electron–nuclear attraction, electron–electron repulsion, and nuclear–nuclear repulsion, respectively. Notice that the energy is zero when the particles are infinitely far apart and not moving. Since the ratio of electron to nuclear masses is at least  $\frac{1}{1820}$ , electronic velocities are much higher than nuclear velocities, and it is common practice to invoke the *Born–Oppenheimer (BO) approximation* of stationary nuclei. The BO approximation works because the electronic distribution can respond almost instantaneously (adiabatically) to changes in the nuclear positions. Thus, the second term on the right-hand side of equation (A.2) is zero and the last term is a constant which one

could work out on a calculator since the nuclear coordinate values are known and fixed. The total energy depends on the nuclear coordinates, which we will represent collectively as  $\mathbf{R}$ :

$$E(\mathbf{R}) = \sum_{i=1}^{N_e} \frac{p_i^2}{2m_e} - \sum_{i=1}^{N_e} \sum_{I=1}^{N_N} \frac{Z_I e^2}{r_{iI}} + \sum_{i=1}^{N_e-1} \sum_{j=i+1}^{N_e} \frac{e^2}{r_{ij}} + \sum_{I=1}^{N_N-1} \sum_{J=I+1}^{N_N} \frac{Z_I Z_J e^2}{R_{IJ}} \quad (\text{A.3})$$

The electronic *Hamiltonian operator*  $H^e$  may be derived from the classical energy expression by replacing all momenta  $p_i$  by the derivative operator,  $p_i \Rightarrow -i\hbar\nabla(i) = -i\hbar(\partial/\partial r_i)$ , where the first “ $i$ ” is the square root of  $-1$ . Thus,

$$H^e(\mathbf{R}) = - \sum_{i=1}^{N_e} \frac{\hbar^2}{2m_e} \nabla(i)^2 - \sum_{i=1}^{N_e} \sum_{I=1}^{N_N} \frac{Z_I e^2}{r_{iI}} + \sum_{i=1}^{N_e-1} \sum_{j=i+1}^{N_e} \frac{e^2}{r_{ij}} \quad (\text{A.4})$$

$$= \sum_{i=1}^{N_e} h(i) + \sum_{i=1}^{N_e-1} \sum_{j=i+1}^{N_e} \frac{e^2}{r_{ij}} \quad (\text{A.5})$$

where the one-electron Hamiltonian (core Hamiltonian) for the  $i$ th electron,  $h(i)$ , is given by

$$h(i) = - \frac{\hbar^2}{2m_e} \nabla(i)^2 - \sum_{I=1}^{N_N} \frac{Z_I e^2}{r_{iI}} \quad (\text{A.6})$$

The explicit dependence on  $\mathbf{R}$  is not shown for equation (A.6) and will not be given in subsequent equations, it being understood that unless stated otherwise, we are working within the BO approximation. The Laplacian operator  $\nabla(i)^2$  in Cartesian coordinates for the  $i$ th electron is given by

$$\nabla(i)^2 = \frac{\partial^2}{\partial x_i^2} + \frac{\partial^2}{\partial y_i^2} + \frac{\partial^2}{\partial z_i^2} \quad (\text{A.7})$$

## ELECTRONIC SCHRÖDINGER EQUATION

The total energy of the molecule is the sum of the electronic energy  $E^e$  and the nuclear energy [the last term of equation (A.3)], which is constant within the BO approximation. The electronic energy  $E^e$  must be obtained by solution of the electronic Schrödinger equation (A.1). Unfortunately, no *exact* solution for equation (A.1) exists, except for systems consisting of only one electron. Nevertheless, it can be shown that there are an infinite number of solutions, that is, wave functions  $\Psi_n$  each corresponding to a different distribution of electrons with energy  $E_n^e$ , and that there is a *lowest* energy distribution, which is customarily denoted  $\Psi_0$  with associated energy  $E_0^e$ . Henceforth, the superscript denoting “electronic” will be omitted. Unless stated otherwise, all quantities will be electronic quantities. The sole exception is the total energy of the molecule, which is obtained by adding the constant nuclear energy to the electronic energy.

## EXPECTATION VALUES

It is one of the postulates of quantum mechanics that for every observable quantity  $o$  there is a corresponding operator  $O$  such that an average or *expectation* value of the observable may be obtained by evaluating the expression

$$o = \frac{\int \Psi O \Psi d\tau}{\int \Psi^2 d\tau} \quad (\text{A.8})$$

In equation (A.8),  $\Psi$  is the wave function which describes the distribution of particles in the system. It may be the exact wave function [the solution to equation (A.1)] or a reasonable approximate wave function. For most molecules, the ground electronic state wave function is real, and in writing the expectation value in the form of equation (A.8), we have made this simplifying (though not necessary) assumption. The electronic energy is an observable of the system, and the corresponding operator is the Hamiltonian operator. Therefore, one may obtain an estimate for the energy even if one does not know the exact wave function but only an approximate one,  $\Psi^*$ , that is,

$$E^* = \frac{\int \Psi^* H \Psi^* d\tau}{\int |\Psi^*|^2 d\tau} \quad (\text{A.9})$$

It can be proved that for the ground state,  $E^*$  is always greater than or equal to the exact energy  $E_0$  and that the two are equal only if  $\Psi^* = \Psi_0$ . This fact provides a prescription for obtaining a solution to equation (A.1) which is as accurate as possible. The procedure is called the *variation method* and is as follows: (1) construct a wave function with the correct form to describe the system, building in flexibility in the form of a set of parameters; (2) differentiate  $E^*$  [equation (A.9)] with respect to each of the parameters and set the resulting equation to zero; and (3) solve the resulting set of simultaneous equations to obtain the optimum set of parameters which give the lowest energy (closest to the exact energy). The wave function constructed using these parameters then should be as close to the exact wave function as the original choice of form and parameters allow. The first task is the construction of the wave function.

## MANY-ELECTRON WAVE FUNCTION

The minimum requirements for a many-electron wave function, namely, antisymmetry with respect to interchange of electrons and indistinguishability of electrons, are satisfied by an antisymmetrized sum of products of one-electron wave functions (orbitals),  $\phi(1)$ ,

$$\Phi(1, 2, \dots, N_e) = (N_e!)^{-1/2} \sum_{p=0}^{N_e!-1} (-1)^p P^p [\phi_1(1)\phi_2(2) \cdots \phi_{N_e}(N_e)] \quad (\text{A.10})$$

The term in square brackets is a Hartree product. The numbers in round brackets refer to particular electrons, or more specifically, to the  $x$ ,  $y$ ,  $z$ , and spin coordinates of those

electrons. The subscripts refer to the characteristics of the individual orbital (spatial distribution and spin). There is a different orbital for each of the  $N_e$  electrons. This is required by the Pauli exclusion principle. The Hartree product represents a particular assignment of the electrons to orbitals. Any other assignment of the electrons to the same orbital set is equally likely and must be allowed to preserve indistinguishability of the electrons. The permutation operator  $P$  permutes the coordinates of two electrons, that is, the electrons swap orbitals. Successive powers of  $P$  accomplish other interchanges; even and odd powers accomplish even and odd numbers of interchanges. There are  $N_e!$  possible permutations of  $N_e$  electrons among  $N_e$  orbitals; the sum over  $N_e!$  terms accomplishes this. The antisymmetry requirement for electronic wave functions is satisfied by the factor  $(-1)^p$ . The orbitals form an orthonormal set; that is, for any pair  $\phi_a$  and  $\phi_b$ ,

$$\int \phi_a(1)\phi_b(1) d\tau_1 = \delta_{ab} \quad (\text{A.11})$$

where the integration is over all possible values of the three spatial coordinates  $x$ ,  $y$ , and  $z$  and the "spin coordinate"  $s$  and  $d\tau_1$  represents the volume element  $dx_1 dy_1 dz_1 ds_1$ . The factor  $(N_e!)^{-1/2}$  in equation (A.10) ensures that  $\Phi(1, 2, \dots, N_e)$  is also normalized. Equation (A.10) may be expressed in determinantal form and is often referred to as a determinantal wave function:

$$\Phi(1, 2, \dots, N_e) = (N_e!)^{-1/2} \begin{vmatrix} \phi_1(1) & \phi_2(1) & \phi_3(1) & \cdots & \phi_{N_e}(1) \\ \phi_1(2) & \phi_2(2) & \phi_3(2) & \cdots & \phi_{N_e}(2) \\ \phi_1(3) & \phi_2(3) & \phi_3(3) & \cdots & \phi_{N_e}(3) \\ \vdots & \vdots & \vdots & \ddots & \vdots \\ \phi_1(N_e) & \phi_2(N_e) & \phi_3(N_e) & \cdots & \phi_{N_e}(N_e) \end{vmatrix} \quad (\text{A.12})$$

Equation (A.10) (or (A.12)) has an inherent restriction built into it since other wave functions of the same form are possible if one could select any  $N_e$  orbitals from an infinite number of them rather than the  $N_e$  used in (A.10). One could thus generate an infinite number of determinantal wave functions of the form (A.10), and without approximation, the *exact* wave function  $\Psi(1, 2, \dots, N_e)$  could be expressed as a linear combination of them:

$$\Psi(1, 2, \dots, N_e) = \sum_{a=0}^{\infty} d_a \Phi_a \quad (\text{A.13})$$

## ELECTRONIC HARTREE-FOCK ENERGY

Although in principle an exact solution to the Schrödinger equation can be expressed in the form of equation (A.13), the wave functions  $\Phi_a$  and coefficients  $d_a$  cannot be determined for an infinitely large set. In the *Hartree-Fock approximation*, it is assumed that the summation in equation (A.13) may be approximated by a single term, that is, that the correct wave function may be approximated by a single determinantal wave function  $\Phi_0$ , the first term of equation (A.13). The method of variations is used to determine the

conditions which lead to an optimum  $\Phi_0$ , which will then be designated  $\Phi_{\text{HF}}$ :

$$E_0 = \frac{\int \Phi_0 H \Phi_0 d\tau}{\int |\Phi_0|^2 d\tau} = \int \Phi_0 H \Phi_0 d\tau \quad (\text{A.14})$$

The last equality holds since  $\Phi_0$  is normalized and will be constrained to remain so upon variation of the orbitals. Before we substitute equation (A.10) into equation (A.14), a simplifying observation can be made. Equation (A.10) [and (A.12)] can be expressed in terms of the *antisymmetrizer operator*,  $A$ ,

$$\Phi(1, 2, \dots, N_e) = A[\phi_1(1)\phi_2(2) \cdots \phi_{N_e}(N_e)] \quad (\text{A.15})$$

where

$$A = (N_e!)^{-1/2} \sum_{p=0}^{N_e!-1} (-1)^p P^p \quad (\text{A.16})$$

Our first objective is to derive a simpler expression for the electronic energy. We can do this by using the properties of the antisymmetrizer operator indicated at the right. Thus,

$$\begin{aligned} E_0 &= \int A[\phi_1(1)\phi_2(2) \cdots \phi_{N_e}(N_e)] H A[\phi_1(1)\phi_2(2) \cdots \phi_{N_e}(N_e)] d\tau \\ &= \int \phi_1(1)\phi_2(2) \cdots \phi_{N_e}(N_e) H A^2[\phi_1(1)\phi_2(2) \cdots \phi_{N_e}(N_e)] d\tau \quad [A, H] = 0 \\ &= (N_e!)^{1/2} \int \phi_1(1)\phi_2(2) \cdots \phi_{N_e}(N_e) H A[\phi_1(1)\phi_2(2) \cdots \phi_{N_e}(N_e)] d\tau \quad A^2 = (N_e!)^{1/2} A \\ &= \int \phi_1(1)\phi_2(2) \cdots \phi_{N_e}(N_e) H \sum_{p=0}^{N_e!-1} (-1)^p P^p [\phi_1(1)\phi_2(2) \cdots \phi_{N_e}(N_e)] d\tau \quad (\text{A.17}) \end{aligned}$$

Finally,

$$\begin{aligned} E_0 &= \int \phi_1(1)\phi_2(2) \cdots \phi_{N_e}(N_e) \sum_{i=1}^{N_e} h(i) \sum_{p=0}^{N_e!-1} (-1)^p P^p [\phi_1(1)\phi_2(2) \cdots \phi_{N_e}(N_e)] d\tau \\ &\quad + \int \phi_1(1)\phi_2(2) \cdots \phi_{N_e}(N_e) \sum_{i=1}^{N_e-1} \sum_{j=i+1}^{N_e} \frac{e^2}{r_{ij}} \sum_{p=0}^{N_e!-1} (-1)^p P^p [\phi_1(1)\phi_2(2) \cdots \phi_{N_e}(N_e)] d\tau \quad (\text{A.18}) \end{aligned}$$

Consider the first term in equation (A.18). Specifically, take the term for the  $i$ th electron and the “do-nothing” permutation ( $p = 0$ ):

$$\begin{aligned} &\int \phi_1(1)\phi_2(2) \cdots \phi_{N_e}(N_e) h(i) (-1)^0 P^0 [\phi_1(1)\phi_2(2) \cdots \phi_{N_e}(N_e)] d\tau \\ &= \int \phi_1(1)\phi_2(2) \cdots \phi_{N_e}(N_e) h(i) \phi_1(1)\phi_2(2) \cdots \phi_{N_e}(N_e) d\tau_1 d\tau_2 \cdots d\tau_{N_e} \end{aligned}$$

$$\begin{aligned}
 &= \int \phi_1(1)\phi_1(1) d\tau_1 \int \phi_2(2)\phi_2(2) d\tau_2 \cdots \int \phi_i(i)h(i)\phi_i(i) d\tau_i \cdots \int \phi_{N_e}(N_e)\phi_{N_e}(N_e) d\tau_{N_e} \\
 &= 1 \cdot 1 \cdots \int \phi_i(i)h(i)\phi_i(i) d\tau_i \cdots 1 \\
 &= \int \phi_i(i)h(i)\phi_i(i) d\tau_i \\
 &= h_i
 \end{aligned} \tag{A.19}$$

Notice that, although we focused on the  $i$ th electron, the subscript of  $h$  refers to the particular orbital (i.e., the spatial characteristics of the orbital). Integration over the coordinates of *any* electron with the same distribution would have produced the same result. The quantity  $h_i$  is the sum of the kinetic energy and the potential energy of attraction to all of the nuclei of any electron which has the distribution  $\phi_i$ .

Another permutation, say  $P^k$ , may interchange electrons  $i$  and  $j$ . For that term, the integration becomes

$$\begin{aligned}
 &\int \phi_1(1)\phi_2(2) \cdots \phi_i(i) \cdots \phi_j(j) \cdots \phi_{N_e}(N_e)h(i)(-1)^k P^k[\phi_1(1)\phi_2(2) \cdots \\
 &\quad \phi_i(i) \cdots \phi_j(j) \cdots \phi_{N_e}(N_e)] d\tau \\
 &= - \int \phi_1(1)\phi_2(2) \cdots \phi_i(i) \cdots \phi_j(j) \cdots \phi_{N_e}(N_e)h(i)\phi_1(1)\phi_2(2) \cdots \\
 &\quad \phi_i(j) \cdots \phi_j(i) \cdots \phi_{N_e}(N_e) d\tau_1 d\tau_2 \cdots d\tau_{N_e} \\
 &= - \int \phi_1(1)\phi_1(1) d\tau_1 \int \phi_2(2)\phi_2(2) d\tau_2 \cdots \int \phi_i(i)h(i)\phi_j(i) d\tau_i \cdots \\
 &\quad \int \phi_j(j)\phi_i(j) d\tau_j \cdots \int \phi_{N_e}(N_e)\phi_{N_e}(N_e) d\tau_{N_e} \\
 &= -1 \cdot 1 \cdots \int \phi_i(i)h(i)\phi_j(i) d\tau_i \cdots 0 \cdots 1 \\
 &= 0
 \end{aligned} \tag{A.20}$$

The negative sign in the second line arises because, by construction, all permutations which yield a single interchange of electrons will be generated by an odd power of the permutation operator ( $k$  is odd). The “zero” result arises from the orthogonality of the orbitals [equation (A.11)]. Indeed, all other permutations will give identically zero for the same reason. Since each electron is in a different orbital, the entire first term of equation (A.18) becomes

$$\begin{aligned}
 &\int \phi_1(1)\phi_2(2) \cdots \phi_{N_e}(N_e) \sum_{i=1}^{N_e} h(i) \sum_{p=0}^{N_e!-1} (-1)^p P^p[\phi_1(1)\phi_2(2) \cdots \phi_{N_e}(N_e)] d\tau \\
 &= \sum_{a=1}^{N_e} h_a
 \end{aligned} \tag{A.21}$$

where we have changed the subscript to  $a$  to indicate that the sum now extends over orbitals rather than electrons (although the number of each is the same). It is worthwhile

stating  $h_a$  explicitly using equation (A.6):

$$h_a = \int \phi_a(1) \left( -\frac{\hbar^2}{2m_e} \nabla(1)^2 - \sum_{I=1}^{N_N} \frac{Z_I e^2}{r_{1I}} \right) \phi_a(1) d\tau_1 \quad (\text{A.22})$$

Equation (A.22) is the energy of a single electron with spatial distribution given by the MO  $\phi_a$ . Equation (A.21) is the total “one-electron” contribution to the total electronic energy.

The “two-electron” contribution is derived in the same way from the second term in equation (A.18). Consider an arbitrary pair of electrons,  $i$  and  $j$ , and two permutations, the do-nothing permutation ( $p = 0$ ) and the specific permutation,  $P^p$ , which interchanges just the  $i$ th and  $j$ th electron. For the second permutation,  $p$  is odd and  $(-1)^p$  will yield a minus sign. Thus,

$$\begin{aligned} & \int \phi_1(1)\phi_2(2)\cdots\phi_{N_e}(N_e) \frac{e^2}{r_{ij}} [1 - P_{ij}][\phi_1(1)\phi_2(2)\cdots\phi_{N_e}(N_e)] d\tau \\ &= \int \phi_1(1)\phi_1(1) d\tau_1 \int \phi_2(2)\phi_2(2) d\tau_2 \cdots \iint \phi_i(i)\phi_j(j) \frac{e^2}{r_{ij}} \phi_i(i)\phi_j(j) d\tau_i d\tau_j \cdots \\ & \quad - \int \phi_{N_e}(N_e)\phi_{N_e}(N_e) d\tau_{N_e} - \int \phi_1(1)\phi_1(1) d\tau_1 \int \phi_2(2)\phi_2(2) d\tau_2 \cdots \\ & \quad - \iint \phi_i(i)\phi_j(j) \frac{e^2}{r_{ij}} \phi_i(j)\phi_j(i) d\tau_i d\tau_j \cdots \int \phi_{N_e}(N_e)\phi_{N_e}(N_e) d\tau_{N_e} \\ &= \iint \phi_i(i)\phi_j(j) \frac{e^2}{r_{ij}} \phi_i(i)\phi_j(j) d\tau_i d\tau_j - \iint \phi_i(i)\phi_j(j) \frac{e^2}{r_{ij}} \phi_i(j)\phi_j(i) d\tau_i d\tau_j \\ &= J_{ij} - K_{ij} \end{aligned} \quad (\text{A.23})$$

All other permutations give identically zero terms due to the orthogonality of the orbitals. The total two-electron contribution to the electronic energy is

$$\begin{aligned} & \int \phi_1(1)\phi_2(2)\cdots\phi_{N_e}(N_e) \sum_{i=1}^{N_e-1} \sum_{j=i+1}^{N_e} \frac{e^2}{r_{ij}} \sum_{p=0}^{N_e!-1} (-1)^p P^p [\phi_1(1)\phi_2(2)\cdots\phi_{N_e}(N_e)] d\tau \\ &= \sum_{a=1}^{N_e-1} \sum_{b=a+1}^{N_e} (J_{ab} - K_{ab}) \end{aligned} \quad (\text{A.24})$$

As above, we have changed the subscripts to indicate that the summations run over the orbitals rather than the electrons. The two-electron repulsion integrals  $J_{ab}$  and  $K_{ab}$  are formally defined as

$$J_{ab} = \iint \phi_a(1)\phi_b(2) \frac{e^2}{r_{12}} \phi_a(1)\phi_b(2) d\tau_1 d\tau_2 \quad (\text{A.25})$$

$$K_{ab} = \iint \phi_a(1)\phi_b(2) \frac{e^2}{r_{12}} \phi_a(2)\phi_b(1) d\tau_1 d\tau_2 \quad (\text{A.26})$$

and are the *Coulomb* and *exchange* integrals, respectively. Thus,

$$E_0 = \sum_{a=1}^{N_e} h_a + \frac{1}{2} \sum_{a=1}^{N_e} \sum_{b=1}^{N_e} (J_{ab} - K_{ab}) \quad (\text{A.27})$$

Notice that the restriction on the second sums can be released and the factor of  $\frac{1}{2}$  introduced since  $J_{aa} = K_{aa}$ .

Once the orbitals have been “optimized” (see below) to yield the lowest possible value of the energy [equation (A.27)], the energy will be the Hartree-Fock energy  $E_{\text{HF}}$ . We will call it that from now on.

### VARIATION OF $E_{\text{HF}}$

Variation of  $E_{\text{HF}}$  [equation (A.27)] with respect to variation of the orbitals is formally carried out as

$$\delta E_{\text{HF}} = \sum_{a=1}^{N_e} \delta h_a + \frac{1}{2} \sum_{a=1}^{N_e} \sum_{b=1}^{N_e} (\delta J_{ab} - \delta K_{ab}) = 0 \quad (\text{A.28})$$

where

$$\begin{aligned} \delta h_a &= \int \phi_a(1) h(1) \delta \phi_a(1) d\tau_1 + \int \delta \phi_a(1) h(1) \phi_a(1) d\tau_1 \\ &= 2 \int \delta \phi_a(1) h(1) \phi_a(1) d\tau_1 \end{aligned} \quad (\text{A.29})$$

$$\begin{aligned} \delta J_{ab} &= \iint \delta \phi_a(1) \phi_b(2) \frac{e^2}{r_{12}} \phi_a(1) \phi_b(2) d\tau_1 d\tau_2 + \iint \phi_a(1) \delta \phi_b(2) \frac{e^2}{r_{12}} \phi_a(1) \phi_b(2) d\tau_1 d\tau_2 \\ &+ \iint \phi_a(1) \phi_b(2) \frac{e^2}{r_{12}} \delta \phi_a(1) \phi_b(2) d\tau_1 d\tau_2 + \iint \phi_a(1) \phi_b(2) \frac{e^2}{r_{12}} \phi_a(1) \delta \phi_b(2) d\tau_1 d\tau_2 \\ &= 2 \iint \delta \phi_a(1) \phi_b(2) \frac{e^2}{r_{12}} \phi_a(1) \phi_b(2) d\tau_1 d\tau_2 + 2 \iint \delta \phi_b(1) \phi_a(2) \frac{e^2}{r_{12}} \phi_a(2) \phi_b(1) d\tau_1 d\tau_2 \end{aligned} \quad (\text{A.30})$$

and

$$\begin{aligned} \delta K_{ab} &= \iint \delta \phi_a(1) \phi_b(2) \frac{e^2}{r_{12}} \phi_a(2) \phi_b(1) d\tau_1 d\tau_2 + \iint \phi_a(1) \delta \phi_b(2) \frac{e^2}{r_{12}} \phi_a(2) \phi_b(1) d\tau_1 d\tau_2 \\ &+ \iint \phi_a(1) \phi_b(2) \frac{e^2}{r_{12}} \delta \phi_a(2) \phi_b(1) d\tau_1 d\tau_2 + \iint \phi_a(1) \phi_b(2) \frac{e^2}{r_{12}} \phi_a(2) \delta \phi_b(1) d\tau_1 d\tau_2 \\ &= 2 \iint \delta \phi_a(1) \phi_b(2) \frac{e^2}{r_{12}} \phi_a(2) \phi_b(1) d\tau_1 d\tau_2 + 2 \iint \delta \phi_b(1) \phi_a(2) \frac{e^2}{r_{12}} \phi_b(2) \phi_a(1) d\tau_1 d\tau_2 \end{aligned} \quad (\text{A.31})$$



Note that the collection of terms takes advantage of the *Hermitian* nature of the operators, that is,

$$\iint \phi_a(1)\phi_b(2) \frac{e^2}{r_{12}} \delta\phi_a(2)\phi_b(1) d\tau_1 d\tau_2 = \iint \delta\phi_a(2)\phi_b(1) \frac{e^2}{r_{12}} \phi_a(1)\phi_b(2) d\tau_1 d\tau_2$$

and the indistinguishability of electrons, that is,

$$\iint \delta\phi_a(2)\phi_b(1) \frac{e^2}{r_{12}} \phi_a(1)\phi_b(2) d\tau_1 d\tau_2 = \iint \delta\phi_a(1)\phi_b(2) \frac{e^2}{r_{12}} \phi_a(2)\phi_b(1) d\tau_1 d\tau_2$$

Not all variations of the orbital set are allowed. The variations are subject to the constraint that the orbitals remain orthonormal [equation (A.11)]. Thus, for all pairs of orbitals  $a$  and  $b$ ,

$$\int \delta\phi_a(1)\phi_b(1) d\tau_1 + \int \phi_a(1) \delta\phi_b(1) d\tau_1 = 0 \quad (\text{A.32})$$

Constraints may be imposed on a set of simultaneous linear equations by the method of Lagrangian multipliers. Let the Lagrangian multipliers be  $-\varepsilon_{ab}$ . Therefore, add to equation (A.28) the quantity

$$\sum_{a=1}^{N_e} \sum_{b=1}^{N_e} (-\varepsilon_{ab}) \left[ \int \delta\phi_a(1)\phi_b(1) d\tau_1 + \int \delta\phi_b(1)\phi_a(1) d\tau_1 \right] \quad (\text{A.33})$$

Thus, the complete set of simultaneous equations for the variation are

$$\begin{aligned} 0 = & 2 \sum_{a=1}^{N_e} \int \delta\phi_a(1)h(1)\phi_a(1) d\tau_1 \\ & + \sum_{a=1}^{N_e} \sum_{b=1}^{N_e} \iint \delta\phi_a(1)\phi_b(2) \frac{e^2}{r_{12}} \phi_a(1)\phi_b(2) d\tau_1 d\tau_2 \\ & + \sum_{a=1}^{N_e} \sum_{b=1}^{N_e} \iint \delta\phi_b(1)\phi_a(2) \frac{e^2}{r_{12}} \phi_a(2)\phi_b(1) d\tau_1 d\tau_2 \\ & - \sum_{a=1}^{N_e} \sum_{b=1}^{N_e} \iint \delta\phi_a(1)\phi_b(2) \frac{e^2}{r_{12}} \phi_a(2)\phi_b(1) d\tau_1 d\tau_2 \\ & - \sum_{a=1}^{N_e} \sum_{b=1}^{N_e} \iint \delta\phi_b(1)\phi_a(2) \frac{e^2}{r_{12}} \phi_b(2)\phi_a(1) d\tau_1 d\tau_2 \\ & - \sum_{a=1}^{N_e} \sum_{b=1}^{N_e} \varepsilon_{ab} \int \delta\phi_a(1)\phi_b(1) d\tau_1 - \sum_{a=1}^{N_e} \sum_{b=1}^{N_e} \varepsilon_{ab} \int \delta\phi_b(1)\phi_a(1) d\tau_1 \end{aligned} \quad (\text{A.34})$$

or

$$\begin{aligned}
 0 = & 2 \sum_{a=1}^{N_e} \int \delta\phi_a(1) h(1) \phi_a(1) d\tau_1 \\
 & + 2 \sum_{a=1}^{N_e} \sum_{b=1}^{N_e} \iint \delta\phi_a(1) \phi_b(2) \frac{e^2}{r_{12}} \phi_a(1) \phi_b(2) d\tau_1 d\tau_2 \\
 & - 2 \sum_{a=1}^{N_e} \sum_{b=1}^{N_e} \iint \delta\phi_a(1) \phi_b(2) \frac{e^2}{r_{12}} \phi_a(2) \phi_b(1) d\tau_1 d\tau_2 \\
 & - 2 \sum_{a=1}^{N_e} \sum_{b=1}^{N_e} \varepsilon_{ab} \int \delta\phi_a(1) \phi_b(1) d\tau_1
 \end{aligned} \tag{A.35}$$

In deriving equation (A.35) from equation (A.34), we have made use of the fact that the indices of the sums are arbitrary and have switched  $a$  and  $b$  in the second terms of the last three lines of equation (A.34). We have also adopted without proof the *hermiticity* of the Lagrangian multipliers, that is,  $\varepsilon_{ab} = \varepsilon_{ba}$ . Canceling the 2's and collecting terms yield the result

$$0 = \sum_{a=1}^{N_e} \int d\tau_1 \delta\phi_a(1) \left[ \left( h(1) + \sum_{b=1}^{N_e} [J_b(1) - K_b(1)] \right) \phi_a(1) - \sum_{b=1}^{N_e} \varepsilon_{ab} \phi_b(1) \right] \tag{A.36}$$

where we have introduced the Coulomb and exchange one-electron operators  $J_b(1)$  and  $K_b(1)$ , which are defined by their action, namely,

$$\int \phi_a(1) J_b(1) \phi_a(1) d\tau_1 = \int \phi_a(1) \left( \int \frac{\phi_b(2) \phi_b(2) e^2}{r_{12}} d\tau_2 \right) \phi_a(1) d\tau_1 = J_{ab} \tag{A.37}$$

$$\int \phi_a(1) K_b(1) \phi_a(1) d\tau_1 = \int \phi_a(1) \left( \int \frac{\phi_b(2) \phi_a(2) e^2}{r_{12}} d\tau_2 \right) \phi_b(1) d\tau_1 = K_{ab} \tag{A.38}$$

*Exercise A.1.* Verify by direct substitution of equations (A.37) and (A.38) into equation (A.36) that equations (A.36) and (A.35) are equivalent.

Since the individual variations of the orbitals are linearly independent, equation (A.36) can only be true if the quantity inside the large square brackets is zero for every value of  $a$ , namely

$$\left( h(1) + \sum_{b=1}^{N_e} [J_b(1) - K_b(1)] \right) \phi_a(1) - \sum_{b=1}^{N_e} \varepsilon_{ab} \phi_b(1) = 0 \tag{A.39}$$

Without loss of generality, the set of orbitals may be rotated so that the  $\varepsilon$  matrix becomes diagonal, that is,

$$\left( h(1) + \sum_{b=1}^{N_e} [J_b(1) - K_b(1)] \right) \phi_a(1) - \varepsilon_a \phi_a(1) = 0 \tag{A.40}$$

The quantity in large parentheses is the Fock operator,  $F(1)$ ,

$$F(1) = h(1) + \sum_{b=1}^{N_e} [J_b(1) - K_b(1)] \quad (\text{A.41})$$

Therefore, the condition that the orbitals yield a stationary point (hopefully a minimum) on the energy hypersurface with respect to variations is that the orbitals are eigenfunctions of the Fock operator, with associated orbital energy,  $\varepsilon$ ,

$$F(1)\phi_a(1) = \varepsilon_a\phi_a(1) \quad (\text{A.42})$$

In summary, to obtain a many-electron wave function of the single determinantal form [equation (A.12)] which will give the lowest electronic energy [equation (A.14) or (A.27)], one must use one-electron wave functions (orbitals) which are eigenfunctions of the one-electron Fock operator according to equation (A.42). There are many, possibly an infinite number of, solutions to equation (A.42). We need the lowest  $N_e$  of them, one for each electron, for equation (A.12) [or (A.27)]. When the  $N_e$  MOs of lowest energy satisfy equation (A.42), then  $E_0 \equiv E_{\text{HF}}$  [equation (A.27)] and  $\Phi_0 \equiv \Phi_{\text{HF}}$  [equation (A.12)].

## LCAO SOLUTION OF FOCK EQUATIONS

We must now bite the bullet and specify what form the MOs must have. We expand the MOs as a linear combination of a number of linearly independent functions, the *basis set*:

$$\phi_a(1) = \sum_{i=1}^n \chi_i(1)c_{ia} \quad \phi = \chi\mathbf{c} \text{ (in matrix form)} \quad (\text{A.43})$$

Such an expansion can always be made *without approximation* if the set of functions is mathematically *complete*. We must necessarily use a finite (and therefore incomplete) set. We will discuss the characteristics of the *basis set* below. For now let us take the  $\chi_i$  as known and proceed to determining the expansion *coefficients*  $c_{ia}$ . Substitution of equation (A.43) into equation (A.42) yields

$$F(1) \sum_{i=1}^n \chi_i(1)c_{ia} = \varepsilon_a \sum_{i=1}^n \chi_i(1)c_{ia} \quad (\text{A.44})$$

Multiplication on the left by  $\chi_j$  and integration over the range of the coordinates of the electron give

$$\sum_{i=1}^n \int \chi_j(1)F(1)\chi_i(1) d\tau_1 c_{ia} = \varepsilon_a \sum_{i=1}^n \int \chi_j(1)\chi_i(1) d\tau_1 c_{ia} \quad (\text{A.45})$$

or

$$\sum_{i=1}^n F_{ji}c_{ia} = \sum_{i=1}^n S_{ji}c_{ia}\varepsilon_a \quad (\text{A.46})$$

Equation (A.46) may be cast as a matrix equation

$$\mathbf{F}\mathbf{c} = \mathbf{S}\mathbf{c}\mathbf{e} \quad (\text{A.47})$$

The *overlap matrix*  $\mathbf{S}$  is defined as

$$\mathbf{S}_{ij} = \int \chi_i(1)\chi_j(1) d\tau_1 \quad (\text{A.48})$$

The basis functions are normalized so that  $\mathbf{S}_{ii} = 1$ , but are not orthogonal, that is,  $\mathbf{S}_{ij} \neq 0$  in general.

The *Fock matrix*  $\mathbf{F}$  is given as

$$\begin{aligned} \mathbf{F}_{ij} &= \int \chi_i(1)\mathbf{F}(1)\chi_j(1) d\tau_1 \\ &= \int \chi_i(1) \left[ h(1) + \sum_{b=1}^{N_e} [J_b(1) - K_b(1)] \right] \chi_j(1) d\tau_1 \\ &= \int \chi_i(1)h(1)\chi_j(1) d\tau_1 + \sum_{b=1}^{N_e} \left[ \int \chi_i(1)J_b(1)\chi_j(1) d\tau_1 - \int \chi_i(1)K_b(1)\chi_j(1) d\tau_1 \right] \\ &= \int \chi_i(1)h(1)\chi_j(1) d\tau_1 + \sum_{b=1}^{N_e} \left[ \iint \chi_i(1)\phi_b(2) \frac{e^2}{r_{12}} \phi_b(2)\chi_j(1) d\tau_2 d\tau_1 \right. \\ &\quad \left. - \iint \chi_i(1)\phi_b(2) \frac{e^2}{r_{12}} \chi_j(2)\phi_b(1) d\tau_2 d\tau_1 \right] \quad (\text{A.49}) \end{aligned}$$

To construct the Fock matrix, one must already know the molecular orbitals (!) since the electron repulsion integrals require them. For this reason, the Fock equation (A.47) must be solved iteratively. One makes an initial guess at the molecular orbitals and uses this guess to construct an approximate Fock matrix. Solution of the Fock equations will produce a set of MOs from which a better Fock matrix can be constructed. After repeating this operation a number of times, if everything goes well, a point will be reached where the MOs obtained from solution of the Fock equations are the same as were obtained from the previous cycle and used to make up the Fock matrix. When this point is reached, one is said to have reached *self-consistency* or to have reached a *self-consistent field (SCF)*. In practice, solution of the Fock equations proceeds as follows. First transform the basis set  $\{\chi\}$  into an orthonormal set  $\{\lambda\}$  by means of a unitary transformation (a *rotation in  $n$  dimensions*),

$$\begin{aligned} \lambda_j &= \sum_{i=1}^n \chi_i u_{ij} & \mathbf{S}_{ij}^\lambda &= \int \lambda_i(1)\lambda_j(1) d\tau_1 = \sum_{k=1}^n \sum_{l=1}^n u_{ki} S_{kl}^\chi u_{lj} = \delta_{ij} \\ & & \mathbf{S}^\lambda &= \mathbf{u}^T \mathbf{S}^\chi \mathbf{u} = \mathbf{I} \end{aligned} \quad (\text{A.50})$$

The inverse transformation is given by

$$\begin{aligned} \chi_j &= \sum_{i=1}^n \lambda_i u_{ij}^{-1} & \mathbf{S}_{ij}^\chi &= \int \chi_i(1)\chi_j(1) d\tau_1 = \sum_{k=1}^n \sum_{l=1}^n u_{ki}^{-1} S_{kl}^\lambda u_{lj}^{-1} = \sum_{k=1}^n (u^{-1})_{ik}^T u_{kj}^{-1} \\ & & \mathbf{S}^\chi &= (\mathbf{u}^{-1})^T \mathbf{u}^{-1} \end{aligned} \quad (\text{A.51})$$

Substitution of the reverse transformation into the definition for the Fock matrix yields

$$\mathbf{F}_{ij}^{\lambda} = \int \chi_i(1) F(1) \chi_j(1) d\tau_1 = \sum_{k=1}^n \sum_{l=1}^n (\mathbf{u}^{-1})_{ik}^T \int \chi_k(1) F \chi_l(1) d\tau_1 \mathbf{u}_{lj}^{-1} \quad (\text{A.52})$$

$$\mathbf{F}^{\lambda} = (\mathbf{u}^{-1})^T \mathbf{F}^{\lambda} \mathbf{u}^{-1}$$

Substitution of equations (A.50) and (A.51) into equation (A.46) and multiplication on the left by  $\mathbf{c}^T$  yield

$$\mathbf{F}^{\lambda} \mathbf{c} = \mathbf{S}^{\lambda} \mathbf{c} \mathbf{e} \quad (\text{A.47})$$

$$(\mathbf{u}^{-1})^T \mathbf{F}^{\lambda} \mathbf{u}^{-1} \mathbf{c} = (\mathbf{u}^{-1})^T \mathbf{u}^{-1} \mathbf{c} \mathbf{e} \quad (\text{A.53})$$

$$\mathbf{c}^T (\mathbf{u}^{-1})^T \mathbf{F}^{\lambda} \mathbf{u}^{-1} \mathbf{c} = \mathbf{c}^T (\mathbf{u}^{-1})^T \mathbf{u}^{-1} \mathbf{c} \mathbf{e} \quad (\text{A.54})$$

$$\mathbf{V}^T \mathbf{F}^{\lambda} \mathbf{V} = \mathbf{V}^T \mathbf{V} \mathbf{e} = \mathbf{e} \quad \mathbf{V} = \mathbf{u}^{-1} \mathbf{c} \quad (\text{A.55})$$

Thus the Fock matrix in the  $\lambda$  basis is diagonalized by standard methods to yield the MO energies  $\varepsilon$  and the matrix  $\mathbf{V}$  from which the coefficient matrix  $\mathbf{c}$  may be obtained by  $\mathbf{c} = \mathbf{u}\mathbf{V}$ . There are several ways in which the matrix  $\mathbf{u}$  and its inverse may be determined. The most commonly used is the *symmetric orthogonalization* due to Löwdin, which involves diagonalization of the overlap matrix. We will not discuss this further.

## INTEGRALS

Solution of the Fock equations requires integrals involving the basis functions, either in pairs or four at a time. Some of these we have already seen. The simplest are the *overlap integrals*, stored in the form of the overlap matrix  $\mathbf{S}$ , whose elements are given by equation (A.48) as

$$\mathbf{S}_{ij} = \int \chi_i(1) \chi_j(1) d\tau_1$$

The Fock integrals first encountered in equation (A.45) are constructed from *kinetic energy* integrals, *nuclear-electron attraction* integrals, and *two-electron repulsion* integrals, as follows, continuing from equation (A.49):

$$\begin{aligned} \mathbf{F}_{ij} = & \int \chi_i(1) \left[ \frac{-\hbar^2}{2m} \nabla^2(1) \right] \chi_j(1) d\tau_1 + \int \chi_i(1) \left[ \sum_{I=1}^{N_N} \frac{-Z_I e^2}{r_{1I}} \right] \chi_j(1) d\tau_1 + \sum_{k=1}^n \sum_{l=1}^n \sum_{b=1}^{N_e} c_{kb} c_{lb} \\ & \left[ \iint \chi_i(1) \chi_k(2) \frac{e^2}{r_{12}} \chi_l(2) \chi_j(1) d\tau_2 d\tau_1 - \iint \chi_i(1) \chi_k(2) \frac{e^2}{r_{12}} \chi_j(2) \chi_l(1) d\tau_2 d\tau_1 \right] \end{aligned} \quad (\text{A.56})$$

$$= \mathbf{T}_{ij} + \mathbf{V}_{ij}^{ne} + \sum_{k=1}^n \sum_{l=1}^n \mathbf{P}_{kl} \mathbf{G}_{ijkl} \quad (\text{A.57})$$

The kinetic energy integrals are collected as the matrix  $\mathbf{T}$ , whose elements are defined by

$$\mathbf{T}_{ij} = \frac{-\hbar^2}{2m} \int \chi_i(1) \nabla^2(1) \chi_j(1) d\tau_1 \quad (\text{A.58})$$

The nuclear–electron attraction integrals are collected as the matrix  $\mathbf{V}^{ne}$ , whose elements are defined by

$$\mathbf{V}_{ij}^{ne} = - \sum_{I=1}^{N_N} Z_I e^2 \int \chi_i(1) \frac{1}{r_{1I}} \chi_j(1) d\tau_1 \quad (\text{A.59})$$

The supermatrix  $\mathbf{G}$ , which contains the two-electron repulsion integrals, has elements defined by

$$\mathbf{G}_{ijkl} = \iint \chi_i(1) \chi_k(2) \frac{e^2}{r_{12}} \chi_l(2) \chi_j(1) d\tau_2 d\tau_1 - \iint \chi_i(1) \chi_k(2) \frac{e^2}{r_{12}} \chi_j(2) \chi_l(1) d\tau_2 d\tau_1 \quad (\text{A.60})$$

In equation (A.57) we also introduced a useful matrix, the *density matrix*  $\mathbf{P}$ , whose elements are defined by

$$\mathbf{P}_{ij} = \sum_{a=1}^{N_e} c_{ia} c_{ja} \quad (\text{A.61})$$

where the sum runs over all of the occupied MOs. One of the limiting factors in ab initio MO calculations is the computation and possibly storage and reading of the two-electron integrals. Their number is approximately proportional to  $n^4$ , where  $n$  is the size of the basis set. It is highly desirable to keep  $n$  as small as possible! Much care must be taken in the choice of basis set. The choice of basis set has been called the *original sin* of computational quantum chemistry.

## THE BASIS SET (STO-3G, 6-31G\*, AND ALL THAT)

The requirement that the basis functions should describe as closely as possible the correct distribution of electrons in the vicinity of nuclei is easily satisfied by choosing hydrogen-like atom wave functions,  $\eta$ , the solutions to the Schrödinger equation for one-electron atoms for which exact solutions are available:

$$\eta_j(1) = N_j^\eta f(r_{1I}, \theta, \phi) e^{-\zeta_j r_{1I}} \quad (\text{A.62})$$

Unfortunately, the exponential radial dependence of the hydrogenic functions makes the evaluation of the necessary integrals exceedingly difficult and time consuming for general computation, and so another set of functions is now universally adopted. These are *Cartesian Gaussian functions* centered on nuclei. Thus,  $g_j(1)$  is a function centered on atom  $I$ :

$$g_j(1) = N_j (x_1 - X_I)^{n_x} (y_1 - Y_I)^{n_y} (z_1 - Z_I)^{n_z} e^{-a_j r_{1I}^2} \quad (\text{A.63})$$

The superscripts,  $n_x$ ,  $n_y$ , and  $n_z$ , are simple positive integers or zero. Their values determine whether the function is  $s$ -type ( $n_x = n_y = n_z = 0$ ),  $p$ -type ( $n_x + n_y + n_z = 1$  in three

**TABLE A.1. The STO-3G Basis Set Corresponding to an STO Exponent of Unity**

$\alpha_{1s}$	$d_{1s}$	$\alpha_{2sp}$	$d_{2s}$	$d_{2p}$
0.109818	0.444635	0.0751386	0.700115	0.391957
0.405771	0.535328	0.231031	0.399513	0.607684
2.22766	0.154329	0.994203	-0.999672	0.155916

ways),  $d$ -type ( $n_x + n_y + n_z = 2$  in six ways), and so on. Specifically, for a nucleus situated at the origin of coordinates,

$$g_{1s}(1) = \left(\frac{8\alpha^3}{\pi^3}\right)^{1/4} e^{-\alpha r_1^2}$$

$$g_{2p_x}(1) = \left(\frac{128\alpha^5}{\pi^3}\right)^{1/4} x_1 e^{-\alpha r_1^2}$$

$$g_{3d_{xy}}(1) = \left(\frac{2048\alpha^7}{\pi^3}\right)^{1/4} x_1 y_1 e^{-\alpha r_1^2}$$

The correct limiting radial behavior of the hydrogen-like atom orbital is as a simple exponential, as in (A.62). Orbitals based on this radial dependence are called Slater-type orbitals (STOs). Gaussian functions are rounded at the nucleus and decrease faster than desirable (Figure 2.2*b*). Therefore, the actual basis functions are constructed by taking fixed linear combinations of the primitive Gaussian functions in such a way as to mimic exponential behavior, that is, resemble atomic orbitals. Thus

$$\chi_i(1) = \sum_{j=1}^{n_g} g_j(1) d_{ji} \tag{A.64}$$

where all of the primitive Gaussian functions are of the same type and the coefficients  $d_{ji}$  are chosen in such a way that  $\chi$  resembles  $\eta$ , that is, has approximate exponential radial dependence (Figure 2.2*c*).

The STO-nG basis sets are made up this way. Table A.1 gives the STO-3G expansions of STOs of  $1s$ ,  $2s$ , and  $2p$  type, with exponents of unity. To obtain other STOs with other exponents  $\xi$ , one needs only to multiply the exponents of the primitive Gaussians given in Table A.1 by the square of  $\xi$ .

A similar philosophy of *contraction* is applied to the “split-valence” basis sets. More flexibility in the basis set is accomplished by systematic addition of *polarization* functions to the split-valence basis set, usually the 6-31G basis. These are designated 6-31G(d) and 6-31G(d,p). These are described more fully in Chapter 2 and are illustrated in Figure 2.3

## INTERPRETATION OF SOLUTIONS OF HF EQUATIONS

### Orbital Energies and Total Electronic Energy

Solution of the HF equations yields MOs and their associated energies. The energy of  $\phi_a$  is

$$\varepsilon_a = \int \phi_a(1)F(1)\phi_a(1) d\tau_1 = h_a + \sum_{b=1}^{N_e} (J_{ab} - K_{ab}) \quad (\text{A.65})$$

where the integrals  $h_a$ ,  $J_{ab}$ , and  $K_{ab}$  were defined in equations (A.19), (A.25), and (A.26), respectively. The orbital energy is the kinetic energy of a single electron with the distribution specified by the MO, its attraction to all of the nuclei, and its repulsion in an averaged way with all of the other electrons in the molecule. The total electronic energy in terms of the same integrals was defined in equation (A.27) as

$$E_{\text{HF}} = \sum_{a=1}^{N_e} h_a + \frac{1}{2} \sum_{a=1}^{N_e} \sum_{b=1}^{N_e} (J_{ab} - K_{ab})$$

It is clear that

$$E_{\text{HF}} = \sum_{a=1}^{N_e} \varepsilon_a - \frac{1}{2} \sum_{a=1}^{N_e} \sum_{b=1}^{N_e} (J_{ab} - K_{ab}) \quad (\text{A.66})$$

The total electronic energy is not simply the sum of the orbital energies, which by themselves would overcount the electron–electron repulsion.

## RESTRICTED HARTREE–FOCK THEORY

The version of HF theory we have been studying is called *unrestricted* Hartree–Fock (UHF) theory. It is appropriate to all molecules, regardless of the number of electrons and the distribution of electron spins (which specify the electronic state of the molecule). The spin must be taken into account when the exchange integrals are being evaluated since if the two spin orbitals involved in this integral did not have the same spin function,  $\alpha$  or  $\beta$ , the integral value is zero by virtue of the orthonormality of the electron spin functions

$$\int \alpha(1)\alpha(1) d\sigma_1 = \int \beta(1)\beta(1) d\sigma_1 = 1 \quad \int \alpha(1)\beta(1) d\sigma_1 = \int \beta(1)\alpha(1) d\sigma_1 = 0 \quad (\text{A.67})$$

As it happens, if a molecule has the same number of electrons with spin up ( $\alpha$ ) as with spin down ( $\beta$ ), the solution of the HF equations in the vicinity of the equilibrium geometry and for the ground electronic state yields the result that the spatial part of the MOs describing  $\alpha$  and  $\beta$  electrons are equal in pairs. In other words, for the vast majority of molecules ( $\text{F}_2$  is an exception), the HF determinantal wave function may be written as

$$\Phi_{\text{RHF}}(1, 2, 3, \dots, N_e) = (N_e!)^{-1/2} |\phi'_1(1)\alpha(1)\phi'_1(2)\beta(2)\phi'_2(3)\alpha(3) \cdots \phi'_M(N_e)\beta(N_e)| \quad (\text{A.68})$$

which yields the familiar picture of MOs “occupied” by two electrons of opposite spins. Here  $M$  is the number of doubly occupied MOs, that is,  $M = \frac{1}{2}N_e$ . If one reformulates the HF equations and total energy expression for a wave function which must have the form of equation (A.68), then one is doing *restricted* HF (RHF) theory. There are con-



siderable computational advantages to RHF theory, so, unless one has some reason to suspect that the RHF solution is not the lowest energy solution, RHF is the obvious starting point. The RHF electronic energy is

$$E_{\text{RHF}} = 2 \sum_{a=1}^M \varepsilon_a - \sum_{a=1}^M \sum_{b=1}^M (2J_{ab} - K_{ab}) \quad (\text{A.69})$$

and the MO energy is given by

$$\varepsilon_a = \int \phi'_a(1) F(1) \phi'_a(1) d\tau_1 = h_a + \sum_{b=1}^M (2J_{ab} - K_{ab}) \quad (\text{A.70})$$

Alternative formulations of the total RHF electronic energy are

$$E_{\text{RHF}} = 2 \sum_{a=1}^M h_a + \sum_{a=1}^M \sum_{b=1}^M (2J_{ab} - K_{ab}) \quad (\text{A.71})$$

and

$$E_{\text{RHF}} = \sum_{a=1}^M (h_a + \varepsilon_a) \quad (\text{A.72})$$

Notice that the energy of the HF determinantal wave function, equation (A.68), and for that matter for any single determinantal wave function, can be written by inspection: Each spatial orbital contributes  $h_a$  or  $2h_a$  according to its occupancy, and each orbital contributes  $2J - K$  in its interaction with every other molecular orbital. Thus, the energy of the determinant for the molecular ion,  $M^+$ , obtained by removing an electron from orbital  $o$  of the RHF determinant, is given as

$$\begin{aligned} \Phi_{\text{RHF}}^{M^+}(1, \dots, N_e - 1) \\ = [(N_e - 1)!]^{-1/2} |\phi'_1(1)\alpha(1)\phi'_1(1)\beta(1) \cdots \\ \phi'_o(o)\alpha(o)\phi'_{o+1}(o+1)\alpha(o+1) \cdots \phi'_M(N_e - 1)\beta(N_e - 1)| \end{aligned} \quad (\text{A.73})$$

is given by

$$E_{\text{RHF}}^{M^+} = 2 \sum_{a \neq o}^M h_a + h_o + \sum_{a \neq o}^M \sum_{b \neq o}^M (2J_{ab} - K_{ab}) + \sum_{b \neq o}^M (2J_{bo} - K_{bo}) \quad (\text{A.74})$$

The energy of the molecule itself, equation (A.71), could have been written as

$$E_{\text{RHF}}^M = 2 \sum_{a \neq o}^M h_a + 2h_o + \sum_{a \neq o}^M \sum_{b \neq o}^M (2J_{ab} - K_{ab}) + 2 \sum_{b \neq o}^M (2J_{bo} - K_{bo}) + J_{oo} \quad (\text{A.75})$$

Then the energy difference becomes

$$\begin{aligned}
 E_{\text{RHF}}^{\text{M}^+} - E_{\text{RHF}}^{\text{M}} &= -h_o - \sum_{b \neq o}^M (2J_{bo} - K_{bo}) - J_{oo} \\
 &= -h_o - \sum_{b=1}^M (2J_{bo} - K_{bo}) \\
 &= -\varepsilon_o
 \end{aligned} \tag{A.76}$$

Thus the ionization potential corresponding to removal of the electron from occupied MO  $o$  is just the negative of that MO's energy. This observation is known as Koopmans' theorem. One can similarly show that the energy of the lowest unoccupied MO is an estimate of the electron affinity of the molecule. In fact, ionization potentials estimated by Koopmans' theorem are fairly accurate, but the electron affinities calculated this way are much less so.

### MULLIKEN POPULATION ANALYSIS

The Mulliken population analysis is a simple way of gaining some useful information about the distribution of the electrons in the molecule. Let us assume again a UHF wave function:

$$\begin{aligned}
 N_e &= \sum_{a=1}^{N_e} \int \phi_a(1) \phi_a(1) d\tau_1 \\
 &= \sum_{i=1}^n \sum_{j=1}^n \sum_{a=1}^{N_e} c_{ia} c_{ja} \int \chi_i(1) \chi_j(1) d\tau_1 \\
 &= \sum_{i=1}^n \sum_{j=1}^n \mathbf{P}_{ij} \mathbf{S}_{ij} \\
 &= \sum_{i=1}^n P_i \quad \text{where } P_i = \sum_{j=1}^n \mathbf{P}_{ij} \mathbf{S}_{ij}
 \end{aligned} \tag{A.77}$$

$$= \sum_{I=1}^{N_A} P_I \quad \text{where } P_I = \sum_i^I P_i \tag{A.78}$$

In equation (A.77) is defined the atomic orbital population  $P_i$ . Summing all of the  $P_i$  that belong to the same atom,  $I$ , yields the atomic population  $P_I$  [equation (A.78)]. The net charge  $q_I$  on atom  $I$  is just the difference between the nuclear charge  $Z_I$  and the atomic population,

$$q_I = Z_I - P_I \tag{A.79}$$

### DIPOLE MOMENTS

The quantum mechanical dipole moment operator is equivalent to the classical dipole moment due to a collection of point charges,

$$\hat{\mu} = - \sum_{i=1}^{N_e} e r_i + \sum_{I=1}^{N_N} Z_I e R_I \quad (\text{A.80})$$

Notice that in equation (A.80) the dipole moment operator and the distances  $r_i$  and  $R_I$  are vectors which are usually expressed in Cartesian coordinates. The molecular dipole moment within the BO approximation is evaluated as an expectation value [recall equation (A.8)],

$$\begin{aligned} \mu &= \int \Phi_{\text{HF}}(1, 2, \dots, N_e) \hat{\mu} \Phi_{\text{HF}}(1, 2, \dots, N_e) d\tau \\ &= \int \Phi_{\text{HF}}(1, 2, \dots, N_e) \sum_{i=1}^{N_e} e r_i \Phi_{\text{HF}}(1, 2, \dots, N_e) d\tau + \sum_{I=1}^{N_N} Z_I e R_I \\ &= \sum_{a=1}^{N_e} \int \phi_a(1) e r_1 \phi_a(1) d\tau_1 + \sum_{I=1}^{N_N} Z_I e R_I \\ &= \sum_{i=1}^n \sum_{j=1}^n \mathbf{P}_{ij} \int \chi_i(1) e r_1 \chi_j(1) d\tau_1 + \sum_{I=1}^{N_N} Z_I e R_I \end{aligned} \quad (\text{A.81})$$

The derivation of the second line of equation (A.81) follows the same reasoning as was used to obtain the one-electron part of the electronic energy [equation (A.21)], since both  $\mu$  and  $h$  are sums of single-particle operators. The dipole moment integrals over basis functions in the last line of equation (A.81) are easily evaluated. Within the HF approximation, dipole moments may be calculated to about 10% accuracy provided a large basis set is used.

## TOTAL ENERGIES

The total energy is the sum of the total electronic energy and the nuclear–nuclear repulsion,

$$E = E_{\text{HF}} + \sum_{I=1}^{N_N-1} \sum_{J=I+1}^{N_N} \frac{Z_I Z_J e^2}{R_{IJ}} \quad (\text{A.82})$$

Since the second term is constant for a given geometry, the total energy depends on the choice of basis set through the HF energy. This dependence is illustrated in Table 2.1.

## CONFIGURATION ENERGIES

Allen has suggested that the familiar two-dimensional periodic table of the elements has a missing third dimension, with units of energy [108, 317, 318]. In part, he reasons that the elements of the periodic table are grouped according to valence electron configurations by quantum numbers  $n$  and  $l$ , which indicate orbital size and shape but whose primary purpose is to specify energy. It is proposed that the missing third dimension is

the configuration energy (CE) (also previously called *spectroscopic electronegativity* [318]), the average one-electron valence shell energy of a ground state free atom, which may be defined as follows:

$$\text{CE} = \frac{a\varepsilon_s + b\varepsilon_p}{a + b} \quad (\text{A.83})$$

where  $a$  and  $b$  are the occupancies of the valence shell  $s$  and  $p$  orbitals, respectively, and  $\varepsilon_s$  and  $\varepsilon_p$  are the multiplet-averaged  $s$  and  $p$  shell ionization potentials. The latter may be measured spectroscopically or identified by Koopmans' theorem with the atomic orbital energies. For the  $d$ -block transition elements, a parallel definition applies, namely,

$$\text{CE} = \frac{a\varepsilon_s + b\varepsilon_d}{a + b} \quad (\text{A.84})$$

although the occupancy of the  $d$  shell may be difficult to assign. Values of CE closely parallel the established electronegativity scales of Pauling [319] and Allred and Rochow [320]. A comparison of the three electronegativity scales for selected main group elements is presented in Table A.2 [321].

**TABLE A.2. Comparison of Configuration Energy with Electronegativity Scales of Pauling ( $\chi_P$ ) and Allred and Rochow ( $\chi_{A\&R}$ )<sup>a</sup>**

	H							
CE	2.300							
$\chi_P$	2.20							
$\chi_{A\&R}$	2.20							
	Li	Be	B	C	N	O	F	Ne
CE	0.912	1.576	2.051	2.544	3.066	3.610	4.193	4.787
$\chi_P$	0.98	1.57	2.04	2.55	3.04	3.44	3.98	
$\chi_{A\&R}$	0.97	1.47	2.01	2.50	3.07	3.50	4.10	
	Na	Mg	Al	Si	P	S	Cl	Ar
CE	0.869	1.293	1.613	1.916	2.253	2.589	2.869	3.242
$\chi_P$	0.93	1.31	1.61	1.90	2.19	2.58	3.16	
$\chi_{A\&R}$	1.01	1.23	1.47	1.74	2.06	2.44	2.83	
	K	Ca	Ga	Ge	As	Se	Br	Kr
CE	0.734	1.034	1.756	1.994	2.211	2.424	2.685	2.966
$\chi_P$	0.82	1.00	1.81	2.01	2.18	2.55	2.96	
$\chi_{A\&R}$	0.91	1.04	1.82	2.02	2.20	2.48	2.74	
	Rb	Sr	In	Sn	Sb	Te	I	Xe
CE	0.706	0.963	1.656	1.824	1.984	2.158	2.359	2.582
$\chi_P$	0.82	0.95	1.78	1.96	2.05	2.10	2.66	
$\chi_{A\&R}$	0.89	0.99	1.49	1.72	1.82	2.01	2.21	

<sup>a</sup>Ref. 318.

## POST-HARTREE-FOCK METHODS

Although HF theory is useful in its own right for many kinds of investigations, there are some applications for which the neglect of electron correlation or the assumption that the error is constant (and so will cancel) is not warranted. Post-Hartree-Fock methods seek to improve the description of the electron-electron interactions using HF theory as a reference point. Improvements to HF theory can be made in a variety of ways, including the method of *configuration interaction (CI)* and by use of *many-body perturbation theory (MBPT)*. It is beyond the scope of this text to treat CI and MBPT methods in any but the most cursory manner. However, both methods can be introduced from aspects of the theory already discussed.

## CONFIGURATION INTERACTION THEORY

Earlier it was argued that the many-electron wave function (the true solution to the electronic Schrödinger equation) could be expanded in terms of an infinite series of single determinantal wave functions [Equation (A.13)]:

$$\Psi(1, 2, \dots, N_e) = \sum_{a=1}^{\infty} d_a \Phi_a$$

where each of the determinants is of the form [equation (A.85)]

$$\Phi(1, 2, \dots, N_e) = (N_e!)^{-1/2} \begin{vmatrix} \phi_1(1) & \phi_2(1) & \phi_3(1) & \cdots & \phi_{N_e}(1) \\ \phi_1(2) & \phi_2(2) & \phi_3(2) & \cdots & \phi_{N_e}(2) \\ \phi_1(3) & \phi_2(3) & \phi_3(3) & \cdots & \phi_{N_e}(3) \\ \vdots & \vdots & \vdots & \ddots & \vdots \\ \phi_1(N_e) & \phi_2(N_e) & \phi_3(N_e) & \cdots & \phi_{N_e}(N_e) \end{vmatrix} \quad (\text{A.85})$$

differing only in their composition in terms of the MOs. If the MOs form an infinite complete orthonormal set, then so do the determinants constructed from them. The HF equations were solved in a finite basis of dimension,  $n$ , and so yielded  $n$  MOs which form an orthonormal set. Since  $n > N_e$ , ( $> \frac{1}{2}N_e$ , in the case of RHF), the “extra” MOs can be used to generate new determinants from the HF determinant (which is constructed from the  $N_e$  MOs of lowest energy) by replacement of the occupied (in  $\Phi_{\text{HF}}$ ) MOs by empty (“virtual”) MOs. The determinants are called electron *configurations* because they describe the distribution of all of the electrons. A configuration constructed from  $\Phi_{\text{HF}}$  by replacement of a single occupied MO by a virtual MO is called a *singly excited configuration* because one can imagine it arising from the excitation of an electron from an occupied MO to an empty MO. If determinants are constructed from all possible single excitations, the number of singly excited determinants would be  $N_e \times (n - N_e)$ . For example, a calculation on the water molecule with the 6-31G\* basis set would generate 19 MOs and 90 singly excited configurations (70 in an RHF calculation). If one generated the list of determinants from all possible replacements among the set of MOs, the set of configurations so obtained is said to be *complete* and forms a finite complete ortho-

normal set with dimension determined by the number of electrons and the number of MOs. The number,  $n_{\text{CI}}$ , is the same as the number of permutations of  $N_e$  objects among  $n$  bins with no more than one object per bin, namely  $n_{\text{CI}} = n!/N_e!(n - N_e)!$ . The many-electron wave function may be expanded in this finite set in the manner of equation (A.13) to yield a CI wave function,

$$\Psi^{\text{CI}}(1, 2, \dots, N_e) = \sum_{a=1}^{n_{\text{CI}}} d_a \Phi_a \quad (\text{A.86})$$

The variational method is used to find the optimum expansion in terms of the configurations; that is, the energy is expressed as an expectation value as was done in equation (A.9),

$$E^{\text{CI}} = \frac{\int \Psi^{\text{CI}} H \Psi^{\text{CI}} d\tau}{\int |\Psi^{\text{CI}}|^2 d\tau} = \frac{\sum_{a=1}^{n_{\text{CI}}} \sum_{b=1}^{c_{\text{CI}}} d_a d_b \int \Phi_a H \Phi_b d\tau}{\sum_{a=1}^{n_{\text{CI}}} d_a^2} \quad (\text{A.87})$$

and differentiated with respect to each of the coefficients,  $d_a$ , and setting the result equal to zero,

$$\frac{\partial E^{\text{CI}}}{\partial d_a} = 2 \sum_{b=1}^{n_{\text{CI}}} d_b \left( \int \Phi_a H \Phi_b d\tau - E^{\text{CI}} \delta_{ab} \right) = 0 \quad (\text{A.88})$$

The set of  $n_{\text{CI}}$  linear equations must then be solved for the energies and coefficients. This is accomplished by diagonalization of the *Hamiltonian matrix*  $\mathbf{H}$ , whose elements are defined by

$$\mathbf{H}_{ab} = \int \Phi_a H \Phi_b d\tau \quad (\text{A.89})$$

The elements of the Hamiltonian matrix can be expressed in terms of the MO energies and core, Coulomb, and exchange integrals between the MOs involved in the “excitations” which generated each configuration. The eigenvalues of  $\mathbf{H}$  are the energies of different electronic states, the lowest energy being the energy of the ground state. Matrix diagonalization is a straightforward procedure for small matrices but is a formidable task for large matrices. Techniques exist to extract the lowest few eigenvalues of large matrices, but in practice, complete CI calculations cannot be carried out except for the smallest molecules and some systematic selection procedure to reduce the size of  $n_{\text{CI}}$  must be used. It can be shown that most of the correlation error in HF theory, namely that associated with pairs of electrons in the same orbital, may be corrected if one includes in the CI calculation all singly and doubly excited configurations (SDCI). GAUSSIAN codes [315] will perform SDCI if asked. The truncation of the CI expansion introduces an anomaly called a *size consistency* error. In other words, the sum of the (for example) SDCI energies for A and B calculated separately are not *exactly* the same as the SDCI energy of A and B handled as a single system. The size consistency error in SDCI is usually small and largely corrected by addition of the effects of some quadruple excitations by the *Davidson correction* [322]. The correlation errors of most ground-state

calculations are largely corrected by SDCI calculation with the Davidson correction. The computational time involved is approximately proportional to  $n^6$ .

## EXCITED STATES FROM CI CALCULATIONS

Excited-state energies and wave functions are automatically obtained from CI calculations. However, the quality of the wave functions is more difficult to achieve. The equivalent of the HF description for the ground state requires an all-singles CI (SCI). Singly excited configurations do not mix with the HF determinant, that is,

$$\mathbf{H}_{\text{HF},b} = \int \Phi_{\text{HF}} H \Phi_b^{\text{SE}} d\tau = 0 \quad (\text{Brillouin's theorem}) \quad (\text{A.90})$$

The SCI may provide a very reasonable description for the electronic excitation process and of the excited-state potential energy surface from which to study photochemical processes. The GAUSSIAN suite [315] is the first widely available quantum chemistry program which allows geometry optimization on SCI excited-state potential energy surfaces. A description for an excited state which is equivalent to the SDCI description of the ground state requires all single, all double, and many of the triple excitations. Some of these may be added by perturbation theory in a manner which is beyond the scope of the present approach. Quite accurate electronic transition energies and transition dipole and optical rotatory strengths may be calculated at this level of theory.

## MANY-BODY PERTURBATION THEORY

There are many variations of many-body perturbation theories. In this book we will only touch on one of these, the Møller–Plesset (MP) variation of Rayleigh–Schrödinger (RS) perturbation theory. Simply stated, perturbation theories attempt to describe differences between systems, rather than to describe the systems separately and then take the difference. The image is of a reference system which is suddenly subjected to a perturbation. The object is to describe the system in the presence of the perturbation in relation to the unperturbed system. The perturbation may be a real perturbation, such as an electric or magnetic field, electromagnetic radiation, the presence of another molecule or medium, a change in the geometry, and so on, or it may be a conceptual device, such as a system in which the electrons did not interact, the perturbation being the turning on of the electron–electron interaction.

## RAYLEIGH–SCHRÖDINGER PERTURBATION THEORY

If the solutions (energies  $E_n^{(0)}$  and wave functions  $\Psi_n^{(0)}$ ) of the Schrödinger equation for the unperturbed system  $H^{(0)}\Psi_n^{(0)} = E_n^{(0)}\Psi_n^{(0)}$  are known, and the operator form of the perturbation,  $H^p$ , can be specified, the Rayleigh–Schrödinger perturbation theory will provide a description of the perturbed system in terms of the unperturbed system. Thus, for the perturbed system, the SE is

$$H\Psi_n = (H^{(0)} + \lambda H^p)\Psi_n = E_n\Psi_n \quad (\text{A.91})$$

The parameter  $\lambda$  is introduced to keep track of the order of the perturbation series, as will become clear. Indeed, one can perform a Taylor series expansion of the perturbed wave functions and perturbed energies using  $\lambda$  to keep track of the order of the expansions. Since the set of eigenfunctions of the unperturbed SE form a complete and orthonormal set, the perturbed wave functions can be expanded in terms of them. Thus,

$$\Psi_n = \Psi_n^{(0)} + \lambda\Psi_n^{(1)} + \lambda^2\Psi_n^{(2)} + \dots \quad (\text{A.92})$$

$$E_n = E_n^{(0)} + \lambda E_n^{(1)} + \lambda^2 E_n^{(2)} + \dots \quad (\text{A.93})$$

The superscripts in parentheses indicate successive levels of correction. If the perturbation is small, this series will converge. Substitution of equations (A.92) and (A.93) into equation (A.91) and collecting powers of  $\lambda$  yields

$$\begin{aligned} & (H^{(0)} + \lambda H^P)(\Psi_n^{(0)} + \lambda\Psi_n^{(1)} + \lambda^2\Psi_n^{(2)} + \dots) \\ & = (E_n^{(0)} + \lambda E_n^{(1)} + \lambda^2 E_n^{(2)} + \dots)(\Psi_n^{(0)} + \lambda\Psi_n^{(1)} + \lambda^2\Psi_n^{(2)} + \dots) \end{aligned} \quad (\text{A.94})$$

$$\begin{aligned} & (H^{(0)}\Psi_n^{(0)} - E_n^{(0)}\Psi_n^{(0)})\lambda^0 + (H^{(0)}\Psi_n^{(1)} + H^P\Psi_n^{(0)} - E_n^{(0)}\Psi_n^{(1)} - E_n^{(1)}\Psi_n^{(0)})\lambda^1 \\ & + (H^{(0)}\Psi_n^{(2)} + H^P\Psi_n^{(1)} - E_n^{(0)}\Psi_n^{(2)} - E_n^{(1)}\Psi_n^{(1)} - E_n^{(2)}\Psi_n^{(0)})\lambda^2 + \dots = 0 \end{aligned} \quad (\text{A.95})$$

Equation (A.95) is a power series in  $\lambda$  which can only be true if the coefficients in front of each term are individually zero. Thus,

$$H^{(0)}\Psi_n^{(0)} - E_n^{(0)}\Psi_n^{(0)} = 0 \quad (\text{A.96})$$

$$H^{(0)}\Psi_n^{(1)} + H^P\Psi_n^{(0)} - E_n^{(0)}\Psi_n^{(1)} - E_n^{(1)}\Psi_n^{(0)} = 0 \quad (\text{A.97})$$

$$H^{(0)}\Psi_n^{(2)} + H^P\Psi_n^{(1)} - E_n^{(0)}\Psi_n^{(2)} - E_n^{(1)}\Psi_n^{(1)} - E_n^{(2)}\Psi_n^{(0)} = 0 \quad (\text{A.98})$$

Equation (A.96) is just the Schrödinger equation for the unperturbed system. Equation (A.97) is the first-order equation. Multiplying each term of equation (A.97) on the left by  $\Psi_n^0$  and integrating yield

$$\int \Psi_n^{(0)} H^{(0)} \Psi_n^{(1)} d\tau + \int \Psi_n^{(0)} H^P \Psi_n^{(0)} d\tau - \int \Psi_n^{(0)} E_n^{(0)} \Psi_n^{(1)} d\tau - E_n^{(1)} \int |\Psi_n^{(0)}|^2 d\tau = 0 \quad (\text{A.99})$$

Since  $H^{(0)}$  is a Hermitian operator and  $\Psi_n^0$  is an eigenfunction of it, the first and third integrals are equal and cancel, leaving an expression for the first-order correction to the energy,

$$E_n^{(1)} = \int \Psi_n^{(0)} H^P \Psi_n^{(0)} d\tau \quad (\text{A.100})$$

Multiplication of equation (A.97) by  $\Psi_m^0$  ( $m \neq n$ ) and integrating give

$$\int \Psi_m^{(0)} H^{(0)} \Psi_n^{(1)} d\tau + \int \Psi_m^{(0)} H^P \Psi_n^{(0)} d\tau - \int \Psi_m^{(0)} E_n^{(0)} \Psi_n^{(1)} d\tau - E_n^{(1)} \int \Psi_m^{(0)} \Psi_n^{(0)} d\tau = 0 \quad (\text{A.101})$$



The last integral is zero because of the orthogonality of the unperturbed wave functions. Equation (A.101) simplifies to

$$\int \Psi_m^{(0)} \Psi_n^{(1)} d\tau = - \frac{\int \Psi_m^{(0)} H^p \Psi_n^{(0)} d\tau}{E_m^{(0)} - E_n^{(0)}} \quad (\text{A.102})$$

Let the first-order correction to the perturbed wave function be expanded as a linear combination of unperturbed wave functions, that is,

$$\Psi_n^{(1)} = \sum_{l=0}^{\infty} \Psi_l^{(0)} a_{ln} \quad (\text{A.103})$$

Substitution of equation (A.103) into equation (A.102) yields an expression for the expansion coefficient, namely,

$$\sum_{l=0}^{\infty} a_{ln} \int \Psi_m^{(0)} \Psi_l^{(0)} d\tau = a_{mn} = - \frac{\int \Psi_m^{(0)} H^p \Psi_n^{(0)} d\tau}{E_m^{(0)} - E_n^{(0)}} \quad (\text{A.104})$$

Thus, the first-order correction to the zero-order (unperturbed) wave function is obtained by substituting equation (A.104) into equation (A.103) and changing the summation index:

$$\Psi_n^{(1)} = - \sum_{m \neq n}^{\infty} \frac{\int \Psi_m^{(0)} H^p \Psi_n^{(0)} d\tau}{E_m^{(0)} - E_n^{(0)}} \Psi_m^{(0)} \quad (\text{A.105})$$

The diagonal term  $m = n$  is excluded from the summation in equation (A.105) since that wave function is the zero-order term. The summation should converge at some finite value of  $m$  as the energy difference in the denominator becomes large.

It is generally believed that a correction to the energy which is comparable to the first-order correction to the wave function would involve the second-order term  $E_n^{(2)}$ , which may be extracted from the second-order equation (A.98). Multiply every term on the left by  $\Psi_n^0$  and integrate:

$$\begin{aligned} & \int \Psi_n^{(0)} H^{(0)} \Psi_n^{(2)} d\tau + \int \Psi_n^{(0)} H^p \Psi_n^{(1)} d\tau - E_n^{(0)} \int \Psi_n^{(0)} \Psi_n^{(2)} d\tau \\ & - E_n^{(1)} \int \Psi_n^{(0)} \Psi_n^{(1)} d\tau - E_n^{(2)} \int |\Psi_n^{(0)}|^2 d\tau = 0 \end{aligned} \quad (\text{A.106})$$

As before, the first term and the third term are equal and cancel. The fourth term also is zero, as can be verified by substitution of equation (A.105) into it. Thus,

$$E_n^{(2)} = \int \Psi_n^{(0)} H^p \Psi_n^{(1)} d\tau \quad (\text{A.107})$$

Substitution of equation (A.105) into equation (A.107) yields the usual expression for the second-order correction to the energy:

$$E_n^{(2)} = - \sum_{m \neq n}^{\infty} \frac{\left| \int \Psi_m^{(0)} H^p \Psi_n^{(0)} d\tau \right|^2}{E_m^{(0)} - E_n^{(0)}} \quad (\text{A.108})$$

In summary, the wave function correct to first order and the energy correct to second order are

$$\Psi_n = \Psi_n^{(0)} - \sum_{m \neq n} \frac{\int E_m^{(0)} H^p \Psi_n^{(0)} d\tau}{E_m^{(0)} - E_n^{(0)}} \Psi_m^{(0)} \quad (\text{correct to first order}) \quad (\text{A.109})$$

$$E_n = E_n^{(0)} + \int \Psi_n^{(0)} H^p \Psi_n^{(0)} d\tau - \sum_{m \neq n}^{\infty} \frac{\left| \int \Psi_m^{(0)} H^p \Psi_n^{(0)} d\tau \right|^2}{E_m^{(0)} - E_n^{(0)}} \quad (\text{correct to second order}) \quad (\text{A.110})$$

The parameter  $\lambda$  has been embedded in the definition of  $H^p$ . The wave function from perturbation theory [equation (A.109)] is not normalized and must be renormalized. The energy of a truncated perturbation expansion [equation (A.110)] is not variational, and it may be possible to calculate energies lower than “experimental.”

## MØLLER–PLESSET PERTURBATION THEORY

Møller–Plesset perturbation theory (MPPT) aims to recover the correlation error incurred in Hartree–Fock theory for the ground state whose zero-order description is  $\Phi_{\text{HF}}$ . The Møller–Plesset zero-order Hamiltonian is the sum of Fock operators, and the zero-order wave functions are determinantal wave functions constructed from HF MOs. Thus the zero-order energies are simply the appropriate sums of MO energies. The “perturbation” is defined as the difference between the sum of Fock operators and the exact Hamiltonian:

$$\begin{aligned} H^{(0)} &= \sum_{i=1}^{N_e} F(i) \\ &= \sum_{i=1}^{N_e} \left( h(i) + \sum_{b=1}^{N_e} [J_b(i) - K_b(i)] \right) \end{aligned} \quad (\text{A.111})$$

$$H^p = \sum_{i=1}^{N_e-1} \sum_{j=i+1}^{N_e} \frac{1}{r_{ij}} - \sum_{i=1}^{N_e} \sum_{b=1}^{N_e} [J_b(i) - K_b(i)] \quad (\text{A.112})$$

We state without further derivation that the electronic energy corrected to second order in Møller–Plesset perturbation theory,  $E_{\text{MP2}}$ , is

$$\begin{aligned}
 E_{\text{MP2}} = & \sum_{a=1}^{N_e} \varepsilon_a - \frac{1}{2} \sum_{a=1}^{N_e} \sum_{b=1}^{N_e} (J_{ab} - K_{ab}) \\
 & + \frac{1}{4} \sum_{a=1}^{N_e} \sum_{b=1}^{N_e} \sum_{u=N_e+1}^n \sum_{v=N_e+1}^n \frac{|\langle ab||uv \rangle|^2}{\varepsilon_a + \varepsilon_b - \varepsilon_u - \varepsilon_v}
 \end{aligned} \tag{A.113}$$

where the notation  $\langle ab||uv \rangle$  means

$$\begin{aligned}
 \langle ab||uv \rangle = & \iint \phi_a(1)\phi_b(2) \frac{1}{r_{12}} \phi_u(1)\phi_v(2) d\tau_1 d\tau_2 \\
 & - \iint \phi_a(1)\phi_b(2) \frac{1}{r_{12}} \phi_v(1)\phi_u(2) d\tau_1 d\tau_2
 \end{aligned} \tag{A.114}$$

Notice that the first two terms correspond to the Hartree–Fock energy, equation (A.66). The last term is the sum of all doubly excited configurations.

## DENSITY FUNCTIONAL THEORY

In 1964 Hohenburg and Kohn proved that the ground-state energy of a molecule is uniquely determined by the electronic density [46], supporting earlier formulations, notably by Slater [323], in which the energy of a system was expressed as a functional of the density. The electron density-dependent energy could be expressed in terms of a kinetic energy,  $[T_e]$ , a Coulomb energy,

$$E(\rho) = [T_e] + [V_c] + E_{\text{xc}}(\rho) + [V_n] \tag{A.115}$$

$[V_c]$ , an exchange-correlation term,  $E_{\text{xc}}(\rho)$ , and an external potential,  $[V_n]$ , which arises primarily from nuclear–electron attraction but could include extramolecular perturbations, such as electric and magnetic fields. If the electronic wave function were expressed as a determinantal wave function, as in HF theory, then a set of equations functionally equivalent to the HF equations (A.40) emerges [324]. Thus

$$\{h(1) + J(1) + V_{\text{xc}}(1)\}\phi_a(1) - \varepsilon_a\phi_a(1) = 0 \tag{A.116}$$

In the Kohn–Sham equations (A.116) [324, 325], the core Hamiltonian operator  $h(1)$  has the same definition as in HF theory (equation A.6), as does the Coulomb operator,  $J(1)$ , although the latter is usually expressed as

$$J(1) = \int \frac{\rho(2)}{r_{12}} d\tau_2$$

where

$$\rho(2) = \sum_{b=1}^{N_e} \phi_b(2)\phi_b(2)$$

The Kohn–Sham equations are distinguished from the HF equations by the treatment of the “exchange” term, which in principle incorporates electron–electron correlation,

$$V_{xc}(1) = \frac{\partial E_{xc}(\rho)}{\partial \rho} \quad (\text{A.117})$$

Of course, because the exchange term will be different from HF theory, the DFT orbitals will also be different.

An early approximation to  $V_{xc}(1)$  was to assume that it arises from a uniform (homogeneous) electron gas:

$$V_{xc} \approx V_x^{\text{hg}} = -3\alpha \left( \frac{3}{8\pi} \right)^{-1/3} \rho^{-1/3} \quad (\text{A.118})$$

where  $\alpha$  is an empirical constant whose value is approximately 0.7. Use of equation (A.118) is known as the Hartree-Fock-Slater (HFS), or  $X\alpha$  method [323]. The  $X\alpha$  method neglects the correlation part. It is the simplest “local density approximation” (LDA). However, the accepted usage of the term, LDA incorporates a correlation functional of the form

$$E_c^{\text{hg}} = \int \rho(1) \epsilon_c^{\text{hg}}(\rho) d\tau_1 \quad (\text{A.119})$$

where the correlation energy per electron for a homogeneous gas,  $\epsilon_c^{\text{hg}}$ , has been tabulated from accurate calculations, or parametrized [326]. The LDA method is “local” in the sense that the energy depends directly on the local value of the electron density. “Non-local” corrections, which incorporate the gradient of the electron density, have been introduced to both the exchange [327] and correlation [328, 329, 330, 331] functionals. The exact form of the exchange and correlation functionals is not known. Fully correlated ab initio calculations have been used as a guide to modeling these functionals [332].

For most exchange-correlational functionals, the integrations required for their contribution to the total energy or to the Fock-like matrix elements must be evaluated numerically. If integration of the multicenter two-electron integrals required for the Coulomb term can also be avoided by numerical integration techniques, then the principal reason for adopting Gaussian basis sets is obviated. The Amsterdam density functional (ADF) computer program [333] uses the physically more realistic STO basis sets. An additional benefit is that computational time does not scale as  $n^4$ , as required for the evaluation of two-electron integrals, but rather as  $n^3$ , being limited by the time required for matrix diagonalizations. The DFT calculations in a Gaussian basis set are available in GAUSSIAN [315] and elsewhere.

Becke has argued that combination of the HF exchange and critically selected empirical exchange and correlational functionals should provide a very accurate description of the true exchange-correlation part of the energy. A number of such hybrid HF/DFT models, including the popular variant Becke3LYP (or B3LYP) [334], are available in the GAUSSIAN [315] series of programs.

The B3LYP functional form is

$$(1 - a_0)E_X^{\text{LSDA}} + a_0E_X^{\text{HF}} + a_X\Delta E_X^{\text{B88}} + a_C E_C^{\text{LYP}} + (1 - a_C)E_C^{\text{VWN}} \quad (\text{A.120})$$

where the energy terms are the Slater exchange, the HF exchange, Becke’s 1988 exchange functional correction [331], the gradient-corrected correlation functional of Lee et al. [330], and the local correlation functional of Vosko et al. [326], respectively. The values of the coefficients determined by Becke are

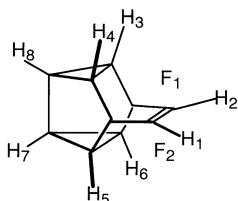
$$a_0 = 0.20 \quad a_X = 0.72 \quad a_C = 0.81$$

## APPENDIX B

# EXERCISES

### Chapter 1

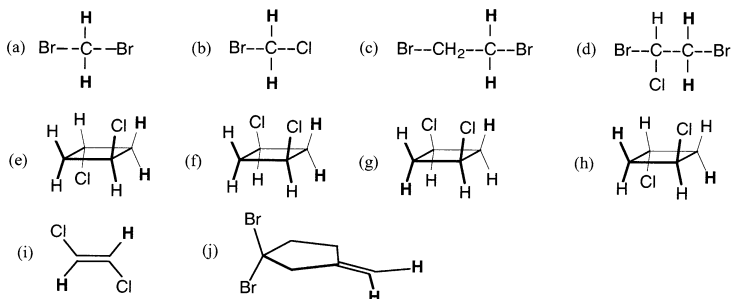
1. The snoutene skeleton is shown below. Locate all of the elements of symmetry (state the point group if you know it), and identify the stereochemical relationship between the specified pairs of groups or faces.



- (a) H<sub>1</sub> and H<sub>2</sub>  
 (b) H<sub>3</sub> and H<sub>4</sub>  
 (c) H<sub>3</sub> and H<sub>5</sub>  
 (d) H<sub>3</sub> and H<sub>6</sub>  
 (e) H<sub>3</sub> and H<sub>7</sub>  
 (f) F<sub>1</sub> and F<sub>2</sub> (faces of the π bond)

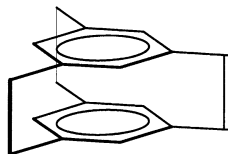
**Answers.** (a) Homotopic; (b) enantiotopic; (c) homotopic; (d) enantiotopic; (e) heterotopic; (f) homotopic.

2. Label the pairs of protons shown in boldface in each of the following compounds as *homotopic*, *enantiotopic*, or *diastereotopic*, as required. Assume normal rotational barriers and observations at room temperature.



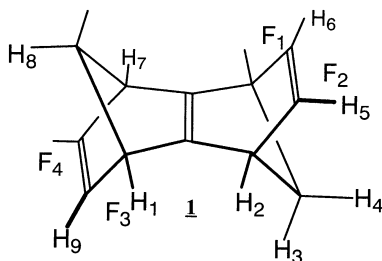
**Answers.** (a) Homotopic; (b) enantiotopic; (c) enantiotopic; (d) diastereotopic; (e) homotopic; (f) diastereotopic; (g) diastereotopic; (h) enantiotopic; (i) homotopic; (j) diastereotopic.

3. The unsaturated [2.2.2](1,3,5)cyclophane, compound C, has been synthesized. (Boekelheide, V.; Hollins, R. A., *J. Am. Chem. Soc.*, **1973**, *95*, 3201.)



COMPOUND C

- (a) Locate all elements of symmetry.  
 (b) Analyze the stereotopic relationships among the hydrogen atoms.  
 (c) Predict and fully assign the  $^1\text{H}$  NMR spectrum.  
 (d) The UV and NMR spectra are unusual in several respects. Can you explain?
4. Analyze the stereochemical relationships between the methyl groups of hexamethyl (Dewar benzene). Identify at least one *pair* of methyl groups in which the methyl groups are homotopic, enantiotopic, diastereotopic, or heterotopic. *Note:* If there are no pairs of a given kind, say so.
5. The following questions deal with the symmetry and spectroscopic relationships of groups within *anti*-sesquinorbornatriene **1**.



- (a) What is the molecular point group? If you cannot remember the name of the point group, locate all elements of symmetry.
- (b) In your answers to the questions, use only those hydrogen atoms or faces which are explicitly labeled (if no groups have the specified relationship, say so). Identify a pair of hydrogen atoms which are:
- (i) Homotopic
  - (ii) Diastereotopic
  - (iii) Enantiotopic
  - (iv) Constitutionally heterotopic

Identify a pair of faces which are:

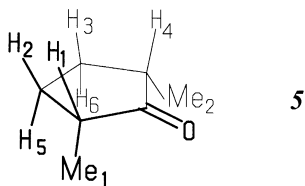
- (v) Homotopic
- (vi) Diastereotopic
- (vii) Enantiotopic

What is the relationship between:

- (viii) H<sub>2</sub> and H<sub>7</sub>?
  - (ix) H<sub>3</sub> and H<sub>8</sub>?
  - (x) H<sub>5</sub> and H<sub>9</sub>?
  - (xi) F<sub>2</sub> and F<sub>3</sub>?
- (c) How many separate <sup>13</sup>C NMR chemical shifts should one observe
- (i) Under *achiral* conditions?
  - (ii) Under *chiral* conditions?
- (d) Replace two H atoms by D in such a way that:
- (i) The only symmetry element is a mirror plane  $\sigma$ .
  - (ii) The only symmetry element is a C<sub>2</sub> axis.
  - (iii) The only symmetry element is a center of inversion  $i$ .
  - (iv) The molecule is asymmetric.

**Answers.** (a) C<sub>2h</sub>; (b) (i) H<sub>1</sub>, H<sub>2</sub>, (ii) H<sub>3</sub>, H<sub>4</sub>, (iii) H<sub>6</sub>, H<sub>9</sub>, (iv) H<sub>1</sub>, H<sub>8</sub>, (v) F<sub>1</sub>, F<sub>3</sub>, (vi) F<sub>1</sub>, F<sub>2</sub>, (vii) none, (viii) enantiotopic, (ix) diastereotopic, (x) homotopic, (xi) diastereotopic; (c) (i) four (uncoupled), (ii) six (uncoupled); (d) (i) H<sub>5</sub>, H<sub>6</sub>, (ii) H<sub>5</sub>, H<sub>9</sub>, (iii) H<sub>6</sub>, H<sub>9</sub>, (iv) H<sub>1</sub>, H<sub>9</sub>.

6. Analyze the stereochemical relationships between the groups of *cis*-2,5-dimethylcyclopentanone **5**. Specifically, identify at least one *pair* of groups for each of the following relationships: homotopic, enantiotopic, diastereotopic, or constitutionally heterotopic. *Note:* if there are no pairs of a given kind, say so.



## Chapter 2 and Appendix A

1. Choose a small molecule and carry out a HF/STO-3G calculation, including a geometry optimization. Repeat, using the B3LYP/6-31G\* level of theory.
  - (a) State the name of the compound and draw a clear representation of its structure, correctly oriented in the coordinate system (standard orientation). What is its molecular point group?
  - (b) Plot the valence MO energy levels, including a few of the unoccupied MOs. Identify the HOMO and LUMO. Make note of the position of the core levels.
  - (c) Sketch the two highest occupied and two lowest unoccupied molecular orbitals on the basis of the STO-3G MO coefficients. Note which atoms have the largest coefficients in each MO. Is there any significance to this? Do the MOs transform according to the irreducible representations of the molecular point group?
  - (d) Comment on the population analysis. Is it reasonable in view of the elemental composition, concepts of electronegativity and resonance, and the molecular symmetry? Compare population analyses for the two levels of theory.

- (e) Find literature references to previous experimental and theoretical work on the compound you chose. Compare the computed properties (geometry, IP, dipole moment, total energy) with experimental and/or other theoretical studies.
- (f) Prepare a 10-min discourse based on the points of the above questions (with a brief introduction) for presentation before the class. Include discussion of the technical aspects of the calculation.
2. Write a one-page essay on the properties and use of *orbitals* in the description of many-electron systems. Your answer should include at least *ten* distinct points. Use of equations is encouraged, but the equations should be verbally interpreted.

**Answer.** Orbitals are one-electron wave functions,  $\phi(1)$ . The fact that electrons are *fermions* requires that each electron be described by a different orbital. The simplest form of a many-electron wave function,  $\Psi(1, 2, \dots, N_e)$ , is a simple product of orbitals (a Hartree product),  $\phi_1(1)\phi_2(2)\phi_3(3) \cdots \phi_{N_e}(N_e)$ . However, the fact that electrons are fermions also imposes the requirement that the many-electron wave function be antisymmetric toward the exchange of any two electrons. All of the physical requirements, including the indistinguishability of electrons, are met by a determinantal wave function, that is, an antisymmetrized sum of Hartree products,  $\Phi(1, 2, 3, \dots, N_e) = |\phi_1(1)\phi_2(2)\phi_3(3) \cdots \phi_{N_e}(N_e)|$ . If  $\Phi(1, 2, 3, \dots, N_e)$  is taken as an approximation of  $\Psi(1, 2, \dots, N_e)$ , i.e., the Hartree–Fock approximation, and the orbitals varied so as to minimize the energy expectation value,

$$E = \frac{\int \Phi H \Phi d\tau}{\int \Phi \cdot \Phi d\tau}$$

where  $H$  is the correct electronic Hamiltonian, one finds that the orbitals must be eigenfunctions of a one-electron operator, the Fock operator  $F(1)$ :

$$F(1)\phi_a(1) = \varepsilon_a\phi_a(1)$$

where  $\varepsilon_a$  is the orbital energy, and

$$F(1) = h(1) + \sum_b^{N_e} [J_b(1) - K_b(1)]$$

In the Fock operator, the “core” Hamiltonian  $h(1)$  does not depend on the orbitals, but the Coulomb and exchange operators  $J_b(1)$  and  $K_b(1)$  depend on  $\phi_b(1)$ . If  $\Phi(1, 2, 3, \dots, N_e)$  is constructed from the lowest energy  $N_e$  orbitals, one has the lowest possible total electronic energy. By Koopmans’ theorem, the negative of the orbital energy is equal to one of the ionization potentials of the molecule or atom.

If one is dealing with a molecule, the orbital is called a molecular orbital (MO) and is constructed as a linear combination of atom-centered basis functions, the coefficients (weights) of which are also determined by application of the variational method to minimize the MO energies.

3. Write one paragraph on the application of the variational principle using each of the following words or phrases in the correct context (not necessarily in the order given; underline each occurrence):



- (a) Schrödinger equation
  - (b) Expectation value
  - (c) CI wave function
  - (d) Single determinantal wave function
  - (e) Hamiltonian matrix
4. Write one paragraph on any aspect of Hartree–Fock theory but incorporate each of the following words or phrases in the correct context (not necessarily in the order given; underline each occurrence):
- (a) Single determinantal wave function
  - (b) Fock operator
  - (c) Molecular orbital energy
  - (d) Exchange integrals
  - (e) Basis set
5. The following questions deal with a specific application of ab initio RHF theory to ethylene ( $C_2H_4$ ).
- (a) Using summation notation, write the electronic nonrelativistic Hamiltonian operator for ethylene.
  - (b) Using any notation which makes it clear, show a single determinantal RHF wave function for ethylene.
  - (c) Assuming that the spatial MOs of part (b) are expanded in a STO-3G basis set:
    - (i) What is the size of the basis set?
    - (ii) Which basis functions are likely to have the largest coefficients in the lowest occupied MO? in the highest occupied MO? Explain briefly.
6. In Hartree–Fock theory, the many-electron wave function is expressed as a single Slater determinant, conveniently abbreviated as

$$\Phi(1, 2, \dots, N_e) = A[\phi_1(1)\phi_2(2) \cdots \phi_{N_e}(N_e)] \quad (1)$$

The molecular orbitals  $\phi_i$  are, by convention, listed in order of increasing energy.

- (a) Why is (1) a satisfactory representation of a many-electron wave function?
- (b) What conditions must be satisfied by the MOs in order that (1) represents the single determinantal wave function of lowest possible energy?
- (c) State some mathematical properties of the MOs (involving integration).
- (d) State some relationships involving the MOs of (1) if (1) were a *restricted* Hartree–Fock wave function.
- (e) The set of MOs are usually expressed as a coefficient matrix. Why?
- (f) Explain the relationship between MO energy, total electronic energy, and total molecular energy (which defines the Born–Oppenheimer potential energy hypersurface).
- (g) Write a single determinantal wave function for the molecular ion,  $M^+$ , in its ground state. What is its energy relative to the energy of (1).
- (h) What are *virtual* or *unoccupied* MOs?

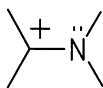
- (i) Write a single determinantal wave function for the molecule in its lowest excited state. What is its energy relative to the energy of (1).  
 (j) Express the permanent dipole moment of a molecule in terms of MOs.

### Chapter 3

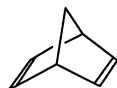
1. Draw a general two-orbital interaction diagram in which the two unperturbed orbitals are of different energy. Label the diagram and indicate relationships which exist between the labeled components.
2. Use a two-orbital interaction diagram to explain or predict some feature of each of the following molecules:



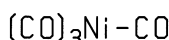
(i)



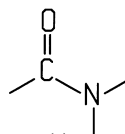
(ii)



(iii)



(iv)



(v)

**Answer to 2(ii).** We note that the structure as drawn has one side which is a carbocation and the other an amine. We should immediately ask whether the presence of the amino group modifies the Lewis acidity of the cationic center using methyl carbocation as a reference and whether the properties of the amine, compared to, for example, ammonia, might be affected by the presence of the cationic site. Amines, like ammonia, have a pyramidal (nonplanar) geometry and are moderately basic. How do the properties of this species compare to these properties which are characteristic of amines? The two ends are connected by a single bond. Single bonds exhibit relatively unhindered rotation and have characteristic lengths and stretching vibrational frequencies. Do these properties compare with those of methylamine, or are they significantly different? Is the C—N bond longer or shorter? Is rotation more or less hindered? Is the C—N stretching frequency higher or lower? All of these questions may be answered using the simple interaction diagram in Figure B3.1, constructed from frontier orbitals of the two interacting fragments, both of which are tricoordinated centers and therefore have only one valence orbital each. On the left-hand side is the empty  $2p$  orbital of the cationic center, and on the right is the nonbonded orbital of the amine, which may also be a  $2p$  orbital if the amine is planar or it may be the  $sp^n$  hybrid orbital of a nonplanar tricoordinated center. What does the diagram tell us? We note immediately that there are two electrons and so the interaction is favorable. The geometry will change in such a way as to maximize the interaction. In other words, the N atom will become planar and one end of the C—N bond will rotate relative to the other to maximize the interaction, bringing both ends into coplanarity. There is appreciable  $\pi$  bond character between the C and the N. Thus the bond will be *shorter* than a typical C—N single bond, as in methylamine. The barrier to torsion about the bond will be substantially *higher*, and the stretching frequency will also be *higher*. In terms of basicity, since the nitrogen lone pair has decreased in energy and the coefficient at N is smaller (it would have been 1 before the interaction), the basicity is less than that of a typical amine. In terms of Lewis acidity, the LUMO is higher in energy than in our reference methyl cation, the coefficient at C is smaller (it also would have been 1 before

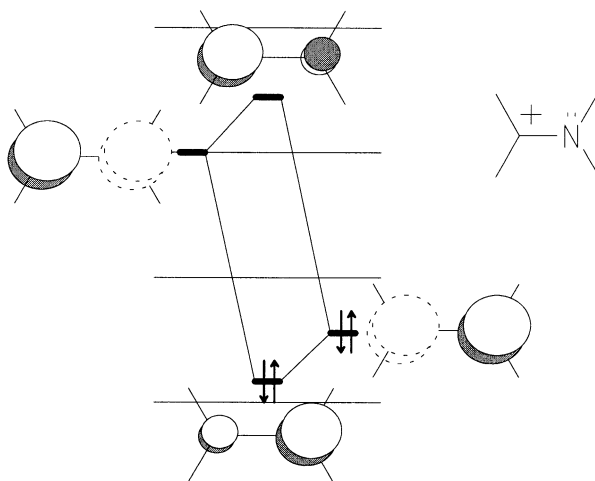
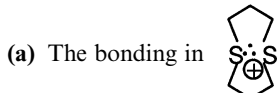


Figure B3.1. Interaction diagram for  $[\text{H}_2\text{C}-\text{NH}_2]^+$ .

the interaction), and the Lewis acidity and electrophilicity will have decreased. By the same token, it is more difficult to reduce (add a electron) than a methyl cation.

3. Use simple orbital interaction diagrams to explain each of the following:

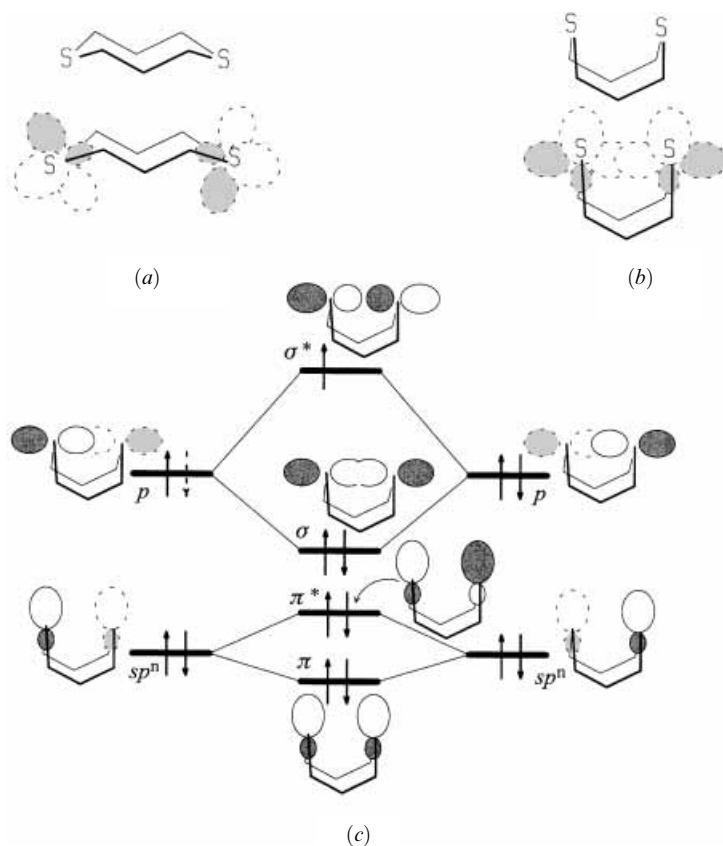


(b) Bonazzola and co-workers (Bonazzola, L.; Michaut, J. P.; Roncin, J., *Can. J. Chem.*, **1988**, *66*, 3050) have shown by ESR spectroscopy that the singly ionized thiirane cation radical,  $[\text{thiirane}]^+$ , forms a 1:1 complex with thiirane itself. Suggest a structure for the complex. *Note:* Thiirane is thiacyclopropane

(c) Hydrazine,  $\text{N}_2\text{H}_4$ , has a dihedral angle close to  $90^\circ$ : For a discus-

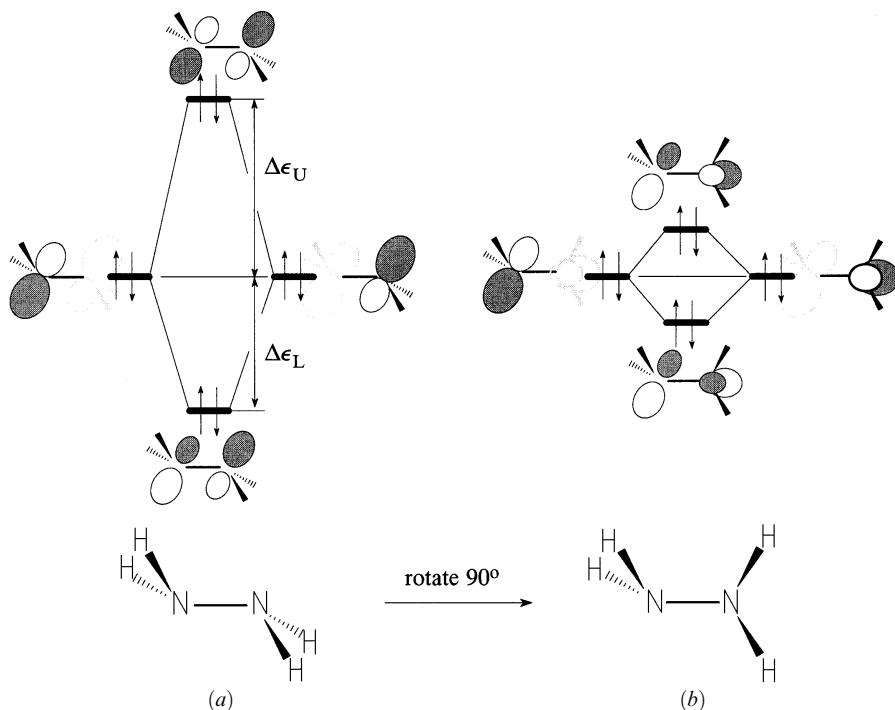
sion of the structures of hydrazines and their ionization potentials, see Klesinger, M.; Rademacher, P., *Angew. Chem. Int. Ed. Engl.*, **1979**, *18*, 826.

**Answer to 3(a).** We are asked here to provide an interaction diagram which will illustrate the nature of the molecular orbitals which contain the three electrons which are involved in binding together the two sulfur atoms. We note that in the absence of an interaction between them, each sulfur atom is a bent dicoordinated atom and as such has two frontier orbitals, a pure  $p$  orbital perpendicular to the plane of the  $\sigma$  bonds to S and an  $sp^n$  hybrid orbital of lower energy directed along the line bisecting the angle made by the  $\sigma$  bonds and in the same plane. In the case of sulfur the  $p$  orbital is  $3p$ , and the  $sp^n$  hybrid has rather little “ $p$ ” character ( $n < 1$ ). To set up the interaction diagram, one must have an appreciation of the limitations imposed by the  $\sigma$  framework, which form an 8-membered ring. Inspection



**Figure B3.2.** 1,5-Dithiacyclooctane: (a) staggered conformation; (b) folded conformation. (c) Interaction diagram in answer to question 3(a) for the bonding in the radical cation.

of molecular models quickly reveals that among the possible conformations of the 8-membered ring are two, as shown in Figures B3.2a and B3.2b, with the valence orbitals superimposed on the molecular skeleton. In the staggered conformation, the sulfur atoms are too far apart to interact. This is the desirable situation in the neutral molecule since all of the nonbonding orbitals are filled and any interaction would be of the four-electron, two-orbital type, which is repulsive. Maximum interaction occurs in the folded conformation (Figure B3.2b). The interaction diagram is shown in Figure B3.2c. The  $sp^n$  orbitals suffer a weak  $\pi$ -type interaction while the  $p$  orbitals interact more strongly in a  $\sigma$  fashion. If one, as in this case, or two electrons [see question 4(b)] are missing, then the interaction is favorable and the cation (or dication) will adopt the folded geometry. The three-electron “bond” has two electrons in the  $\sigma$  orbital and one in the  $\sigma^*$  orbital, for a net attraction. The strength of the three-electron “S—S bond” is approximately 115 kJ/mol (James, M. A.; Illies, A. J., *J. Phys. Chem.*, **1996**, *100*, 15794–15799). A suitable answer to this question could have ignored the weaker interactions of the  $sp^n$  orbitals. Note that diseleno

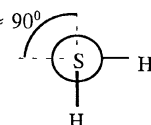



**Figure B3.3.** Interaction diagrams for (a) staggered and (b) perpendicular conformations of hydrazine.

radical cations undergo similar bonding (Cordova-Reyes, I.; Hu, H.; Gu, J.-H.; VandenHoven, E.; Mohammed, A.; Holdcroft, S.; Pinto, B. M., *Can. J. Chem.*, **1996**, *74*, 533–543).

**Answer to 3(c).** Each nitrogen atom of hydrazine is tricoordinated and pyramidal. The frontier valence orbital at each site is an  $sp^2$  hybrid directed along the axis of the trigonal pyramid. Both are doubly occupied, and the two  $sp^2$  orbitals suffer a repulsive four-electron, two-orbital interaction, as shown in Figure B3.3. If the lone-pair orbitals are aligned as shown in Figure B3.3a, the intrinsic interaction is larger because the overlap is larger than in the case depicted in Figure B3.3b, where the two hybrid orbitals are almost perpendicular to each other and therefore overlap less. *Larger overlap is accompanied by a larger difference between  $\Delta\epsilon_U$  and  $\Delta\epsilon_L$ , that is, a larger repulsion.* Therefore, hydrazine adopts the apparently more crowded perpendicular conformation to minimize the repulsive interaction.

- Use *two-orbital* interaction diagrams to explain the *observed* features of the following systems. *Note:* A clear orbital interaction diagram includes pictures of the orbitals before and after the interaction and shows the disposition of the electrons. A brief verbal explanation of the diagram is also desirable. If more than two orbitals seem to be involved, use your judgment to choose the two most important orbitals.

- (a) Hydrogen disulfide,  $S_2H_2$ , has a dihedral angle close to  $90^\circ$ :
- 
- (b) The two sulfur atoms in 1,5-dithiacyclooctyl dication are sufficiently close to say that a bond exists between them [see answer to 3(a)]:
- 
- (c) Ammonia is more basic than phosphine. (*Hint*: Use a proton as the Lewis acid for your answer.)
- (d) The  $NH_2$  group of formamide,  $NH_2CHO$ , is flat, whereas the nitrogen atom of most amines is pyramidal.
- (e) Nucleophilic attack on the carbonyl group of ketones,  $R_2C=O$ , is catalyzed by Lewis acids.

**Answer to 4(c).** The two-orbital interaction diagrams for  $NH_3 + H^+$  and  $PH_3 + H^+$  must be compared (see Figure B3.4). These should be drawn on the same energy scale. Thus the energy of the  $1s$  orbital of  $H$  is at the same level in both diagrams, the nonbonded orbital  $n_N$  of ammonia is lower in energy, and  $n_P$ , the nonbonded orbital of  $PH_3$ , is in between. Because  $P$  is a third-row element, the intrinsic interaction matrix element  $h_{PH}$  will be substantially less than  $h_{NH}$ , and both  $\Delta\epsilon_L$  and  $\Delta\epsilon_U$  will depend on it rather than on the energy difference (see the discussion of the halogens in Chapter 4). Two consequences ensue from the small  $\Delta\epsilon_L$ . The  $P-H$  bond is intrinsically weaker toward both homolytic and heterolytic dissociation. The

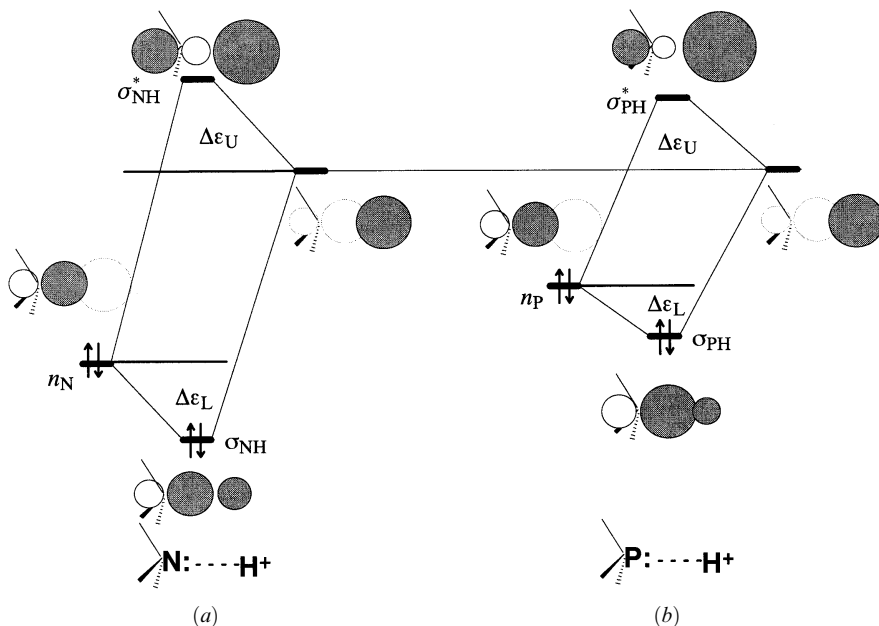


**Figure B3.4.** Two-electron, two-orbital interaction diagrams for (a)  $NH_3 + H^+$  and (b)  $PH_3 + H^+$ .

antibonding orbital  $\sigma_{\text{PH}}^*$  is lower in energy and more polarized than  $\sigma_{\text{NH}}^*$ , as a consequence of which phosphonium ( $\text{PH}_4^+$ ) is more acidic than ammonium ( $\text{NH}_4^+$ ). Both results are consistent with higher basicity for ammonia than phosphine.

**Answer to 4(d).** This question asks us to explain a structural change, pyramidal to planar, that distinguishes the tricoordinated nitrogen atom of amides from amines in general. Structural changes may ensue from a minimization of repulsive interactions (four-electron, two-orbital) and/or maximization of attractive interactions (two-electron, two-orbital). The latter is almost always the case, although question 3(c) dealt with an exception. We therefore adopt a two-electron, two-orbital interaction diagram where the “interacting” fragment orbitals are the LUMO of the carbonyl group and the occupied valence orbital of a neighboring tricoordinated nitrogen. Since one of the interacting orbitals (the carbonyl group orbital) is a complex orbital, the interaction will be treated as coming entirely from the orbitals of the two atoms closest to each other, the N and the C. According to general principles, the LUMO of the C=O group is the  $\pi_{\text{CO}}^*$ , which is polarized toward C (the less electronegative end), and so should interact strongly with the single orbital of N. This is  $p$  if the nitrogen is planar and  $sp^n$  if it is pyramidal. The two situations are depicted in Figures B3.5a and B3.5b. The interaction is more favorable if the overlap is maximized. The  $\pi$ -type overlap is maximized if the two orbitals are both  $p$  orbitals with their axes parallel (Figure B3.5b). As a consequence, the nitrogen becomes planar and the plane of the  $\text{NH}_2$  group coincides with the plane of the carbonyl group. The preceding discussion is sufficient to answer the question of nitrogen planarity. Many other properties of the amide group can be explained on the basis of the same diagram. The amide group is discussed in greater detail in Chapter 8 and a more general interaction diagram is provided there (Figure 8.6a).

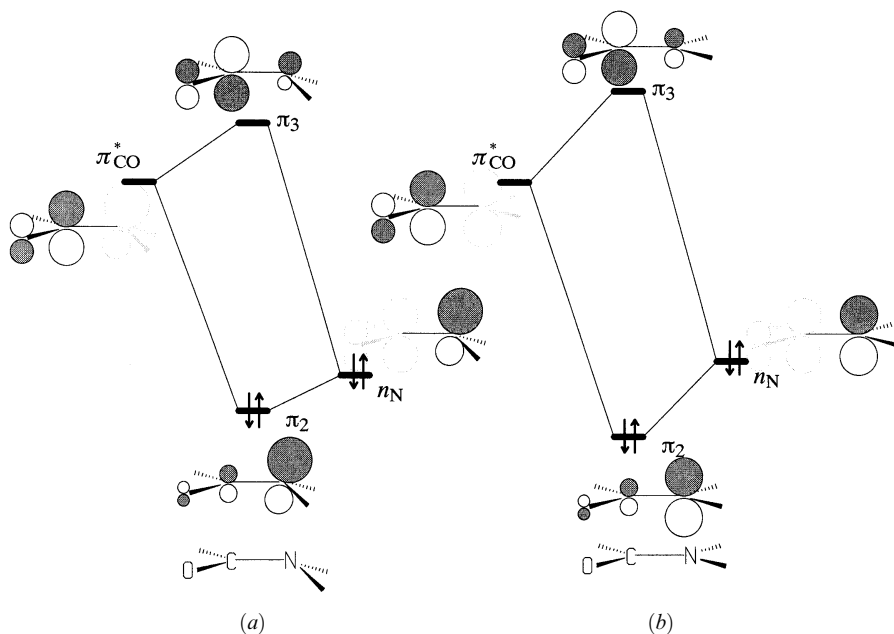


**Figure B3.5.** Two-electron, two-orbital interaction diagrams for (a) pyramidal N and (b) planar N.

5. Rohlfling and Hay recently determined the geometry of FOOF, the fluoro analog of hydrogen peroxide (Rohlfling, C. M.; Hay, P. J., *J. Chem. Phys.*, **1987**, *86*, 4518–4522). The geometry is unusual in three respects: (a) the O—F bonds are unusually long (1.575 Å compared to 1.41 Å in most oxyfluorides), (b) the O—O bond is unusually short (1.217 Å compared to 1.42 Å in HOOH), and (c) the FOOF torsion angle is almost 90° (87.5°). Explain all three features.

**Answer.** This question asks us to explain structural features in FOOF which are unusual compared to HOOH (or alkyl peroxides for that matter). The underlying reason is the maximization of an attractive two-orbital, two-electron interaction between a nonbonded  $p$  orbital of one oxygen and a low-lying  $\sigma_{\text{OF}}^*$  orbital of the adjacent O—F bond. This interaction is analogous to that exhibited in the anomeric effect in sugars. The interaction is mirrored for the other O—OF pair. The orbital interaction diagram is shown in Figure B3.6. The characteristics of the  $\sigma$  O—F bond may be deduced from the orbital interaction diagram shown in Figure B3.6a. The LUMO is low lying and polarized toward the less electronegative O atom. Since neither O nor F undergoes significant hybridization, the orbitals involved in this bond are essentially  $2p$  orbitals. The dicoordinated oxygen has two valence orbitals, a higher occupied  $2p$  orbital (which is elevated somewhat by being involved in a four-electron, two-orbital interaction with the F atom) and a lower occupied orbital which is formally an  $sp^n$  hybrid, but which in fact is essentially the unhybridized  $2s$  orbital of oxygen. The primary interaction, shown in Figure B3.6b, is between the  $2p$  valence orbitals of oxygen atom ( $n_{\text{O}}$ ) and the adjacent  $\sigma_{\text{OF}}^*$  unoccupied orbital. This

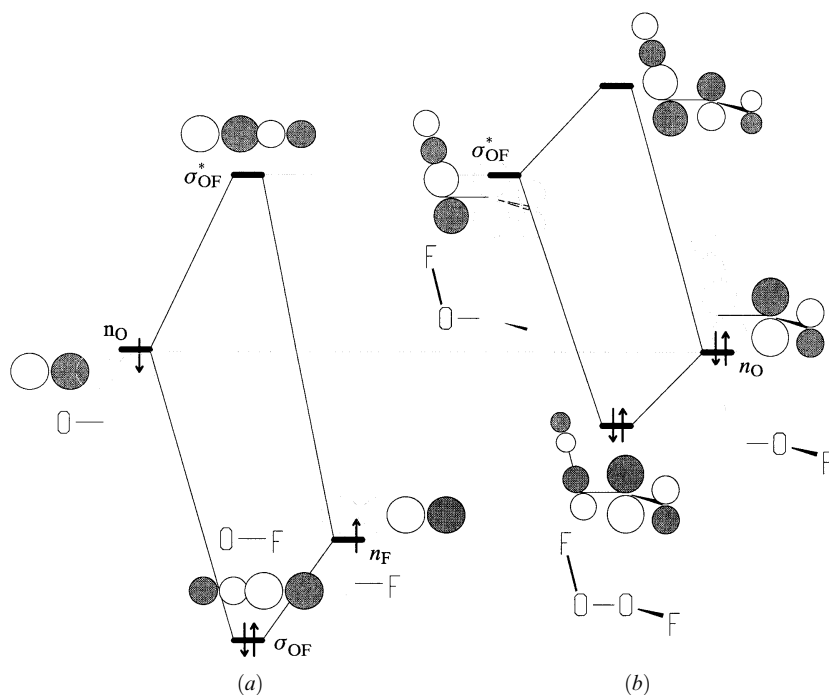
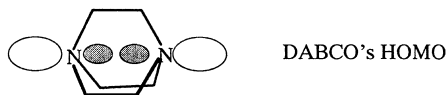


**Figure B3.6.** (a) Two electron, two-orbital interaction diagrams for an O—F bond; (b) two-electron, two-orbital interaction diagram for the donor–acceptor interaction in FOOF.



$\pi$ -type interaction is maximized if the two orbitals are coplanar, that is, if the OF bond is perpendicular to the OOF plane. The occupied orbital that results from the interaction is bonding in the O—O region and antibonding in the O—F region, thus accounting for the shortened O—O separation and the increased OF separation. The interaction is mirrored by the other O—OF pair, and the two pairs of interactions are synergistic, that is, they feed on each other. Transfer of electrons from one end to the other raises the  $n_{\text{O}}$  orbital energy of the acceptor side and lowers the  $\sigma_{\text{OF}}^*$  on the donor side, thereby promoting the back donation of charge.

6. The properties of DABCO (1,4-diazabicyclo[2.2.2]octane) are of considerable interest. The in- and out-of-phase interaction of the two occupied  $sp^3$  hybridized lone pairs on the two nitrogen atoms may be described by an interaction diagram such as shown in Figure 3.5b.



As expected, DABCO is a much stronger base than triethylamine, has two ionization potentials separated by several electron-volts, and is more easily oxidized than trimethylamine. What is unusual about DABCO is that the *in-phase* combination of the nonbonded pairs is the HOMO, the lowest IP is *lower* than that of trimethylamine, and the next higher IP is *higher* than that of trimethylamine. Explain.

**Answer.** This question asks us to explain some unexpected features of a fairly simple molecule. Based on the simplest application of orbital interaction theory, as shown in Figure B3.7a, one would expect the HOMO and HOMO-1 of DABCO to be the out-of-phase ( $a_2''$ ) and in-phase ( $a_1'$ ) combinations of the interacting nitrogen lone pairs, respectively. The reference point may be taken to be the energy of one of the N lone pairs,  $n_{\text{N}}$ , which can also be taken as the energy of the HOMO of trimethylamine, that is, the IP by Koopmans' theorem. Each nitrogen atom is a *pyramidal* tricoordinated atom, and the single remaining valence orbital is an  $sp^n$  hybrid directed away from the point of the pyramid. The two interacting  $sp^n$  hybrid orbitals are pointed away from each other and so will interact only weakly through the smaller back lobes. Nevertheless, one would expect to observe that DABCO has one IP which is lower than that of trimethylamine (ionization from the HOMO) and one which is higher (ionization from the HOMO-1). Everything is as expected until one realizes that the actual symmetries of HOMO and HOMO-1 of DABCO are reversed! The explanation must be that there is a secondary interaction with the C—C sigma bonds which cannot be neglected. This is shown in Figure B3.7b. Because of the threefold symmetry, the three C—C bonding orbitals interact to give three group orbitals, one of which has  $a_1'$  symmetry and a degenerate pair of  $e'$  symmetry. Likewise, the  $\sigma_{\text{CC}}^*$  orbitals combine to form an orbital of symmetry  $a_2''$  and a degenerate pair of symmetry  $e''$ . These are given on the right-hand side of Figure B3.7b, although only the  $a_1'$  and  $a_2''$  combinations are drawn out explicitly. Interaction of the occupied  $a_1'$  combination of  $n_{\text{N}}$  with the occupied  $a_1'$  combination of  $\sigma_{\text{CC}}$  effectively raises the  $a_1' n_{\text{N}}$  combination, mixed out of phase with the  $a_1' \sigma_{\text{CC}}$  combination. At the same time, the occupied  $a_2'' n_{\text{N}}$  combination is lowered by in-phase interaction of the  $a_2'' \sigma_{\text{CC}}^*$  combination, evidently enough to end up below the raised  $a_1'$  orbital. This interaction with the  $\sigma$  bonding orbitals is strong enough to “undo” the weaker primary  $n_{\text{N}}-n_{\text{N}}$  interaction.

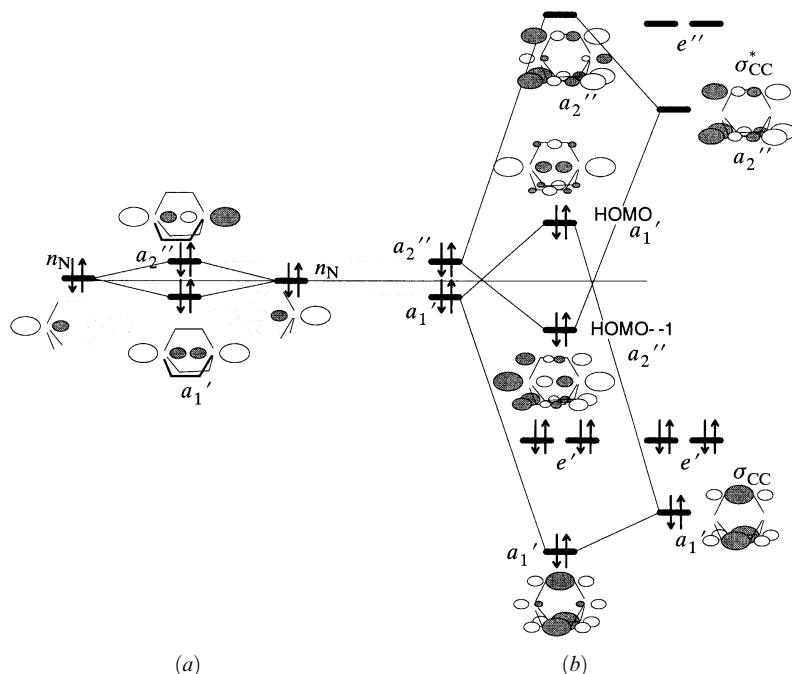


**Figure B3.7.** (a) Four-electron, two-orbital interaction diagram for the N lone pairs,  $n_N$ ; (b) secondary interactions with the in-phase combinations of the C—C  $\sigma$  and  $\sigma^*$  orbitals which reverse the order of the HOMO and HOMO-1. The orbitals symmetries are specified in  $D_{3h}$ .

7. (a) Draw a *two-orbital* interaction diagram for the B—C bond, as in  $\text{H}_2\text{B—CH}_3$ . Label the diagram clearly. Sketch all of the orbitals. Identify the orbitals (e.g.,  $n$ ,  $\pi$ ,  $\pi^*$ ,  $\sigma$ ,  $\sigma^*$ , etc., as appropriate).
- (b) Draw a separate *two-orbital* interaction diagram for  $\text{H}_2\text{B—CH}_3$ , and explain on the basis of the diagram how the presence of the  $\text{BH}_2$  group may serve to acidify a CH bond toward proton donation.
8. Use a *two-orbital* interaction diagram to explain the *observed* feature of any one of the following systems. *Note:* A clear orbital interaction diagram includes pictures of the orbitals before and after the interaction and shows the disposition of the electrons. A brief verbal explanation of the diagram, in addition to the interpretation, is also desirable. If more than two orbitals seem to be involved, use your judgment to choose the two most important orbitals.
  - (a) The barrier to rotation about the C—N bond of formamide,  $\text{NH}_2\text{CHO}$ , is 80 kJ/mol, substantially larger than the value usually found for a C—N single bond, 8 kJ/mol.
  - (b) Reaction of alkenes with  $\text{BrCl}$  proceeds via the intermediate  $[\text{alkene-Br}]^+$  rather than the intermediate  $[\text{alkene-Cl}]^+$ .
  - (c) Ammonia and  $\text{ClF}$  form a 1 : 1 complex in the gas phase. Predict the structure of the donor–acceptor complex.

9. The structure of the radical cation of ethylene,  $[\text{CH}_2\text{CH}_2]^+$ , is not  $D_{2h}$ , like ethylene, but rather  $D_2$ , with a twist of  $25^\circ$  (Merer, A. J.; Schoonveld, L., *Can. J. Phys.*, **1969**, *47*, 1731. See also (a) Köppel, H.; Domcke, W.; Cederbaum, L. S.; von Niessen, W., *J. Chem. Phys.*, **1978**, *69*, 4252–4263. (b) Eriksson, L. A.; Lunell, S.; Boyd, R. J., *J. Am. Chem. Soc.*, **1993**, *115*, 6896–6900). The equilibrium geometry of the  $\pi-\pi^*$  state of ethylene has  $D_{2d}$  symmetry. Explain, in terms of orbital interaction theory.
10. Photoexcitation, in orbital terms, can be described as the promotion of a single electron from HOMO to LUMO by the interaction with light. When either *trans*- or *cis*-2-butene is subjected to UV light, the same mixture of *cis* and *trans* isomers results. Explain.

**Answer to 9 and 10.** The orbital interaction diagram for the bonding is shown in Figure B3.8. The geometric changes described for ethylene, its cation radical, and its excited state reinforce our conclusions regarding the effect of overlap, namely that

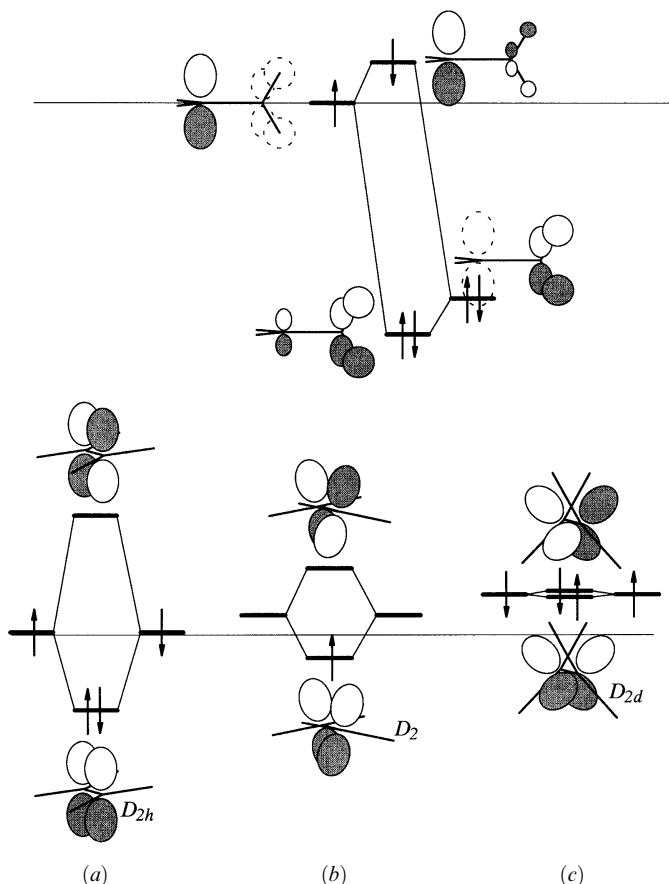


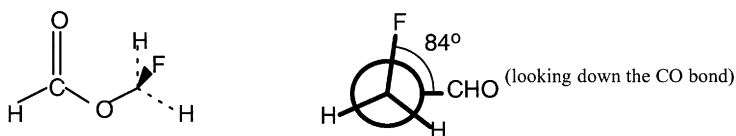
**Figure B3.8.** Interaction diagrams: (a) between  $2p$  orbital with the antisymmetric group orbital of the adjacent  $\text{CH}_2$  group; (b) of  $\pi$  orbitals ethylene in its ground state; (c) of twisted ethylene cation; (d) of the  $\pi-\pi^*$  state of ethylene.

$\Delta\epsilon_U > \Delta\epsilon_L$ . It would be sufficient to explain the change in geometry of the  $\pi$ - $\pi^*$  state on this basis. The  $\pi$ - $\pi^*$  state has one electron in each of the  $\pi$  and  $\pi^*$  orbitals. If the electrons must be separated, it would be energetically better not to have the interaction between the  $\pi$  orbitals so the geometry changes to  $D_{2d}$  where the  $p$  orbitals are at right angles and do not overlap by symmetry (Figure B3.8d). However, if this were the whole story, then the geometry of the ethylene radical cation should also be planar, like ethylene itself. The surprising twisted geometry reveals that a second interaction, forbidden by symmetry in the planar  $D_{2h}$  structure, is turned on as twisting about the C—C bond takes place. This is the interaction between a  $p$  orbital of one C atom with the  $p$ -like group orbital of the adjacent  $\sigma$  bonds which reaches a maximum in the  $90^\circ$   $D_{2d}$  geometry (Figure B3.8a). This interaction occurs at each end (only one is shown in Figure B3.8a). It raises the energy of the  $p$  orbital and is attractive with two or three electrons, although in the latter case, less so than a full-fledged  $\pi$  interaction. Evidently, in the case of the cation radical, the loss of a single electron's worth of  $\pi$  bonding is partially compensated by the interaction with the  $\sigma$  bonds, hence the twisting. The situation in the case of the photoexcited *cis*- or *trans*-2-butene is explained by Figures B3.8b and B3.8d. Both reach the same  $\pi$ - $\pi^*$  state geometry, which deviates slightly from local  $D_{2d}$  symmetry toward the *trans*-2-butene structure because of the steric interaction between the methyl groups. When it reverts to the ground state (both electrons go into the same orbital), more of it becomes *trans* than *cis*. Actually, in pure alkene, isomerism takes second place to another much faster photoreaction, dimerization. This reaction is also readily understood in orbital terms, but discussion of it is reserved until Chapter 14.

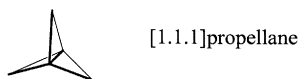
## Chapter 4

- This question deals with the description of a typical dative bond.
  - Draw a *two-orbital* interaction diagram for the B—N bond, as in  $\text{H}_3\text{B}^- - \text{N}^+\text{H}_3$ . Label the diagram clearly.
  - Sketch all of the orbitals. Identify the orbitals (e.g.,  $n, \pi, \pi^*, \sigma, \sigma^*$ , etc., as appropriate).
  - Comment on the polarity of the B—N bond. Why is the boron atom shown with a formal charge of  $-1$ ?
- Reaction of alkenes with BrCl proceeds via the intermediate  $[\text{alkene-Br}]^+$  rather than the intermediate  $[\text{alkene-Cl}]^+$ . Explain using a two-orbital interaction diagram. (The structure of the complex between ethylene and BrCl in the gas phase has been determined by microwave spectroscopy. It is T-shaped, with the BrCl molecule lying perpendicular to the ethylene plane and pointing bromine-end first toward the midpoint of the C=C bond: Legon, A. C.; Bloemink, H. I.; Hinds, K.; Thorn, J. C., *Chem. Eng. News*, **1994** Nov. 7, 26–29.)
- Suggest a reason for the rapid expulsion of atomic bromine upon one-electron reduction of *N*-bromosuccinimide (Lind, J.; Shen, X.; Eriksen, T. E.; Merényi, G.; Ebersson, L., *J. Am. Chem. Soc.*, **1991**, 113, 4629).
- Predict the structures and bonding in donor–acceptor complexes of ammonia with  $\text{F}_2$ ,  $\text{Cl}_2$ , and  $\text{ClF}$ . What are the expected relative bond strengths? Are your predictions in accord with the results of high-level theoretical calculations of Røggen and Dahl (Røggen, I.; Dahl, T., *J. Am. Chem. Soc.*, **1992**, 114, 511)?

5. In the dihalogenated ethanes, 1,2-dichloroethane and 1,2-dibromoethane preferentially adopt the conformation in which the two halogens are anti to each other as expected on the basis of steric repulsions. On the other hand, 1,2-difluoroethane exists predominantly in the gauche conformation (Friesen, D.; Hedberg, K., *J. Am. Chem. Soc.*, **1980**, *102*, 3987). This unexpected behavior has been explained as a manifestation of the *gauche effect* (Wolfe, S., *Acc. Chem. Res.*, **1972**, *5*, 102) from the formation of “bent” bonds (Wiberg, K. B.; Murcko, M. A.; Laidig, K. E.; MacDougall, P. J., *J. Phys. Chem.*, **1990**, *94*, 6956) or as due to hyperconjugative interaction between the C—F and C—H bonds (Radom, L., *Prog. Theor. Org. Chem.*, **1982**, *3*, 1). The last explanation relies on orbital interaction theory. Can you reproduce the arguments?
6. In a microwave investigation, Lopata and Kuczkowski (Lopata, A. D.; Kuczkowski, R. L., *J. Am. Chem. Soc.*, **1981**, *103*, 3304–3309) determined that the equilibrium geometry of FCH<sub>2</sub>—O—CHO was as shown below. Explain the near 90° orientation of the CF bond relative to the plane of the rest of the molecule (the explanation is the same as for the anomeric effect in sugars.)



7. Low-energy electron impact spectroscopy of [1.1.1]propellane reveals an unusually low energy for electron capture to form the radical anion (2.04 eV compared to about 6 eV for most alkanes):



In addition, appreciable lengthening of the interbridgehead C—C bond is indicated (Schafer, O.; Allan, M.; Szeimies, G.; Sanktjohanser, M., *J. Am. Chem. Soc.*, **1992**, *114*, 8180–8186). Can you explain these observations on the basis of orbital interaction theory? Compare your explanation with that offered in the reference.

**Answer.** The orbitals of a normal C—C bond and of the central C—C bond of [1.1.1]propellane are shown in Figures B4.1a and B4.1b, respectively. For both systems, the interacting orbitals are *sp*<sup>n</sup> hybrids at about the same energy. The direction of polarization is dictated by the rest of the  $\sigma$  framework. In the case of the propellane, the hybrid orbitals are pointed away from each other and therefore interact much more weakly, resulting in a much lower  $\sigma^*$  as LUMO. This accounts for the ease of capture of an electron. The anion would have an electron in this orbital, thereby reducing the bond order and weakening the bond further.

8. Solve the HMO equations for the  $\sigma$  orbitals and orbital energies of the C—C and C—O bonds: assume that  $h(O) = h(C) - |h_{CO}|$ ,  $h_{CC} = h_{CO}$ , and  $S_{CO} = 0$ . Sketch the results in the form of an interaction diagram. Which bond is stronger? Calculate the homolytic bond dissociation energies in units of  $|h_{CC}|$ . What is the net charge on O, assuming that it arises solely from the polarization of the  $\sigma$  bond?

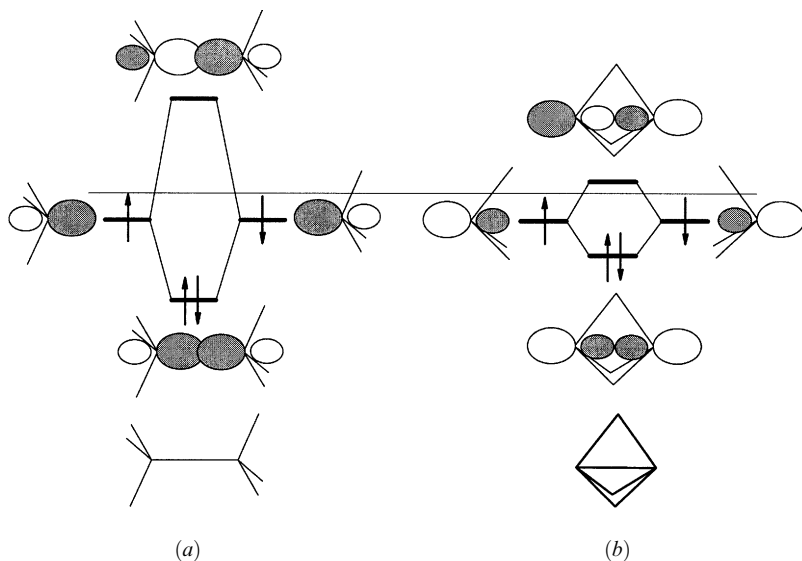


**Figure B4.1.** Interaction diagrams: (a) normal C—C  $\sigma$  bond; (b)  $\sigma$  and  $\sigma^*$  orbitals of central bond of [1.1.1]propellane.

**Answer.**  $E(L) = h_C - 1.618|h_{CO}$ ;  $E(U) = h_C + 0.618|h_{CO}$ ;  $\psi(L) = 0.851 sp^n(O) + 0.526 sp^n(C)$ ;  $\psi(U) = 0.526 sp^n(O) - 0.851 sp^n(C)$ .

(a) Bond energy:  $\alpha(C) + \alpha(O) - 2E(L) = -2.236\beta = 2.236|\beta|$ .

(b) Ionization potential:  $-E(L) = -(\alpha - 1.618\beta) = |\alpha| + 1.618|\beta|$ .

(c) Electronic excitation ( $\pi$ - $\pi^*$ ):  $E(U) - E(L) = -2.236\beta = 2.236|\beta|$ .

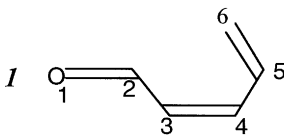
(d) Bond order:  $2(0.851)(0.526) = 0.895$ .

(d) Net charges: on O,  $-2(0.851)^2 + 1 = -0.447$ ; on C,  $-2(0.526)^2 + 1 = +0.447$ .

## Chapter 5

- This question deals with the compound on which you chose to do the SHMO calculation.
  - State the name of the compound and draw a clear representation of its structure.
  - Do a sketch of the energy levels on the usual  $\alpha$ ,  $\beta$  energy scale. Identify the HOMO and LUMO.
  - Sketch the two highest occupied and two lowest unoccupied molecular orbitals.
  - Comment on the Lewis acidity and basicity. Is one expected to dominate in typical chemical reactions? Indicate the probable site(s) of reaction with appropriate reagents (nucleophiles/electrophiles).
  - Give the equation of any reaction of the compound which you have found in the literature or a text book (in either case, cite the reference).
  - Compare known characteristics (reactivity, polarity, color, etc.) of the compound with what you might expect on the basis of the SHMO calculation.

2. The results of an SHMO calculation on (*Z*)-pentadienone, **1**, are given below (*Note*:  $\alpha_{\text{O}} = \alpha - 0.97|\beta|$ ,  $\beta_{\text{CO}} = -1.09|\beta|$ ):



$$\begin{array}{ll}
 \varepsilon_1 = \alpha - 1.968|\beta| & \phi_1 = 0.57p_1 + 0.53p_2 + 0.45p_3 + 0.35p_4 + 0.24p_5 + 0.12p_6 \\
 \varepsilon_2 = \alpha - 1.505|\beta| & \phi_2 = -0.49p_1 - 0.25p_2 + 0.15p_3 + 0.47p_4 + 0.56p_5 + 0.37p_6 \\
 \varepsilon_3 = \alpha - 0.696|\beta| & \phi_3 = 0.45p_1 - 0.12p_2 - 0.55p_3 - 0.27p_4 + 0.37p_5 + 0.52p_6 \\
 \varepsilon_4 = \alpha + 0.265|\beta| & \phi_4 = -0.38p_1 + 0.44p_2 + 0.28p_3 - 0.51p_4 - 0.15p_5 + 0.55p_6 \\
 \varepsilon_5 = \alpha + 1.156|\beta| & \phi_5 = -0.28p_1 + 0.55p_2 - 0.35p_3 - 0.15p_4 + 0.52p_5 - 0.45p_6 \\
 \varepsilon_6 = \alpha + 1.778|\beta| & \phi_6 = -0.15p_1 + 0.38p_2 - 0.52p_3 + 0.56p_4 - 0.45p_5 + 0.25p_6
 \end{array}$$

- Sketch the highest occupied molecular orbital (HOMO) and the lowest unoccupied molecular orbital (LUMO) on the basis of the calculation.
- Assuming that **1** were to react with an electrophile, where is the most likely site of attack? Compare the Lewis basicity of **1** to that of ethylene.
- Assuming that **1** were to react with a nucleophile, where is the most likely site of attack? Compare the Lewis acidity of **1** to that of ethylene.
- In terms of  $|\beta|$ , estimate the energy of the lowest  $\pi-\pi^*$  electronic excitation of **1**. Is the  $\pi-\pi^*$  state likely to be higher or lower than the  $n-\pi^*$  state? Explain in less than three lines.
- Calculate the  $\pi$  bond order of the  $\text{C}_2-\text{C}_3$  bond of **1**. What is the net charge on  $\text{O}_1$ ?
- Show the most likely product from a Diels–Alder reaction of **1** with 1,3-butadiene. Pay attention to all relevant aspects of stereo- and regioselectivity.

**Answer.** There are a number of questions of this type which are primarily concerned with the interpretation of the results of MO calculations and their relationship with the ideas of orbital interaction theory. The data are derived from a calculation using SHMO.

- Pentadienone **1** has six  $\pi$  electrons. A “sketch” of the frontier MOs is shown in Figure B5.1. The relative sizes of the atomic orbital are proportional to the sizes of the MO coefficients and the relative phases are shown by shading. The convention is adopted that a positive signed coefficient corresponds to a  $p$  orbital with the unshaded lobe up and a negative coefficient is portrayed by a  $p$  orbital with the shaded lobe up. The actual convention you use is unimportant, but you must be consistent.
- Attack by an electrophile will be directed to the part of the HOMO which has the largest coefficient, in this case, atom 3. Atom 6 is a close second. Basicity relative to ethylene is governed by the relative energy of the HOMO and by the relative magnitudes of the largest coefficients. The HOMO is substantially higher, suggesting greater basicity, but the largest coefficient (0.55) is smaller

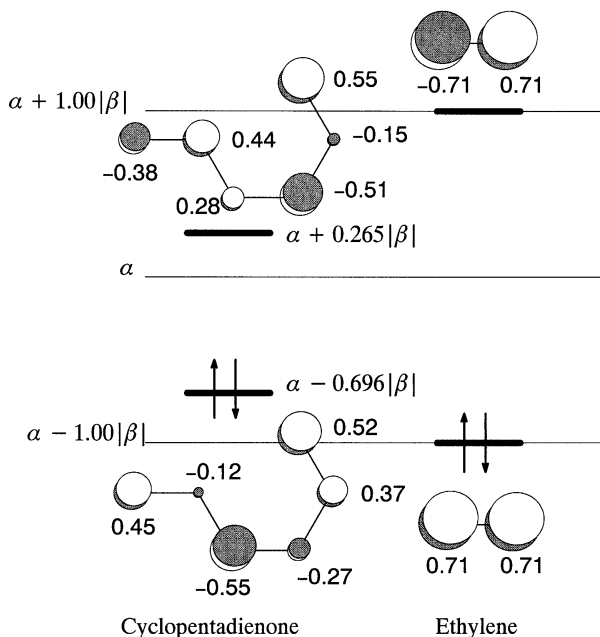


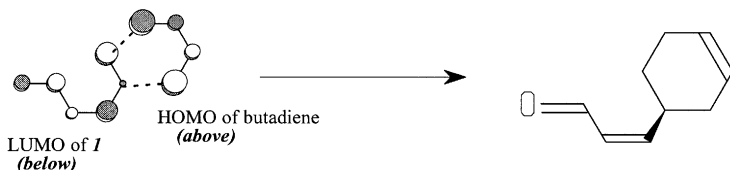
**Figure B5.1.** The HOMO and LUMO of pentadienone and ethylene (SHMO).

than in ethylene (0.71), suggesting lower basicity. Since the two factors are in opposition, one might expect that the basicity will be similar, perhaps slightly greater than that of ethylene.

- (c) Attack by a nucleophile will be directed to the part of the LUMO which has the largest coefficient, in this case, atom 6. Atom 4 is second. Acidity in the Lewis sense relative to ethylene is governed by the relative energy of the LUMO and by the relative magnitudes of the largest coefficients. The LUMO is much lower, suggesting significantly greater acidity. Again, the largest coefficient (0.55) is smaller than in ethylene (0.71), suggesting lower acidity. Although the two factors are again in opposition, one might expect that the large energy difference will dominate and that the acidity will be greater than that of ethylene. (In fact, it is extremely difficult to do a nucleophilic attack on ethylene.)
- (d) The energy of the  $\pi$ - $\pi^*$  excitation in SHMO theory is just the difference of the LUMO and HOMO orbital energies,  $0.961|\beta|$ . The “ $n$ ” orbital is a nonbonding orbital on oxygen which lies in the plane of the molecule and is not part of the  $\pi$  system. Its energy is that of a  $p$  orbital on a monocoordinated oxygen,  $\alpha - 0.97|\beta|$ . Since the  $n$  orbital is lower than the highest occupied  $\pi$  orbital, the excitation should have lower energy than the  $n$ - $\pi^*$  excitation so the  $\pi$ - $\pi^*$  state will be lower in energy than the  $n$ - $\pi^*$  state.
- (e) The bond order of the  $C_2$ - $C_3$  bond is  $2(0.53)(0.45) + 2(-0.25)(0.15) + 2(-0.12)(-0.55) = 0.53$ . The total electron population on atom 1 is  $2(0.57)^2 + 2(-0.49)^2 + 2(0.45)^2 = 1.535$ . Since a monocoordinated oxygen atom is neutral with one electron in the  $\pi$  system, the net charge is  $1 - 1.535 = -0.535$ .

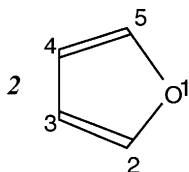


- (f) The important orbital interaction for the Diels–Alder reaction is the LUMO-(pentadienone)–HOMO(butadiene). The strongest interaction (best overlap) originates if the two molecules are oriented as follows:



The interaction is driven by the overlap of the orbitals with the largest coefficients of each MO.

3. The results of an SHMO calculation on furan, **2**, are given below (Note:  $\alpha_O = \alpha_C - 2.09|\beta_{CC}|$ ,  $\beta_{CO} = -0.66|\beta_{CC}|$ ):



$$\epsilon_1 = \alpha - 2.548|\beta| \quad \phi_1 = 0.86p_1 + 0.30p_2 + 0.19p_3 + 0.19p_4 + 0.30p_5$$

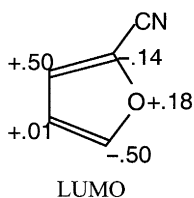
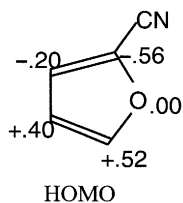
$$\epsilon_2 = \alpha - 1.383|\beta| \quad \phi_2 = 0.43p_1 - 0.23p_2 - 0.60p_3 - 0.60p_4 - 0.23p_5$$

$$\epsilon_3 = \alpha - 0.618|\beta| \quad \phi_3 = -0.60p_2 - 0.37p_3 + 0.37p_4 + 0.60p_5$$

$$\epsilon_4 = \alpha + 0.846|\beta| \quad \phi_4 = 0.27p_1 - 0.60p_2 + 0.33p_3 + 0.33p_4 - 0.60p_5$$

$$\epsilon_5 = \alpha + 1.618|\beta| \quad \phi_5 = -0.37p_2 + 0.60p_3 - 0.60p_4 + 0.37p_5$$

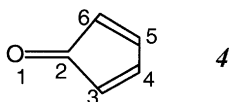
- (a) Sketch the highest occupied molecular orbital (HOMO) and the lowest unoccupied molecular orbital (LUMO) on the basis of the calculation.
- (b) Assuming that **2** were to react with an electrophile, where is the most likely site of attack? Compare the Lewis basicity of **2** to that of ethylene. Show the products of such a reaction (pick a specific electrophile).
- (c) Assuming that **2** were to react with a nucleophile, where is the most likely site of attack? Compare the Lewis acidity of **2** to that of ethylene. Show the products of such a reaction (pick a specific nucleophile).
- (d) Consider an equimolar mixture of **2** and 2-cyanofuran, **3**. A Diels–Alder product is obtained from the mixture. Predict the structure of the product. The HOMO and LUMO of **3** are shown below.



$$\epsilon_{\text{HOMO}} = \alpha - .796 |\beta|$$

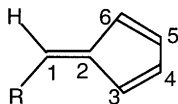
$$\epsilon_{\text{LUMO}} = \alpha + .254 |\beta|$$

- (e) In terms of  $\alpha$  and/or  $|\beta|$ , provide an estimate for the lowest ionization potential of **2** according to the calculation.
- (f) In terms of  $|\beta|$ , estimate the energy of the lowest  $\pi-\pi^*$  electronic excitation of **2**.
- (g) Furan **2** belongs to the point group  $C_{2v}$ . Indicate whether the HOMO is symmetric or antisymmetric with respect to each of the three symmetry elements of **2**. Do the same for the LUMO. Do the same for the lowest  $\pi-\pi^*$  state of **2**.
- (h) Calculate the net charge on the oxygen atom of **2**.
- (i) Calculate the  $\pi$  bond order of the C—O bond of **2**.
4. The results of a SHMO calculation on cyclopentadienone, **4**, are given below (*Note:*  $\alpha_O = \alpha - 0.97|\beta|$ ,  $\beta_{CO} = -1.09|\beta|$ ):



$$\begin{aligned} \varepsilon_1 &= \alpha - 2.252|\beta| & \phi_1 &= 0.46p_1 + 0.56p_2 + 0.38p_3 + 0.31p_4 + 0.31p_5 + 0.38p_6 \\ \varepsilon_2 &= \alpha - 1.366|\beta| & \phi_2 &= 0.64p_1 + 0.24p_2 - 0.18p_3 - 0.48p_4 - 0.48p_5 - 0.18p_6 \\ \varepsilon_3 &= \alpha - 0.618|\beta| & \phi_3 &= -0.60p_3 - 0.37p_4 + 0.37p_5 + 0.60p_6 \\ \varepsilon_4 &= \alpha - 0.148|\beta| & \phi_4 &= 0.56p_1 - 0.43p_2 - 0.33p_3 + 0.38p_4 + 0.38p_5 - 0.33p_6 \\ \varepsilon_5 &= \alpha + 1.618|\beta| & \phi_5 &= -0.37p_3 + 0.60p_4 - 0.60p_5 + 0.37p_6 \\ \varepsilon_6 &= \alpha + 1.796|\beta| & \phi_6 &= 0.26p_1 - 0.67p_2 + 0.46p_3 - 0.17p_4 - 0.17p_5 + 0.46p_6 \end{aligned}$$

- (a) Sketch the highest occupied molecular orbital (HOMO) and the lowest unoccupied molecular orbital (LUMO) on the basis of the calculation.
- (b) Assuming that **4** were to react with an electrophile, where is the most likely site of attack? Compare the Lewis basicity of **4** to that of ethylene.
- (c) Assuming that **4** were to react with a nucleophile, where is the most likely site of attack? Compare the Lewis acidity of **4** to that of ethylene.
- (d) In terms of  $|\beta|$ , estimate the energy of the lowest  $\pi-\pi^*$  electronic excitation of **4**. Is the  $\pi-\pi^*$  state likely to be higher or lower than the  $n-\pi^*$  state? Explain in less than three lines. Is it plausible that compounds with this structure might be colored (recall tetraphenylcyclopentadienone)?
- (e) Calculate the  $\pi$  bond order of the C<sub>2</sub>—C<sub>3</sub> bond of **4**.
- (f) Show the most likely product from a Diels–Alder reaction of **4** with 1,3-butadiene. Pay attention to all relevant aspects of stereo- and regioselectivity (recall your laboratory chemistry with the tetraphenyl derivative).
- (g) Compound **4** is expected to be very reactive and has never been synthesized. Can you suggest a reason? You made a tetraphenyl derivative of **4** in the laboratory. Suggest the manner in which the phenyl groups might stabilize the compound.
5. The results of a SHMO calculation on fulvene, **5** (R = H), are given below:



$$\begin{aligned}
 \epsilon_1 &= \alpha - 2.115|\beta| & \phi_1 &= 0.25p_1 + 0.52p_2 + 0.43p_3 + 0.38p_4 + 0.38p_5 + 0.43p_6 \\
 \epsilon_2 &= \alpha - 1.000|\beta| & \phi_2 &= 0.50p_1 + 0.50p_2 - 0.50p_4 - 0.50p_5 \\
 \epsilon_3 &= \alpha - 0.618|\beta| & \phi_3 &= -0.60p_3 - 0.37p_4 + 0.37p_5 + 0.60p_6 \\
 \epsilon_4 &= \alpha + 0.254|\beta| & \phi_4 &= 0.75p_1 - 0.19p_2 - 0.35p_3 + 0.28p_4 + 0.28p_5 - 0.35p_6 \\
 \epsilon_5 &= \alpha + 1.618|\beta| & \phi_5 &= -0.37p_3 + 0.60p_4 - 0.60p_5 + 0.37p_6 \\
 \epsilon_6 &= \alpha + 1.861|\beta| & \phi_6 &= 0.36p_1 - 0.66p_2 + 0.44p_3 - 0.15p_4 - 0.15p_5 + 0.44p_6
 \end{aligned}$$

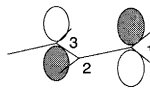
- (a) Sketch the highest occupied molecular orbital (HOMO) and the lowest unoccupied molecular orbital (LUMO) on the basis of the calculation.
- (b) Assuming that **5** (R = H) were to react with an electrophile, where is the most likely site of attack? Compare the Lewis basicity of **5** (R = H) to that of ethylene.
- (c) Assuming that **5** (R = H) were to react with a nucleophile, where is the most likely site of attack? Compare the Lewis acidity of **5** (R = H) to that of ethylene.
- (d) In terms of  $|\beta|$ , estimate the energy of the lowest  $\pi$ - $\pi^*$  electronic excitation of **5** (R = H). Is it plausible that compounds with this structure might be colored? Explain in three lines or less.
- (e) Calculate the  $\pi$  bond order of the C<sub>1</sub>—C<sub>2</sub> bond of **5** (R = H).
- (f) Calculate the *net charge* of atom C<sub>1</sub> of **5** (R = H).
- (g) Choose a suitable reagent and show the most likely product in a reaction between it and fulvene, **5** (R = H).
6. Use principles of orbital interaction theory to explain the lower Lewis acidity of the allyl cation, [CH<sub>2</sub>CHCH<sub>2</sub>]<sup>+</sup>, compared to the methyl cation, [CH<sub>3</sub>]<sup>+</sup>.

**Answer.** The Lewis acidity depends on the interaction energy ( $\Delta\epsilon_L$ ) from the interaction of the LUMO of the acid with the HOMO of the nucleophile. The interaction is of  $\sigma$  type, with the base HOMO (usually a nonbonded  $p$  or  $sp^n$  hybrid) interacting end on with the LUMO, which for the methyl cation is a single  $2p$  orbital and for the allyl system is a linear combination of  $2p$  orbitals. The LUMOs of the two systems are shown below.

Allyl LUMO

$$\epsilon = \alpha + 0.0|\beta|$$

$$\phi = 0.707p_1 - 0.707p_3$$



Methyl LUMO

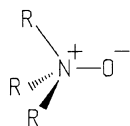
$$\epsilon = \alpha + 0.0|\beta|$$

$$\phi = 1.0p$$



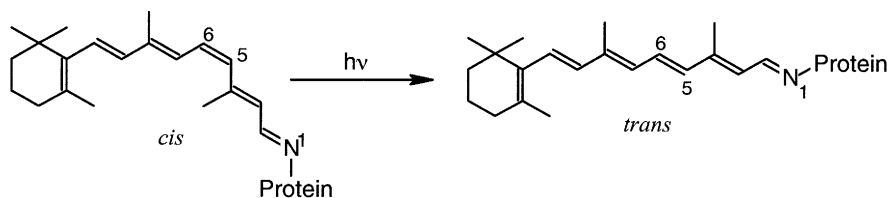
The magnitude of interaction,  $\Delta\epsilon_L \approx h_{AB}^2 / (\epsilon_{LUMO} - \epsilon_{HOMO})$ , depends inversely on the orbital energy differences and directly on the square of the intrinsic interaction matrix element, which in turn is approximately proportional to the overlap of the two orbitals. The LUMO energies of methyl and allyl are the same. The difference in reactivity, as measured by  $\Delta\epsilon_L$  does not arise from the orbital energy differences, but rather from the magnitude of  $h_{AB} \approx kS_{AB}$ . Since the nucleophile's HOMO can only overlap with one  $p$  orbital of the LUMO in each case, the overlap with the allyl LUMO will be smaller because the magnitude of the coefficient (0.707) is smaller (it is 1.0 in the case of methyl).

7. Using simple orbital interaction considerations, explain the polarity of the N—O bond in amine oxides.



**Answer.** This question pertains to the  $\sigma$  bond between a tricoordinated nitrogen atom and a zero-coordinated oxygen atom. It is in *this* chapter rather than the previous one because the student can use the SHMO heteroatom parameters in Table 5.1 as a guide to position the interacting orbitals correctly on the same energy scale. It is evident that a  $p$  orbital on a tricoordinated nitrogen ( $\alpha_N = \alpha - 1.37|\beta|$ ) is *lower* in energy than a  $p$  orbital of a monocoordinated oxygen ( $\alpha_O = \alpha - 0.97|\beta|$ ). The  $sp^n$  hybrid character of the orbital of the N and the *zero* coordination of the oxygen will exaggerate the difference in energies. The correct interaction diagram for the N—O bond of the amine oxide is shown in Figure B5.2. Notice that the N—O  $\sigma$  bond is polarized toward nitrogen. Since nitrogen provides both electrons for this dative bond, it loses a fraction of these to the oxygen atom. This is reflected in the formal charges.

8. The chromophore (light-absorbing part of the molecule) of rhodopsin, the protein responsible for vision, is a polyunsaturated imine with one of the double bonds in the less stable (*Z*) configuration.



the chromophore of rhodopsin  
(the imine of retinal)

Upon absorption of light, a rapid *cis*–*trans* isomerization takes place, together with the generation of an electrical pulse. The electrical pulse corresponds to a large change in the molecular dipole moment upon photoexcitation. Answer the following questions using SHMO.

- Explain the mechanism of isomerization. Does examination of the HOMO and LUMO  $\pi$  orbitals of the chromophore suggest why it is the 5,6 double bond which isomerizes?
- In the transition state (TS) for rotation, the conjugation is broken at the *cis* double-bond position. It is this point that is thought to have a very large dipole moment. Do the SHMO orbitals provide an explanation? What is the predicted direction of the dipole moment?

**Answer.** The  $\pi$  system chromophore of rhodopsin consists of 12 atoms in an unbranched arrangement, with a dicoordinated N atom at one end. Remember that SHMO theory cannot distinguish between isomers. A good model for the chromophore is a 12-atom  $\pi$  system, 1-aza-1,3,5,7,9,11-dodecahexaene (Figure B5.3).

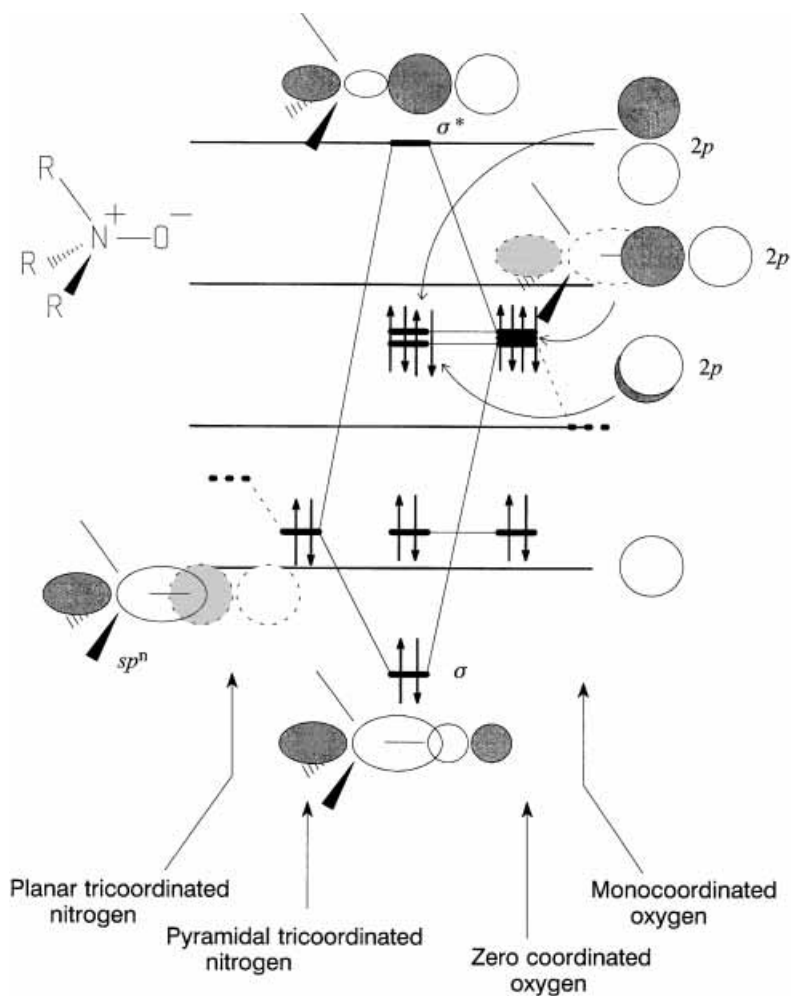


Figure B5.2. Interaction diagram for an amine oxide.

Although not relevant for the SHMO calculation, the *cis* double bond would be in the 5,6-position.

- According to the SHMO program's data table, this double bond has the lowest  $\pi$  bond order of the six formal  $\pi$  bonds in the molecule. This fact that the LUMO is particularly antibonding between the 5- and 6-positions, with coefficients of +0.255 and  $-0.324$ , respectively, and the strain inherent in the *cis* configuration may be an explanation why this bond, and not one of the others, is the one which isomerizes.
- In the middle of the 5,6 bond rotation, conjugation is lost and the system becomes two independent  $\pi$  systems, a heptatrienyl fragment and a 1-azapentadienyl fragment. This change is readily simulated in the SHMO program by erasing the

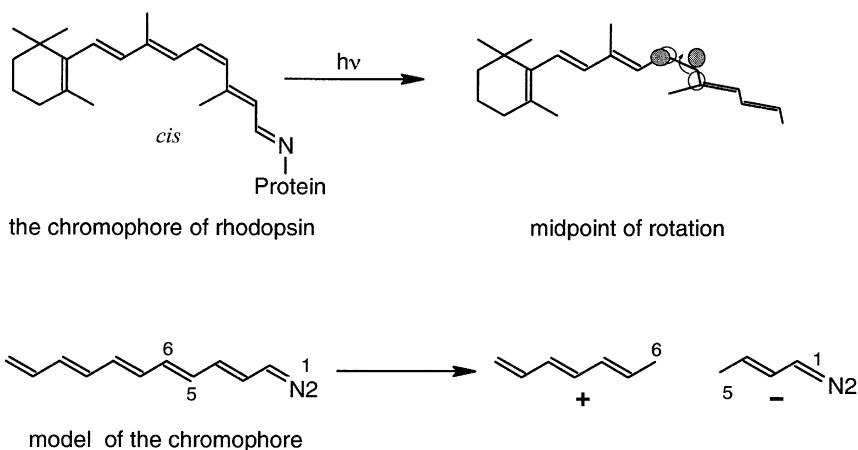


Figure B5.3.

5,6 bond. In the absence of the N atom, both of the odd-numbered  $\pi$  systems would be neutral with a SOMO at  $\alpha$ . However, the presence of the N atom lowers the third orbital of the five-atom part, and this orbital will be doubly occupied, leaving six electrons for the heptadienyl part. Thus a formal charge separation is predicted—the rotational TS consists of a heptadienyl cation and a 1-azapentadienyl anion. This “sudden polarization” is responsible for the large change in dipole moment and hence the electrical pulse responsible for vision. For a detailed experimental study of the mechanism of the isomerization, see Haran, G.; Morlino, E. A.; Matthes, J.; Callender, R. H.; Hochstrasser, R. M., *J. Phys. Chem. A*, **1999**, *103*, 2202–2207. Also see Kandori, H.; Sasabe, H.; Nakanishi, K.; Yoshizawa, T.; Mizukami, T.; Shichida, Y., *J. Am. Chem. Soc.*, **1996**, *118*, 1002–1005.

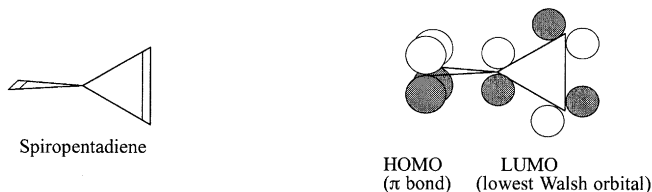
## Chapter 6

1. A recent study (Seeman, J. I.; Grassian, V. H.; Bernstein, E. R., *J. Am. Chem. Soc.*, **1988**, *110*, 8542) has demonstrated that  $\alpha$ -methylstyrene is nonplanar in the ground state but is planar in its first excited state. This may be interpreted as evidence that the  $\pi$  bond order of the bond connecting the vinyl group to the ring is greater in the lowest  $\pi$ - $\pi^*$  state than in the ground state. Can you offer an explanation for this observation by considering the properties of styrene to arise from the interaction of a benzene ring with ethylene?

**Answer.** The HOMOs and LUMOs of benzene and ethylene have the same SHMO energies,  $\alpha - |\beta|$  and  $\alpha + |\beta|$ , respectively. These HOMOs interact, the out-of-phase combination becoming the HOMO of styrene. Thus the HOMO of styrene is antibonding across the bond connecting the vinyl group to the ring. Upon photoexcitation, one electron leaves this orbital, resulting in a net increase of the  $\pi$  bond order of this bond. The LUMO of styrene corresponds to the in-phase combination of the LUMOs of ethylene and benzene and therefore contributes a positive contribution to the  $\pi$  bond order of the connecting bond when it receives the photoexcited electron.

- Use an orbital interaction diagram to explain the observation that tetracyanoethylene is very easily reduced to its radical anion.
- The highly strained olefin, spiropentadiene, has been synthesized (Billups, W. E.; Haley, M. M., *J. Am. Chem. Soc.*, **1991**, *113*, 5084) after more than a decade of theoretical investigations which predicted significant *spiroconjugation*. Discuss the  $\pi$  bonding of this compound.

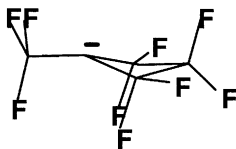
**Answer.** The high symmetry of spiropentadiene ( $D_{2d}$ ) limits the possibilities for interaction of orbitals of one ring with orbitals of the other. Thus the  $\pi$  bonding orbital of one ring cannot interact by symmetry with either the  $\pi$  or  $\pi^*$  orbitals of the other ring. Only the  $\pi^*$  orbitals of the two rings can interact, but as both are unoccupied, no stabilization ensues from this interaction. However, a plausible interaction which may lead to extra stabilization is the interaction of the occupied  $\pi$  orbital of one ring with the unoccupied Walsh orbital of the other, as shown below, leading to two two-electron, two-orbital stabilizations, a form of homoconjugation.



- Octamethyl-1,4-cyclohexadiene has been shown to form a long-lived complex with  $\text{NO}^+$  (Borodkin, G. I.; Elanov, I. R.; Podryvanov, V. A.; Shakirov, M. M.; Shubin, V. G., *J. Am. Chem. Soc.*, **1995**, *117*, 12863–12864). Dynamic  $^{13}\text{C}$  NMR evidence indicates that the complex is fluxional. A structure was postulated, based on semi-empirical calculations, in which the  $\text{NO}^+$  is attached to a single  $\pi$  bond. Use principles of orbital interaction theory to discuss the structure and bonding of such a complex (see also Figure 4.8 and question 4, Chapter 11).

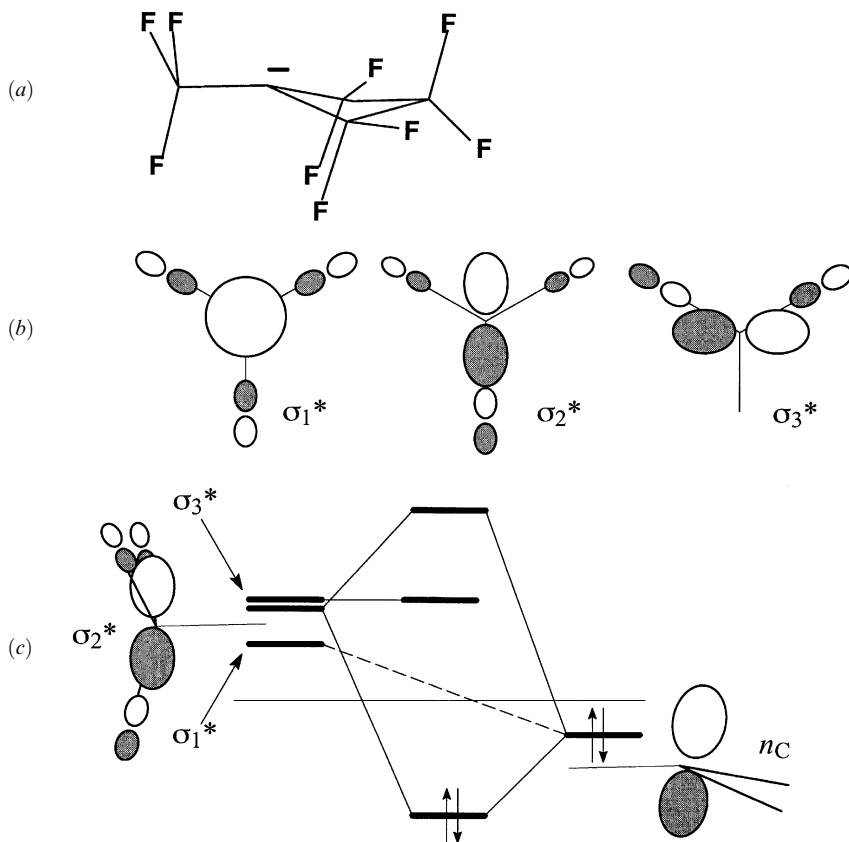
## Chapter 7

- The tertiary carbanion perfluoro-1-methyl-1-cyclobutyl is considerably more stable than most carbanions.



Explain the role of adjacent fluorine atoms in carbanion stabilization. Use the group orbitals of the trifluoromethyl group in your orbital analysis. What kind of group (X, “C,” or Z) is  $-\text{CF}_3$ ? (See Farnham, W. B.; Dixon, D. A.; Calabrese, J. C., *J. Am. Chem. Soc.*, **1988**, *110*, 2607–2611.)

**Answer.** Two factors contribute to the stabilization of carbanions by an adjacent trifluoromethyl group or other perfluorinated groups. Most obviously, the strong inductive effect of the highly electronegative fluorine atoms will tend to increase the

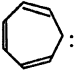


**Figure B7.1.** (a) 1-Trifluoromethylperfluorocyclobutyl carbanion. (b) The group antibonding orbitals of the CF<sub>3</sub> group. (c) Orbital interaction diagram showing the dominant interaction between  $\sigma_2^*$  and  $n_C$  and the secondary interaction of  $n_C$  with  $\sigma_1^*$  (dashed line).

effective electronegativity of nearby carbon atoms and therefore stabilize a negative charge. An orbital interaction diagram for stabilization by  $\pi$ -type delocalization of the carbanionic lone pair is shown in Figure B7.1c. All C—F bonds  $\beta$  to the carbanion site stabilize the carbanion by negative hyperconjugation. The group molecular orbitals of the trifluoromethyl group are shown in Figure B7.1b, as seen down the three-fold symmetry axis (see also Figure 3.20). Because of the electronegativity difference between C and F, the C—F antibonding orbitals are highly polarized toward the carbon atom and are low lying; both factors strengthen the  $\pi$ -type interaction between  $n_C$  and one of the degenerate pairs of  $\sigma^*$  orbitals. It usually happens that the degeneracy is broken, with one bond being selected,  $\sigma_2^*$  in this case. The broken three fold symmetry and pyramidalization at the carbanion site (i.e.,  $n_C$  is  $sp^n$  rather than pure  $p$ ) permit a favorable secondary interaction with the lowest-lying empty group orbital,  $\sigma_1^*$ , shown by a dashed line in Figure B7.1c. Because the dominant interaction is  $\pi$  type, and because the bonding orbitals (not shown) are



very low lying and polarized away from C, one can legitimately regard the  $-\text{CF}_3$  group as a Z-type substituent.

- Use orbital interaction analysis to explain stabilization of a carbocationic center by a cyclopropyl group. What kind of substituent (X, "C," or Z) is cyclopropyl? Explain. Predict the orientation of the planar cationic center relative to the cyclopropyl ring.
- By considering the  $\pi$  MOs of the cyclopentadienyl system ( $\text{C}_5\text{H}_5$ ) to result from an interaction between *cis*-butadiene  $\pi$  MOs and an  $sp^2$  hybridized C atom, explain the stability of the cyclopentadienyl anion and the instability of the cyclopentadienyl cation.
- Use simple orbital interaction arguments (i.e., orbital correlation diagrams) to explain the following:
  - Stabilization of a carbocation by C—H hyperconjugation
  - Stabilization of a carbanion by C—F negative hyperconjugation
  - Triplet ground state of phenyl carbene,  $\text{C}_6\text{H}_5-\text{C}-\text{H}$
  - Singlet nature of cycloheptatrienyliene, :
  - Nucleophilicity of N,N-dimethylaminocarbinyl radical,  $(\text{CH}_3)_2\text{N}\dot{\text{C}}\text{H}_2$

**Answer to 4(d).** We can consider the orbitals of cycloheptatrienyliene to arise from the interaction of the  $\pi$  orbitals of hexatriene and the valence orbitals of a di-coordinated carbon atom (a  $2p$  orbital and an  $sp^n$  hybrid orbital). The  $\pi$  orbitals of hexatriene may be obtained from an SHMO calculation. The interaction diagram is shown in Figure B7.2. The  $p$  orbital of the carbene site is raised as a result of the dominant interaction with  $\pi_3$  of hexatriene. The orbital  $\pi_4$ , which is closest in energy to the carbene's  $p$  orbital, does not interact because of symmetry, and  $\pi_5$  interacts less strongly because the coefficients at the terminal positions of the hexatriene are smaller. The larger HOMO ( $sp^n$ )–LUMO ( $\pi'_4$  or  $\pi'_5$ ) gap permits the ground state to be singlet.

- Use orbital interaction analysis to suggest a reason that tropylium cation  $\text{C}_7\text{H}_7^+$  is such a stable cation. This may be done in either of two ways: by considering the interaction of a simple carbocation with 1,3,5-hexatriene or the interaction of an allyl cation with butadiene, both held in the 7-membered planar ring geometry of tropylium. In either case, attention must be paid to orbital symmetry.
- Use orbital interaction analysis to predict the structure of a complex between  $\text{H}_2\text{O}$  and  $:\text{CH}_2$ . The structure was determined by ab initio MO theory (Moreno, M.; Lluch, J. M.; Oliva, A.; Bertrán, J., *Can. J. Chem.*, **1987**, *65*, 2774–2778).
- Methyl methoxy carbene,  $\text{CH}_3-\text{C}-\text{OCH}_3$ , was described recently (Sheridan, R. S.; Moss, R. A.; Wilk, B. K.; Shen, S.; Wlostowski, M.; Kesselmayr, M. A.; Subramanian, R.; Kmiecik-Lawrynowicz, G.; Krogh-Jespersen, K., *J. Am. Chem. Soc.*, **1988**, *110*, 7563–7564) as a remarkably selective nucleophile. Explain why the carbene,  $\text{CH}_3-\text{C}-\text{OCH}_3$ , has a singlet ground state and determine the basis for its "nucleophilicity."
- Benzynes is considered to be the intermediate in strong base-catalyzed nucleophilic aromatic substitution.

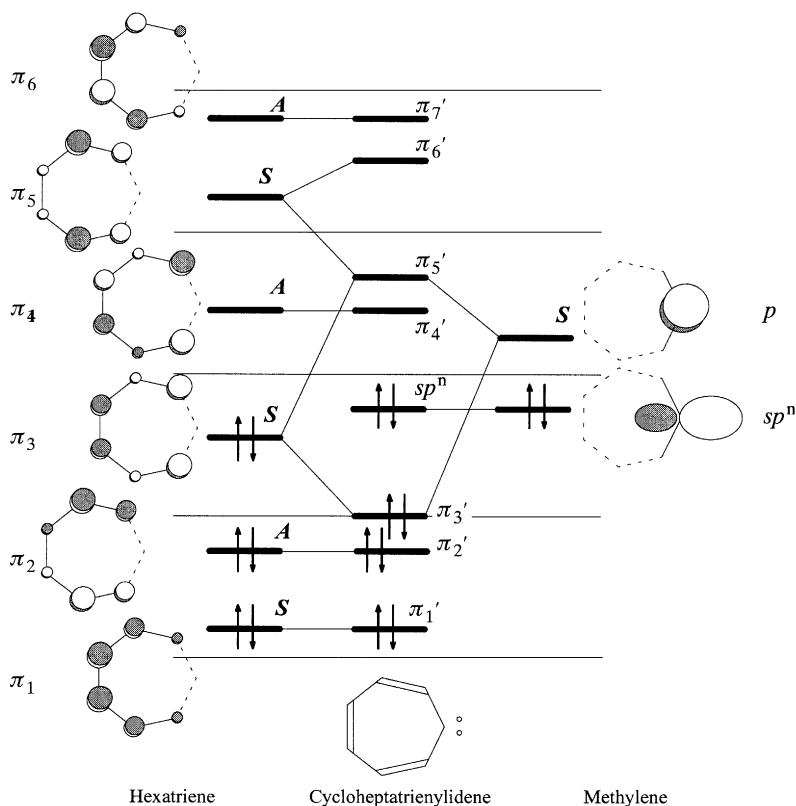
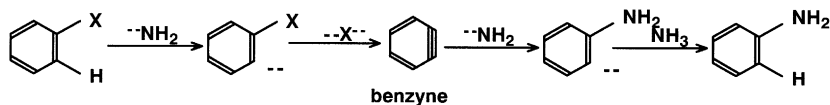


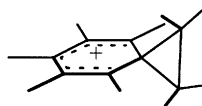
**Figure B7.2.** Electronic structure of cycloheptatrienyldiene from the interaction of the orbitals of hexatriene and methylene. Symmetry labels refer to the  $p$  and  $\pi$  orbitals and a vertical mirror.



- Suggest a reason for the ease of formation of the carbanion in step 1.
- Suggest a reason for the ease of departure of  $X^-$  in step 2.
- Suggest a reason for the ease of nucleophilic addition to the double bond in benzyne.

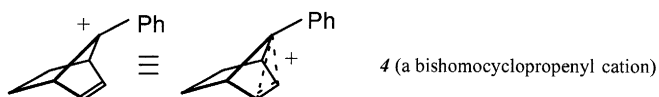
(The MW and IR spectra of benzyne have been measured: MW, Brown, R. D.; Godfrey, P. D.; Rodler, M., *J. Am. Chem. Soc.*, **1986**, *108*, 1296–1297; IR, Radziszewski, J. G.; Hess, Jr., B. A.; Zahradnik, R., *J. Am. Chem. Soc.*, **1992**, *114*, 52–57.)

- Use orbital interaction analysis to derive the bonding molecular orbitals of ethylbenzenium ion. Consider ethylbenzenium ion to be the result of the interaction of a phenyl group,  $C_6H_5$ , and ethylene,  $C_2H_4$ , with the appropriate number of electrons. (Direct evidence for the existence of ethylbenzenium ion was obtained by Fornarini, S.; Muraglia, V., *J. Am. Chem. Soc.*, **1989**, *111*, 873.)

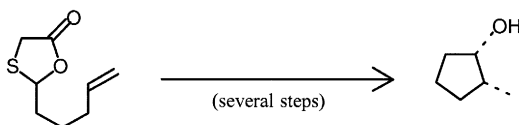


ethylbenzenium ion (all substituents are H)

10. Use orbital interaction analysis to derive the bonding molecular orbitals of bishomocyclopropenyl cations, such as **4**. The X-ray structure of the hexafluoroantimonate salt of **4** was recently determined by Laube, T., *J. Am. Chem. Soc.*, **1989**, *111*, 9224.

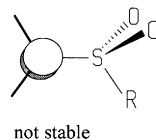
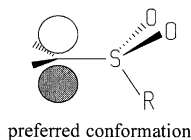


11. Explain Markovnikov's rule, that is, in an electrophilic addition of HX to an olefin, the hydrogen goes to the carbon atom which has the most hydrogens.
12. Cycloalkanols may be synthesized by free-radical intramolecular cyclization (Yadav, V.; Fallis, A. G., *Can. J. Chem.*, **1991**, *69*, 779–789).

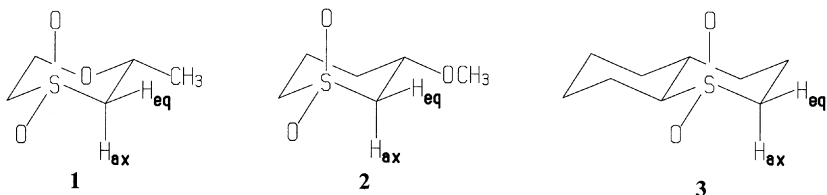


Analyze the reaction, paying close attention to substituent effects. Suggest a reason based on orbital interaction criteria for the formation of 5-membered rings rather than 6-membered rings.

13. Discuss stabilization of free radicals by the *captodative* effect. [See, e.g., (a) Kosower, E. M.; Waits, H. P.; Teuerstein, A.; Butler, L. C., *J. Org. Chem.*, **1978**, *43*, 800. (b) Olson, J. B.; Koch, T. H., *J. Am. Chem. Soc.*, **1986**, *108*, 756. (c) Brook, D. J. R.; Haltiwanger, R. C.; Koch, T. H., *J. Am. Chem. Soc.*, **1991**, *113*, 5910.]
14. (a) Offer a rationale for the preferred orientation of an  $\alpha$ -sulfonyl carbanion (it is not necessary to invoke the use of *d* orbitals). For a review of  $\alpha$ -sulfonyl carbanions, see Boche, G., *Angew. Chem. Int. Ed. Engl.*, **1989**, *28*, 277–297.



- (b) The observation of part (a) explains why the equatorial  $\alpha$  proton ( $H_{eq}$ ) in 6-membered cyclic sulfones is selectively abstracted under basic conditions. Suggest a reason that the rate of H/D exchange in NaOD/D<sub>2</sub>O of  $\alpha$ - $H_{eq}$  is 36 times faster in **1** than in **2** and about 10,000 times faster than in **3** (King, J. F.; Rathore, R., *J. Am. Chem. Soc.*, **1990**, *112*, 2001).



## Chapter 8

1. Solve the SHMO equation for the  $\pi$  orbitals and orbital energies of the carbonyl group:  $\alpha(\text{O}) = \alpha(\text{C}) - |\beta(\text{CC})|$ ,  $\beta(\text{CO}) = \beta(\text{CC})$ . Sketch the results in the form of an interaction diagram.

**Answer.**  $E(L) = \alpha + 1.618\beta$ ;  $E(U) = \alpha - 0.618\beta$ ;  $\psi(L) = 0.851p(\text{O}) + 0.526p(\text{C})$ ;  $\psi(U) = 0.526p(\text{O}) - 0.851p(\text{C})$ .

Bond energy:  $\alpha(\text{C}) + \alpha(\text{O}) - 2E(L) = -1.236\beta = 1.236|\beta|$ .

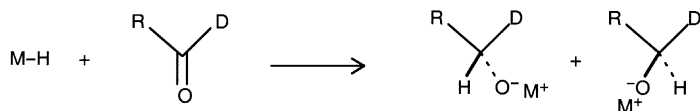
Ionization potential:  $-E(L) = -(\alpha - 0.618\beta) = |\alpha| + 0.618|\beta|$ .

Electronic excitation ( $\pi \rightarrow \pi^*$ ):  $E(U) - E(L) = -2.236\beta = 2.236|\beta|$ .

Bond order:  $2(0.851)(0.526) = 0.895$ .

Net charges: on O,  $-2(0.851)^2 + 1 = -0.447$ ; on C,  $-2(0.526)^2 + 1 = +0.447$ .

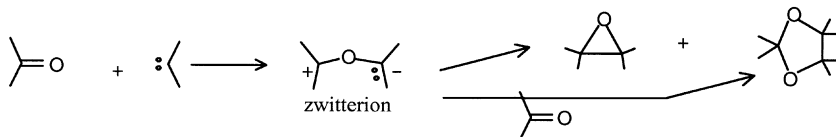
2. Develop an orbital diagram for the amide group from the interaction of the C=O and N moieties. Explain the positioning of the C=O and N orbitals before and after they interact. In developing the interactions, consider both the relative energies of the interacting orbitals and the polarization of the C=O  $\pi$  orbitals. Don't forget the higher nonbonded electron pair on O. What features of the amide functional group are consistent with what you would expect from the perturbative MO analysis?
3. 2,5-Dimethylborolane has been shown to be effective in asymmetric reduction of ketones (Imai, T.; Tamura, T.; Yamamuro, A.; Sato, T.; Wollmann, T. A.; Kennedy, R. M.; Masamune, S., *J. Am. Chem. Soc.*, **1986**, *108*, 7402–7404). Using the frontier orbitals of a borolane and a ketone, show the probable course of the initial interaction between the two.
4. Metal hydrides are often used to reduce aldehydes and ketones:



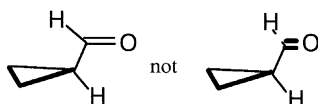
The rate-determining step, “M,” may be a single metal such as Na or Li or a complex such as  $\text{AlH}_3$  (as in  $\text{LiAlH}_4$ ). Using a two-orbital interaction diagram (assume  $\text{M} = \text{Li}$ ), show which orbitals are involved in the above step. Predict the most favorable geometry for the approach of the reagents. (For an interesting variation of this reaction using a chiral aluminum hydride to effect enantioselective reduction, see Noyori, R.; Tomino, I.; Yamada, M.; Nishizawa, M., *J. Am. Chem. Soc.*, **1984**, *106*, 6717–6725.)

5. Explain the higher reactivity of acetone (propanone) compared to methyl acetate ( $\text{CH}_3\text{CO}_2\text{CH}_3$ ) toward reduction by sodium borohydride.

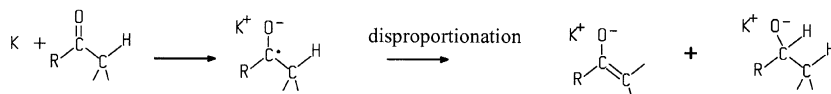
6. Singlet carbenes react with carbonyl compounds to produce zwitterionic intermediates which can cyclize to epoxides or react further with another carbonyl to form 1,3-dioxacyclopentanes. Show which orbitals are involved and predict the geometry of approach of the carbene and carbonyl compound in the *initial interaction* that produces the zwitterion.



7. Explain the bisected geometry of cyclopropyl aldehyde.

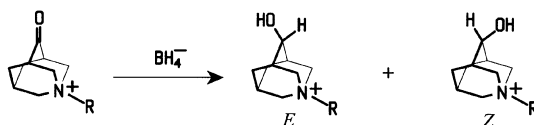


8. Alkali metal reduction of ketones may involve the following steps:



- (a) Discuss the electronic structure of each intermediate in terms of the orbitals involved.
- (b) Show a plausible geometry for the transition state for the disproportionation step, according to orbital interaction theory.
- (c) What additional features emerge from the study by Rautenstrauch et al. (Rautenstrauch, V.; Mégard, P.; Bourdin, B.; Furrer, A., *J. Am. Chem. Soc.*, **1992**, *114*, 1418) on the reduction of camphors with potassium in liquid ammonia?
- (d) Present a brief summary of stereochemical considerations in metal reductions of carbonyls as deduced in the theoretical study of Wu and Houk (Wu, Y.-D.; Houk, K. N., *J. Am. Chem. Soc.*, **1992**, *114*, 1656).
9. Hahn and le Noble have discovered strongly enhanced stereoselectivity in the reduction of 5-substituted adamantanones where the substitution at C<sub>5</sub> is by positive nitrogen (Hahn, J. M.; le Noble, W. J., *J. Am. Chem. Soc.*, **1992**, *114*, 1916). Thus *E/Z* ratios for borohydride reduction of compounds 1–3 were in the range 20–25. Suggest a possible reason for these observations on the basis of orbital interaction theory.

- 1 R = CH<sub>3</sub> I<sup>-</sup>  
 2 R = O<sup>-</sup>  
 3 R = CH<sub>2</sub>CO<sub>2</sub><sup>-</sup>



**Answer.** A possible explanation for the observed diastereoselectivity of nucleophilic addition to the carbonyl involves a static distortion of the carbonyl group so as to improve  $\pi$  donation of the  $\beta$   $\sigma$  C—C bonds into the  $\pi^*$  orbital of the carbonyl

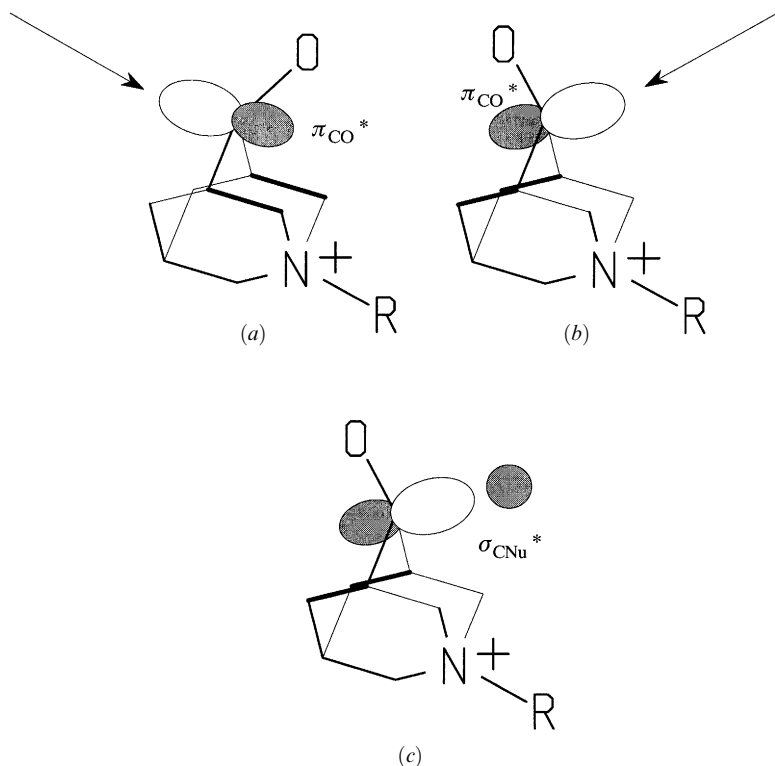


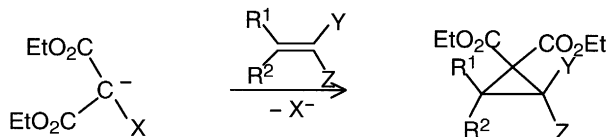
**Figure B8.1.** (a, b) Static distortion of carbonyl group to favor overlap with the highlighted bonds. The bonds in (a) are poorer  $\pi$  donors because of electrostatic effects of the quaternary N center and interaction with  $\sigma_{\text{NR}}^*$ . Thus interaction (b) is favored. (c) Distortion in the transition state to favor donation into  $\sigma_{\text{CNu}}^*$  bond.

group, as shown in Figure B8.1. The consequent polarization of the orbital at carbon results in more favorable overlap with the HOMO of the nucleophile ( $\text{H}^-$  or  $\text{H}-\text{BH}_3^-$ , in the present case) and attack from the direction indicated by the arrow. Just such a distortion was observed theoretically in 2-adamantyl cation (Dutler, R.; Rauk, A.; Sorensen, T. S.; Whitworth, S. M., *J. Am. Chem. Soc.*, **1989**, *111*, 9024–9029). It may be argued that the static distortion in the ground state of the carbonyl is insufficient to account for the high selectivity observed. According to the theory of Cieplak et al. (Cieplak, A. S.; Tait, B. D.; Johnson, C. R., *J. Am. Chem. Soc.*, **1989**, *111*, 8447–8462), the distortion occurs naturally as one approaches the transition state, one  $\pi$  face being preferred by donation into the  $\sigma_{\text{CNu}}^*$  orbital (Figure B8.1c).

10. Unlike carbonyl compounds, thiocarbonyl compounds such as thioketones,  $\text{R}_1\text{R}_2\text{C}=\text{S}$ , are very reactive and often impossible to isolate in a pure state. Apply principles of orbital interaction theory to explain:
- The high reactivity of thioketones toward nucleophiles
  - The tendency of thioketones to dimerize. Predict the structure of the dimer.

## Chapter 9

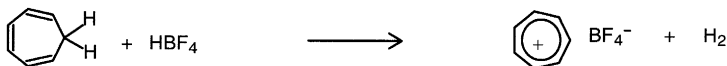
1. Cyclopropanes may be obtained from the Michael condensation of bromo- and chloromalonate carbanions (Le Menn, J.-C.; Tallec, A.; Sarrazin, J., *Can. J. Chem.*, **1991**, *69*, 761–767).



The mechanism involves nucleophilic addition to a Z-substituted olefin followed by an intramolecular bimolecular nucleophilic substitution. Several side reactions also occur. Discuss the chemistry involved in this reaction, pointing out substituent effects at each stage.

## Chapter 10

- Predict the structure of the complex formed between oxirane and HCl. Use orbital interaction arguments and draw an orbital interaction diagram. How does your prediction compare with the experimental structure (Legon, A. C.; Rego, C. A.; Wallwork, A. L., *J. Chem. Phys.*, **1992**, *97*, 3050–3059)?
- In principle, an alkyl halide,  $R^1R^2CH-CCIR^3R^4$ , may react with a nucleophile,  $Nu^-$ , by  $S_N1$ ,  $S_N2$ , E1, E1cb, or E2 mechanisms. Choose  $R^1$ ,  $R^2$ ,  $R^3$ ,  $R^4$ , and  $Nu^-$  so that the course of the reaction may be expected to follow *each* of the mechanisms. The groups and nucleophile should be sufficiently different so that the stereochemical consequences of the reaction are obvious in your answer. Justify your choices using perturbative MO arguments but do not draw orbital interaction diagrams.
- Suggest a reason that fluoboric acid is a very strong acid.
  - Why does  $Ph_3C-OH$  dehydrate in the presence of  $HBf_4$ ? Would  $CH_3OH$  do the same thing?
  - What is the function of acetic anhydride in the  $Ph_3C^+$  synthesis?
  - Why does cycloheptatriene lose hydride readily? Would cyclopentadiene do the same?
  - Why can one not prepare tropylium tetrafluoroborate by the more straightforward route shown below?



- Suggest an explanation based on orbital interactions for the observed stereochemistry for E2 elimination reactions, that is, the strong stereoelectronic preference that the C—H and C—X bonds be anti-coplanar.
- Using simple orbital interaction considerations, explain the following observations. Use orbital interaction diagrams and show the orbitals clearly.
  - The acidity of the C—H bond in cyclopentadiene ( $pK_a = 16$ ).

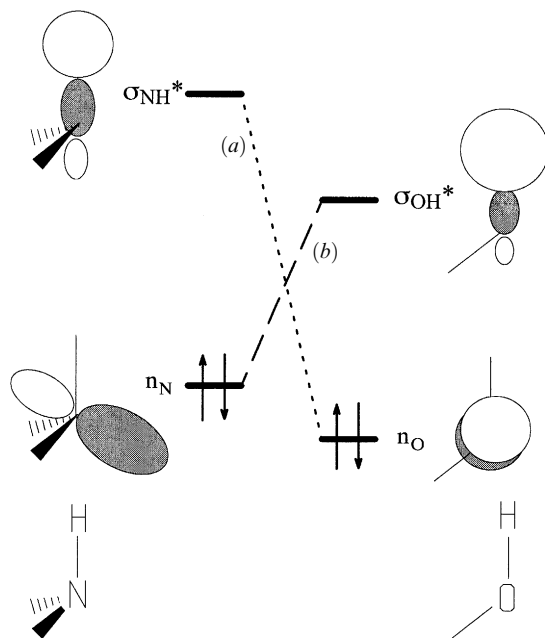
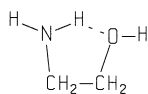
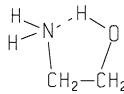


**Figure B10.1.** The frontier orbitals of an  $\text{—NH}_2$  group and an  $\text{—OH}$  group. The stronger hydrogen-bonding interaction (b) determines the most stable conformation of ethanolamine.

- (b) Ethanolamine exists in a number of hydrogen-bonded conformations, two of which are shown below.



**a**



**b**

One of the two is substantially more stable than the other. Which is more stable? Explain. (Räsänen, M.; Aspiala, A.; Homanen, L.; Murto, J., *J. Mol. Struct.*, **1982**, *96*, 81.)

**Answer to 5(b).** The orbitals and orbital energies of generic  $\text{—NH}_2$  and  $\text{—OH}$  groups are shown side by side in Figure B10.1. Conformations *a* and *b* exhibit hydrogen-bonding interactions *a* and *b*, respectively. Interaction *b* is favored by the smaller energy gap and additionally by increased polarization of both  $n_{\text{N}}$  and  $\sigma_{\text{OH}}^*$  orbitals.

6. The bond dissociation energy (BDE) and acidity constant ( $\text{p}K_{\text{a}}$ ) of cubane ( $\text{Cub—H}$ ) have been determined experimentally by Eaton and co-workers (Hare, M.; Emrick, T.; Eaton, P. E.; Kass, S. R., *J. Am. Chem. Soc.*, **1997**, *119*, 237–238). The BDE is unusually high for a tertiary C—H bond, 427 kJ/mol, about 25 kJ/mol higher than in isobutane. The C—H bond is also quite acidic, comparable to the acidity of the N—H bond in ammonia,  $\text{p}K_{\text{a}} = 36$ , indicating an unusual stability for the anion



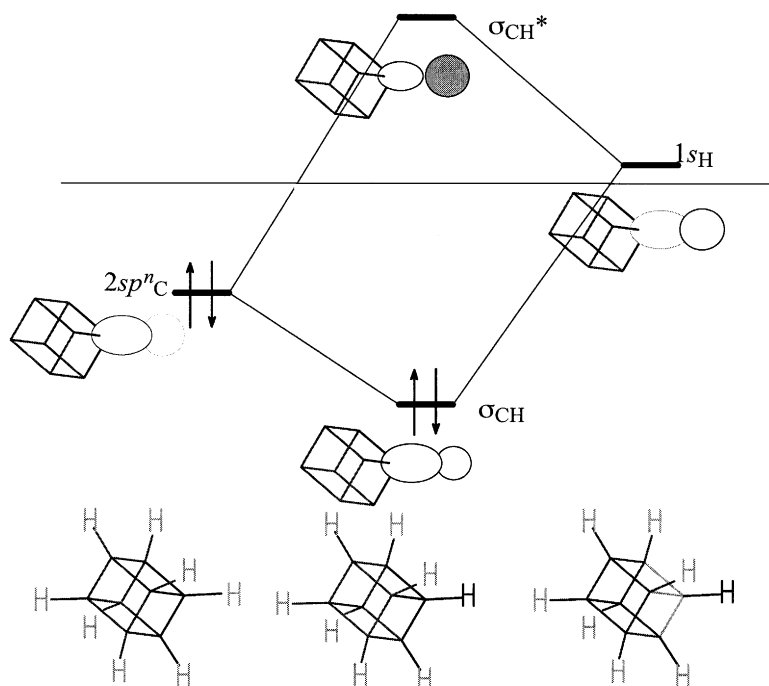
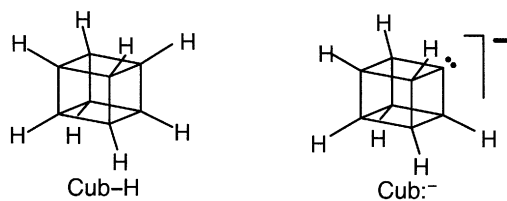


**Figure B10.2.** Frontier orbitals of a C—H bond in cubane. The high  $s$  character of the C orbital leads to a lower energy  $\sigma_{\text{CH}}^*$ .

Cub<sup>-</sup>. The normal  $\text{p}K_{\text{a}}$  for a hydrocarbon is about 50. Use orbital interaction diagrams to explain these features.



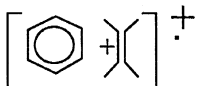
**Answer.** The orbitals and orbital energies of a C—H bond of cubane are shown in Figure B10.2. The key here is the nearly  $90^\circ$  angles of the C—C sigma bonds. This suggests a high  $p$  character in the C—C bonding orbitals and high  $s$  character for formally  $sp^n$  orbital of the C—H bond. As a consequence of the greater energy separation of the C and H orbitals, the  $\sigma_{\text{CH}}^*$  orbital is lower in energy and more polarized than for a normal alkyl C—H bond, and therefore more susceptible to attack by a base (more kinetic acidity). The resulting carbanion is more stable because of the lower energy of the  $sp^n$  orbital. The lower energy of this orbital, and consequently the lower energy of the  $\sigma_{\text{CH}}$  orbital, implies the greater C—H bond dissociation energy of the cubane C—H bond. The arguments respecting the acidity and BDE of the cubane C—H bond are derived from the discussion of heterolytic and

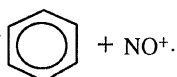
homolytic bond dissociations in Chapter 4. Entirely analogous arguments apply to the increasing acidity and increasing BDEs of C—H bonds in the series, alkyl CH, alkenyl CH, and alkynyl CH in Chapter 10. In this series, increased *s* character is due to the hybridization state of the C atom.

7. The Lewis acid–base complex  $\text{BH}_3\text{NH}_3$  crystallizes in a form which has a short  $\text{H}\cdots\text{H}$  distance ( $d_{\text{HH}} = 2.02 \text{ \AA}$ ), which has been described as a “dihydrogen bond” (Klooster, W. T.; Koetzle, T. F.; Siegbahn, P. E. M.; Richardson, T. B.; Crabtree, R. H., *J. Am. Chem. Soc.*, **1999**, *121*, 6337–6343). Provide a description of the  $\text{B—H}\cdots\text{H—N}$  “bond” using orbital interaction theory. Does your description also explain why the geometry is bent at  $\text{B—H}\cdots\text{H}$  and nearly linear at  $\text{H}\cdots\text{H—N}$ ?

## Chapter 11

- Use orbital interaction diagrams to explain why methoxybenzene (anisole) prefers a conformation in which the methyl group lies in the plane of the aromatic ring.
- Use orbital interaction diagrams to explain why benzyne is an excellent dienophile in Diels–Alder reactions.

3. Use orbital interaction diagrams to propose a possible structure of . Indicate the probable orbitals involved in the 680 nm absorption of this species.

4. Use orbital interaction diagrams to propose a possible structure of .

Indicate the probable orbitals involved in the 343 and 500 nm absorption of this species (see Kim, E. K.; Kochi, J. K., *J. Am. Chem. Soc.*, **1991**, *113*, 4962).

**Answer.** We postulate that the structure of the complex will be that which provides the most favorable HOMO–LUMO interaction(s), while minimizing interactions between occupied orbitals. The  $\text{NO}^+$  is isoelectronic with CO. Its LUMO will be very low lying, a degenerate pair of  $\pi^*$  orbitals polarized toward the nitrogen atom. The benzene HOMOs also are a degenerate pair with a single nodal surface bisecting the ring. Two structures may be postulated for the complex. An attractive possibility involves both HOMOs and both LUMOs, as shown in Figure B11.1a, analogous to transition metal carbonyl complexes. This complex, which has symmetry  $C_{6v}$ , has two serious strikes against it. First, there is no obvious bonding contribution from the *sp* hybrid orbital on N, as there is in transition metal carbonyl complexes, since the benzene LUMO has the wrong symmetry to interact with it. The *sp* hybrid orbital interactions are destabilizing. Second, the  $\pi^*$  orbitals of  $\text{NO}^+$  are not as highly polarized as they are in CO, leaving more of the orbital not involved in bonding. An alternative structure which does not have these disadvantages but uses only one of the HOMO–LUMO pairs for bonding is shown in Figure B11.1b. The corresponding interaction diagram (Figure B11.1c) suggests a possible secondary interaction of the component LUMOs, which lowers the LUMO for the system. Proposals for the 343- and 500-nm transitions are shown as dashed lines.

5. The cyclopentadienyl cation **1** has been studied extensively both theoretically and experimentally and was recently generated under solvolytic conditions (Allen, A. D.;

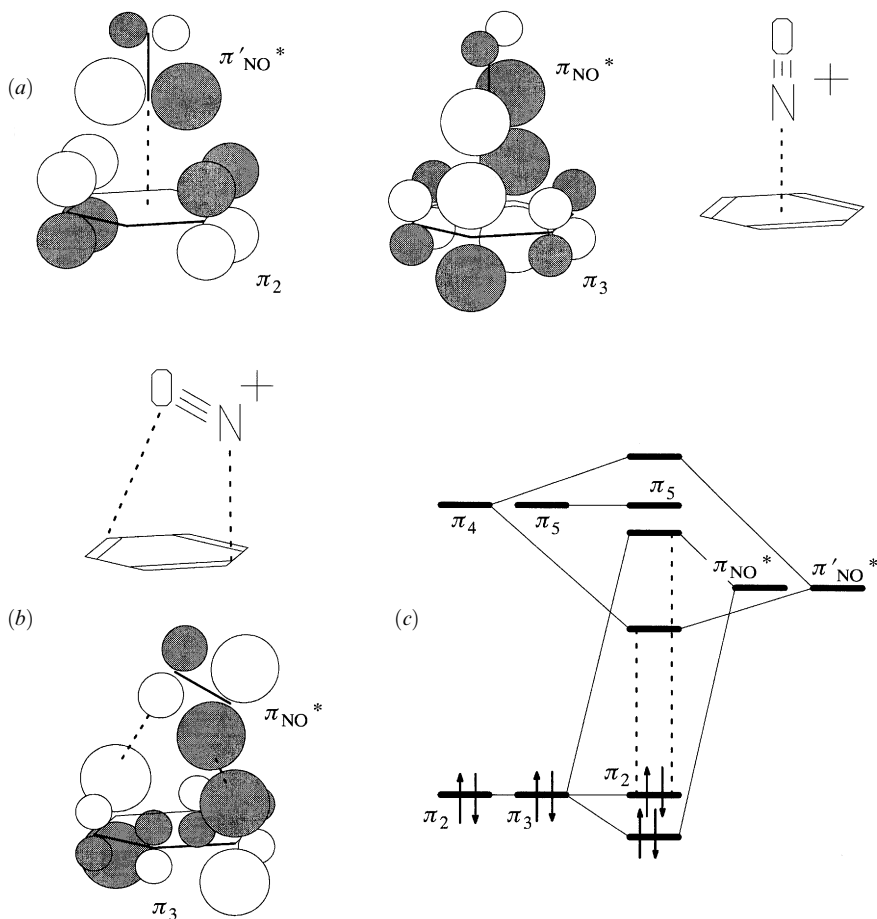
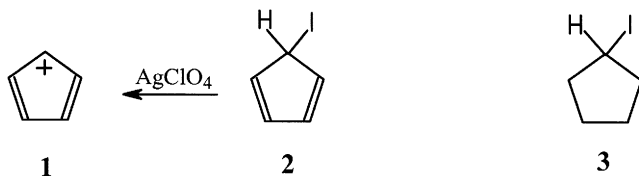


**Figure B11.1.** (a) Bonding interactions and structure of benzene- $\text{NO}^+$  complex with  $C_{6v}$  symmetry. (b) Bonding interactions and structure of benzene- $\text{NO}^+$  complex with  $C_s$  symmetry. (c) Interaction diagram for the  $C_s$  complex. The dashed lines correspond to possible assignments for the two lowest transitions.

Sumonja, M.; Tidwell, T. T., *J. Am. Chem. Soc.*, **1997**, *119*, 2371–2375, and references therein). It has the properties expected of an antiaromatic compound. It is very difficult to generate **1** under solvolytic ( $\text{S}_{\text{N}}1$ ) conditions from the precursor iodide **2**. Nevertheless, **2** undergoes  $\text{S}_{\text{N}}2$  reaction unusually rapidly (**2** reacts with bromide ion about 10 times faster than **3**).



Use principles of orbital interaction theory to explain:

- (a) Why the ground state of **1** is not singlet but triplet
  - (b) Why the  $C_5H_5$  ring is usually found as an *anion*
  - (c) Why nucleophilic substitution of **2** by bromide ion may be faster than substitution of the saturated compound cyclopentyl iodide **3** by bromide
6. A study by Abu-Raqabah and Symons (Abu-Raqabah, A.; Symons, M. C. R., *J. Am. Chem. Soc.*, **1990**, *112*, 8614) has characterized the pyridine–chlorine atom three-electron bonded species  $Py \leftarrow Cl$  by ESR and UV spectroscopy. In an earlier paper, Breslow and co-workers (Breslow, R.; Brandl, M.; Hunger, J.; Adams, A. D., *J. Am. Chem. Soc.*, **1987**, *109*, 3799) considered ring acylated pyridine–chlorine radicals to be  $\pi$  radicals and anticipated special stability for the 4-carboalkoxypyridine–chlorine radical.
- (a) Using an orbital interaction diagram, provide a bonding description that explains the red-shifted  $\sigma \rightarrow \sigma^*$  UV absorption and the increased length of the N–Cl bond.
  - (b) Show by means of orbital interaction arguments whether Breslow’s expectation is justified or not. In other words, would a Z substituent in the 4-position stabilize a pyridine–chlorine  $\pi$  radical?

**Answer to 6(a).** We consider the radical to be derived by addition of an electron to N-chloropyridinium cation. The character of the radical is in doubt because it is uncertain whether the LUMO of the *N*-chloropyridinium cation will be one of the  $\pi^*$  orbitals, or  $\sigma_{NCl}^*$ . While  $\sigma^*$  orbitals will, as a rule, be higher than  $\pi^*$  orbitals, this may not be the case here because of two factors: (a) the two orbitals involved in the  $\sigma$ -type interaction,  $n_N$  and  $3p_{Cl}$ , are both low in energy to start with and (b) the fact that a  $3p$  rather than a  $2p$  orbital is involved reduces the magnitude of the intrinsic interaction matrix element as explained in Chapter 4. The experimental evidence of Abu-Raqabah and Symons is consistent with a  $\sigma$ -type radical as shown in Figure B11.2. Occupancy of the  $\sigma_{NCl}^*$  orbital would lead to a substantial reduction in the N–Cl bond order. The consequent lengthening of the N–Cl bond is accompanied by reduction of the  $\sigma$ – $\sigma^*$  gap, which is seen as a red shift of the  $\sigma$ – $\sigma^*$  UV absorption.

**Answer to 6(b).** The  $\pi^*$  orbitals of *N*-chloropyridinium cation as calculated by SHMO are shown in Figure B11.3. An extra electron has been added to the LUMO  $\pi_4$ . Since  $\pi_4$  has its largest coefficient at the 4-position, it is clear that Breslow’s expectation is correct; the SOMO of a  $\pi$  radical would interact favorably with a Z substituent at the 4-position. This is readily verified by an SHMO calculation on the *N*-chloropyridinyl radical with a Z-substituent at this position.

7. The “inorganic benzene” borazine has been shown to undergo electrophilic substitution in a manner very similar to benzene itself. Does the electrophile attack at B or N? Use orbital interaction theory to predict the site of attack. Compare this with the prediction on the basis of an SHMO calculation and experimental findings (Chivarino, B.; Crestoni, M. E.; Di Marzio, A.; Fornarini, S.; Rosi, M., *J. Am. Chem. Soc.*, **1999**, *121*, 11204–11210).

**Answer.** This is a bit of a trick question since the “Kekule resonance structure” of borazine tends to imply that the positively charged electrophile should go for the negatively charged boron atoms. Consideration of the orbital interactions shown in Figure B11.4 quickly assures us that the occupied MO electron density is almost

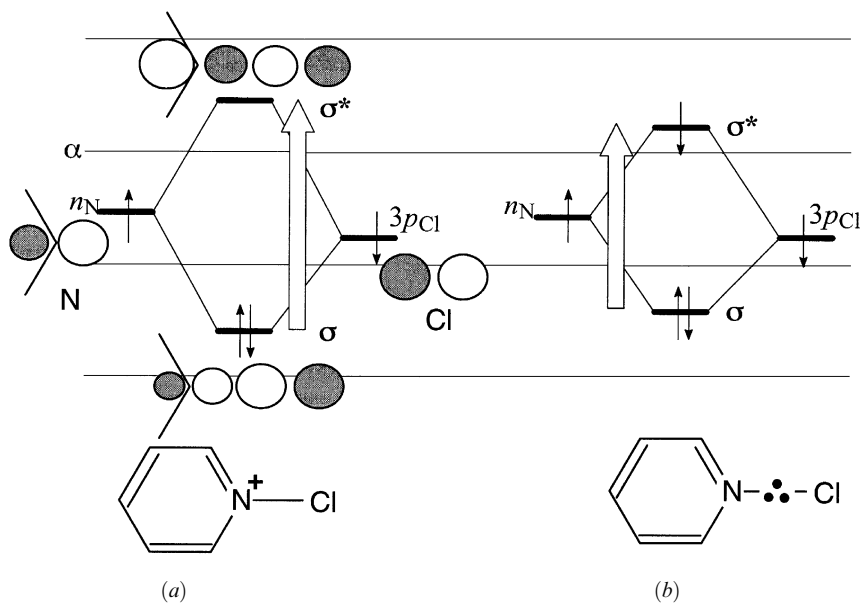


**Figure B11.2.** The sigma orbitals of the cation (a) and radical (b) of N-chloropyridine. The partial occupancy of the  $\sigma^*$  orbital leads to a longer N—Cl bond, a reduction of the  $\sigma$ — $\sigma^*$  separation, and a red shift in the  $\sigma$ — $\sigma^*$  electronic excitation (vertical white arrow).

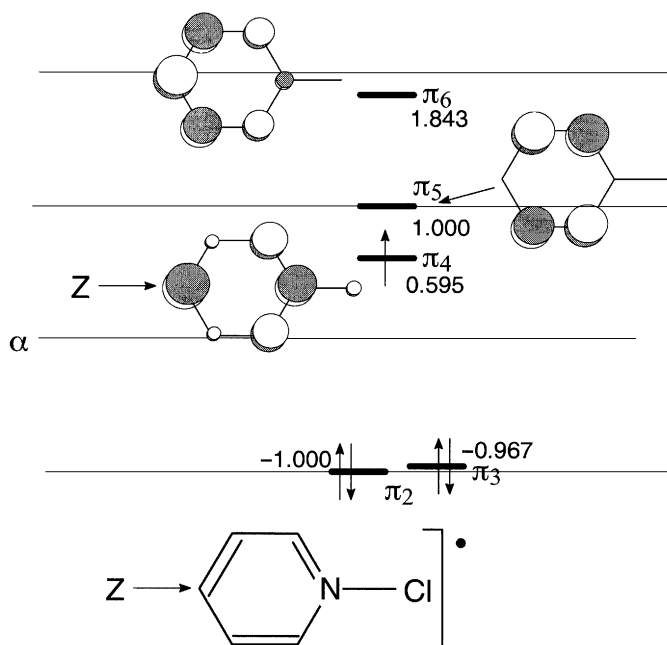


**Figure B11.3.** The SHMO  $\pi$  orbitals of N-chloropyridinyl  $\pi$  radical.

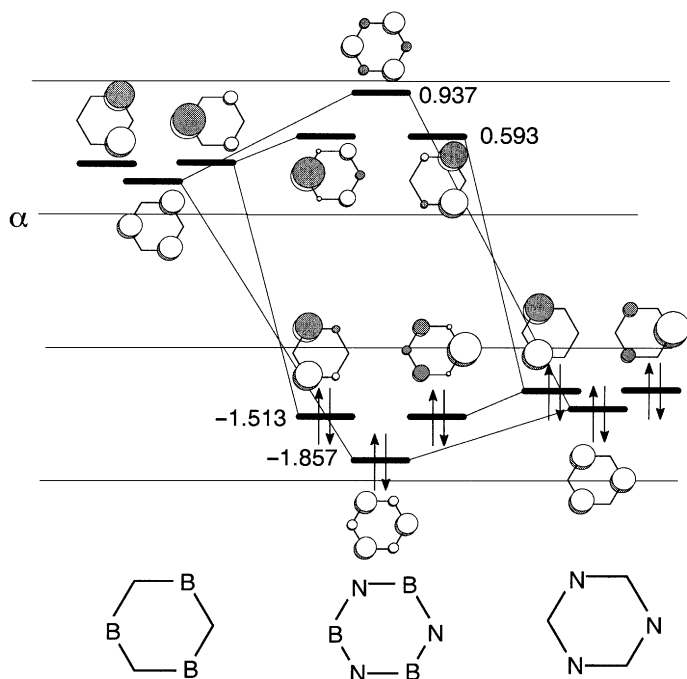
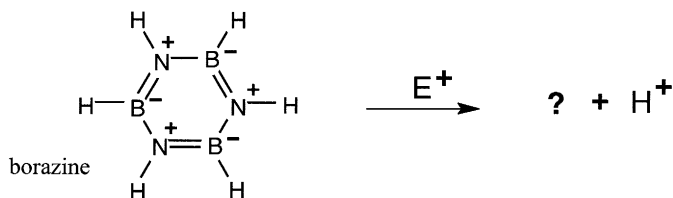


**Figure B11.4.** The SHMO  $\pi$  orbitals and orbital energies of borazine, shown as the result of orbital interactions between symmetrized group orbitals of an  $N_3$  equilateral triangle and a  $B_3$  equilateral triangle.

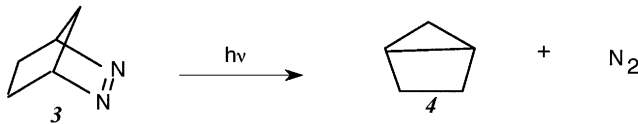
entirely on the N atoms, so this must be the site of electrophilic attack. The energies and orbital sizes shown in the figure are readily derived by use of the SHMO program using parameters appropriate for tricoordinated boron and nitrogen atoms.



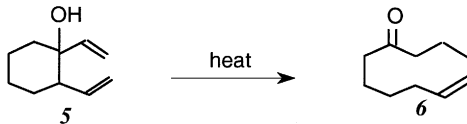
## Chapter 12

- In a Diels–Alder reaction, when both  $\pi$  systems are polarized, the more favorable overlap, and therefore the stronger interaction, occurs when the ends with the larger coefficients get together and the smaller coefficients get together. Predict the major product of each of the following cycloaddition reactions:
  - (*1E*)-1-phenyl-1,3-butadiene + acrolein  $\rightarrow$
  - (*3E*)-2-methyl-1,3-pentadiene + formaldehyde  $\rightarrow$

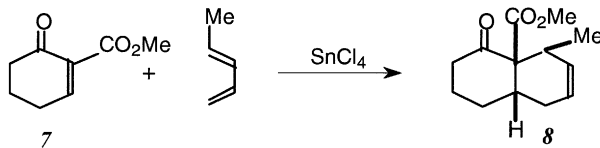
- (c) 1-carbomethoxycyclopentadiene + ethenol acetate  $\rightarrow$   
 (d) acrolein + ethenol acetate  $\rightarrow$  (an oxacyclohexene)  
 (e) methyl 1,3-butadien-1-yl ether + methyl propynoate  $\rightarrow$
2. Provide a general classification in terms of “s” and “a” components for each of the reactions given below. Verify, using the “odd sum” rule, that the reaction is *allowed* under the specified reaction conditions.
- (a) 2,3-Diazabicyclo[2.2.1]hept-2-ene **3** yields bicyclo[2.1.0]pent-2-ene **4** upon photolysis.



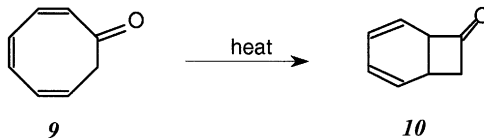
- (b) Compound **5** yields **6** upon heating (*Hint*: there is an enol intermediate).



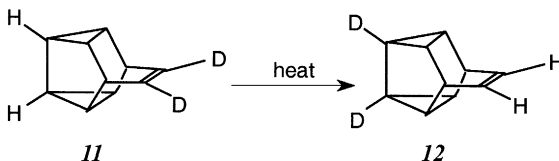
- (c) 2-Carbomethoxy-2-cyclohexen-1-one **7** reacts with (*E*)-1,3-pentadiene to yield the bicyclic product **8** as the major product. What is the role of stannic chloride in the reaction?



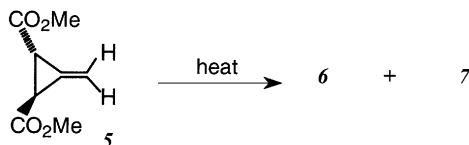
- (d) Cyclooctatrienone **9** is converted smoothly to the bicyclic dienone **10** upon heating.



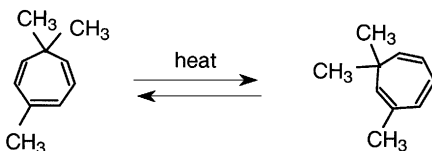
- (e) 9,10-Dideuteriosnoutene **11** is transformed to 7,8-dideuteriosnoutene **12** upon heating.



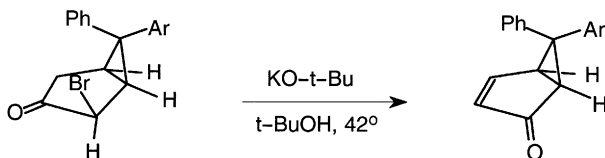
- (f) What are the two optically active products produced upon thermal rearrangement of Feist's ester **5**?



- (g) The following rearrangement of cycloheptatrienes is not concerted but proceeds by thermally allowed steps. Suggest a mechanism.



- (h) Propose a mechanism for the following reaction.



3. Classify the following reactions by the *component analysis* method (e.g.,  $\pi 4_s + \sigma 2_a + \dots$ ). Decide whether the reaction *as shown* is thermally allowed. Show clearly the orbitals on which you base your analysis.

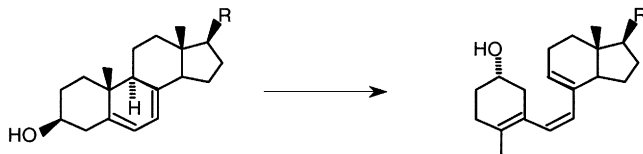
- (a) The cycloaddition of acetylene to cyclobutadiene to give Dewar benzene:



- (b) The rearrangement of Dewar benzene to benzene:



- (c) The electrocyclic opening of the steroid-derived cyclohexadiene:

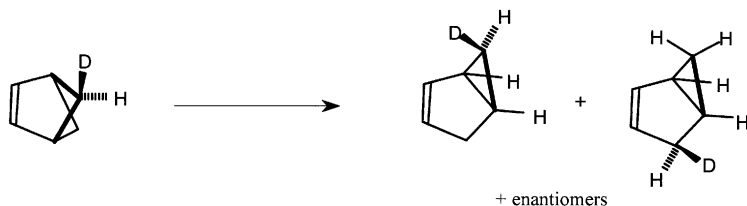


- (d) The opening of cyclopropyl cations to allyl cations:

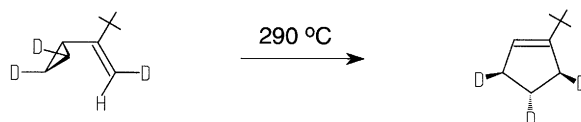


- (e) The sigmatropic rearrangement of bicyclo[2.1.1]hex-2-ene to bicyclo[3.1.0]hex-2-ene:





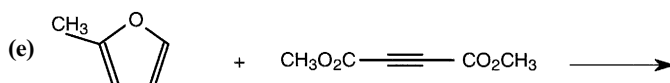
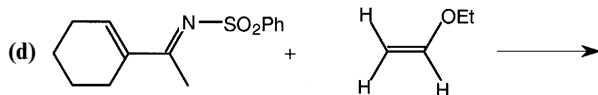
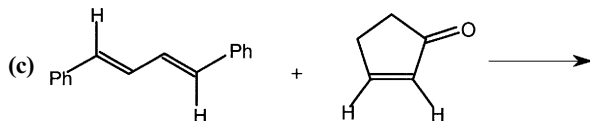
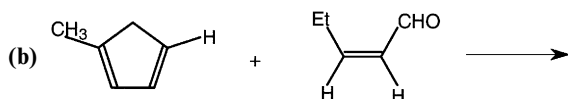
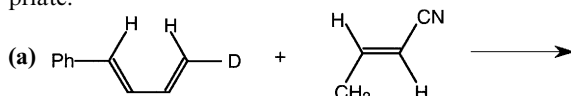
- (f) The following stereochemistry was recently established for the thermal vinylcyclopropane to cyclopentene rearrangement (Gajewski, J. J.; Olson, L. P.; Willcott III, M. R., *J. Am. Chem. Soc.*, **1996**, *118*, 299–306). Using whatever method you wish, decide whether the experimental result is consistent with a concerted allowed [1,3] sigmatropic rearrangement.



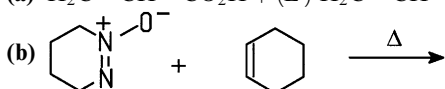
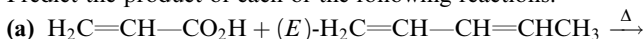
4. Use orbital interaction diagrams to explain the following observations:
- Benzynes is an excellent dienophile in Diels–Alder reactions.
  - A mixture of cyclopentadiene and ethene yields only dicyclopentadiene and not norbornene (bicyclo[2.2.1]hept-2-ene).
  - 2-Methylpropenyl cation adds to cyclopentadiene to form **1**.



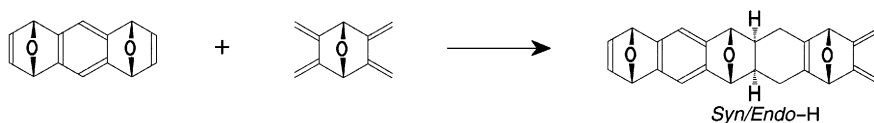
5. Show the expected products of the following Diels–Alder reactions. Pay careful attention to stereochemistry and regioselectivity if these considerations are appropriate.



6. Predict the product of each of the following reactions:

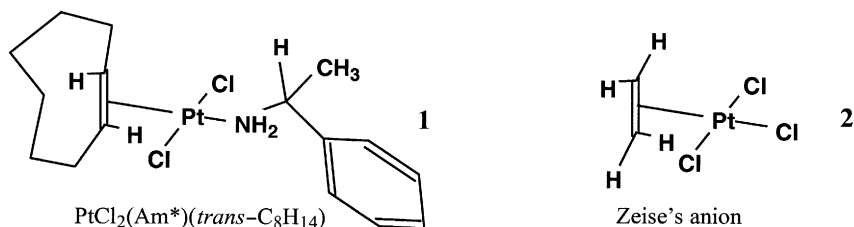


7. The origin of the diastereoselectivity found for the Diels–Alder reaction, has been attributed to a dominance of interactions between the occupied MOs of the reactants, that is, to four-electron, two-orbital interactions rather than to the usual secondary aspect of the HOMO–LUMO interaction. Show by suitable orbital interaction diagrams why this may be the case. The relevant references are found in Ashton, P. R.; Brown, G. R.; Isaacs, N. S.; Giuffrida, D.; Kohnke, F. H.; Mathias, J. P.; Slawin, A. M. Z.; Smith, D. R.; Stoddart, J. F.; Williams, D. J., *J. Am. Chem. Soc.*, **1992**, *114*, 6330–6353. *Note:* The process shown in the following reaction forms the basis for the construction of larger stereoregular molecules and has been termed *molecular LEGO*.



## Chapter 13

1. (a) An optically active complex,  $\text{PtCl}_2(\text{Am}^*)(\text{C}_2\text{H}_4)$  **1** ( $\text{Am}^* = \alpha$ -methylbenzylamine), derived from Zeise's anion **2**, was used in the first optical resolution of *trans*-cyclooctene. The ethylene could be exchanged for *trans*-cyclooctene to give both diastereomers of  $\text{PtCl}_2(\text{Am}^*)(\text{trans-C}_8\text{H}_{14})$ , which could be separated (Cope, A. C.; Ganellin, C. R.; Johnson, Jr., H. W.; Van Auken, T. V.; Winkler, H. J. S., *J. Am. Chem. Soc.*, **1963**, *85*, 3276–3279). Derive a bonding picture for the metal-to-distorted alkene part of the complex **1**.



(b) Exchange of the alkene in complexes such as **1** or **2** have been shown (Plutino, M. R.; Otto, S.; Roodt, A.; Elding, L. I., *Inorg. Chem.*, **1999**, *38*, 1233–1238) to take place by an associative mechanism involving displacement of the labile *trans* ligand. On the basis of the frontier orbitals of **2**, suggest a structure for the initial associative complex between **2** and ethylene.

2. The commercially important Wacker process for the oxidation of ethylene is shown in Figure B13.1 (see Shriver, D. F.; Atkins, P. W.; Langford, C. H., *Inorganic Chemistry*, Oxford University Press, Oxford, 1994, p. 728).

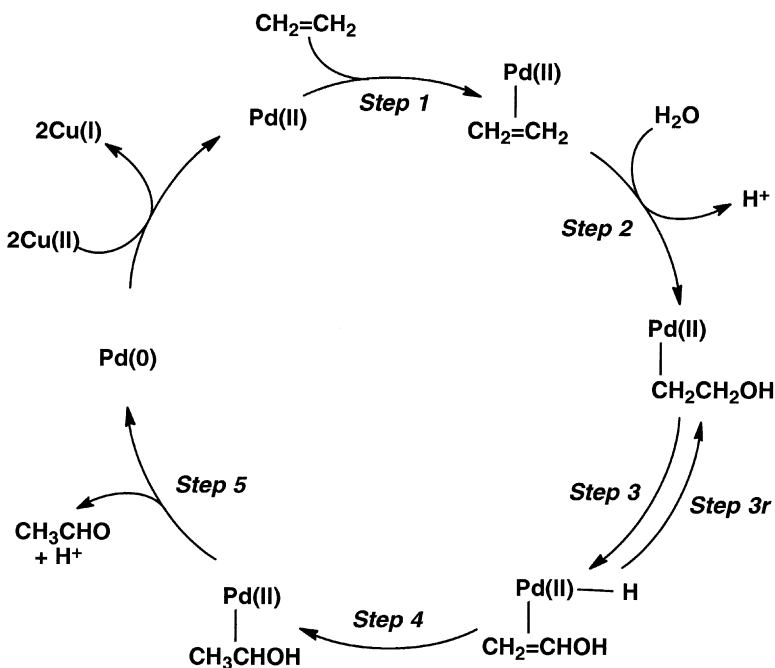
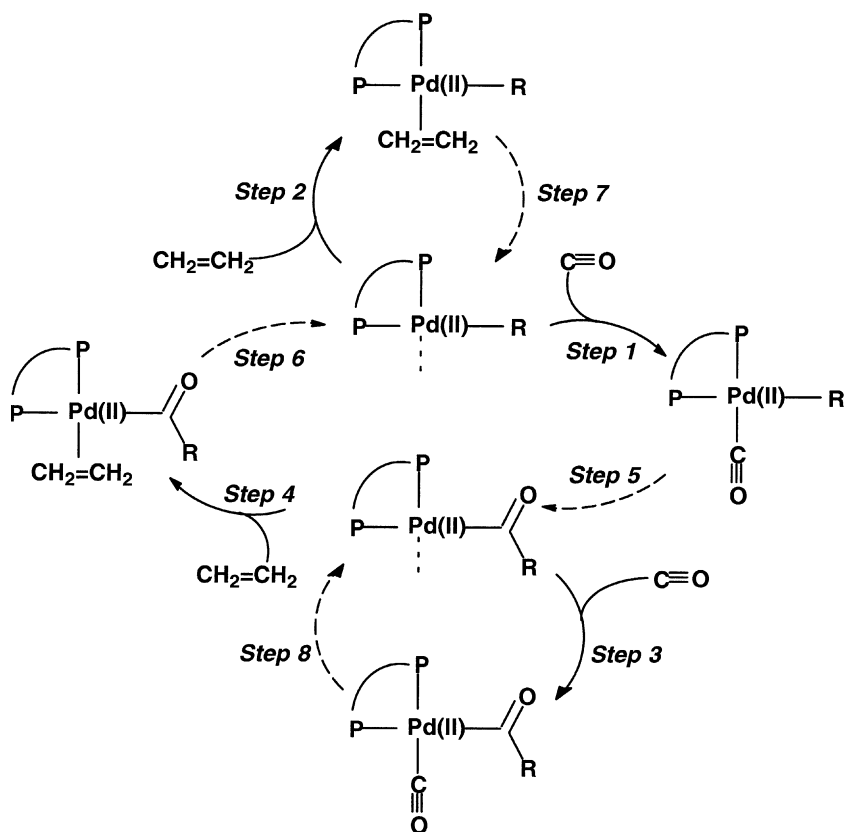


Figure B13.1. Schematic of the Wacker process for the oxidation of ethylene.

- In step 2, show the orbitals involved in the nucleophilic addition of water to the complex.
  - Discuss step 3 in terms of anchimeric assistance by the hydroxyl group.
  - Compare steps 3r and 4. Which should be the more probable based on orbital interaction theory?
  - Discuss step 5 in terms of anchimeric assistance by the hydroxyl group.
3. A catalytic system based on bisphosphine-substituted  $\text{Pd(II)}$  in the presence of both  $\text{CO}$  and an alkene leads to the formation of alternating olefin-CO copolymers,  $(\text{CH}_2\text{CH}_2\text{C(O)-})_n$ , rather than homopolymers. The system has been studied theoretically (Margl. P.; Ziegler, T., *J. Am. Chem. Soc.*, **1996**, *118*, 7337–7344). A schematic is shown in Figure B13.2. According to the study, the alternation arises from the lower activation energies for steps 5 (48 kJ/mol) and 6 (58 kJ/mol) compared to step 7 (65 kJ/mol) and the greater exothermicity of  $\text{CO}$  attachment (step 1,  $-219$  kJ/mol) over ethylene attachment (step 2,  $-200$  kJ/mol). Apply principles of orbital interaction theory to rationalize the trends in activation energies and binding energies.

**Answer.** Three aspects of the scheme shown in Figure B13.2 may be examined by orbital interaction theory: (a) the binding of  $\text{CO}$  compared to ethylene; (b) the reactivity of coordinated carbonyl compared to ethylene with respect to reactivity toward intramolecular nucleophilic attack; and (c) the migratory aptitude of alkyl versus carbonyl groups.



**Figure B13.2.** Schematic of the copolymerization of CO and ethylene. The dashed arrows (steps 5–8) represent intramolecular rearrangement processes.

- (a) Figure B13.3a shows the possible interactions between a tricoordinated Pd(II) complex and ethylene or CO. The binding of ethylene is entirely analogous to Zeise's salt, which was discussed in Chapter 13 (Figure 13.7). Only the positions of the ethylene donor ( $\pi_{CC}$ ) and acceptor ( $\pi_{CC}^*$ ) are shown for reference. Carbon monoxide, having a higher donor orbital ( $n_{CO}$ ), and a pair of lower energy acceptor orbitals ( $\pi_{CO}^*$ ) will bind more strongly to the metal, in spite of the less favorable four-electron, two-orbital interaction with the  $ndz^2$  orbital. In other words, the carbonyl donor and acceptor interactions, i and ii, respectively, will both be more favorable than the corresponding interactions for ethylene, iii and iv, respectively, but the repulsive interaction with  $ndz^2$  will also be stronger for CO. Thus, with reference to Figure B13.2, step 1 is more exothermic than step 2, and step 3 is more exothermic than step 4.
- (b) For an assessment of the acceptor aptitude of ethylene compared to carbonyl (acyl or CO) ligands on the metal, one needs to consider the energy of the  $\pi_{CC}^*$  and  $\pi_{CO}^*$  orbitals and the possible  $\sigma$ -type overlap with a group in the cis position

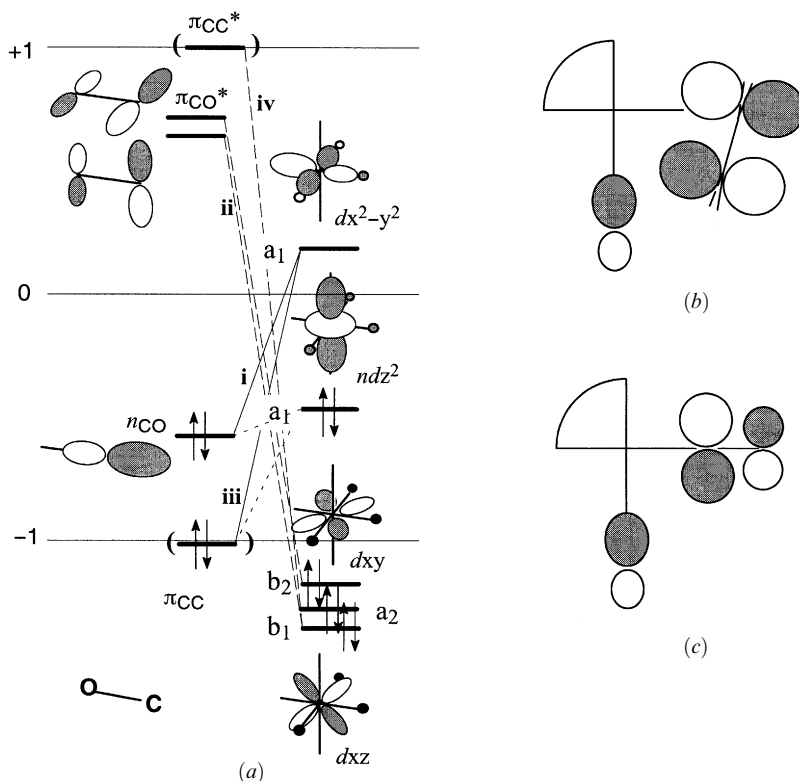


**Figure B13.3.** (a) Comparison of bonding of CO and ethylene to Pd(II). (b) Distortion of bound ethylene to favor interaction between  $\pi_{CC}^*$  and a cis ligand. (c) Compared to interaction with  $\pi_{CO}^*$  of ligated CO or acyl group.

of the metal. In consideration of the relative energies, you may ignore the presence of the metal since  $\pi$  backbonding in these cationic complexes is weak. Energy considerations dictate that the acceptor ability of the acyl or carbonyl group should be better than that of ethylene simply because the  $\pi_{CO}^*$  orbital is at lower energy than  $\pi_{CC}^*$ . However, and unfortunately, geometric considerations have the opposite effect, as shown graphically in Figures B13.3*b,c*. The ethylene can readily shift to improve overlap of the  $\pi_{CC}^*$  orbital with a cis ligand while maintaining bonding to the metal through the opposite C atom.

- (c) The migratory aptitude of the alkyl group should be greater than of acyl because the  $\sigma$  bond to alkyl (which resembles a nonbonded orbital on  $sp^3$  hybridized carbon) is higher in energy than the  $\sigma$  bond to acyl (which resembles a nonbonded orbital of  $sp^2$  hybridized carbon). Thus, with reference to Figure B13.2, step 5, in which an alkyl group migrates to carbonyl, is more facile than step 7, in which an alkyl group migrates to ethylene. To obtain the observed alternation in copolymerization, step 6, in which an acyl group migrates to ethylene, yielding a longer alkyl-like segment, must be easier than step 7, and also step 8, in

which an acyl group migrates to carbonyl, yielding adjacent carbonyl groups in the polymer chain. The theoretical calculations yield this result, but it cannot be deduced from simple orbital interaction considerations.

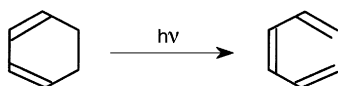
## Chapter 14

1. A key step in one route to the synthesis of hexamethyl Dewar benzene is the cycloaddition of 2-butyne to tetramethylcyclobutadiene (stabilized by Al cation). Using the parent compounds (no methyls), develop a Woodward–Hoffmann orbital correlation diagram for the reaction and determine whether the reaction is thermally allowed.
2. This question requires you to construct an orbital correlation diagram of the Woodward–Hoffmann type.
  - (a) Show that the rearrangement of Dewar benzene to benzene is a thermally forbidden process.



[Breslow et al. (Breslow, R.; Napierski, J.; Schmidt, A. H., *J. Am. Chem. Soc.*, **1972**, *94*, 5906–5907) have determined that the activation energy for the rearrangement is 96.2 kJ/mol.]

- (b) Show that the photochemical electrocyclic ring opening of 1,3-cyclohexadiene to *cis*-1,3,5-hexatriene should occur by conrotatory motion.



[Although long predicted by the Woodward–Hoffmann rules, this was first demonstrated experimentally in 1987 (Trulson, M. O.; Dollinger, G. D.; Mathies, R. A., *J. Am. Chem. Soc.*, **1987**, *109*, 586–587).]

- (c) Cyclopropyl cations open to allyl cations spontaneously and stereospecifically. Predict the stereochemical course of ring opening, disrotatory or conrotatory?



- (d) Further to (c) above, it has been shown both experimentally and theoretically that 2,3-dialkyl-1,1-difluorocyclopropanes isomerize thermally in a disrotatory manner (Tian, F.; Lewis, S. B.; Bartberger, M. D.; Dolbier, Jr., W. R.; Borden, W. T., *J. Am. Chem. Soc.*, **1998**, *120*, 6187–6188). Explain why these compounds would be expected to behave analogously to cyclopropyl cations.

**Answer to 2(b).** The orbital correlation diagram for the rearrangement of Dewar benzene to benzene is shown in Figure B14.1. This is a special case of electrocyclic ring opening. The bridgehead carbon atoms must rotate in a disrotatory fashion, preserving a single mirror plane of symmetry,  $\sigma_1$ . A second mirror plane,  $\sigma_2$ , is also preserved, but this does not determine the allowedness of the reaction.

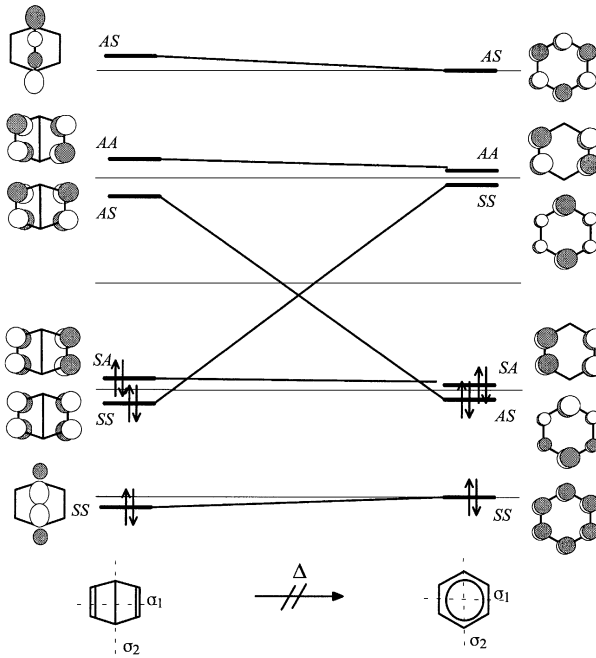


**Figure B14.1.** Orbital correlation diagram for rearrangement of Dewar benzene to benzene. Two vertical planes of symmetry are preserved.

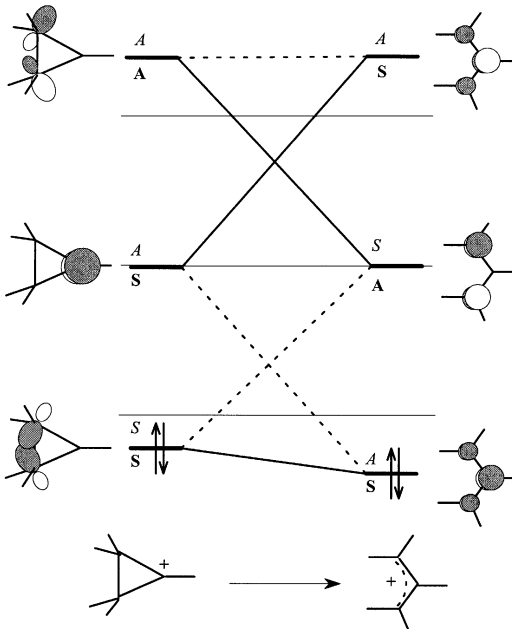
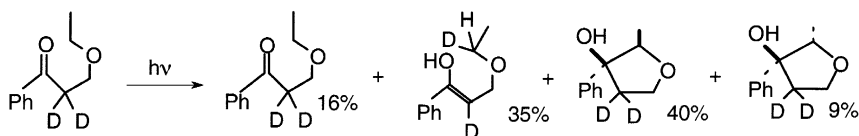


**Figure B14.2.** Orbital correlation diagram for electrocyclic opening of cyclopropyl cation: S, A and solid lines indicate disrotatory opening; S, A and dotted lines indicate conrotatory opening.

**Answer to 2(d).** This question illustrates that it is the number of electrons, not the number of nuclei, that is important. The orbital correlation diagram is shown in Figure B14.2. In disrotatory opening, a mirror plane of symmetry is preserved. This correlation is with bold symmetry labels and solid correlation lines. Italic symmetry labels and dotted correlation lines denote the preserved rotational axis of symmetry for conrotatory ring opening. For the cation, the disrotatory mode is the thermally allowed mode. It corresponds to a  $\sigma_{2s} + \omega_0s$  pericyclic reaction.

## Chapter 15

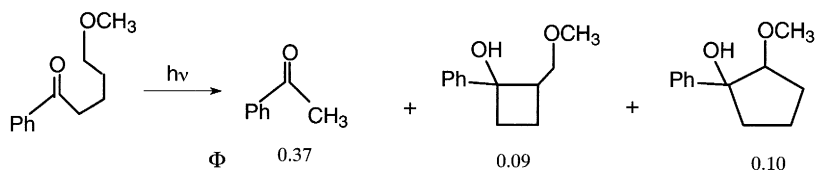
1. In a recent article on photoexcited ketones, Wagner reported the following overall reaction (Wagner, P. J., *Acc. Chem. Res.*, **1989**, 22, 83), a mechanism thought to involve a diradical intermediate:



- (a) Draw the structure of the intermediate diradical and explain how each of the products could be derived from it.
- (b) Produce a state correlation diagram of the Dauben–Salem–Turro type and analyze the reaction in terms of the carbonyl electronic states which are likely to be involved (you may ignore the effect of the phenyl group on the carbonyl and radical orbitals; it will not change the relative energies of the states).

**Answer.** All of the products can be directly derived from the diradical shown in Figure B15.1a. The state correlation diagram for the Norrish Type II reaction is shown in Figure B15.1b. The insert shows the two product orbitals and the configuration of the  $^3D$  state. Both the singlet and triplet  $n\pi^*$  states of the carbonyl group descend to product diradical ground states. Efficient intersystem crossing (IC) on the singlet manifold may account for the 16% yield of recovered starting material.

2. In the article mentioned in question 1, Wagner reported the following overall reaction, a mechanism thought to involve two different diradical intermediates:



- (a) Draw the structures of the intermediate diradicals and explain how each of the products could be derived from it.
- (b) Produce a state correlation diagram of the Dauben–Salem–Turro type and analyze the reaction in terms of the carbonyl electronic states which are likely to be involved (you may ignore the effect of the phenyl group on the carbonyl and radical orbitals; it will not change the relative energies of the states).
3. This question involves the analysis of carbonyl photochemistry using Dauben–Salem–Turro state correlation diagrams.



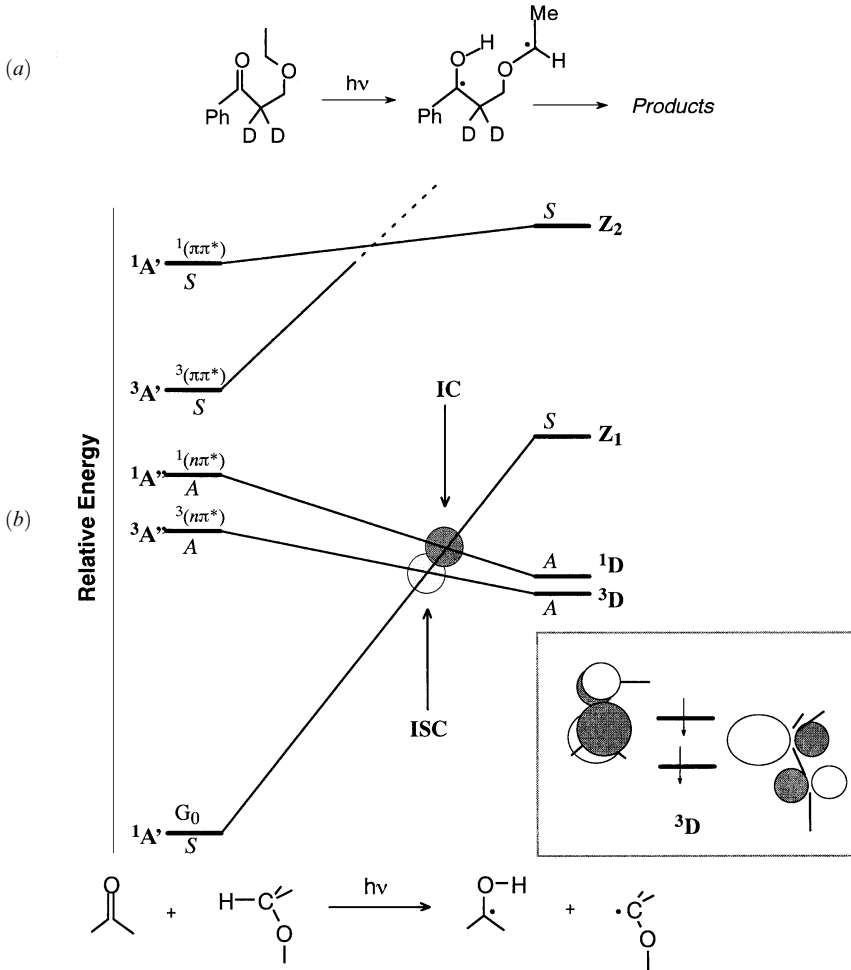
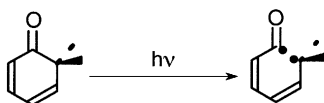


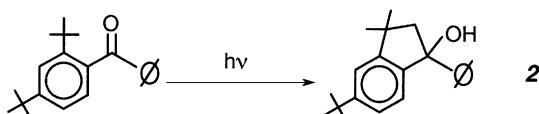
**Figure B15.1.** (a) Intermediate diradical. (b) State correlation diagram for the Norrish Type II reaction.

- (a) Provide an analysis of the photoreduction of benzophenone to benzpinacol in isopropyl alcohol (the reaction you carried out in the laboratory). What was the photoreactive state for the reaction? What was the effect of added naphthalene and why did it have this effect?
- (b) A characteristic of the photochemistry of cyclohexadienones is cleavage of the C—C bond next to the carbonyl, as shown below for 2,2-dimethyl-2,4-cyclohexadienone. Develop a Dauben–Salem–Turro state correlation diagram for the photochemical step shown and, on the basis of your diagram, discuss the efficiency of the reaction on the singlet and triplet manifold [see also question 1(d)].

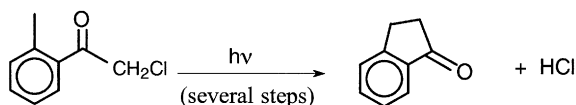


4. This question involves the analysis of carbonyl photochemistry using Dauben–Salem–Turro state correlation diagrams.

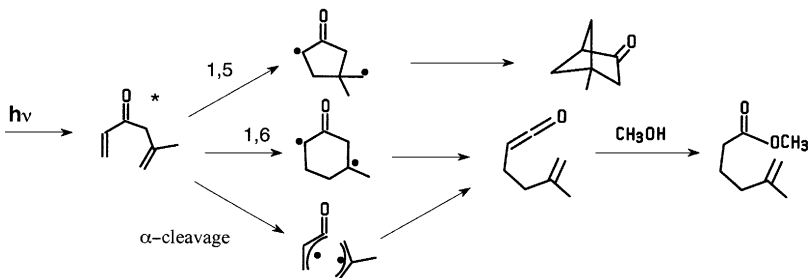
(a) 2,4-Di-*t*-butylbenzophenone yields the benzocyclopentanol **2** upon photolysis. An intermediate diradical is involved. Show the structure of the intermediate diradical. Develop a Dauben–Salem–Turro state correlation diagram for the photochemical step and, on the basis of your diagram, discuss the efficiency of the reaction on the singlet and triplet manifold.



5. Photolysis of  $\alpha$ -chloro-*o*-methylacetophenones yields 1-indanones. The mechanism has been studied by laser flash photolysis (Netto-Ferreira, J. C.; Scaiano, J. C., *J. Am. Chem. Soc.*, **1991**, *113*, 5800). Develop a Dauben–Salem–Turro state correlation diagram for the photochemical step and, on the basis of your diagram, discuss the efficiency of the reaction on the singlet and triplet manifold. Do the experimental results agree with your analysis?

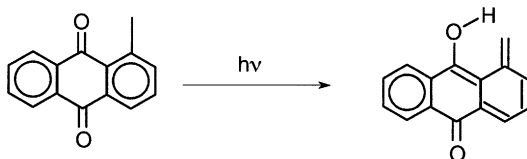


6. The photochemistry of 1,5-hexadien-3-ones has been examined by Dauben and co-workers. A relatively rare dependence of the intramolecular enone–olefin photoaddition of several derivatives has been observed. Discuss the mechanistic possibilities in terms of Dauben–Salem–Turro state correlation diagrams. (See Dauben, W. G.; Cogen, J. M.; Ganzer, G. A.; Behar, V., *J. Am. Chem. Soc.*, **1991**, *113*, 5817.)

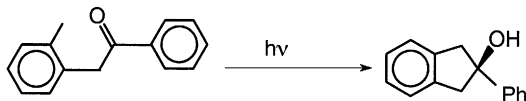


7. The mechanism of photoenolization in 1-methylantraquinone has been studied in detail (Gritsan, N. P.; Khmelinski, I. V.; Usov, O. M., *J. Am. Chem. Soc.*, **1991**, *113*, 9615). The reaction was found to occur in both the singlet and triplet ( $n\pi^*$ ) states. Develop a Dauben–Salem–Turro state correlation diagram for the photochemical step and, on the basis of your diagram, discuss the efficiency of the reaction

on the singlet and triplet manifold. Do the experimental results agree with your analysis?

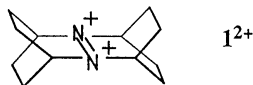


8. The mechanism of photocyclization of  $\alpha$ -(*o*-tolyl)acetophenones has been explored [(a) Wagner, P. J.; Meador, M. A.; Zhou, B.; Park, B.-S., *J. Am. Chem. Soc.*, **1991**, *113*, 9630. (b) Wagner, P. J.; Zhou, B.; Hasegawa, T.; Ward, D. L., *J. Am. Chem. Soc.*, **1991**, *113*, 9640]. Develop a Dauben–Salem–Turro state correlation diagram for the photochemical step and, on the basis of your diagram, discuss the efficiency of the reaction on the singlet and triplet manifold. Do the experimental results agree with your analysis?



### Miscellaneous

1. Using orbital interaction theory wherever appropriate, discuss the chemistry of the diazenium dication of 2,7-diazatetracyclo[6.2.2.2<sup>3,6</sup>.2<sup>7</sup>]tetradecane  $1^{2+}$  (see Nelsen, S. F.; Wang, Y., *J. Am. Chem. Soc.*, **1991**, *113*, 5905).



2. Discuss the mechanism of action of brewer's yeast pyruvate decarboxylase using orbital interaction theory wherever appropriate. For the mechanism, see Zeng, X.; Chung, A.; Haran, M.; Jordan, F., *J. Am. Chem. Soc.*, **1991**, *113*, 5842.

**Answer.** The mechanism of pyruvate decarboxylase involves use of the cofactor thiamine pyrophosphate TPP (called thiamine diphosphate; TDP in the reference) which contains the thiazolium ring. It is shown in Figure B.1. Each of the five steps involves some aspect that can be addressed by orbital interaction theory. In step 1, a zwitterionic carbanion is generated. This may alternatively be regarded as a carbene (not zwitterionic at all!) stabilized by two X:-type substituents. Such carbenes are nucleophilic, as we have seen in Chapter 7. In step 2, nucleophilic attack occurs at the keto carbonyl group. The principles governing carbonyl reactivity were discussed in Chapter 8. Alternatively, an SHMO calculation reveals that pyruvate has a very low LUMO ( $\alpha + 0.266|\beta|$ ) and the largest coefficient of the LUMO is at this carbon atom (0.60 vs. 0.39 at C1). Loss of CO<sub>2</sub> in step 3 is facile if the C—C bond can adopt a position perpendicular to the plane of the ring, since then overlap with the highly polarized and low LUMO of the aminium group is maximized and electron transfer can occur. The resulting species, shown as a zwitterionic carbanion, may also be viewed as a neutral enolamine, which by SHMO is seen to have a very high HOMO ( $\alpha - 0.471|\beta|$ ) and the largest coefficient on the carbon shown as being protonated by the enzyme in step 4. E2 elimination of acetaldehyde in step 5 is possible if the C—C bond and OH bonds can adopt a coplanar arrangement.

3. Allylic acetals rearrange under acid catalysis to produce tetrahydrofurans.

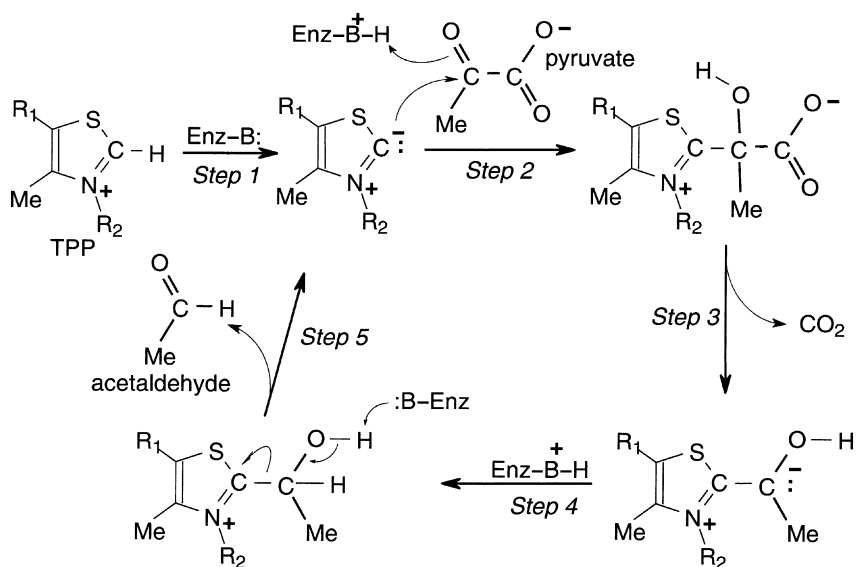
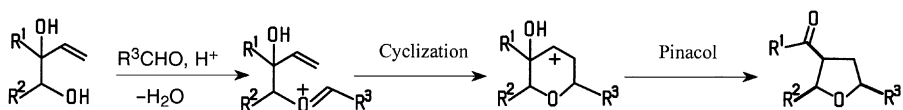


**Figure B.1.** Mechanism for the conversion of pyruvic acid to acetaldehyde and CO<sub>2</sub> by pyruvate decarboxylase.



The mechanism has been shown to involve a cyclization step followed by a pinacol rearrangement (Hopkins, M. H.; Overman, L. E.; Rishton, G. M., *J. Am. Chem. Soc.*, **1991**, *113*, 5354; see also Bach et al., p. 5365, and Woods et al., p. 5378, mentioned in questions 4 and 5, respectively). Provide a detailed mechanism for the reaction and discuss features of the steps and intermediates from the point of view of orbital interactions.

- The mechanism of oxidation of amines by hydrogen peroxide has been investigated theoretically (Bach, R. D.; Owensby, A. L.; Gonzalez, C.; Schlegel, H. B.; McDouall, J. J. W., *J. Am. Chem. Soc.*, **1991**, *113*, 6001) and has been shown to be analogous to an S<sub>N</sub>2 attack by nitrogen on the O—O bond with simultaneous transfer of hydrogen. Compare the ab initio results of Bach et al. to expectations based on orbital interaction theory.
- The mechanism of epoxidation of olefins by peroxyacids has been probed by an “endocyclic restriction test” (Woods, K. W.; Beak, P., *J. Am. Chem. Soc.*, **1991**, *113*, 6281):



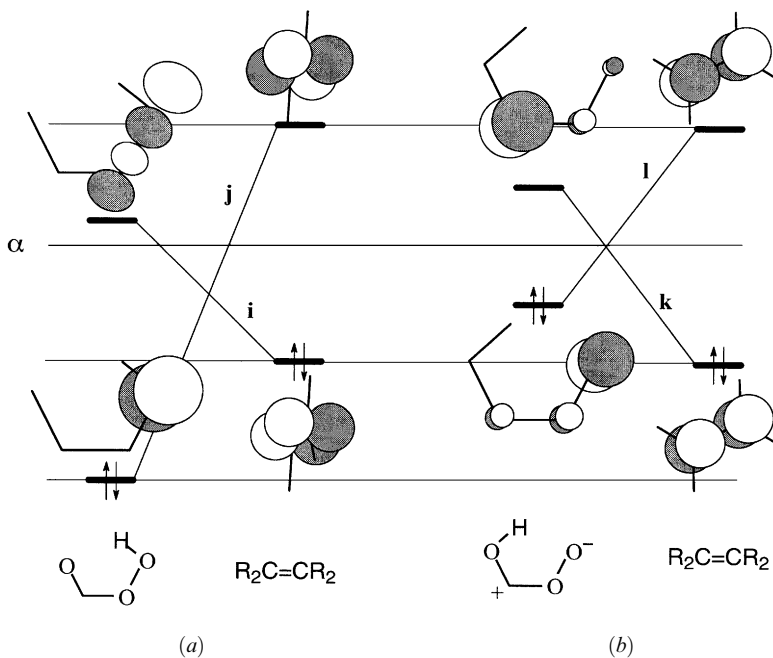


**Figure B.2.** (a) Orbital interactions for a nucleophilic attack by  $\pi_{CC}$  on  $\sigma_{OO}^*$ . (b) 1,3 Dipolar addition to alkene.

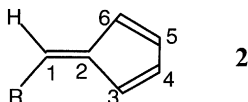
It was established that the oxygen transfer takes place via an  $S_N2$ -like transition state (a), rather than a pathway which resembles a 1,3-dipolar addition (b). Comment on the relative merits of the two transition states using principles of orbital interaction theory. A spiro structure similar to (a) for the transition state has been located by ab initio calculations (Bach, R. D.; Owensby, A. L.; Gonzalez, C.; Schlegel, H. B.; McDouall, J. J. W., *J. Am. Chem. Soc.*, **1991**, *113*, 2338).

**Answer.** The orbital interaction diagram for path (a) is shown in Figure B.2a. The LUMO of the peracid is the  $\sigma_{OO}^*$  orbital. It is placed near  $\alpha$  since the two oxygen atoms are very electronegative. The primary interaction, *i*, is with the HOMO of the alkene. The perpendicular orientation of the alkene (leading to a spiro transition state) is dictated not by  $\sigma_{OO}^*$  but by the nonbonded orbital on the oxygen of the OH group. In this orientation, a favorable secondary interaction, *j*, is maximized. Path (a) would be further enhanced by X<sup>-</sup> or "C"<sup>-</sup> type substituents on the alkene. Path (b) is possible if the proton is transferred to the carbonyl oxygen. The SHMO orbitals of the zwitterionic form are shown in Figure B.2b. It is clear that a 1,3 dipolar cycloaddition mode is also favored since both HOMO-LUMO interactions, *k* and *l*, are favored by one large coefficient. One must conclude that path (b) is not seen due to the low abundance of the tautomeric form of the peracid.

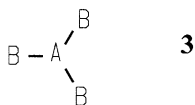
6. The photochemical elimination of  $H_2$  from 1,4-cyclohexadiene has been shown experimentally to proceed through a transition state with  $C_{2v}$  or  $C_2$  symmetry (Cromwell, E. F.; Liu, D.-J.; Vrakking, M. J. J.; Kung, A. H.; Lee, Y. T., *J. Chem. Phys.*,

1991, 95, 297). Decide on the basis of orbital and state correlation diagrams whether or not the reaction is photolytically allowed.

7. Predict the structure of the van der Waals complex between ozone and acetylene. Indicate which frontier orbital interactions should be most important. How does your prediction compare with the experimental structure (Gillies, J. Z.; Gillies, C. W.; Lovas, F. J.; Matsumura, K.; Suenram, R. D.; Kraka, E.; Cremer, D., *J. Am. Chem. Soc.*, **1991**, *113*, 6408)?
8. The laboratory preparation of azulene [(a) Lemal, D. M.; Goldman, G. D., *J. Chem. Ed.*, **1988**, *65*, 923. (b) Brieger, G., *J. Chem. Ed.*, **1992**, *69*, A262] involves as a key reagent, dimethylaminofulvene, **2** ( $R = NMe_2$ ), which is used in a reaction with thiophene-1,1-dioxide to assemble the final azulene skeleton. Unsubstituted fulvene, **2** ( $R = H$ ), is a very reactive compound. It forms a *dimer* via a cycloaddition reaction in manner entirely analogous to the reaction between dimethylaminofulvene and thiophene-1,1-dioxide.



- (a) Show the most likely product of a reaction of fulvene with itself (i.e., the dimerization). *Hint*: Postulate a transition state for the reaction based on the most favorable interaction of the frontier orbitals, and from it deduce the structure of the most likely product.
- (b) Develop a *two*-orbital interaction diagram for the amino-substituted fulvene, **2** ( $R = NMe_2$ ) (for the purposes of the diagram you may treat the methyl groups as if they were H atoms). Show clearly the relative positions of the initial and final orbitals (recall that for a tricoordinated nitrogen atom,  $\alpha_N = \alpha - 1.37|\beta|$ ), and sketch the initial and final orbitals in the correct orientation.
- (c) Use your orbital interaction diagram to discuss the effect of the dimethylamino group on the reactivity of the fulvene.
9. “Y”-conjugation is often discussed in the literature as a different kind of “aromaticity” because of the prevalence of structures such as  $NO_3^-$ ,  $CO_3^{2-}$ , and urea ( $NH_2C(O)NH_2$ ). Develop a bonding scheme for the  $\pi$  orbitals of **3**, in which A and B can each donate one *p* orbital to the  $\pi$  system and A is less electronegative than B.



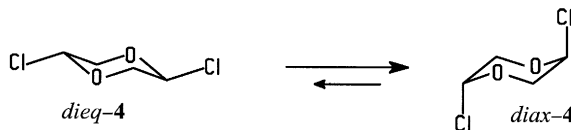
Discuss the optimum number of electrons (two, four, or six). Why is it desirable that A is the less electronegative element or group? Do  $BF_3$  and *tert*-butyl cation fit the pattern? *Hint*: The compound has threefold symmetry and some MOs will be degenerate.

10. Predict the structure of the van der Waals complexes between  $BF_3$  and CO. Both 1:1 and 1:2 complexes have been observed (Sluyts, E. J.; van der Veken, B. J., *J. Am. Chem. Soc.*, **1996**, *118*, 440–445) by IR spectroscopy in liquid argon and

enthalpies of complexation determined ( $-7.6$  and  $-14.5$  kJ/mol, respectively). Why is it reasonable that the second CO binds almost as strongly as the first?

11. Dative bonded complexes between alane ( $\text{AlH}_3$ ) and amines have long been known. Complexes with one and two amines are common. For example, bis-(trimethylamine) alane,  $\text{AlH}_3(\text{N}(\text{CH}_3)_3)_2$ , is a white crystalline solid with a low vapor pressure. Using ammonia as a model for trimethylamine, apply orbital interaction analysis to describe the bonding in the 1:1 and 1:2 complexes. Theoretical studies on the ammonia complexes of  $\text{AlH}_3$  have led to the conclusion that there is little dative bonding (as judged by the amount of charge transfer) (Marsh, C. M. B.; Schaefer III, H. F., *J. Phys. Chem.*, **1995**, *99*, 14309–14315). Comment on the theoretical results.
12. Use orbital interaction diagrams to explain each of the following (show the orbitals clearly):

- (a) Describe the N—N bond in hydrazinium dichloride,  $\text{H}_3\text{N}^+ - \text{N}^+\text{H}_3 \cdot 2\text{Cl}^-$ .
- (b) Account for the fact that *trans*-2,5-dichloro-1,4-dioxane **4** preferentially adopts the diaxial conformation (Koritsánszky, T.; Strumpel, M. K.; Buschmann, J.; Luger, P.; Hansen, N. K.; PichonPesme, V., *J. Am. Chem. Soc.*, **1991**, *113*, 9148). *Hint*: This is an example of the anomeric effect in operation.



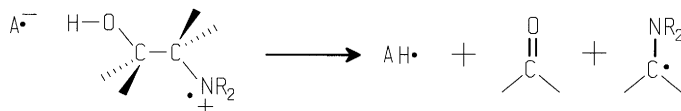
- (c) Offer an explanation for the observation that the lowest ionization potential for the diacetylene **5** (IP = 8.47 eV) is lower than the corresponding IP of **6** (9.13 eV) (Gleiter, R.; Kratz, D.; Schäfer, W.; Schehlmann, V., *J. Am. Chem. Soc.*, **1991**, *113*, 9258).



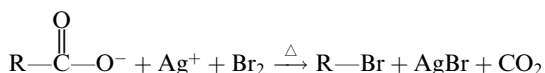
- (d) Show why C—H bonds next to a carbocationic center are especially acidic and why proton abstraction yields olefins.



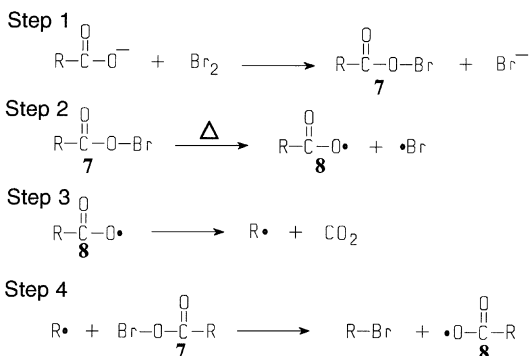
13. The mechanism for the oxidative photofragmentation of  $\alpha,\beta$ -amino alcohols is consistent with a preference for anti geometry in the cleavage step (Ci, X.; Kellett, M. A.; Whitten, D. G., *J. Am. Chem. Soc.*, **1991**, *113*, 3893). Provide a rationalization based on the frontier orbitals of the system.



14. Carboxylic acids may be converted to alkyl bromides with the loss of one carbon atom by the Hunsdiecker reaction:



The mechanism is a free-radical chain reaction which is believed to involve the following steps:



The reaction is initiated in step 2 and propagated by steps 3 and 4. Analyze each of the steps of the Hunsdiecker reaction in terms of simple orbital interaction theory.

- Using a two-orbital interaction diagram, show the interaction which results in the formation of the bromoxy acid, **7**, and displacement of bromide ion in step 1.
- Use an appropriate orbital interaction diagram to describe the O—Br bond of **7**, which ruptures upon heating in step 2. Why is it feasible that this is the weakest bond in this compound?
- Show the electronic structure of the acyloxy free radical, **8**, which is produced in step 2. Is it a  $\sigma$  or  $\pi$  radical? *Hint*: You may wish to construct the MOs of **8** from the interaction of two monocoordinated oxygen atoms, bearing in mind the local symmetry of the carboxylate group.
- Use your bonding description from part (b) to explain why the alkyl radical should attack at the Br atom of **7** and not at some other site in step 4.

#### Answer

- This is a simple nucleophilic substitution on  $\text{Br}_2$ . The Br—Br  $\sigma$ -type interaction is very weak, and as a consequence, the LUMO ( $\sigma_{\text{BrBr}}^*$ ) is low in energy. The interaction is of the two-electron, two-orbital type, the other orbital being the HOMO of the carboxylate group, the out-of-phase combination of the in-plane nonbonded orbitals of the oxygen atoms [ $\pi_2$  will be a little lower; see part (c)].
- The  $\sigma$  bond of the bromoxy acid is very weak because of the poor intrinsic interaction between a  $2p$  orbital and a  $4p$  orbital.
- The interaction diagram for the carboxylate group is shown in Figure B.3. Because the in-plane  $p$  orbitals ( $p_\sigma$ ) overlap more strongly than the out-of-plane orbitals ( $p_\pi$ ), the HOMO of the carboxylate anion will be a  $\sigma^*$  orbital, and the neutral carboxylate free radical is predicted to be a  $\sigma$  radical.



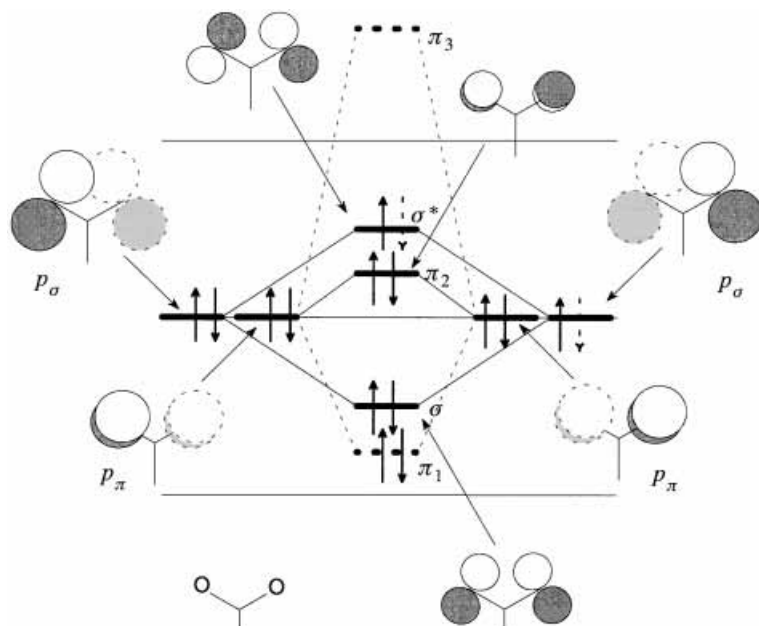
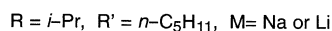
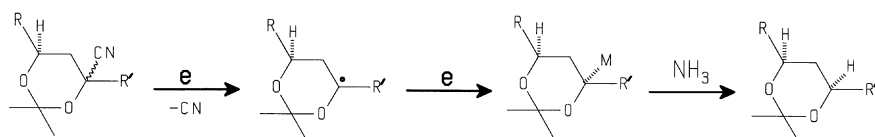


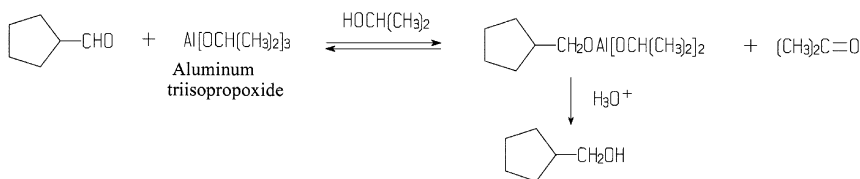
**Figure B.3.** The MOs of a carboxylate anion and free radical. The dashed lines indicate the result of interaction with the central carbon  $2p$  orbital.

- (d) To understand why the Br atom is abstracted, we must realize that bromine is less electronegative than oxygen. Therefore the LUMO which is the  $\sigma_{\text{BrO}}^*$  orbital is polarized toward Br. Since the alkyl radical SOMO is high in energy (i.e., at  $\alpha$ ), the SOMO–LUMO interaction will be more important than any interaction with the occupied orbitals.

15. Reductive decyanations of 2-cyanotetrahydropyran derivatives with sodium in ammonia yield predominantly axially protonated products. The observations are consistent with the reductive decyanation proceeding via the pyramidal, axial radical which accepts a second electron to give a configurationally stable carbanion, which in turn abstracts a proton from ammonia with retention of configuration (Rychnovsky, S. D.; Powers, J. P.; LePage, T. J., *J. Am. Chem. Soc.*, **1992**, *114*, 8375–8384). Provide an explanation for the axial preference of the intermediate free radical on the basis of orbital interactions. *Hint:* The title of the paper by Rychnovsky et al. is “Conformation and Reactivity of Anomeric Radicals.”



16. Cyclopentadienyl iodide (5-iodo-1,3-cyclopentadiene) reacts approximately 10 times as rapidly as cyclopentenyl iodide (3-iodocyclopentene) with tetrabutylammonium bromide under the same conditions (Breslow, R.; Canary, J. W., *J. Am. Chem. Soc.*, **1991**, *113*, 3950). Under solvolysis conditions ( $S_N1$ ), the reactivity order is reversed. Provide a rationalization based on the frontier orbitals of the system. What would you predict for the analogous 3- and 7-membered ring systems?
17. The Meerwein–Pondorf–Verley reaction involves transfer of a hydride from the oxygen-substituted carbon atom of an isopropoxide group to a carbonyl group, thus effecting the reduction of the carbonyl compound to an alcohol.



Without the aluminum triisopropoxide, the reaction does not proceed. Show the structure of the intermediate in which the hydride transfer occurs and use ideas from orbital interaction theory to discuss the factors which enhance the hydride transfer in this reaction.

**Answer.** Three factors combine to make this reaction facile: (a) activation of the carbonyl group toward nucleophilic addition as a result of coordination to the Lewis acid (aluminum triisopropoxide), as discussed in Chapter 8; (b) activation of the secondary C—H bond as a  $\sigma$  donor by the presence of the very good X: substituent ( $—O—Al$ , which resembles  $—O^-$ ), as discussed in Chapter 4; and (c) *opportunity* presented by the coordination within the complex shown in Figure B.4,

18. An *exciplex* is a complex between two molecules, one of which has been photoexcited, that is,  $A^* \cdots \cdots B$ . Show, using orbital interaction diagrams, the possible bonding in an exciplex. An *excimer* is an exciplex of the type  $A^* \cdots \cdots A$ . In general, would you expect stronger or weaker bonding in an excimer? Explain. [Of interest: In a recent study of the Diels–Alder reaction, it was found that some enantioselectivity could be achieved by tying up one of the two prochiral (enantiotopic) faces of the dienophile, a trans-substituted alkene as an exciplex with an optically active

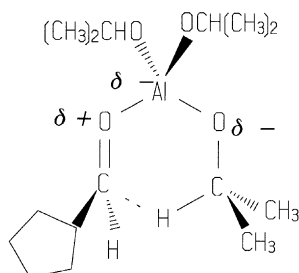
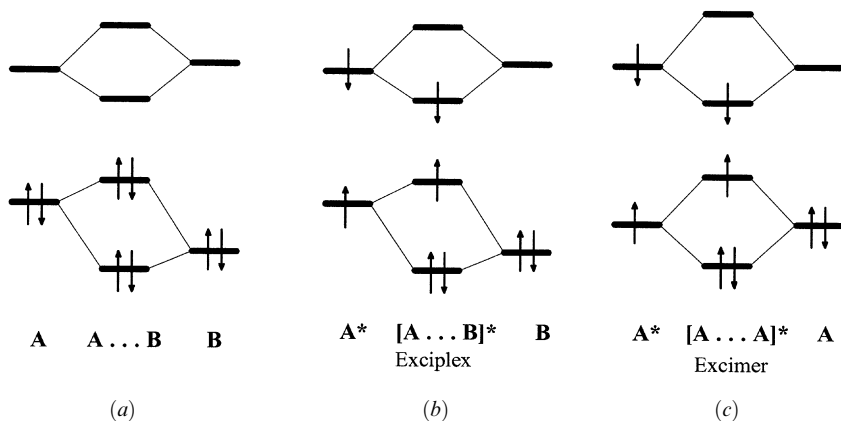


Figure B.4. Intermediate in the Meerwein–Ponndorf–Verley reaction.



**Figure B.5.** (a) Interaction of two molecules in their ground state. (b) three-electron and one-electron bonding in an exciplex. (c) Bonding in an excimer.

sensitizer, a twisted binaphthyl (Kim, J.-I.; Schuster, G. B., *J. Am. Chem. Soc.*, **1992**, *114*, 9309–9317).]

**Answer.** The interaction between two ground-state molecules in close approach is shown schematically in Figure B.5a. The energy interaction is dominated by the four-electron, two-orbital case, which is repulsive. The interaction of the LUMOs, which may be large, has no consequence to the energy, *unless* one of the molecules is photoexcited. In this case, shown in Figure B.5b, the LUMO–LUMO and the HOMO–HOMO interactions become attractive. The overall energy gain depends on the energy separations and the extent of orbital overlap in the two interactions. A perfect match in nodal characteristics and energies is achieved when the two molecules are identical (Figure B.5c). Therefore an excimer would be expected to be more stable in general than an exciplex.

- Use orbital interaction theory to develop the  $\pi$  orbitals of the 2-oxaallyl system,  $R_2C=O-CR_2$ , also known as a carbonyl ylide. Show why 2-oxaallyl readily reacts with alkenes and alkyne in a  $4 + 2$  cycloaddition reaction (an example may be found in El-Saidi, M.; Kassam, K.; Pole, D. L.; Tadey, T.; Warkentin, J., *J. Am. Chem. Soc.*, **1992**, *114*, 8751–8752).
- The photochemistry of previtamin  $D_3$  has been intensively studied (for leading references, see Dauben, W. G.; Disanayaka, B.; Funhoff, D. J. H.; Kohler, B. E.; Schilke, D. E.; Zhou, B., *J. Am. Chem. Soc.*, **1991**, *113*, 8367, and Enas, J. D.; Shen, G.-Y.; Okamura, W. H., *J. Am. Chem. Soc.*, **1991**, *113*, 3873). The thermal and photoreactions are summarized in Figure B.6. Discuss the various conversions using the descriptive terminology of pericyclic reactions.
- Cyclobutadiene has been shown to have a rectangular geometry by competitive trapping of the two valence tautomeric 1,2-dideuteriocyclobutadienes using methyl 3-cyanoacrylate in a Diels–Alder reaction. [(a) Whitman, D. W.; Carpenter, B. K., *J. Am. Chem. Soc.*, **1982**, *104*, 6473–6474. (b) Whitman, D. W.; Carpenter, B. K., *J. Am. Chem. Soc.*, **1980**, *102*, 4272–4274.]

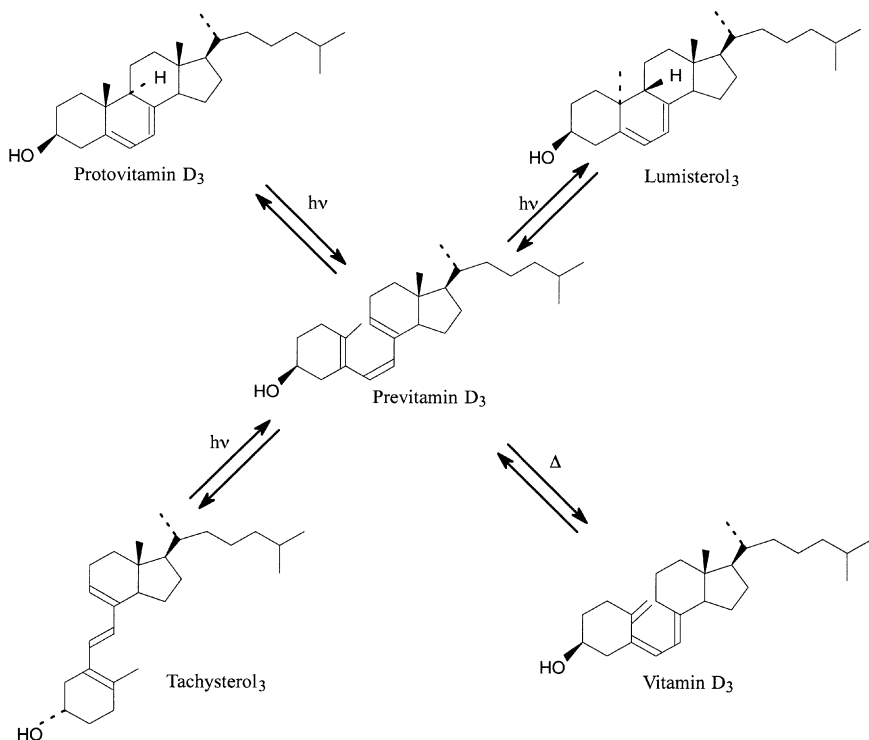
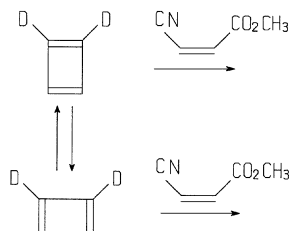


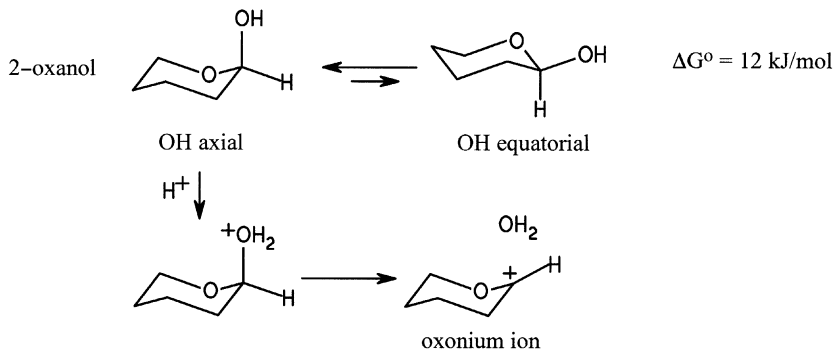
Figure B.6. Photoreactions of previtamin D<sub>3</sub>.



Show the products expected from the Diels–Alder reactions. Use orbital interaction theory to develop a bonding scheme for rectangular cyclobutadiene and explain why rectangular cyclobutadiene may be exceptionally reactive as a diene in Diels–Alder reactions.

22. The operation of the anomeric effect and the stabilization of carbocations are beautifully illustrated in a conformational study of 2-oxanol (2-oxacyclohexanol) (Smith, B. J., *J. Am. Chem. Soc.*, **1997**, *119*, 2699–2706). 2-Oxanol prefers the OH axial form by 12 kJ/mol and, upon protonation of the OH group, spontaneously loses water to form the oxonium ion. Use principles of orbital interaction theory to explain:

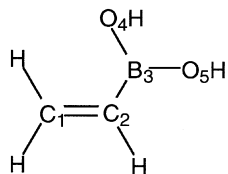
- (a) The stabilization of the carbocation center by the oxygen  
 (b) The preference for the OH axial form (the anomeric effect)  
 (c) Why it is plausible that loss of water would be easy from the protonated form



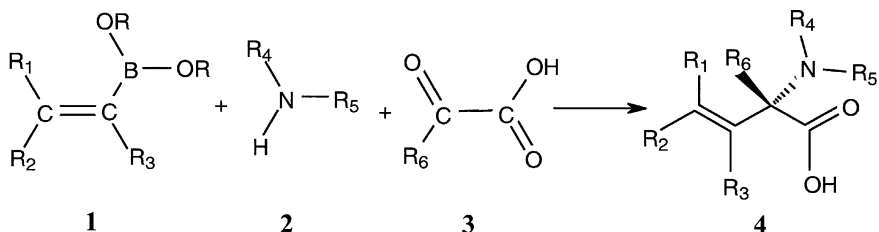
23. Vinylboronic acids have found use in a multicomponent one-step synthesis of  $\alpha$ -amino acids (see question 24). The HOMO and LUMO of the parent compound,  $\text{CH}_2=\text{CHB}(\text{OH})_2$ , from an SHMO calculation are

$$\epsilon_{\text{HOMO}} = \alpha - 1.153|\beta|: \quad \phi_{\text{HOMO}} = 0.62\chi_1 + 0.72\chi_2 + 0.28\chi_3 - 0.10\chi_4 - 0.10\chi_5$$

$$\epsilon_{\text{LUMO}} = \alpha + 0.343|\beta|: \quad \phi_{\text{LUMO}} = -0.62\chi_1 + 0.21\chi_2 + 0.74\chi_3 - 0.11\chi_4 - 0.11\chi_5$$



- (a) Draw the HOMO and LUMO.  
 (b) Would you expect vinylboronic acid to be more or less reactive toward electrophilic attack than ethylene? Where would be the site of attack? Explain.  
 (c) Would you expect vinylboronic acid to be more or less reactive toward nucleophilic attack than ethylene? Where would be the site of attack? Explain.  
 (d) Define  $\alpha$ ,  $\beta$ , and  $\chi_1$ .
24. Petasis and Zavialov have developed the following new synthesis of  $\alpha$ -amino acids 4 (Petasis, N. A.; Zavialov, I. A., *J. Am. Chem. Soc.*, **1997**, *119*, 445–446):



The reaction is initiated by addition of the amine **2** to the  $\alpha$  keto acid **3**, catalyzed by the vinyl boronic acid derivative **1**. Use orbital interaction theoretical arguments to explain the following features of this synthesis:

- (a) The amine attacks the carbonyl of the keto group of **3** rather than the carbonyl of the acid group.
- (b) The nucleophilic attack on carbonyl may be catalyzed by the vinylboronic acid **1**. How?
- (c) The amine attacks the  $\alpha$  keto acid **3** rather than the vinylboronic acid **1**. Why? (By SHMO, the LUMO of an  $\alpha$  keto acid is at  $\alpha + 0.122|\beta|$ ; see also question 23).

## REFERENCES AND NOTES

---

1. Fukui, K., *Acc. Chem. Res.*, **1971**, *4*, 57.
2. (a) Fukui, K., *Angew. Chem. Int. Ed. Engl.*, **1982**, *21*, 801. (b) Fukui, K., selected papers, *Frontier Orbitals and Reaction Paths*, Fukui, K.; Fujimoto, H., Eds., World Scientific London, 1997.
3. (a) Woodward, R. B.; Hoffmann, R., *The Conservation of Orbital Symmetry*, Verlag Chemie, Weinheim, 1970. (b) Woodward, R. B.; Hoffmann, R., *Angew. Chem. Int. Ed. Engl.*, **1969**, *8*, 781. (c) Woodward, R. B.; Hoffmann, R., *Acc. Chem. Res.*, **1968**, *1*, 17.
4. Klopman, G., *J. Am. Chem. Soc.*, **1968**, *90*, 223.
5. Salem, L., *J. Am. Chem. Soc.*, **1968**, *90*, 543, 553.
6. Hoffmann, R., *Acc. Chem. Res.*, **1971**, *4*, 1–9.
7. Fleming, I., *Frontier Orbitals and Organic Chemical Reactions*, Wiley, New York, 1976.
8. Hoffmann, R., *J. Mol. Struct. (Theochem.)*, **1998**, *424*, 1–6.
9. (a) Shaik, S. S., *J. Am. Chem. Soc.*, **1981**, *103*, 3692. (b) Pross, A.; Shaik, S. S., *Acc. Chem. Res.*, **1983**, *16*, 363. (c) Shaik, S. S., *Prog. Phys. Org. Chem.*, **1985**, *15*, 197. (d) Pross, A., *Adv. Phys. Org. Chem.*, **1985**, *21*, 99.
10. (a) Halevi, E. A., *Helvet. Chim. Acta*, **1975**, *58*, 2136. (b) Halevi, E. A., *Angew. Chem. Int. Ed. Engl.*, **1976**, *15*, 593. (c) Halevi, E. A., *Nouv. J. Chim.*, **1976**, *15*, 593. (d) Katriel, J.; Halevi, E. A., *Theoret. Chim. Acta*, **1975**, *40*, 1. (e) Bachler, V.; Halevi, E. A., *Theoret. Chim. Acta*, **1981**, *59*, 595. (f) Halevi, E. A.; Thiel, W., *J. Photochemistry*, **1985**, *28*, 373. (g) Halevi, E. A.; Rom, R., *Israel J. Chem.*, **1989**, *29*, 311.
11. Halevi, E. A., *Orbital Symmetry and Reaction Mechanism: The OCAMS Way*, Springer-Verlag, New York, 1992.
12. Rauk, A.; Cannings, R., *SHMO*, A Simple Huckel Molecular Orbital Theory Calculator, <http://www.chem.ucalgary.ca/SHMO/>.
13. (a) Dauben, W. G.; Salem, L.; Turro, N. J., *Acc. Chem. Res.*, **1975**, *8*, 41. (b) Turro, N. J., *J. Mol. Struct. (Theochem.)*, **1998**, *424*, 77–82.
14. Michl, J.; Bonacic-Koutecky, V., *Electronic Aspects of Organic Photochemistry*, Wiley, New York, 1990.

15. Turro, N. J., *Modern Molecular Photochemistry*, University Science Books, Mill Valley, CA, 1991.
16. Gilbert, A.; Baggott, J. E., *Essentials of Molecular Photochemistry*, CRC Press, Boca Raton, FL, 1991.
17. Many of the ideas and examples in Chapter 1 have been extracted from notes of a course given by Kurt Mislow to a class of Princeton graduate students in 1968.
18. Jaffe, H. H.; Orchin, M., *Symmetry in Chemistry*, Wiley, New York, 1965.
19. (a) Masamune, S.; Kennedy, R. M.; Petersen, J. S.; Houk, K. N.; Wu, Y.-D., *J. Am. Chem. Soc.*, **1986**, *108*, 7404–7405. (b) Imai, T.; Tamura, T.; Yamamuro, A.; Sato, T.; Wollmann, T. A.; Kennedy, R. M.; Masamune, S., *J. Am. Chem. Soc.*, **1986**, *108*, 7402–7404.
20. Luger, P.; Buschmann, J.; McMullan, R. K.; Ruble, J. R.; Matias, P.; Jeffrey, G. A., *J. Am. Chem. Soc.*, **1986**, *108*, 7825.
21. Stair, P. C., *J. Am. Chem. Soc.*, **1982**, *104*, 4044.
22. Kuck, D.; Bögge, H., *J. Am. Chem. Soc.*, **1986**, *108*, 8107.
23. de Boer, J. A. A.; Reinhoudt, D. N.; Harkema, S.; van Hummel, G. J.; de Jong, F., *J. Am. Chem. Soc.*, **1982**, *104*, 4073.
24. Eaton, P. E.; Cole, Jr., T. W., *J. Am. Chem. Soc.*, **1964**, *86*, 3157.
25. Paquette, L. A.; Ternansky, R. J.; Balogh, D. W.; Kentgen, G., *J. Am. Chem. Soc.*, **1983**, *105*, 5446.
26. Shanzer, A.; Libman, J.; Gottlieb, H.; Frolov, F., *J. Am. Chem. Soc.*, **1982**, *104*, 4220.
27. For a review, see Buda, A. B.; Auf der Heyde, T.; Mislow, K., *Angew. Chem. Int. Ed. Engl.*, **1992**, *31*, 989–1007.
28. (a) Zabrodsky, H.; Peleg, S.; Avnir, D., *J. Am. Chem. Soc.*, **1992**, *114*, 7843–7851. (b) Ferrarini, A.; Nordio, P. L., *J. Chem. Soc. Perkin*, **1998**, *2*, 455–460.
29. Mislow, K., *Introduction to Stereochemistry*, W. A. Benjamin, New York, 1965.
30. (a) Mislow, K., *Bull. Soc. Chim. Belg.*, **1977**, *86*, 595. (b) Mislow, K.; Siegel, J., *J. Am. Chem. Soc.*, **1984**, *106*, 3319.
31. Juaristi, E., *Stereochemistry and Conformational Analysis*, Wiley-Interscience, New York, 1991.
32. Eliel, E. L.; Wilen, S. H.; Mander, L. N., *Stereochemistry of Organic Compounds*, Wiley-Interscience, New York, 1994.
33. Morrison, J. D., Ed., *Asymmetric Synthesis*, Vols. 2 and 3, Academic, Orlando, FL, 1983.
34. Marckwald, W., *Ber.*, **1904**, *37*, 349.
35. (a) Katsuki, T.; Sharpless, K. B., *J. Am. Chem. Soc.*, **1980**, *102*, 5974. (b) Rossiter, B. E.; Katsuki, T.; Sharpless, K. B., *J. Am. Chem. Soc.*, **1981**, *103*, 464.
36. (a) Finn, M. G.; Sharpless, K. B., *J. Am. Chem. Soc.*, **1991**, *113*, 113. (b) Woodward, S. S.; Finn, M. G.; Sharpless, K. B., *J. Am. Chem. Soc.*, **1991**, *113*, 106.
37. Atta-ur-Rahman; Shah, Z., *Stereoselective Synthesis in Organic Chemistry*, Springer-Verlag, New York, 1993.
38. Kolb, H. C.; Van Nieuwenhze, M. S.; Sharpless, K. B., *Chem. Rev.*, **1994**, *94*, 2483–2547.
39. Heathcock, C. H., in *Asymmetric Reactions and Processes in Chemistry*, Eliel, E. L.; Otsuka, S., Eds., ACS Symposium Series 185, American Chemical Society, Washington, DC, 1982, p. 55.
40. Brown, H. C., *Hydroboration*, Benjamin, New York, 1963.
41. Midland, M. M., *Chem. Rev.*, **1989**, *89*, 1553.
42. Pirkle, W. H.; Beare, S. D., *J. Am. Chem. Soc.*, **1968**, *90*, 6250.
43. Pirkle, W. H.; Beare, S. D., *J. Am. Chem. Soc.*, **1969**, *91*, 5150, and references therein.
44. Hofer, O., *Top. Stereochem.*, **1976**, *9*, 111.



45. Takeuchi, Y.; Itoh, N.; Note, H.; Koizumi, T.; Yamaguchi, K., *J. Am. Chem. Soc.*, **1991**, *113*, 6318.
46. Hohenberg, P.; Kohn, W., *Phys. Rev. B*, **1964**, *136*, 864–871.
47. Szabo, A.; Ostlund, N. S., *Modern Quantum Chemistry: Introduction to Advanced Electronic Structure Theory*, MacMillan, New York, 1982, p. 192.
48. Hariharan, P. C.; Pople, J. A., *Theoret. Chim. Acta*, **1973**, *28*, 213.
49. Baker, J.; Muir, M.; Andzelm, J., *J. Chem. Phys.*, **1995**, *102*, 2063–2079. B3LYP is called ACM (adiabatic connection model) in this paper.
50. Mebel, A. M.; Morokuma, K.; Lin, M. C., *J. Chem. Phys.*, **1995**, *103*, 7414–7421.
51. Qin, Y.; Wheeler, R. A., *J. Phys. Chem.*, **1996**, *100*, 10554–10566.
52. Barone, V.; Adamo, C.; Lelj, F., *J. Chem. Phys.*, **1995**, *102*, 364–370. (b)
53. Armstrong, D. A.; Yu, D.; Rauk, A., *Can. J. Chem.*, **1996**, *76*, 1192–1199.
54. Schlegel, H. B., *J. Comput. Chem.*, **1982**, *3*, 214.
55. Hehre, W. J.; Radom, L.; Schleyer, P. v. R.; Pople, J. A., *Ab Initio Molecular Orbital Theory*, Wiley, New York, 1986.
56. *JANAF Thermochemical Tables*, 2nd ed., Natl. Stand. Ref. Data Ser. NSRDS-NBS 31, U.S. Government Printing Office, Washington, DC, 1971.
57. An *ab initio* form of PMO theory has been developed: (a) Bernardi, F.; Bottoni, A., *Theor. Chim. Acta*, **1981**, *58*, 245. (b) Bernardi, F.; Bottoni, A., in *Computational Theoretical Organic Chemistry*, Csizmadia, I. G.; Daudel, R., Eds., Reidel, Dordrecht, 1981, pp. 197–231. (c) Bernardi, F.; Bottoni, A.; Fossey, J.; Sorba, J., *Tetrahedron*, **1986**, *42*, 5567–5580.
58. Albright, T. A.; Burdett, J. K.; Whangbo, M.-H., *Orbital Interactions in Chemistry*, Wiley-Interscience, New York, 1985.
59. Wolfsberg, M.; Helmholz, L., *J. Chem. Phys.*, **1952**, *20*, 837.
60. Hoffmann, R., *J. Chem. Phys.*, **1963**, *39*, 1397.
61. Woolley, R. G., *Nouv. J. Chim.*, **1981**, *5*, 219, 227.
62. (a) Bischof, P.; Hashmall, J. A.; Heilbronner, E.; Hornung, V., *Helv. Chim. Acta*, **1969**, *52*, 1745. (b) Haselbach, E.; Heilbronner, E.; Schroder, G., *Helv. Chim. Acta*, **1971**, *54*, 153.
63. Masclat, P.; Grosjean, D.; Mouvier, G.; Dubois, J., *J. Electron Spectrosc. Relat. Phenom.*, **1973**, *2*, 225.
64. Robin, M. B., *Higher Excited States of Polyatomic Molecules*, vols. I, II, III, Academic, New York, 1975.
65. Baird, N. C., *J. Chem. Ed.*, **1977**, *54*, 291–293.
66. Kim, E. K.; Kochi, J. K., *J. Am. Chem. Soc.*, **1991**, *113*, 4962.
67. Bingham, R. C., *J. Am. Chem. Soc.*, **1975**, *97*, 6743.
68. Chen, Y.; Tschuikow-Roux, E.; Rauk, A., *J. Phys. Chem.*, **1991**, *95*, 9832.
69. Gill, P. M. W.; Radom, L., *J. Am. Chem. Soc.*, **1988**, *110*, 4931–4941.
70. Tachikawa, H.; Ogasawara, M., *J. Phys. Chem.*, **1990**, *94*, 1746.
71. Barnett, R. N.; Landman, U.; Dhar, S.; Kestner, N. R.; Jortner, J.; Nitzan, A., *J. Chem. Phys.*, **1989**, *91*, 7797.
72. Van der Waals forces are very complex and manifest themselves even at distances at which it is unreasonable to assume that orbital interactions can occur. An explanation due to London in terms of the mutual attraction of induced dipoles (dispersion forces) accounts for the long-range behavior. The unoccupied–occupied orbital interactions will be the dominant component of van der Waals forces at short range. See Kauzmann, W., *Quantum Chemistry*, Academic, New York, 1957, Chapter 13, for a discussion of dispersion forces.
73. Gimarc, B. M., *Acc. Chem. Res.*, **1974**, *7*, 384.
74. Walsh, A. D., *J. Chem. Soc.*, **1953**, 2260; and papers immediately following.

75. (a) Peyerimhoff, S. D.; Buenker, R. J.; Allen, L. C., *J. Chem. Phys.*, **1966**, *45*, 734. (b) Allen, L. C.; Russell, J. D., *J. Chem. Phys.*, **1967**, *46*, 1029.
76. (a) Ritchie, C. D., *J. Am. Chem. Soc.*, **1983**, *105*, 7313–7318. (b) Ritchie, C. D., in *Nucleophilicity*, Harris, J. M.; McManus, S. P., Eds., Advances in Chemistry Series, American Chemical Society, Washington, DC, 1986.
77. Armentrout, P. B.; Simons, J., *J. Am. Chem. Soc.*, **1992**, *114*, 8627–8633.
78. Shaik, S. S., *J. Org. Chem.*, **1987**, *52*, 1563–1568.
79. Safi, B.; Choho, K.; De Proft, F.; Geerlings, P., *J. Phys. Chem. A*, **1998**, *102*, 5253–5259.
80. Rauk, A.; Sorensen, T. S.; Maerker, C.; de Carneiro, J. W.; Sieber, S.; Schleyer, P. v. R., *J. Am. Chem. Soc.*, **1996**, *118*, 3761–3762.
81. Maerker, C.; Schleyer, P. v. R.; Koch, W.; Rauk, A.; Sorensen, T. S.; Mareda, J., *J. Am. Chem. Soc.*, in press.
82. (a) Schmidt, H.; Schweig, A., *Tetrahedron Lett.*, **1973**, 981. (b) Schmidt, H.; Schweig, A., *Angew. Chem. Int. Ed. Engl.*, **1973**, *12*, 307.
83. (a) Benson, S. W., *J. Chem. Ed.*, **1965**, *42*, 502. (b) Kerr, J. A., *Chem. Rev.*, **1966**, *66*, 465.
84. Hoffmann, R.; Imamura, A.; Hehre, W. J., *J. Am. Chem. Soc.*, **1968**, *90*, 1499, and references therein.
85. Paulson, B. P.; Curtiss, L. A.; Bal, B.; Closs, G. L.; Miller, J. R., *J. Am. Chem. Soc.*, **1996**, *118*, 378–387, and references therein.
86. Schleyer, P. v. R.; Kaupp, M.; Hampel, F.; Bremer, M.; Mislow, K., *J. Am. Chem. Soc.*, **1992**, *114*, 6791–6797.
87. Brundle, C. R.; Robin, M. B.; Kuebler, N. A.; Basch, H., *J. Am. Chem. Soc.*, **1972**, *94*, 1451.
88. Kobayashi, T.; Miki, S.; Yoshida, Z.; Asako, Y.; Kajimoto, C., *J. Am. Chem. Soc.*, **1988**, *110*, 5622.
89. Honegger, E.; Yang, Z. Z.; Heilbronner, E.; Alder, R. W.; Moss, R. E.; Sessions, R. B., *J. Elect. Spectrosc. Rel. Phenom.*, **1985**, *36*, 297.
90. Kimura, K.; Katsumata, S.; Achiba, Y.; Yamazaki, T.; Iwata, S., *Handbook of He I Photoelectron Spectra of Fundamental Organic Molecules*, Halsted, New York, 1981.
91. (a) Badger, R. M., *J. Chem. Phys.*, **1934**, *2*, 128. (b) Badger, R. M., *J. Chem. Phys.*, **1935**, *3*, 710. (c) Gordy, W., *J. Chem. Phys.*, **1946**, *14*, 305.
92. (a) Mack, H. G.; Christen, D.; Oberhammer, H., *J. Mol. Struct.*, **1988**, *190*, 215. (b) Christen, D.; Gupta, O. D.; Kadel, J.; Kirchmeier, R. L.; Mack, H. G.; Oberhammer, H.; Shreeve, J. M., *J. Am. Chem. Soc.*, **1991**, *113*, 9131.
93. Roggen, I.; Dahl, T., *J. Am. Chem. Soc.*, **1992**, *114*, 511, and references therein.
94. David, S.; Eisenstein, O.; Hehre, W. J.; Salem, L.; Hoffmann, R., *J. Am. Chem. Soc.*, **1973**, *95*, 3806.
95. Laube, T.; Hollenstein, S., *J. Am. Chem. Soc.*, **1992**, *114*, 8812–8817, and references therein.
96. For a review of the structural consequences of hyperconjugation, see Radom, L., *Prog. Theor. Org. Chem.*, **1982**, *3*, 1.
97. Zurawski, B.; Ahlrichs, R.; Kutzelnigg, W., *Chem. Phys. Lett.*, **1973**, *21*, 309.
98. (a) Raghavachari, K.; Haddon, R. C.; Schleyer, P. v. R.; Schaefer III, H. F., *J. Am. Chem. Soc.*, **1983**, *105*, 5915. (b) Yoshimine, M.; McLean, A. D.; Liu, B.; DeFrees, D. J.; Binkley, J. S., *J. Am. Chem. Soc.*, **1983**, *105*, 6185.
99. (a) Hawthorne, M. F., *Acc. Chem. Res.*, **1968**, *1*, 281. (b) Lipscomb, W. N., *Acc. Chem. Res.*, **1973**, *6*, 257.
100. Walsh, A. D., *Trans. Faraday Soc.*, **1949**, *45*, 179.
101. For a discussion of the bonding in cyclopropane and other molecules with “bent” bonds, see Wiberg, K. B., *Acc. Chem. Res.*, **1996**, *29*, 229–234.

102. SHMO is written in Java and is available on the internet at <http://www.chem.ucalgary.ca/SHMO/>.
103. (a) Whitman, D. W.; Carpenter, B. K., *J. Am. Chem. Soc.*, **1982**, *104*, 6473–6474. (b) Carpenter, B. K., *J. Am. Chem. Soc.*, **1983**, *105*, 1700–1701. (c) Whitman, D. W.; Carpenter, B. K., *J. Am. Chem. Soc.*, **1980**, *102*, 4272–4274.
104. Borden, W. T.; Davidson, E. R.; Hart, P., *J. Am. Chem. Soc.*, **1978**, *100*, 388–392.
105. Van Catledge, F. A., *J. Org. Chem.*, **1980**, *45*, 4801.
106. Mullay, J., *J. Am. Chem. Soc.*, **1985**, *107*, 7271–7275.
107. Boyd, R. J.; Edgecombe, K. E., *J. Am. Chem. Soc.*, **1988**, *110*, 4182–4186.
108. Reed, L. H.; Allen, L. C., *J. Phys. Chem.*, **1992**, *96*, 157.
109. Meot-Ner (Mautner), M.; Sieck, L. W., *J. Am. Chem. Soc.*, **1991**, *113*, 4448.
110. Lias, S. G.; Liebman, J. F.; Levin, R. D., *J. Phys. Chem. Ref. Data*, **1984**, *13*, 695; proton affinities of 800 compounds.
111. Bailey, W. F.; Nurmi, T. T.; Patricia, J. J.; Wang, W., *J. Am. Chem. Soc.*, **1987**, *109*, 2442–2448.
112. Bailey, W. F.; Khanolkar, A. D.; Gavaskar, K. V., *J. Am. Chem. Soc.*, **1992**, *114*, 8053–8060.
113. Bailey, W. F.; Khanolkar, A. D.; Gavaskar, K. V.; Ovaska, T. V.; Rossi, K.; Thiel, Y.; Wiberg, K. B., *J. Am. Chem. Soc.*, **1991**, *113*, 5720.
114. For a review of electrophilic additions to alkenes and alkynes, see Fahey, R. C., *Top. Stereochem.*, **1968**, *3*, 237–342.
115. Rauk, A.; Barriol, J. M., *Chem. Phys.*, **1977**, *25*, 409.
116. Shea, K. J.; Kim, J.-S., *J. Am. Chem. Soc.*, **1992**, *114*, 3044–3051.
117. Traetteberg, M., *Acta Chem. Scand.*, **1975**, *B29*, 29.
118. Wijsman, G. W.; de Wolf, W. H.; Bickelhaupt, F., *J. Am. Chem. Soc.*, **1992**, *114*, 9191–9192.
119. March, J., *Advanced Organic Chemistry: Reactions, Mechanisms and Structure*, 3rd ed., Wiley, New York, 1985.
120. Raabe, G.; Michl, J., *Chem. Rev.*, **1985**, *85*, 419.
121. Gaspar, P. P., in *Reactive Intermediates*, vol. 3, Jones, M.; Moss, R. A., Eds., Wiley, New York, 1985, Chapter 9.
122. Maier, G.; Mihm, G.; Reisenauer, H. P.; Littman, D., *Chem. Ber.*, **1984**, *117*, 2351.
123. Shin, S. K.; Irikura, K. K.; Beauchamp, J. L.; Goddard III, W. A., *J. Am. Chem. Soc.*, **1988**, *110*, 24–30.
124. Wang, Y.; Poirier, R. A., *Can. J. Chem.*, **1998**, *76*, 477–482.
125. Determined indirectly, see ref. 123.
126. (a) West, R.; Fink, M. J.; Michl, J., *Science*, **1981**, *214*, 1343. (b) Tokitoh, N.; Suzuki, H.; Okazaki, R., *J. Am. Chem. Soc.*, **1993**, *115*, 10428–10429.
127. Stams, D. A.; Thomas, T. D.; MacLaren, D. C.; Ji, D.; Morton, T. H., *J. Am. Chem. Soc.*, **1990**, *112*, 1427–1434.
128. (a) Creary, X.; Mehrsheikh-Mohammadi, M. E.; Eggers, M. D., *J. Am. Chem. Soc.*, **1987**, *109*, 2435–2442. (b) Creary, X., *Acc. Chem. Res.*, **1985**, *18*, 3–8.
129. Fornarini, S.; Muraglia, V., *J. Am. Chem. Soc.*, **1989**, *111*, 873.
130. (a) Olah, G. A.; Liang, G.; Mateescu, G. D.; Riemenschneider, J. L., *J. Am. Chem. Soc.*, **1973**, *95*, 8698. (b) Saunders, M.; Kates, M. R., *J. Am. Chem. Soc.*, **1983**, *105*, 3571.
131. Olah, G. A.; Rasul, G.; Prakash, G. K. S., *J. Am. Chem. Soc.*, **1999**, *121*, 9615–9617.
132. Lambert, J. B.; Zhao, Y., *Angew. Chem. Int. Ed. Engl.*, **1997**, *36*, 400.
133. For a review of gas phase carbanion chemistry, see Squires, R. R., *Acc. Chem. Res.*, **1992**, *25*, 461–467.

134. For a review of carbanions generated next to heteroatoms, including nitrogen, see Kessar, S. V.; Singh, P., *Chem. Rev.*, **1997**, *97*, 721–738.
135. Farnham, W. B.; Dixon, D. A.; Calabrese, J. C., *J. Am. Chem. Soc.*, **1988**, *110*, 2607–2611.
136. (a) Boese, R.; Paetzold, P.; Tapper, A.; Ziembinski, R., *Chem. Ber.*, **1989**, *122*, 1057. (b) Olmsted, M. M.; Power, P. P.; Weese, K. J.; Doedens, R. J., *J. Am. Chem. Soc.*, **1987**, *109*, 2541. (c) Locquenghien, K. H. v.; Baceiredo, A.; Boese, R.; Bertrand, G., *J. Am. Chem. Soc.*, **1991**, *113*, 5062.
137. Freriks, I. L.; de Koning, L. J.; Nibbering, N. M. M., *J. Am. Chem. Soc.*, **1991**, *113*, 9119–9124.
138. Bickelhaupt, F. M.; Ziegler, T.; Schleyer, P. v. R., *Organometallics*, **1996**, *15*, 1477–1487.
139. Abell, P. I., in *Free Radicals*, vol. II, Kochi, J. K., Ed., Wiley, New York, 1973, p. 96.
140. McMillen, D. F.; Golden, D. M., *Ann. Rev. Phys. Chem.*, **1982**, *33*, 493–532, and references therein.
141. Bordwell, F. G.; Cheng, J.-P.; Ji, G.-Z.; Satish, A. V.; Zhang, X., *J. Am. Chem. Soc.*, **1991**, *113*, 9790–9795, and references therein.
142. Sustmann, R.; Korth, H.-G., *Adv. Phys. Org. Chem.*, **1990**, *26*, 131–178.
143. Bordwell, F. G.; Zhang, X. M.; Alnajjar, M. S., *J. Am. Chem. Soc.*, **1992**, *114*, 7623–7629.
144. Berkowitz, J.; Ellison, G. B.; Gutman, D., *J. Phys. Chem.*, **1994**, *98*, 2744.
145. Griller, D.; Lossing, F. P., *J. Am. Chem. Soc.*, **1981**, *103*, 1586.
146. Leroy, G.; Sana, M.; Wilante, C., *J. Mol. Struct.*, **1991**, *228*, 37–45.
147. Ruscic, B.; Berkowitz, J., *J. Chem. Phys.*, **1992**, *97*, 1818–1823.
148. Viehe, H.-G.; Janousek, Z.; Merényi, R.; Stella, L., *Acc. Chem. Res.*, **1985**, *18*, 148–154.
149. Yu, D.; Rauk, A.; Armstrong, D. A., *J. Am. Chem. Soc.*, **1995**, *117*, 1789–1796.
150. Rauk, A.; Yu, D.; Taylor, J.; Shustov, G. V.; Block, D. A.; Armstrong, D. A., *Biochemistry*, **1999**, *38*, 9089–9096.
151. Jensen, P.; Bunker, P. R., *J. Chem. Phys.*, **1988**, *89*, 1327, and earlier references.
152. Bauschlicher, Jr., C. W.; Schaefer III, H. F.; Bagus, P. S., *J. Am. Chem. Soc.*, **1977**, *99*, 7106–7110.
153. Wasserman, E.; Kuck, V. J.; Hutton, R. S.; Anderson, E. D.; Yager, W. A., *J. Chem. Phys.*, **1971**, *54*, 4120.
154. Murray, K. K.; Leopold, D. G.; Miller, T. M.; Lineberger, W. C., *J. Chem. Phys.*, **1988**, *89*, 5442.
155. (a) Koda, S., *Chem. Phys. Lett.*, **1978**, *55*, 353. (b) Koda, S., *Chem. Phys.*, **1982**, *66*, 383.
156. Kim, S.-J.; Hamilton, T. P.; Schaefer III, H. F., *J. Chem. Phys.*, **1991**, *94*, 2063.
157. Russo, N.; Sicilia, E.; Toscano, M., *J. Chem. Phys.*, **1992**, *97*, 5031–5036.
158. Kesselmayer, M. A.; Sheridan, R. S., *J. Am. Chem. Soc.*, **1986**, *108*, 99.
159. Du, X.-M.; Fan, H.; Goodman, J. L.; Kesselmayer, M. A.; Krogh-Jespersen, K.; La Villa, J. A.; Moss, R. A.; Shen, S.; Sheridan, R. S., *J. Am. Chem. Soc.*, **1990**, *112*, 1920.
160. Suh, D.; Pole, D. L.; Warkentin, J.; Terlouw, J. K., *Can. J. Chem.*, **1996**, *74*, 544–558.
161. Arduengo III, A. J.; Harlow, R. L.; Kline, M., *J. Am. Chem. Soc.*, **1991**, *113*, 361.
162. Arduengo III, A. J.; Dias, H. V. R.; Harlow, R. L.; Kline, M., *J. Am. Chem. Soc.*, **1992**, *114*, 5530.
163. Richards, Jr., C. A.; Kim, S. J.; Yamaguchi, Y.; Schaefer III, H. F., *J. Am. Chem. Soc.*, **1995**, *117*, 10104–10107.
164. McMahon, R. J.; Abelt, C. J.; Chapman, O. L.; Johnson, J. W.; Kreil, C. L.; LeRoux, J.-P.; Mooring, A. M.; West, P. R., *J. Am. Chem. Soc.*, **1987**, *109*, 2456.
165. Maier, G.; Reisenaur, H. P.; Schwab, W.; Carsky, P.; Hess, Jr., B. A.; Schaad, L. J., *J. Am. Chem. Soc.*, **1987**, *109*, 5183.

166. Tomioka, H.; Hirai, K.; Tabayashi, K.; Murata, S.; Izawa, Y.; Inagaki, S.; Okajima, T., *J. Am. Chem. Soc.*, **1990**, *112*, 7692.
167. Gosavi, R. K.; Torres, M.; Strausz, O. P., *Can. J. Chem.*, **1991**, *69*, 1630.
168. For a review, see Gaspar, P. P.; West, R., in *The Chemistry of Organic Silicon Compounds*, 2nd ed., Rappoport, Z.; Apeloig, Y., Eds., Wiley, New York, 1999, Part 3, pp. 2463–2568.
169. Kira, M.; Ishida, S.; Iwamoto, T.; Kabuto, C., *J. Am. Chem. Soc.*, **1999**, *121*, 9722–9723, and references therein.
170. (a) Suchard, S. N., *Selected Spectroscopic Constants for Selected Heteronuclear Diatomic Molecules*, Air Force Report No. SANSO-TR-74-82, U. S. Government Printing Office, Washington, DC, 1974. (b) Gilles, A.; Masanet, J.; Vermeil, C., *Chem. Phys. Lett.*, **1974**, *25*, 346.
171. Davis, J. H.; Goddard III, W. A., *J. Am. Chem. Soc.*, **1977**, *99*, 7111–7121.
172. Back, T. G.; Kerr, R. G., *Can. J. Chem.*, **1982**, *60*, 2711, and references therein.
173. Rauk, A.; Alewood, P. F., *Can. J. Chem.*, **1977**, *55*, 1498, and references therein.
174. Hrovat, D. A.; Waali, E. E.; Borden, W. T., *J. Am. Chem. Soc.*, **1992**, *114*, 8698–8699.
175. Kim, S.-J.; Hamilton, T. P.; Schaefer III, H. F., *J. Am. Chem. Soc.*, **1992**, *114*, 5349–5355.
176. Travers, M. J.; Cowles, D. C.; Clifford, E. P.; Ellison, G. B., *J. Am. Chem. Soc.*, **1992**, *114*, 8699–8701.
177. For a review of nitrenium ions, see Scott, A. P., Ph. D. Dissertation, The University of New England, Armidale, N. S. W., Australia, 1991.
178. Gibson, S. T.; Greene, J. P.; Berkowitz, J., *J. Chem. Phys.*, **1985**, *83*, 4319.
179. Ford, G. P.; Herman, P. S., *J. Am. Chem. Soc.*, **1989**, *111*, 3987.
180. (a) *Multiple Bonds and Low Coordination in Phosphorus Chemistry*, Regitz, M.; Scherer, O. J., Eds., Georg Thieme Verlag, Stuttgart, 1990. (b) Cowley, A. H.; Kemp, R. A., *Chem. Rev.*, **1985**, *85*, 367.
181. Burford, N.; Parks, T. M.; Royan, B. W.; Borecka, B.; Cameron, T. S.; Richardson, J. F.; Gabe, E. J.; Hynes, R., *J. Am. Chem. Soc.*, **1992**, *114*, 8147–8153.
182. Ford, G. P.; Scribner, J. D., *J. Am. Chem. Soc.*, **1981**, *103*, 4281.
183. (a) Li, Y.; Abramovitch, R. A.; Houk, K. N., *J. Org. Chem.*, **1989**, *54*, 2911. (b) Ohwada, T.; Shudo, K., *J. Am. Chem. Soc.*, **1989**, *111*, 34.
184. Worthington, S. E.; Cramer, C. J.; Dulles, F. J.; Storer, J. W., <http://pollux.chem.umn./STgaps/>.
185. Elevation of the HOMO,  $n_O$ , of the carbonyl group above  $\alpha - |\beta|$  is expected on the basis of the orbital interactions, and the SHMO energy of the  $2p$  orbital of a monocoordinated oxygen atom (Table 5.1, Chapter 5). This is consistent with increased basicity of the carbonyl oxygen relative to the  $\pi$  bond of ethylene but is not consistent with the observed ionization potentials (IPs) of carbonyls and structurally related alkenes. For instance, the IP of formaldehyde is 10.88 eV and that of ethylene is 10.51 eV. It may be that SHMO expectations are in error here and that the greater basicity of the carbonyl oxygen is simply a reflection of the greater stability of the protonated carbonyl intermediate as compared to the protonated alkene, as discussed in Chapter 7.
186. Besseau, F.; Lucon, M.; Laurence, C.; Berthelot, M., *J. Chem. Soc. Perkin*, **1998**, *2*, 101–108.
187. Saied, O.; Bachand, B.; Wuest, J. D., *Can. J. Chem.*, **1998**, *76*, 490–497.
188. Rauk, A.; Hunt, I. R.; Keay, B. A., *J. Org. Chem.*, **1994**, *59*, 6808–6816.
189. For a study of hydride reductions, see Wu, Y.-D.; Tucker, J. A.; Houk, K. N., *J. Am. Chem. Soc.*, **1991**, *113*, 5018, and references therein.
190. Liebman, J. F.; Pollack, R. M., *J. Org. Chem.*, **1973**, *38*, 3444.
191. Hoz, S., *J. Org. Chem.*, **1982**, *47*, 3545.
192. Shustov, G. V., *Acad. Sci. U. S. S. R. Proc. Chem.*, **1985**, *280*, 80.

193. (a) Cieplak, A. S., *J. Am. Chem. Soc.*, **1981**, *103*, 4540–4552. (b) Cieplak, A. S.; Tait, B. D.; Johnson, C. R., *J. Am. Chem. Soc.*, **1989**, *111*, 8447–8462.
194. (a) Wu, Y.-D.; Houk, K. N., *J. Am. Chem. Soc.*, **1987**, *109*, 908–910. (b) Houk, K. N.; Wu, Y.-D., in *Stereochemistry of Organic and Bioorganic Transformations*, Bartmann, W.; Sharpless, K. B., Eds., VCH, Weinheim, Germany, 1987, pp. 247–260.
195. (a) Klein, J., *Tetrahedron*, **1974**, *30*, 3349–3353. (b) Klein, J., *Tetrahedron Lett.*, **1973**, 4307–4310.
196. Chérest, M.; Felkin, H.; Prudent, N., *Tetrahedron Lett.*, **1968**, 2199–2204. (b) Chérest, M.; Felkin, H., *Tetrahedron Lett.*, **1968**, 2205–2208.
197. (a) Anh, N. T.; Eistenstein, O., *Nouv. J. Chim.*, **1977**, *1*, 61–70. (b) Anh, N. T., *Top. Curr. Chem.*, **1980**, *88*, 145–162.
198. Sorensen, T. S., to be published.
199. Dannenberg, J. J., *Chem. Rev.*, **1999**, *99*, 1225–1242.
200. Li, Y.; Garrell, R. L.; Houk, K. N., *J. Am. Chem. Soc.*, **1991**, *113*, 5895.
201. Pranata, J.; Davis, G. D., *J. Phys. Chem.*, **1995**, *99*, 14340–14346.
202. Involvement of the N lone pair in “resonance” with the carbonyl group has been a subject of some controversy. For a review, see Bennet, A. J.; Somayaji, V.; Brown, R. S.; Santarsiero, B. D., *J. Am. Chem. Soc.*, **1991**, *113*, 7563.
203. Jackman, L. M., in *Dynamic NMR Spectroscopy*, Jackman, L. M.; Cotton, F. A., Eds., Academic, New York, 1975, p. 203.
204. Tortajada, J.; Leon, E.; Morizer, J.-P.; Luna, A.; Mo, O.; Yanez, M., *J. Phys. Chem.*, **1995**, *99*, 13890–13898.
205. For a discussion of the mechanism of acid and base catalyzed hydrolysis of amides, see Brown, R. S.; Bennet, A. J.; Slobock-Tilk, H., *Acc. Chem. Res.*, **1992**, *25*, 481–488.
206. Wang, Q.-P.; Bennet, A. J.; Brown, R. S.; Santarsiero, B. D., *J. Am. Chem. Soc.*, **1991**, *113*, 5757.
207. For a review of nonplanar and strained amides, see Greenberg, A., in *Structure and Reactivity*, Liebman, J. F.; Greenberg, A., Eds., VCH, New York, 1988, Chapter 4, pp. 138–179.
208. Wiberg, K. B.; Hadad, C. M.; Rablen, P. R.; Cioslowski, J., *J. Am. Chem. Soc.*, **1992**, *114*, 8644–8654.
209. Richard, J. P.; Amyes, T. L.; Vontor, T., *J. Am. Chem. Soc.*, **1991**, *113*, 5871, and references therein.
210. Shaik, S. S.; Schlegel, H. B.; Wolfe, S., *Theoretical Aspects of Physical Organic Chemistry: The S<sub>N</sub>2 Mechanism*, Wiley-Interscience, New York, 1992.
211. For leading references, see (a) Cyr, D. M.; Posey, L. A.; Bishea, G. A.; Han, C.-C.; Johnson, M. A., *J. Am. Chem. Soc.*, **1991**, *113*, 9697. (b) Wilbur, J. L.; Brauman, J. I., *J. Am. Chem. Soc.*, **1991**, *113*, 9699.
212. Wladkowski, B. D.; Lim, K. F.; Allen, W. D.; Brauman, J. I., *J. Am. Chem. Soc.*, **1992**, *114*, 9136–9153.
213. For a detailed discussion, see reference 119, pp. 304–310.
214. Abboud, J.-L.; Notario, R.; Bertrán, J.; Taft, R. W., *J. Am. Chem. Soc.*, **1991**, *113*, 4738, and references therein.
215. Winstein, S.; Savedoff, L. G.; Smith, S.; Stevens, I. D. R.; Gall, J. S., *Tetrahedron Lett.*, **1960**, *9*, 24.
216. Olmstead, W. N.; Brauman, J. I., *J. Am. Chem. Soc.*, **1977**, *99*, 4129–4228.
217. (a) Edwards, J. O.; Pearson, R. G., *J. Am. Chem. Soc.*, **1962**, *84*, 16. (b) Grekov, A. P.; Veselov, V. Ya., *Usp. Khim.*, **1978**, *47*, 1200.
218. (a) Shaik, S. S.; Pross, A., *J. Am. Chem. Soc.*, **1982**, *104*, 2708. (b) Shaik, S. S., *Nouv. J. Chim.*, **1982**, *6*, 159.

219. Shaik, S. S., *J. Am. Chem. Soc.*, **1983**, *105*, 4358–4367.
220. Shaik, S. S., *J. Am. Chem. Soc.*, **1984**, *106*, 1227.
221. Pimentel, G. C.; McClellan, A. L., *The Hydrogen Bond*, W. H. Freeman, San Francisco, 1960.
222. Hanessian, S.; Simard, M.; Roelans, S., *J. Am. Chem. Soc.*, **1995**, *117*, 7630–7645.
223. Herbine, P.; Hu, T. A.; Johnson, G.; Dyke, T. R., *J. Chem. Phys.*, **1990**, *93*, 5485, and references therein.
224. As of this writing, there is some controversy about the gas phase structure of the ammonia dimer (Baum, R. M., *Chem. Eng. News*, **1992**, *October 19*, 20–23). The traditional view of the dimer, containing a “linear” hydrogen bond, which is supported by most theoretical and experimental studies, has been questioned by Klemperer and co-workers on the basis of microwave measurements (Klemperer, W.; Nelson Jr., D. D.; Fraser, G. T., *Science*, **1987**, *238*, 1670).
225. Curtiss, L. A.; Frurip, D. J.; Blander, M., *J. Chem. Phys.*, **1979**, *71*, 2703.
226. Van Duijneveldt-van de Rijdt, J. G. C. M.; van Duijneveldt, F. B., *J. Chem. Phys.*, **1992**, *97*, 5019–5030.
227. Pugliano, N.; Saykally, R. J., *Science*, **1992**, *257*, 1937.
228. Fowler, J. E.; Schaefer III, H. F., *J. Am. Chem. Soc.*, **1995**, *117*, 446–452, and references therein.
229. Perrin, C. L.; Thoburn, J. D., *J. Am. Chem. Soc.*, **1992**, *114*, 8559–8565.
230. Sponer, J.; Hobza, P., *J. Am. Chem. Soc.*, **1994**, *116*, 709–714, and references therein.
231. Winningham, M. J.; Sogah, D. Y., *J. Am. Chem. Soc.*, **1994**, *116*, 11173–11174, and references therein.
232. Lesburg, C. A.; Christianson, D. W., *J. Am. Chem. Soc.*, **1995**, *117*, 6838–6844.
233. Newton, M. D.; Jeffrey, G. A.; Tagaki, S., *J. Am. Chem. Soc.*, **1979**, *101*, 1997–2002.
234. Gronert, S., *J. Am. Chem. Soc.*, **1991**, *113*, 6041.
235. Sunner, J. A.; Hirao, K.; Kebarle, P., *J. Phys. Chem.*, **1989**, *93*, 4010.
236. (a) Kirchen, R. P.; Ranganayakulu, K.; Rauk, A.; Singh, B. P.; Sorensen, T. S., *J. Am. Chem. Soc.*, **1981**, *103*, 588. (b) Kirchen, R. P.; Okazawa, N.; Ranganayakulu, K.; Rauk, A.; Sorensen, T. S., *J. Am. Chem. Soc.*, **1981**, *103*, 597. (c) Sorensen, T. S.; Whitworth, S. M., *J. Am. Chem. Soc.*, **1990**, *112*, 8135.
237. Dorigo, A. E.; McCarrick, M. A.; Loncharich, R. J.; Houk, K. N., *J. Am. Chem. Soc.*, **1990**, *112*, 7508–7514. Erratum: *J. Am. Chem. Soc.*, **1991**, *113*, 4368.
238. (a) Tsang, W., *Int. J. Chem. Kinet.*, **1978**, *10*, 821. (b) Tsang, W., *J. Am. Chem. Soc.*, **1985**, *107*, 2872.
239. (a) Russell, J. J.; Seetula, J. A.; Senkan, S. M.; Gutman, D., *Int. J. Chem. Kinet.*, **1988**, *20*, 759. (b) Russell, J. J.; Seetula, J. A.; Timonen, R. S.; Gutman, D.; Nava, D. F., *J. Am. Chem. Soc.*, **1988**, *110*, 3084. (c) Russell, J. J.; Seetula, J. A.; Gutman, D., *J. Am. Chem. Soc.*, **1988**, *110*, 3092. (d) Seetula, J. A.; Russell, J. J.; Gutman, D., *J. Am. Chem. Soc.*, **1990**, *112*, 1347.
240. Roberts, B. P.; Steel, A. J., *J. Chem. Soc. Perkin Trans.*, **1994**, *2*, 2155–2162.
241. (a) Zavitsas, A. A., *J. Chem. Soc. Perkin Trans.*, **1998**, *2*, 499–502, and references therein. (b) Zavitsas, A. A., *J. Chem. Soc. Perkin Trans.*, **1996**, *2*, 391–394.
242. Griller, D.; Ingold, K. U., *J. Am. Chem. Soc.*, **1974**, *96*, 630.
243. Alnajjar, M. S.; Garrossian, M. S.; Autrey, S. T.; Ferris, K. F.; Franz, J. A., *J. Phys. Chem.*, **1992**, *96*, 7037.
244. *Handbook of Bimolecular and Termolecular Gas Reactions*, Kerr, J. A., Ed., CRC Press, Boca Raton, FL, 1981.
245. Liu, B., *J. Phys. Chem.*, **1984**, *80*, 581.
246. Estimated from ab initio calculations: Gordon, M. S.; Nguyen, K. A.; Truhlar, D. G., *J. Phys. Chem.*, **1989**, *93*, 7356.

247. Schiesser, C. H.; Skidmore, M. A., *J. Chem. Soc. Perkin Trans.*, **1998**, 2, 2329–2333.
248. For a discussion on efforts to localize the  $\pi$  electrons of benzene, see *Chem. Eng. News*, **1996**, April 1, 27–31.
249. Burgi, H.-B.; Baldrige, K. K.; Hardcastle, F.; Frank, N. L.; Gantzel, P.; Siegel, J. S.; Ziller, J., *Angew. Chem. Int. Ed. Engl.*, **1995**, 34, 1454–1455.
250. Boese, R.; Blaser, D.; Billups, W. D.; Haley, M. M.; Maulitz, A. H.; Mohler, D. L.; Vollhardt, K. P. C., *Angew. Chem. Int. Ed. Engl.*, **1994**, 33, 313–316.
251. Frank, N. L.; Baldrige, K. K.; Siegel, J. S., *J. Am. Chem. Soc.*, **1995**, 117, 2102–2103.
252. Diederich, F.; Rubin, Y.; Knobler, C. B.; Whetten, R. L.; Schriver, K. E.; Houk, K. N.; Li, Y., *Science*, **1989**, 245, 1088.
253. (a) Krätschmer, W.; Lamb, L. D.; Fostiropoulos, K.; Huffman, D. R., *Nature*, **1990**, 347, 354. (b) Taylor, R.; Hare, J. P.; Abdul-Sada, A. K.; Kroto, H. W., *J. Chem. Soc. Chem. Commun.*, **1990**, 1423.
254. Parasuk, V.; Almlöf, J.; Feyereisen, M. W., *J. Am. Chem. Soc.*, **1991**, 113, 1049.
255. For a special edition on Buckminsterfullerenes, see *Acc. Chem. Res.*, **1992**, 25, 98–175.
256. Haddon, R. C.; Brus, L. E.; Raghavachari, K., *Chem. Phys. Lett.*, **1986**, 125, 459.
257. Cremer, D.; Reichel, F.; Kraka, E., *J. Am. Chem. Soc.*, **1991**, 113, 9459.
258. For a review of secondary orbital interactions, see Ginsburg, D., *Tetrahedron*, **1983**, 39, 2095–2135.
259. Dewar, M. J. S., *Angewante Chemie Int. Ed. Engl.*, **1971**, 10, 761–870.
260. Houk, K. N.; Lin, Y.-T.; Brown, F. K., *J. Am. Chem. Soc.*, **1986**, 108, 554, and references therein.
261. Bernardi, F.; Bottoni, A.; Robb, M. A.; Field, M. J.; Hillier, I. H.; Guest, M. F., *J. Chem. Soc. Chem. Commun.*, **1985**, 1051.
262. Doering, W. von E.; Toscano, V. G.; Beasley, G. H., *Tetrahedron*, **1971**, 27, 5299–5306.
263. (a) Morokuma, K.; Borden, W. T.; Hrovat, D. A., *J. Am. Chem. Soc.*, **1988**, 110, 4474. (b)
264. Maluendes, S. A.; Dupuis, M., *J. Chem. Phys.*, **1990**, 93, 5902.
265. Lee, E.; Shin, I.-J.; Kim, T.-S., *J. Am. Chem. Soc.*, **1990**, 112, 260.
266. Luger, P.; Buschmann, J.; McMullan, R. K.; Ruble, J. R.; Matias, P.; Jeffrey, G. A., *J. Am. Chem. Soc.*, **1986**, 108, 7825.
267. Meier, B. H.; Earl, W. L., *J. Am. Chem. Soc.*, **1985**, 107, 5553.
268. Padwa, A., *1,3-Dipolar Cycloaddition Chemistry*, vols. 1 and 2, Wiley, New York, 1984.
269. Samuilov, Y. D.; Konovalov, A. I., *Russ. Chem. Rev.*, **1984**, 53, 332.
270. For a review of 1,3-dipolar reactions, see Gothelf, K. V.; Jorgensen, K. A., *Chem. Rev.*, **1998**, 863–909.
271. Houk, K. N.; Sims, J.; Watts, C. R.; Luskus, L. J., *J. Am. Chem. Soc.*, **1973**, 95, 7301.
272. Houk, K. N.; Sims, J.; Duke, Jr., R. E.; Strozier, R. W.; George, J. K., *J. Am. Chem. Soc.*, **1973**, 95, 7287.
273. Bridson-Jones, F. S.; Buckley, G. D.; Cross, L. H.; Driver, A. P., *J. Chem. Soc.*, **1951**, 2999.
274. Herzberg, G., *Molecular Spectra and Molecular Structure III. Electronic Spectra and Electronic Structure of Polyatomic Molecules*, D. Van Nostrand, Toronto, 1967.
275. (a) Elian, M.; Chen, M. M.; Mingos, D. M. P.; Hoffmann, R., *Inorg. Chem.*, **1976**, 15, 1148. (b) Hoffmann, R., *Angew. Chem. Int. Ed. Engl.*, **1982**, 21, 711.
276. Moore, C. E., *Atomic Energy Levels*, vols. 1–3, NBS Circular 467, U.S. Government Printing Office, Washington, DC, 1958.
277. Clementi, E.; Roetti, C., *Atomic Data and Nuclear Data Tables*, **1974**, 14, 177–478.
278. Cotton, F. A.; Wilkinson, G., *Advanced Inorganic Chemistry*, 5th ed., Wiley-Interscience, New York, 1988.



279. See, e.g., Summerville, R. H.; Hoffmann, R., *J. Am. Chem. Soc.*, **1976**, *98*, 7240–7254.
280. Shriver, D. F.; Atkins, P. W.; Langford, C. H., *Inorganic Chemistry*, Oxford University Press, Oxford, 1994, pp. 247, 626.
281. Jarvis, J. A. J.; Kilbourn, B. T.; Owston, P. G., *Acta Cryst.*, **1971**, *B27*, 366–372.
282. Ziegler, T.; Rauk, A., *Inorg. Chem.*, **1979**, *18*, 1558.
283. Stromberg, S.; Svensson, M.; Zetterberg, K., *Organometallics*, **1997**, *16*, 3165–3168.
284. Hill, G. S.; Puddephatt, R. J., *Organometallics*, **1998**, *17*, 1478–1486.
285. Stahl, S. S.; Labinger, J. A.; Bercaw, J. E., *J. Am. Chem. Soc.*, **1996**, *118*, 5961–5976.
286. Holloway, C. E.; Hulley, G.; Johnson, B. F. G.; Lewis, J., *J. Chem. Soc. A*, **1969**, 53–60.
287. Regioselectivity of H attack.
288. (a) Ziegler, K.; Holzkamp, E.; Breil, H.; Martin, H., *Angew. Chemie*, **1955**, *67*, 541. (b) Natta, G.; Pino, P.; Corradini, P.; Danusso, F.; Mantica, E.; Mazzanti, G.; Moraglio, G., *J. Am. Chem. Soc.*, **1955**, *77*, 1708. (c) Brintzinger, H. H.; Fischer, D.; Mulhaupt, R.; Rieger, B.; Waymouth, R. M., *Angew. Chemie*, **1995**, *34*, 1143–1170. (d) Druliner, J. D., *Organometallics*, **1984**, *3*, 205.
289. For an example of activation by  $B(CF_3)_3$ , see Chan, M. S. W.; Vanka, K.; Pye, C. C.; Ziegler, T., *Organometallics*, **1999**, *18*, 4624–4636.
290. Andersen, A.; Cordes, H.-G.; Herwig, J.; Kaminsky, W.; Merck, A.; Mottweiler, P.; Pein, J.; Sinn, H.; Vollmer, H.-J., *Angew. Chemie*, **1976**, *15*, 630.
291. Lohrenz, J. C. W.; Woo, T. K.; Ziegler, T., *J. Am. Chem. Soc.*, **1995**, *117*, 12793–12800.
292. Margl, P.; Deng, L.; Ziegler, T., *J. Am. Chem. Soc.*, **1999**, *121*, 154–162, and references therein.
293. Macgregor, S. A.; Eisenstein, O.; Whittlesey, M. K.; Peritz, R. N., *J. Chem. Soc. Dalton Trans.*, **1998**, 291–300.
294. Ziegler, T.; Tschinke, V.; Fan, L.; Becke, A. D., *J. Am. Chem. Soc.*, **1989**, *111*, 9177.
295. Wang, W.; Narducci, A. A.; House, P. G.; Weitz, E., *J. Am. Chem. Soc.*, **1996**, *118*, 8654–8657.
296. Han, Y.; Deng, L.; Ziegler, T., *J. Am. Chem. Soc.*, **1997**, *119*, 5939–5945.
297. Review: Marvell, E. N., *Thermal Electrocyclic Reactions*, Academic, New York, 1980.
298. Thomas IV, B. E.; Evanseck, J. D.; Houk, K. N., *J. Am. Chem. Soc.*, **1993**, *115*, 4165–4169, and references therein.
299. (a) Ziegenbein, W., *Chem. Ber.*, **1965**, *96*, 1427. (b) Goldfarb, T. D.; Landquist, L. J., *J. Am. Chem. Soc.*, **1967**, *89*, 4588.
300. Fowler, J. E.; Alberts, I. L.; Schaefer III, H. F., *J. Am. Chem. Soc.*, **1991**, *113*, 4768, and references therein.
301. (a) Yamazaki, H.; Cvetanovic, R. J., *J. Am. Chem. Soc.*, **1969**, *91*, 520–522. (b) Yamazaki, H.; Cvetanovic, R. J.; Irwin, R. S., *J. Am. Chem. Soc.*, **1976**, *98*, 2198–2205.
302. Ikezawa, H.; Kutal, C.; Yasufuku, K.; Yamazaki, H., *J. Am. Chem. Soc.*, **1986**, *108*, 1589–1594, and references therein.
303. (a) Clark, K. B.; Leigh, W. J., *J. Am. Chem. Soc.*, **1987**, *109*, 6086. (b) Leigh, W. J.; Zheng, K.; Clark, K. B., *Can. J. Chem.*, **1990**, *68*, **1988**.
304. Leigh, W. J.; Zheng, K., *J. Am. Chem. Soc.*, **1991**, *113*, 4019; Erratum: *J. Am. Chem. Soc.*, **1992**, *114*, 796.
305. Bernardi, F.; Olivucci, M.; Ragazos, I. N.; Robb, M. A., *J. Am. Chem. Soc.*, **1992**, *114*, 2752–2754.
306. Trulson, M. O.; Dollinger, G. D.; Mathies, R. A., *J. Am. Chem. Soc.*, **1987**, *109*, 586–587.
307. Martin, H.-D.; Urbanek, T.; Pfohler, P.; Walsh, R., *J. Chem. Soc. Chem. Commun.*, **1985**, 964–965.

308. (a) Hoffmann, R., *J. Am. Chem. Soc.*, **1968**, *90*, 1475. (b) Fueno, T.; Nagase, S.; Tatsumi, K.; Yamaguchi, K., *Theor. Chim. Acta*, **1972**, *26*, 43.
309. (a) Houk, K. N.; Rondan, N. G.; Mareda, J., *J. Am. Chem. Soc.*, **1984**, *106*, 4291. (b) Houk, K. N.; Rondan, N. G., *J. Am. Chem. Soc.*, **1984**, *106*, 4293.
310. Dobson, R. C.; Hayes, D. M.; Hoffmann, R., *J. Am. Chem. Soc.*, **1971**, *93*, 6188.
311. Hoffmann, R.; Gleiter, R.; Mallory, F. B., *J. Am. Chem. Soc.*, **1970**, *92*, 1460.
312. See, for example, Zaklika, K. A.; Thayer, A. L.; Schaap, A. P., *J. Am. Chem. Soc.*, **1978**, *100*, 4916–4918.
313. Dewar, M. J. S.; Kirschner, S., *J. Am. Chem. Soc.*, **1974**, *96*, 7578–7579, and references therein.
314. Calvert, J. G.; Pitts, Jr., J. N., *Photochemistry*, Wiley, New York, 1966, p. 280.
315. (a) Frisch, M. J.; Trucks, G. W.; Head-Gordon, M.; Gill, P. M. W.; Wong, M. W.; Foresman, J. B.; Johnson, B. G.; Schlegel, H. B.; Robb, M. A.; Repogle, E. S.; Gomperts, R.; Andres, J. L.; Raghavachari, K.; Binkley, J. S.; Gonzalez, C.; Martin, R. L.; Fox, D. J.; Defrees, D. J.; Baker, J.; Stewart, J. J. P.; Pople, J. A., *Gaussian 92, Revision A*, Gaussian, Pittsburgh, PA, 1992. (b) Frisch, M. J.; Trucks, G. W.; Schlegel, H. B.; Gill, P. M. W.; Johnson, B. G.; Robb, M. A.; Cheeseman, J. R.; Keith, T. A.; Petersson, G. A.; Montgomery, J. A.; Raghavachari, K.; Al-Laham, M. A.; Zakrewski, V. G.; Ortiz, J. V.; Foresman, J. B.; Cioslowski, J.; Stefanov, B. B.; Nanayakkara, A.; Challacombe, M.; Peng, C. Y.; Ayala, P. Y.; Chen, W.; Wong, M. W.; Andres, J. L.; Repogle, E. S.; Gomperts, R.; Martin, R. L.; Fox, D. J.; Binkley, J. S.; Defrees, D. J.; Baker, J.; Stewart, J. P.; Head-Gordon, M.; Gonzalez, C.; Pople, J. A., *Gaussian 94, (SGI-Revision B.3)*, Gaussian, Pittsburgh PA, 1995.
316. Jensen, F., *Introduction to Computational Chemistry*, Wiley, New York, 1999.
317. Allen, L. C., *J. Am. Chem. Soc.*, **1992**, *114*, 1510.
318. Allen, L. C., *J. Am. Chem. Soc.*, **1989**, *111*, 9003.
319. (a) Pauling, L., *J. Am. Chem. Soc.*, **1932**, *54*, 3570. (b) Allred, A. L., *J. Inorg. Nucl. Chem.*, **1961**, *17*, 215.
320. Allred, A. L.; Rochow, E. G., *J. Inorg. Nucl. Chem.*, **1957**, *5*, 264.
321. For an additional discussion of electronegativities and an extensive list of references, see Luo, Y.-R.; Benson, S. W., *Acc. Chem. Res.*, **1992**, *25*, 375.
322. Langhoff, S. R.; Davidson, E. R., *Int. J. Quantum Chem.*, **1974**, *8*, 61.
323. Slater, J. C., *Phys. Rev.*, **1951**, *81*, 385.
324. Kohn, W.; Sham, L. J., *Phys. Rev. A*, **1965**, *140*, 1133–1138.
325. Pople, J. A.; Gill, P. M. W.; Johnson, B. G., *Chem. Phys. Lett.*, **1992**, *199*, 557–560.
326. Vosko, S. H.; Wilk, L.; Nusair, M., *Can. J. Phys.*, **1980**, *2*, 1200.
327. Becke, A. D., *Phys. Rev. A*, **1988**, *38*, 3098.
328. (a) Perdew, J. P., *Phys. Rev. B*, **1986**, *33*, 8822. (b) Perdew, J. P., *Phys. Rev. B*, **1986**, *34*, 7046.
329. Colle, R.; Salvetti, O., *J. Chem. Phys.*, **1983**, *79*, 1404.
330. Lee, C.; Yang, W.; Parr, R. G., *Phys. Rev. B*, **1988**, *37*, 785–789.
331. Becke, A. D., *J. Chem. Phys.*, **1988**, *88*, 1053.
332. Sule, P.; Gritsenko, O. V.; Nagy, A.; Baerends, E. J., *J. Chem. Phys.*, **1995**, *103*, 10085–10094.
333. (a) Baerends, E. J.; Ellis, D. E.; Ros, P., *Chem. Phys.*, **1973**, *2*, 41. (b) teVelde, G.; Baerends, E. J., *J. Comp. Phys.*, **1992**, *99*, 84.
334. Becke, A. D., *J. Chem. Phys.*, **1993**, *98*, 5648–5652.

## INDEX

---

- Absorption, 211
- Acetaldehyde  
  in aldol reaction, 100  
  BF<sub>3</sub> affinity, 123  
  IP, 123  
  PA, 123  
  p*K*<sub>b</sub>, 123  
  pyruvate decarboxylase, 302  
  by Wacker process, 293
- Acetic anhydride, 281
- Acetoacetone  
  asymmetric reduction of, 12  
  p*K*<sub>a</sub>, 142
- Acetone, 278  
  BF<sub>3</sub> affinity, 123  
  IP, 123  
  PA, 123  
  p*K*<sub>a</sub>, 142  
  p*K*<sub>b</sub>, 123
- Acetonitrile  
  p*K*<sub>a</sub>, 142
- Acetylene  
  complex with ozone, 304  
  p*K*<sub>a</sub>, 142  
  point group of, 5
- Acetylenes  
  cyclic di-, IP, 305
- Acetylacetonate (*acac*)  
  as chelating ligand, 186
- Achiral  
  definition, 1, 8
- Aconitic acid, 12
- Acrolein  
  BF<sub>3</sub> affinity, 123  
  PA, 123
- Acrylonitrile, 101
- Activation energies  
  H• + H—H—H, 149  
  H<sub>3</sub>C• + H—H—CH<sub>3</sub>, 149  
  negative, 148  
  RO• + H—H—OR  
  RS• + H—H—SR, 149
- Acyl hydrolysis, 105
- Acylnitrenium ions, 120
- Acyloxy radicals, 112
- Adamantanones, 279, 280
- 2-Adamantyl cation, 280
- Adenine, 138
- Agostic interaction, 191
- Alane (AlH<sub>3</sub>), 278  
  complex with amines, 305
- Alcohols  
  from carbocations, 107  
  reaction with RO•, 149
- Aldehydes  
  reduction by metal hydrides, 278
- Alkenes, 98–104  
  electrophilic additions, 98–99

- Alkenes (*Continued*)  
 nonplanar, 102
- Alkoxides  
 bases and nucleophiles, 97
- Alkoxy radicals  
 with H—OR, 149
- Alkyl azides, 172
- Alkyl halides  
 acids and electrophiles, 97  
 from carbocations, 107  
 reactions, 281  
 in  $S_N1$ , 129–130, 134  
 in  $S_N2$ , 130–131, 134  
 LUMO, 131, 133
- Alkyl peroxides, 258
- Alkylammonium salts  
 from carbocations, 107
- Alkynes, 103
- Allene  
 point group of, 6
- Allyl  
 SHMO, 89
- Allyl anion  
 from cyclopropyl anion, 200  
 HOMO, 100
- Allyl cation  
 acidity relative to methyl cation, 268  
 from cyclopropyl cation, 200  
 LUMO, 100
- Allylic alcohols  
 epoxidation, 11
- Alpha, in SHMO, 92–96  
 effect of coordination number, 93  
 heteroatoms, 93  
 reference energy, 92  
 table of, 94
- Alpha effect, 132
- Alpine-Borane, 11, 12
- Alternant systems, 91
- Aluminum triisopropoxide, 308
- Alumoxane, 193
- Amide group, 126–127  
 barrier to rotation, 127  
 basicity of, 127  
 interaction diagram, 127  
 nonplanar, 127  
 SHMO, 126
- Amides  
 bases and nucleophiles, 97
- Amine oxides, 270  
 interaction diagram, 271
- Amines  
 complex with  $AlH_3$ , 305  
 oxidation by  $H_2O_2$ , 302
- $\alpha$ -Amino acids  
 synthesis, 311
- $\alpha,\beta$ -Aminoalcohols  
 photofragmentation, 305
- Aminocarbocation, 252  
 interaction diagram, 253
- Aminonitrene, 118
- Ammonia ( $NH_3$ )  
 basicity relative to phosphine, 256  
 BDE, 76  
 complex with  $F_2$ ,  $Cl_2$ ,  $ClF$ , 82, 262  
 dative bond with  $BH_3$ , 262  
 dimer, 321  
 effect on  $\Delta_O$ , 181  
 geometry of, 32  
 H-bonded complexes, 138  
 interaction diagram, 256  
 infrared intensities of, 32  
 IP, 81  
 as L: ligand, 176  
 nonbonded orbital of, 27  
 normal coordinates of, 32  
 orbital energies, 26  
 point group of, 5  
 reaction with  $BF_3$ , 49  
 total energy, 29  
 trans effect, 181
- Ammonium ( $NH_4^+$ ), 257
- Amsterdam density functional (ADF)  
 computer program, 246
- Anchimeric assistance, 82
- Aniline  
 SHMO, 153
- Anomeric effect, 82, 310–311, 305
- Antarafacial, 163  
 examples, 164  
 sigma bonds, 167
- Anti-Bredt olefin, 102
- Approximations of MO theory  
 Born–Oppenheimer, 22  
 Hartree–Fock, 222  
 Hückel, 35, 86  
 independent electron, 35  
 LCAO, 229  
 nonrelativistic, 22  
 SHMO, 87  
 Wolfsberg–Helmholtz, 43  
 zero-overlap, 38, 40
- Aromaticity, 150
- Aromatic compounds, 150–160
- Arsenium ions, 119
- Asymmetric synthesis  
 definition, 9
- Avoided crossing, 206

- 1-Aza-1,3,5,7,9,11-dodecahexaene, 270
- Azides  
to nitrenes, 116
- Aziridines  
ring opening, 200
- Azo compounds  
from nitrenes, 117
- Azoxyalkane, 174
- Azulene, 304  
synthesis, 304
- B3LYP, 31  
functional, 246
- Baker's yeast pyruvate decarboxylase, 301–302  
mechanism, 302
- Basicities  
gas phase, 97
- Basis set, 23, 229, 232–233  
exponential, 232  
Gaussian functions, 24–25  
Cartesian, 232  
primitive, 233  
contracted, 233  
exponents, 233  
polarized, 233  
split valence, 25, 233
- 9-BBN, 11, 12
- BDE, see Bond dissociation energy
- Benzaldehyde  
asymmetric reduction of, 12  
SHMO, 153
- Benzene  
from benzvalene, 203, 204  
complex with ethylene cation radical, 284  
complex with  $\text{NO}^+$ , 284  
interaction diagram, 285  
as ligand, 187  
point group of, 5  
SHMO, 90, 151
- Benzenes, substituted  
electrophilic substitutions, 152  
“C” substituent, 155–156  
X: substituent, 153–154  
Z substituent, 154–155  
nucleophilic substitutions, 157–160  
Z substituent, 158
- Benzocyclopentanol, 300
- Benzophenone  
photoreduction, 299
- Benzpinacol, 299
- Benzvalene, 204  
barrier to benzene, 203  
correlation diagram, 204
- Benzyl alcohol, (*R*)- $\alpha$ -d, preparation, 12
- Benzyl carbocation, 106
- Benzynes, 159–160, 275–276  
in Diels–Alder reaction, 160  
E1cb, 159  
interaction diagram, 159  
MW and IR spectra, 276  
nucleophilic substitution, 159
- Beta, in SHMO, 92–96  
effect of coordination number, 93  
effect of twisting, 102  
energy scale, 92  
heteroatoms, 93  
table of, 94
- $\text{BF}_3$  affinity  
acetaldehyde, 123  
acetone, 123  
acrolein, 123  
butenone, 123  
dimethyl ether, 123  
dimethylacrolein, 123  
formaldehyde, 123  
methanol, 123  
methyl acetate, 123  
methyl acrylate, 123  
(*E*)-methylacrolein, 123  
nucleophilicity, 123  
oxetane, 123  
table of, 123  
tetrahydrofuran, 123  
water, 123
- $\text{BH}_3\text{NH}_3$ , 284  
structure, 284
- Bicyclo[3.1.0]hex-2-ene, 291  
sigmatropic rearrangement, 290–291
- Bicyclo[2.1.0]pent-2-ene, 289
- Bishomocyclopropenyl cation, 277
- Bond, definition of, 50
- Bond angles  
geometric relationship between, 15
- Bond dissociation energy  
relationship with  $\text{p}K_a$  and  $E_{\text{ox}}$ , 112–113
- Bond Dissociation Energy (BDE)  
cubane C—H, 282  
cysteine S—H, 113  
glycine  $^{\alpha}\text{C}$ —H, 113  
glutathione S—H, 113  
M—H bonds, 195  
methane, 113  
table, 76  
three-electron S—S bond, 254
- Bond energy,  $\pi$  bonds  
disilene, 104  
ethylene, 104  
silaethene, 104

- Bond order, SHMO, 91–92  
 Bond strength, see Bond dissociation energy  
 9-Borabicyclo[3.3.1]nonane (9-BBN), 12  
 Borane (BH<sub>3</sub>)  
   dative bond with NH<sub>3</sub>, 262  
 Boranes, 84  
   acids and electrophiles, 97  
 Borazine, 286, 288  
   SHMO, 288  
   interaction diagram, 288  
 Boric acid  
   point group of, 5  
 Boron trifluoride (BF<sub>3</sub>), see also BF<sub>3</sub>  
   complex with CO, 304–305  
   reaction with NH<sub>3</sub>, 49  
   “Y”-conjugation, 304  
 Born–Oppenheimer approximation, 22, 219  
 Bound state, 209–210  
 BrCl, with alkenes, 260  
 Brillouin’s theorem, 241  
 Bromide ion (Br<sup>−</sup>)  
   effect on Δ<sub>O</sub>, 181  
   trans effect, 181  
   as X<sup>−</sup> ligand, 176  
 Bromine (Br<sub>2</sub>)  
   sigma bond, 77  
 Bromochloromethane, 13  
 11-Bromo-*endo*-9-chloro-7-ethoxybicyclo[5.3.1]undec-1(11)-ene, 102–103  
 Bromomalonate carbanion, 281  
 Bromomethane  
   BDE, 76  
 Bromonium ion, 108  
 N-Bromosuccinimide, 262  
 Brucine, in asymmetric synthesis, 10, 11  
 Buckminsterfullerene (C<sub>60</sub>)  
   point group of, 6  
 Bullvalene, 170, 171  
   point group of, 4  
 Butadiene  
   Diels–Alder, 198, 201  
   with ethylene, 169  
   SHMO, 89  
 Butadienes  
   from cyclobutenes, 198–200, 202  
 2-Butene  
   photodimerization, 202  
   photolysis, 261  
 (*Z*)-2-Butene  
   IP of, 48, 80  
 Butenone  
   BF<sub>3</sub> affinity, 123  
   IP, 123  
   PA, 123  
*tert*-Butyl cation  
   “Y”-conjugation, 304  
*tert*-Butyl carbanion, 109  
*tert*-Butylhydroperoxide, 11  
 2-Butyne, 296  
 “C” substituents  
   electrophilic addition  
     alkenes, 101–102  
     benzenes, 155–156  
   interaction with  
     C=C, 100  
     C–H, 143, 145  
     C=O, 122  
     carbanion, 109  
     carbene, 115  
     carbocation, 106  
     carbon radical, 111  
     nitrene, 117  
     nitrenium, 119  
   list of, 102  
 C<sub>18</sub>, 151  
 C<sub>60</sub>, 151  
 Cannizzaro reaction, 84, 146  
   formaldehyde, 146  
 Captodative effect, 113, 277  
 Carbalkoxycarbenes (:CRCO<sub>2</sub>R), 116  
 Carbanions, 108–110  
   bases and nucleophiles, 97  
   gas phase, 109  
   substituents on, 109  
   *a*-sulfonyl, 277  
 Carbene, see also Methylene  
   :CBR<sub>2</sub>, 115  
   :C(CH<sub>3</sub>)<sub>2</sub>, 116  
   :CCl<sub>2</sub>, 115  
   :CClOCH<sub>3</sub>, 115  
   :CF<sub>2</sub>, 115  
   :CFOCH<sub>3</sub>, 115  
   :CHCCH, 116  
   :CHC<sub>6</sub>H<sub>5</sub>, 116  
   :CHCHO, 116  
   :CHF, 115  
   :CI<sub>2</sub>, 115  
   :C(OCH<sub>3</sub>)<sub>2</sub>, 115  
   :CRCO<sub>2</sub>R, 116  
 Carbenes, 114–116  
   addition to alkenes, 207–208  
   C–H insertion, 208  
   dimerization, 208  
   electronic states, 114  
   singlet  
     reaction with carbonyl, 279

- Carbenes (*Continued*)  
 substituents on, 115
- Carbocations, 105–108  
 acids and electrophiles, 97  
 dialkoxy, 105  
 ethyl, 84  
 fluoro, 105  
 norbornyl, 84  
 reactions, 107  
 substituents on, 106
- 2-Carbomethoxy-2-cyclohexen-1-one, 289
- Carbon dioxide  
 point group of, 5
- Carbon monoxide (CO)  
 complex with  $\text{BF}_3$ , 304  
 effect on  $\Delta_{\text{O}}$ , 181  
 as L: ligand, 176  
 point group of, 5  
 trans effect, 181
- Carbonyl compounds, 121–128  
 acids and electrophiles, 97  
 electrophilic attack, 121–123  
 photochemistry  
 Norrish type I, 215–217  
 Norrish type II, 213–215  
 stability of, 127–128  
 UV spectra, 214
- Carbonyl group  
 basicity of O, 122–123  
 interaction diagram, 122  
 IP of, 123  
 nucleophilic attack on, 68, 124–126  
 nucleophilicity of O, 122–123  
 $\pi^*$  antibond, SHMO, 124  
 $\pi$  bond, SHMO, 121  
 reactions, 125
- Carbonyl imine, 174
- Carbonyl oxide, 174
- Carbonyl ylide, 174
- Carboranes, 84
- Carboxyalkyl radicals, 112
- Carboxylate group  
 interaction diagram, 307
- Cartesian Gaussian functions, in basis set, 24–25
- Catalytic cracking, 146
- CCSD(T), 30
- $\text{CF}_3$ , see Trifluoromethyl
- CFPA, 14
- C—H bonds, 141–143  
 activation by X:; “C” substituents, 145  
 activation by Z, “C” substituents, 142  
 hybridization, 141  
 $\text{p}K_{\text{a}}$  values, 142
- Chelotropic reactions, 163, 165–166, 201  
 butadienes +  $\text{SO}_2$ , 164, 166  
 carbene addition to alkene, 164, 166  
 orbital correlation diagram, 200  
 stereochemistry, 165–166
- Chemiluminescence, 208
- Chiral  
 definition, 1, 8
- Chiral auxiliary, 11
- Chloride ion ( $\text{Cl}^-$ )  
 effect on  $\Delta_{\text{O}}$ , 181  
 trans effect, 181  
 as X: ligand, 176
- Chlorine ( $\text{Cl}_2$ )  
 complex with ammonia, 82  
 sigma bond, 77
- Chlorine fluoride (ClF)  
 complex with ammonia, 82
- Chloroethane  
 gas phase  $\text{S}_{\text{N}}2$ , E2, 144
- Chloroform  
 point group of, 5
- Chloromalonate carbanion, 281
- Chloromethane  
 BDE, 76
- Chloromethoxycarbene ( $:\text{CClOCH}_3$ ), 115
- o*-Chloro-*o*-methylacetophenone, 300
- m*-Chloroperbenzoic acid  
 epoxidation by, 102
- N*-Chloropyridine, 287  
 interaction diagram, 287  
 SHMO, 287  
 three-electron bond, 286
- Chromium pentacarbonyl ( $\text{Cr}(\text{CO})_5$ ), 177
- Cl, see Configuration interaction
- Citric acid, 12
- ClF, with ammonia, 260
- Coefficients, 229
- Component analysis, 167–168  
 rule for, 168
- Configuration, electronic, 205
- Configuration interaction (CI), 30  
 doubly excited configurations, 240  
 electronic transition energies, 241  
 optical rotatory strengths, 241  
 singly excited configurations, 241  
 theory, 239–241  
 transition dipole, 241
- Conrotatory, 165
- Constitutional isomers, 8
- Constitutionally heterotopic groups, 9
- Contraction, 233
- Cope rearrangement, 170–171  
 bullvalene, 170  
 divinylcyclopropane, 170

- Cope rearrangement (*Continued*)  
 1,5-hexadiene, 170  
 interaction diagram, 171  
 orbital analysis, 170–171  
 oxy-Cope, 170
- Copolymerization  
 CO + alkenes, 293–296  
 interaction diagram, 295
- Core Hamiltonian, 35
- Correlation diagrams  
 general principles, 196–197  
 orbital, 196–203  
 state, 203–208
- Coulomb integral, alpha  
 effect of coordination number, 93  
 heteroatoms, 93  
 reference energy, 92  
 table of, 94
- Coulomb's law, 219
- Coupling Constant,  $C^{13}$ —H, 16
- Cyanide ion ( $CN^-$ )  
 effect on  $\Delta_o$ , 181  
 trans effect, 181  
 as  $X^-$  ligand, 176
- $\alpha$ -Cyano- $\alpha$ -fluorophenylacetic acid, CFPA,  
 14
- 2-Cyanofuran, 267  
 SHMO, 267
- 2-Cyanotetrahydropyran  
 reduction, 307
- Cycloaddition reactions, 162–165, 197–198  
 component analysis, 168  
 Diels–Alder, 162, 198  
 ethylene + ethylene, 198  
 orbital correlation diagram, 198  
 stereochemistry, 162–163
- Cycloalkanols, synthesis, 277
- Cyclobutadiene  
 barrier, 91  
 ground state, 91  
 point group of, 5  
 self-reactivity, 97  
 SHMO, 151  
 structure, 309–310
- Cyclobutane  
 ethylene dimerization, 198, 201  
 point group of, 5, 6
- Cyclobutanes  
 photodimerization of alkenes, 202
- Cyclobutanone  
 group designations, 9
- Cyclobutenes  
 from butadienes, 198–200  
 photolysis, 203
- Cyclodec-5-en-1-one, 289
- Cyclodecyl cation  
 hydride bridge, 147
- 1,4-Cycloheptadiene, 170, 171
- Cycloheptatriene, 281
- Cycloheptatrienes  
 rearrangements, 290
- Cycloheptatrienylidene, 275  
 interaction diagram, 276
- 1,3-Cyclohexadiene  
 electrocyclic reaction, 296  
 photolysis, 203
- 1,3-Cyclohexadienes  
 electrocyclic reactions, 290
- 1,4-Cyclohexadiene  
 HOMO, 80  
 interaction diagram, 80
- Cyclohexadienones  
 photochemistry, 299–300
- Cyclohexane  
 point group of, 6  
 symmetry elements, 7
- Cyclohexanones, 84  
 nucleophilic addition, 125, 126
- Cyclohexene  
 IP, 48, 102
- Cyclohexenes  
 from Diels–Alder, 170
- 1,5-Cyclooctadiene, 11, 187  
 as ligand, 187
- Cyclooctatetraene  
 from cubane, 203  
 point group of, 6
- Cyclooctatrienone, 289
- cis*-Cyclooctene  
 IP, 102
- trans*-Cyclooctene  
 geometry, 102  
 IP, 102  
 optical resolution, 292
- Cyclopentadiene, 291  
 dimerization, 97, 291  
 with 2-methylpropenyl cation  
 $pK_a$ , 142, 281
- Cyclopentadienone, 268  
 SHMO, 268
- Cyclopentadienyl  
 anion, 151  
 versus cation, 275  
 as ligand, 187, 193  
 cation, 285  
 point group of, 5  
 SHMO, 151
- Cyclopentene, 291  
 sigmatropic rearrangement, 291
- [2.2.2](1,3,5)Cyclophane, 248



- Cyclopropane  
 bond angle, 16  
 bonding, 84–85  
 correlation diagrams, 207  
 electronic states, 207  
 hybridization, 16  
 point group of, 5  
 structure of, 16, 84  
 Walsh orbitals, 85
- Cyclopropanes  
 from halomalonate carbanions, 281
- Cyclopropenyl  
 SHMO, 90, 151
- Cyclopropyl aldehyde, 279
- Cyclopropyl anion  
 ring opening, 200
- Cyclopropyl cation  
 ring opening, 200
- Cyclopropyl cations  
 electrocyclic reaction, 290, 296–297  
 interaction diagram, 297
- Cycloreversions, 162–165  
 stereochemistry, 162–163
- Cysteine  
 BDE(S—H), 113
- Cytosine, 138
- Cubane  
 from cyclooctatetraene, 203  
 interaction diagram, 283  
 $pK_a$ , 282  
 point group of, 4
- Curtius rearrangement, 118
- DABCO, see 1,4-Diazabicyclo[2.2.2]octane
- Dative bond, 49, 262
- Dauben–Turro–Salem analysis, 212–213  
 Norrish type I, 215–217  
 Norrish type II, 213–215  
 orbital interaction diagram, 213
- Davidson correction, 240
- Density, 22
- Density functional theory, 21, 31, 245–246  
 B3LYP functional, 246  
 Hartree–Fock–Slater exchange, 246  
 Kohn–Sham equations, 245  
 local density approximation, 246  
 nonlocal corrections, 246
- Density matrix, 232
- Determinantal wave function, 23
- Dewar benzene, 290  
 from acetylene + cyclobutadiene, 290  
 interaction diagram, 297  
 rearrangement to benzene, 290, 296–297
- DFT, see Density functional theory
- 1,3-Di-1-adamantylimidazol-2-ylidene, 116
- Dialkoxycarbenes, 116
- 2,3-Dialkyl-1,1-difluorocyclopropanes, 296
- trans*-1,2-Diaminocyclohexane, 138
- Diastereomers, 8
- Diastereotopic groups, 9
- 2,3-Diazabicyclo[2.2.1]hept-2-ene, 289
- 1,4-Diazabicyclo[2.2.2]octane (DABCO), 259  
 HOMO, 80  
 interaction diagram, 260  
 IP, 81
- 2,7-Diazatetracyclo[6.2.2.2<sup>3,6</sup>.0<sup>2,7</sup>]tetradecane  
 dication, 301
- 1,1-Diazine, 118
- Diazoalkanes, 172
- Diborane, 147  
 point group of, 5
- Dibromocarbene (:CBr<sub>2</sub>), 115
- 1,2-Dibromoethane, 263
- 2,4-Di-*t*-butylbenzophenone, 300
- Dicarboxylic acids  
 symmetrical H-bonds in, 140
- Dichlorocarbene (:CCl<sub>2</sub>), 115
- trans*-2,5-Dichloro-1,4-dioxane, 305
- 1,2-Dichloroethane, 263  
 point group of, 4
- 1,2-Dichloroethene  
 point group of, 5
- Dicyclopentadiene, 291
- Dienophiles, 169  
 benzyne, 160
- Diels–Alder reaction, 169–170  
 aromatic TS, 151  
 benzyne, 160  
 butadiene + ethylene, 169  
 diastereoselectivity, 292  
 interaction diagram, 169  
 orbital analysis, 169–170  
 orbital correlation diagram, 198, 201  
 reverse demand, 169  
 substituent effects, 169–170
- Diethyl tartrate, 11
- Difluorocarbene (:CF<sub>2</sub>), 115
- 1,2-Difluoroethane, 263
- Diiodocarbene (:CI<sub>2</sub>), 115
- Dimanganese decacarbonyl (Mn<sub>2</sub>(CO)<sub>10</sub>),  
 177
- Dimethoxycarbene (:C(OCH<sub>3</sub>)<sub>2</sub>), 115
- 2,2-Dimethyl-2,4-cyclohexadienone, 300  
 photochemistry, 299–300
- Dimethyl ether  
 BF<sub>3</sub> affinity, 123  
 IP, 123  
 PA, 123  
 $pK_b$ , 123
- Dimethyl fumarate, 111–112

- Dimethylacrolein  
   BF<sub>3</sub> affinity, 123  
   PA, 123  
*N,N*-Dimethylaminocarbonyl radical, 275  
 Dimethylaminofulvene, 304  
 2,5-Dimethylborolane, 278  
 Dimethylcarbene (:C(CH<sub>3</sub>)<sub>2</sub>), 116  
 2,5-Dimethylcyclopentanone, 249  
   group designations, 9  
*N,N*-Dimethylformamide  
   barrier to rotation, 127  
 Dimethylnitrenium ion, 119  
 Dimethylsulfone  
   p*K*<sub>a</sub>, 142  
 Dimethylsulfoxide, 13  
 1,3-Dioxacyclopentanes, 279  
 Dioxetanes, 208  
   activation energy, 208  
   pyrolysis, 208  
 1,3-Dipolar cycloadditions, 171–174  
   aziridines, 174  
   oxiranes, 174  
   ozonolysis, 174  
 1,3-Dipoles, 172–174  
   eighteen-electron, 174  
   SHMO, 173  
   sixteen-electron, 172  
 Dipole moment, 236–237  
   Hartree-Fock, 237  
 Diradical state, 212  
 1,5-Dithiacyclooctane, 254  
   cation, 253  
   dication, 256  
   interaction diagram, 254  
 Disilane  
   from silyl radical + silane, 149  
 Disilene  
   pi bond energy, 104  
 Disilenes, 103–104  
 Disrotatory, 165  
 Dissociative state, 210  
 1,2-Divinylcyclohexanol, 289  
 Divinylcyclopropane, 170, 171  
 DNA  
   H-bonds in, 138, 140  
 Dodecahedrane  
   point group of, 4  
  
 E1 mechanism, 144  
   carbocation intermediates in, 106  
 E1cb mechanism, 144  
 E2 reaction, 143–144  
   gas phase, 144  
   and SN<sub>2</sub>, 143  
  
 Electrocyclic reactions, 163, 165  
   butadienes to cyclobutenes, 164–165  
   component analysis, 168  
   stereochemistry, 165  
 Electron  
   as a fermion, 19  
   hydrated, 51, 53  
   liquid ammonia, 53  
 Electron affinity  
   and Lewis acidity, 69  
   and LUMO, 26  
 Electron density, 21  
 Electronegativity scales, table, 238  
   Allred and Rochow, 238  
   configuration energy, 238  
   Pauling, 238  
 Electronic states  
   of carbonyl group, 205  
   of cyclopropane, 207  
   from MOs, 205–206  
   singlet, 206  
   symmetry, 206  
   triplet, 206  
 Electrophiles  
   hard and soft, 110  
 Electrophilic radicals, 111  
 Electrostatic effects, 55  
   on orbital energies, 56  
 Elimination reaction  
   E1, 106, 144  
   E1cb, 82  
   E2, 143–144  
 Enamine, 101  
 Enantiotopic groups, 9  
 Enantiomers, 8  
 Energies, orbital  
   CH<sub>4</sub>, 26  
   HF, 26  
   H<sub>2</sub>O, 26  
   NH<sub>3</sub>, 26  
 Energy  
   configuration, 237–238  
   kinetic, 219  
   orbital, 229, 233–234  
     RHF, 235  
   potential, 21  
   RHF, 235  
   total, 219, 237  
   total electronic, 233–234  
 Enol  
   SHMO, 95  
 Enolate anion  
   in aldol reaction, 100  
   SHMO, 95

- Enolate anion (*Continued*)  
 SHMO HOMO, 110
- Epoxidation  
 interaction diagram, 303  
 by peroxy acids, 302–303
- Epoxides, 279
- Esters  
 from carbocations, 107  
 from dimethoxycarbenes, 116
- Ethanal, see Acetaldehyde
- Ethane  
 BDE, 76  
 interaction diagram, 264  
 $pK_a$ , 142  
 point group of, 6  
 protonated ( $C_2H_7^+$ ), 147
- Ethanolamine, 282  
 interaction diagram, 282
- Ethene, see Ethylene
- Ethers  
 from carbocations, 107
- Ethyl carbanion, 109
- Ethyl cation  
 structure, 108, 147
- Ethylbenzenium ion, 108, 277
- Ethylene  
 complex with BrCl, 262  
 Diels–Alder with butadiene, 169  
 dimerization to cyclobutane, 198, 201  
 interaction diagram, 88, 159  
 IP, 80  
 localized orbitals of, 18  
 oxidation by Wacker process, 292–293  
 $\pi$  bond energy, 104  
 $\pi$ - $\pi^*$  state, 261  
 interaction diagram, 261  
 $pK_a$ , 142  
 point group of, 5  
 reactivity, 98  
 RHF, 251  
 SHMO, 88  
 twisted  
 point group of, 5  
 in Zeise's salt, 189
- Ethylene radical cation, 261  
 interaction diagram, 261
- Ethylenediamine (*en*)  
 as chelating ligand, 186  
 effect on  $\Delta_O$ , 181
- Ethynylcarbene ( $:CHCCH$ ), 116
- Excimer, 308–309  
 interaction diagram, 309
- Exciplex, 308–309  
 interaction diagram, 309
- Expectation value, 221
- Extended Hückel theory, 43
- Feist's ester, 289–290  
 sigmatropic rearrangement, 290
- Fermions  
 electronic wave functions, 19, 23
- FHF<sup>-</sup>, 139
- Fluoboric acid ( $HBF_4$ ), 281
- Fluorescence, 211  
 lifetime, 212
- Fluoride ion ( $F^-$ )  
 effect on  $\Delta_O$ , 181  
 as X: ligand, 176
- Fluorine ( $F_2$ )  
 complex with ammonia, 82  
 sigma bond, 77
- Fluorocarbene ( $:CHF$ ), 115
- Fluoromethane  
 BDE, 76
- Fluoromethoxycarbene ( $:CFOCH_3$ ), 115
- Fluoromethyl formate, 263  
 structure, 263
- Fock equations, 23
- Fock operator, 35
- FOOF, 258  
 interaction diagram, 258  
 structure, 258
- Formal oxidation state, 176  
 effect on  $\Delta_O$ , 181
- Formaldehyde  
 $BF_3$  affinity, 123  
 IP, 123, 319  
 PA, 123  
 $pK_b$ , 123  
 point group of, 5
- Formamide, 252  
 interaction diagram, 257  
 rotation barrier, 260  
 structure, 256
- Formylcarbene ( $:CHCHO$ ), 116
- Free Radicals, carbon, 110–114  
 RSE, table of, 114  
 structure, 110  
 substituents on, 111
- Frequency analysis, 32–33  
 scale factors, 33
- Fulvene, 268  
 SHMO, 268
- Furan, 267  
 SHMO, 267
- Gauche effect, 263
- GAUSSIAN computer program, 240

## INDEX

---

- Absorption, 211
- Acetaldehyde  
  in aldol reaction, 100  
  BF<sub>3</sub> affinity, 123  
  IP, 123  
  PA, 123  
  p*K*<sub>b</sub>, 123  
  pyruvate decarboxylase, 302  
  by Wacker process, 293
- Acetic anhydride, 281
- Acetoacetone  
  asymmetric reduction of, 12  
  p*K*<sub>a</sub>, 142
- Acetone, 278  
  BF<sub>3</sub> affinity, 123  
  IP, 123  
  PA, 123  
  p*K*<sub>a</sub>, 142  
  p*K*<sub>b</sub>, 123
- Acetonitrile  
  p*K*<sub>a</sub>, 142
- Acetylene  
  complex with ozone, 304  
  p*K*<sub>a</sub>, 142  
  point group of, 5
- Acetylenes  
  cyclic di-, IP, 305
- Acetylacetonate (*acac*)  
  as chelating ligand, 186
- Achiral  
  definition, 1, 8
- Aconitic acid, 12
- Acrolein  
  BF<sub>3</sub> affinity, 123  
  PA, 123
- Acrylonitrile, 101
- Activation energies  
  H• + H—H—H, 149  
  H<sub>3</sub>C• + H—H—CH<sub>3</sub>, 149  
  negative, 148  
  RO• + H—H—OR  
  RS• + H—H—SR, 149
- Acyl hydrolysis, 105
- Acylnitrenium ions, 120
- Acyloxy radicals, 112
- Adamantanones, 279, 280
- 2-Adamantyl cation, 280
- Adenine, 138
- Agostic interaction, 191
- Alane (AlH<sub>3</sub>), 278  
  complex with amines, 305
- Alcohols  
  from carbocations, 107  
  reaction with RO•, 149
- Aldehydes  
  reduction by metal hydrides, 278
- Alkenes, 98–104  
  electrophilic additions, 98–99

- Alkenes (*Continued*)  
 nonplanar, 102
- Alkoxides  
 bases and nucleophiles, 97
- Alkoxy radicals  
 with H—OR, 149
- Alkyl azides, 172
- Alkyl halides  
 acids and electrophiles, 97  
 from carbocations, 107  
 reactions, 281  
 in  $S_N1$ , 129–130, 134  
 in  $S_N2$ , 130–131, 134  
 LUMO, 131, 133
- Alkyl peroxides, 258
- Alkylammonium salts  
 from carbocations, 107
- Alkynes, 103
- Allene  
 point group of, 6
- Allyl  
 SHMO, 89
- Allyl anion  
 from cyclopropyl anion, 200  
 HOMO, 100
- Allyl cation  
 acidity relative to methyl cation, 268  
 from cyclopropyl cation, 200  
 LUMO, 100
- Allylic alcohols  
 epoxidation, 11
- Alpha, in SHMO, 92–96  
 effect of coordination number, 93  
 heteroatoms, 93  
 reference energy, 92  
 table of, 94
- Alpha effect, 132
- Alpine-Borane, 11, 12
- Alternant systems, 91
- Aluminum triisopropoxide, 308
- Alumoxane, 193
- Amide group, 126–127  
 barrier to rotation, 127  
 basicity of, 127  
 interaction diagram, 127  
 nonplanar, 127  
 SHMO, 126
- Amides  
 bases and nucleophiles, 97
- Amine oxides, 270  
 interaction diagram, 271
- Amines  
 complex with  $AlH_3$ , 305  
 oxidation by  $H_2O_2$ , 302
- $\alpha$ -Amino acids  
 synthesis, 311
- $\alpha,\beta$ -Aminoalcohols  
 photofragmentation, 305
- Aminocarbocation, 252  
 interaction diagram, 253
- Aminonitrene, 118
- Ammonia ( $NH_3$ )  
 basicity relative to phosphine, 256  
 BDE, 76  
 complex with  $F_2$ ,  $Cl_2$ ,  $ClF$ , 82, 262  
 dative bond with  $BH_3$ , 262  
 dimer, 321  
 effect on  $\Delta_O$ , 181  
 geometry of, 32  
 H-bonded complexes, 138  
 interaction diagram, 256  
 infrared intensities of, 32  
 IP, 81  
 as L: ligand, 176  
 nonbonded orbital of, 27  
 normal coordinates of, 32  
 orbital energies, 26  
 point group of, 5  
 reaction with  $BF_3$ , 49  
 total energy, 29  
 trans effect, 181
- Ammonium ( $NH_4^+$ ), 257
- Amsterdam density functional (ADF)  
 computer program, 246
- Anchimeric assistance, 82
- Aniline  
 SHMO, 153
- Anomeric effect, 82, 310–311, 305
- Antarafacial, 163  
 examples, 164  
 sigma bonds, 167
- Anti-Bredt olefin, 102
- Approximations of MO theory  
 Born–Oppenheimer, 22  
 Hartree–Fock, 222  
 Hückel, 35, 86  
 independent electron, 35  
 LCAO, 229  
 nonrelativistic, 22  
 SHMO, 87  
 Wolfsberg–Helmholtz, 43  
 zero-overlap, 38, 40
- Aromaticity, 150
- Aromatic compounds, 150–160
- Arsenium ions, 119
- Asymmetric synthesis  
 definition, 9
- Avoided crossing, 206

- 1-Aza-1,3,5,7,9,11-dodecahexaene, 270
- Azides  
to nitrenes, 116
- Aziridines  
ring opening, 200
- Azo compounds  
from nitrenes, 117
- Azoxyalkane, 174
- Azulene, 304  
synthesis, 304
- B3LYP, 31  
functional, 246
- Baker's yeast pyruvate decarboxylase, 301–302  
mechanism, 302
- Basicities  
gas phase, 97
- Basis set, 23, 229, 232–233  
exponential, 232  
Gaussian functions, 24–25  
Cartesian, 232  
primitive, 233  
contracted, 233  
exponents, 233  
polarized, 233  
split valence, 25, 233
- 9-BBN, 11, 12
- BDE, see Bond dissociation energy
- Benzaldehyde  
asymmetric reduction of, 12  
SHMO, 153
- Benzene  
from benzvalene, 203, 204  
complex with ethylene cation radical, 284  
complex with  $\text{NO}^+$ , 284  
interaction diagram, 285  
as ligand, 187  
point group of, 5  
SHMO, 90, 151
- Benzenes, substituted  
electrophilic substitutions, 152  
“C” substituent, 155–156  
X: substituent, 153–154  
Z substituent, 154–155  
nucleophilic substitutions, 157–160  
Z substituent, 158
- Benzocyclopentanol, 300
- Benzophenone  
photoreduction, 299
- Benzpinacol, 299
- Benzvalene, 204  
barrier to benzene, 203  
correlation diagram, 204
- Benzyl alcohol, (*R*)- $\alpha$ -d, preparation, 12
- Benzyl carbocation, 106
- Benzynes, 159–160, 275–276  
in Diels–Alder reaction, 160  
E1cb, 159  
interaction diagram, 159  
MW and IR spectra, 276  
nucleophilic substitution, 159
- Beta, in SHMO, 92–96  
effect of coordination number, 93  
effect of twisting, 102  
energy scale, 92  
heteroatoms, 93  
table of, 94
- $\text{BF}_3$  affinity  
acetaldehyde, 123  
acetone, 123  
acrolein, 123  
butenone, 123  
dimethyl ether, 123  
dimethylacrolein, 123  
formaldehyde, 123  
methanol, 123  
methyl acetate, 123  
methyl acrylate, 123  
(*E*)-methylacrolein, 123  
nucleophilicity, 123  
oxetane, 123  
table of, 123  
tetrahydrofuran, 123  
water, 123
- $\text{BH}_3\text{NH}_3$ , 284  
structure, 284
- Bicyclo[3.1.0]hex-2-ene, 291  
sigmatropic rearrangement, 290–291
- Bicyclo[2.1.0]pent-2-ene, 289
- Bishomocyclopropenyl cation, 277
- Bond, definition of, 50
- Bond angles  
geometric relationship between, 15
- Bond dissociation energy  
relationship with  $\text{p}K_a$  and  $E_{\text{ox}}$ , 112–113
- Bond Dissociation Energy (BDE)  
cubane C—H, 282  
cysteine S—H, 113  
glycine  $^{\alpha}\text{C}$ —H, 113  
glutathione S—H, 113  
M—H bonds, 195  
methane, 113  
table, 76  
three-electron S—S bond, 254
- Bond energy,  $\pi$  bonds  
disilene, 104  
ethylene, 104  
silaethene, 104

- Bond order, SHMO, 91–92  
 Bond strength, see Bond dissociation energy  
 9-Borabicyclo[3.3.1]nonane (9-BBN), 12  
 Borane (BH<sub>3</sub>)  
   dative bond with NH<sub>3</sub>, 262  
 Boranes, 84  
   acids and electrophiles, 97  
 Borazine, 286, 288  
   SHMO, 288  
   interaction diagram, 288  
 Boric acid  
   point group of, 5  
 Boron trifluoride (BF<sub>3</sub>), see also BF<sub>3</sub>  
   complex with CO, 304–305  
   reaction with NH<sub>3</sub>, 49  
   “Y”-conjugation, 304  
 Born–Oppenheimer approximation, 22, 219  
 Bound state, 209–210  
 BrCl, with alkenes, 260  
 Brillouin’s theorem, 241  
 Bromide ion (Br<sup>−</sup>)  
   effect on Δ<sub>O</sub>, 181  
   trans effect, 181  
   as X<sup>−</sup> ligand, 176  
 Bromine (Br<sub>2</sub>)  
   sigma bond, 77  
 Bromochloromethane, 13  
 11-Bromo-*endo*-9-chloro-7-ethoxybicyclo[5.3.1]undec-1(11)-ene, 102–103  
 Bromomalonate carbanion, 281  
 Bromomethane  
   BDE, 76  
 Bromonium ion, 108  
 N-Bromosuccinimide, 262  
 Brucine, in asymmetric synthesis, 10, 11  
 Buckminsterfullerene (C<sub>60</sub>)  
   point group of, 6  
 Bullvalene, 170, 171  
   point group of, 4  
 Butadiene  
   Diels–Alder, 198, 201  
   with ethylene, 169  
   SHMO, 89  
 Butadienes  
   from cyclobutenes, 198–200, 202  
 2-Butene  
   photodimerization, 202  
   photolysis, 261  
 (*Z*)-2-Butene  
   IP of, 48, 80  
 Butenone  
   BF<sub>3</sub> affinity, 123  
   IP, 123  
   PA, 123  
   *tert*-Butyl cation  
   “Y”-conjugation, 304  
   *tert*-Butyl carbanion, 109  
   *tert*-Butylhydroperoxide, 11  
   2-Butyne, 296  
 “C” substituents  
   electrophilic addition  
     alkenes, 101–102  
     benzenes, 155–156  
   interaction with  
     C=C, 100  
     C–H, 143, 145  
     C=O, 122  
     carbanion, 109  
     carbene, 115  
     carbocation, 106  
     carbon radical, 111  
     nitrene, 117  
     nitrenium, 119  
   list of, 102  
 C<sub>18</sub>, 151  
 C<sub>60</sub>, 151  
 Cannizzaro reaction, 84, 146  
   formaldehyde, 146  
 Captodative effect, 113, 277  
 Carbalkoxycarbenes (:CRCO<sub>2</sub>R), 116  
 Carbanions, 108–110  
   bases and nucleophiles, 97  
   gas phase, 109  
   substituents on, 109  
   *a*-sulfonyl, 277  
 Carbene, see also Methylene  
   :CBR<sub>2</sub>, 115  
   :C(CH<sub>3</sub>)<sub>2</sub>, 116  
   :CCl<sub>2</sub>, 115  
   :CClOCH<sub>3</sub>, 115  
   :CF<sub>2</sub>, 115  
   :CFOCH<sub>3</sub>, 115  
   :CHCCH, 116  
   :CHC<sub>6</sub>H<sub>5</sub>, 116  
   :CHCHO, 116  
   :CHF, 115  
   :CI<sub>2</sub>, 115  
   :C(OCH<sub>3</sub>)<sub>2</sub>, 115  
   :CRCO<sub>2</sub>R, 116  
 Carbenes, 114–116  
   addition to alkenes, 207–208  
   C–H insertion, 208  
   dimerization, 208  
   electronic states, 114  
   singlet  
     reaction with carbonyl, 279

- Carbenes (*Continued*)  
 substituents on, 115
- Carbocations, 105–108  
 acids and electrophiles, 97  
 dialkoxy, 105  
 ethyl, 84  
 fluoro, 105  
 norbornyl, 84  
 reactions, 107  
 substituents on, 106
- 2-Carbomethoxy-2-cyclohexen-1-one, 289
- Carbon dioxide  
 point group of, 5
- Carbon monoxide (CO)  
 complex with  $\text{BF}_3$ , 304  
 effect on  $\Delta_{\text{O}}$ , 181  
 as L: ligand, 176  
 point group of, 5  
 trans effect, 181
- Carbonyl compounds, 121–128  
 acids and electrophiles, 97  
 electrophilic attack, 121–123  
 photochemistry  
   Norrish type I, 215–217  
   Norrish type II, 213–215  
 stability of, 127–128  
 UV spectra, 214
- Carbonyl group  
 basicity of O, 122–123  
 interaction diagram, 122  
 IP of, 123  
 nucleophilic attack on, 68, 124–126  
 nucleophilicity of O, 122–123  
 $\pi^*$  antibond, SHMO, 124  
 $\pi$  bond, SHMO, 121  
 reactions, 125
- Carbonyl imine, 174
- Carbonyl oxide, 174
- Carbonyl ylide, 174
- Carboranes, 84
- Carboxyalkyl radicals, 112
- Carboxylate group  
 interaction diagram, 307
- Cartesian Gaussian functions, in basis set, 24–25
- Catalytic cracking, 146
- CCSD(T), 30
- $\text{CF}_3$ , see Trifluoromethyl
- CFPA, 14
- C—H bonds, 141–143  
 activation by X:; “C” substituents, 145  
 activation by Z, “C” substituents, 142  
 hybridization, 141  
 $\text{p}K_{\text{a}}$  values, 142
- Chelotropic reactions, 163, 165–166, 201  
 butadienes +  $\text{SO}_2$ , 164, 166  
 carbene addition to alkene, 164, 166  
 orbital correlation diagram, 200  
 stereochemistry, 165–166
- Chemiluminescence, 208
- Chiral  
 definition, 1, 8
- Chiral auxiliary, 11
- Chloride ion ( $\text{Cl}^-$ )  
 effect on  $\Delta_{\text{O}}$ , 181  
 trans effect, 181  
 as X: ligand, 176
- Chlorine ( $\text{Cl}_2$ )  
 complex with ammonia, 82  
 sigma bond, 77
- Chlorine fluoride (ClF)  
 complex with ammonia, 82
- Chloroethane  
 gas phase  $\text{S}_{\text{N}}2$ , E2, 144
- Chloroform  
 point group of, 5
- Chloromalonate carbanion, 281
- Chloromethane  
 BDE, 76
- Chloromethoxycarbene ( $:\text{CClOCH}_3$ ), 115
- o*-Chloro-*o*-methylacetophenone, 300
- m*-Chloroperbenzoic acid  
 epoxidation by, 102
- N*-Chloropyridine, 287  
 interaction diagram, 287  
 SHMO, 287  
 three-electron bond, 286
- Chromium pentacarbonyl ( $\text{Cr}(\text{CO})_5$ ), 177
- CI, see Configuration interaction
- Citric acid, 12
- ClF, with ammonia, 260
- Coefficients, 229
- Component analysis, 167–168  
 rule for, 168
- Configuration, electronic, 205
- Configuration interaction (CI), 30  
 doubly excited configurations, 240  
 electronic transition energies, 241  
 optical rotatory strengths, 241  
 singly excited configurations, 241  
 theory, 239–241  
 transition dipole, 241
- Conrotatory, 165
- Constitutional isomers, 8
- Constitutionally heterotopic groups, 9
- Contraction, 233
- Cope rearrangement, 170–171  
 bullvalene, 170  
 divinylcyclopropane, 170



- Cope rearrangement (*Continued*)  
 1,5-hexadiene, 170  
 interaction diagram, 171  
 orbital analysis, 170–171  
 oxy-Cope, 170
- Copolymerization  
 CO + alkenes, 293–296  
 interaction diagram, 295
- Core Hamiltonian, 35
- Correlation diagrams  
 general principles, 196–197  
 orbital, 196–203  
 state, 203–208
- Coulomb integral, alpha  
 effect of coordination number, 93  
 heteroatoms, 93  
 reference energy, 92  
 table of, 94
- Coulomb's law, 219
- Coupling Constant,  $C^{13}$ —H, 16
- Cyanide ion ( $CN^-$ )  
 effect on  $\Delta_o$ , 181  
 trans effect, 181  
 as  $X^-$  ligand, 176
- $\alpha$ -Cyano- $\alpha$ -fluorophenylacetic acid, CFPA,  
 14
- 2-Cyanofuran, 267  
 SHMO, 267
- 2-Cyanotetrahydropyran  
 reduction, 307
- Cycloaddition reactions, 162–165, 197–198  
 component analysis, 168  
 Diels–Alder, 162, 198  
 ethylene + ethylene, 198  
 orbital correlation diagram, 198  
 stereochemistry, 162–163
- Cycloalkanols, synthesis, 277
- Cyclobutadiene  
 barrier, 91  
 ground state, 91  
 point group of, 5  
 self-reactivity, 97  
 SHMO, 151  
 structure, 309–310
- Cyclobutane  
 ethylene dimerization, 198, 201  
 point group of, 5, 6
- Cyclobutanes  
 photodimerization of alkenes, 202
- Cyclobutanone  
 group designations, 9
- Cyclobutenes  
 from butadienes, 198–200  
 photolysis, 203
- Cyclodec-5-en-1-one, 289
- Cyclodecyl cation  
 hydride bridge, 147
- 1,4-Cycloheptadiene, 170, 171
- Cycloheptatriene, 281
- Cycloheptatrienes  
 rearrangements, 290
- Cycloheptatrienylidene, 275  
 interaction diagram, 276
- 1,3-Cyclohexadiene  
 electrocyclic reaction, 296  
 photolysis, 203
- 1,3-Cyclohexadienes  
 electrocyclic reactions, 290
- 1,4-Cyclohexadiene  
 HOMO, 80  
 interaction diagram, 80
- Cyclohexadienones  
 photochemistry, 299–300
- Cyclohexane  
 point group of, 6  
 symmetry elements, 7
- Cyclohexanones, 84  
 nucleophilic addition, 125, 126
- Cyclohexene  
 IP, 48, 102
- Cyclohexenes  
 from Diels–Alder, 170
- 1,5-Cyclooctadiene, 11, 187  
 as ligand, 187
- Cyclooctatetraene  
 from cubane, 203  
 point group of, 6
- Cyclooctatrienone, 289
- cis*-Cyclooctene  
 IP, 102
- trans*-Cyclooctene  
 geometry, 102  
 IP, 102  
 optical resolution, 292
- Cyclopentadiene, 291  
 dimerization, 97, 291  
 with 2-methylpropenyl cation  
 $pK_a$ , 142, 281
- Cyclopentadienone, 268  
 SHMO, 268
- Cyclopentadienyl  
 anion, 151  
 versus cation, 275  
 as ligand, 187, 193  
 cation, 285  
 point group of, 5  
 SHMO, 151
- Cyclopentene, 291  
 sigmatropic rearrangement, 291
- [2.2.2](1,3,5)Cyclophane, 248

- Cyclopropane  
 bond angle, 16  
 bonding, 84–85  
 correlation diagrams, 207  
 electronic states, 207  
 hybridization, 16  
 point group of, 5  
 structure of, 16, 84  
 Walsh orbitals, 85
- Cyclopropanes  
 from halomalonate carbanions, 281
- Cyclopropenyl  
 SHMO, 90, 151
- Cyclopropyl aldehyde, 279
- Cyclopropyl anion  
 ring opening, 200
- Cyclopropyl cation  
 ring opening, 200
- Cyclopropyl cations  
 electrocyclic reaction, 290, 296–297  
 interaction diagram, 297
- Cycloreversions, 162–165  
 stereochemistry, 162–163
- Cysteine  
 BDE(S—H), 113
- Cytosine, 138
- Cubane  
 from cyclooctatetraene, 203  
 interaction diagram, 283  
 $pK_a$ , 282  
 point group of, 4
- Curtius rearrangement, 118
- DABCO, see 1,4-Diazabicyclo[2.2.2]octane
- Dative bond, 49, 262
- Dauben–Turro–Salem analysis, 212–213  
 Norrish type I, 215–217  
 Norrish type II, 213–215  
 orbital interaction diagram, 213
- Davidson correction, 240
- Density, 22
- Density functional theory, 21, 31, 245–246  
 B3LYP functional, 246  
 Hartree–Fock–Slater exchange, 246  
 Kohn–Sham equations, 245  
 local density approximation, 246  
 nonlocal corrections, 246
- Density matrix, 232
- Determinantal wave function, 23
- Dewar benzene, 290  
 from acetylene + cyclobutadiene, 290  
 interaction diagram, 297  
 rearrangement to benzene, 290, 296–297
- DFT, see Density functional theory
- 1,3-Di-1-adamantylimidazol-2-ylidene, 116
- Dialkoxycarbenes, 116
- 2,3-Dialkyl-1,1-difluorocyclopropanes, 296
- trans*-1,2-Diaminocyclohexane, 138
- Diastereomers, 8
- Diastereotopic groups, 9
- 2,3-Diazabicyclo[2.2.1]hept-2-ene, 289
- 1,4-Diazabicyclo[2.2.2]octane (DABCO), 259  
 HOMO, 80  
 interaction diagram, 260  
 IP, 81
- 2,7-Diazatetracyclo[6.2.2.2<sup>3,6</sup>.0<sup>2,7</sup>]tetradecane  
 dication, 301
- 1,1-Diazine, 118
- Diazoalkanes, 172
- Diborane, 147  
 point group of, 5
- Dibromocarbene (:CBr<sub>2</sub>), 115
- 1,2-Dibromoethane, 263
- 2,4-Di-*t*-butylbenzophenone, 300
- Dicarboxylic acids  
 symmetrical H-bonds in, 140
- Dichlorocarbene (:CCl<sub>2</sub>), 115
- trans*-2,5-Dichloro-1,4-dioxane, 305
- 1,2-Dichloroethane, 263  
 point group of, 4
- 1,2-Dichloroethene  
 point group of, 5
- Dicyclopentadiene, 291
- Dienophiles, 169  
 benzyne, 160
- Diels–Alder reaction, 169–170  
 aromatic TS, 151  
 benzyne, 160  
 butadiene + ethylene, 169  
 diastereoselectivity, 292  
 interaction diagram, 169  
 orbital analysis, 169–170  
 orbital correlation diagram, 198, 201  
 reverse demand, 169  
 substituent effects, 169–170
- Diethyl tartrate, 11
- Difluorocarbene (:CF<sub>2</sub>), 115
- 1,2-Difluoroethane, 263
- Diiodocarbene (:CI<sub>2</sub>), 115
- Dimanganese decacarbonyl (Mn<sub>2</sub>(CO)<sub>10</sub>),  
 177
- Dimethoxycarbene (:C(OCH<sub>3</sub>)<sub>2</sub>), 115
- 2,2-Dimethyl-2,4-cyclohexadienone, 300  
 photochemistry, 299–300
- Dimethyl ether  
 BF<sub>3</sub> affinity, 123  
 IP, 123  
 PA, 123  
 $pK_b$ , 123
- Dimethyl fumarate, 111–112

- Dimethylacrolein  
 BF<sub>3</sub> affinity, 123  
 PA, 123  
*N,N*-Dimethylaminocarbinyl radical, 275  
 Dimethylaminofulvene, 304  
 2,5-Dimethylborolane, 278  
 Dimethylcarbene (:C(CH<sub>3</sub>)<sub>2</sub>), 116  
 2,5-Dimethylcyclopentanone, 249  
 group designations, 9  
*N,N*-Dimethylformamide  
 barrier to rotation, 127  
 Dimethylnitrenium ion, 119  
 Dimethylsulfone  
 p*K*<sub>a</sub>, 142  
 Dimethylsulfoxide, 13  
 1,3-Dioxacyclopentanes, 279  
 Dioxetanes, 208  
 activation energy, 208  
 pyrolysis, 208  
 1,3-Dipolar cycloadditions, 171–174  
 aziridines, 174  
 oxiranes, 174  
 ozonolysis, 174  
 1,3-Dipoles, 172–174  
 eighteen-electron, 174  
 SHMO, 173  
 sixteen-electron, 172  
 Dipole moment, 236–237  
 Hartree-Fock, 237  
 Diradical state, 212  
 1,5-Dithiacyclooctane, 254  
 cation, 253  
 dication, 256  
 interaction diagram, 254  
 Disilane  
 from silyl radical + silane, 149  
 Disilene  
 pi bond energy, 104  
 Disilenes, 103–104  
 Disrotatory, 165  
 Dissociative state, 210  
 1,2-Divinylcyclohexanol, 289  
 Divinylcyclopropane, 170, 171  
 DNA  
 H-bonds in, 138, 140  
 Dodecahedrane  
 point group of, 4  
 E1 mechanism, 144  
 carbocation intermediates in, 106  
 E1cb mechanism, 144  
 E2 reaction, 143–144  
 gas phase, 144  
 and SN<sub>2</sub>, 143  
 Electrocyclic reactions, 163, 165  
 butadienes to cyclobutenes, 164–165  
 component analysis, 168  
 stereochemistry, 165  
 Electron  
 as a fermion, 19  
 hydrated, 51, 53  
 liquid ammonia, 53  
 Electron affinity  
 and Lewis acidity, 69  
 and LUMO, 26  
 Electron density, 21  
 Electronegativity scales, table, 238  
 Allred and Rochow, 238  
 configuration energy, 238  
 Pauling, 238  
 Electronic states  
 of carbonyl group, 205  
 of cyclopropane, 207  
 from MOs, 205–206  
 singlet, 206  
 symmetry, 206  
 triplet, 206  
 Electrophiles  
 hard and soft, 110  
 Electrophilic radicals, 111  
 Electrostatic effects, 55  
 on orbital energies, 56  
 Elimination reaction  
 E1, 106, 144  
 E1cb, 82  
 E2, 143–144  
 Enamine, 101  
 Enantiotopic groups, 9  
 Enantiomers, 8  
 Energies, orbital  
 CH<sub>4</sub>, 26  
 HF, 26  
 H<sub>2</sub>O, 26  
 NH<sub>3</sub>, 26  
 Energy  
 configuration, 237–238  
 kinetic, 219  
 orbital, 229, 233–234  
 RHF, 235  
 potential, 21  
 RHF, 235  
 total, 219, 237  
 total electronic, 233–234  
 Enol  
 SHMO, 95  
 Enolate anion  
 in aldol reaction, 100  
 SHMO, 95

- Enolate anion (*Continued*)  
 SHMO HOMO, 110
- Epoxidation  
 interaction diagram, 303  
 by peroxy acids, 302–303
- Epoxides, 279
- Esters  
 from carbocations, 107  
 from dimethoxycarbenes, 116
- Ethanal, see Acetaldehyde
- Ethane  
 BDE, 76  
 interaction diagram, 264  
 $pK_a$ , 142  
 point group of, 6  
 protonated ( $C_2H_7^+$ ), 147
- Ethanolamine, 282  
 interaction diagram, 282
- Ethene, see Ethylene
- Ethers  
 from carbocations, 107
- Ethyl carbanion, 109
- Ethyl cation  
 structure, 108, 147
- Ethylbenzenium ion, 108, 277
- Ethylene  
 complex with BrCl, 262  
 Diels–Alder with butadiene, 169  
 dimerization to cyclobutane, 198, 201  
 interaction diagram, 88, 159  
 IP, 80  
 localized orbitals of, 18  
 oxidation by Wacker process, 292–293  
 $\pi$  bond energy, 104  
 $\pi$ - $\pi^*$  state, 261  
 interaction diagram, 261  
 $pK_a$ , 142  
 point group of, 5  
 reactivity, 98  
 RHF, 251  
 SHMO, 88  
 twisted  
 point group of, 5  
 in Zeise's salt, 189
- Ethylene radical cation, 261  
 interaction diagram, 261
- Ethylenediamine (*en*)  
 as chelating ligand, 186  
 effect on  $\Delta_O$ , 181
- Ethynylcarbene ( $:CHCCH$ ), 116
- Excimer, 308–309  
 interaction diagram, 309
- Exciplex, 308–309  
 interaction diagram, 309
- Expectation value, 221
- Extended Hückel theory, 43
- Feist's ester, 289–290  
 sigmatropic rearrangement, 290
- Fermions  
 electronic wave functions, 19, 23
- FHF<sup>-</sup>, 139
- Fluoboric acid ( $HBF_4$ ), 281
- Fluorescence, 211  
 lifetime, 212
- Fluoride ion ( $F^-$ )  
 effect on  $\Delta_O$ , 181  
 as X: ligand, 176
- Fluorine ( $F_2$ )  
 complex with ammonia, 82  
 sigma bond, 77
- Fluorocarbene ( $:CHF$ ), 115
- Fluoromethane  
 BDE, 76
- Fluoromethoxycarbene ( $:CFOCH_3$ ), 115
- Fluoromethyl formate, 263  
 structure, 263
- Fock equations, 23
- Fock operator, 35
- FOOF, 258  
 interaction diagram, 258  
 structure, 258
- Formal oxidation state, 176  
 effect on  $\Delta_O$ , 181
- Formaldehyde  
 $BF_3$  affinity, 123  
 IP, 123, 319  
 PA, 123  
 $pK_b$ , 123  
 point group of, 5
- Formamide, 252  
 interaction diagram, 257  
 rotation barrier, 260  
 structure, 256
- Formylcarbene ( $:CHCHO$ ), 116
- Free Radicals, carbon, 110–114  
 RSE, table of, 114  
 structure, 110  
 substituents on, 111
- Frequency analysis, 32–33  
 scale factors, 33
- Fulvene, 268  
 SHMO, 268
- Furan, 267  
 SHMO, 267
- Gauche effect, 263
- GAUSSIAN computer program, 240

- Gaussian functions, in basis set, 24–25
- Geometric isomers, 8
- Geometry  
of first row hydrides, 32
- Geometry optimization, 31–32
- Group  
definition, 2
- Group orbitals, 56–61  
atoms, 56–57  
dicoordinated atoms, 58–59  
hexacoordinated metals, 177  
methyl, 60–61  
methylene, 59–61  
monocoordinated atoms, 57–58  
pentacoordinated metals, 185–186  
tetraordinated metals, 182, 184  
tricoordinated atoms, 59  
tricoordinated metals, 182, 183
- Groups  
stereotopic relationships, 9
- Glycine  
BDE( $^{\circ}\text{C}-\text{H}$ ), 113
- Glutathione  
BDE( $\text{S}-\text{H}$ ), 113
- Guanine, 138
- Guanidinium ion, 105
- Halides  
leaving groups, 130  
nucleophilicity, 130
- Hamiltonian, 219–220  
classical, 219  
operator, 220
- Hamiltonian matrix, 240
- Hammond principle, 105
- Hapto number, 187
- Hard electrophiles, 110  
reaction with enolate, 110
- Harmonic Frequency Analysis, 32–33  
scale factors, 33
- Hartree product, 23, 221
- Hartree–Fock limit, 29  
of first row hydrides, 29
- Hartree–Fock theory, 20–32, 218–231  
approximation, 222  
energy, 222–226  
restricted (RHF), 234–236  
successes and failures, 29–30  
unrestricted (UHF), 222–234  
wave function, 223
- Hessian matrix, 31
- Heterotopic groups, 9
- 1,4-Hexadiene  
photolytic loss of  $\text{H}_2$ , 303–304
- 1,5-Hexadiene, 170
- 1,5-Hexadien-3-ones, 300  
photochemistry, 300
- Hexamethyl Dewar benzene  
synthesis, 296
- 1,3,5-Hexatriene, 275, 276
- (Z)-1,3,5-hexatriene, 200, 296  
electrocyclic reaction, 296  
photolysis of cyclohexadiene, 203
- Hexatrienes  
electrocyclic reaction, 198–199, 202
- Hofmann rearrangement, 118
- Homotopic groups, 9
- Homotropylium, 152
- Hückel array, 85
- Hückel MO theory, 35, 86
- Hückel  $4n + 2$  rule, 150, 151
- Hund's rule, 114
- Hunsdiecker reaction, 305–307
- Hybridization, 15, 16  
of cyclopropane, 16  
of metals, 180  
SHMO, 96
- Hydrazine ( $\text{N}_2\text{H}_4$ )  
interaction diagram, 255  
structure, 253
- Hydrazines, 132  
conformation, 77
- Hydrazinium dichloride, 305
- Hydride ( $\text{H}^-$ )  
trans effect, 181  
as  $\text{X}^-$  ligand, 176
- Hydride abstraction, 145–147  
interaction diagram, 145
- Hydride bridging, 145, 147  
cyclodecyl cation, 147  
diborane, 147  
ethyl cation, 147  
protonated ethane, 147
- 1,2-Hydride shift, 84  
in carbenes, 115  
in carbocations, 107  
in nitrenes, 118  
in nitrenium ions, 120
- Hydrogen ( $\text{H}_2$ )  
reaction with H atom, 149
- Hydrogen atom  
with  $\text{H}_2$ , 149
- Hydrogen atom transfer, 148–149  
barriers, 149
- Hydrogen bond, 82
- Hydrogen bonding in, 50  
ammonia complexes, 138  
aqueous HF, 138

- Hydrogen bonding in (*Continued*)  
 diamine, diol mixtures, 138  
 ethanolamine, 282  
 nucleic acids, 137–138  
 proteins, 137–138  
 water dimer, 138  
 water trimer, 139
- Hydrogen bonds, 137–141  
 bifurcated, 139–140  
 symmetrical, 139–140
- Hydrogen-bridged radicals, 147–148
- Hydrogen bromide (HBr)  
 BDE, 76  
 and methyl radical, 51
- Hydrogen chloride (HCl)  
 BDE, 76  
 complex with oxirane, 281  
 and methyl radical, 51  
 point group of, 5
- Hydrogen disulfide (H<sub>2</sub>S<sub>2</sub>)  
 structure, 256
- Hydrogen fluoride (HF)  
 aqueous, p*K*<sub>a</sub>, 139  
 BDE, 76  
 geometry of, 32  
 orbital energies, 26  
 total energy, 29
- Hydrogen peroxide (H<sub>2</sub>O<sub>2</sub>), 258  
 oxidation of amines, 302  
 point group of, 4  
 structure, 258
- Hydrogenation of alkenes, 192
- Hydroxide (OH<sup>-</sup>)  
 trans effect, 181
- Hydroxylamines, 132
- Hyperconjugation, 84, 263
- Imine ylide, 174
- Imines  
 acids and electrophiles, 97
- 1-Indanone, 300
- Independent electron approximation, 35
- Integrals  
 Coulomb, 225–226  
 exchange, 225–226  
 intrinsic interaction, 37, 52  
 kinetic energy, 231  
 nuclear-electron attraction, 231  
 overlap, 37, 52, 231  
 two-electron repulsion, 225, 232
- Intended correlations, 206
- Interaction diagram, 62–71  
 construction, 62–65  
 interpretation, 65–69
- Interaction diagram, specific groups  
 amide group, 127  
 Br—Br bond, 77  
 carbonyl group, 63  
 carboxylate, 307  
 C—Br bond, 74  
 C=C with substituents, 100  
 C—C  $\pi$  bond, 88  
 C—C  $\sigma$  bond, 73, 76  
 C—Cl bond, 74  
 C—H bonds, 141, 145  
 C—M (metal), 83  
 C—N bond, 73  
 C—O bond, 73  
 C—F bond, 73, 74  
 C—I bond, 74  
 Cl—Cl bond, 77  
 cyclopropane, 85  
 F—F bond, 76, 77  
 H-bond, symmetrical, 139  
 H-bond, three-center, 140  
 I—I bond, 77  
 N—N bond, 76  
 O—O bond, 76
- Intermolecular interactions, 46, 53–55
- Internal conversion, 211
- Intersystem crossing, 208, 211  
 time scale, 212
- Intrinsic interaction integral  
 effect of twisting of C=C, 102  
 general principles, 52  
 in M—C, M—H, 180–182  
 and  $\Delta_{\text{O}}$ , 181  
 and overlap, 55
- Iodide ion (I<sup>-</sup>)  
 effect on  $\Delta_{\text{O}}$ , 181  
 trans effect, 181
- Iodocyclopentane, 285
- 5-Iodocyclopentadiene, 285, 308
- 3-Iodocyclopentene, 308
- 6-Iodo-1-hexene, 98
- Iodomethane  
 BDE, 76
- Ionization potential  
 bond, 73  
 and HOMO, 26  
 Koopmans' theorem, 80, 236  
 nucleophilicity, 69  
 table of, 123
- Ionization potential of  
 acetaldehyde, 123  
 acetone, 123  
 ammonia, 81  
 (z)-2-butene, 48

- Ionization potential of (*Continued*)  
   butenone, 123  
   cyclic diacetylenes, 305  
   cyclohexene, 48, 102  
   *cis*-cyclooctene, 102  
   *trans*-cyclooctene, 102  
   DABCO, 81  
   dimethyl ether, 123  
   ethylene, 80, 319  
   formaldehyde, 123, 319  
   hydrogen atom, 55, 75  
   methanol, 123  
   methyl acetate, 123  
   methyl acrylate, 123  
   nitrous oxide (N<sub>2</sub>O), 172  
   norbornadiene, 48  
   norbornene, 48  
   oxetane, 123  
   tetrahydrofuran, 123  
   trimethylamine, 81  
   water, 123
- Iron pentacarbonyl (Fe(CO)<sub>5</sub>), 177
- Isocyanates  
   from acyl nitrenes, 118
- Isomers  
   definition, 8
- Isopropyl alcohol, 299
- Jablonski diagram, 210–211
- Katsuki–Sharpless epoxidation, 11
- Ketones  
   Norrish type I, 215–217  
     state correlation diagram, 216  
   Norrish type II, 213–215  
     state correlation diagram, 215, 299  
   nucleophilic attack, 124–126  
   photochemistry, 298–301  
   reduction by metal hydrides, 278  
   reduction by alkali metals, 279
- Kinetic energy, 219
- Kohn–Sham equations, 245
- Koopmans' theorem, 80, 236
- L: ligands, list, 176
- Lagrangian multipliers, 227, 228
- Lanthanide chemical shift reagents, 13
- LCAO, 229
- Lewis acid, xiii
- Lewis acidity, allyl and methyl cations, 269
- Lewis acids  
   AlCl<sub>3</sub>, 130, 146  
   BF<sub>3</sub>, 130  
   catalytic cracking, 146  
   FeCl<sub>3</sub>, 130
- Lewis base, xiii
- Lifetime  
   fluorescence, 212
- Lifetimes, table of, 7
- Ligands, 176  
   carbon, 186–187  
   chelating, 187  
     *en* (ethylenediamine), 187  
     *acac* (acetylacetonate), 187  
   L: ligands, 176  
   X: ligands, 176
- Lithium aluminium hydride, 83, 278
- Lossen rearrangement, 118
- Lumisterol<sub>3</sub>, 310
- Manganese pentacarbonyl (Mn(CO)<sub>5</sub>), 177
- Markovnikov's rule, 277
- McLafferty rearrangement, 65
- MCPBA, see *m*-Chloroperbenzoic acid
- Meerwein–Ponndorf–Verley reaction, 84, 308
- Metal cations  
   acids and electrophiles, 97
- Metal hydrides  
   reduction of aldehydes and ketones, 278
- Methanamine, see Methylamine
- Methane  
   BDE, 76, 113  
   geometry of, 32  
   orbital energies, 26  
   point group of, 6  
   reaction with methyl radical, 149  
   total energy, 29
- Methanol  
   BDE, 76  
   BF<sub>3</sub> affinity, 123  
   IP, 123  
   PA, 123  
   p*K*<sub>b</sub>, 123  
   point group, 3
- α-Methoxy-α-trifluoromethylphenylacetic acid,  
   MTPA, 14
- Methyl acetate, 278  
   IP, 123  
   BF<sub>3</sub> affinity, 123  
   PA, 123  
   p*K*<sub>a</sub>, 142  
   p*K*<sub>b</sub>, 123
- Methyl acrylate  
   BF<sub>3</sub> affinity, 123  
   PA, 123  
   p*K*<sub>b</sub>, 123
- Methyl alanine, 13
- Methyl anion (CH<sub>3</sub><sup>-</sup>), see also Carbanions  
   gas phase, 109  
   trans effect, 181

- Methyl anion ( $\text{CH}_3^-$ ) (*Continued*)  
 as  $\text{X}^\cdot$  ligand, 176
- Methyl bromide  
 BDE, 76
- Methyl cation, 105, see also Carbocations
- Methyl chloride  
 BDE, 76
- Methyl fluoride  
 BDE, 76
- Methyl iodide, 131–132  
 BDE, 76
- Methyl methoxy carbene, 275
- Methyl radical, see also Free Radicals,  
 carbon  
 with HCl, HBr, 51, 148  
 with methane, 149  
 RSE, 113  
 structure, 110
- (*E*)-Methylacrolein  
 $\text{BF}_3$  affinity, 123  
 PA, 123
- Methylamine  
 BDE, 76
- 1-Methylantraquinone, 300–301
- Methylborane ( $\text{CH}_3\text{BH}_2$ ), 260
- 1-Methylcyclohexyl cation, 71
- Methylene, see also Carbenes  
 complex with water, 275  
 electronic states, 114  
 S—T gap, 114  
 structure, 114
- Methylene chloride  
 point group of, 5
- Methylnitrenium ion, 119
- 2-Methylpropenyl cation, 291  
 with cyclopentadiene, 291
- $\alpha$ -Methylstyrene, 272
- Michael addition, 101
- Möbius array, 85
- Molecular ion  
 RHF energy, 235  
 wave function, 235
- Molecular LEGO, 292
- Molecular orbital  
 energy of, 36  
 equation for, 36, 38
- Molecular orbital theory, 20–32
- Molecular orbitals  
 ammonia, 28  
 representations of, 27
- Molozonide, 174
- Møller-Plesset perturbation theory, 30, 241,  
 244–245  
 energy to second order, (MP2) 245  
 zero-order Hamiltonian, 244
- Monosaccharides  
 H-bonds in, 140
- MPPT, see Møller–Plesset perturbation  
 theory
- MTPA, 14
- Mulliken population analysis, 91, 236
- Naphthalene, 299  
 point group of, 5
- Negative hyperconjugation, 274, 275
- Neighboring group effect, 82
- Net Charge  
 SHMO, 91–92  
 Mulliken, 236
- Nickel tetracarbonyl, 252
- Nitrene (HN)  
 electronic states, 116–117  
 S—T gap, 116
- Nitrenes, 116–118, see also Nitrene (HN)  
 aminonitrenes, 118  
 from azide photolysis, 116  
 phenylnitrene, 118  
 substituents on, 117
- Nitrenium ion ( $\text{NH}_2^+$ )  
 electronic states, 118–119
- Nitrenium ions, 118–120, see also Nitrenium  
 ion ( $\text{NH}_2^+$ )  
 dimethylnitrenium ion, 11  
 1,2-hydride shift, 119  
 methylnitrenium ion, 119  
 phenylnitrenium ion, 120  
 substituents on, 119
- Nitrile imines, 172
- Nitrile oxides, 172
- Nitrile ylides, 172
- Nitriles  
 acids and electrophiles, 97
- Nitro compounds, 174
- Nitromethane  
 $pK_a$ , 142
- Nitrone, 174
- Nitrosyl imine, 174
- Nitrosyl oxide, 174
- Nitrous oxide ( $\text{N}_2\text{O}$ )  
 in 1,3-dipolar addition, 172  
 IP, 172
- Norbornadiene, 203, 252  
 interaction in, 48  
 IP of, 48  
 photochemistry, 202–203
- Norbornadione, 200
- Norbornene  
 IP, 48
- 2-Norbornyl cation  
 structure, 108



- Norrish type I, 66  
 Norrish type II, 66  
 Nucleophiles  
   alpha effect, 132  
   hydrazines, 132  
   hydroxylamines, 132  
   peroxides, 132
- OCAMS, xiv, 197
- Octahedral coordination, 177  
   orbitals, 177
- Octahedral crystal-field splitting ( $\Delta_O$ ), 181  
   effect of formal oxidation state, 182  
   effect of ligands on, 181  
   effect of type of metal, 181
- Octamethyl-1,4-cyclohexadiene, 273  
   complex with  $\text{NO}^+$ , 273
- (3*Z*,5*Z*)-Octatetraene, 200
- Olefins, see Alkenes
- Operator  
   Coulomb, 228, 245  
   dipole moment, 237  
   exchange, 228  
   exchange-correlation, 246  
   Fock, 229  
   Hamiltonian, 218, 220  
   Laplacian, 220  
   antisymmetrizer, 223  
   properties, 223
- Optical purity, by NMR, 13, 14
- Orbital correlation diagrams, 196–203  
   cycloaddition reactions, 197–196  
     Diels–Alder, 198  
     ethylene + ethylene, 198  
   electrocyclic reactions, 198–200  
     butadienes, 199  
     hexatrienes, 199  
   limitations, 203  
   photochemical, 201  
   Woodward–Hoffmann, 197
- Orbital energies, see also Energies, orbital  
   degeneracy, 27, 90
- Orbital interaction theory, 34–71  
   diagram, 40, 42, 47  
   limitations, 69–71  
   sigma bonds, 72–86
- Orbitals  
   atomic, and symmetry, 16–17  
   hydrogen-like atomic, 233  
   molecular, and symmetry, 17–18  
   properties and uses, 250
- Organometallic compounds, 175–195
- Orthonormal set, 222
- Overlap, effect of, 44–45  
   general principles, 52  
   integrals, 37  
   matrix, 230  
   sigma versus pi, 45
- 2-Oxaallyl, 309
- 2-Oxacyclohexanol, 310–311
- Oxaloacetic acid, 12
- 2-Oxanol, 310–311
- Oxetane  
    $\text{BF}_3$  affinity, 123  
   IP, 123  
   PA, 123
- Oxidation  
   by hydride abstraction, 145
- Oxidation potential  
   relationship with BDE and  $\text{p}K_a$ , 112–113
- Oxidation state, formal, 176  
   effect on  $\Delta_O$ , 181
- Oxidative addition, 175, 176  
    $\text{H}_2$  from  $\text{Fe}(\text{CO})_4\text{H}_2$ , 195  
   to  $\text{H}-\text{H}$  and  $\text{C}-\text{H}$  bonds, 194–195  
    $\text{M}(\text{PH}_3)_4 + \text{H}_2$ , 195  
    $\text{Ru}(\text{CO})_4 + \text{CH}_4$ , 195
- Oxidizing agents, 77
- Oxirane  
   complex with  $\text{HCl}$ , 281
- Oxiranes  
   ring opening, 200
- Oxonium ion, 311
- Ozone, 174  
   complex with acetylene, 304
- Ozonolysis  
   as 1,3-dipolar addition, 174
- Pentacoordinated metals  
    $\text{Cr}(\text{CO})_5$ , 177  
    $\text{Fe}(\text{CO})_5$ , 177  
    $\text{KPtCl}_3(\eta^2-\text{C}_2\text{H}_4)$ , 187  
    $\text{Mn}(\text{CO})_5$ , 177  
   orbitals of, 185
- (*E*)-1,3-Pentadiene
- (*Z*)-Pentadienone, 265  
   Diels–Alder with butadiene, 266, 267  
   SHMO, 265, 266
- Pentadienyl  
   SHMO, 89  
   amino, 154  
   formyl, 155  
   vinyl, 156
- Pericyclic reactions, 161–174  
   cheletropic, 165–166  
   component analysis, 167–168  
   rule for, 168

- Pericyclic reactions (*Continued*)  
 cycloadditions, 162–165  
 cycloreversions, 162–165  
 electrocyclic, 165  
 general considerations, 161  
 sigmatropic, 166–167
- Peroxides, 132  
 conformation, 77
- Peroxy acids, 302–303  
 and alkenes  
 interaction diagram, 303
- Perturbation theory, 241–245  
 and orbital interaction theory, 45
- Perturbative MO theory, 34
- (*S*)-1-Phenylethanol, preparation, 12
- Phenyl carbene (:CHC<sub>6</sub>H<sub>5</sub>), 116, 275
- Phenyl nitrene (C<sub>6</sub>H<sub>5</sub>N), 118
- Phenyl nitrenium ion, 120
- [4]Phenylene, 150
- 1-Phenyl-2,2,2-trifluoroethanol, 13
- Phosphenium ions, 119
- Phosphine (PH<sub>3</sub>)  
 basicity relative to ammonia, 256  
 interaction diagram, 256
- Phosphonium (PH<sub>4</sub><sup>+</sup>), 257
- Phosphorescence, 208, 211  
 time scale, 212
- Photochemistry, 209–217  
 Dauben–Salem–Turro, 212–213  
 from orbital correlation diagrams, 201–203  
 quenching, 215  
 sensitization, 215
- Photodimerization, 202
- Photoexcitation, 209–210  
 time scale, 212
- (+)- $\alpha$ -Pinene, 11
- $pK_a$   
 acetoacetone, 142  
 acetone, 142  
 acetonitrile, 142  
 acetylene, 142  
 cyclopentadiene, 142, 281  
 cubane, 282  
 dimethylsulfone, 142  
 ethane, 142  
 ethylene, 142  
 HF(aq), 139  
 hydrocarbons, 283  
 methyl acetate, 142  
 nitromethane, 142  
 propene, 142  
 relationship with BDE and  $E_{ox}$ , 112–113  
 toluene, 142
- $pK_b$   
 acetaldehyde, 123  
 acetone, 123  
 dimethyl ether, 123  
 formaldehyde, 123  
 methanol, 123  
 methyl acetate, 123  
 methyl acrylate, 123  
 table of, 123  
 water, 123
- Point groups, molecular, 3–6
- Polarization functions, 25, 233
- Polyethylene, 193
- Polymerization  
 Kaminsky, 193  
 Ziegler–Natta, 192
- Population analysis  
 Mulliken, 91, 236  
 SHMO, 91–92
- Post–Hartree–Fock methods, 239–245
- Potential energy, 219
- Potential energy surface, 210
- Previtamin D<sub>3</sub>, 309–310
- Probability  
 and wave function, 21
- [1.1.1]propellane, 263  
 interaction diagram, 264
- Propene, 100  
 $pK_a$ , 142
- 2-Propyl carbanion, 109
- Proteins  
 H-bonds in, 138, 140
- Proton abstractions  
 parallel to S<sub>N</sub>2, 141
- Proton affinities, 97
- Proton affinity (PA)  
 acetaldehyde, 123  
 acetone, 123  
 acrolein, 123  
 butenone, 123  
 dimethyl ether, 123  
 dimethylacrolein, 123  
 formaldehyde, 123  
 methanol, 123  
 methyl acetate, 123  
 methyl acrylate, 123  
 (*E*)-methylacrolein, 123  
 oxetane, 123  
 table of, 123  
 tetrahydrofuran, 123  
 water, 123
- Protovitamin D<sub>3</sub>, 310
- Pyridine  
 nucleophilic attack, 158

- Pyridine (*Continued*)  
 SHMO, 156  
 three-electron bond to chlorine atom, 286  
 interaction diagram, 287  
 SHMO, 287
- Pyridinium ion  
 nucleophilic attack, 158  
 SHMO, 156
- Pyrrole  
 nucleophilic attack, 158  
 SHMO, 156
- Pyruvate decarboxylase, 301–302  
 mechanism, 302
- Pyruvic acid, 301–302  
 pyruvate decarboxylase, 302
- Quadratic formula, roots, 43
- Quadricyclene, 203  
 photochemistry, 202–203
- QCISD(T), 30
- Rabbit ears, 17, 27
- Radical  
 electrophilic, 111  
 nucleophilic, 49, 111  
 one-electron, 51  
 three-electron, 49
- Radical stabilization energy, 113–114  
 and BDE, 113  
 table of, 114
- Radicals  
 hydrogen bridged, 147–148
- Rayleigh–Schrödinger perturbation theory, 31,  
 241–244  
 energy to first order, 242  
 energy to second order, 244  
 wave function to first order, 243
- Reactivity  
 acidity, 68–69  
 basicity, 66–68  
 electrophilicity, 68–69  
 from interaction diagrams, 66–69  
 nucleophilicity, 66–68
- Reductive elimination, 176
- Resonance integral, beta  
 energy scale, 92  
 effect of coordination number, 93  
 heteroatoms, 93  
 table of, 94
- Restricted Hartree–Fock theory (RHF), 23,  
 234–236  
 energy, 35  
 operator, 35
- Retinal imine, 270, 272
- Rhodopsin, 270, 272
- Rotation barrier  
 ethane-like molecules, 78
- Rotational levels, 210
- RSE, see Radical stabilization energy
- Schoenflies notation, 2–3
- SCF Energies  
 of first row hydrides, 29
- Schrödinger equation, 21, 218  
 electronic, 220
- Self-consistent field (SCF), 230  
 anti-Sesquinorbornatriene, 248  
 SHMO, see also Simple Hückel molecular  
 orbital theory  
 allyl, 89  
 amide group, 126  
 aniline, 153  
 benzaldehyde, 153  
 benzene, 90, 151  
 borazine, 288  
 butadiene, 89  
 carbonyl, 121, 124, 278  
 N-chloropyridine, 287  
 2-cyanofuran, 267  
 cyclobutadiene, 90, 151  
 cyclopentadienone, 268  
 cyclopentadienyl, 90, 151  
 cyclopropenyl, 90, 151  
 enol, 95  
 enolate, 95  
 ethylene, 88, 266  
 fulvene, 268  
 furan, 267  
 pentadienone, 265, 266  
 pentadienyl, 89, 151  
 amino, 154  
 formyl, 155  
 vinyl, 156  
 pyridine, 156  
 pyridine-*N*-oxide, 156  
 pyridinium ion, 156  
 pyrrole, 156  
 styrene, 153  
 tropylium, 151  
 vinylboronic acid, 311
- SHMO computer program, xiv
- Sigma bonds  
 C—X, 72–74  
 cleavage, 74  
 electron acceptors, 81–82  
 electron donors, 83–84  
 pi interactions of, 78, 79  
 SHMO, 96  
 strengths, table, 76
- Sigmatropic reactions, 163, 166–167

- Sigmatropic reactions (*Continued*)  
 stereochemistry, 166–167  
 Cope rearrangement, 164, 166  
 component analysis, 168
- Silaethene  
 $\pi$  bond energy, 104
- Silaethenes, 103–104
- Silane  
 reaction with silyl radical, 149  
 reaction with thiyl radical, 149
- Silyl cations, 108
- Silyl radical  
 reaction with silane, 149
- Silylenes, 116
- Simple Hückel molecular orbital theory, 86–97  
 alpha, 87  
 approximations, 87  
 beta, 87
- Slater determinant, 251, see also Determinantal wave function
- $S_N1$  mechanism, 129–130  
 alkyl halides, 129  
 carbocation intermediates in, 106  
 leaving group, 130  
 Lewis acid catalysis, 130
- $S_N2$  mechanism, 130–136  
 alkyl halides, 130  
 carbocation intermediates in, 106  
 and E2, 143  
 gas phase, 144  
 geometry of approach, 131  
 leaving group, 130, 132  
 nucleophilicity, 131–132  
 substituent effects, 132–134  
 transition state, 132, 133  
 VBCM description, 134–135
- Snoutene, 247  
 rearrangement, 289
- Sodium borohydride, 83, 278
- Sodium hydride, 83
- Soft Electrophiles, 110  
 reaction with enolate, 110
- Spin function, 234
- Spin-Spin Coupling, and *ss* character, 16
- Spiropentadiene, 273
- Split valence basis set, 24–25
- State correlation diagrams, 203–208  
 carbene to alkene, 207  
 Dauben–Salem–Turro, 212–213  
 Norrish type I, 215–217  
 Norrish type II, 213–215  
 from orbital correlation, 203–206  
 rules for, 206
- Stationary point, 209
- Steric interaction, 47
- Stereoisomers, 8
- Stereoheterotopic groups, 9
- STO-nG, 24
- Structures  
 of first row hydrides, 32
- Styrene  
 SHMO, 153
- Substituent types, 99  
 see “C” substituents  
 see X: substituents  
 see Z substituents
- Sudden polarization, 272
- $\alpha$ -Sulfonyl carbanion, 277–278
- Sulfuric acid, 100
- Suprafacial, 163  
 examples, 164  
 sigma bonds, 167
- Synthesis, asymmetric, definition, 9
- Tachysterol<sub>3</sub>, 310
- Tetracoordinated metals  
 FeCl<sub>4</sub>, 184  
 Fe(CO)<sub>4</sub>, 184  
 Ni(CO)<sub>4</sub>, 184  
 orbitals of, 182–184
- Tetracyanoethylene, 273
- Tetrahydrofuran  
 BF<sub>3</sub> affinity, 123  
 IP, 123  
 PA, 123
- Tetramesityldisilene, 104
- Tetramethylcyclobutadiene, 296
- Tetrazenes, 118
- Thiirane, 253  
 cation, 253
- Thiiranes  
 ring opening, 200
- Thiocarbonyl compounds, 280
- Thioethers  
 from carbocations, 107
- Thioketones, 280
- Thiols  
 from carbocations, 107  
 reaction with RS<sup>+</sup>, 149
- Thiyl radical  
 with RSH, 149  
 with silane, 149
- Thiophene, 1,1-dioxide, 304
- Thymine, 138
- Time scales, 211–212  
 electronic excitation, 212
- Titanium tetraisopropoxide, 11
- Toluene  
 p*K*<sub>a</sub>, 142  
 $\alpha$ -(*o*-tolyl)acetophenones, 301

- Trifluoromethyl  
 radical, RSE, 113  
 as *Z* substituent, 109
- Trimesitylsilicenium cation, 108
- bis*-(Trimethylamine)alane, 305
- Trans effect, 181  
 effect of ligands, 181
- Transition metal bonding  
 orbitals, 176–178
- Transition metals, 175–176  
 orbital energies, 178–179  
 and  $|\beta|$  scale, 179  
 table, 176  
 valence orbitals, 179–180  
 reaction with C—H, H—H, 186
- Tricarboxylic acid cycle, 12
- Tricoordinated metals  
 HFe(CO)CH<sub>3</sub>, 182  
 MC<sub>3</sub><sup>−</sup> + ethylene, 189–191  
 Ni(C<sub>2</sub>H<sub>4</sub>)<sub>3</sub>, 182  
 orbitals of, 182, 183
- Tricyclobutabenzene, 150
- Tricyclo[3.1.0.0<sup>2,4</sup>]hexane  
 group designations, 9
- 1-Trifluoromethylperfluoro-1-cyclobutyl  
 carbanion, 273  
 interaction diagram, 274
- Trimethylamine  
 IP, 81
- Triphenylcarbinol (Ph<sub>3</sub>COH), 281
- Triphenylmethyl carbocation, 106, 146, 281
- Triphenylphosphine (PPh<sub>3</sub>)  
 effect on Δ<sub>O</sub>, 181  
 as L: ligand, 176  
 trans effect, 181
- Trisbicyclo[2.1.1]hexabenzene, 150
- Tris(ethylenediamine) complexes  
 point group of, 5
- Tropylium cation, 275  
 synthesis, 146
- Tropylium tetrafluoroborate, 281
- Twistane  
 point group of, 4
- Two-orbital interaction, 35–43
- Unbound state, 209–210
- Unrestricted Hartree–Fock theory (UHF), 23,  
 222–234
- Urea, 304
- Valence bond configuration mixing (VBCM),  
 xiv  
 relation to orbital interaction theory, 69–70  
 S<sub>N</sub>2 reaction, 134–135
- Van der Waals  
 attraction, 50, 53  
 forces, 315  
 surface, 53
- Variation method, 37, 221, 240
- Vertical excitation, 210
- VBCM, see Valence bond configuration mixing  
 theory
- Vibrational cascade, 211  
 time scale, 212
- Vinyl acetate, 111–112
- Vinylboronic acids, 311–312  
 SHMO, 311
- Vinylcyclopropane, 291  
 sigmatropic rearrangement, 291
- Vitamin D<sub>3</sub>, 310
- Wacker process, 292–293
- Wagner–Meerwein rearrangement, 84  
 in carbocations, 107
- Water (H<sub>2</sub>O)  
 BDE, 76  
 BF<sub>3</sub> affinity, 123  
 complex with :CH<sub>2</sub>, 275  
 dimer, 138  
 effect on Δ<sub>O</sub>, 181  
 geometry of, 32  
 IP, 123  
 as L: ligand, 176  
 localized orbitals of, 18  
 orbital energies, 26  
 PA, 123  
 p*K*<sub>b</sub>, 123  
 point group of, 5  
 total energy, 29  
 trimer, 139
- Wave function, 218  
 many-electron, 221  
 determinantal, 23, 222  
 RHF, 234  
 UHF, 222  
 one-electron, 221, see also Orbitals  
 orbital, 22  
 probability, 21
- Woodward–Hoffmann correlation, 197
- X: ligands, list, 176
- X: substituents  
 Cope rearrangement, 171  
 electrophilic addition  
 alkenes, 99–101  
 benzenes, 153–154  
 interaction with  
 C=C, 100

X: substituents (*Continued*)

- C—H, 145
- C=O, 122
- carbanion, 109
- carbon radical, 111
- carbocation, 106
- carbene, 115
- nitrene, 117
- nitrenium, 119
- list of, 100
- on nucleophiles, 125

## “Y”-Conjugation, 304

## Ylides

- phosphonium, 109–110
- sulfonium, 109–110

## Z substituents

- boron, trigonal, as, 110
- Cope rearrangement, 171
- electrophilic addition
  - alkenes, 101
  - benzenes, 154–155

## interaction with

- C=C, 100
- C—H, 143
- C=O, 122
- carbanion, 109
- carbon radical, 111
- carbocation, 106
- carbene, 115
- nitrene, 117
- nitrenium, 119

## list of, 101

trifluoromethyl as, 109, 275

Zeise's anion, 292

Zeise's salt ( $\text{KPtCl}_3(\eta^2\text{-C}_2\text{H}_4)$ ), 187

- barrier to rotation, 189
- binding energy, 186
- bonding, 187–191
- interaction diagram, 188
- structure, 189

Zero-point vibrational energy, 33

Ziegler–Natta polymerization, 192–194

ZPVE, see Zero-point vibrational energy

Zwitterionic state, 212